

# **WET STEAM TURBINES**

## **FOR NUCLEAR POWER PLANTS**



Alexander Leyzerovich, PH.D.

# Wet-Steam Turbines for Nuclear Power Plants

Alexander S. Leyzerovich



Copyright © 2005  
PennWell Corporation  
1421 South Sheridan Road  
Tulsa, Oklahoma 74112  
1-800-752-9764  
[sales@pennwell.com](mailto:sales@pennwell.com)  
[www.pennwell.com](http://www.pennwell.com)  
[www.pennwell-store.com](http://www.pennwell-store.com)  
Managing Editor: Stephen Hill  
Cover Designer:  
Book Designer: Clark Bell

Library of Congress Cataloging-in-Publication Data  
Leyzerovich, A. Sh. (Aleksandr Shaulovich)  
Wet-steam turbines for nuclear power plants / by Alexander S.  
Leyzerovich.—1st American ed.

p. cm.

Includes bibliographical references and index.

ISBN 1-59370-032-6

1. Boiling water reactors—Equipment and supplies.
2. Steam-turbines. I.Title.

TK9203.B6L45 2005

621.48'3—dc22

2005009821

All rights reserved. No part of this book may be reproduced, stored in a retrieval system, or transcribed in any form or by any means, electronic or mechanical including photocopying or recording, without the prior permission of the publisher.

Printed in the United States of America

1 2 3 4 5 09 08 07 06 05

Chinese, 1985) and *Technological Fundamentals of Power Steam Turbine Start-Up Automation* (1985), as well as in many papers published in various power engineering periodicals, in both Russian and English.

I would like to express my deep gratitude to E. R. Plotkin, N. S. Tchernetsky, V. B. Kirillov, A. D. Melamed, N. A. Rusanova, E. N. Sergiyevskaya, V.A. Panfilov, N. I. Davydov, B. N. Lyudomirsky, and others of my collaborators at VTI, as well as many of my colleagues from the turbine manufacturers and nuclear power plants with whom I was working in close contact during those years. I would also like to thank all of the colleagues from various countries who have helped me in gathering materials for this book.

*Dr Alexander S. Leyzerovich*

# Contents

List of Illustrations .....	xi
List of Tables.....	xxvii
Preface .....	xxix
<b>1. The Nuclear Power Industry at the Turn of the 21st Century.....</b>	<b>1</b>
The Early History of Nuclear Wet-Steam Turbines .....	1
Operating Performances in the Nuclear Power Industry.....	5
Main Types of Reactors Used for Power Production.....	18
The Nearest Prospects for Wet-Steam Turbine-Based Nuclear Power Plants .....	26
References.....	31
Bibliography.....	35
<b>2. The Thermal Process in Wet-Steam Turbines .....</b>	<b>39</b>
Initial, Partition, and End Steam Conditions.....	39
Features of Wet-Steam Flow in the Turbine Steam Path.....	53
Wet-steam flow in turbine blade rows .....	54
The influence of wetness on wet-steam turbine efficiency .....	63
Experimental research of wet-steam flow in turbines .....	74
References.....	93
Bibliography.....	97

<b>3. Design.....</b>	<b>101</b>
General Design Features of Wet-Steam Turbines .....	104
Influence of single capacity and rotation speed on turbine design ..	104
Blading, gland seals, and protection against erosion-corrosion wear.	136
Steam admission elements.....	148
Bearings .....	157
Last Stage Blades.....	161
Length of the last stage blades.....	161
Roots, shrouds, and snubbers.....	170
Aerodynamics of LSBs .....	180
Last stage blade protection against WDE .....	190
Water Removal from Turbines.....	194
Peripheral moisture separation and removal between the stage rows.....	195
Intrachannel moisture separation.....	199
Moisture separating stages, or stage-separators .....	204
External moisture separators and reheaters .....	206
References.....	217
Bibliography.....	225
<b>4. Operation.....</b>	<b>233</b>
Operating Conditions of Wet-Steam Turbines .....	233
Efficiency of Wet-Steam Turbines and Heat-Rate Performance Tests .....	258
Some Generic Damages of Wet-Steam Turbines and Their Causes.....	276
Stress-corrosion and corrosion-fatigue cracking .....	279
Erosion-corrosion of turbine casings.....	293
Damages to blading .....	296

Protection and Preservation of Steam/Water Paths Using Microadditives of Amines-Based Surfactant .....	305
Experimental Research and Calculation of Transients for Wet-Steam Turbines .....	310
Start-up tests of wet-steam turbines .....	310
Calculation of temperature fields for main turbine design elements..	337
Calculated optimization of start-up diagrams .....	343
Information Support for Operators and Automated Control During Turbine Transients.....	356
References.....	375
Bibliography.....	385
<b>5. Refurbishment .....</b>	<b>395</b>
Retrofitting Versus Repairing .....	395
Retrofitting IP Cylinders.....	402
Replacing disk-type rotors with welded ones (experience of ALSTOM).....	402
Replacing LP disk-type rotors with solid ones (experience of Westinghouse) .....	408
Retrofitting LP cylinders with disk-type rotors (experience of Siemens) .....	411
Complete Upgrading of Turbines Including Both HP and LP Cylinders .....	415
Upgrade Experience of Siemens.....	415
Upgrade Experience of Mitsubishi Heavy Industries .....	419
Upgrade Experience of ALSTOM at SONGS .....	421
References.....	427
Bibliography.....	431

<b>Appendix. List of Abbreviations and Symbols.....</b>	<b>435</b>
Abbreviations of Institutions in the Power Industry.....	435
Acronyms.....	436
Symbols .....	438
Subscripts and Superscripts.....	440
Criteria of Similarity.....	441
Conversion Table for Main Units Used.....	442
Index .....	443

# 1

---

---

# The Nuclear Power Industry at the Turn of the 21st Century

## The Early History of Nuclear Wet-Steam Turbines

The first kilowatt-hours of electricity from nuclear energy were produced on December 20, 1951, in the United States by a steam turbine generator fed with steam from Experimental Breeder Reactor-I (EBR-I). The turbine had a rated output of 200 kW and initial steam conditions of 2.8 MPa and 220°C (405 psi, 429°F). In 1953, tests began at the shore-based prototype of a steam-turbine unit for the first nuclear-powered U.S. submarine, the *Nautilus*, and in 1954, the Soviet Union launched the first experimental nuclear power installation, with a rated output of 5 MW. The first commercial power generating unit with a nuclear reactor as a steam supply source was placed in service in 1957 at Shippingport.<sup>1</sup> The Westinghouse turbine of this unit was designed for a rotation speed of 1,800 rpm and a maximum capability rating of 100 MW. It was fed with saturated dry steam, with the inlet steam pressure varying from 3.8 MPa (545 psi) at the maximum load to 5.9 MPa (850 psi) when the reactor was at idle. As shown in Figure 1-1, the turbine was a single-cylinder, single-exhaust machine with 40-inch last stage blades.

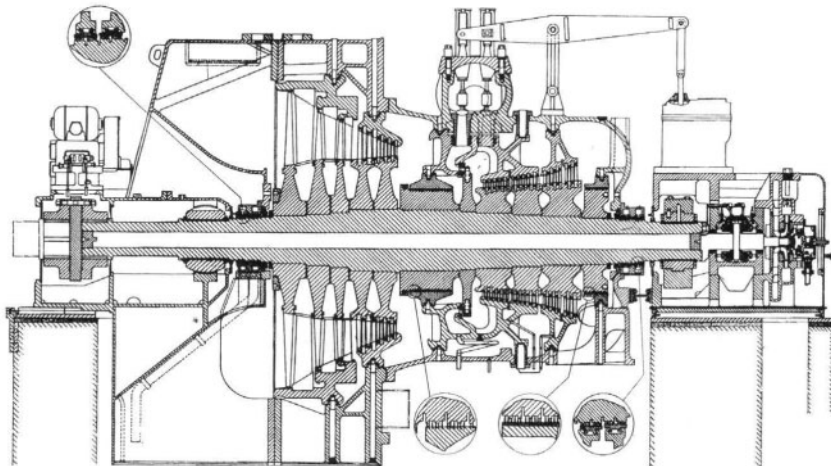


**Fig. 1-1.** Westinghouse nuclear wet-steam turbine (100-MW, 1,800 rpm) used at Shippingport Station, 1957

Source: J.A. Carlson<sup>2</sup>

It was the first relatively large wet-steam turbine developed for nuclear power plants. It worked with the steam expansion process occurring primarily in the moisture region. The major problem in this case is the increase of the moisture content as the steam expands. Excessive moisture primarily contributes to turbine blade erosion and blade efficiency losses. If steam at a dry and saturated condition expanded directly to the steam pressure in the condenser, the moisture content at the turbine exhaust could reach 20–25%, depending on the inlet pressure and vacuum conditions.

The first nuclear wet-steam turbines were developed from a base of design and operation experience accumulated with fossil fuel non-reheat steam turbines dating back to the 1920s and 1930s. In particular, of significance was the experience gained from bottoming turbines operated on the exhaust steam of piston engines or technology processes. However, because of essentially low initial steam pressure, the final moisture content for all of those turbines was not so great, and the rather low temperatures mitigated the intensity of the corrosion and erosion processes. In addition, all of those old turbines were inadequate in terms of capacity for turbines to be used in nuclear

power units, whose output should be counted in hundreds of megawatts. Relatively low initial steam pressure and a comparatively small heat drop would result in extremely large volumetric flow amounts at both the turbine inlet and exhaust, and this scale effect had to be taken into consideration.

Most of the first nuclear steam turbines, beginning with the one at Shippingport, were designed as low-speed turbines (with a rotation speed of 1,800 or 1,500 rpm). The large physical size of such turbines provided the necessary inlet and exhaust annular areas of the steam path without an excessive increase in the circumferential speed of the rotating blades. In order to decrease the final moisture content at the turbine exhaust and improve the cycle efficiency, the turbines were designed with mechanical moisture separation between the high-pressure (HP) and low-pressure (LP) sections. The moisture separator for the Shippingport turbine was a stationary, centrifugal type, and the quality of steam entering the LP section was about 99%.

One of the design requirements for the Shippingport turbine was that the highest turbine efficiency should be at partial loads, because the initial reactor core was expected to have a capability of only about 60 MW (it was later replaced to achieve a 100-MW capability). To meet this requirement, the turbine was designed with a bypass-type steam control. The first group of five control valves admitted steam in sequence to separate nozzle chambers under a group nozzle control for loads of up to 80 MW. For greater loads, steam was admitted additionally to the first-stage chamber through a second group of four control valves operating in parallel, bypassing the first turbine stage. All nine control valves were mounted on two crossbars in the steam chest at the top of the turbine. The turbine was designed with opposite steam flow directions in the HP and LP sections. This made it possible to locate both the HP and LP steam admission parts at the central section of the turbine and decrease the diameter of the dummy (balance) piston required to balance the axial thrust. This also resulted in reduced balance piston leakages. To prevent intense erosion of the rotating blades, their inlet (leading) edges were protected with Stellite strips for all the blades, with the tip speed exceeding 270 m/s (900 ft/s).

Many of the first nuclear power units were designed with two or more steam turbines fed with steam in parallel from the same reactor. Double-turbine nuclear power units (with two steam turbines operating in parallel) have been used up until recently. In particular, such a project decision makes it possible to limit the turbine sizes and prevent forced reactor outage in the case of a turbine failure. However, with the increased experience and growing confidence in wet-steam turbine reliability, the single-turbine scheme has become the most widespread. With the increase in reactor capability and steam turbine capacity, nuclear turbines have been designed as multi-cylinder machines. So, for example, the next Westinghouse wet-steam turbine after Shippingport (built for Yankee Atomic Electric Company), with a rated output of 145 MW, was designed with two cylinders (double-flow HP and LP cylinders) and throttle steam control. This steam flow control type became rather typical for nuclear steam turbines, as they are supposed to work mainly with invariable maximum loads. The very first nuclear steam turbines were usually designed with shrunk-on wheel discs in both the HP and LP sections (see Fig. 1-1). Later, this concept gave way to forged and welded rotors, and the combined rotors (with shrunk-on wheel discs), if any, have been employed only in the LP sections.

The earlier nuclear wet-steam turbines (up to General Electric's 1,100-MW, 1,800-rpm turbine used at Browns Ferry in Alabama, which began operation in 1974) mostly employed moisture separation without reheat. There was even a turbine (AEG's 670-MW, 1,500-rpm turbine at Würgassen, Germany, 1971) with two-stage separation at two different pressure levels. However, most of the later wet-steam turbines have been designed with one- or two-stage steam reheat after the HP section. It is rather difficult to reheat steam inside the reactor. In particular, it would necessitate penetrating the reactor containment twice (for the cold and hot reheat steam lines). That is why for nuclear wet-steam turbines, reheating has been carried out in steam-to-steam reheaters. Reheat by main (live) steam was first used at the Italian power plant Trino Vercellese (Tosi's 187-MW, 1,500-rpm turbine, 1964), and reheat by bled steam was first incorporated in AEI's 100-MW, 3,000-rpm turbine for the British Winfrith Heath nuclear power plant. Along with this, many wet-steam turbines for nuclear power plants employ two-stage reheat (with both main and bled steam); this concept was first used in 1969 in the United States for General Electric's turbines at Oyster Creek and Nine Mile Point

(641 MW and 620 MW, respectively, both 1,800 rpm). This steam-to-steam reheat does not improve the thermal efficiency of the cycle, as distinguished from *fire reheat* for fossil fuel power units. Nevertheless, this reheat is very useful in reducing steam wetness in the LP section, and providing in this way some improvement in its efficiency, as well as mitigating erosion problems.

For a grid frequency of 60 Hz, wet-steam turbines have been designed predominantly with a rotation speed of 1,800 rpm. By the early 1980s, the largest of these were in service in the United States at Grand Gulf (Siemens/KWU's 1,306-MW turbine) and Palo Verde (General Electric's 1,359-MW turbine). For a 50-Hz grid frequency, smaller centrifugal forces allowed an economic choice between the half-speed and somewhat cheaper (because of smaller sizes) full-speed concepts. In 1984, the largest 3,000-rpm nuclear turbines were operated in Switzerland at Gösgen (Siemens/KWU's 970-MW turbine) and Leibstadt (BBC's 1,000-MW turbine), and the largest half-speed (1,500-rpm) turbines were in operation at Paluel in France (CEM's 1,347-MW turbine) and Krümmel in Germany (Siemens/KWU's 1,316 MW turbine).<sup>3</sup>

Experience in design and operation of nuclear wet-steam turbines accumulated during the first decades of their existence was reflected in some valuable monographs and articles issued in the 1960s, 1970s, and early 1980s.

## Operating Performances in the Nuclear Power Industry

By the end of 2000—about 40 years after the first experience in deriving electricity from nuclear energy—according to the International Atomic Energy Agency (IAEA), there were 438 nuclear power reactors operating in the world, with a total net electric power generation capacity of 351,327 MW. These values seem somewhat understated, not taking into account for various reasons a few nuclear power units under operation in several countries, that may or may not be IAEA members, as well as some nuclear power units that were

temporarily out of service. In 2000, six new reactors with a total capacity of 3,056 MW(e) were commissioned in Brazil, the Czech Republic, India, and Pakistan, and 33 more nuclear power reactors were reported as being under construction, including seven in Asia.<sup>4</sup> Along with the launching of new power units, some old ones were decommissioned and are permanently or temporarily out of service. As a result, by the end of 2002, the IAEA counted only 441 nuclear power reactors in the world, with a total net power generation capacity of 358,660 MW. This was despite six new reactors with the total capacity of 5,013 MW becoming operational in 2002 in the Czech Republic, China, and South Korea.<sup>5</sup>

Even though in recent years the annual increases in the world's nuclear power capacity have remained rather low, nuclear power plants have generated a significant part of the world's electricity (about 16% in 2002<sup>6</sup>), made a great contribution to the power industry in many countries, and practically dominated the power industry in some of them. Table 1-1 shows nuclear electricity production for some countries with the highest reliance on nuclear power. France and Lithuania are most dependent on it, with over 70% of their electricity generated by nuclear power plants; the next six countries on the list receive 40–60% of their total energy from nuclear power; and for eight countries, including the United States, this percentage ranges from 10% to 40%.<sup>7</sup>

The 50 nuclear power units worldwide with the greatest power production in 2001 are listed in Table 1-2.

**Table 1-1.** Nuclear electricity production in various countries (1999)

Country	Number Of Reactors In Service (Reactors Under Construction Are Indicated In Parentheses)	Nuclear Electricity Production (TWh)	Percentage Of Total Electricity Production
France	59 (0)	375.0	75.0
Lithuania	2 (0)	9.9	73.1
Belgium	7 (0)	46.6	57.7
Bulgaria	6 (0)	14.5	47.1

Slovakia	6 (2)	13.1	47.0
Sweden	11 (0)	70.1	46.8
Ukraine	14 (4)	67.4	43.8
South Korea	16 (4)	97.8	42.8
Hungary	4 (0)	14.1	38.3
Armenia	1 (0)	2.1	36.4
Japan	53 (4)	306.9	36.0
Germany	19 (0)	160.4	31.2
United Kingdom	35 (0)	91.2	28.9
United States	104 (0)	727.7	19.8
Russia	29 (3)	110.9	14.4
Canada	14 (0)	70.4	12.4
South Africa	2 (0)	13.5	7.1
India	11 (3)	11.4	2.7
China	3 (7)	14.1	1.1

Source: "Four New Plants Added to World Nuclear Fleet in 1999," *Power Engineering* 104(9): 26.

**Table 1–2.** Top 50 nuclear power plant units ranked by power production (2001)

Rank	Country	Power Plant Name, Unit	Type of Reactor	Gross Unit Capacity (MW)	Gross Power Production (GWh)
1	Germany	Isar, 2	PWR	1,475	12,396
2	Germany	Brokdorf	PWR	1,440	11,791
3	Germany	Grohnde	PWR	1,430	11,560
4	Germany	Emsland	PWR	1,400	11,526
5	Germany	Unterweser	PWR	1,410	11,206
6	Germany	Neckar, 2	PWR	1,365	11,172
7	Germany	Grafenrheinfeld	PWR	1,345	11,154

8	United States	South Texas Project, 1	PWR	1,315	10,804
9	Germany	Gundremmingen, B	BWR	1,344	10,784
10	United States	Byron, 1	PWR	1,242	10,754
11	United States	Wolf Creek, 1	PWR	1,226	10,726
12	United States	Palo Verde, 2	PWR	1,307	10,667
13	United States	Vogtle, 1	PWR	1,215	10,597
14	France	Chooz-B, 2	PWR	1,516	10,585
15	United States	Catawba, 1	PWR	1,205	10,520
16	Brazil	Angra, 2	PWR	1,350	10,498
17	United States	Limerick, 1	BWR	1,163	10,466
18	France	Flamanville, 1	PWR	1,382	10,459
19	Japan	Kashiwazaki-Kariwa, 7	BWR	1,356	10,422
20	Germany	Gundremmingen, C	BWR	1,344	10,320
21	United States	Grand Gulf, 1	BWR	1,306	10,319
22	United States	Comanche Peak, 2	PWR	1,173	10,268
23	United States	Sequoyah, 2	PWR	1,181	10,257
24	United States	McGuire, 2	PWR	1,225	10,252
25	France	Penly, 1	PWR	1,382	10,245
26	France	Paluel, 1	PWR	1,382	10,227
27	United States	LaSalle County, 1	BWR	1,137	10,142
28	United States	Palo Verde, 1	PWR	1,307	10,128
29	United States	Byron, 2	PWR	1,210	10,125
30	Germany	Biblis, A	PWR	1,225	10,093
31	United States	Watts Bar, 1	PWR	1,210	10,073
32	United States	Browns Ferry, 3	BWR	1,155	10,025
33	United States	San Onofre, 2	PWR	1,181	9,993

34	United States	Braidwood, 2	PWR	1,210	9,987
35	United States	South Texas Project, 2	PWR	1,315	9,985
36	United States	LaSalle County, 2	BWR	1,137	9,981
37	France	Belleville, 1	PWR	1,363	9,965
38	France	Chooz-B, 1	PWR	1,516	9,949
39	United States	Diablo Canyon, 1	PWR	1,164	9,948
40	United States	Waterford, 3	PWR	1,153	9,948
41	United States	Braidwood, 1	PWR	1,242	9,923
42	United States	Salem, 2	PWR	1,170	9,914
43	United States	Vogtle, 2	PWR	1,215	9,889
44	France	Nogent, 2	PWR	1,363	9,798
45	France	Cattenom, 1	PWR	1,362	9,732
46	United States	Palo Verde, 3	PWR	1,307	9,726
47	United Kingdom	Sizewell-B, 1	PWR	1,250	9,704
48	Japan	Ohi, 1	PWR	1,175	9,697
49	France	St. Alban, 1	PWR	1,381	9,691
50	Japan	Ohi, 4	PWR	1,180	9,652

Source: B. Schwieger, M. Leonard, S. Taylor, et al.

The nuclear power plants in operation have three outstanding attributes:

- 1) they do not pollute the atmosphere with greenhouse gas emissions;
- 2) they feature high operating availability; and
- 3) their electric power production is relatively cheap.

According to the Nuclear Energy Institute (NEI), power generation from nuclear power plants in the United States annually precludes the emission into the atmosphere of 3.4 million tons of sulfur dioxide ( $\text{SO}_2$ ), 1.4 million tons of nitric and nitrous oxides ( $\text{NO}_x$ ), and 694 million tons of carbon dioxide ( $\text{CO}_2$ ), the major greenhouse gas. The use of nuclear power avoids emission of as much  $\text{CO}_2$  as is released from approximately 50% of all U.S. passenger cars and light trucks. If nuclear power were not employed and were replaced by fossil fuel power plants, approximately 123 million passenger cars or 88 million light trucks would have to be eliminated to keep U.S.  $\text{CO}_2$  emissions at the current level.

For years, U.S. nuclear power plants have consistently maintained high operating performances with regard to safety, availability and economics, steadily improving them in recent years (Fig. 1-2). In 2000, according to the data released by the Energy Information Administration (EIA) of the U.S. Department of Energy, nuclear power plants in the United States generated 753.9 billion kWh, 3.5% more than the previous record in 1999.<sup>8</sup> In other words, due to raising operating performances, U.S. nuclear power plants increased their output in 2000 by an amount equivalent to more than three new 1,000-MW power units. During the 10-year period from 1990 to 2000, nuclear power production in the United States increased from 574 billion kWh to almost 754 billion kWh, while the number of nuclear power units in service actually decreased from 111 units in 1990 to 103 units in 2000 due to the decommissioning of eight old units. In 1999, for the first time, nuclear power production costs dropped below those of coal.<sup>9</sup> Nuclear power production averaged 1.83 cents/kWh (as compared with 2.13 in 1998); power production from coal remained steady at 2.07 cents/kWh; and power production from oil-fired and gas-fired power plants averaged 3.18 cents/kWh and 3.52 cents/kWh, respectively. The Exelon electric power utility, which owns 17 nuclear power units in the United States, declared nuclear power production costs of less than 2.5 cents/kWh, as compared with 3.5–4.5 cents/kWh for gas-fired power plants, assuming a gas price of \$3–4 per million BTUs.<sup>10</sup> According to *International Journal for Nuclear Power*, the cost of electricity produced at U.S. nuclear power plants decreased from 3.4 cents/kWh in the 1980s to about 1.7 cents/kWh in 2001,<sup>11</sup> and according to the NEI, in 2002 the cost was 1.67 cents/kWh.<sup>12</sup>

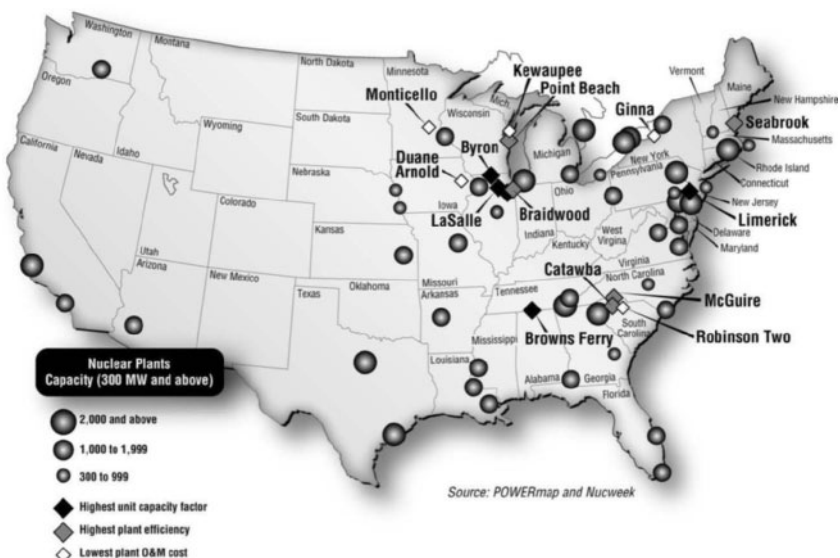


**Fig. 1–2.** U.S. nuclear power plants

Source: B. Schwieger, M. Leonard, S. Taylor, et al.<sup>13</sup>

Similar trends are also evident in other countries. For example, in Japan, the electricity production cost for nuclear power plants in the 1990s was 9 yen/kWh, compared with 10 yen/kWh for fossil fuel power plants operating on coal and liquefied natural gas (LNG) and 11 yen/kWh for oil-fired power plants.<sup>14</sup> Experts in Finland estimated that by 2000, nuclear power plants became the cheapest power producers in the country—electricity generated by them cost about 2.4 euro cents/kWh, compared with 3.2 euro cents/kWh for coal-fired power plants and 3.05 euro cents/kWh for gas-fired power plants.<sup>15</sup>

The 20 U.S. nuclear power plants with the highest efficiency are presented in Table 1–3, with ranking based on power plant data averaged for the period 1999–2001. Note that the values in the table are given with more precision than the accuracy of the initial data measurements. For all 20 plants, the heat rate variations are within 1.7% of the average, and taking into account the actual power plant instrumentation accuracy, these data can be considered statistically equal. Therefore, the data presented in the table are of concern not for comparing the individual power plant efficiency values, but for demonstrating their general level.

**Table 1–3.** Top 20 U.S. nuclear power plants ranked by efficiency (1999–2001)

Rank	Power Plant Name, Unit	State	No. and Type of Reactors	Net Capacity (MW)	Average Heat Rate (Btu/kWh [kJ/kWh])
1	Point Beach	WI	2 PWRs	994	10,046 (10,599)
2	Seabrook	NH	1 PWR	449	10,054 (10,608)
3	Catawba	SC	2 PWRs	2,258	10,068 (10,622)
4	McGuire	NC	2 PWRs	2,258	10,180 (10,741)
4	Braidwood	IL	2 PWRs	2,235	10,180 (10,741)
6	Sequoyah	TN	2 PWRs	2,238	10,230 (10,793)
7	Millstone, 3	CT	1 PWR	1,159	10,238 (10,802)
8	Watts Bar	TN	1 PWR	1,218	10,250 (10,814)
9	Byron	IL	2 PWRs	2,296	10,254 (10,819)
10	Crystal River, 3	FL	1 PWR	825	10,268 (10,833)
11	Summer	SC	1 PWR	954	10,276 (10,842)
12	Oconee	SC	3 PWRs	2,538	10,277 (10,843)
13	Wolf Creek	KS	1 PWR	1,170	10,282 (10,848)
14	Ginna	NY	1 PWR	517	10,285 (10,851)
15	Limerick	PA	2 BWRs	2,310	10,301 (10,868)
16	Farley	AL	2 PWRs	1,658	10,322 (10,890)
17	Columbia, 2	WI	1 BWR	1,100	10,331 (10,900)
18	Monticello	MN	1 BWR	545	10,350 (10,920)
19	Fermi, 2	MI	1 BWR	1,094	10,364 (10,935)
20	South Texas Project	TX	2 PWRs	2,500	10,386 (10,958)

Source: B. Schwieger, M. Leonard, S. Taylor, et al.

Nearly 75% of the production costs for a nuclear power plant are attributed to labor, whereas for coal-fired power plants, the production costs are predominately composed of fuel charges—as much as about 85%. The 20 U.S. nuclear power plants with the lowest non-fuel operation and maintenance (O&M) costs are ranked in Table 1–4. The presented data allow thinking that these expenditures can probably be further reduced.

**Table 1–4.** Top 20 U.S. nuclear power plants ranked by lowest non-fuel O&M costs (1999–2001)

Rank	Power Plant Name, Unit	State	No. and Type of Reactors	Net Capacity (MW)	Average Non-Fuel O&M cost (\$ million/yr)
1	Keweenaw	WI	1 PWR	563	53.9
2	Ginna	NY	1 PWR	517	53.9
3	Monticello	MN	1 BWR	545	55.7
4	H. B. Robinson, 2	SC	1 PWR	739	58.8
5	Duane Arnold	IA	1 BWR	614	61.9
6	Shearon-Harris	NC	1 PWR	950	67.1
7	Summer	SC	1 PWR	1,005	79.6
8	Nine Mile Point, 1	NY	1 BWR	640	82.3
9	Columbia, 2	WA	1 BWR	1,100	85.5
10	Watts Bar, 1	TN	1 PWR	1,210	87.7
11	Prairie Island	MN	2 PWRs	1,120	89.1
12	Fort Calhoun	NE	1 PWR	501	89.2
13	River Bend	LA	1 BWR	936	94.3
14	Vermont Yankee	VT	1 BWR	540	96.1
15	Callaway	MO	1 PWR	1,192	96.6
16	Grand Gulf	MS	1 BWR	1,306	96.9
17	Davis-Besse	OH	1 PWR	925	97.3
18	Waterford, 3	LA	1 PWR	1,153	99.3
19	North Anna	VA	2 PWRs	1,934	101.4
20	Fitzpatrick	NY	1 BWR	849	102.2

Source: B. Schwieger, M. Leonard, S. Taylor, et al.

The top 20 U.S. nuclear power plants ranked by annual power generation are listed in Table 1–5. The average capacity factor for U.S. nuclear power units in 1999 was more than 87%, and according to the EIA, it exceeded 90% in 2002.<sup>16</sup> According to the NEI's president, Joe Colvin, the average capacity factors for the U.S. nuclear power industry for 2001 and 2002 were 90.7% and 91.9%, respectively, and the preliminary data for 2003 gave a figure of 89.4%.<sup>17</sup> Explaining 2003's slight drop-off in performance, Colvin said, "We expect these small year-to-year variations" and expressed the hope that current

inspections, replacements, and repairs would further improve industry performances in future years.

Even more important is that the increases in availability are coupled with equally impressive improvements in safety indices. The number of “unusual events” reported to the U.S. Nuclear Regulatory Commission (NRC) dropped from 151 in 1990 to just 18 in 2000. During the same period, the median number of annual unplanned automatic shutdowns per unit dropped from 1.2 to 0, according to the Institute of Nuclear Power Operations (INPO) in Atlanta.

**Table 1–5.** Top 20 U.S. nuclear power plants ranked by power generation (2001)

Rank	Power Plant Name, Unit	State	No. and Type of Reactors	Net Capacity (MW)	Net Power Generation (GWh)	Capacity Factor (%)
1	Palo Verde	AZ	3 PWRs	3,742	28,724	87.6
2	Braidwood	IL	2 PWRs	2,235	20,241	103.4
3	South Texas Project	TX	2 PWRs	2,500	19,841	90.6
4	Vogtle	GA	2 PWRs	2,297	19,601	97.4
5	Byron	IL	2 PWRs	2,296	19,443	96.7
6	Oconee	SC	3 PWRs	2,538	19,040	85.6
7	Sequoyah	TN	2 PWRs	2,238	18,950	96.7
8	LaSalle County	IL	2 BWRs	2,200	18,584	96.4
9	McGuire	NC	2 PWRs	2,258	18,563	93.8
10	Catawba	SC	2 PWRs	2,258	18,551	93.8
11	Limerick	PA	2 BWRs	2,310	18,491	91.4
12	Comanche Peak	TX	2 PWRs	2,300	18,322	90.9
13	Browns Ferry	AL	3 BWRs	2,236	18,217	93.0
14	Diablo Canyon	CA	2 PWRs	2,160	18,078	95.5
15	Salem	NJ	2 PWRs	2,230	17,202	88.1
16	Peach Bottom	PA	2BWRs	2,186	17,049	89.0
17	Susquehanna	PA	2 BWRs	2,265	16,867	85.0
18	Donald C. Cook	MI	2 PWRs	2,130	15,824	84.8
19	San Onofre	CA	2 PWRs	2,150	15,142	80.4
20	Arkansas Nuclear One, 1	AR	2 PWRs	1,694	14,781	99.6

Source: P. Boschee, “Industry Report,” *Electric Light & Power* 80 (11): 21–24.

Table 1–6 shows similar trends in data of nuclear power generation worldwide over the last few years. Nuclear power plant capacity factor values are higher than that for the United States in seven countries, with Finland having the best three-year average capacity factor of 93.17%.

**Table 1–6.** Nuclear power generation by countries (2001).

Country	No. of Units	Total Gross Nuclear Capacity (MW(e))	Total Gross Nuclear Power Generation (2001) (GWh)	Capacity Factor (2001) (%)	Average Annual Gross Nuclear Power Generation (1999–2001) (GWh)	Average Capacity Factor (1999–2001) (%)
Argentina	2	1,005	7,059	73.10	6,781	71.15
Armenia	1	408	1,700	51.99	1,881	55.59
Belgium	7	5,995	46,349	88.81	47,841	91.18
Brazil	2	2,007	14,352	77.86	8,129	67.04
Bulgaria	4	2,880	20,020	N/A	N/A	N/A
Canada	21	15,795	77,491	53.44	69,703	50.93
China	2	1,968	14,990	86.95	14,786	85.69
Czech Republic	4	1,760	13,593	88.17	13,513	87.56
Finland	4	2,760	22,773	93.44	22,742	93.17
France	57	62,920	409,361	73.14	394,476	72.16
Germany	19	22,365	171,258	87.16	170,204	87.15
Hungary	4	1,866	14,126	86.39	14,141	87.05
India	14	2,720	19,195	78.47	15,916	69.34
Japan	52	45,082	319,345	79.43	318,930	79.16
Lithuania	2	3,000	11,362	43.24	9,685	37.71
Mexico	2	1,350	8,726	73.79	8,983	75.90
Netherlands	1	480	3,975	94.36	3,911	92.76
Pakistan	2	462	2,169	48.99	886	29.84
Romania	1	706	5,446	88.06	5,367	88.69
Russia	30	22,266	134,488	67.28	127,302	65.19
Slovakia	6	2,640	17,094	73.92	14,700	71.08

Slovenia	1	707	5,257	84.88	4,905	82.41
South Africa	2	1,930	11,293	66.79	12,797	75.62
South Korea	16	13,768	112,052	92.56	105,078	90.35
Spain	9	7,815	63,715	91.56	61,590	89.77
Sweden	11	9,844	72,232	83.65	67,575	75.94
Switzerland	5	3,352	26,673	90.00	25,945	88.08
Taiwan	6	5,144	35,486	79.76	37,472	83.41
Ukraine	13	11,880	76,175	74.26	75,236	69.42
United Kingdom	27	14,612	90,512	67.21	89,307	63.78
United States	104	103,759	794,505	88.12	781,626	86.67
Totals	427	370,366	2,602,752	—	2,531,838	—

Source: Data from B. Schwieger, M. Leonard, S. Taylor, et al.

Because of greater capital expenditures and lesser electricity costs as compared to fossil fuel plants, it is more profitable to operate nuclear power plants in a base-load mode, in which case the capacity factor value is primarily determined by the power plant's reliability and characterizes its availability. For the countries where nuclear power plants account for a significant part of the total installed power generation capacity, some nuclear plants should lower their output during the night and weekend ebbs of power consumption in order to considerably decrease their capacity factor values (Table 1-1).

France is second in the world after the United States in the number of nuclear power units in operation (see Tables 1-1 and 1-6). From 1992 to 1997, the availability of French standard nuclear power units with pressurized water reactors (PWRs) increased from 71.2% to 82.6% (20 units with 900-MW capacity and 34 units with 1,300-MW capacity).<sup>18</sup> Simultaneously, their operating expenses decreased from 5.05 to 4.48 centimes/kWh, and the average number of automatic and unplanned shutdowns per 7,000 operating hours fell from 2.9 to 1.4.

The safety level of German nuclear power plants has been raised considerably over the years, enough so that their safety record can

compare favorably with other countries.<sup>19</sup> Operating performances for German nuclear power units in 2002 are shown in Table 1-7. In 2003, 19 German nuclear power plants generated a total of 165.1 TWh of electricity, with an average capacity factor of 87.7%. This is more than 50% of the required power production in the country.<sup>20</sup>

Likewise, high levels of operating performances are recorded for nuclear power plants in Japan, Russia, South Korea, Finland, Belgium, and other countries.

**Table 1-7.** Operating performances for German nuclear power units (2002)

Power Plant Name, Unit	Reactor Type	Gross Rated Output (MW)	Gross Power Generation (GWh)	Time Availability Factor (%)	Unplanned Outages (%)	Capacity Factor (%)
Obrigheim	PWR	357	2,996	96.0	0.1	95.4
Stade	PWR	672	4,948	86.3	7.8	84.0
Biblis, A	PWR	1,225	6,558	68.3	2.7	60.3
Biblis, B	PWR	1,300	10,745	95.6	0.0	93.7
Neckar, 1	PWR	840	6,672	94.1	1.3	90.7
Neckar, 2	PWR	1,365	10,489	88.8	6.3	88.0
Brunsbüttel	BWR	806	897	13.3	80.6	12.7
Isar, 1	BWR	912	7,870	99.7	0.7	98.5
Isar, 2	PWR	1,475	12,166	95.3	0.1	94.0
Unterweser	PWR	1,410	7,114	60.6	32.6	57.5
Philippensburg, 1	BWR	926	6,896	90.0	4.0	84.2
Philippensburg, 2	PWR	1,458	11,650	92.9	0.4	90.6
Grafenrheinfeld	PWR	1,345	10,432	91.1	1.5	88.7
Krümmel	BWR	1,316	8,854	80.7	0.8	91.6
Gundremmingen, B	BWR	1,344	10,503	92.9	0.2	90.6
Gundremmingen, C	BWR	1,344	10,825	94.8	1.4	91.6
Grohnde	PWR	1,430	11,429	94.0	1.8	90.6
Brokdorf	PWR	1,440	11,922	95.9	0.0	94.5
Emsland	PWR	1,400	11,862	97.0	0.1	96.6

Source: "Operating results of nuclear power plants in 2002" (in German), *VGB PowerTech* 83 (5): 37-73.

## Main Types of Reactors Used for Power Production

The vast majority of the nuclear power units in service are equipped with light-water reactors (LWRs), which use light water as both coolant and moderator.<sup>21</sup> There are two main types of LWRs: pressurized water reactors (PWRs) and boiling water reactors (BWRs). Pressurized-water reactor versions developed in the former Soviet Union (FSU) are commonly designated as VVER, or WWER. In PWRs, the primary circuit's water is pumped at relatively high pressure into the reactor vessel where it is heated and then passed to heat exchangers (steam generators), where it boils the secondary circuit's water, which in turn evaporates and passes to the turbine (Fig. 1-3). In BWRs, the water in the reactor core is allowed to boil, and the produced steam passes directly to the turbine (Fig. 1-4). The nuclear power units with PWRs represent indirect, or two-circuit, cycles, whereas power units with BWRs employ a direct, or single-circuit, cycle. The fuel for both of these reactor types is enriched uranium dioxide, which is clad in zirconium alloy tube assemblies.

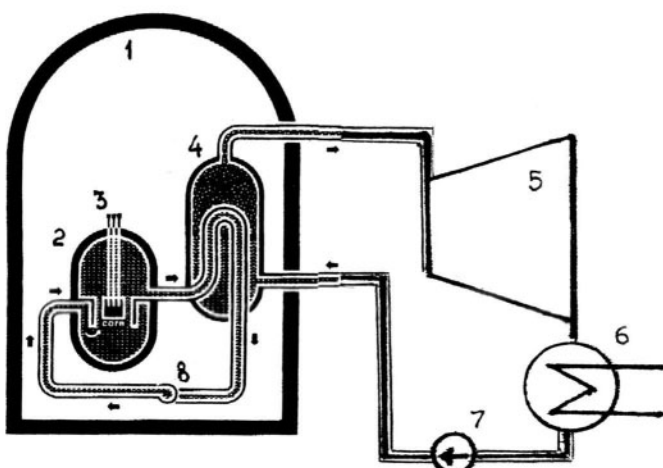


**Fig. 1-3.** Schematic diagram for a nuclear power unit with PWR (1: reactor containment structure; 2: pressure vessel; 3: control rods; 4: steam generator(s); 5: steam turbine; 6: condenser; 7: feed water pump(s); 8: main circulating pump(s))

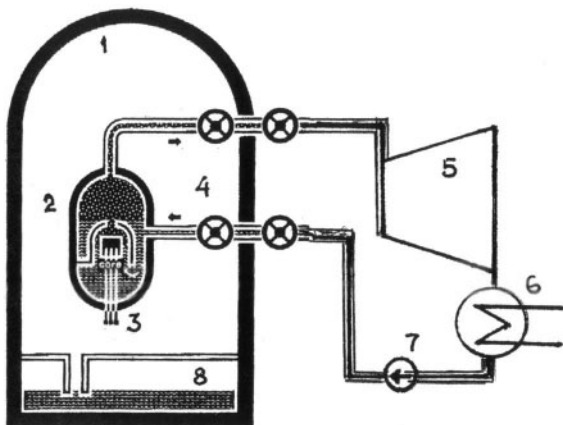


**Fig. 1-4.** Schematic diagram for a nuclear power unit with BWR (1: reactor containment structure; 2: pressure vessel and steam separator; 3: control rods; 4: isolation valves; 5: steam turbine; 6: condenser; 7: feed water pump(s); 8: water pool)

LWRs (both PWRs and BWRs) are the most widespread reactors employed by nuclear power plants throughout the world, with PWRs slightly outnumbering BWRs. The individual electric capacity of power units with LWRs presently reaches 1,400–1,500 MW (Table 1-2). A considerable amount of operating experience with these reactors has been accumulated over the last five decades. They feature high reliability and are economically competitive with fossil fuel power plants in many energy markets. Their greatest advantage is the use of ordinary, inexpensive water as moderator and coolant.

LWRs—both PWRs and BWRs—should be periodically shut down for refueling. Refueling cannot be accomplished under load, while the reactor is working. Commonly, for large-capacity LWRs, refueling takes place at intervals of about 12 to 18 months, and about a third of the core is replaced at each refueling. Thus, the fuel elements must

be capable of lasting from three to five years before discharge. For refueling, the reactor has to be shut down and brought to a cold condition. The vessel cover is then removed, allowing the fuel element assemblies to be replaced. In the process of refueling, some of the fuel assemblies in the core are removed and others are moved to different positions so that new fuel assemblies can be loaded. During refueling, it is desirable to undertake all preventive maintenance and repair operations on the unit's equipment, including any repairs or refurbishment required for the turbine. Therefore, the maintenance schedule should be closely tied with the refueling schedule. In the early 1990s, the reactor refueling process could take up to 90 days. Reducing the amount of refueling time has been one of the main sources of raising availability and capacity factors of nuclear power plants. In 1999, the median refueling time for U.S. nuclear power units with PWRs dropped to 39 days, and some power plant operators have been able to complete refueling procedures in as few as 21 days.<sup>22</sup> In 2000, Hope Creek managed to complete the refueling of its 1,000-MW BWR in 32 days and 18 hours—15 days quicker than the plant's previous best.<sup>23</sup>

Extending the time interval between refuelings is another way to improve a power unit's availability and lower the operating costs, along with optimizing maintenance and shortening the duration of the refueling process. Since 1998, the fuel replacement interval has been extended from one year to 18 months for 15 out of 20 standard French 1,300-MW PWR-based nuclear power units, as well as for 16 out of 34 French 900-MW units.<sup>24</sup>

Both PWRs and BWRs have massive steel pressure vessels that are only manufactured in a small number of countries with highly developed heavy industry technologies. Because of high power density in the core, a PWR pressure vessel is relatively small, with thick steel walls. The highly pressurized primary circulation system of PWRs is extensive and increases the possibility of a major rupture. The PWR steam generators also often show susceptibility for breaking down. The PWR coolant system becomes highly radioactive during use, and adequate shielding of the operational personnel is an important requirement. BWR-based power units have a single circuit, and the coolant is pumped into the reactor vessel at a lower pressure than in PWR-based units. For a comparable output, a BWR reactor vessel is considerably larger and heavier than one in a PWR,

even though the reactor vessel wall is thinner. The primary coolant system for a BWR, though smaller than that for a PWR, is still very expensive and poses a potential hazard of radioactive leakage. Radioactive steam passing to the turbine also requires special countermeasures for protecting the operational personnel.

In addition to the previously mentioned issues, the main generic disadvantage of all LWRs is the use of enriched uranium, calling for either international supply or domestic industrial enrichment capability. To avoid the need for enriched nuclear fuel, Canada has designed and built a heavy-water-moderated reactor fueled with natural uranium—the Canada deuterium uranium (CANDU) pressurized heavy-water reactor (PHWR). As of 2000, 34 PHWRs and CANDU reactors were in operation at nuclear power plants in various countries: Canada (14 units with net individual electric power capacity of up to 750 MW); India (12 units with individual electric power capacity of about 200–220 MW); South Korea (four units of about 700 MW capacity each); China (two 665-MW units); Argentina (two units of 319 MW and 600 MW capacity); Romania (one unit of 660 MW capacity); and Pakistan (one unit of 125 MW capacity). Similar steam-generating heavy-water reactors (SGHWRs) also used to be developed and installed in the United Kingdom, Japan, and Italy.

In the initial CANDU-based projects, heavy water was used as both moderator and coolant, circulating in separate circuits, with the heavy water in the primary circuit collected in a tubed tank, called a *calandria*. In the PHWR (advanced CANDU) and SGHWR, heavy water is used only as moderator, with light water used as coolant (Fig. 1-5). The fuel, which is natural uranium dioxide, is arranged in horizontal pressure tubes made of Zircaloy. The use of natural uranium results in much lower fuel fabrication expenditures. With natural uranium, the reactor does not have a high excess of reactivity as it does in reactors using enriched nuclear fuel, and this helps to reduce the likelihood of major power trips. The use of pressure tubes for the fuel in the reactor core allows the coolant to be pressurized without the need for a large steel pressure vessel. In addition, the large core of natural uranium allows for on-load refueling without having to stop operating the unit. Owing to this, the availability and capacity factors of PHWR-based nuclear power units can reach very high values. PHWRs also are efficient producers of plutonium. All of these merits would make the PHWR highly competitive with the LWR, were heavy

water not so expensive. The CANDU-type reactors typically exhibit intensive xenon poisoning, accumulating xenon in the reactor core about one hour after a reactor trip. This sometimes makes it difficult to restart the reactor quickly after unplanned, occasional trips. After reactor trips, to enable prompt restarts and shorten the duration of preliminary technological operations, it is desirable to keep the turbine running at the synchronous rotation speed driven by the generator as a motor for about an hour. In addition, the minimal continuous load provided by the CANDU-type reactors is remarkably higher than that for LWRs (about 60% versus 25%).

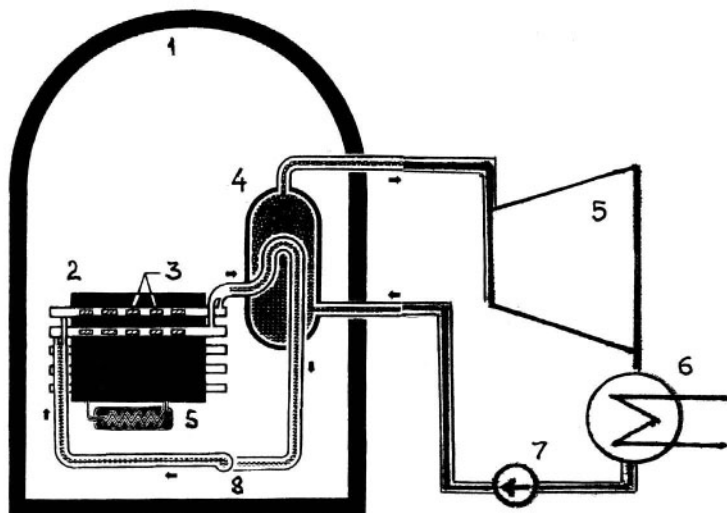


**Fig. 1–5.** Schematic diagram for a nuclear power unit with PHWR (1: reactor containment structure; 2: calandria; 3: fuel; 4: steam generator(s); 5: steam turbine; 6: condenser; 7: feed water pump(s); 8: main circulating pump(s); 9: moderator heat exchanger)

The list of the most widespread nuclear power reactors could be supplemented by light-water-cooled graphite-moderated reactors (LWGRs), which are also called pressure-tube graphite reactors (PTGRs). They were designed, constructed, and installed only in the former Soviet Union under the name RBMK—the abbreviation for the Russian term “channel reactor of large capacity.” The ill-fated

Chernobyl Unit 4 reactor was of this type, and by 2000, 14 units of this type, somewhat refurbished and made safer, were in operation in Russia, Lithuania, and Ukraine. The LWGR works with enriched uranium dioxide clad in zirconium alloy tubes and cooled by ordinary water, which is allowed to boil (Fig. 1-6). The water flows through the numerous pressure tubes arranged in channels in the body of graphite, which serves as moderator. The reactor is refueled on-load. The chief merit of this design is the possibility of achieving a large individual power capacity (an electric output of 1,500 MW or more) without using a steel pressure vessel, which is very expensive and laborious to manufacture. Its main disadvantage is that poorly controlled water flows through the numerous channels. In addition, as the Chernobyl catastrophe showed, LWGRs tend toward potential instability under certain circumstances.

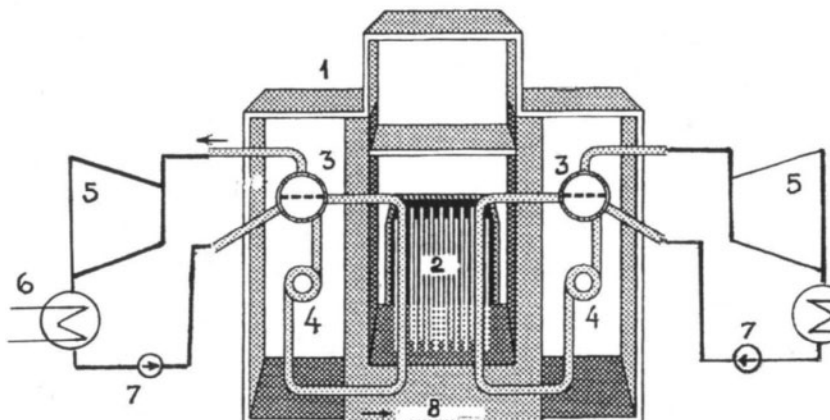


**Fig. 1-6.** Schematic diagram for a nuclear power unit with LWGR (RBMK) (1: reactor building; 2: core; 3: steam separators; 4: circulating pumps, 5: steam turbines; 6: condensers; 7: feed water pumps; 8: water to core)

All of the previously mentioned reactor types have saturated or slightly superheated steam at their outlet, and this steam produced by the reactor passes to the power unit's turbine or turbines (some nuclear power units are equipped with two or more turbines working

in parallel). The use of saturated steam requires specially designed wet-steam turbines. For two-circuit nuclear power units with PWRs or PHWRs, the steam passing into the turbine(s) does not pass through the reactor core and is not radioactive. For the single-circuit units with BWRs or LWGRs, the working steam goes to the turbine(s) just after passing through the reactor, and this places additional requirements on the turbine materials and design.

Along with the previously mentioned reactors with saturated steam at the outlet, there also exist other reactor types that have not gained as wide an acceptance, primarily including gas-cooled, graphite-moderated reactors developed in the United Kingdom and France. France quickly abandoned these reactors in favor of PWRs, but their development and application continued in the United Kingdom. According to the IAEA as of 2001, nuclear power plants in the United Kingdom utilized 13 advanced gas-cooled reactors (AGR), with an individual electric capacity of 660 MW, as well as 10 older Magnox reactors.<sup>25</sup> Magnox reactors were so named because the natural uranium oxide fuel is enclosed in a magnesium alloy canister. This reactor design was eventually superseded by the AGR, which, with higher steam pressure and temperature, operates at higher efficiency. For AGRs, CO<sub>2</sub> is employed as the coolant, and the outlet temperature is about 650°C (1,200°F). These reactors use enriched ceramic uranium dioxide fuel in stainless steel shells and have a much more effective fuel burnup than their Magnox predecessors. The early Magnox reactors used steel pressure vessels. But the later ones, as well as AGRs, were equipped with pre-stressed concrete vessels lined with mild steel and integrated into the radiation shielding to form a concrete shell over 5 m thick. An AGR can be refueled while operating under load, and its fuel elements can remain in the core for up to five years. All of these gas-cooled reactors have superheated steam at their outlet, with the steam parameters close to those employed at many fossil fuel power plants of 1960s-1980s vintage (16 MPa, 538/538°C [2,320 psi, 1,000/1,000°F]). In particular, the turbines of British nuclear power plants with these types of reactors (Dungeness-B, Hartlepool, Heysham, Hinkley Point, Hunterston-B) do not differ from those operated at British fossil fuel power plants. Owing to the higher steam conditions, the gas-cooled graphite-moderated reactors provide higher thermal efficiency as compared to those reactors producing saturated steam. In addition, the AGR is inherently a safe reactor and does not require special additional containment besides the main reinforced concrete pressure vessel. However, it requires heavy industry to support its technology, uses enriched uranium, and has not demonstrated

sufficient economic advantages to warrant acceptance outside the United Kingdom in competition with the PWR, BWR, and PHWR.

High-temperature gas-cooled reactors (HTGRs) are another further development of the gas-cooled reactor concept. The idea is to achieve higher steam temperatures at the reactor outlet by using helium as the coolant and graphite-coated spheres of enriched uranium dioxide as fuel. Experimental and prototype versions were built in the United Kingdom, the United States, and Germany, but all of them were eventually decommissioned, including the largest one—the 330-MW(e) nuclear power unit at Fort St. Vrain, with output steam parameters of 16.6 MPa and 538/538°C (2,407 psi, 1,000/1,000°F)—in 1989.<sup>26</sup>

A further development of this concept is tied to the direct use of a gaseous coolant (helium) as the working fluid for gas turbines in the Brayton cycle. Two more advanced reactor projects are based on this idea: the gas turbine-modular helium reactor (GT-MHR), developed by General Atomics, and the pebble bed modular reactor (PBMR), developed by Eskom, a large South African utility.<sup>27</sup> It might be well to note that, while typical nuclear power units with LWRs have a thermal efficiency of about 33%, a heat efficiency of more than 40% is anticipated for the basic PBMR project.<sup>28</sup> A further increase in the fuel performance leading to higher outlet gas temperatures offers the prospect of up to 50% efficiency. The world's first experimental PBMR with a capacity of 10 MW is operated in China, and a project of a 195-MW reactor is underway. Eskom plans to launch a pilot 110-MW PBMR at Koeberg nuclear plant in 2007, and Exelon has indicated an intention to apply for a license to construct the first PBMR unit in the United States.

Great expectations were set on the development of fast breeder reactors (FBRs). The FBR is not a thermal reactor, as it has no moderator and works with fast (instead of "thermal") neutrons. Worldwide, there were only a few such reactors built and put into operation, including the 250-MW Phénix and 1,242-MW Super-Phénix in France, the BN-350 and BN-600 in the former Soviet Union (with the rated electric outputs of 350 and 600 MW, respectively), and the 270-MW Dounreay in the United Kingdom. With the use of liquid sodium employed as coolant (for liquid-metal FSBs—LMFSBs), heat discharged in the fission process within the reactor core is carried away by the liquid sodium circulating within a large pool with built-in intermediate heat exchangers, which transfer the heat to

liquid sodium in the secondary, intermediate circuit. In turn, the heat transfers to the steam generators, where it is transferred to the third circuit's water, thus making superheated steam to drive the turbine. Because the core contains no moderator, the neutrons involved in the fission process are not slowed down and retain their fast speeds (hence the term "fast" neutrons). The central core region consists of a mixed uranium-plutonium oxide fuel (containing U-235, Pu-239, and U-238) surrounded by a blanket of U-238. Once launched, the FBR is self-sufficient and may even produce excess plutonium (hence the appellation "breeder"). The outlet steam conditions for such reactors (as, for example, Phénix) are approximately 16 MPa and 510/510°C (2,320 psi, 950/950°F). The FBR-based power units in service employ steam turbines hardly differing in their design from those of fossil fuel plants with the same output and steam parameters.

Research in recent years has inspired a renewed interest in the development of FBRs, as well as LWRs, with supercritical outlet steam conditions, but for the time being they remain more theoretical in nature.<sup>29</sup>

## The Nearest Prospects for Wet-Steam Turbine-Based Nuclear Power Plants

In view of the worldwide energy situation, there is no doubt that the importance of nuclear energy will continue to grow in the foreseeable future. Nuclear power plants currently make, and will have to continue to make, a vital contribution toward reducing CO<sub>2</sub> emissions into the atmosphere and conserving fossil fuel energy resources. Because of this, a new generation of power reactors is currently being implemented in newly constructed nuclear power units. Using the terminology of the U.S. Department of Energy, as proposed by the NEI, they belong to a Generation III reactor technology, embracing new design concepts developed since 2000 and certified by the NRC. Some experts have also coined a term for an intermediate Generation III+, intended for newly developed designs not yet certified by the NRC.<sup>30</sup> The next generation of technology, Generation IV,

should include unique new designs assumed to be deployable by 2030, such as supercritical water-cooled reactors, gas-cooled and lead-cooled fast reactors, and others.<sup>31</sup>

The advanced BWR (ABWR) project was developed by GE. The project's features make it more reliable, and also improve the power unit's ability to meet the power market's demands. The ABWR's compact design results in a building volume that is only 70% as large as earlier BWR projects. Similarly, the Westinghouse AP600, a Generation III reactor intended for medium-capacity nuclear power units, also uses a boiling water design, but is smaller and simpler than older BWRs, with improved safety and 50% less building space required. The Westinghouse AP1000 project is similar to the AP600 and is intended for nuclear power units with an electric output of about 1,100 MW. The NRC has also certified three other standard reactor projects, all of them targeted for capital expenditures of about \$1,000/kW.<sup>32</sup>

An essential advantage of boiling water reactors, as well as other single-circuit reactors, is the absence of the great amount of equipment normally required for the secondary circuit. The basic ABWR project was developed by an international team of BWR suppliers from Japan, the United States, Sweden, and Italy, for the 1,356 MW Kashiwazaki-Kariwa Units 6 and 7 in Japan.<sup>33</sup> Put into commercial operation in 1996 and 1997, they became the world's first nuclear power units that could rightfully be considered belonging to Generation III. Performance tests conducted at Unit 6 showed a thermal efficiency of 34.5%—the highest level yet measured at any Japanese BWR-based nuclear power plant. Two other similar units are presently under construction and scheduled to be put into operation in 2005 and 2006 (Hamaoka Unit 5 and Shika Unit 2), and four others are planned for construction in the next 10 years. In addition, Japan is scheduled to build two 1,540-MW nuclear power units with APWRs by 2011. In Western Europe, no new nuclear power units had been ordered between 1991, when France authorized construction of its latest reactor (which was finally commissioned in 1996), and December 2003, when a contract was signed for Finland's fifth nuclear power unit. According to the Finnish Ministry of Trade and Industry, six projects were bid: three with advanced BWRs (one developed by GE in the United States with a rated electric output of 1,400 MW; the Westinghouse/BNFL BWR90+ model developed in Sweden with a rated output of 1,500 MW; and Framatome ANP's 1,000-MW

SWR1000 model, developed in Germany), and three with advanced PWRs (Westinghouse/BNFL's 1,000-MW AP1000/EP; Framatome ANP's EPR, developed jointly by France and Germany, with an individual electric capacity of over 1,500 MW; and the Russian 1,000-MW VVER 91/99).<sup>34</sup> Electric energy from the new nuclear power units will be cheaper than that produced by fossil fuel power plants: 2.15 cents/kWh versus 2.41 cents/kWh for coal-fired power units, 2.61 cents/kWh for natural gas, and 3.09 cents/kWh for peat. In addition to the joint French-German EPR project, Siemens has proposed a new project, currently under consideration, known as the SWR.<sup>35</sup> In December 2003, Teollisuuden Voima Oy (TVO), developer, owner, and operator of the Olkiluoto nuclear power plant, signed a turnkey contract with the Framatome ANP-Siemens consortium for construction of the plant's Unit 3, which would be the largest nuclear power unit ever. The unit is scheduled to be commissioned in 2009, and will have a net individual capacity of 1,600 MW(e).<sup>36</sup>

South Korea has announced plans for constructing a series of Korean advanced PWRs, or Korean next generation reactors (KNGRs), also known as the APR1400.<sup>37</sup> The first two APR1400 units will be Shin-Kori Units 3 and 4. Their commercial operation is scheduled to commence in 2010 or 2011. The APR1400, with an electric output of 1,400 MW, has evolved from the 1,000-MW Korean standard nuclear plant (KSNP) project. Two KSNP units, Ulchin Units 3 and 4, have been in operation since 1998 and 1999. Yonggwang Units 5 and 6 were put into operation in 2002 and 2003, and Ulchin Units 5 and 6, currently under construction, are scheduled to be commissioned in 2005 and 2006. The economic target for the APR1400 is a 20% cost advantage over coal-fired power plants. The units are designed for a lifetime of 60 years, with a refueling interval of 18 to 24 months and an availability factor expected to be more than 90%.

Atomic Energy of Canada Limited (AECL) has proposed the next generation CANDU project (NG CANDU). It is envisaged as a medium-sized reactor with an individual electric capacity of about 650 MW, realizing a capital cost reduction of 40% relative to current nuclear power plants.<sup>38</sup> The aim is to achieve a capital expenditure level of \$1,000/kW. In this project, heavy water is used only as coolant. Among other improvements, the reactor is operated with somewhat higher outlet steam pressure that raises the unit's thermal efficiency. The NG CANDU design should replace its predecessor, CANDU 6, which is used as the

basis for two 665-MW units of the Chinese Qinshan Phase 3 (Units 4 and 5) nuclear power plant project, completed in 2003.<sup>39</sup>

Generation III nuclear power units are designed for a lifetime of 60 years, instead of the 40 years or less attributed to their Generation II predecessors. The rated lifetime for the Russian VVER and RBMK Generation II reactors was 30 years, and these units began reaching that milestone in the early 2000s, begging the question of their fate. In the next few years, the same problem will arise for some Eastern European nuclear power units constructed after Soviet projects. Evidence shows that for most of them, their lifetime can be considerably prolonged.<sup>40</sup>

By the end of 2000, 11 Japanese BWR-based power plant units had been operated for 20 years or more, and this number will almost double to 19 by 2010.<sup>41</sup> In the United States and Western Europe, several Generation II nuclear power units have also already been decommissioned, shut down, and partially or completely dismantled.<sup>42</sup> The latest example is the 662-MW(e) Stade nuclear power plant in Germany, commissioned in 1972. It was shut down on November 1, 2003. Work on dismantling its reactor is due to begin in 2005, once its fuel has been removed.<sup>43</sup>

By 2015, the NRC's operating license for more than three-dozen U.S. nuclear power units will have expired. Although it is possible that many of these units could be decommissioned, there is also a possibility of prolonging their operation. The recent 20-year license extensions granted to the two-unit, 1,700-MW Calvert Cliffs, the 2,500-MW Oconee, and the Arkansas Nuclear One nuclear power units were widely applauded and have given a shot in the arm to proponents of renewing the licenses for other aging power units. By the early 2000s, approximately 40 nuclear power units have either filed their license renewal applications or informed the NRC of their intention to do so. Many analysts believe that "the future of the U.S. nuclear power industry is brighter today than at any time since the 1979 Three Mile Island accident."<sup>44</sup> Most experts consider it desirable, and quite possible, to continue operation of existing nuclear power plants for 20 additional years beyond their original 40-year license term, which would reduce the number of new base-load nuclear and fossil fuel power plants needed to be built, thereby avoiding substantial carbon emissions.<sup>45</sup>

Many experts now consider it reasonable even to restart some nuclear power units that were shut down earlier.<sup>46</sup> In 2002, the Tennessee Valley Authority (TVA) announced that it would restart its 1,100-MW Browns Ferry Unit 1, shut down in the mid-1980s along with two others at Browns Ferry and two at Sequoyah. All five of these units were restarted and have demonstrated excellent operating performances.<sup>47</sup> These successes have made it possible to consider completing the construction of some unfinished nuclear power units. Thus, the TVA has expressed its intention to complete construction of the two-unit Bellefonte nuclear power plant and Watts Bar Unit 2.

Relicensing and restarting of existing nuclear power plants commonly happens in parallel with their uprating. Uprating involves increasing the power unit's capacity over the initially assessed value. This can also be commonly done for other, more recent, nuclear power units in service, and can be performed in two ways. First, although a given nuclear power unit may only produce as much power as licensed by the NRC, most reactors (as well as other main power equipment, including the turbines) have the design margin to produce more energy than specified by the current license. Recently, the NRC has evaluated these design margins and relaxed its policy. As a result, many nuclear power plant operators have applied for an uprating and received authorization to increase the reactor output. Second, nuclear power plants can increase their electric capacity without increasing the reactor's output by initiating technological improvements in "traditional" (non-nuclear) equipment—primarily steam turbines. The refurbishment of turbines can yield an increase in the unit output of at least 1.4–1.7% for even relatively modern turbines with the same reactor capacity.

## References

- 1 Bannister, R. L., and G. J. Silvestri, Jr. 1989. The evolution of central station steam turbines. *Mechanical Engineering* 111(2): 70–78.
- 2 Carlson, J. A. 1958. Steam turbines for nuclear power plants. *Proceedings of the American Power Conference* 20: 225–231.
- 3 Harris, F. R. 1984. The Parsons centenary—A hundred years of steam turbines. *Proceedings of the Institute of Mechanical Engineers* 198A(9): 183–223.
- 4 2001. *Operating Experience with Nuclear Power Stations in Member States in 2000*. Vienna: International Atomic Energy Agency.
- 5 2003. *Operating Experience with Nuclear Power Stations in Member States in 2002*. Vienna: International Atomic Energy Agency.
- 6 Hohlefelder, W. 2003. Nuclear power: Memorandum of understanding implications for Germany's energy sector. *VGB PowerTech* 83(5): 1.
- 7 2000. Four new plants added to world nuclear fleet in 1999. *Power Engineering* 104(9): 26.
- 8 Zink, J. C. 2001. Nukes' performance may encourage bright future. *Power Engineering* 105(6): 26.
- 9 2001. Nuclear costs less than coal. *Nuclear Engineering International* 46(559): 2.
- 10 Davis, K. 2001. Nuclear reigns as hot commodity. *Electric Light & Power* 79(6): 1.
- 11 Wesselmann, C. 2003. Nuclear power production (in German). *BWK* 55(6): 40–47.
- 12 Rigby, P. 2003. Can Washington jump-start new U.S. nuclear plants? *Platts Energy Business & Technology* 20–24.
- 13 Schwieger, B., M. Leonard, S. Taylor, et al. 2002. First annual top plants survey. *Power* 146(4): 27–70.
- 14 Sekine, Y. 1993. Nuclear power generation in Japan—Present status and future prospects. *Proceedings of the Institute of Mechanical Engineers, Part A: Journal of Power and Energy* 207: 233–246.
- 15 Toivola, A. 2004. Nuclear power as part of the Finnish electricity supply. *VGB PowerTech* 84(1/2): 52–55.
- 16 Rigby, Can Washington jump-start new U.S. nuclear plants?, 20–24.
- 17 Peltier, R. 2004. Nuclear renaissance continues. *Power* 148(5): 32–40.
- 18 Serres, R., and D. Carbonnier. 1999. French nuclear power plants—Results and outlooks. *VGB PowerTech* 79(8): 16–19.

### 32 Wet-Steam Turbines for Nuclear Power Plants

- 19 von Weiche, G., and H. Pamme. 2003. Safety culture in nuclear power plants (in German). *VGB PowerTech* 83(3): 55-58.
- 20 Zaiss, W. 2004. Performance of German nuclear power plants in 2003. *VGB PowerTech* 84(5): 2.
- 21 El-Wakil, M. M. 1984. Powerplant Technology. New York: McGraw-Hill.
- 22 2000. Nuclear power embarks on a renaissance. *Power* 144(3): 6-7.
- 23 Schimmoller, B. K. 2000. Accelerating outages & extending intervals. *Power Engineering* 104(11): 42-50.
- 24 Serres, French nuclear power plants, 16-19.
- 25 2001. *Operating Experience with Nuclear Power Stations in Member States in 2000*.
- 26 Hylko, J. M. 2002. Nuclear operators weigh decommissioning, relicensing options. *Power* 146(3): 64-70.
- 27 Gautschi, F. 2003. Nuclear power return may hinge on advanced gas-cooled reactor design. *Power Engineering* 107(3): 45-48.
- 28 Ferreira, T. 2001. PMBR: The future is now. *Modern Power Systems* 21(8): 43-44.
- 29 Generation IV: To 2030 and beyond. 2003. *Modern Power Systems* 23(2): 28-29.
- 30 Thomas, M. 2002. Nuclear power bids for wider acceptance. *EnergyTech* 2: 8-11, 52.
- 31 Generation IV: To 2030 and beyond, 28-29.
- 32 Kennedy, E. H., and R. P. Vijuk. 2003. AP1000: A passive future for the PWR. *Modern Power Systems* 23 (8): 49-52.
- 33 Moriya, K., M. Ohtsuka, M. Aoyama, and M. Matsuura. 2001. Development study of nuclear power plants for the 21st century. *Hitachi Review* 50(3): 61-67.
- 34 2002. Finland's fifth unit hangs in the parliamentary balance. *Modern Power Systems* 22(2): 26-27.
- 35 Liersch, G., J. Mattern, and R. Danisch. 1999. The new generation of nuclear power plant reactors: EPR and SWR1000. *VGB PowerTech* 79(8): 63-67.
- 36 Site work underway on Finland's 1600 MWe EPR. 2004. *Modern Power Systems* 24(3): 30-34.
- 37 2001. Koreans prepare to build the first advanced PWR. *Modern Power Systems* 21(8): 37-41.
- 38 Hopwood, J., K. Hedges, and M. Pakan. 2002. Next-generation CANDU technology. *Nuclear Plant Journal* (5): 35-38.
- 39 Haraguchi, M., Q. Liu, and S. Oda. 2001. Steam-turbine equipment for Qinshan phase-III nuclear power station in China. *Hitachi Review* 50(3): 95-99.

- 40 Riegg, G. 1999. Decommissioning in the Russian Federation: Rules, planning and concepts. *Nuclear Engineering International* 44(11): 27-29.
- 41 Ikegami, T., T. Shimura, and M. Koike. 2001. Plant life management technologies for nuclear power plants. *Hitachi Review* 50 (3): 84-88.
- 42 Wild, E. 2002. The prospects for nuclear power in Europe. *VGB PowerTech* 82(5): 69-71.
- 43 From Stade to finish. 2004. *Nuclear Engineering International* 49(595): 32-35.
- 44 Hylko, Nuclear operators weigh decommissioning, 64-70.
- 45 Moore, T. 2002. License renewal revitalizes the nuclear industry. *EPRI Journal* 27 (3): 9-17.
- 46 Swanekamp, R. 2003. License renewal, plant upgrades brighten nuclear's future. *Power* 147(1): 25-31.
- 47 Schwieger, First annual top plants survey, 27-70.

## Bibliography

- Aubert, M. 1974. Phénix 4 fast breeder power plant. *Nuclear Engineering* (218): 563–566.
- Aubry, P., S. Bayard, and A. Anis. 1986. Nuclear LP turbine design and operating experience. *Proceedings of the American Power Conference* 48: 166–171.
- Bannister, R. L., and G. J. Silvestri, Jr. 1989. The evolution of central station steam turbines. *Mechanical Engineering* 111(2): 70–78.
- Boschee, P. 2002. Industry report. *Electric Light & Power* 80(11): 21–24.
- Carlson, J. A. 1958. Steam turbines for nuclear power plants. *Proceedings of the American Power Conference* 20: 225–231.
- Davis, K. 2001. Nuclear reigns as hot commodity. *Electric Light & Power* 79(6): 1.
- El-Wakil, M. M. 1984. *Powerplant Technology*. New York: McGraw-Hill, 1984.
- Elliot, T. C., K. Chen, and R. C. Swanekamp, eds. 1998. *Standard Handbook of Powerplant Engineering*, 2d ed. New York: McGraw-Hill, 1998.
- Ferreira, T. 2001. PMBR: The future is now. *Modern Power Systems* 21(8): 43–44.
- Filippov, G. A., O. A. Povarov, and V. V. Pryakhin. 1973. *Researches and Calculations for Wet-Steam Turbines* (in Russian). Moscow: Energiya, 1973.
- Finland's fifth unit hangs in the parliamentary balance. 2002. *Modern Power Systems* 22(2): 26–27.
- Four new plants added to world nuclear fleet in 1999. 2000. *Power Engineering* 104(9): 26.
- From Stade to finish. 2004. *Nuclear Engineering International* 49(595): 32–35.
- Gautschi, F. 2003. Nuclear power return may hinge on advanced gas-cooled reactor design. *Power Engineering* 107(3): 45–48.
- Generation IV: To 2030 and beyond. 2003. *Modern Power Systems* 23(2): 28–29.
- Gyamarthy, G. 1962. *A Theory of Wet-Steam Turbines* (in German). Zurich: Juris-Verlag, 1962.
- . 1976. Basic notions. In *Two-Phase Steam Flow in Turbines and Separators: Theory, Instrumentation, Engineering*, ed. M. J. Moore and C. H. Sieverding, 1–57. Washington, D.C.: Hemisphere Publishing Corp., 1976.
- Haraguchi, M., Q. Liu, and S. Oda. 2001. Steam-turbine equipment for Qinshan phase-III nuclear power station in China. *Hitachi Review* 50(3): 95–99.
- Harris, F. R. 1984. The Parsons centenary—A hundred years of steam turbines. *Proceedings of the Institute of Mechanical Engineers* 198A(9): 183–223.
- Hohlefelder, W. 2003. Nuclear power: Memorandum of understanding implications for Germany's energy sector. *VGB PowerTech* 83(5): 1.

- Hopwood, J., K. Hedges, and M. Pakan. 2002. Next-generation CANDU technology. *Nuclear Plant Journal* (5): 35–38.
- Hylko, J. M. 2002. Nuclear operators weigh decommissioning, relicensing options. *Power* 146(3): 64–70.
- Ikegami, T., T. Shimura, and M. Koike. 2001. Plant life management technologies for nuclear power plants. *Hitachi Review* 50(3): 84–88.
- International Atomic Energy Agency. 2001. *Operating Experience with Nuclear Power Stations in Member States in 2000*. Vienna: International Atomic Energy Agency, 2001.
- . 2003. *Operating Experience with Nuclear Power Stations in Member States in 2002*. Vienna: International Atomic Energy Agency, 2003.
- Kalderon, K. 1971. Large steam turbines for conventional power plants. *Journal of Science and Technology* (1): 21–29.
- Kennedy, E. H., and R. P. Vijuk. 2003. AP1000: A passive future for the PWR. *Modern Power Systems* 23(8): 49–52.
- Kirillov, P. L. 2001. Changing over to supercritical parameters: The way to advance nuclear power stations with water cooled reactors. *Thermal Engineering* 48(12): 973–978.
- Koreans prepare to build the first advanced PWR. 2001. *Modern Power Systems* 21(8):37 –41.
- Kosyak, Y. F., ed. 1978. *Steam-Turbine Installations for Nuclear Power Plants* (in Russian). Moscow: Energiya, 1978.
- , V. N. Galatsan, and V. A. Paley. 1983. *Operating Nuclear Power Plant Turbines* (in Russian). Moscow: Energoatomizdat.
- Liersch, G., J. Mattern, and R. Danisch. 1999. The new generation of nuclear power plant reactors: EPR and SWR1000. *VGB PowerTech* 79(8): 63–67.
- Moore, M. J., and C. H. Sieverding, eds. 1976. *Two-Phase Steam Flow in Turbines and Separators: Theory, Instrumentation, Engineering*. Washington, D.C.: Hemisphere Publishing Corp., 1976.
- Moore, T. 2002. License renewal revitalizes the nuclear industry. *EPRI Journal* 27(3): 9–17.
- Moriya, K., M. Ohtsuka, M. Aoyama, and M. Matsuura. 2001. Development study of nuclear power plants for the 21st century. *Hitachi Review* 50(3): 61–67.
- Mounfield, P. R. 1991. *World Nuclear Power*. London: Routledge, 1991.
- Min, K. H., and D. R. Chari. 2004. My brilliant Korea. *Modern Power Systems* 24(3): 34–36.
- Nedderman, J. 1997. Kashiwazaki-Kariwa Unit 6 fulfills ABWR promise. *Modern Power Systems* 17(3): 50–52.
- Next generation aims to combine best of CANDU and PWR. 2002. *Modern Power Systems* 22(2): 29–30.

- Nuclear costs less than coal. 2001. *Nuclear Engineering International* 46(559): 2.
- Nuclear power embarks on a renaissance. 2000. *Power* 144(3): 6-7.
- Operating results of nuclear power plants in 2002 (in German). 2003. *VGB PowerTech* 83(5):37-73.
- Peltier, R. 2004. Nuclear renaissance continues. *Power* 148(5): 32-40.
- Proceedings of the First International Symposium on Supercritical Water-Cooled Reactors.* 2000. Tokyo, Japan, 2000.
- Riegg, G. 1999. Decommissioning in the Russian Federation: Rules, planning and concepts. *Nuclear Engineering International* 44(11): 27-29.
- Rigby, P. 2003. Can Washington jump-start new U.S. nuclear plants? *Platts Energy Business & Technology* 2003: 20-24.
- Schimmoller, B. K. 2000. Accelerating outages & extending intervals. *Power Engineering* 104(11): 42-50.
- Schwieger, B., M. Leonard, S. Taylor, et al. 2002. First annual top plants survey. *Power* 146(4): 27-70.
- Sekine, Y. 1993. Nuclear power generation in Japan—Present status and future prospects. *Proceedings of the Institute of Mechanical Engineers, Part A: Journal of Power and Energy* 207: 233-246.
- Serres, R., and D. Carbonnier. 1999. French nuclear power plants—Results and outlooks. *VGB PowerTech* 79(8): 16-19.
- Site work underway on Finland's 1600 MWe EPR. 2004. *Modern Power Systems* 24(3): 30-34.
- Spalthoff, F. J., H. Haas, and F. Heindrichs. 1976. First year of operation of the world's largest tandem compound turbine-generator. *Proceedings of the American Power Conference* 38: 555-569.
- Swanekamp, R. 2003. License renewal, plant upgrades brighten nuclear's future. *Power* 147(1): 25-31.
- Thomas, M. 2002. Nuclear power bids for wider acceptance. *EnergyTech* 2: 8-11, 52.
- Three US power providers looking at additional nuclear units. 2002. *Power Engineering* 106(5): 14.
- Toivola, A. 2004. Nuclear power as part of the Finnish electricity supply. *VGB PowerTech* 84(1/2): 52-55.
- Traupel, W. 1977. *Thermal Turbomachinery*. 3d ed. (in German). Heidelberg: Springer, 1977.
- Troyanovsky, B. M. 1978. *Turbines for Nuclear Power Plants*. 2d ed. (in Russian). Moscow: Energiya, 1978.
- Tsuji, A., A. Endoh, and Y. Asada. 1998. Completion of ABWR plant—Kashiwazaki-Kariwa nuclear power station Unit Nos. 6 and 7. *Hitachi Review* 47(5): 157-163.

- von Weiche, G., and H. Pamme. 2003. Safety culture in nuclear power plants (in German). *VGB PowerTech* 83(3): 55–58.
- Voronin, L. M. 2000. Prospects for the development of nuclear power engineering in Russia in the XXI century. *Thermal Engineering* 47(12): 868–872.
- , B. Y. Berezin, and I. M. Kisil. 1997. Extending the service life of power-generating units at nuclear power stations in Russia. *Thermal Engineering* 44(8): 639–642.
- Wesselmann, C. 2003. Nuclear power production (in German). *BWK* 55(6): 40–47.
- Wild, E. 2002. The prospects for nuclear power in Europe. *VGB PowerTech* 82(5): 69–71.
- Zaiss, W. 2004. Performance of German nuclear power plants in 2003. *VGB PowerTech* 84(5): 2.
- Zink, J. C. 2001. Nukes' performance may encourage bright future. *Power Engineering* 105(6): 26.

## 2

---

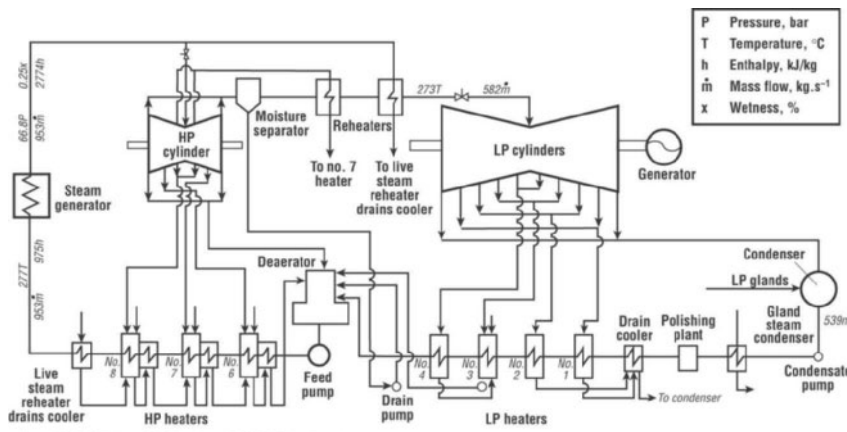
---

# The Thermal Process in Wet-steam Turbines

## Initial, Partition, and End Steam Conditions

A characteristic schematic diagram for a turboset of a typical modern nuclear power unit (for example, with a PWR), with the working fluid's operating conditions corresponding to its 100% maximum continuous rating (MCR), is shown in Figure 2-1. The main (live) steam leaves the reactor's steam generator(s) with a steam pressure of 6.68 MPa (969 psi) and moisture content of 0.25% and enters the double-flow HP cylinder. After this, it passes through the moisture separators (MS) and two-stage reheaters (R) and reaches two or three double-flow, double-exhaust LP cylinders, being superheated to 273°C (523°F) by steam extracted from the HP cylinder (the first reheat stage) and a portion of main steam (the second reheat stage). After the LP cylinders, the working steam passes to the condensers. The resultant steam condensate is pumped through the LP regenerative heaters to the deaerator, from which the feed water is directed by the feed pump(s) back into the steam generator(s) through the HP heaters. The LP and HP regenerative heaters and deaerator are fed with steam from the turbine's steam extractions (bleedings). The turbine's regenerative system also comprises the gland steam condenser and drain coolers. If the feed pumps are driven by steam turbines, the driving turbines are also fed with steam from the turbine's bleedings, most commonly located after the steam reheater. Due to all the

steam and water extractions, the rated steam flow amount at the LP cylinder exhausts makes up about 55% of the main steam flow from the steam generators. This simplifies designing the last LP stage blades (LSBs), improves their operating conditions, and reduces the energy losses with the exhaust velocity. Because of the low initial steam parameters and, as a result, less available energy as compared to that for fossil fuel power units, enormous steam flow amounts are needed to provide comparable power output—nearly 1.7 tons/s (about 3,750 lbs/s) for a 1,000-MW output.



After: T.H. McCloskey, R.B. Dooley, and W.P. McNaughton

**Fig. 2-1.** Schematic diagram of a large double-circuit nuclear power unit turboset with operating conditions corresponding to 100% MCR

Source: T. H. McCloskey, R. B. Dooley, and W. P. McNaughton<sup>1</sup>

The thermal (or steam expansion) processes for wet-steam turbines of nuclear power plants differ considerably from those of fossil fuel power units. First of all, this difference is determined by different initial steam conditions and, correspondingly, a different initial position on the Mollier (h-s) diagram: substantially superheated high-pressure steam for fossil fuel power units versus saturated steam of much lower pressure for nuclear power plants (Fig. 2-2). For wet-steam turbines, to decrease the steam wetness in the last LP stages, particular attention is given to measures of internal (that is, within the steam path) moisture separation. In addition, wet-steam turbines are commonly furnished with external moisture separators and reheat (Fig. 2-1). Owing to steam reheat, a certain portion of the steam

expansion line for the first LP stages lies above the saturation curve in the Mollier diagram, and the corresponding turbine stages work on superheated steam. Nevertheless, all of the HP-section stages and at least a considerable part of the LP stages work with wet steam.

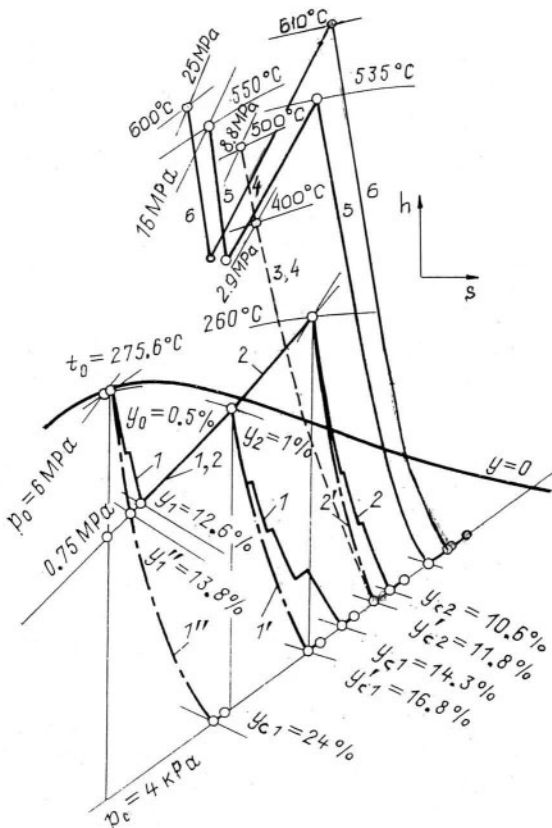


**Fig. 2-2.** Mollier diagram with characteristic steam expansion lines for wet-steam turbines compared to superheated steam turbines of fossil fuel plants (1": a hypothetical wet-steam turbine without any moisture separation; 1: a wet-steam turbine with an external moisture separator; 2: a wet-steam turbine with an external moisture separator and additional steam reheat; 3 and 4: non-reheat superheated steam turbines of the 1920s and 1940s, respectively; 5: a reheat steam turbine of a subcritical-pressure fossil fuel power unit of the 1960s; 6: a modern reheat turbine of a supercritical-pressure fossil fuel power unit with elevated main and reheat steam temperatures; 1' and 2': predicted expansion lines ignoring internal moisture removal)

The steam expansion process in wet-steam turbines is somewhat similar to the steam expansion process for non-reheat steam turbines of fossil fuel power plants of the period between the mid-1920s and mid-1940s, with rather moderate (from our present point of view) steam pressure and relatively high (from the standpoint of that time) steam temperatures: 2.9 MPa and 400°C (420 psi, 750°F) and 8.8 MPa and 500°C (1,276 psi, 932°F) (see lines 3 and 4 in Fig. 2-2). The steam wetness in the LP stages and the final moisture content of the exhausted steam of both those old non-reheat steam turbines and modern wet-steam turbines are approximately the same. However, if the wet-steam turbines did not have moisture separation and steam reheat, their last LP stages would have to work with steam containing up to 24% moisture. The post-World War II progress in fossil fuel steam turbine power units—raising the initial steam pressure up to supercritical and ultra-supercritical levels, the use of steam reheat, and the sharp elevation of the main and reheat steam temperatures up to 600°C (1,112°F) and even higher—has resulted in a substantial decrease in the exhaust steam wetness for these turbines with advanced steam conditions (see lines 5 and 6 in Fig. 2-2). As for nuclear wet-steam turbines, raising the initial steam pressure to improve the turbine efficiency increases the degree of wetness in the turbine steam path, shifting the steam expansion process lines to the left on the Mollier diagram. This effect is especially noticeable for the HP steam path.

The presence of moisture in the steam flow lowers the turbine efficiency, and it also poses a danger of intense erosion to the turbine's steam path elements. First of all, this concerns water drop erosion (WDE) of rotating blades. Intensity of this erosion is approximately in proportion to the steam wetness. In turn, water erosion in the turbine steam path is accompanied with corrosive processes caused by the presence of corrosive impurities such as chlorides, sulfates, carbon dioxide, organic impurities, and so on, in the working fluid. When steam condenses in the turbine, during the transition to two-phase conditions, these impurities are distributed among the vapor and the small amounts of water droplets that are formed. Most of the low-volatile impurities, in particular the chlorides and sulfates, almost completely pass into the water droplets. As the amount of this primary condensate is small, the concentration of impurities in it can be relatively high. When this moisture precipitates at the nearby surfaces, it forms liquid films with a high content of corrosive impurities. This problem is inherent in the processes of moisture formation in

turbines. Some experimental data also indicate that the intensity of corrosion processes in steam turbines increases if the condensation zone reciprocates.<sup>2</sup> For wet-steam turbines, there exist certain regions in the Mollier diagram that are characterized by extreme, intense, or moderate severity of erosion-corrosion wearing (ECW) (Fig. 2-3). Without steam reheat, significant portions of the HP and LP stages would work within the severe erosion-corrosion zone. For reheat wet-steam turbines with appropriate correlations of the initial and reheat steam pressure, the turbine's steam path only partially crosses the severe erosion-corrosion zone, but, nevertheless, a considerable portion of the HP stages remains in the intense erosion-corrosion zone.

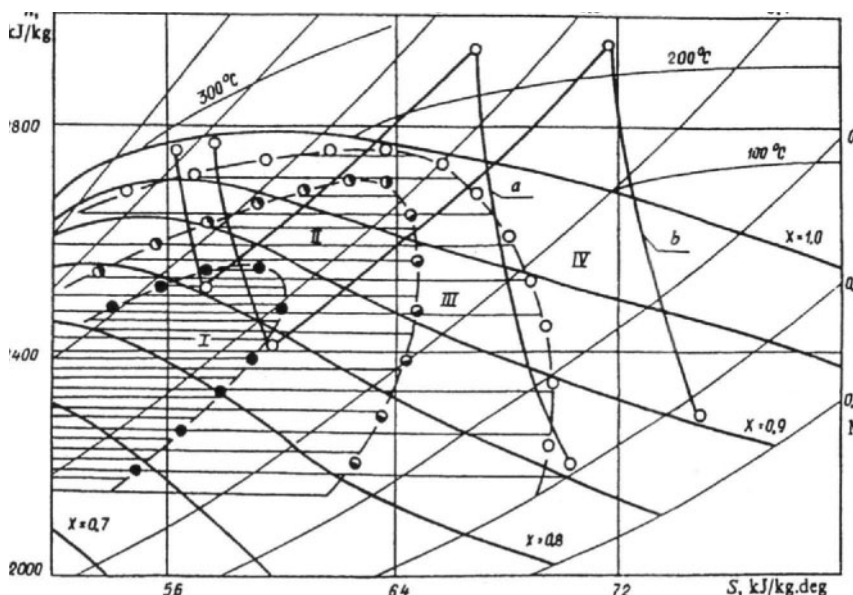


**Fig. 2-3.** Areas of various levels intensity of erosion-corrosion processes in the wet-steam region for turbine stator elements made of carbon steels (ECW rates: I: > 2.5 mm/yr, II: > 1.5 mm/yr, III: > 1.0 mm/yr, IV: < 1.0 mm/yr; *a* and *b*: steam expansion processes for TurboAtom K-1000-60/1500 and K-220-44 turbines, respectively)

Source: O. A. Povarov, G. V. Tomarov, and V. N. Zharov<sup>3</sup>

Despite all the countermeasures, the moisture content for the wet-steam turbines' last LP stages is usually greater than that for fossil fuel reheat turbines of superheated steam. The predicted exit

steam wetness for the wet-steam reheat turbines could reach 12–17%, however, the actual values are about 11–14%, thanks to the internal moisture removal in the steam path. Steam wetness after the turbines' HP section is measured at approximately the same levels as at the LP cylinder's exit. Thus, the problems of both energy losses due to wetness and erosion of the steam path components require equal attention to both the HP and LP sections. The mean diameters and lengths of the HP section's blades are smaller than those for the LP cylinder, so they work with smaller circumferential velocities. This circumstance somewhat moderates the energy losses. On the other hand, steam in the HP section stages is much denser, because of its higher pressure, and can impair the turbine performances in terms of energy losses and erosion damages to a greater extent.

Because of the energy losses due to wetness, the internal efficiency values of the wet-steam turbine sections are lower than those for fossil fuel reheat turbines of superheated steam: about 82% for the HP sections of wet-steam turbines versus 86–92% for the HP sections of superheated-steam turbines; and 85–87% for the LP sections of wet-steam turbines versus 89–94% for the intermediate-pressure (IP) sections and 90–91% for the LP sections of reheat steam turbines for fossil fuel power plants.

The most characteristic fossil fuel steam-turbine-based power units in the second half of the 20th century were designed with sub-critical main steam pressure—for example, about 16 MPa (2,320 psi), as shown in Figure 2–2, and main/reheat steam temperatures in the range between 530°C (985°F) and 565°C (1,050°F). Along with this, in many countries (the United States, the former Soviet Union, Germany, Italy, Denmark, Japan, South Korea, and China), a large number of supercritical-pressure steam turbine units with a main steam pressure of about 24–25 MPa have been created. In recent years, Germany, Japan, and Denmark have been developing and implementing a new generation of modern units with ultra-supercritical (USC) main steam pressure of up to 31 MPa (4,500 psi) and elevated steam temperatures of up to 600–610°C (1,112–1,130°F).<sup>4</sup>

The first fossil fuel steam-turbine power units with USC steam pressure and advanced steam temperatures were designed, constructed, and launched as early as the late 1950s and early 1960s:

for example, 125-MW Philo Unit no. 6 in Ohio, with a double-reheat turbine of GE and steam parameters of 31 MPa and 621/565/538°C (4,500 psi, 1,150/1,050/1,000°F); 325-MW Eddystone Unit 2 in Pennsylvania, with a double-reheat turbine of Westinghouse and steam conditions of 34.5 MPa and 650/565/565°C (5,000 psi, 1,200/1,050/1,050°F); the 100-MW back-pressure turbine at Kashira power plant near Moscow, with steam conditions of 29.4 MPa and 650/565°C (4,350 psi, 1,200/1,050°F); and 107-MW Hattingen Units 3 and 4 in Germany, with an ordinary supercritical steam pressure, but elevated main steam temperature of 600°C (1,112°C). However, even though all of these units operated successfully, they were somewhat premature, and the design was not copied and did not gain further acceptance.<sup>5</sup>

In 2000, two new coal-fired USC units exhibited the highest thermal efficiency level yet seen.<sup>6</sup> These two are the German 907-MW unit at the Boxberg power plant, with steam conditions of 26.6 MPa and 545/581°C (3,860 psi, 1,013/1,078°F), and the Japanese Tachibana-wan Unit 2, with a capacity of 1,050 MW and steam conditions of 25 MPa and 600/610°C (3,625 psi, 1,112/1,130°F). The Boxberg unit's net efficiency was recorded at 47.2%, and the gross efficiency of its Siemens turbine was 48.5%. The turbine's acceptance tests demonstrated an internal efficiency for the HP and IP cylinders of 94.2% and 96.1%, respectively. With a gross efficiency of 49.0%, the Tachibana-wan unit's steam turbine, produced by Mitsubishi Heavy Industries (MHI), has been acclaimed as the most efficient worldwide.

The previous highest gross efficiency values for modern steam turbines were recorded at the following power units:

- 47.4%—Japan's Hekinan 700-MW Unit 3, with MHI's turbine for steam conditions of 24 MPa and 538/593°C (3,480 psi, 1,000/1,099°F);
- 47.6%—Germany's Hessler 720-MW power unit, with ALSTOM's turbine for steam conditions of 27.5 MPa and 578/600°C (3,990 psi, 1,072/1,112°F), and
- 48.4%—Japan's Kawagoe 700-MW Units 1 and 2 , with Toshiba's turbine for steam conditions of 31 MPa and 566/566/566°C (4,496 psi, 1,051/1,051/1,051°F)

Even though the efficiency levels reached at Boxberg and Tachibana-wan look very impressive, they likely represent only interim benchmarks. A new efficiency record could be achieved by the Siemens turbine at Germany's Niederaussem Unit K, with steam conditions of 27.5 MPa and 580/600°C (3,990 psi, 1,076/1,112°F). This unit's turbine has a lower condenser pressure compared with the Boxberg unit and a 25% larger exhaust area due to the use of longer LSBs. The unit, commissioned in September 2002, was designed to reach 45.2% thermal efficiency. Even higher efficiency values are targeted for the Avedøre 530-MW Unit 2 in Denmark, with steam conditions of 30 MPa and 580/600°C (4,350 psi, 1,076/1,112°F), and Westafalen 350-MW Unit D in Germany, with steam conditions of 29 MPa and 600/620°C (4,210 psi, 1,112/1,148°F). Higher performances are also expected from new Japanese power units to be commissioned by 2005, due to even further heightened steam conditions—up to 30 MPa and 630/630°C (4,350 psi, 1,166/1,166°F)—and turbine steam path advances.<sup>7</sup> It is currently considered technologically feasible, as well as economically advisable, to raise the steam parameters for future fossil fuel steam-turbine-based power units up to 35 MPa and 700/720°C (5,075 psi, 1,292/1,328°F). This promises to increase the net efficiency of such units to as much as 50–51% and to make them effective in combating the rise of fuel prices by lowering the costs of power generation.<sup>8</sup>

Against the background of these figures, the thermal efficiency data for nuclear wet-steam turbines, with a best gross efficiency of about 36%, look rather modest. Because nuclear power units of the nearest future, just like their predecessors, are mostly designed with a moderate initial steam pressure of up to 7.5 MPa, it is not likely any radical increases in thermal efficiency will be achieved, except for gains due to improvements in the steam path design and reduction of internal energy losses.

In theory, the thermal efficiency of the wet-steam turbine's simple cycle (without regeneration, special moisture removal, and steam reheat) would grow by increasing the initial steam pressure up to 16–17 MPa (2,320–2,465 psi), although it would decrease slightly with any further increase in initial steam pressure.<sup>9</sup> In reality, the choice of the initial pressure value for nuclear power plants is mainly dictated by the strength of the reactor's pressure vessel for single-circuit units and heat transfer conditions for the boiling coolant for double-circuit units with BWRs or IWGRs. The pressure vessels of

modern PWRs are commonly designed for an internal pressure of about 15–16 MPa (2,175–2,320 psi). With regard to the underheating of the primary circuit water in reference to its saturation temperature and the terminal temperature difference (TTD) between the primary circuit water temperature at the reactor's outlet and the secondary circuit water's saturation temperature in the steam generator, the primary circuit pressure creates a steam pressure provided by the steam generator at a level of about 5–7.5 MPa (725–1,085 psi). The best heat transfer conditions for boiling water take place with a pressure of about 7 MPa (1,015 psi), so nuclear power plants with BWRs or LWGRs are commonly designed with an outlet steam pressure of about 6.5–7.3 MPa (940–1,060 psi).<sup>10</sup>

An increase of the initial steam pressure entails an undesirable increase in the steam wetness in the HP section stages when the turbine works under partial loads, because of throttling of the main steam in the HP control valves. First-generation wet-steam turbines with lower initial steam pressures (as, for example, TurboAtom's widespread wet-steam turbines K-220-44 with a rated electric output of 220 MW and initial steam pressure of 44 atm [4.32 MPa; 626 psi] used with Soviet PWR-type VVER-440 reactors) have somewhat more favorable conditions during start-ups and deep load changes, because the initial thermal process point due to throttling extends into the superheated steam region. However, such a low initial steam pressure was derived from quite different reasons—primarily because of the strength of the reactor's pressure vessel.

Generally, it is desirable to decrease the turbine's end pressure (pressure in the condenser) in order to increase the turbine's available energy and improve the thermal cycle's efficiency. For characteristic wet-steam turbines, reduction of the end pressure from 4 kPa to 3 kPa (from 0.58 to 0.435 psi) could increase the thermal efficiency by approximately 2–3%.<sup>11</sup> Because nuclear power plants do not require continual voluminous fuel deliveries, the developers have more freedom in choosing a desirable location for a plant that provides better cooling. As a result, the average end pressure for turbines of nuclear power plants is commonly somewhat lower than that for fossil fuel power plants located in the same region, even though some nuclear power plants in industrial zones have to operate with cooling towers and a relatively high pressure in the condenser. At the same time, deeper vacuum in the condenser (lower end pressure) increases

the volumetric steam flow amount at the turbine exit and requires longer LSBs or a greater number of exhaust flows to limit the exhaust energy losses. If the turbine's exit area is not sufficiently large and the exhaust steam velocity is relatively high, the gain in efficiency reachable due to a lower end pressure decreases considerably. Besides, a lower end pressure means greater steam wetness for the LSBs and hence additional energy losses.

This influence of the end pressure in the condenser,  $p_c$ , with regard to the steam flow amount through the turbine (or the turbine output,  $N$ ) related to the exhaust area value,  $F$ , is illustrated in Figure 2-4. The exhaust area is taken equal to the total annular area of the LSBs:

$$F = n \times \pi d_m L, \quad (2.1)$$

where  $n$  is the number of the LP exhaust flows, and  $L$  and  $d_m$  are the LSB's length and median diameter, respectively.

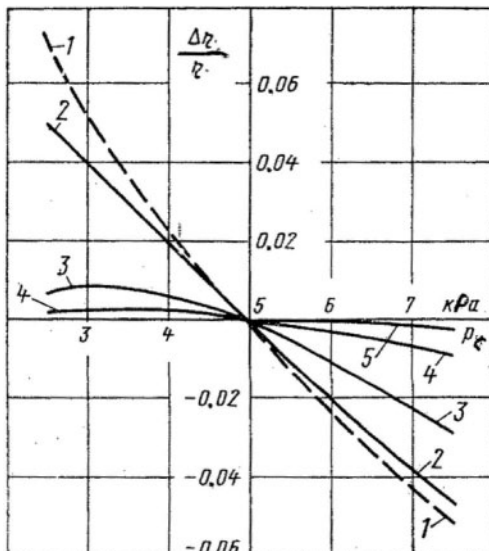


**Fig. 2-4.** Influence of the end steam pressure in the condenser,  $p_c$ , on wet-steam turbine thermal efficiency (initial steam pressure,  $p_0 = 7$  MPa [1,015 psi]; 1: invariable outlet steam velocity,  $G_c \times v_c / F$ ; 2, 3, 4, and 5:  $N/F = 5, 10, 15$  and  $20 \text{ MW/m}^2$ , respectively)  
Source: B. M. Troyanovskii<sup>12</sup>

Large steam flow amounts of wet-steam turbines require vast exhaust areas (significantly greater than those for superheated-steam turbines of a comparable output). Wet-steam turbines are designed with more LP cylinders (up to four) or as low-speed machines (with a rotation speed of 1,800 or 1,500 rpm) to have a possibility of increasing the LSB length without sacrificing the LSB strength.

For large wet-steam turbines with several LP cylinders and condensers, additional efficiency gains can be achieved by connecting the condensers successively with the cooling water. As a result, the average end pressure would be lower than if the condensers were connected in parallel. This results in a greater turbine output with the same steam flow amount and cooling water inlet temperature and flow amount. Successive connection of condensers was first proposed for Westinghouse turbines.<sup>13</sup> As an example, Figure 2-5 shows how the gains in LP cylinder outputs and total turbine efficiency change with the cooling water inlet temperature, as applied to a 750-MW low-speed wet-steam turbine with three serially connected condensers. Even though the last (third) LP cylinder is underloaded because of warmer cooling water and higher end pressure, this loss is more than compensated by the gain in the output of the first two cylinders, whose condensers are cooled by colder water and provide deeper vacuum. Under favorable conditions, successive connection of the condensers can bring an increase in the turbine's output or efficiency as much as 0.45%.<sup>14</sup> Unfortunately, this gain is notable only for relatively warm cooling water, although it increases when the turbine operates under partial loads.

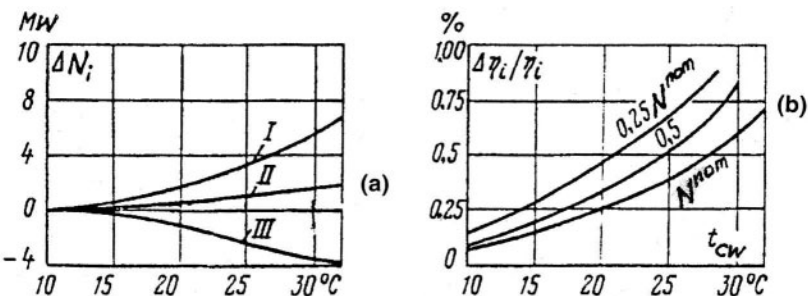


**Fig. 2-5.** Gain in the output (a) and efficiency (b) for a 750-MW wet-steam turbine with three serially connected condensers, related to the turbine load and cooling water inlet temperature (I, II, and III: gain in the output for the first, second, and third LP cylinders, respectively, with the turbine working under full load)

Source: R. L. Coit<sup>15</sup>

If the working steam were to expand within the turbine directly from the initial point to the end pressure, the steam wetness in the last stages would reach inadmissibly high values of about 24% (Fig. 2-2). This would bring about large energy losses and, more importantly, cause intense erosion in the steam path. To reduce the degree of wetness in the LP section and prevent these effects, wet-steam turbines are equipped with external moisture separators and reheat. Different turbine configurations with the moisture separators and one- and two-stage reheaters are shown in Figure 2-6. Sometimes designers furnish a turbine with an additional MS stage and, in addition to the HP and LP sections, introduce an intermediate-pressure (IP) section (or cylinder) situated between two moisture separators, as shown in Figure 2-6d. However, the most widespread configuration for modern wet-steam turbines comprises a single set of one or more moisture separator and reheat (MSRs) placed between the HP and LP cylinders (Figs. 2-6b and 2-6c). Sometimes, even with this configuration, the first stages after the MSR are placed in a separate IP section.

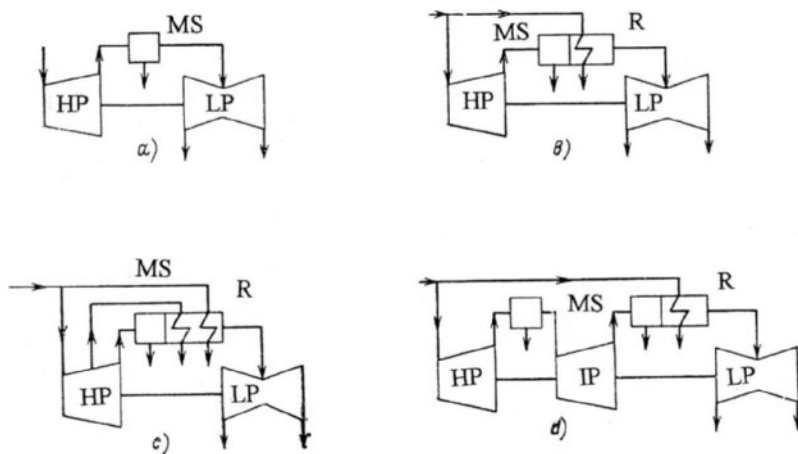


**Fig. 2-6.** Configurations of wet-steam turbines with different combinations of external moisture separators (MS) and single-stage and two-stage reheaters (R)

The influence of the partition, or splitting, pressure (the pressure after the HP section), related to the initial steam pressure ( $p_{part}/p_0$ ) on the turbine efficiency as applied to low-speed wet-steam turbines, according to GE, is shown in Figure 2-7. The choice of the partition pressure also influences the separator's and re heater's overall dimensions, so with regard to capital expenditures, power production costs turn out to be less dependent on the aforesaid pressure ratio. In addition, capital expenditures also depend on various other subsidiary circumstances.<sup>16</sup> The choice of the partition pressure also considerably influences the steam wetness in the last stages of both the HP and LP sections: a reduction of the partition pressure increases the exit wetness in the HP section and decreases it in the LP cylinders, and an increase in the partition pressure has the opposite effects. All of these contradictory considerations result in a large spread of values for the partition-to-initial steam pressure ratio for wet-steam turbines of different designs. This ratio normally falls in the range of 0.08–0.2. In the schematic diagram shown in Figure 2-1, this ratio is 0.088, and for the steam expansion process shown in Figure 2-2, it is equal to 0.125.

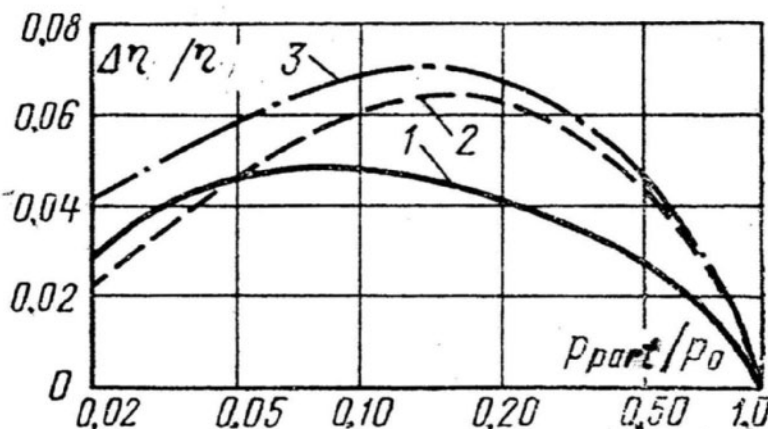


**Fig. 2-7.** Influence of partition steam pressure (between the HP and LP cylinders) on wet-steam turbine efficiency, according to GE (1: with separator only, as shown in Figure 2-6a; 2: with separator and one-stage reheat, as shown in Figure 2-6b; 3: with separator and two-stage reheat, as shown in Figure 2-6c)

Source: F. G. Baily, J. A. Booth, K. C. Cotton, and E. H. Miller<sup>17</sup>

Wet-steam turbines' steam reheat does not directly cause any increase in the thermal efficiency as it takes place for fossil fuel power units, in which steam reheat is provided by external heat. For wet-steam turbines, steam is reheated by highly potential steam extracted from the HP section, as well as a portion of the main steam not used in the turbine. In other words, the heating steam is used ineffectively. Thus, steam reheat for wet-steam turbines is needed only to decrease the steam wetness in the LP section, and it raises the turbine's efficiency indirectly—by reducing the energy losses because of wetness. Wet-steam turbines are commonly provided with highly developed regenerative systems, which are designed and calculated like those of fossil fuel power units<sup>18</sup> (Fig. 2-1).

## Features of Wet-Steam Flow in the Turbine Steam Path

When superheated steam flows through the turbine's steam path, its expansion is accompanied by the release of the energy of superheating until it reaches a saturated condition. With further expansion, the flowing steam releases a portion of its latent heat of evaporation. This results in conceiving particles of water that are drawn by the parent steam through the steam path until they either pass to the condenser (or bleedings) or fall onto nearby surfaces. Except for a few stages of the turbine section immediately after the MSR that operate on superheated steam, all of the wet-steam turbine's rest stages (in both the HP and LP sections) work on wet steam (Fig. 2-2). The working fluid for these stages is a two-phase steam-water mixture. The liquid component of this flow exists in the forms of fog (fine droplets), drops of different diameters, water films and rivulets moving along the solid surfaces, and water streams separated from these surfaces (Fig. 2-8). A portion of this liquid separates from the steam path and passes into bleedings, peripheral water catcher belts, special slots in hollow vanes, and so on.

The two-phase mixture can exist in states of stable or metastable thermodynamic equilibrium or phase transition (that is, condensing or evaporating). In the stable state, the thermodynamic conditions of wet steam are described by: 1) its wetness,  $y$ , which characterizes the relative mass of the liquid component in the unit volume as  $y = m'/m = m'/(m'+m'')$ , where  $m'$  and  $m''$  are the masses of the liquid and vapor phases, respectively; or 2) its dryness,  $x = (1 - y)$ . The water drops drawn by the wet-steam flow vary in their size from fine particles with diameters of about 0.01 mkm ( $0.4 \times 10^{-4}$  mil) to coarse-grained drops with diameters of about 100 mkm (4 mil). Small droplets can merge and agglomerate, and on the contrary, large drops can lose stability and divide. The drop stability, characterized by the Weber number, depends on the liquid's surface tension, density, and flow velocity. For more detailed discussion of the fluid dynamics of wet steam and the motion of two-phase mediums in turbine steam path elements, there are a number of basic monographs on these subjects.<sup>19</sup>

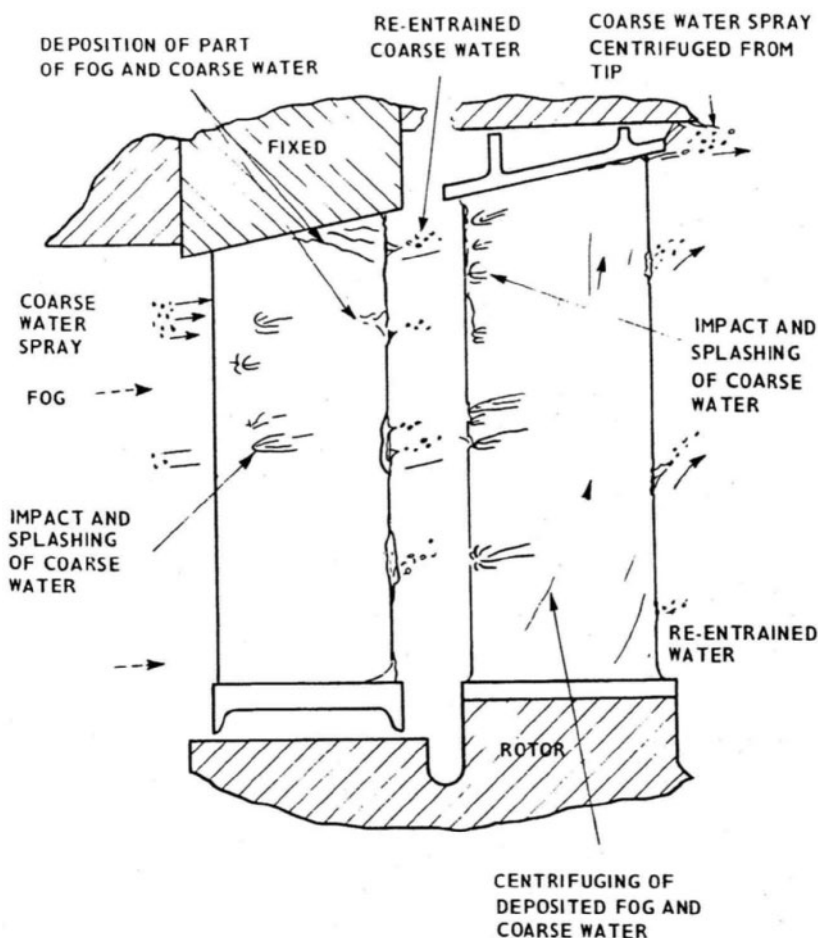


**Fig. 2-8.** Various forms of water existing in a wet-steam turbine stage  
*Source: M. J. Moore<sup>20</sup>*

### Wet-steam flow in turbine blade rows

When the final point of steam expansion in a turbine row lies in the wet region (that is, below the saturation curve delineated by  $x = 1$ ), it is significant whether the process begins at a point lying above this curve or below it. In the first case, the superheated steam usually does not have time to condense; the expansion process occurs without creating a liquid phase and discharging the latent heat of evaporation. As a result, the final steam temperature,  $t_2$  turns out to be less than the

saturation temperature,  $t_{sat}$ , at the pressure after the turbine row,  $p_2$ . This temperature difference,  $\Delta t = t_{sat} - t_2$ , is known as the degree of subcooling, or supersaturation. It is related to the velocity of steam expansion:

$$\dot{p} = \frac{1}{p} \times \frac{\partial p}{\partial \tau}, \quad (2.2)$$

where  $\tau$  is time. If  $da$  is the length differential in the axial direction, then

$$\dot{p} = \frac{1}{p} \times \frac{\partial p}{\partial a} \times \frac{da}{d\tau} = -\frac{c_a}{p} \times \frac{\partial p}{\partial a}, \quad (2.2a)$$

where  $\frac{da}{d\tau} = c_a$  is the axial stream velocity. The greater the value  $\dot{p}$ , the greater the degree of subcooling. It also depends on the initial steam pressure, decreasing when it increases. Subcooling values of 15–25°C were already obtained in the 1930s by Aurel Stodola,<sup>21</sup> but modern supersonic nozzles have made it possible to increase this value to 30–45°C. The specific volume of subcooled steam is less than that in the case of equilibrium expansion, resulting in a decrease of the available energy. The relative value of this decrease is called the subcooling loss.

The subcooled steam is not in a stable state. It occurs only in the course of a dynamic process and disappears as soon as thermodynamic equilibrium is established. Subcooled steam, being in a metastable state, passes into a thermodynamically stable state as the liquid phase arises. The condensation process commences spontaneously (that is, without any external forces acting on the steam) as a quantum change around the water microdroplets, which appear randomly in the flow and act as condensation centers, provided their diameters exceed a certain critical value. This critical diameter decreases with an increase of subcooling. Presently, researchers accept indisputably that just spontaneous nucleation after a limited degree of supersaturation is the main process responsible for creation of the liquid phase in the turbine steam flow. With the increase in enthalpy difference in the wet-steam region, the degree of steam subcooling increases, and the microdroplets' critical diameter decreases. This promotes creation of the condensation centers and initiates *condensation shocks*, which are similar to compression shocks in aerodynamics. As the critical diameter of the condensation centers decreases, the average diameter of drops

provoking spontaneous condensation also decreases. Some generalized dependencies relating to the change of the maximum achievable subcooling degree,  $\Delta t = t_{sat} - t_2$ , and the critical droplet radius,  $r_{cr}$  with the steam expansion velocity,  $\dot{p}$ , and initial saturated steam pressure,  $p_{0s}$ , (as applied to the LP stage channels) are shown in Figure 2-9.

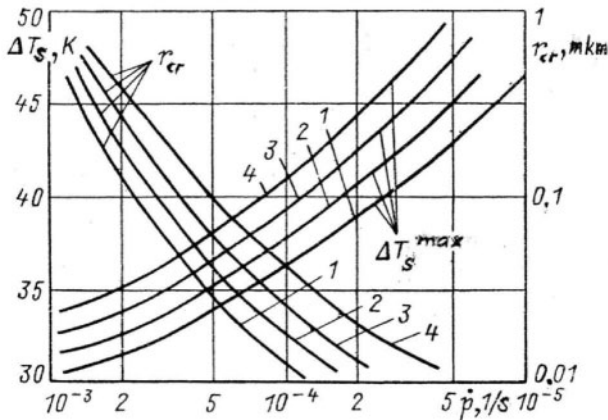


**Fig. 2-9.** Changes of maximum achievable subcooling temperature and critical droplet radius with initial saturated steam pressure,  $p_{0s}$ , and steam expansion velocity (1:  $p_{0s} = 0.1$  MPa; 2:  $p_{0s} = 0.05$  MPa; 3:  $p_{0s} = 0.03$  MPa; 4:  $p_{0s} = 0.02$  MPa) *Source:* B. M. Troyanovskii, G. A. Filippov, and A. E. Bulkin<sup>22</sup>

Subcooled (supersaturated) dry steam is described by the same thermodynamic state equations as superheated steam. This means that the Mollier diagram for this medium is obtained by extrapolating the curvilinear isobars and isotherms that apply for the superheated range. Because of the considerable delay related to subcooling, steam begins to condense not at  $x = 1$ , but at the steam dryness value corresponding to the diagram steam conditions  $x_w < 1$ . The family of curves for constant values of  $x_w$  are known as Wilson lines. Because the value of  $x_w$  depends on the pressure decline rate,  $\dot{p}$  (which, in turn, depends on the blade row's size and profiles, stream conditions, and steam pressure), it is more reasonable to talk about a certain Wilson region enclosed by the lines corresponding to the actual characteristic values  $\dot{p}$ ; that is,  $x_w(\dot{p})$ . In the range of  $\dot{p}$  values between 10 and 10,000 sec<sup>-1</sup>, the Wilson region occupies the range of steam dryness values  $x_w = 0.977-0.963$  (Fig. 2-10a).

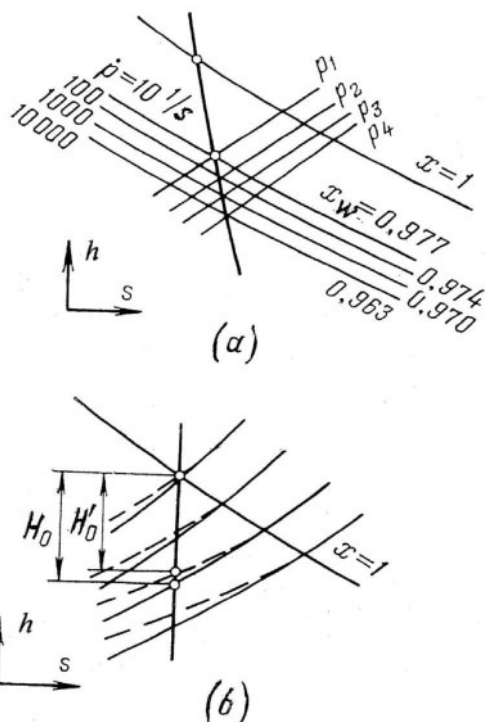


**Fig. 2-10.** Steam expansion process with subcooling shown on h-s axes  
(a: Wilson lines  $x_w = \text{const}$  depending on  $p$ , isobars in the wet-steam region for subcooled steam)

In calculating values in the zone between the saturation curve where  $x = 1$  and the Wilson line,  $x_w$ , it is acceptable to take thermodynamic steam properties like those for superheated steam. It is also possible to draw conventional isobars for subcooled steam within this zone in order to obtain the values of the actual available energy,  $H'_0$ , taking into account the subcooling loss calculated as:

$$\zeta_{sc} = (H_0 - H'_0) / H_0, \quad (2.3)$$

where  $H_0$  is the available energy of the process, and  $H'_0$  is the enthalpy difference corresponding to the isentropic expansion process, but reduced because of the smaller steam temperature and specific volume (Fig. 2-10b). According to theoretical estimates, if the initial pressure,  $p_0$ , is not too great, this value can be calculated as:

$$\zeta_{sc} = 1 - \frac{k}{k-1} \times \frac{p_0 v_0}{H_0} (1 - \varepsilon^{\frac{k-1}{k}}), \quad (2.3a)$$

where  $p_0$  and  $v_0$  are the initial pressure and specific volume of steam, respectively,  $\varepsilon = p/p_0$  is the steam pressure ratio, and  $k$  is the isentropic index, which can be taken equal to that for superheated steam under the initial pressure  $p_0$ . If  $p_0 > p_{sat}$ , the pressure ratio is assumed to be related to  $p_{sat}$ , and all of the steam parameters in Equation 2.3a are taken for the saturation curve. This equation can be approximated with good accuracy by the following empirical expression:

$$\zeta_{sc} = 0.12 - 0.2 \times \varepsilon + 0.08 \times \varepsilon^2 \quad (2.3b)$$

For  $\varepsilon = 0.5$ ,  $\zeta_{sc} = 0.4$ . A further reduction of  $\varepsilon < 0.5$  corresponds to conditions of spontaneous condensation (Fig. 2-11).

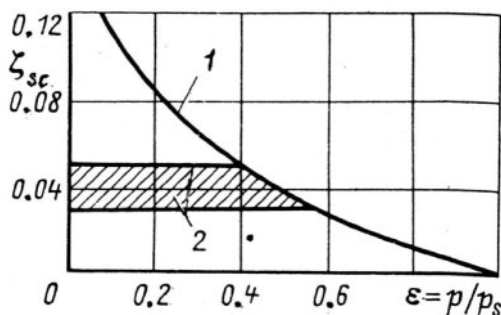


**Fig. 2-11.** Energy loss with subcooling of wet steam depending on pressure ratio (1: calculated data for subcooling; 2: zone in which spontaneous condensation begins)  
Source: A.V. Shcheglyev<sup>23</sup>

Computation techniques have been developed by different research institutions and turbine manufacturers for simulating the expansion processes for saturated steam with non-equilibrium spontaneous condensation.<sup>24</sup> Their results show good agreement with experimental data, indicating that these techniques can be used for designing turbine blade profiles that operate near the Wilson region with minimal subcooling losses.

If the expansion process begins at the point with initial steam wetness (as it does for most stages of wet-steam turbines), condensation is also influenced by the steam conditions at the row inlet. The most influential factor in this process is the size of water drops. For a two-phase steam-water mixture as the working fluid, the thermal processes in rows and cascades are somewhat ambiguous and intricate, because of variations in the liquid concentration and drop sizes, their uneven dispersion at the row inlet, and the differences in stream direction and velocity between the water drops and the steam stream. The drop traces within the row channels are materially different, depending on the drop diameter,  $d$  (Fig. 2-12). The smallest drops (with  $d < 1\text{-}5 \text{ mkm}$ , or  $0.04\text{-}0.2 \text{ mil}$ ) closely follow the main stream and pass through the channel without colliding against the profile surfaces and settling on them. The larger drops deviate from the stream lines to a degree depending on the drop's size—the larger the drop, the greater the deviation. And, finally, the largest drops ( $d > 50\text{-}100 \text{ mkm}$ , or  $2\text{-}4 \text{ mil}$ ) can move through the row channel almost independently of the steam stream line and come onto the concave profile face; some of them break up against the profile edges. These drops slip along the concave profile surface generating water films, separate from the surface, collide against the opposite surface, and are reflected back again. A general pattern of their flow is shown in Figure 2-13. The drops in streams 1 and 2 of this sketch have the largest size and the smallest velocity.

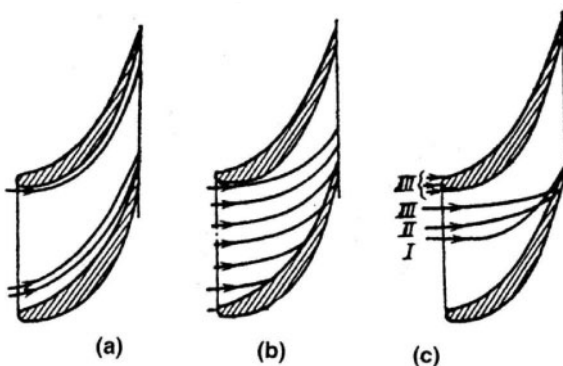


**Fig. 2-12.** Drop paths of water in a nozzle channel depending on the drop size (a: inlet drop  $d < 1$  mkm; b: inlet drop  $d \approx 10$  mkm; c-I: inlet drop  $d = 2$  mkm; c-II: inlet drop  $d = 20$  mkm, c-III: inlet drop  $d = 200$  mkm)

Source: A.V. Shcheglyev<sup>25</sup>

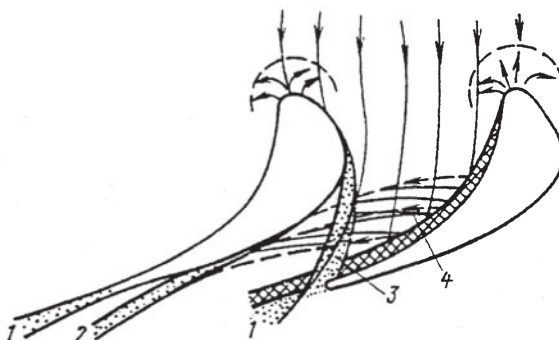


**Fig. 2-13.** General pattern of water motion within a nozzle channel (1: water drops along the edges; 2 and 3: water drops separating from the convex blade surface; 4: droplets reflected off the concave blade surface)

Source: A.V. Shcheglyev<sup>26</sup>

Variations in the energy losses in an annular nozzle row placed behind the preceding turbine stage, based on the initial steam wetness and drop size, are shown in Figure 2-14a. A characteristic feature is an increase in energy losses if the expansion process commences near the saturation curve. This is explained by the substantial instability of the liquid condensation process. With transference of the saturation curve and the appearance of fine-droplet liquid in the preceding stage, the energy losses in the row sharply decrease because of less subcooling and more balanced condensation. The energy losses

begin to increase again with further increases in the initial wetness ( $y_0 > 0.03$ ). This is mainly related to mechanical interaction between the phases. Larger water drops at the stage inlet cause greater energy losses, which increase with greater steam wetness values.

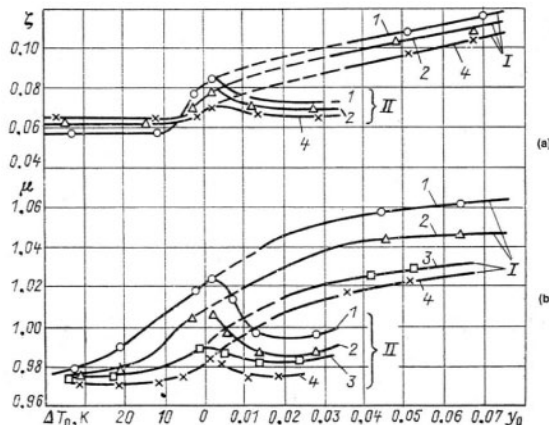


**Fig. 2-14.** Experimental characteristics of energy losses (a) and flow amount factor (b) for slightly superheated and wet steam (I: critical drop  $d \approx 40$  mkm; II: critical drop  $d \approx 0.4$  mkm; 1: water drop  $r = 500$  mkm; 2: water drop  $r = 200$  mkm; 3: water drop  $r = 100$  mkm; 4: water drop  $r = 10$  mkm)

Source: B. M. Troyanovskii, G.A. Filippov, and A. E. Bulkin<sup>27</sup>

The flow amount factor values for wet steam also differ from those for superheated steam. This factor,  $\mu$ , is the ratio between the actual steam flow amount through the row and the flow amount for the steam expansion process if it were isentropic. For the nozzle rows with superheated steam, the flow amount factor value,  $\mu_1$ , can be accepted equal to approximately 0.97, and for the rotating blade rows, it varies between 0.89 and 0.97, depending on the relative blade length,  $l/b$ , and the flow turn angle,  $\Delta\beta$ . The longer the blades and the smaller the flow turn angle, the less the aerodynamic resistance of the channels and the closer the flow amount factor value to 1.0. Experiments show that for wet steam this factor is greater than that for superheated steam (Fig. 2-14b). This effect also increases with an increase in the water drop diameter.

As a first approximation for the nozzle rows, the flow amount factor ratio for wet and superheated steam can be presented by the following equation:<sup>28</sup>

$$(\mu_1^{\text{wet}}/\mu_1^{\text{s.h.}}) = 1/(\sqrt{x_1}), \quad (2.4)$$

where  $x_1$  is the steam dryness downstream of the row at equilibrium expansion. For rotating blades of impulse-type stages, the flow amount factor depends on the enthalpy drop. If the steam pressure values upstream and downstream of the blade row are equal (that is, the channel has a constant section area and the stage is purely of an impulse type), the flow amount factors for wet and superheated steam are approximately equal. In a general way, this dependence is shown in Figure 2-15, and can be approximated by the following equation:

$$(\mu_2^{\text{wet}}/\mu_2^{\text{s.h.}}) = x_2^{-Y/2} \quad (2.5)$$

where  $Y = 1 - (\sin\beta_2/\sin\beta_1)$ . It is important that for wet steam the flow amount factor  $\mu > 1.0$ . The explanation for this lies in the fact that the actual specific volume of wet steam is less than that assumed for thermodynamic equilibrium, and this effect outweighs the influence of the decreased velocity and a certain obstruction of flow by water streams.

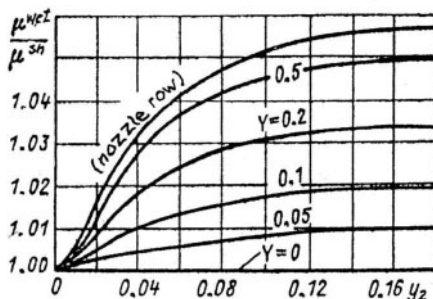


**Fig. 2-15.** Influence of wetness in the exit section of a turbine blade row on the flow amount factor, where  $Y = 1 - \sin\beta_2 / \sin\beta_1$   
Source: A. V. Shcheglyaev<sup>29</sup>

Another important characteristic of a two-phase flow that influences the blade row performance is a slide factor, which is determined

as the ratio between the average velocities of the water drops and the steam:  $v = c'/c''$ . This factor has an important influence on the efficiency and erosion reliability of the turbine stages, as well as influencing the possibility of water separation within the turbine steam path. An analysis of water distribution and its dispersion downstream of the turbine rows shows that a substantial portion of the liquid phase in the flowing steam-water mixture is in the form of large drops, and their mechanical interaction with the steam and the profile surfaces is essential. This influence is largely determined by the steam wetness,  $y$ , and the specific volume ratio for the steam and water phases, which in turn depends on the steam pressure. This specific volume ratio decreases with an increase in steam density. These relationships are confirmed by experimental data (Fig. 2-16).

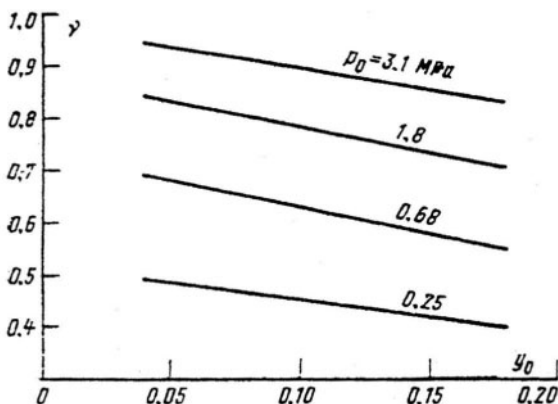


**Fig. 2-16.** Influence of initial steam pressure,  $p_0$ , and wetness,  $y_0$ , on the slide factor for a supersonic nozzle  
Source: B. M. Troyanovskii<sup>30</sup>

### The influence of wetness on wet-steam turbine efficiency

The amount of steam wetness significantly affects all turbine row characteristics: the amount of energy losses, flow amount factors, flow exit angles, and so on. The presence of moisture in the steam flow also changes all of the characteristics of wet-steam turbine stages, as compared with stages working on gas or superheated steam.

The water drops leave the nozzle channel with a velocity,  $c'$ , which is less than the steam velocity,  $c''$ , achieved due to expansion. Even if the exit angles of steam flow and liquid motion coincided, the water drops leaving the nozzle channel with a lower velocity would move in a different direction relative to the rotating blades, and would hit the back of the turbine blade at an angle of  $\delta\beta_1 = \beta_1'' - \beta_1'$  (Fig. 2-17). As a result, a retarding torque develops that acts on the rotating wheel. This retarding torque increases with the increase of the circumferential speed,  $u$ , reduction of the water velocity, increase of the steam wetness, and growth of water drops hitting the rotating blades. All of these values vary along the height of the stage, and the stage efficiency is affected by factors that, in turn, remarkably depend on the turbine's steam path design features, peculiarities of the wet-steam flow, the wetness dispersion, and so on.

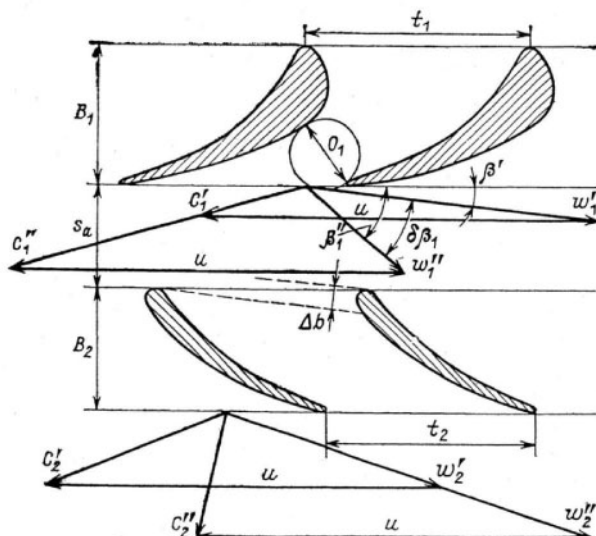


**Fig. 2-17.** Velocity triangles of a wet-steam turbine stage for steam and water

This intricate, multifactor influence is difficult to treat theoretically or to model numerically. In many respects, it is more productive and reliable to investigate these phenomena experimentally, and even the best existing theoretical and computational models need for their verification reliable experimental data on the structure of wet steam flowing in real turbine stages and multistage turbines.

Some results of bench tests for a model turbine stage with variations in the initial steam temperature and wetness are shown in Figure 2-18. The initial wetness was created by a spray providing relatively large drops, with an average diameter of about 50mkm. This diminished the stage efficiency throughout the studied velocity ratio range, simultaneously reducing its optimal value. Increases in wetness resulted in increased stage reactivity (reaction degree). This is predominantly explained by a greater increase in the flow amount factor for the nozzle row,  $\mu_1$ , compared with that for the rotating blades,  $\mu_2$ , as well as by the increase in the exit angle,  $\alpha_1$ , with the degree of wetness. Figure 2-19 demonstrates specific changes in the efficiency for model stages with different median diameter-to-height ratios depending on the initial wetness. The smaller the stage height, the more intensely the wetness diminishes the stage efficiency, because a greater part of the moisture precipitates on the wall surfaces, forming thin water films. These films then divide into drops, but they do not have time to accelerate in the gap between the nozzles and rotating blades and to a large degree hamper the rotating blades. For such stages with a relatively small height, the optimal velocity ratio more noticeably decreases with the increase of the steam wetness. The wetness influence also differs for different blade profiles. It is greater for blade rows with larger turn angles and less for the plane profiles that are characteristic for the tip sections of blades with large length-to-median diameter ratios (Fig. 2-20).<sup>32</sup>

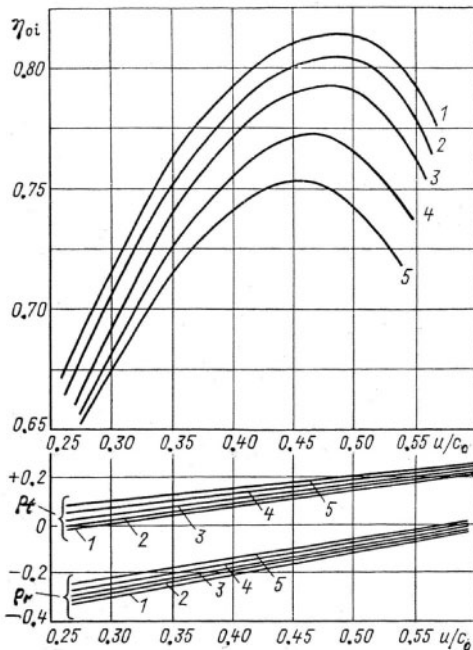


**Fig. 2-18.** Changes in the internal efficiency and reaction degree for tip and root zones ( $\rho_t$  and  $\rho_b$ , respectively) related to velocity ratio and initial steam wetness for an experimental turbine stage (1:  $\Delta t_0 = 150^\circ\text{C}$ ; 2:  $y_0 = 0.005$ ; 3:  $y_0 = 0.02$ ; 4:  $y_0 = 0.042$ ; 5:  $y_0 = 0.068$ )

Source: B. M. Troyanovskii, G. A. Filippov, and A. E. Bulkin<sup>31</sup>

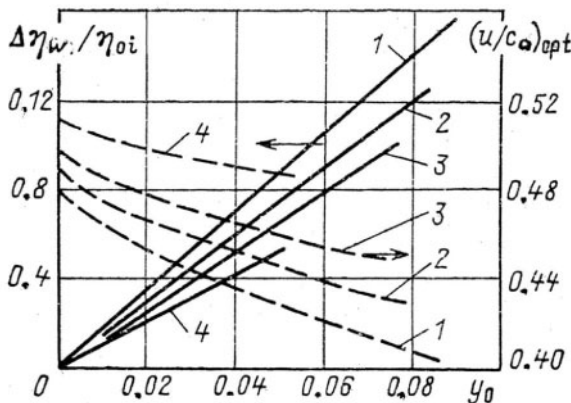


**Fig. 2-19.** Changes in optimal velocity ratio and internal stage efficiency for turbine stages with different median-diameter-to-height ratios, depending on initial wetness (1:  $d/l = 27, l_1 = 15 \text{ mm}$ ; 2:  $d/l = 16, l_1 = 25 \text{ mm}$ ; 3:  $d/l = 8, l_1 = 48 \text{ mm}$ ; 4:  $d/l = 2.7, l_1 = 207 \text{ mm}$ )

Source: B. M. Troyanovskii, G. A. Filippov, and A. E. Bulkin<sup>33</sup>

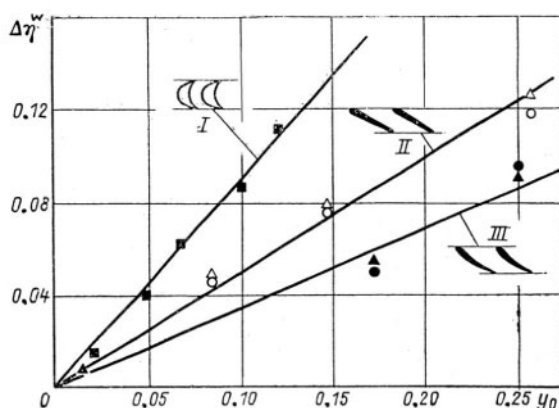


**Fig. 2-20.** Influence of initial wetness on changes in efficiency related to different rotating blade profiles (I:  $u/c_0 = 0.5$ ; II and III:  $u/c_0 = 0.7$ )

Source: B. M. Troyanovskii, G. A. Filippov, and A. E. Bulkin<sup>34</sup>

Calculations of the turbine steam path fulfilled consecutively stage-by-stage must take into consideration the change in steam wetness after the stages due to internal moisture separation. The actual initial wetness for the next stage is less than the outlet wetness after the preceding stage, indicated by  $y_2$ , by the value of

$\Delta y = \psi \times y_2$ , where  $\psi$  is the separation factor, or separation efficiency. Its value depends on various physical, geometrical, and design characteristics of the stage, and on the type of moisture separation used in the stage. According to some experimental data, for typical internal moisture separation devices, a stage's separation efficiency,  $\psi$ , can vary between 0.02 and 0.2, increasing along the steam path during the steam expansion process.<sup>35</sup> Due to moisture separation, the initial point of the steam expansion process for the stage shifts along the initial pressure isobar by  $\Delta y$ , as seen in Figure 2-2 for the LP stages, and the entire steam expansion line assumes a zigzag configuration. Because a certain portion of the steam is captured and removed with the water, the steam flow amount for the stage is additionally decreased. According to GE, this additional steam flow loss amounts to about 0.5%.<sup>36</sup>

The total influence of wetness on the wet-steam turbine's stage efficiency is often approximated by various semi-empirical equations. In so doing, the wet-steam turbine's stage efficiency is related to the efficiency of the same stage as if it worked with superheated steam. One of such semi-empirical equations has been proposed as follows:<sup>37</sup>

$$\eta_{st}^{\text{wet}} = \eta_{st}^{\text{s.h.}} \times [1 - 2 \times (u/c_0) \times (k_1 y_0 + k_2 \Delta y)], \quad (2.6)$$

where  $y = y_2 - y_0$  is the increase in wetness for the stage,  $u/c_0$  is the velocity ratio for the stage, and  $k_1$  and  $k_2$  are empirical coefficients, where  $k_2 \approx 0.35$ , and the value of  $k_1$  is supposed linearly dependent on the share of coarse-grain drops,  $\lambda_{cg}$ :

$$k_1 \approx 0.8 + 0.5 \times \lambda_{cg} \quad (2.7)$$

In turn, the value of  $\lambda_{cg}$  depends on many steam path characteristics. This dependence is also described by various semi-empirical equations. So, for example, for multistage wet-steam turbines, it is advised to take this value in proportion to the number of preceding stages working with wet steam,  $z_w$ .<sup>38</sup>

$$\lambda_{cg} = 0.07 \times (z_w + 1) \times (0.5 - 0.94 \times \ln p_0) \quad (2.8)$$

For stages with slightly superheated steam at the entrance, when the steam expansion line crosses the saturation curve, including the first HP stage, their efficiency is proposed to count as

$$\eta_{st}^{\text{wet}} = \eta_{st}^{\text{s.h.}} \times (1 - \zeta_{sc}), \quad (2.9)$$

where the loss due to wetness corresponds to the subcooling loss, and can be calculated with the help of Equation 2.3b as  $\varepsilon = p_2/p_{0s}$ , where  $p_{0s}$  is the pressure at the point where the steam expansion line crosses the saturation curve.

The overall effect the steam wetness has on wet-steam turbines' efficiency has been empirically proven in numerous bench and field tests at wet-steam turbines of diverse design features. Of particular interest is a greater sensitivity to the wetness of the stages with shrouded, reaction-type rotating blades compared with unshrouded (free-standing) blades (Fig. 2-21). Results of tests performed by GE with low-speed impulse-type turbine stages feature, in particular, rapid declines in efficiency with the first appearance of wetness (mean values up to 0.02), which points out the significance of energy losses with steam subcooling in the process of phase transition (Fig. 2-22). Nonlinear dependencies between energy losses (or decrease in efficiency) and median wetness were also found in other field experiments.<sup>39</sup>

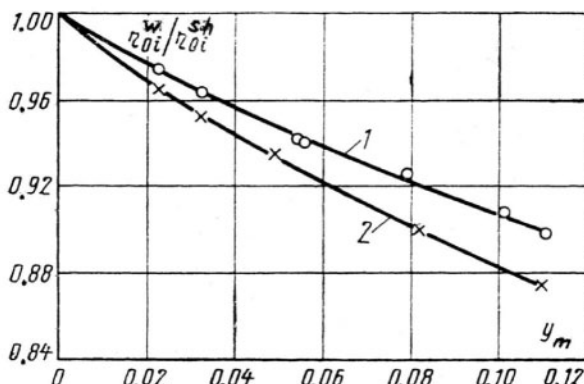


**Fig. 2-21.** Influence of wetness on efficiency for reaction-type turbine stages (1: steam path with shrouded rotating blades; 2: steam path with unshrouded rotating blades)

Source: B.M. Troyanovskii, G.A. Filippov, and A.E. Bulkin<sup>40</sup>

Nevertheless, as the first approximation, the influence of wetness on turbine efficiency is often considered to be linear, and can be described in the simplest form by the Baumann rule:

$$\eta_{st}^{\text{wet}} = \eta_{st}^{\text{s.h.}} \times (1 - \alpha y_m), \quad (2.10)$$

where  $y_m = (y_0 + y_2)/2$  is the average steam wetness for the stage or stage group, and  $\alpha$  is an empirical coefficient known as the Baumann factor. Various experiments carried out on different types of turbines provide a range of values for  $\alpha$ , varying from 0.4 to 2.0, but this factor is usually assumed equal to 1.0, according to Karl Baumann himself.<sup>41</sup> This assumption takes into account not only the previously mentioned energy losses, but also working-fluid mass losses, because the steam converted into water no longer performs work in the considered and subsequent turbine stages. Originally based on experiments carried out on steam turbines in 1921,<sup>42</sup> the Baumann rule has remained as a long-lived empirical rule in the history of turbomachinery. Although the Baumann rule is convenient to apply and in many cases quite commensurate with experimental data as shown in Figure 2-22, it actually provides little insight into the physical nature of wetness as it relates to turbine efficiency. It takes into account the total quantity of moisture in the wet-steam flow, but ignores its structure. At the same time, according to the theory of two-phase wet-steam flow, possible variations in the flow structure can be even more important and influential than the total moisture quantity.

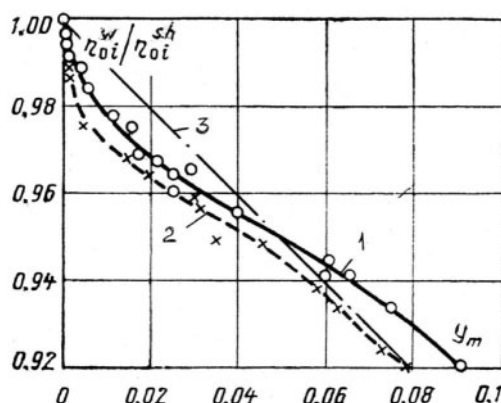


**Fig. 2-22.** Influence of wetness on efficiency for impulse-type turbine stages (1: HP steam path; 2: LP steam path; 3: Baumann rule)

Source: M.J. Moore<sup>43</sup>

All of the previously mentioned approaches are mainly employed for plain steam path calculations. For turbine stages with relatively long blades, the steam expansion process is calculated for a few sections (individual streams) across the stage height. In doing so, the lengthwise wetness distribution following the preceding stage is calculated based on the initial average wetness (for the relevant stage) and the coarse-grain wetness share—as shown in Figure 2-23, for example. It is also conditionally accepted that this share for each section changes in proportion to the total wetness in the relevant section, but cannot be greater than 0.9. As seen in Figure 2-23, it is assumed that the greater the drop size, the more uneven the wetness distribution along the blade length becomes, acquiring an L-shaped appearance.

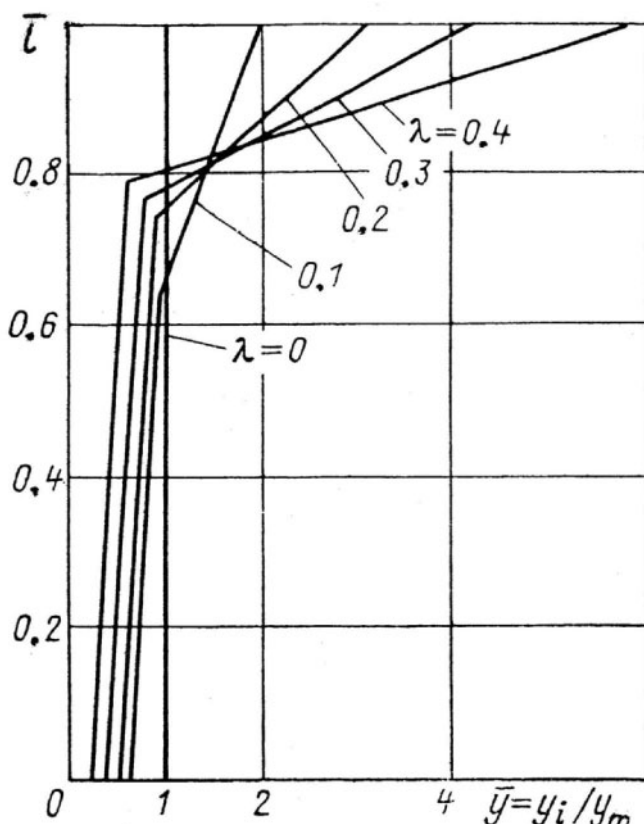


**Fig. 2-23.** Distribution of exit wetness along the height of an individual stage, depending on the coarse-grain wetness portion  
Source: B. M. Troyanovskii, G. A. Filippov, and A. E. Bulkin<sup>44</sup>

Most turbine developers currently calculate and design turbine steam paths with the use of fully three-dimensional (3-D) computational techniques.<sup>45</sup> These 3-D computational techniques are aimed at reducing the secondary energy losses in the turbine stages, along with profile losses. This has led to the development and use of new, sometimes nontraditional, blade profiles, and the creation of 3-D, meridionally profiled steam paths using not only twisted and tapered, but also bowed (curved) and leaned (inclined) vanes and blades. The evolution of reaction-type integrally shrouded HP blades for Siemens turbines shown in Figure 2-24 and Figure 2-25 demonstrates the effect of replacing a classical vane with a curved and inclined one in the last LP stage for Asea Brown Boveri (ABB) turbines.

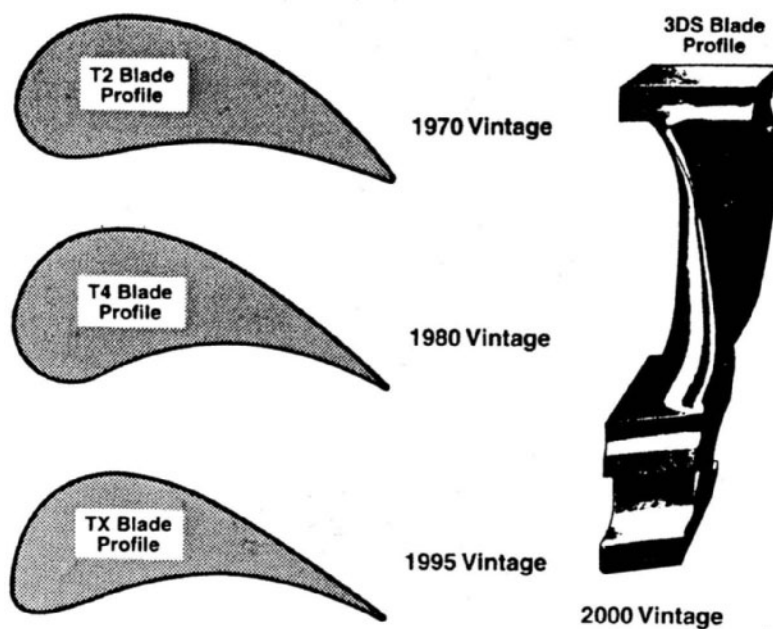


**Fig. 2-24.** Development of reaction-type, integrally shrouded blades for Siemens turbines

Source: H. Oeynhausen, A. Drosdziok, W. Ulm, and H. Termyuehlen<sup>46</sup>

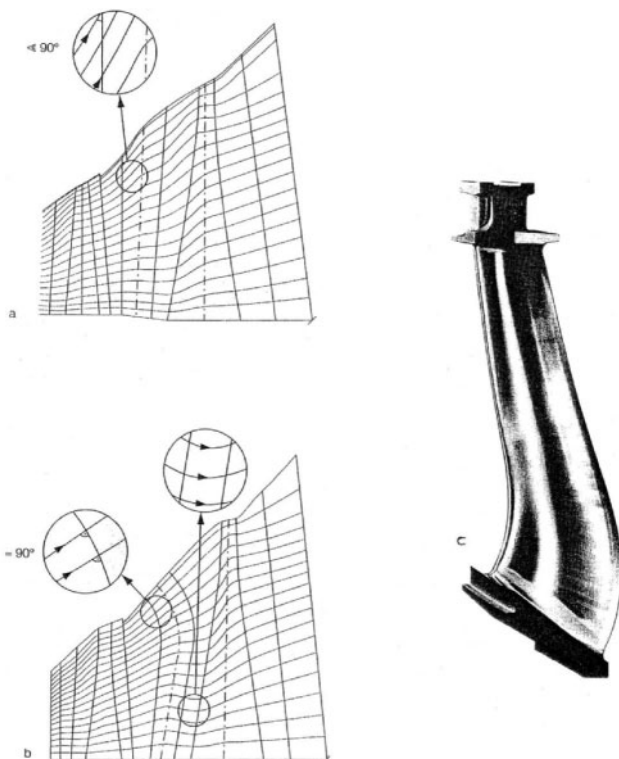


**Fig. 2-25.** Changes in meridional steam flow behavior in LP stages of ABB turbines, due to using 3-D, bowed, and inclined vanes in the last stage (a: classical vane; b: bowed and leaned vane; c: model of advanced 3-D vane)  
Source: A. P. Weiss<sup>47</sup>

Curved and inclined blades, with the angle of inclination decreasing from the blade root to its periphery, were first proposed and investigated at the Moscow Power Engineering Institute by G.A. Filippov and H. Chungchi in 1962.<sup>48</sup> Nowadays, these saber-like vanes and blades have gained widespread acceptance in steam turbines built by almost all the world's major turbine manufacturers. Although initially these vanes and blades were predominantly intended only for LP stages with a large length-to-mean diameter ratio, now such blading is frequently employed in the HP and IP stages.

Advanced computational fluid dynamics (CFD) calculations have also been applied to improve the turbine path in nonbladed areas, with the use of special baffles, razors, and screens to avoid backflows and vortex formation and to reduce extreme energy and pressure losses.

Among other novelties of turbomachinery, of importance is Siemens' initiative to design the turbine steam path optimizing the reaction degree for each stage individually, varying it in a wide range from 10% to 60%.<sup>49</sup> Whereas Siemens has traditionally designed their turbines in a reaction-type mode, GE has traditionally produced impulse-type turbines. Nevertheless, GE currently suggests a "dense pack" turbine design methodology, when the steam path is designed with an increased number of stages and increased reaction degree.<sup>50</sup> In so doing, GE arrived at nearly the same intermediate design decision as Siemens did, but from another direction. The 2000s-vintage turbines also feature reduced steam leakage due to advanced steam gland seals. All of these features make modern turbines much more efficient compared with those of the 1990s.<sup>51</sup>

Even though the mentioned design approaches were mainly developed for fossil fuel power plants, they have been integrated into modern wet-steam turbine design as well. However, the development of wet-steam turbines and computation of their steam paths, in particular, has demanded a better comprehension of moisture behavior in the steam path, as well as the motion of water drops and films with regard to actual turbine design features. Special methods for calculating the wet steam structure have had to be developed. In contrast to old flow analysis techniques, which could only deal with ideal gases, new 3-D calculation methodologies analyze non-equilibrium condensation flows that take into account different steam wetness conditions and phase variations, allowing the designers to estimate the flow rate, loads, and losses of individual turbine stages much more accurately.<sup>52</sup> Nevertheless, these methodologies require further development and improvement.

The mentioned analytical tasks were simultaneously taken up by different groups of prominent scientists in the mid-1970s.<sup>53</sup> Calculation methods for those years as applied to multistage wet-steam turbines were mainly based on extremely simplified notions and did not take into consideration a number of important factors. The shortage of reliable experimental data concerning the structure of the wet-steam flow in actual turbine steam paths was also noted, and developers looked forward to substantial progress in all of the turbine steam path characteristics based on such experimental data. Almost 20 years later, a scientist of a new generation spoke in front of the von Karman Institute for Fluid Dynamics' audience, saying that "our

[Previous Page](#)

## 74 *Wet-Steam Turbines for Nuclear Power Plants*

inability to understand the nucleation process in steam turbines is surprising" and emphasized that "it is evident that the nucleation of water droplets in turbines involves phenomena which are not reproduced by laboratory experiments on nozzles and stationary cascades but nevertheless play a dominating role in the process of phase transition in real machines."<sup>54</sup> He also noted that, despite considerable advances made in aerodynamic design methods, there existed a tendency to consider the wetness loss component as unavoidable. Disputing this point of view, A. Guha declared that more fundamental knowledge of wet-steam flow in turbines could reduce these losses to a minimum. In addition, this should allow more effective removal of water from the steam path and minimize erosion damage. To attain these aims, experimental investigations should be transferred from stationary nozzle rows, cascades, and individual stages to actual or model multistage turbines.

### **Experimental research of wet-steam flow in turbines**

Experimental research of wet-steam flow in turbines in service could be aimed at solving different tasks and using very different techniques. In the simplest case, the wet steam extracted from the steam path is directed into measuring tanks, and measuring the water quantity makes it possible to assess steam conditions by the indirect route. Figure 2-26 shows some results of experimental and computational investigations of wet-steam parameters and moisture separation efficiency for HP stages of the K-220-44 turbine (with a rated output of 220 MW and main steam pressure of 44 atm [4.3 MPa; 626 psi]).<sup>55</sup> The use of measuring tanks connected to different cavities for trapping the water could be quite helpful for investigating and comparing different moisture removal techniques.<sup>56</sup>

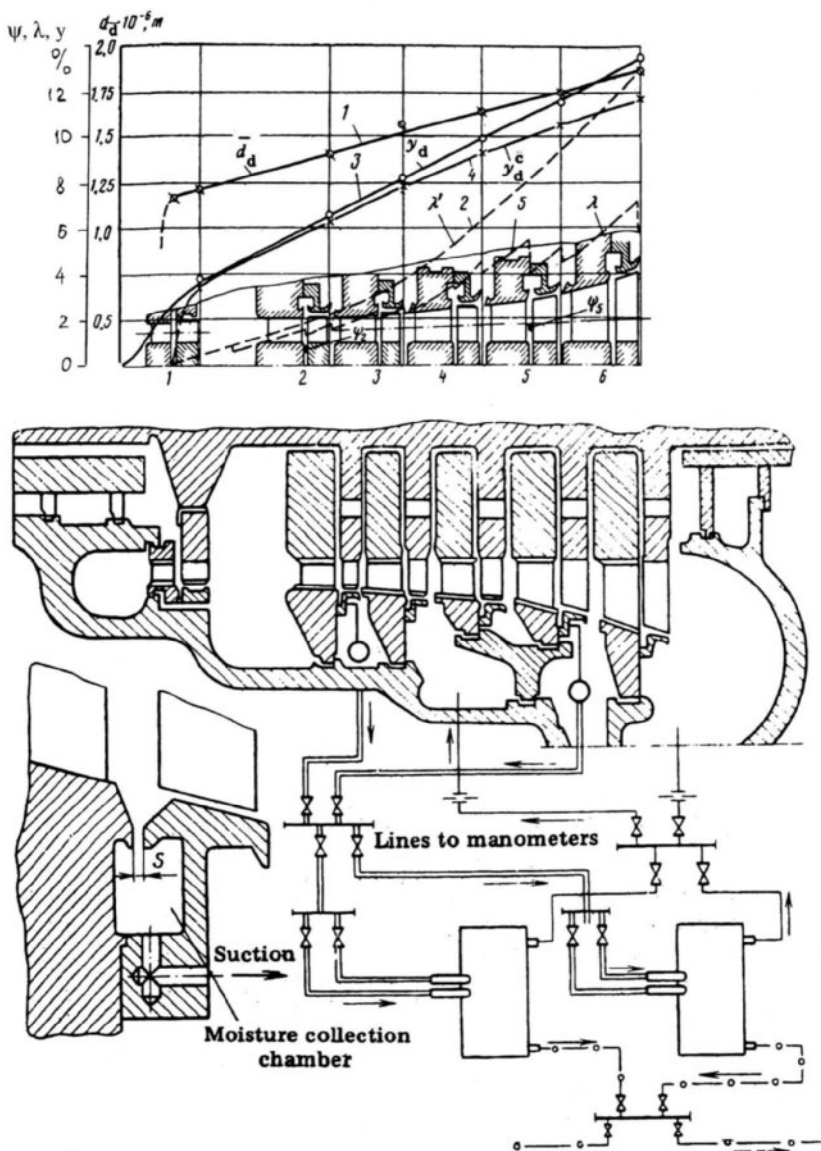


**Fig. 2-26.** Variation in wet-steam conditions along the steam path of the HP cylinder of a K-220-44 turbine (1: average water drop diameter,  $d_d$ ; 2: portion of large drops, ignoring moisture separation,  $\lambda'$ ; 3: total steam wetness,  $y_d$ ; 4: steam wetness for fine water droplets,  $y'_d$ ; 5: portion of large drops, with moisture separation,  $\lambda$ ;  $\psi_2$  and  $\psi_5$  : moisture separation efficiency for the water traps after the second and fifth stages)

Source: Y. F. Kosyak, G. A. Filippov, Y. E. Yushkevich, et al.<sup>57</sup>

Direct measurement and analysis of the moisture conditions in the steam path are commonly performed with the use of long probes inserted into the intracylinder spaces of the operating turbine through accurately positioned guide tubes. A typical installation of such probes between the blade rows of an LP turbine is shown in Figure 2-27. Traversing across the stage height, a probe can provide detailed data about the radial steam condition distribution. The same or similar probes with other heads are also used to measure total and static steam pressure, steam flow direction, and steam velocity in a 3-D field. These probes can also be used for sampling the primary steam condensate from the flow for chemical analysis. Similarly, endoscopes are input into the steam path to observe the motion of the moisture and visually inspect the steam path itself.

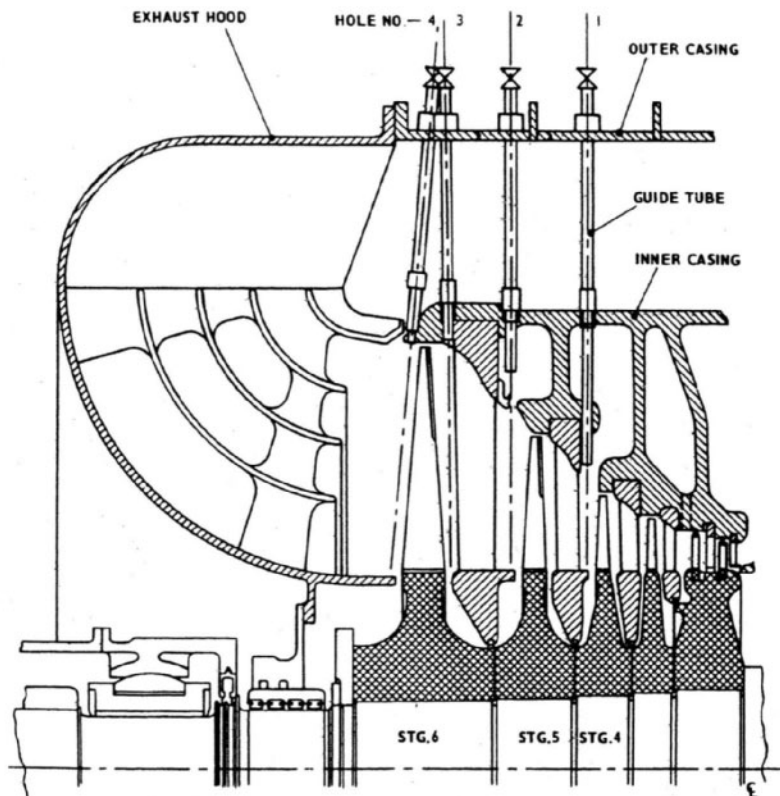


**Fig. 2-27.** Installation of research probes into an LP turbine section  
Source: M. J. Moore<sup>58</sup>

Different methods exist for measuring the various wetness fractions, in particular, those of coarse-grain water. By definition, coarse-grain water consists of large water drops ( $d > 10 \text{ mkm}$ ) drawn by the steam flow or water films and rivulets on the boundary surfaces, which can leave these surfaces and join the steam stream. Mechanical separation and collection of these fractions are therefore feasible, using various separating elements. A typical coarse-grain water distribution between the next-to-last and last stages of a 500-MW turbine is shown in Figure 2-28. Numerous methods have also been developed for measuring the fog wetness fractions.

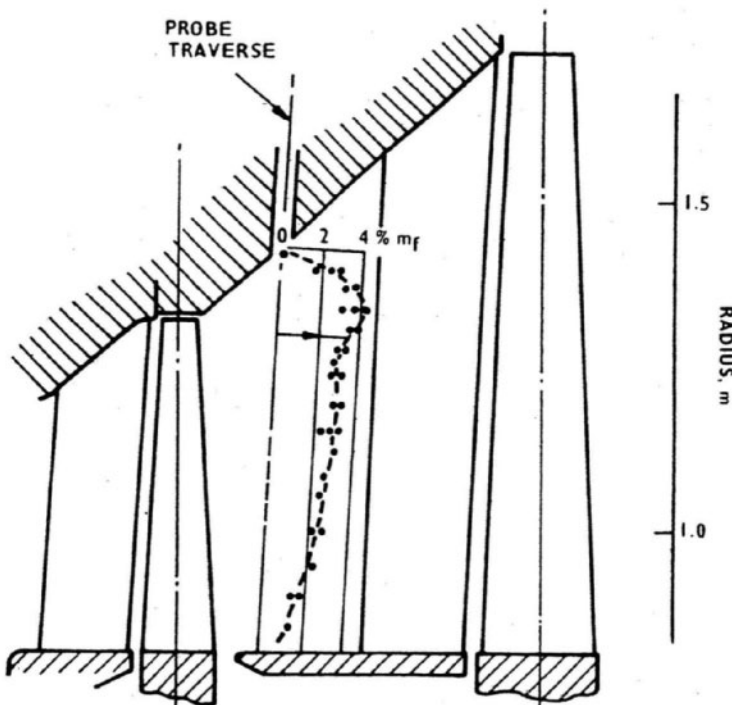


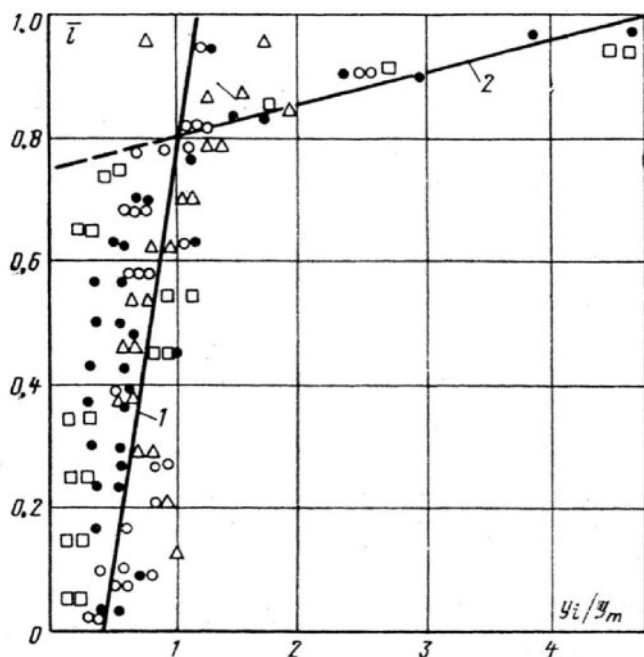
**Fig. 2-28.** Typical distribution of coarse-grain water before the last LP stage of a 500-MW turbine  
Source: M.J. Moore<sup>59</sup>

The simplest method of assessing the steam wetness consists in throttling steam from the two-phase region to a superheated condition. In doing so, the steam wetness is determined by measuring the

temperature and pressure of the superheated steam at the end of the throttling process. Some researchers have also used absorption, dielectrics, psychometrics, and other methods, even though they seem to provide less accurate results.

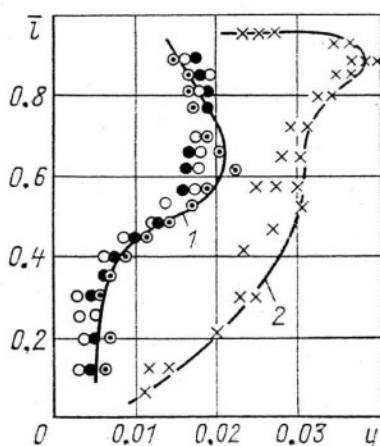
Methods of measuring the drop size also differ for large drops and fog droplets. Among the most widespread and noteworthy is the extinction (also known as light-scattering or light-attenuation) method, which is based on the attenuation of a monochromatic light beam due to its scattering by the drops. The resultant extinction coefficient to be measured can be expressed as a function of the particle size. The indicatrix (a polar diagram) of the scattered light radiation can also be used for measuring the average size of the fog droplets. The main advantages of these and other optical methods are their high degree of sensitivity and lack of inertness.

The steam wetness distribution along the stage height shown in Figure 2-28 is rather typical. It is generally believed that the steam wetness, as well as the modal size of moisture particles and the relative portion of large particles, steadily increases toward the periphery of the stage under the action of centrifugal forces, and experimental data for individual stages commonly confirm this (Fig. 2-29). If the stage has a water extraction belt located after the rotating blades, it promotes this process. Coarse-grain water spray centrifuged from the blade tips can be seen in Figure 2-8. At the same time, there exist numerous experimental data for turbine sections that demonstrate a decrease in the local wetness at the very periphery of the stage, which can be explained mainly by the lower efficiency of the preceding stages at their tip sections, changes of the stage reactivity along the height, as well as some other factors (Fig. 2-30).



**Fig. 2-29.** Steam wetness variation over the height of an individual stage (1: without water extraction after the stage; 2: with water drop trap located after the stage)

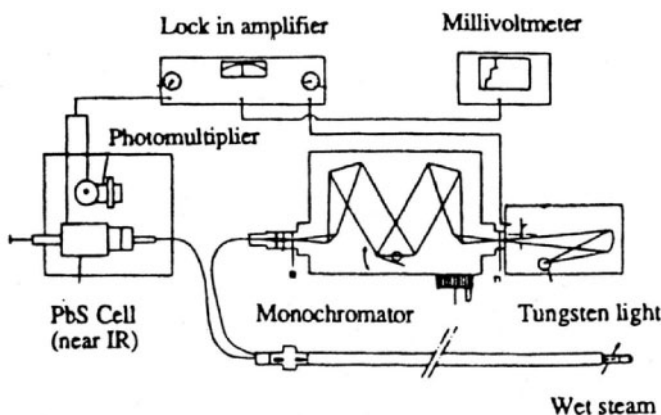
Source: I. I. Kirillov, Y. F. Kosyak, A. I. Nosovitskii, et al.<sup>60</sup>



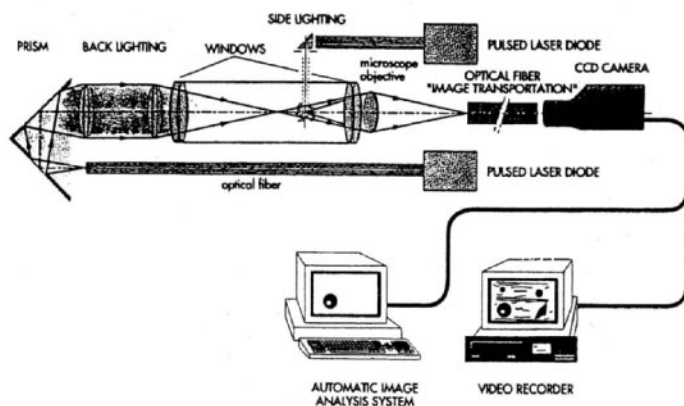
**Fig. 2-30.** Wetness distribution along the length of the last turbine stage inlet, according to experimental data from Westinghouse (1) and AEI (2) turbines

Source: B. M. Troyanovskii<sup>61</sup>

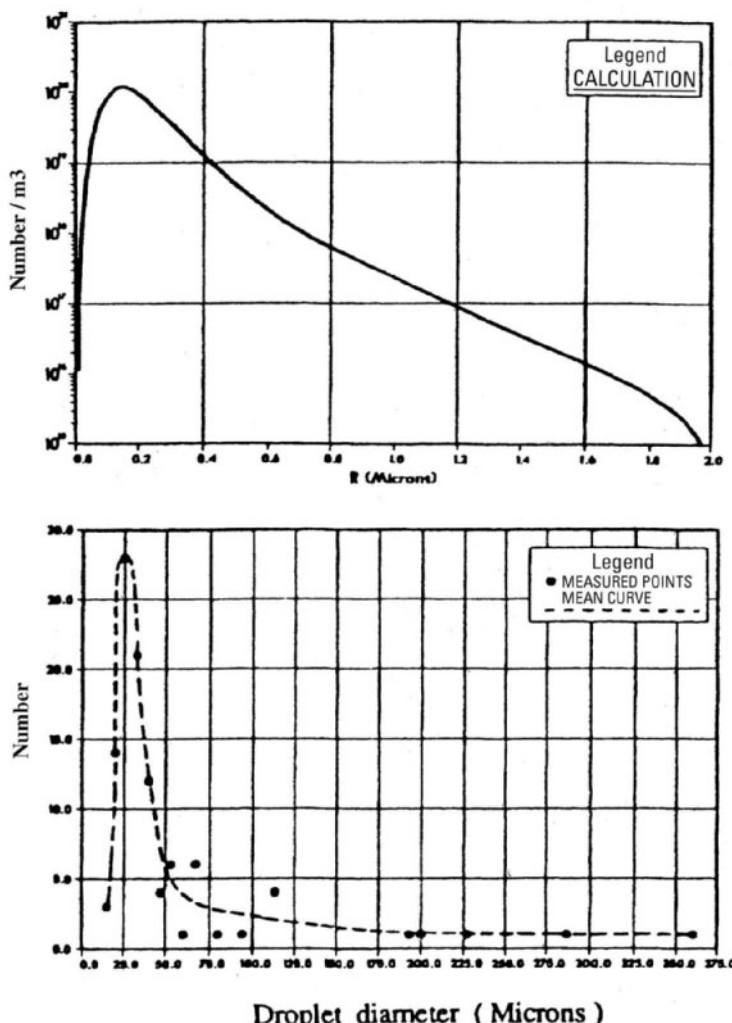
Currently, most experimental researches of wet-steam flow in turbines are produced with the use of optical methods. Figure 2-31 depicts an optical attenuation probe used by researchers of Electricité de France (EdF) for investigations of the wet-steam structure in the LP cylinders applied in 900-MW turbines of nuclear power plants and 600-MW turbines of fossil fuel power plants.<sup>62</sup> The measurements were performed within a wide light wavelength range of 0.35 to 5 mkm, that is, extending up to infrared frequencies. The optical system was incorporated in a 25-mm diameter probe. The wet steam flows through a slot with a length that can be varied from 0 to 200 mm. Purge air is blown on both ends of the slot to prevent deposition of droplets on the sapphire windows. The light, originating from a tungsten lamp, passes through a monochromatic system of interchangeable grating plates; it is then channeled through the probe by a flexible 1 mm silica optical fiber. The changeable detection component could be a photomultiplier for visible light (up to 0.7 mkm), a PbS cell for infrared radiation (0.8 to 2 mkm), or an InSb cell (2 to 5 mkm). A microvideo probe employing back and side lighting methodology is used for coarse-grained drops. This technique was developed for measuring drop sizes greater than 10 mkm (Fig. 2-32). The measured volume is illuminated from two directions: perpendicular to the optical axis, in order to select drops within the focal distance of the magnifying system, and along the axis, with light shining from the rear, in order to determine directly the drop size. This optical system was also incorporated into the same 25-mm diameter tube. To capture the motion of the drops, a pulse diode laser was used as a light source. The images were recorded on a video recorder and then analyzed by the operator (automatic image processing was an anticipated future development). The ultimate goal was to achieve real-time analysis (at a video frequency of 25 Hz) and obtain realistic histograms over a short recording time (1-2 minutes). Experimental distributions of fog droplets and large drops downstream of the last stage blade are shown in Figure 2-33. On the basis of these experimental investigations, the EdF researchers calculated the structure of the energy losses due to wetness for the 900-MW wet-steam turbine's LP stages, including the following components: thermodynamic (related to the non-equilibrium state of the steam), drop acceleration, drop collisions with the rotating blades, water film deposition, action of the centrifugal forces, and additional friction (Fig. 2-34). The calculated losses for the last (seventh) stage are compared with those counted on the basis of the Baumann rule.



**Fig. 2-31.** Optical attenuation probe for measuring fog droplet size  
Source: A. R. Laali, J. J. Courant, and A. Kleitz<sup>63</sup>

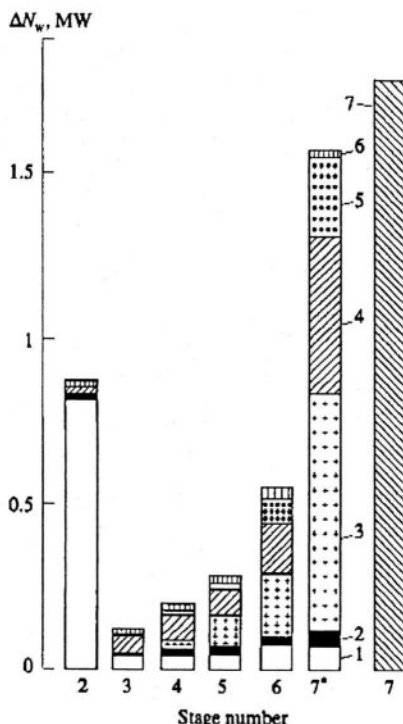


**Fig. 2-32.** Microvideo probe used for coarse-grain water drop measurements  
Source: A. R. Laali, J. J. Courant, and A. Kleitz<sup>64</sup>



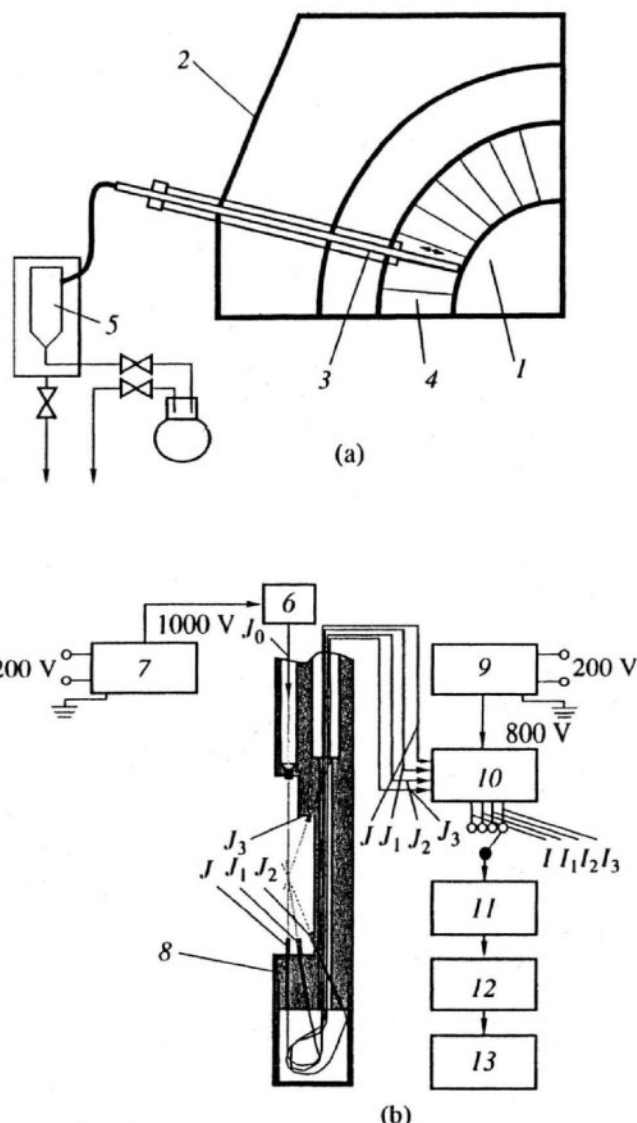
**Fig. 2-33.** Experimental distributions of fog droplets and large drops downstream of the LSB

*Source:* A. R. Laali, J. J. Courant, and A. Kleitz<sup>65</sup>



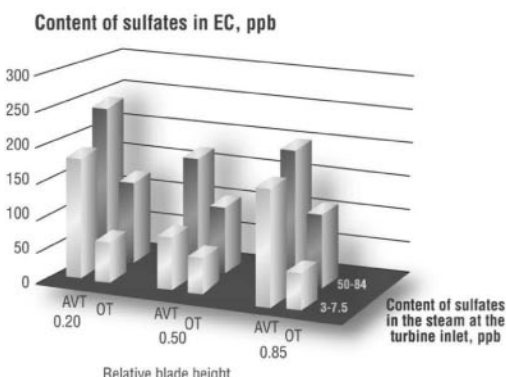
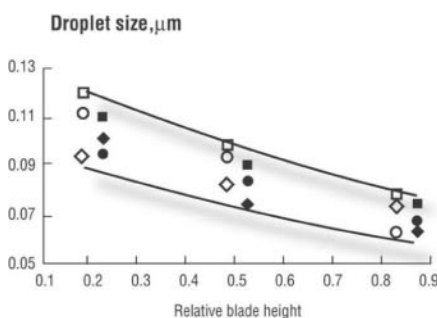
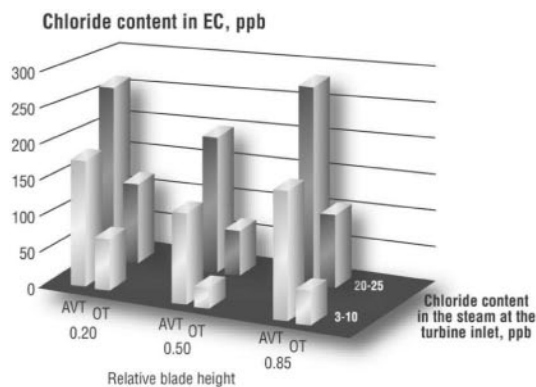
**Fig. 2-34.** Calculated energy losses due to wetness for LP stages of a low-speed 600-MW wet-steam turbine (loss components: 1: thermodynamic (related to the nonequilibrium state of the steam); 2: drop acceleration; 3: drop collisions with the rotating blades; 4: water film deposition; 5: action of the centrifugal forces; 6: additional friction; 7: total energy loss for the seventh stage (calculated on the basis of the Baumann rule))  
Source: B. M. Troyanovskii<sup>66</sup>

Figure 2-35 demonstrates a system developed by Russian scientists at the Moscow Power Engineering Institute, comprising a primary condensate sample trap and a laser probe inserted into the turbine steam flow.<sup>67</sup> The drop size and steam wetness were measured using two optical methods—an asymmetric indicatrix of optical dispersion and light attenuation. A helium-neon laser was used as the light source. The experiments were performed with two different types of water chemistry, all-volatile treatment (AVT) and oxygenated treatment (OT), with automatic processing of all the chemical analysis data. The probe facilitated measurements at several positions along the stage height. Some results of these experiments for different impurity levels in the steam at the turbine inlet are shown in Figure 2-36.



**Fig. 2-35.** System for sampling primary condensate (a) and laser probe (b) for investigating corrosive properties of wet steam on a model turbine (1: turbine rotor; 2: turbine casing; 3: probe and sample trap; 4: turbine stage; 5: sample tank; 6: helium-neon laser; 7: laser power supply; 8: head of the laser probe; 9: photomultiplier power supply; 10: photomultiplier; 11: analog-to-digital transformer; 12: interface; 13: computer;  $J_x$ : radiation intensity;  $I_x$ : current signal)

Source: O. I. Martynova, O. A. Povarov, T. I. Petrova, et al.<sup>68</sup>



**Fig. 2-36.** Content of chlorides (a) and sulfates (c) in primary condensate; variation of droplet size over the stage height for different impurity levels in steam at the turbine inlet (b)

Source: O. I. Martynova, O.A. Povarov, T. I. Petrova, et al.<sup>69</sup>

Japanese scientists of Toshiba employed a combined approach to investigations of wet-steam flow as applied to a new 40-inch titanium LSB developed for the rotation speed of 3,600 rpm and 52-inch steel LSB for low-speed turbines.<sup>70</sup> The steam wetness and water drop size distribution along the stage height were measured with the use of an optical system, as shown in Figure 2-37a. For the measurement, a parallel laser beam was radiated into the steam flow, and the light scattered from the drops was transmitted through 30-channel optical fibers to photodiodes. Computerized analysis of the scattered light intensity distribution enabled calculation of the drop size and moisture mass distribution; some results of the wetness measurements are shown in Figure 2-37b. The tests simultaneously comprised measuring the quantity of water removed from the stage via suction slots on the surfaces of the hollow vane, as well as the relative erosion rate of the LSB's inlet edge (Figs. 2-38a and c). In addition, the steam flow can be viewed through a *boroscope*—a kind of endoscope (Fig. 2-39a). In order to avoid direct contact with the steam, the boroscope was enclosed in a protective sheath (Fig. 2-39b). It was introduced into the steam path downstream of the last stage vane row to observe the steam flow and water motion on the convex vane surface (Fig. 2-39c). Many water films and rivulets stripped off from the outlet edge and atomized in the steam stream were seen along the upper half of the blade height, but these events were relatively rare in the lower half.

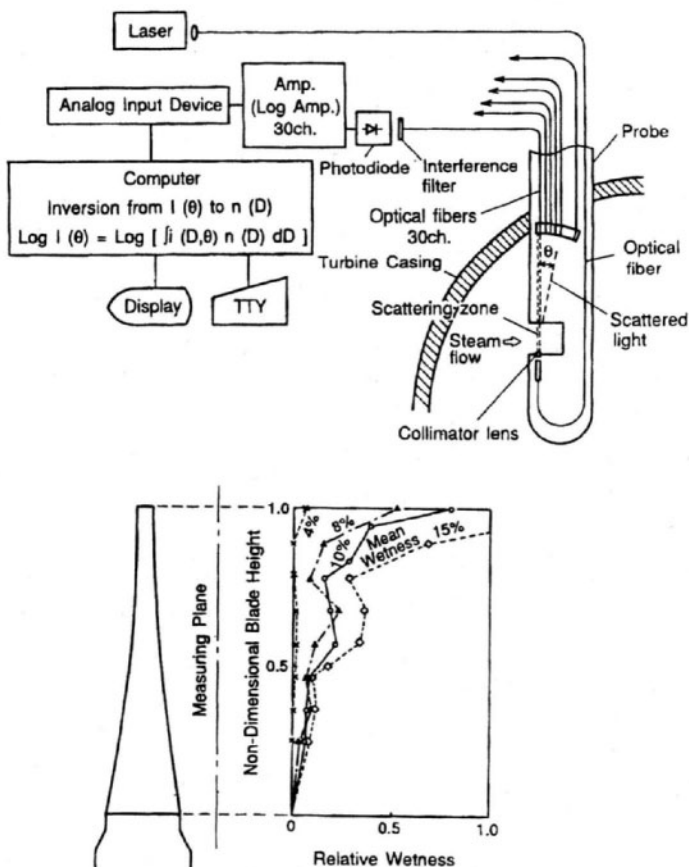


**Fig. 2-37.** Schematic diagram of steam wetness measurement system (a); wetness distribution over the stage height at a model turbine outlet (b)  
 Source: T. Sakamoto, S. Nagao, and T. Tanuma<sup>71</sup>

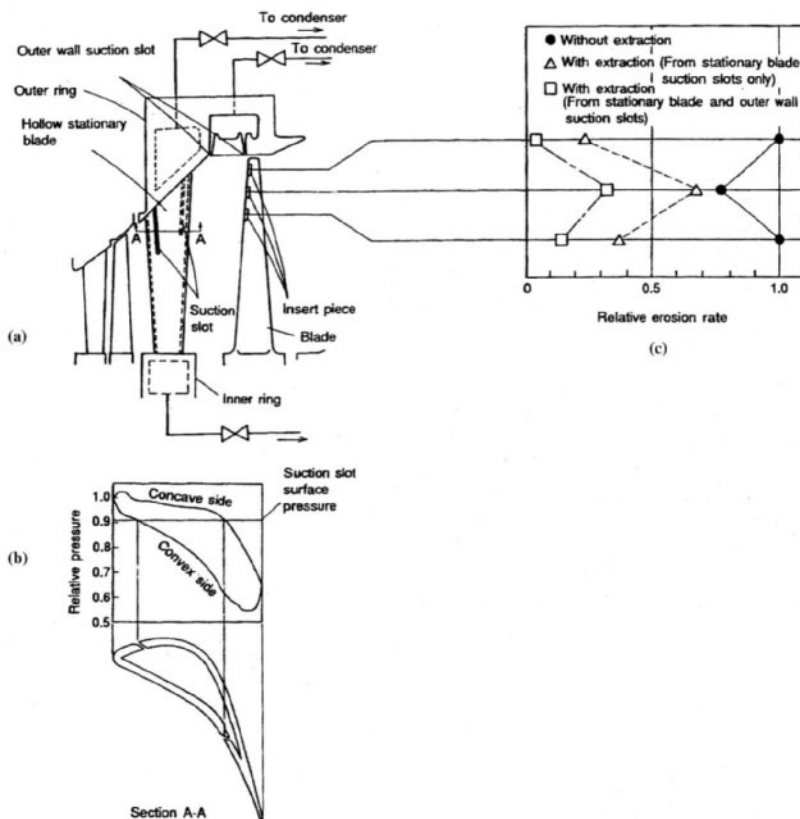


**Fig. 2-38.** Schematic diagram for measuring water quantities withdrawn through suction slots on surfaces of the hollow vane (a); pressure distribution along the vane profile (b); relative erosion rate of the blade inlet edge (c)  
 Source: T. Sakamoto, S. Nagao, and T. Tanuma<sup>72</sup>

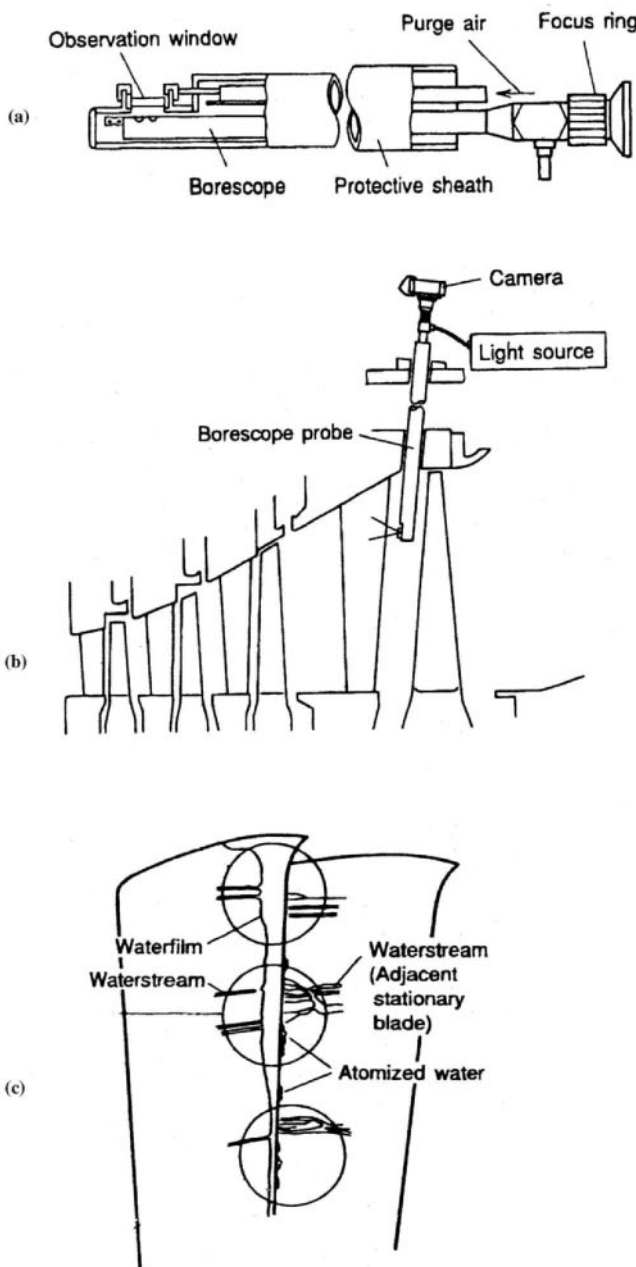


**Fig. 2-39.** Boroscope probe (a); inserted into the model turbine steam path (b); behavior of water flow at outlet edge of the nozzle vane (c)  
Source: H. Kawagishi, S. Nagao, and T. Yamamura<sup>73</sup>

According to endoscopic observations by different researchers, the actual motion of water across the stationary, non-rotating parts of the steam path (nozzle vanes, diaphragm, and casing walls) composes an intricate picture (Fig. 2-40). The pattern to a great degree depends on the pressure and steam-flow fields around the stage, but in many respects, it is rather disordered, although there exists some well-defined radial water motion—for example, along the trailing edges of the stationary blades. These rivulets tend to accumulate and detach at specific sites, thus causing concentrated blade erosion. The water motion across the surface of the rotating blades is difficult to observe, but due to the influence of centrifugal forces, such a motion is much more predictable. The water films are believed to be relatively thin and move predominantly in a nearly radial direction, as determined by centrifugal and Coriolis forces. For typical LP steam path conditions, a film thickness of about 10 mkm is expected, with flow velocities on the order of a few meters per second. A supposed characteristic water flow pattern according to some theoretical treatments is shown in Figure 2-41.

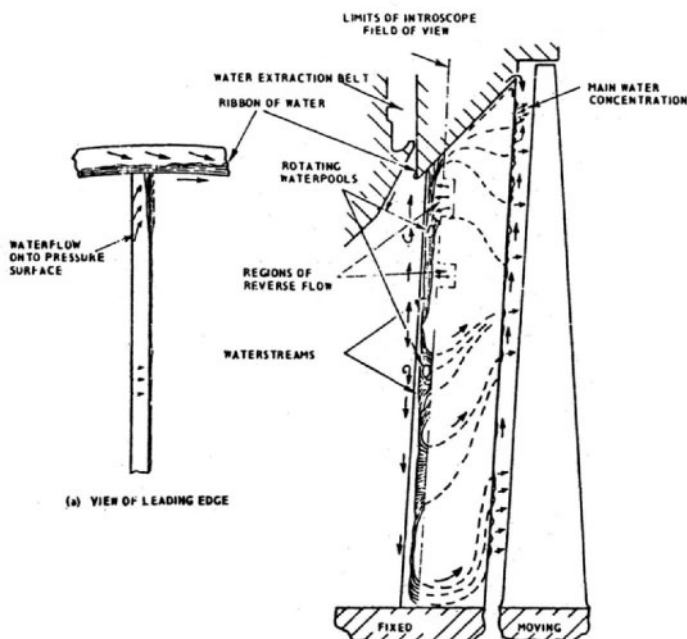


**Fig. 2-40.** Water motion on the pressure surface of the last stage nozzle vane

Source: M. J. Moore<sup>74</sup>

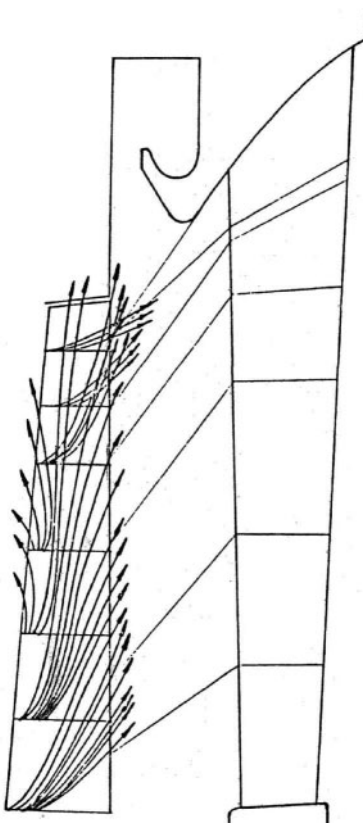


**Fig. 2-41.** Theoretical characteristic water flow field for LP rotating blades  
Source: I. I. Kirillov and R. M. Yablonik<sup>75</sup>

Now it is beyond question that energy losses due to wetness are unavoidable. However, the amount of these losses in modern turbines is decidedly too high and could be significantly decreased. On the other hand, experimental research in the last few years has not radically changed the understanding of steam and moisture flow in wet-steam turbines and discovered new ways to decline these losses generally. New methods of decreasing energy losses due to wetness have been slow in being developed. The accumulation of new knowledge has resulted in gradual improvements to measurements of the steam path and methods for drying the steam. These methods actually increase the working fluid losses with the removed water, but make the steam flow more efficient.

## References

- 1 McCloskey, T. H., R. B. Dooley, and W. P. McNaughton. 1999. *Turbine Steam Path Damage: Theory and Practice*, Vols. 1-2. Palo Alto, Calif.: EPRI, 1999.
- 2 Lindinger, R. J. and R. M. Currant. 1981. Corrosion experience in large steam turbines. *Power Engineering* 85 (10): 76-80.
- 3 Povarov, O. A., G. V. Tomarov, and V. N. Zharov. 1990. Erosion-corrosion of saturated-steam turbine plant elements. *Thermal Engineering* 37(12):643-647.
- 4 Leyzerovich, A. 1997. *Large Power Steam Turbines: Design & Operation*, Vols. 1-2. Tulsa, Okla.: PennWell Publishing, 1997.
- 5 Bannister, R. L. and G. J. Silvestri, Jr. 1989. The evolution of central station steam turbines. *Mechanical Engineering* 111 (2): 70-78.
- 6 Leyzerovich, A. 2000. New benchmarks for steam turbine efficiency. *Power Engineering* 106 (8): 37-42.
- 7 Sakai, K., S. Morita, T. Yamamoto, and T. Tsunura. 1998. Design and operating experience of the latest 1,000-MW coal-fired boiler. *Hitachi Review* 47 (5): 183-187.
- 8 Is 700+°C steam temperature economically viable? *Modern Power Systems* 18(5): 73-77.
- 9 Troyanovskii, B. M. 1978. *Turbines for Nuclear Power Plants*, 2d ed. (in Russian). Moscow: Energiya, 1978.
- 10 Mounfield, P. R. 1991. *World Nuclear Power*. London: Routledge, 1991.
- 11 Troyanovskii, *Turbines for Nuclear Power Plants*.
- 12 Ibid.
- 13 Coit, R. L. 1975. Design trends use utility feed-water heaters and condensers. *Combustion* 46(8): 14-27.
- 14 Arkad'ev, B. A. 1986. *Operating Conditions of Steam Turbosets for Nuclear Power Plants* (in Russian). Moscow: Energoatomizdat, 1986.
- 15 Coit, Design trends, 14-27.
- 16 Zorin, V. M., and V. D. Baibakov. 2003. The optimization of the splitting pressure in the turbines for nuclear power plants. *Thermal Engineering* 50 (10): 844-851.
- 17 Baily, F. G., J. A. Booth, K. C. Cotton, and E. H. Miller. 1973. *Predicting the Performance of 1800-rpm Large Steam Turbine-Generators Operating with Light-Water Power Reactors*. New York: General Electric, 1973.
- 18 El-Wakil, M. M. 1984. *Powerplant Technology*. New York: McGraw-Hill, 1984.
- 19 Deich, M. E., and G. A. Filippov. 1987. *Two-Phase Flows in Elements of Thermal Power Equipment* (in Russian). Moscow: Energoatomizdat, 1987.

- 20 Moore, M. J. 1976. Gas dynamics of wet steam and energy losses in wet-steam turbines. In *Two-Phase Steam Flow in Turbines and Separators: Theory, Instrumentation, Engineering*, ed. M. J. Moore and C.H. Sieverding, 59–126. Washington, D.C.: Hemisphere Publishing Corp., 1976.
- 21 Stodola, A. 1945. *Steam and Gas Turbines*, Vols. 1–2. trans. L. C. Loewenstein. New York: Peter Smith, 1945.
- 22 Troyanovskii, B. M., G. A. Filippov, and A. E. Bulkin. 1985. *Steam and Gas Turbines for Nuclear Power Plants* (in Russian). Moscow: Energoatomizdat, 1985.
- 23 Shcheglyaev, A. V. 1993. *Steam Turbines*, 6th ed., Vols. 1-2 (in Russian). ed. B. M. Troyanovskii. Moscow: Energoatomizdat, 1993.
- 24 Guha, A. 1995. Application of the non-equilibrium theory to steam turbines. In *Two-Phase Flows with Phase Transition*, 73–110. Rhode Saint Genése, Belgium: Institute for Fluid Dynamics, 1995.
- 25 Shcheglyaev, *Steam Turbines*.
- 26 Ibid.
- 27 Troyanovskii, *Steam and Gas Turbines for Nuclear Power Plants*.
- 28 Shcheglyaev, *Steam Turbines*.
- 29 Ibid.
- 30 Troyanovskii, *Turbines for Nuclear Power Plants*.
- 31 Troyanovskii, *Steam and Gas Turbines for Nuclear Power Plants*.
- 32 Ibid.
- 33 Ibid.
- 34 Ibid.
- 35 Ibid.
- 36 Ibid.
- 37 Shcheglyaev, *Steam Turbines*.
- 38 Troyanovskii, *Steam and Gas Turbines for Nuclear Power Plants*.
- 39 Troyanovskii, *Turbines for Nuclear Power Plants*.
- 40 Troyanovskii, *Steam and Gas Turbines for Nuclear Power Plants*.
- 41 Moore, Gas dynamics. 59–126.
- 42 Baumann, K. 1921. Some recent developments in large steam turbine practice. *Engineer* 111: 435–458.
43. Moore, Gas dynamics. 59–126
- 44 Troyanovskii, *Steam and Gas Turbines for Nuclear Power Plants*.

- 45 Troyanovskii, B. M. 1996. Improving the flow path of steam turbines. *Thermal Engineering* 43 (1): 9-18.
- 46 Oeynhausen, H., A. Droszdio, H. Ulm, and H. Termuehlen. 1996. Advanced 1000 MW tandem-compound reheat steam turbines. *Proceedings of the American Power Conference* 58: 686-698.
- 47 Weiss, A. P. 1998. Aerodynamic design of advanced LP steam turbines. *ABB Review* 5: 4-11.
- 48 Deich, M. E., and B. M. Troyanovskii. 1964. *Investigations and Design of Axial-Turbine Stages* (in Russian). Moscow: Mashinostroenie, 1964.
- 49 Simon, V., H. Oeynhausen, R. Bürkner, and K.-J. Eich. 1997. Impulse blading? reaction blading? Variable blading! *VGB Kraftwerkstechnik* 77(9):648-652.
- 50 Maughan, J. R., L.D. Willey, J. M. Hill, and S. Goel. 2000. Development of the dense pack steam turbine: a new design methodology for increased efficiency. In *Proceedings of the International Joint Power Generation Conference*, 1-11. New York: ASME, 2000.
- 51 Nowi, A. and B. R. Haller. 1997. Developments in steam turbine efficiency. *VGB Kraftwerkstechnik* 77 (7): 499-503.
- 52 Laali, A.R., J. J. Courant, and A. Kleitz. 1991. Calculation and measurement of fog droplet size: Comparison between nuclear and fossil fired turbines. In *Design, Repair, and Refurbishment of Steam Turbines*, PWR-Vol. 13, 133-138. New York: ASME, 1991.
- 53 Filippov, G. A., O. A. Povarov, and V. V. Pryakhin. 1973. *Investigations and Calculations for Wet-Steam Turbines* (in Russian). Moscow: Energiya, 1973.
- 54 Guha, Application of the non-equilibrium theory, 73-110.
- 55 Kiryukhin, V. I., G. A. Filippov, O. A. Povarov, and V. I. Dikarev. 1976. Investigation of the structure of wet steam in a multistage turbine. *Thermal Engineering* 23 (5): 26-29.
- 56 Hayes, J. K., S. A. Trovato, S. Misilo, and J. Burger. 1991. An investigation and assessment of methods to improve moisture removal and reheating of PWR cycle steam. In *Design, Repair, and Refurbishment of Steam Turbines*, PWR-Vol. 13, 115-126. New York: ASME, 1991.
- 57 Kosyak, Y. F., G.A. Filippov, Y. E. Yushkevich, et al. 1978. Investigation of moisture separation in the HPC for the K-220-44 turbine. *Thermal Engineering*, 25 (6): 9-12.
- 58 Moore, M. J. 1976. Instrumentation for wet steam. *Two-Phase Steam Flow in Turbines and Separators: Theory, Instrumentation, Engineering*, ed. M.J. Moore and C.H. Sieverding, 191-206. Washington, D.C.: Hemisphere Publishing Corp., 1976.
- 59 Ibid.
- 60 Kirillov, I. I., Y.F. Kosyak, A. I. Novosiltskii, et al. 1970. Effect of wetness on LP stage efficiency in large steam turbines. *Thermal Engineering* 17 (6): 51-54.
- 61 Troyanovskii, *Turbines for Nuclear Power Plants*.

96      *Wet-Steam Turbines for Nuclear Power Plants*

- 62 Laali, Calculation and measurement of fog droplet size, 135–138.
- 63 Ibid.
- 64 Ibid.
- 65 Ibid.
- 66 Troyanovskii, B. M. 1993. Ways of improving the efficiency of steam turbines. *Thermal Engineering* 40(7): 528–536.
- 67 Martynova, O. I., O. A. Povarov, T. I. Petrova, et al. 1998. Formation of corrosive media in the region of the phase transition in steam turbines. *Thermal Engineering* 4(7): 568–574.
- 68 Ibid.
- 69 Ibid.
- 70 Sakamoto, T., S. Nagao, and T. Tanuma. 1992. Investigation of wet steam flow for steam turbine repowering. In *Steam Turbine-Generator Developments for the Power Generation Industry*, PWR-Vol. 18, 33–39. New York: ASME, 1992.
- 71 Ibid.
- 72 Ibid.
- 73 Kawagishi, H., S. Nagao, and T. Yamamura. 1983. Visualization of wet steam flow in turbines by a boroscope (in Japanese). *JSME Paper* 830-7, 41–44.
- 74 Moore, Gas dynamics. 59–126.
- 75 Kirillov, I. I. and R. M. Yablonik. 1968. *Fundamentals of a Theory of Wet-Steam Turbines* (in Russian). Leningrad: Mashinostroenie, 1968.

## Bibliography

- Antoshin, V. I., Y. Y. Kachuriner, Y. V. Nakhman, et al. 1982. The structure of the liquid phase in the low-pressure cylinder of a steam turbine. *Thermal Engineering* 29(7): 371-374.
- Arkad'ev, B. A. 1986. *Operating Conditions of Steam Turbosets for Nuclear Power Plants* (in Russian). Moscow: Energoatomizdat, 1986.
- Baily, F. G., J. A. Booth, K. C. Cotton, and E. H. Miller. 1973. *Predicting the Performance of 1800-rpm Large Steam Turbine-Generators Operating with Light-Water Power Reactors*. New York: General Electric, 1973.
- Bannister, R. L. and G. J. Silvestri, Jr. 1989. The evolution of central station steam turbines. *Mechanical Engineering* 111(2):70-78.
- Baumann K. 1921. Some recent developments in large steam turbine practice, *Engineer* 111:435-458.
- Borisov, F. P., M. Y. Ivanov, A. M. Karelkin, et al. 1993. Steam turbine high-efficiency stage design using ideal and viscous gas-flow calculations. *Thermal Engineering* 40 (5):375-381.
- Cofer, J. I., IV. 1996. Advances in steam path technology. *Journal of Engineering for Gas Turbines and Power. Transactions of the ASME* 118:337-352.
- Coit, R. L. 1975. Design trends use utility feed-water heaters and condensers. *Combustion* 46(8): 14-27.
- Deich, M. E., Y. L. Abramov, and V. I. Glushkov. 1970. Regarding the mechanism of moisture flow in turbine nozzle blade channels. *Thermal Engineering* 17(11): 48-52.
- \_\_\_\_\_, and G. A. Filippov. 1987. *Two-Phase Flows in Elements of Thermal Power Equipment* (in Russian). Moscow: Energoatomizdat, 1987.
- \_\_\_\_\_, and B. M. Troyanovskii. 1964. *Investigations and Design of Axial-Turbine Stages* (in Russian). Moscow: Mashinostroenie, 1964.
- \_\_\_\_\_, B. M. Troyanovskii, and G. A. Filippov. 1990. An effective way of improving the efficiency of turbine stages. *Thermal Engineering* 37(10): 520-523.
- Dobkes, A. L., T. M. Zil'ber, Y. Y. Kachuriner, et al. 1992. Studying the characteristics of wet steam in turbine flow sections. *Thermal Engineering* 39(1): 45-49.
- Drosdziok, A. 1998. Steam turbines (in German). *BWK* 50(4): 120-124.
- El-Wakil, M. M. 1984. *Powerplant Technology*. New York: McGraw-Hill, 1984.
- Engelke, W. 1976. Operating experience of wet-steam turbines. In *Two-Phase Steam Flow in Turbines and Separators: Theory, Instrumentation, Engineering*, ed. M. J. Moore and C. H. Sieverding, 291-315. Washington, D.C.: Hemisphere Publishing Corp., 1976.
- Filippov, G. A., O. A. Povarov, and V. V. Pryakhin. 1973. *Investigations and Calculations for Wet-Steam Turbines* (in Russian). Moscow: Energiya, 1973.
- Giovando, C. 1998. Explore opportunities from today's steam turbines. *Power* 148(4): 28-39.
- Guha, A. 1995. Application of the non-equilibrium theory to steam turbines. In *Two-Phase Flows with Phase Transition*, 73-110. Rhode Saint Genése, Belgium: Institute for Fluid Dynamics, 1995.
- Gyamarthy, G. G. 1962. *A Theory of Wet-Steam Turbines* (in German). Zurich: Juris-Verlag, 1962.

- Hayes, J. K., S. A. Trovato, S. Misilo, and J. Burger. 1991. An investigation and assessment of methods to improve moisture removal and reheating of PWR cycle steam. In *Design, Repair, and Refurbishment of Steam Turbines*, PWR Vol. 13, 115-126. New York: ASME, 1991.
- Hoffstadt, U. 2001. Boxberg achieves world record for efficiency. *Modern Power Systems* 21(10):21-23.
- Is 700+°C steam temperature economically viable? *Modern Power Systems* 18(5): 73-77.
- Kachuriner, Y. Y. 2003. Characteristics of the turbine-blade rows in the initial condensation region. *Thermal Engineering* 50(6): 470-476.
- Kawagishi, H., S. Nagao, and T. Yamamura. 1983. Visualization of wet steam flow in turbines by a boroscope (in Japanese). *JSME Paper* 830-7, 41-44.
- Kirillov, I. I., Y. F. Kosyak, A. I. Novosiltskii, et al. 1970. Effect of wetness on LP stage efficiency in large steam turbines. *Thermal Engineering*. 17(6): 51-54.
- \_\_\_\_\_, V. V. Ris, E. M. Smirnov, and A. E. Khodak. 1993. Calculation of three-dimensional flows in turbomachines based on the solution of the parabolized Navier-Stokes equations. *Thermal Engineering* 40(3): 197-200.
- \_\_\_\_\_, and R. M. Yablonik. 1968. *Fundamentals of a Theory of Wet-Steam Turbines* (in Russian). Leningrad: Mashinostroenie, 1968.
- Kiryukhin, V. I., G. A. Filippov, O. A. Povarov, and V. I. Dikarev. 1976. Investigation of the structure of wet steam in a multistage turbine. *Thermal Engineering*. 23(5):26-29.
- \_\_\_\_\_, V. V. Pryakhin, V. I. Dikarev, and V. V. Ivanov. 1973. Investigation of the efficiency of moisture traps in multistage turbines. *Thermal Engineering*. 20(6):109-113.
- Kjaer, S., F. Klauke, R. Vanstone, et al. 2002. The advanced supercritical 700°C pulverized coal-fired power plant. *VGB PowerTech*. 82 (7): 46-49.
- Kosyak, Y. F., G. A. Filippov, Y. E. Yushkevich, et al. 1978. Investigation of moisture separation in the HPC of the K-220-44 turbine. *Thermal Engineering* 25(6):9-12.
- \_\_\_\_\_, T. M. Zil'ber, Y. V. Kotov, et al. 1973. Investigation of effectiveness of moisture trapping inside channels in the diaphragms of the last stages of the low pressure cylinders of high-capacity steam turbines. *Thermal Engineering* 20(7): 55-58.
- Laali, A. R., and B. Collignan. 1994. Condensation process in high pressure nuclear steam turbines. 1994. *Advances in Steam Turbine Technology for the Power Generation Industry*, PWR-Vol. 26, 49-56. New York: ASME, 1994.
- \_\_\_\_\_, J. J. Courant, and A. Kleitz. 1991. Calculation and measurement of fog droplet size: Comparison between nuclear and fossil fired turbines. 1991. In *Design, Repair, and Refurbishment of Steam Turbines*, PWR-Vol. 13, 133-138. New York: ASME, 1991.
- Leyzerovich, A. 1997. *Large Power Steam Turbines: Design & Operation*, Vols. 1-2. Tulsa, Okla.: PennWell Publishing, 1997.
- \_\_\_\_\_. 2002. New benchmarks for steam turbine efficiency. *Power Engineering* 106(8): 37-42.
- Lindinger, R. J. and R. M. Currant. 1981. Corrosion experience in large steam turbines. *Power Engineering* 85(10): 76-80.
- Logan, T. M. 2002. Tangjin 5 and 6: Korea's first ultrasupercritical units. *Modern Power Systems* 22(10): 23-25.

- Luby, P. 2003. Supercritical systems. *Modern Power Systems* 23(8): 27–32.
- Machida, M., H. Yoda, E. Saito, and K. Namura. 2002. Development of long blades with continuous cover blade structure for steam turbines. *Hitachi Review* 51(5): 143–147.
- Martynova, O. I., O. A. Povarov, T. I. Petrova, et al. 1998. Formation of corrosive media in the region of the phase transition in steam turbines. *Thermal Engineering* 45(7): 568–574.
- Maughan, J. R., L. D. Willey, J. M. Hill, and S. Goel. 2000. Development of the dense pack steam turbine: a new design methodology for increased efficiency. In *Proceedings of the International Joint Power Generation Conference*, 1–11. New York: ASME, 2000.
- McCloskey, T. H., R. B. Dooley, and W. P. McNaughton. 1999. *Turbine Steam Path Damage: Theory and Practice*, Vols. 1–2. Palo Alto, Calif.: EPRI, 1999.
- Miyawaki, T., H. Tashiro, M. Honjo, and E. Watanabe. 1992. Improvement of LP turbine efficiency by fully 3D designed blade. *Steam Turbine-Generator Developments for the Power Generation Industry*, PWR-Vol. 18, 75–80. New York: ASME, 1992.
- Moore, M. J. 1976. Gas dynamics of wet steam and energy losses in wet-steam turbines. In *Two-Phase Steam Flow in Turbines and Separators: Theory, Instrumentation, Engineering*, ed. M. J. Moore and C. H. Sieverding, 59–126. Washington, D.C.: Hemisphere Publishing Corp., 1976.
- . 1976. Instrumentation for wet steam. *Two-Phase Steam Flow in Turbines and Separators: Theory, Instrumentation, Engineering*, ed. M. J. Moore and C. H. Sieverding, 191–206. Washington, D.C.: Hemisphere Publishing Corp., 1976.
- and P. Sculpher. 1970. Conditions producing concentrated erosion in large steam turbines. *Proceedings of the Institute of Mechanical Engineers* 184(3G): 45–56.
- , and C. H. Sieverding, eds. 1976. *Two-Phase Steam Flow in Turbines and Separators: Theory, Instrumentation, Engineering*. Washington, D.C.: Hemisphere Publishing Corp., 1976.
- Mounfield, P. R. 1991. *World Nuclear Power*. London: Routledge, 1991.
- Nowi, A. and B. R. Haller. 1997. Developments in steam turbine efficiency. *VGB Kraftwerkstechnik* 77(7): 499–503.
- Nowi, A., and P. J. Walker. 1999. First test results for steam turbines with state-of-the-art blading. *VGB PowerTech* 79(12): 48–52.
- Oeynhausen, H., A. Droszdioł, H. Ulm, and H. Termuehlen. 1996. Advanced 1000 MW tandem-compound reheat steam turbines. *Proceedings of the American Power Conference* 58: 686–698.
- Povarov, O. A. 1980. Problems of moisture separation in turbine plants of nuclear power stations. *Thermal Engineering* 27(2): 84–89.
- Povarov, O. A., L. A. Fel'dberg, V. N. Semenov, and S. A. Popov. 2000. Measurement of the droplet size and the wetness of the steam in the turbine by the spectral transparency method. *Thermal Engineering* 47(11): 991–996.
- Povarov, O. A., G. V. Tomarov, and V. N. Zharov. 1990. Erosion-corrosion of saturated-steam turbine plant elements. *Thermal Engineering* 37(12): 643–647.
- Sakai, K., S. Morita, T. Yamamoto, and T. Tsunura. 1998. Design and operating experience of the latest 1,000-MW coal-fired boiler. *Hitachi Review* 47(5): 183–187.

- Sakamoto, T., S. Nagao, and T. Tanuma. 1992. Investigation of wet steam flow for steam turbine repowering. *Steam Turbine-Generator Developments for the Power Generation Industry*, PWR-Vol. 18, 33-39. New York: ASME, 1992.
- Saltanov, G. A. 1979. *Unbalanced and Unsteady Processes in Gas Dynamics of One-Phase and Two-Phase Mediums* (in Russian). Moscow: Nauka, 1979.
- Scarlin, B. 1997. Steam turbines (in German). *BWK* 49(4): 91-96.
- Senoo, S., Y. Shikano, and K. Tsubouchi. 1999. Two-dimensional analysis for non-equilibrium homogeneously condensing flows through steam turbines cascades. *Proceedings of the ASME/JSME Fluids Engineering Division Summer Meeting*. New York: ASME, 1999.
- Shcheglyayev, A. V. 1993. *Steam Turbines*, 6th ed., Vols. 1-2 (in Russian). ed. B. M. Troyanovsky. Moscow: Energoatomizdat, 1993.
- Simon, V., and H. Oeynhausen. 1998. 3DV three-dimensional blades—A new generation of steam turbine blading. *Proceedings of International Joint Power Generation Conference*, PWR-Vol. 33-2, 89-96. New York: ASME, 1998.
- \_\_\_\_\_, H. Oeynhausen, R. Bürkner, and K.-J. Eich. 1997. Impulse blading? reaction blading? Variable blading! *VGB Kraftwerkstechnik* 77(9):648-652.
- Smith, D. J. 2001. Steam turbines remain the workhorse for power generation. *Power Engineering* 105(8):44-46.
- Stodola, A. 1945. *Steam and Gas Turbines*, Vols. 1-2. trans. L. C. Loewenstein. New York: Peter Smith, 1945.
- Styrikovich, M. A., V. S. Polonsky, and G. V. Ziklauri. 1982. *Heat-Mass Exchange and Hydrodynamics in Two-Phase Flows at Nuclear Power Plants* (in Russian). Moscow: Nauka, 1982.
- Suzuki, A., S. Hisa, S. Nagao, and H. Ogata. 1986. Development of 52-inch last stage blade for large steam turbines, 1-7. *Paper of the ASME 86-JPGC-Pwr-41*.
- Swanekamp, R. 2002. Return of the supercritical boiler. *Power*: 32-40.
- "Tachibana-van unit 2 takes a supercritical step forward for Japan. 2001. *Modern Power Systems* 21(11): 41-47.
- Tatsuno, K. and S. Nagao. 1986. Water droplet size measurements in an experimental steam turbine using an optical fiber droplet size, 1-8. In *Paper of the ASME 84-WA/HT-57*, 1-8. New York: ASME, 1986.
- Troyanovskii, B. M. 1996. Improving the flow path of steam turbines. *Thermal Engineering* 43(1): 9-18.
- \_\_\_\_\_. 1978. *Turbines for Nuclear Power Plants*, 2d ed. (in Russian). Moscow: Energiya, 1978.
- \_\_\_\_\_. 1993. Ways of improving the efficiency of steam turbines. Part 2. *Thermal Engineering* 40(7): 528-536.
- \_\_\_\_\_, G. A. Filippov, and A. E. Bulkin. 1985. *Steam and Gas Turbines for Nuclear Power Plants* (in Russian). Moscow: Energoatomizdat, 1985.
- \_\_\_\_\_, M. S. Indurskii, L. L. Simoyu, et al. 1985. Calculation for turbine flow sections operating on wet steam. *Thermal Engineering* 32(7): 375-379.
- Weiss, A. P. 1998. Aerodynamic design of advanced LP steam turbines. *ABB Review* 1998(5):4-11.
- Zorin, V. M., and V. D. Baibakov. 2003. The optimization of the splitting pressure in the turbines for nuclear power plants. *Thermal Engineering* 50(10): 844-851.

## 3

---

---

# Design

Wet-steam turbines for nuclear power plants are currently designed and produced by only a few manufacturers worldwide. Several former independent producers of nuclear turbines, including the British manufacturer GEC, which was formed from the merger of AEI and English Electric, French manufacturers Rateau, Alsacienne de Construction Mecanique (SACM), and Campaignie Electromecanique (CEM), and the German firm MAN—all merged to form GEC Alsthom. In turn, GEC Alsthom merged with ABB Kraftwerke AG, which had been formed from the merger of German-Swiss firms Brown Boveri and Escher-Wiss and Swedish manufacturer Stal-Laval, creating the international giant ABB-ALSTOM, presently named merely ALSTOM. In another spate of conglomeration, German firm Kraftwerke Union AG (Siemens/KWU) absorbed the British company NEI Parsons and the German AEG and then merged with Westinghouse to create another huge international concern, Siemens Power Generation (Siemens PG), which includes the U.S. subsidiary Siemens Westinghouse Power Corporation (SWPC).

Among other contemporary producers of wet-steam turbines for nuclear power plants are General Electric in the United States; a trio of Japanese manufacturers—Hitachi, Mitsubishi Heavy

Industries (MHI), and Toshiba; Turboatom (also known as Kharkov Turbine Works, or KhTGZ) in Ukraine; Leningrad Metallic Works (LMZ) in Russia, and Škoda Energo (Skoda) in the Czech Republic. Combined, these companies have provided almost all of the steam turbines for every nuclear power plant in the world. In addition to the companies mentioned, Ansaldo Energia manufactured six turbines for Italian nuclear power plants with a total capacity of 3,530 MW; and Bharat Heavy Electricals Ltd. (BHEL) built a series of eight wet-steam turbines with individual capacities of about 230 MW for Indian nuclear power plants with PHWRs, under license from ALSTOM. Production of large-capacity wet-steam turbines is scheduled to commence in the near future at Donfang Steam Turbine Works and Shanghai Steam Turbine Co., Ltd. in China and at Doosan Heavy Industries & Construction Co. in South Korea.

As of January 2001, at the nuclear power plants of the IAEA's member countries, there were in service at least 440 nuclear wet-steam turbines with individual output of more than 100 MW, not counting those installed in permanently or temporarily decommissioned power units.<sup>1</sup>

Some older nuclear power units were designed to be operated with two (or more) steam turbines fed with main steam in parallel. This explains a certain discrepancy between the above figure and the total number of nuclear power units according to the IAEA data given in chapter 1. This difference (between the number of nuclear wet-steam turbines and the total number of nuclear power units) also takes into account gas-cooled and fast breeder reactors working with superheated-steam turbines. The double-turbine scheme has been widely used at nuclear power units employing former Soviet reactors VVER-440 (31 power units in operation as of 2001, each one with two turbines with a rated output of about 220 MW), the first VVER-1000 (two 500-MW turbines), and RBMK-1000 and RBMK-1500 (14 power units in operation as of 2001, with turbines of rated output of 500 and 750 MW, respectively). In addition, this double-turbine scheme has been employed at some Western European and Asian nuclear power plants with PWR-, BWR-, and PHWR-type reactors. The use of this scheme was primarily intended to decrease the number of forced shutdowns in the case of wet-steam turbine failures, and also allow for the possibility

of more efficient unloading of the units by shutting down one of the two (or more) turbines during power consumption ebbs at nights and on weekends. With regard to double-turbine units, the single capacity spectrum for the wet-steam turbines presented in Table 3-1 looks more logical. Even though the single capacities of nuclear power units are commonly given as net values, as applied to steam turbines it seems more representative to cite the gross capacity data.

**Table 3-1.** Distribution of wet-steam turbines by gross individual capacity (as of 2001)

Gross Capacity (MW)	Number of Turbines							
	U.S.	France	Japan	Russia	Germany	Korea	Others	Total
100—200	—	—	—	—	—	—	2	2
200—400	—	—	2	12	1	1	66	82
400—600	8	—	12	24	—	1	22	67
600—800	8	—	4	—	1	4	20	37
800—1,000	35	34	11	—	4	8	22	114
1,000—1,200	31	—	21	6	—	2	16	76
1,200—1,400	22	20	2	—	7	—	1	52
1,400—1,600	—	4	—	—	6	—	—	10
Total	104	58	52	42	19	16	144	440

Turbines with rated outputs between 200 and 600 MW, which amount to a significant portion of “nuclear” wet-steam turbines, including some of the double-turbine units mentioned previously, are generally referred to as being of moderate capacity. They are especially attractive for modest-sized and developing countries, as well as for relatively autonomous power systems. For industrially developed countries with highly developed power generation grids, larger power units (and turbines) are more attractive, with single capacity of about 1,000 MW or more. Due to larger capital expenditures and lower fuel costs, nuclear power generation costs depend to a greater degree on the installed capacity as compared with fossil fuel plants. Thus, an

increase in capacity from 580 MW to 1,160 MW for a coal-fired plant was determined to decrease its power generation cost by about 8%, whereas the corresponding reduction for nuclear power plants with BWRs was approximately 30%.<sup>2</sup>

Along with a trend toward increasing the single capacity of nuclear power units in the upper-end range of 1,300–1,700 MW and perhaps more in the future, many countries still have a demand for nuclear power plants with units of a moderate and relatively low single capacity.<sup>3</sup> This is due to constrained investment capital and limited power grid capacities. In recent years, many nuclear power projects featuring medium-sized reactors have begun development, and they will need wet-steam turbines of a corresponding capacity. There should be a high degree of freedom in the design of these units in order to match diverse investment capacities and customer needs. When the nuclear power plant output is relatively small, the benefits of improved thermal efficiency become somewhat less noticeable, and for this reason the emphasis is placed on decreasing civil engineering expenditures and simplifying the equipment design and operation rather than raising efficiency. As for simplifying the turbine design, this can first require reducing the number of LP flows and cylinders, and the use of less expensive material than titanium in the last stage blades (LSB). On the other hand, the use of longer titanium LSBs can result in reducing a number of the LP cylinders, and in this case, can adequately pay for itself.

## General Design Features of Wet-Steam Turbines

### Influence of single capacity and rotation speed on turbine design

As distinct from some steam turbines for fossil fuel power plants, all wet-steam turbines for nuclear power plants, up to those of the largest individual capacity, are designed single-shaft, or tandem-compound (TC). This is mainly explained by the fact that both the HP and LP sections of wet-steam turbines work with wet steam, and their

steam paths are exposed to water drop erosion and require similar approaches to coping with this problem. By contrast, many modern steam turbines of fossil fuel power plants, with the single capacity of 700 to 1,300 MW, have been designed as double-shaft, or cross-compound (CC). This is especially typical for countries with the grid frequency of 60 Hz and, correspondingly, requires the full rotation speed of 3,600 rpm, instead of 3,000 rpm for the grid frequency of 50 Hz. The CC turbine configuration is most effective if the LP cylinders are located on a separate low-speed shaft with a four-pole generator, and the HP and IP cylinders are located on a high-speed shaft with a two-pole generator. This scheme helps to cope with large volumetric steam flow amounts at the LP exhausts, not excessively increasing this number and simultaneously providing high efficiency in the HP and IP sections.<sup>4</sup>

Water drop erosion (WDE) of the rotating blades is one of the most important factors influencing the operating reliability of wet-steam turbines and thus also determining their design configuration. There exist different approaches to determining a so-called WDE criterion,  $E$ , as well as different empirical equations that were developed to estimate its value.<sup>5</sup> The simplest and most obvious equation was developed by Hitachi:

$$E = 4.3 \times (0.01u_p - 2.44)^2 y_1^{0.8} \quad (3.1)$$

where  $u_p$  is the circumferential speed of the blades (m/s), and  $y_1$  is the steam wetness in the gap between the nozzle and blade rows (%). The blade longevity is supposed to be assured if  $E < 2$ ; if the value of  $E$  ranges from 2 to 4, the blades are regarded as being exposed to moderate corrosion, and if  $E > 4$ , this condition is treated as inadmissible.

According to another approach proposed by R. Hohl of Escher-Wiss, it is assumed that the longevity of rotating blades is assured if  $E < 1.0$ , where  $E$  is calculated as follows:

$$E = \frac{y_0}{\psi} \times \frac{C_{2a}}{200v_2} \times \left( \frac{u_p}{100} \right)^4 = \frac{y_0}{\psi} \times \frac{G}{200F} \times \left( \frac{u_p}{100} \right)^4 \quad (3.2)$$

where  $y_0$  is the steam wetness at the stage inlet;  $\psi$  is the stage's moisture separation factor, varying from 0.8 to 1.0;  $v_2$  is the specific volume of the steam at the stage outlet ( $\text{m}^3/\text{kg}$ );  $c_{2a}$  is the axial component of the exit steam flow velocity ( $\text{m/s}$ );  $G$  is the steam flow amount through the stage ( $\text{kg/s}$ ); and  $F$  is the annular area of the stage blades ( $\text{m}^2$ ).

Other turbine producers and research institutions in the power industry have proposed many other expressions that are more complex and take into account additional factors, such as the blade length-to-mean diameter ratio, axial clearance between the nozzle and blade rows, portion of coarse-grain drops in the total moisture content, stage reactivity at the blade tip, outlet edge thickness of the nozzles, and the stage's enthalpy drop. The admissible value of  $E$  calculated with the use of these equations also varies. Nevertheless, according to all these approaches, the WDE hazard mainly depends on the steam wetness and circumferential speed of the rotating blades, sharply increasing with the latter. A combination of large steam output and relatively low initial steam pressure for wet-steam turbines results in enormous mass and volumetric steam flow rates, and thus requires blades with large mean diameters and lengths, which aggravates the WDE problem. Therefore, the last stages of the HP and LP sections of wet-steam turbines operate with a steam wetness of about 10–14 % (see Fig. 2–2).

Currently, the maximum rated single gross capacity for nuclear power units in service is about 1,500 MW. In particular, this refers to power units of French nuclear power plants Chooz-B and Civaux (two units each), both commissioned in the late 1990s and equipped with ALSTOM's wet-steam turbine, the *Arabelle*.<sup>6</sup> These machines became and have remained the largest steam turbines in the world. With inlet steam pressure of 7.1 MPa (1,030 psi) and back pressure of 5.5 kPa (0.8 psi), the *Arabelle* also has one of the best gross efficiency performances among wet-steam turbines in operation: 35.7%. The longitudinal section of the HP cylinder and one of three LP cylinders of this turbine are shown in Figure 3–1. It is a low-speed (1,500 rpm) tandem-compound six-exhaust turbine. All of the rotors are welded. The HP cylinder, in addition to the HP section, comprises an intermediate pressure (IP) section. The working steam, after leaving the HP section and before entering the IP section, goes through two horizontal moisture separators and reheaters (MSRs)

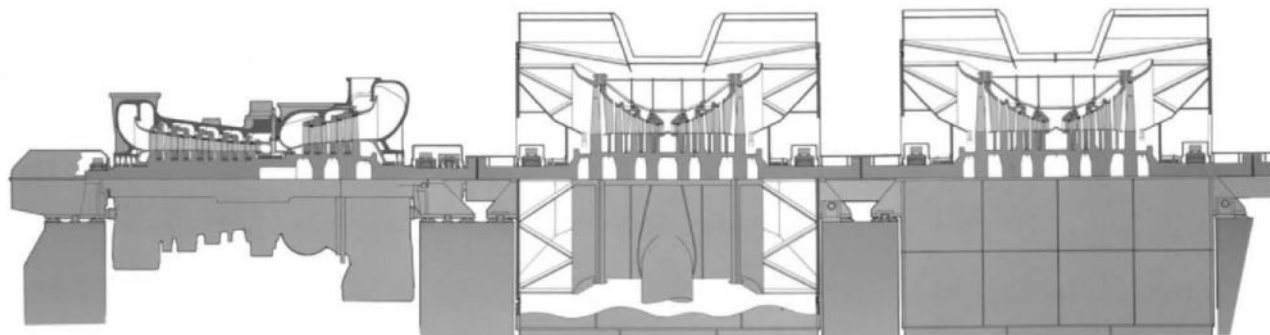


**Fig. 3-1** Longitudinal section of the HP cylinder and two of three LP cylinders of ALSTOM's 1,500-MW 1,500-rpm wet-steam turbine the *Arabelle*  
*Source:* By courtesy of ALSTOM

situated on either side of the turbine. Both the HP and IP sections are single-flow. This provides higher efficiency due to longer blading and reduced so-called secondary energy losses (at endwalls) in the blade rows. The HP and IP steam paths have opposite steam flow directions to counterbalance their static axial thrusts. The turbine has three LP cylinders, with LSBs as long as 1,450 mm (57 in) forming a total annular exhaust area of  $115.2 \text{ m}^2$  ( $1240 \text{ ft}^2$ ).

The same exhaust area value could be achieved with four exhausts using the 1,850-mm (73-inch) LSB developed by ALSTOM a little later. In this case, the turbine, with two LP cylinders, would measure about 6 m (20 ft) shorter. On the other hand, a six-exhaust turbine with the 1,850-mm LSBs would have a total annular exhaust area of about  $172 \text{ m}^2$  ( $1,850 \text{ ft}^2$ ). It would reduce the energy losses with the exit steam velocity to relatively small values, despite an enormous steam flow rate. The circumferential blade tip speed values for the mentioned 1,450-mm and 1,850-mm LSBs are 445 m/s and 534 m/s, respectively.

Later, a smaller version of the *Arabelle* was developed—the *Mirabelle*, a three-cylinder 1,000-MW turbine of the same configuration, which is 14% lighter than 1,000-MW French wet-steam turbines of the previous generation.

As opposed to the *Arabelle*, ALSTOM low-speed turbines of the same class with an individual capacity of about 1,200–1,500 MW for use with the 60-Hz grid frequency due to the greater rotation speed (1,800 rpm) and, as a result, a necessity to limit the HP stage height have been designed with a double-flow HP cylinder and three LP cylinders (Fig. 3-2). Its general outline and plan view are shown in Figure 3-3. With an LSB length of 1,194 mm (47 in) and a circumferential blade tip speed of 449 m/s (almost identical to that of the *Arabelle*), this turbine has a total annular exhaust area of only  $80.4 \text{ m}^2$  ( $865 \text{ ft}^2$ ), which provides significantly larger exhaust energy losses compared to its European 50-Hz analog. At the same time, in order to achieve even a smaller total annular area of  $74.4 \text{ m}^2$ , a full-speed 60-Hz turbine of the same capacity should comprise 12 exhausts (that is, six LP cylinders) with an LSB length of 852 mm (33.5 in), resulting in a considerably greater circumferential speed of 594 m/s. It is obvious that such a six-cylinder, caterpillar-like machine would create numerous

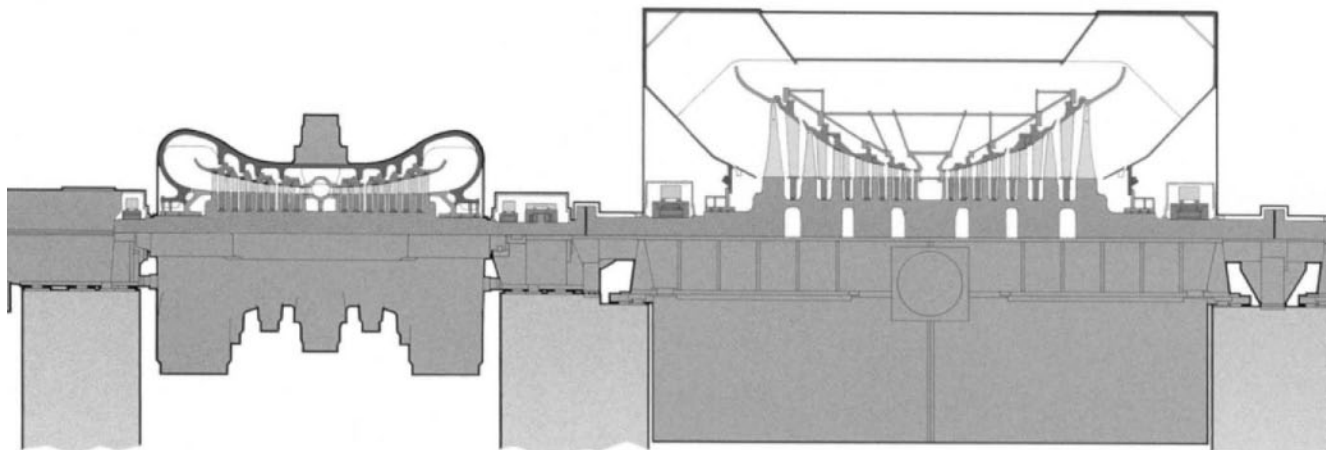


**Fig. 3-2** Longitudinal section of the HP cylinder and one of three LP cylinders  
of ALSTOM's 1,200-to-1,500-MW 1,800-rpm wet-steam turbine  
*Source:* By courtesy of ALSTOM

severe design and operation problems. International experience indicates that the maximum number of cylinders on the shaft should not exceed five.<sup>7</sup> For a smaller single capacity of about 1,000 MW and the rotation speed of 1,800 rpm, ALSTOM also produces four-cylinder turbines, with a single-flow HP cylinder and three double-exhaust LP cylinders. In particular, such turbines were delivered for several nuclear power plants of South Korea.

All of the previously mentioned ALSTOM turbines have cross-over pipes between the MSRs and LP cylinders situated beneath the turbine's horizontal split plane, allowing free access to the LP cylinders and facilitating their inspection, maintenance, and repair

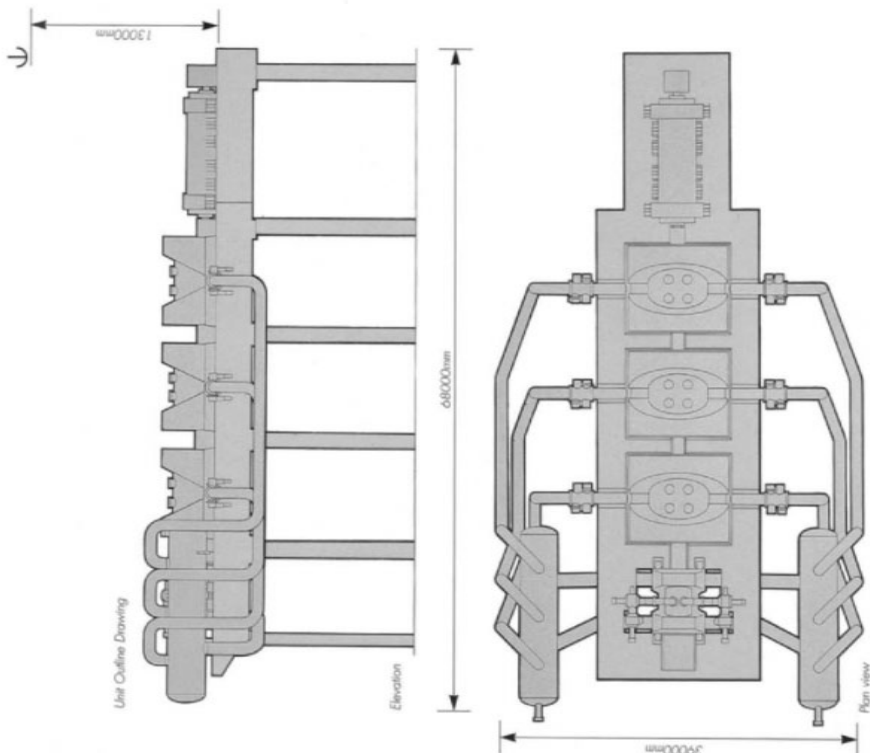


**Fig. 3-3** Outline drawing and plan view of ALSTOM's 1,200-to-1,500-MW 1,800-rpm wet-steam turbine  
Source: By courtesy of ALSTOM

(Fig. 3-3). This approach is characteristic for wet-steam turbines of different manufacturers, even though some turbine types retain more traditional top crossover pipes.

Designing wet-steam turbines begins with choosing either a high (full) or low (half) rotation speed, that is, employing either a two-pole or four-pole generator. With a two-pole generator, the turbine's rotation speed will be 3,000 or 3,600 rpm for the grid frequency of 50 Hz or 60 Hz, respectively; with a four-pole generator, it will be 1,500 or 1,800 rpm for 50 Hz or 60 Hz, respectively. For wet-steam turbines of relatively small output, this design question is traditionally answered in favor of the high-speed option.

The left-hand (small-capacity) portion of the wet-steam turbine individual-capacity spectrum is mainly filled by turbines with an individual capacity of about 200–230 MW (Table 3-1). These are commonly designed as tandem-compound, high-speed, two- or three-cylinder turbines with one or two double-flow LP cylinders. Turboatom's 3,000-rpm K-220-44 turbine with an 852-mm LSB (an annular exhaust area of  $6.25 \text{ m}^2$  per flow), as well as its Škoda analog with an 840-mm LSB (and a slightly larger annular exhaust area of  $7.1 \text{ m}^2$  per flow, due to a greater mean diameter), are both built with three cylinders and four exhausts (Figs. 3-4 and 3-5).<sup>8</sup> Both turbines were designed for a main steam pressure of 4.3 MPa (44 atm; 626 psi) and intended for operation with PWR-type reactors VVER-440. In order to counterbalance the axial thrust, Škoda's HP cylinder is double-flow, whereas the Turboatom turbine has a single-flow HP cylinder that provides somewhat smaller secondary losses (at the raw channel endwalls) due to its greater stage height. The HP rotors for both turbines are made forged with a central axial bore, and the LP rotors are of a welded type.

Unlike most other turbines for nuclear power plants, the Turboatom K-220-44 turbine was initially designed with a nozzle-group steam admission control. In later modifications, these turbines were manufactured with a throttle-type steam admission control, a smoother outline of the HP cylinder casing, and with two cylinders, including a single LP cylinder furnished with a 920-mm (36-in) LSB (Fig. 3-6).<sup>9</sup> Because of the unsteady state thermal stresses that arise in welded LP rotors during turbine start-ups, a new arrangement of the LP rotor

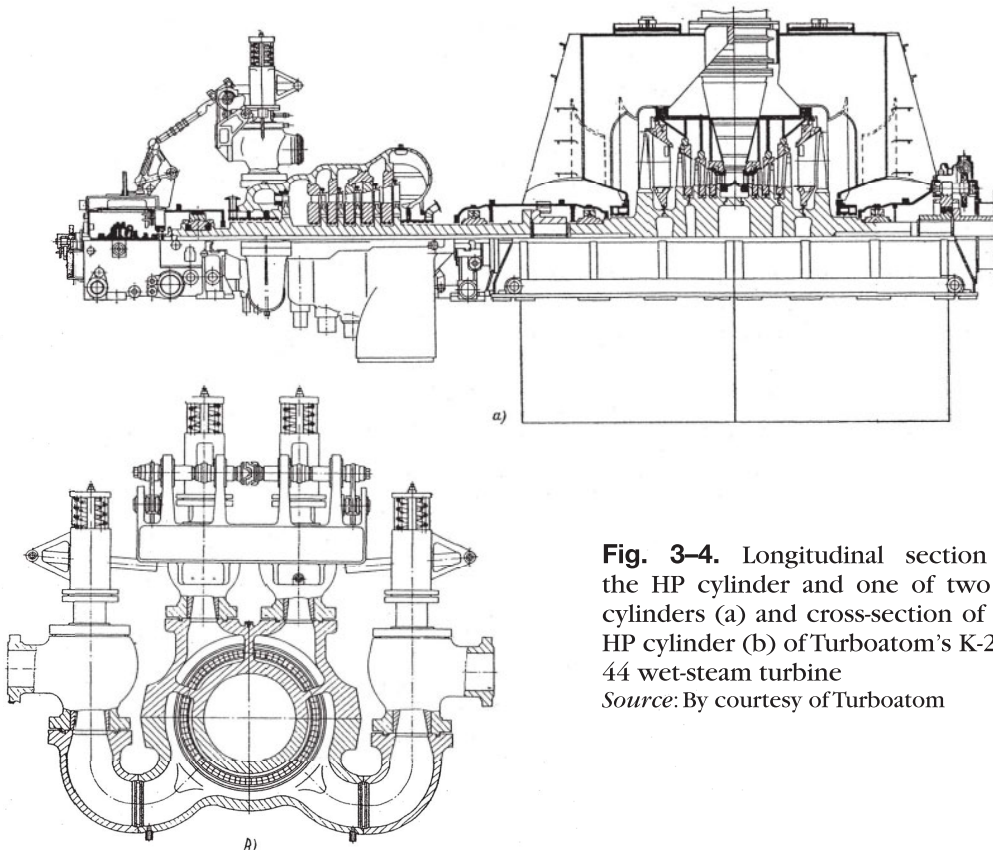


**Fig. 3-4.** Longitudinal section of the HP cylinder and one of two LP cylinders (a) and cross-section of the HP cylinder (b) of Turboatom's K-220-44 wet-steam turbine  
Source: By courtesy of Turboatom

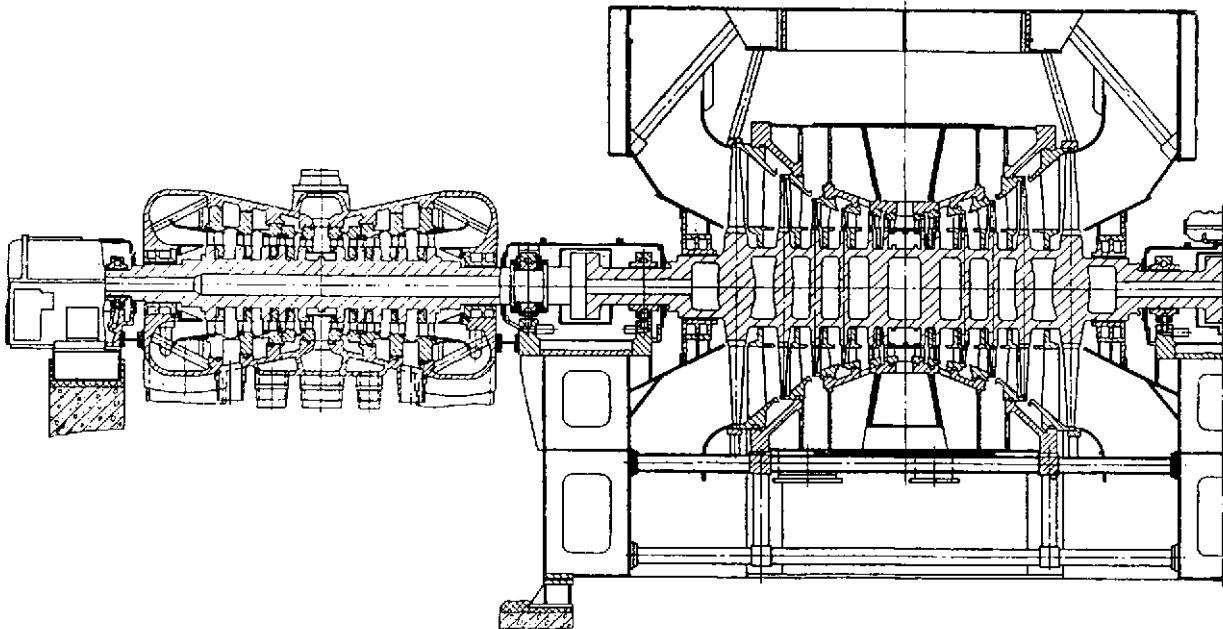


**Fig. 3-5.** Longitudinal section of the HP cylinder and one of two LP cylinders of Skoda's 220-MW 3,000-rpm wet-steam turbine  
Source: B. M. Troyanovskii<sup>10</sup>

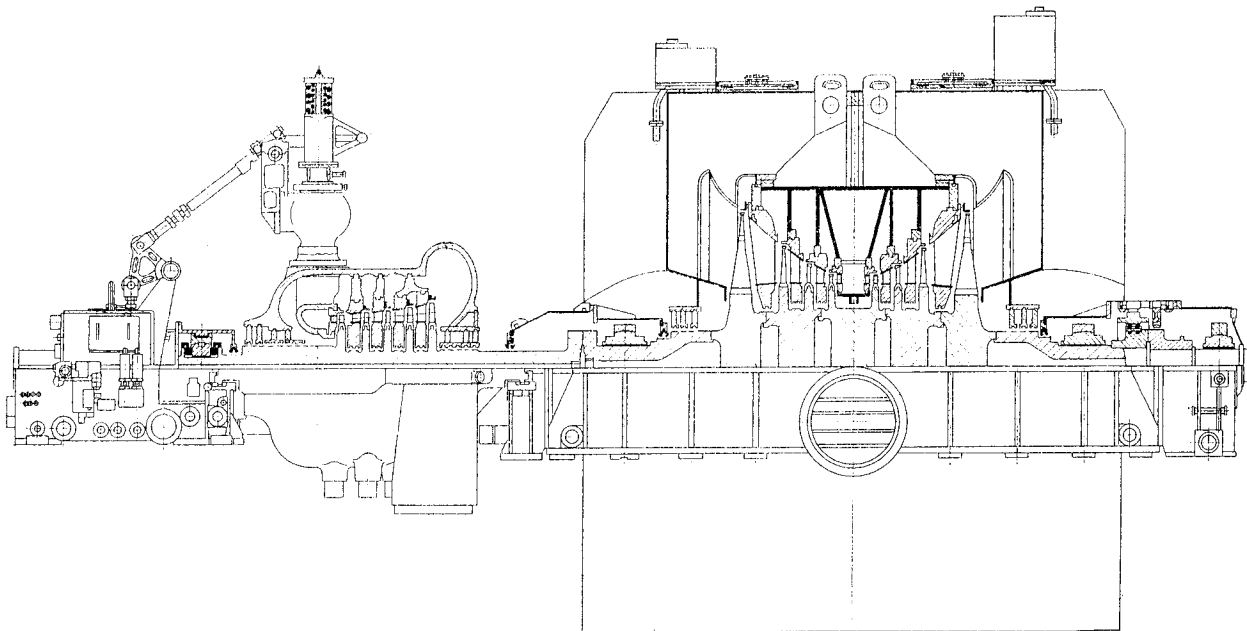


**Fig. 3-6.** Longitudinal section of Turboatom's K-220-44 wet-steam turbine,  
with one LP cylinder and a 920-mm last stage blade

*Source:* By courtesy of Turboatom

disks applied to this turbine seems more favorable due to less intense heat transfer conditions for the central disk at its periphery (see chapter 4). As a result, this disk is heated more evenly, with less radial temperature differences.

The K-220-44 turbines are equipped with an out-of-date mechanical-hydraulic governing system that tells on its appearance. The same should be said about location of the HP control valve steam chests directly on the turbine casing—it is also a legacy of previous designs; whereas, in most modern steam turbines, the valve casings are placed beside the turbine (see, for example, Figs. 3-3 and 3-29 through 3-33). Removal of the HP valve steam chests from the HP casing makes the metal temperature fields more even and decreases the start-up thermal stresses in both the HP casing and valve steam chests. Even with full-arc steam admission, the HP cylinder of K-220-44 retains the nozzle box, which to a degree substitutes for an absent inner casing (shell). As a rule, large-output wet-steam turbines are designed with double-casing HP cylinders. This provides for easier solutions to distortion and corrosion-erosion problems for both the inner and outer casings. Along with this, for example, the HP cylinder of the previously mentioned ALSTOM 1,000-MW 1,800-rpm turbine is designed single-casing, without an inner shell (Fig. 3-2).

With increasing turbine output, the rotation speed choice becomes more ambiguous up to a certain threshold value. For nuclear power units with output greater than this threshold value, the only alternative to the half-speed decision is the use of two half-capacity full-speed turbines, that is, transition to a double-turbine scheme. The main problem with low-speed turbines is that they are more complicated and labor-intensive in the manufacturing process, require heavier machining facilities and larger manufacturing areas, necessitate the use of more up-to-date technologies, and so on. High-speed turbine design is also somewhat more favorable because of the higher internal efficiency of the HP stages with longer vanes and blades—that is why the largest superheated-steam turbines in fossil fuel power plants are designed as cross-compound turbines, with a low-speed shaft for the LP cylinders and a high-speed shaft for the HP and IP cylinders.<sup>11</sup>

The threshold value achievable for full-speed (high-speed) wet-steam turbines without excessive exhaust losses, on one hand, and an absurd increase in the LP flow number, on the other hand, is not constant. It depends on the available LSB length and has tended to grow in time with technology improvements and the appearance of new, longer LSBs. For the 50-Hz grid frequency, this threshold value is currently slightly more than 1,000 MW. Attempts to forcedly increase this threshold value (for example, by using a Baumann stage<sup>12</sup>) appear to be rather ineffective. At the same time, the use of titanium LSBs with a length of 1,500 mm (59 in) would allow designing a full-speed (3,000 rpm) wet-steam turbine with an individual capacity of up to 1,250 MW with two or three LP cylinders, depending on the cooling water temperature.<sup>13</sup> On the other hand, according to estimates by Turboatom, above the single capacity of about 1,070 MW, the specific metal requirement (the turbine's total metal mass related to its output) for a half-speed turbine comes close to that of a full-speed turbine of the same output (approximately 2 kg/ kW).<sup>14</sup>

For the 60-Hz power utilities of the United States, Canada, Southwest Japan, Korea, Saudi Arabia, the Philippines, and some countries in Central and Latin America (such as Mexico, Brazil, and Peru), the threshold value of a maximum individual capacity achievable for full-speed wet-steam turbines is about 1.5 times less. By way of illustration, of interest are the data of the individual capacity and rotation speed for wet-steam turbines manufactured by Siemens for nuclear power plants of different countries presented in Table 3-2. It can be seen that the turbines built for European countries are designed as both half-speed and full-speed up to the rated output of approximately 1,000 MW; the turbines with an output of less than 600 MW are predominantly full-speed, and the turbines with the single capacity of approximately 1,200 MW and greater are always half-speed. For the 60-Hz power grids in the United States and Brazil, all of the large Siemens nuclear wet-steam turbines are half-speed. Similarly, all of the Westinghouse wet-steam turbines for nuclear power plants with the single capacity of up to 1,325 MW (57 60-Hz turbines and six 50-Hz turbines, as of 1989) were half-speed.<sup>15</sup>

**Table 3–2.** Main characteristics of Siemens large wet-steam turbines

Power Plant Name/Unit, Country	Rated Output (MW)	Rotation Speed (rpm)	Turbine Type*	Reactor Type	In Operation Since	Notes
Obrigheim, Germany	345	3,000	TC-6F30	PWR	Apr. 1969	
Stade, Germany	662	1,500	TC-4F54	PWR	Apr. 1972	
Borssele, Netherlands	477	3,000	TC-6F35	PWR	Jun. 1973	Two-stage MSR
Atucha, Argentina	340	3,000	TC-6F27	HWR	Mar. 1974	
Biblis A, Germany	1,204	1,500	TC-6F54	PWR	Feb. 1975	
Würgassen, Germany	670	1,500	TC-4F59	BWR	Nov. 1975	Two-stage MS; currently not in service
Biblis B, Germany	1,300	1,500	TC-6F54	PWR	May 1976	
Brunsbüttel, Germany	840	1,500	TC-4F54	BWR	Jul. 1976	
Neckar 1, Germany	732	3,000	TC-6F35	PWR	Dec. 1976	
Isar 1, Germany	951	1,500	TC-4F54	BWR	Dec. 1977	
Unterweser, Germany	1,300	1,500	TC-6F54	PWR	Mar. 1979	
Gösgen, Switzerland	966	3,000	TC-6F43	PWR	Nov. 1979	
Philippsburg 1, Germany	946	1,500	TC-6F54	BWR	May 1979	
Grafenrheinfeld, Germany	1,300	1,500	TC-6F54	PWR	Dec. 1981	
Krümmel, Germany	1,316	1,500	TC-6F54	BWR	Aug. 1982	
Gundremmingen B, Germany	1,311	1,500	TC-4F54	BWR	Jun. 1983	
Grohnde, Germany	1,361	1,500	TC-6F54	PWR	Mar. 1984	
Gundremmingen C, Germany	1,311	1,500	TC-4F54	BWR	Jun. 1984	
Philippsburg 2, Germany	1,362	1,500	TC-6F54	PWR	Jun. 1984	

Grand Gulf 1, United States	1,309	1,800	TC-6F44	BWR	Jul. 1985	Two-stage MSR
Brokdorf, Germany	1,365	1,500	TC-6F54	PWR	Dec. 1986	
Isar 2, Germany	1,475	1,500	TC-6F54	PWR	Apr. 1988	
Emsland, Germany	1,400	1,500	TC-4F54	PWR	Jun. 1988	
Neckar 2, Germany	1,365	1,500	TC-4F54	PWR	Jun. 1990	
Comanche Peak 1, United States	1,161	1,800	TC-4F44	PWR	Jul. 1990	
Comanche Peak 2, United States	1,161	1,800	TC-4F44	PWR	Mar. 1993	
Trillo, Spain	1,032	3,000	TC-6F43	PWR	Aug. 1988	
Angra 2, Brazil	1,325	1,800	TC-6F44	PWR	Nov. 2000	

Source: G. Jacobsen, H. Oeynhausen, and H. Termuehlen<sup>16</sup>

For comparison, Figures 3–7 and 3–8 show two Siemens turbines of almost the same class: one with an individual capacity of slightly more than 1,000 MW and a rotation speed of 3,000 rpm and the other with the single capacity of approximately 1,300 MW and a rotation speed of 1,500 rpm. In the first case, the turbine is built with an LSB length of 1,080 mm (42.5 in), and in the second case the LSB length is 1,365 mm (54 in). Main characteristics of modern LSB for high-speed and low-speed large steam turbines of various turbine producers are given below in Tables 3–3 and 3–4. The low-speed Siemens turbines, such as the one shown in Figure 3–8, with the single gross capacities of from 1,200 MW (Germany's Biblis Unit A) up to 1,475 MW (Germany's Isar Unit 2) had been the largest in the world until ALSTOM's 1500-MW *Arabelle* was developed. Heat rate field tests of the 1,300-MW turbine at Unterweser in Germany showed a gross efficiency of 35%, which later increased to 36.56% after refurbishment, including the replacement of the LP steam paths.<sup>17</sup> With an LSB of 1,675 mm (66 in), a similar half-speed (1,500 rpm) turbine, developed by Siemens for the European Pressurized Water Reactor (EPR), can provide a gross electric output of up to 1,700 MW. The turbine has two vertical MSRs, which makes it more compact. Its general 3-D view is presented in Figure 3–9. This project won a design competition for the newest European nuclear power unit built in Finland (Olkiluoto Unit 3 to be put into operation in 2009).<sup>18</sup>

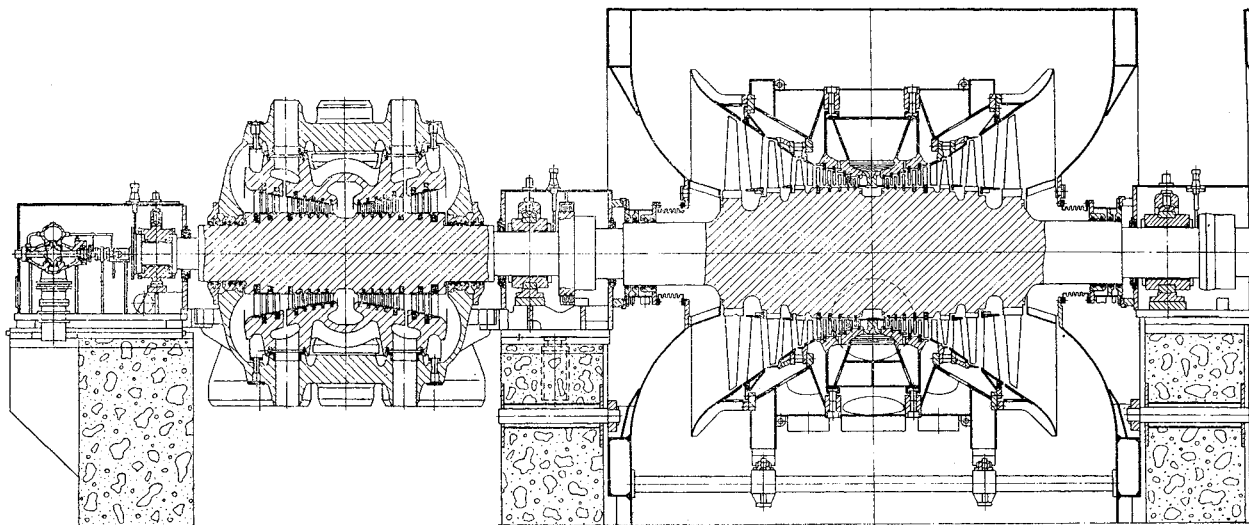


**Fig. 3–7** Longitudinal section of the HP cylinder and one of three LP cylinders of Siemens' 1,040-MW 3,000-rpm wet-steam turbine

Source: F. R. Harris<sup>19</sup>

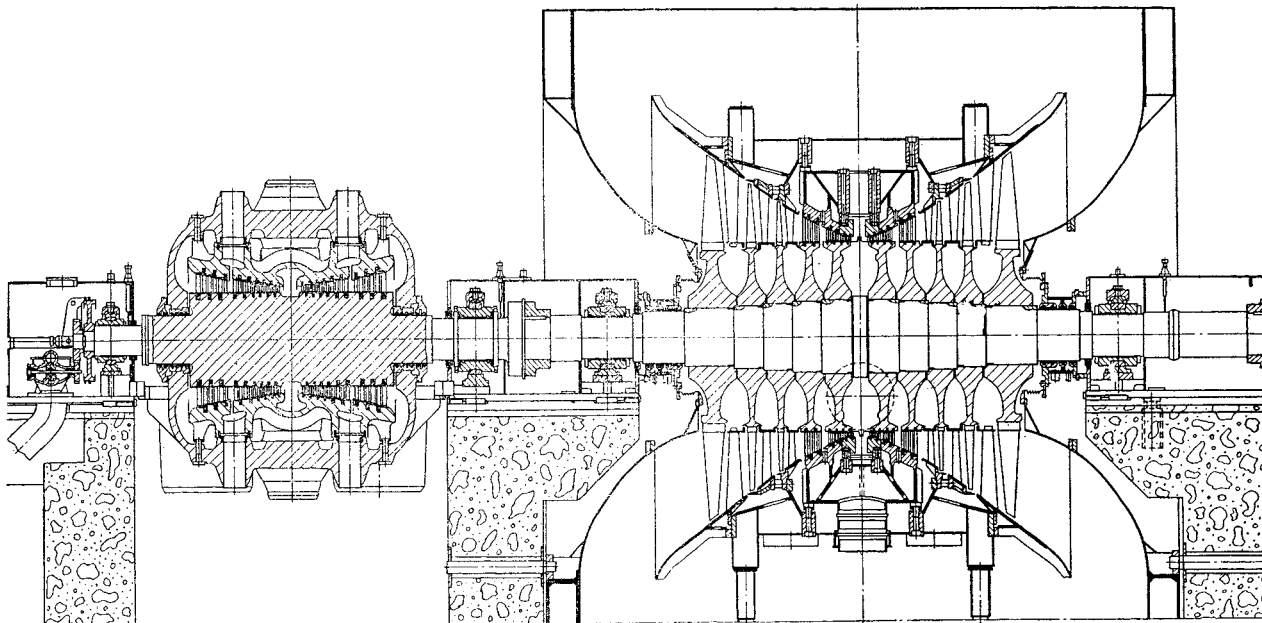


**Fig. 3–8** Longitudinal section of the HP cylinder and one of three LP cylinders of Siemens' 1,300-MW 1,500-rpm wet-steam turbine  
Source: F.J. Spalthoff, H. Haas, and F. Heinrichs<sup>20</sup>

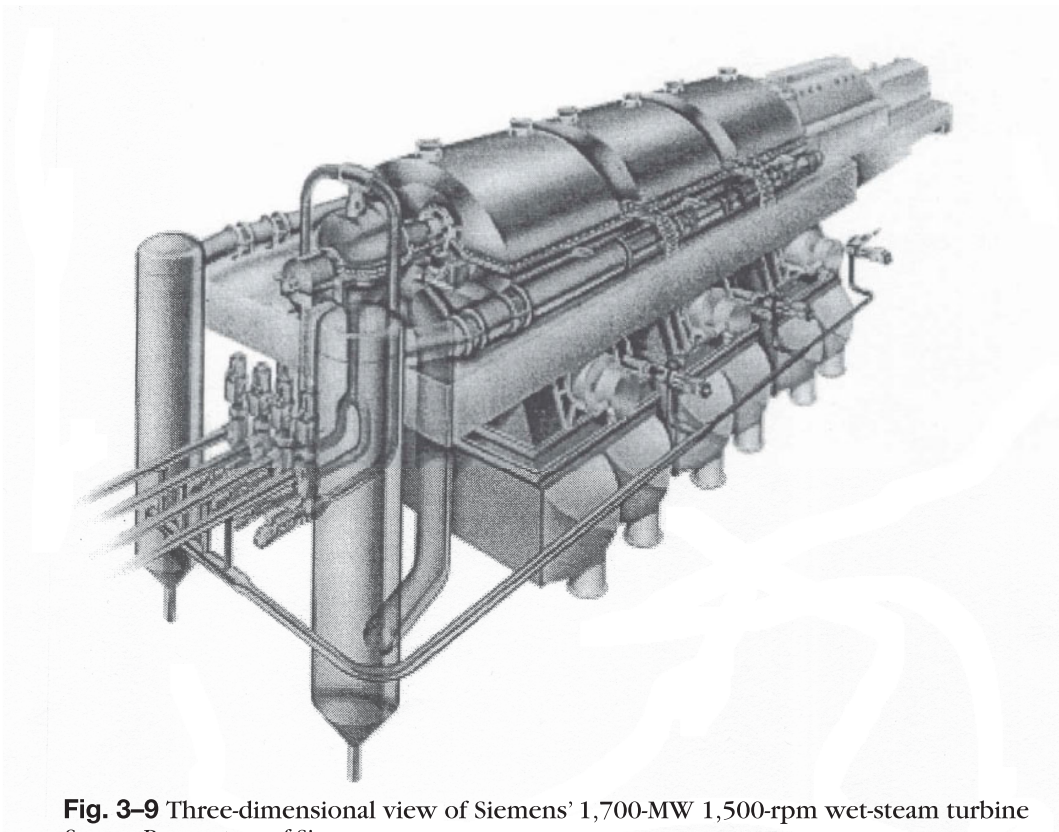


**Fig. 3-9** Three-dimensional view of Siemens' 1,700-MW 1,500-rpm wet-steam turbine  
Source: By courtesy of Siemens

Both Siemens' high-speed and low-speed turbines have one double-flow HP cylinder and three double-exhaust LP cylinders (Figs. 3-7 and 3-8). The turbines are quite similar in appearance, except for their size. The most obvious distinction is the use of LP rotors with shrunk-on wheel disks for the low-speed turbines, as compared with solid, or monoblock (that is, forged without a central axial bore), LP rotors for the high-speed turbines. In principle, the combined rotors (with shrunk-on disks) are prone to stress corrosion cracking (SCC). However, due to special design decisions, Siemens' turbines have not exhibited this problem (see chapter 4). On the other hand, manufacturing enormous solid forgings necessary for the low-speed monoblock LP rotors requires massive expenditures. The second obvious difference between the high- and low-speed Siemens' turbines is that the smaller overall sizes and lighter components of the high-speed turbines allow the use of common bearings for adjacent rotors, whereas the heavier rotors of the low-speed turbines must rest on two separate bearings for each rotor.

Along with this, the main design decisions applied by Brown Boveri (which eventually became ALSTOM) have been practically the same for their high- and low-speed wet-steam turbines, and their appearances do not significantly differ, except for the sizes. Both the HP and LP rotors are welded from forged discs. This design decision is also used by other turbine manufacturers mostly for LP rotors (see, for example, Figs. 3-1, 3-2, 3-4 through 3-6, 3-13, 3-16, 3-18, and 3-19.). The low-speed (1,800 rpm) turbine shown in Figure 3-10, with an output of 1,160 MW, was first manufactured for the Donald C. Cook nuclear power plant in the United States. The general arrangement of the turbine, with its horizontal MSR located along both sides of the LP cylinders, is typical for many large nuclear wet-steam turbines (Fig. 3-10b).

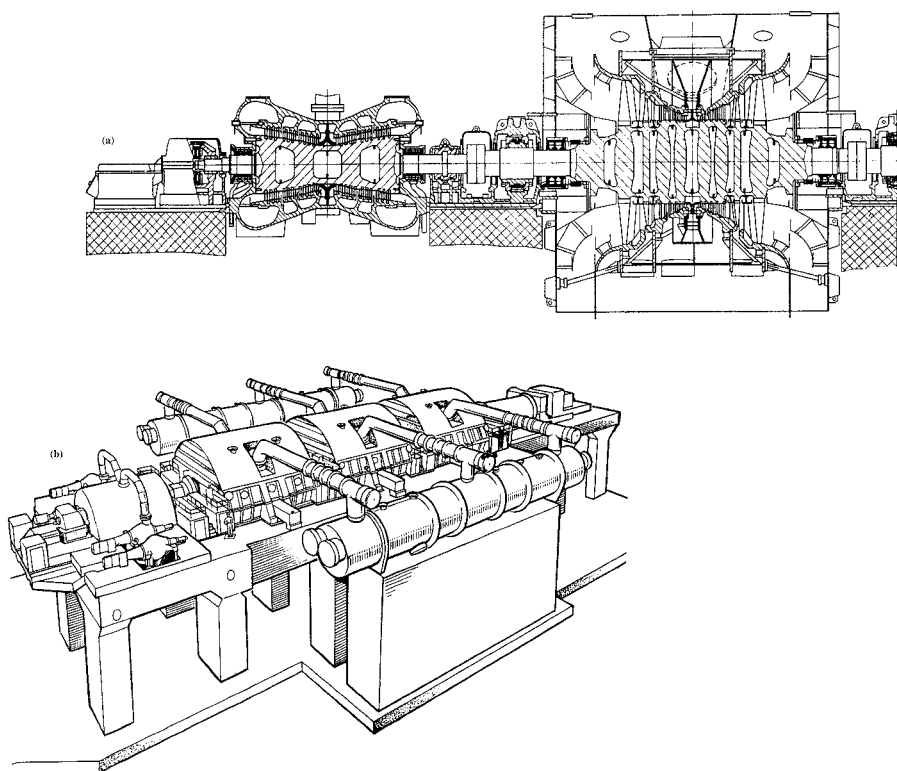


**Fig. 3-10.** Longitudinal section of the HP cylinder and one of three LP cylinders (a) and general view (b) of Brown Boveri's 1,100-to-1,300-MW 1,800-rpm wet-steam turbine  
Source: B. M. Troyanovskii<sup>21</sup>

As distinct from the ALSTOM and Siemens turbines, most Mitsubishi Heavy Industries low-speed nuclear steam turbines are designed with forged rotors in both the HP and LP cylinders. The longitudinal section of such a typical 900-MW turbine is shown in Figure 3-11. Depending on the needs of a particular customer, the turbine can be manufactured and delivered with either bored or solid rotors. The turbine features 3-D reaction blading in the HP cylinder and integrally shrouded blades in all the LP stages up to the LSB.

Another example of a turbine with solid rotors used in both the HP and LP cylinders is the GEC Alsthom 3,000-rpm wet-steam turbine shown in Figure 3-12. This turbine is used in the British double-turbine nuclear power unit Sizewell-B. As distinct from other British nuclear power plants, this unit is equipped with a PWR, in which the secondary circuit incorporates two turbine-generator units, each with 630 MW of nominal output. The turbines have a 945-mm (37-in) LSB. The average cooling water temperature at the plant is 13°C (55°F). For the standard LSB module of that time, with an optimized back pressure of 4.3 kPa ( $\approx 0.62$  psi), the most economic exhaust area would be provided by using three LP cylinders. Each rotor rests on two bearings that are mounted in pedestals supported directly on the low-tuned foundation block. The rotor system's thrust bearing is mounted in the bearing pedestal between the HP cylinder and the first LP cylinder. The MSR vessels are located horizontally at the floor level on each side of the turbine next to the LP cylinders.

Nuclear wet-steam turbines demonstrate the whole diversity of all the rotor types, however high-speed turbines, with their smaller sizes, provide more freedom in choosing the type of rotor used.<sup>22</sup> Solid rotors without a central bore, as well as welded rotors, are characterized by a relatively moderate centrifugal stress level—even the largest LP rotors with the longest LSB. Therefore, the highest stresses for these rotors occur in zones completely isolated from the steam flow. On the other hand, the forged, bored rotors feature easy access to the central part of the rotor, providing the quality control during manufacturing that is important for large forged parts. However, they have high local stresses at the bore surface, even though steam does not sweep these critical zones. Combined rotors with shrunk-on disks also produce high stresses at the bore surfaces, as well as additional stress concentration near the keyways. In addition, steam flow sweeps directly over these areas, which makes such rotors more vulnerable

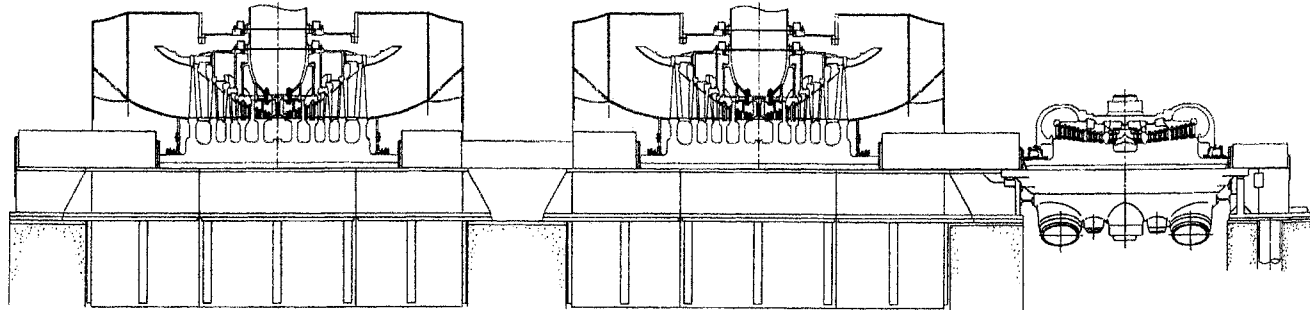


**Fig. 3-11** Longitudinal section of MHI's 900-MW-class low-speed wet-steam turbine  
*Source:* By courtesy of Mitsubishi Heavy Industries

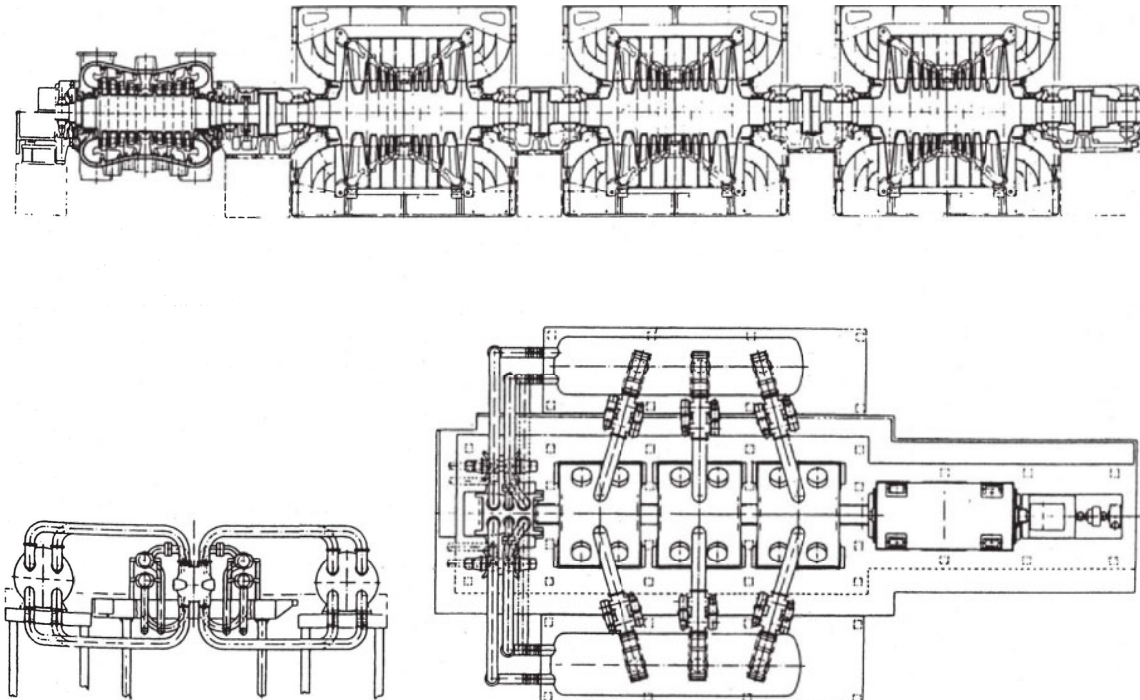


**Fig. 3–12** Longitudinal section and general view of GEC Alsthom's 630-MW 3,000-rpm wet-steam turbine for the double-turbine Sizewell-B nuclear power unit  
Source: J.A. Hesketh and J. Muscroft<sup>23</sup>

to stress corrosion cracking (SCC), especially in the Wilson (phase-transition) region. Advanced disk technology, such as that developed by Siemens, is needed to prevent these rotors from experiencing SCC. As a palliative measure, low-speed LP rotors are sometimes manufactured as solid units with shrunk-on disks added at the very last stages, which allows for a reduction in the size of the forged piece.

The gain in efficiency achievable for half-speed turbines, as compared to full-speed turbines, was demonstrated in efficiency calculations fulfilled by Turboatom as applied to their 1,000-MW 1,500-rpm turbine. It was compared with a similar high-speed (3,000 rpm) turbine designed by LMZ.<sup>24</sup> Both of these turbines were intended to work with PWR-type reactors VVER-1000s, with a main steam pressure of 5.9 MPa (853 psi). The Turboatom K-1000-60/1500-2 turbine comprises a double-flow HP cylinder and three LP cylinders, with a 1,450-mm (57-in) LSB providing an annular exhaust area of 18.9 m<sup>2</sup> (203.4 ft<sup>2</sup>) per flow (Fig. 3-13).<sup>25</sup> All of the rotors are made welded. The LMZ K-1000-60/3000 turbine includes one double-flow HP cylinder and four LP cylinders, with the LSB made of titanium alloy with a length of 1,200 mm (47 in) and an annular exhaust area of 11.3 m<sup>2</sup> (121.6 ft<sup>2</sup>) per flow (Fig. 3-14).<sup>26</sup> This turbine also differs from all of the previously mentioned ones in the location of its LP cylinders—instead of the more common “train” arrangement (with all of the LP cylinders located in series between the HP cylinder and the generator), it uses a “butterfly” scheme, with the LP cylinders symmetrically located on both sides of the HP cylinder. This provides some advantages in the arrangement of the turbine auxiliaries and somewhat decreases the pressure drops in the LP crossover pipes. As with the Siemens 1,000-MW high-speed turbine, the LP rotors are solid (Fig. 3-7). Initially, these rotors were designed to be welded, but creating them as solid units helped to ensure their greater strength.

Calculations showed that due to the larger total exhaust area (113.4 m<sup>2</sup> vs. 90.4 m<sup>2</sup>) and, as a result, smaller energy losses with the exit velocity (28.0 kJ/kg vs. 45.0 kJ/kg, at the steam back pressure of 4 kPa [0.58 psi]), the low-speed 1,000-MW Turboatom turbine could be more efficient by about  $\Delta\eta/\eta = 4\%$ .<sup>27</sup> The acceptance tests of this turbine at the Zaporozhe nuclear power plant in Ukraine proved a gross thermal efficiency of 34.8% at the MCR of 1,010 MW.<sup>28</sup>

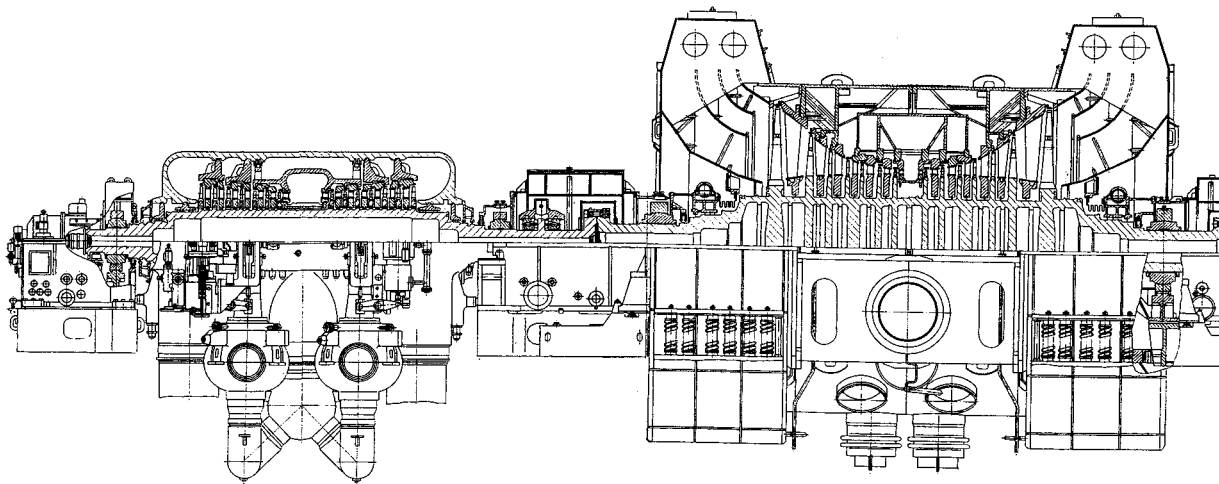


**Fig. 3-13.** Longitudinal section of the HP cylinder and one of three LP cylinders of Turboatom's 1,000-MW 1,500-rpm K-1000-60/1500-2 wet-steam turbine

*Source:* By courtesy of Turboatom

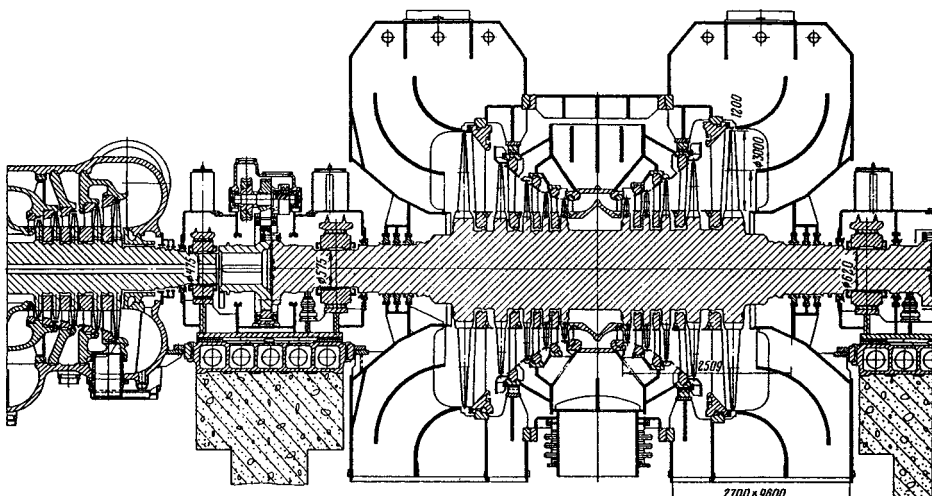


**Fig. 3-14.** Longitudinal section of a half of the HP cylinder and one of four LP cylinders of LMZ's 1,000-MW 3,000-rpm K-1000-60/3000 wet-steam turbine

Source: By courtesy of LMZ

According to Turboatom, the larger overall dimensions of the low-speed turbines provide less pressure drops in the turbine's nonbladed areas. In addition, the larger size also allows designers to increase uncontrolled steam extractions in order to cover the heating demands of adjacent dwelling and industrial regions. This idea materialized in the next version of Turboatom's low-speed 1,000-MW turbine series, the KT-1070-60/1500-3.<sup>29</sup> It was designed with increased uncontrolled bleedings for a heating output of up to 5,000 GJ/h (4.74 billion Btu/h). The schematic diagram of this turboset is shown in Figure 3-15. The turbine is designed with three cylinders, including two LP cylinders, and a 1,650-mm (65-in) LSB. The increased steam

extractions can be also used for desalination of seawater. Although sacrificing approximately 20% in electric output, a steam turbine such as the K-1070-60/1500-3 can provide approximately  $15,000 \text{ m}^3/\text{h}$  of desalinated water, that is, about  $100,000 \text{ m}^3/\text{day}$  if the bleedings are open only at night during the power consumption ebbs.<sup>30</sup>

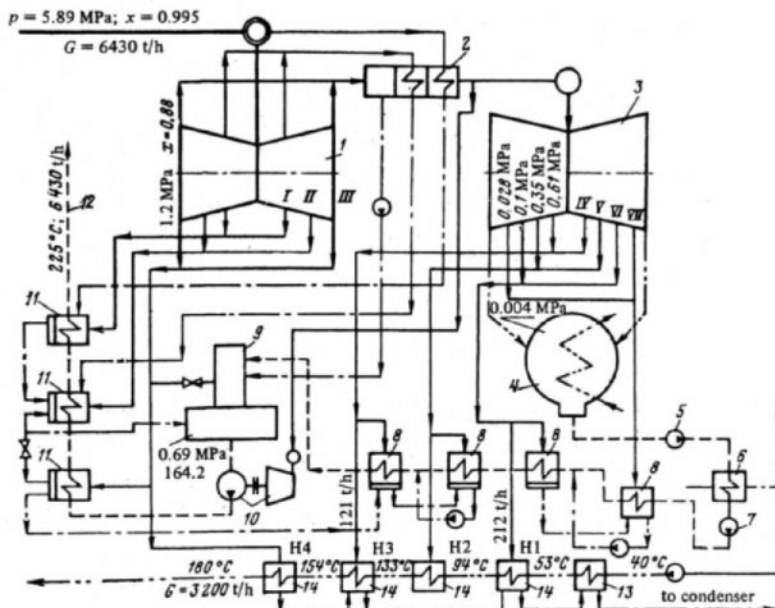


**Fig. 3-15.** Schematic diagram of Turboatom's KT-1070-60/1500-3 1,000-MW wet-steam turbine with four-stage network water heating to  $180^\circ\text{C}$  (1: HP cylinder; 2: MSR; 3: two LP cylinders; 4: condensers; 5: first-stage condensate pumps; 6: steam ejector cooler; 7: second-stage condensate pumps; 8: LP regenerative heaters; 9: deaerators; 10: turbine-driven feed water pumps; 11: HP feed water regenerative heaters; 12: to reactor's steam generators; 13: network water heaters' drain coolers; 14: network water heaters; I: first steam bleeding; II: second steam bleeding, etc.)  
Source: M.A. Virchenko, B.A. Arkad'ev, and V.Y. Ioffe<sup>31</sup>

Modern steam turbines are thoroughly calculated and designed with the use of contemporary methods of computational fluid dynamics (CFD), applied not only to the primary steam paths of the turbines, but also to the nonbladed areas, such as steam admission and extraction chambers, crossover pipes, exhaust ports (hoods), and so on. The efficiency of “nuclear” wet-steam turbines is more sensitive to energy losses in the LP cylinders, because their portion in the turbine output is much more than that of superheated-steam reheat turbines. Hence, the LP exhaust ports of nuclear turbines need special attention to maintain efficiency. At the same time, their design optimization is especially intricate, because of high exit steam velocities after the LSB, significant unevenness of this velocity field across the steam stream, and significant changes in the steam flow patterns depending on the steam flow amount (or turbine load).

The exhaust port efficiency can be characterized by a correlation between the steam pressure values at the port’s exit and entrance (that is, in the condenser,  $p_c$ , and after the LSB,  $p_2$ , respectively) and the energy losses with the exit steam velocity,  $c_2$ . This value, called the relative decompression, or hydraulic resistance factor, can be either negative or positive. It is estimated as follows:

$$\xi_{\text{dec}} = 1 - \zeta = (p_c - p_2) / (c_2^2 / 2v_2)$$

where  $v_2$  is the specific volume of steam after the LSB. If the value of  $\zeta$  is less than 1.0 (that is,  $p_c > p_2$  and  $\xi_{\text{dec}} > 0$ ), this indicates that the energy loss with the exit velocity is partially compensated in the exhaust port. But if  $\zeta > 1.0$ ,  $p_c < p_2$ , and  $\xi_{\text{dec}} < 0$ , the exhaust port energy loss is added to that with the exit velocity. For typical LP cylinder exhaust ports,  $\zeta$  is commonly close to 1.2. The use of a special diffuser configuration for the LP exhaust port makes it possible to decrease this value to approximately 1.0 or even less.<sup>32</sup>

Turboatom’s family of low-speed 1,000-MW turbines also includes the K-1000-60/1500-1 turbine, which differs from the previously mentioned models by the use of a separate double-flow IP cylinder and side condensers (Figs. 3-16 and 3-17). These two design concepts were preliminarily worked out at a model 500-MW low-speed turbine, which was subjected to detailed field tests at the pilot double-turbine Novovoronezh Unit 5 with a prototype VVER-1000 reactor (Fig. 3-18).

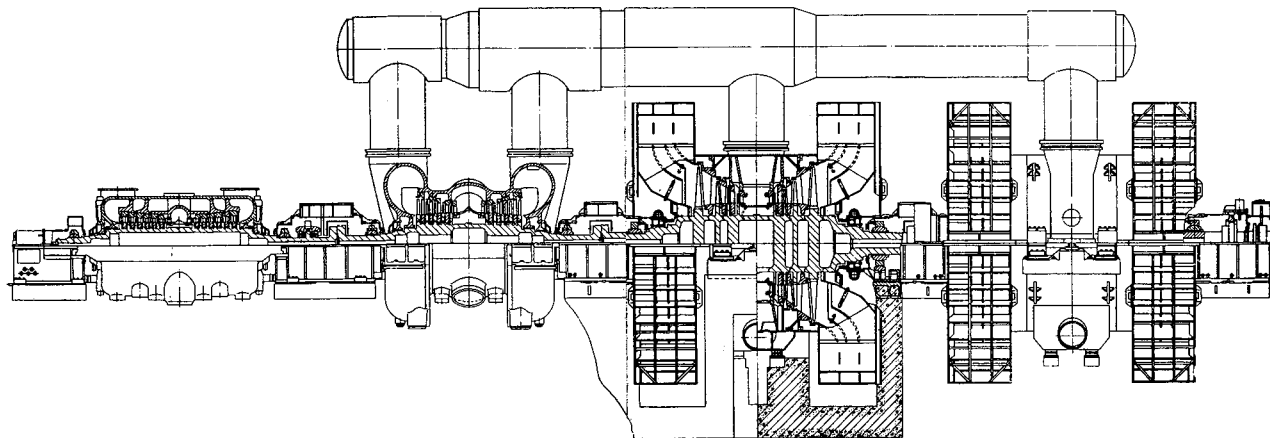


**Fig. 3-16.** Longitudinal section of Turboatom's K-1000-60/1500-1 1,000-MW 1,500-rpm wet-steam turbine with IP cylinder and side condensers  
*Source:* By courtesy of Turboatom

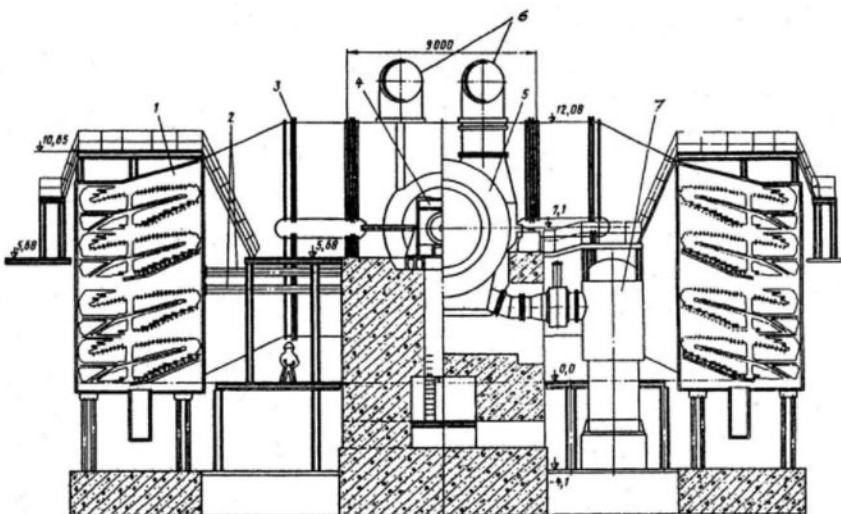


**Fig. 3-17.** Rear-view and cross-section of the LP cylinder for Turboatom's 500- and 1,000-MW 1,500-rpm wet-steam turbines with side condensers (1: condenser; 2: flexible joint; 3: sylphon; 4: bearing casing; 5: LP cylinder's casing; 6: crossover pipes; 7: LP regenerative heater)

Source: By courtesy of Turboatom

All of the rest of previously mentioned turbines, as well as the overwhelming majority of all large steam turbines used in both nuclear and fossil fuel power plants, are equipped with basement condensers. When the exhaust steam leaves the LSB, it disperses in both radial and axial directions and then turns to reach the condenser. Simultaneously, the steam streams, which have been annular in cross section up to this point, develop a rectangular cross section. This process is accompanied by the creation of vortices, rotation of the exhausted steam, and additional pressure drops (see Fig. 5-11). With side condensers, as for the considered K-500-60/1500 and K-1000-60/1500-1 turbines, a space angle of turning for the steam stream is less than that for turbines with basement condensers that results in more even steam conditions after the LSB. Bench tests for the mentioned turbines with side exhaust ports showed a value of  $\zeta$  close to 0.7.<sup>33</sup> Field heat-rate performance tests at the Novovoronezh, South Ukraine, and Kalinin nuclear power plants completely confirmed the higher efficiency ratings of turbines with side exhaust ports. In addition, the side condensers make the turbine foundation simpler and stiffer and allow for a decrease in the overall size of the turbine hall.

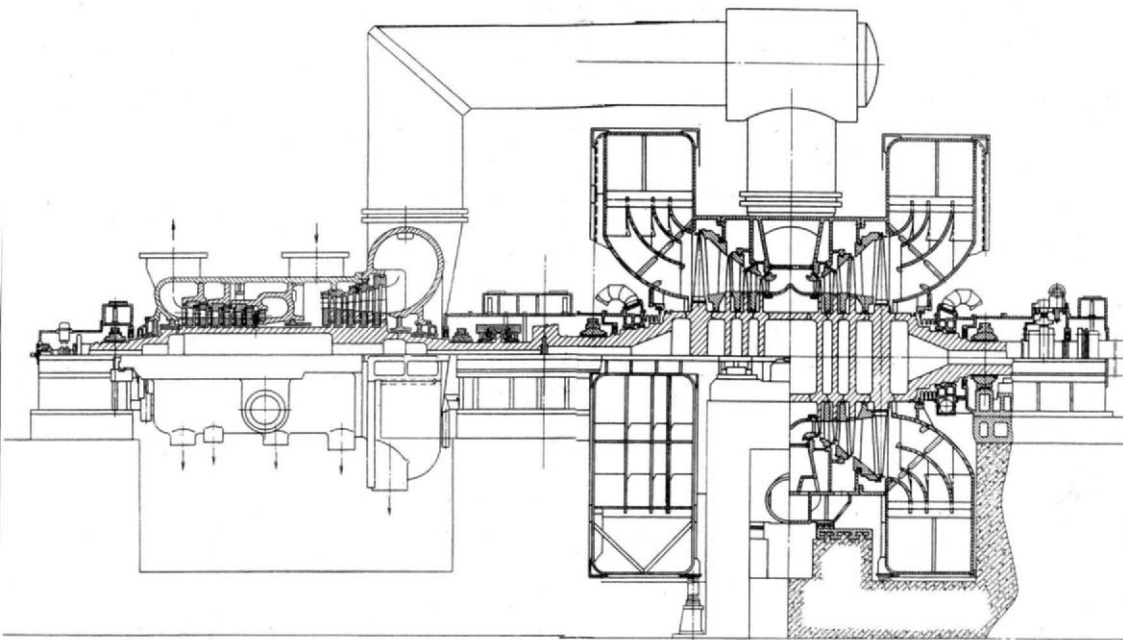


**Fig. 3-18.** Longitudinal section of Turboatom's 500-MW low-speed wet-steam turbine with IP section and side condensers

*Source:* By courtesy of Turboatom

On the other hand, the side exhaust ports are much more prone to air suction because of the greater number and length of joints under vacuum. The danger of water induction into the turbine from the side condensers is also perceptibly higher, and placement of the condensers underneath the turbine provides more freedom for seating the turbine auxiliaries in the basement area.

Some considerations show that with employing an LSB of about 1,800 mm (71 in) long, a low-speed turbine with a rotation speed of 1,500 rpm could theoretically be designed for a rated single capacity of about 2,000 MW. Such a turbine could include four cylinders (a double-flow HP cylinder and three LP cylinders) with a total annular exhaust area of approximately  $163 \text{ m}^2$  ( $1,750 \text{ ft}^2$ ). The LP rotor would have a root diameter of the LSB wheel disk of approximately 3,000 mm (118 in), and the span between the bearing axes would be approximately 10.7 m (35 ft). To transport such a monster by rail, it would have to be made combined, that is, with bolted journals (Fig. 3-19).

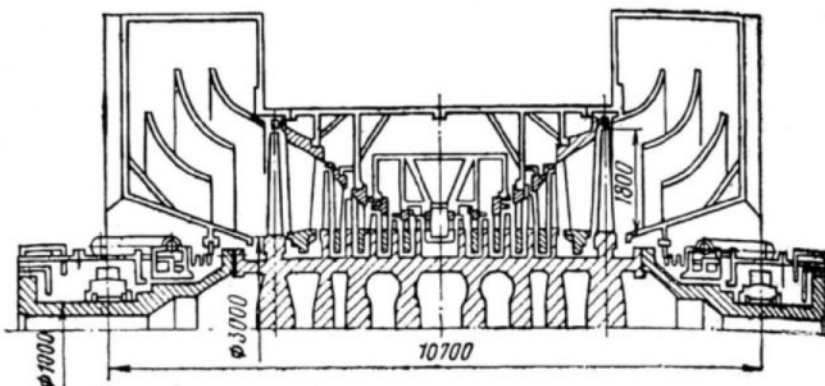


**Fig. 3-19.** Hypothetical LP cylinder with 1,800-mm last stage blades for up to 2,000-MW wet-steam turbine

Source: L. P. Safonov, V. I. Nishnevich, M. V. Bakuradze, et al.<sup>34</sup>

[Previous Page](#)

## 136 Wet-Steam Turbines for Nuclear Power Plants

### Blading, gland seals, and protection against erosion-corrosion wear

Wet-steam turbines are made with both impulse-type and reaction blading in their HP (and IP, if applicable) sections. In impulse-type turbine stages, steam expands only in the nozzle rows (fixed blades), and the rotating blades are moved only due to the change of the steam flow direction in the blade channels. In reaction-type turbine stages, the steam expansion and speed-up of the steam flow take place in both the fixed blade and rotating blade channels approximately to an equal degree. The ratio between the available energy (enthalpy drop) for the blade row and the total available energy of the stage is termed the stage reactivity or reaction degree,  $\rho$ . For a purely impulse-type stage,  $\rho = 0$ , and for a characteristic reaction-type stage,  $\rho = 0.5$ . The optimal velocity ratio (the ratio between the circumferential rotation speed and the fictitious steam velocity corresponding to the stage's available energy) for impulse-type stages is equal to approximately 0.47. For reaction stages ( $\rho = 0.5$ ), it is  $\sqrt{2}$  times more, and hence (because the available energy is in proportion to the velocity ratio squared) the optimal enthalpy drop per stage is double less than that for an impulse stage of the same diameter.

Since the steam flow velocity at the nozzle exit usually has a remarkable circular constituent that arouses the centrifugal force influencing the steam flow, in the gap between the nozzle and blade rows there appears an uneven radial pressure distribution counter-balancing this centrifugal force, and the steam pressure,  $p_1$ , increases along the stage height—from the root section to the tip section. As a result, if the stage is not specially profiled, the stage reaction degree,  $\rho$ , also increases with the radius. The greater the relative blade length  $l/d$  (the blade length related to the mean blade diameter), the more remarkable is this change. The simplest external manifestation of impulse stages is accommodating the rotating blades in the wheel disks. On the contrary, for reaction stages, the rotating blades are mounted directly at the shaft surface because of essential steam pressure difference upstream and downstream from the blade row. With a wheel disk, this would have created a large thrust (axial) force at the shaft and caused large bend stress in the disk. In addition, reaction turbines have more stages as compared with impulse-type turbines, all other things being equal. Manufacturers traditionally designed their turbines with blading of one or another type. Among the consistent promoters

of impulse-type turbines have been GE, Hitachi, LMZ, Škoda, Toshiba, Turbotom, as well as AEI, Alsthom, English Electric, MAN, and Rateau, presently known as ALSTOM. Examples of various impulse-type wet-steam turbines are shown in Figures 3-1, 3-2, 3-4 through 3-6, 3-12 through 3-14, 3-16, 3-18, and 3-20. The last one presents Toshiba's impulse-type wet-steam turbine designed in close collaboration with GE, and this turbine, as well as similar ones of Hitachi, greatly resembles wet-steam turbines for nuclear power plants produced by GE. Reaction-type turbines have been preferred by Brown Boveri (ABB), Mitsubishi Heavy Industries, NEI Parsons, Siemens, and Westinghouse. Typical reaction-type wet-steam turbines are presented in Figures 3-7, 3-8, 3-10, and 3-11. The LP steam path with reaction-type first stages of a typical Westinghouse wet-steam turbine (such as the two 560-MW turbines of Prairie Island or the two 523-MW turbines of Point Beach nuclear power plants) is shown in Figure 3-21. The subsequent LP stages, with their long blades and considerable change in the steam flow characteristics along the stage height, look practically identical in both impulse- and reaction-type turbines. They all have a high reaction degree at the blade tip and low (sometimes even negative) reactivity at the root.

Both impulse- and reaction-type turbines have their inherent strengths and weaknesses. Reaction-type blading has a somewhat better internal efficiency, due to lower mean velocities and a more convergent character of its steam flow. On the other hand, reaction-type stages commonly have somewhat greater steam leakages through the stage seals. In addition, the optimal available energy drop for a reaction-type stage is less than that for an impulse-type stage of the same dimensions, thus resulting in a larger number of stages compared with impulse-type turbines of the same steam conditions and output. Reaction-type turbines are also characterized by a greater axial thrust, which requires special design countermeasures.

However, for modern steam turbines, differences in turbine cost and efficiency depend less on the blading type than on other factors. With today's highly three-dimensional steam path designs, employing either purely impulse- or purely reaction-type blading has ultimately lost initial benefits. Siemens was the first turbine manufacturer to abandon the old paradigm and begin individually setting the reaction of each stage, varying the reaction degree in a wide range from 10% to 60%.<sup>35</sup> On the other hand, GE devised their

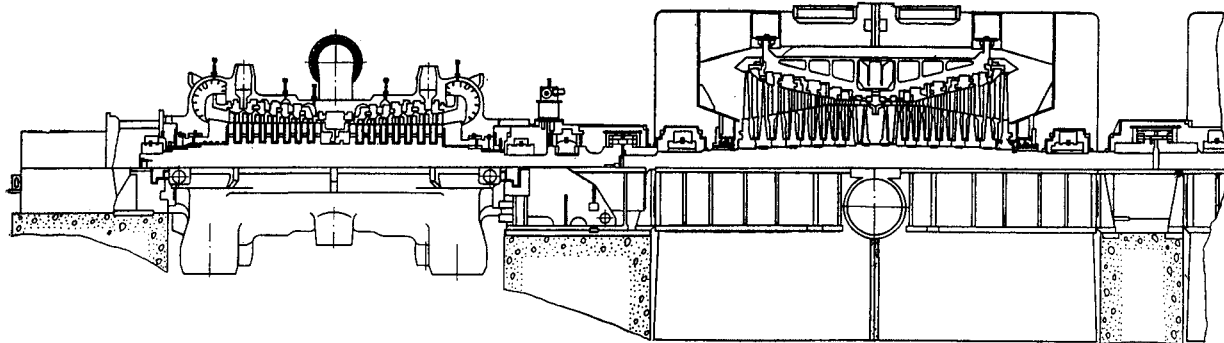


**Fig. 3–20.** Longitudinal section of the HP cylinder and one of the LP cylinders of Toshiba's 800-MW-class low-speed wet-steam turbine

*Source:* By courtesy of Toshiba

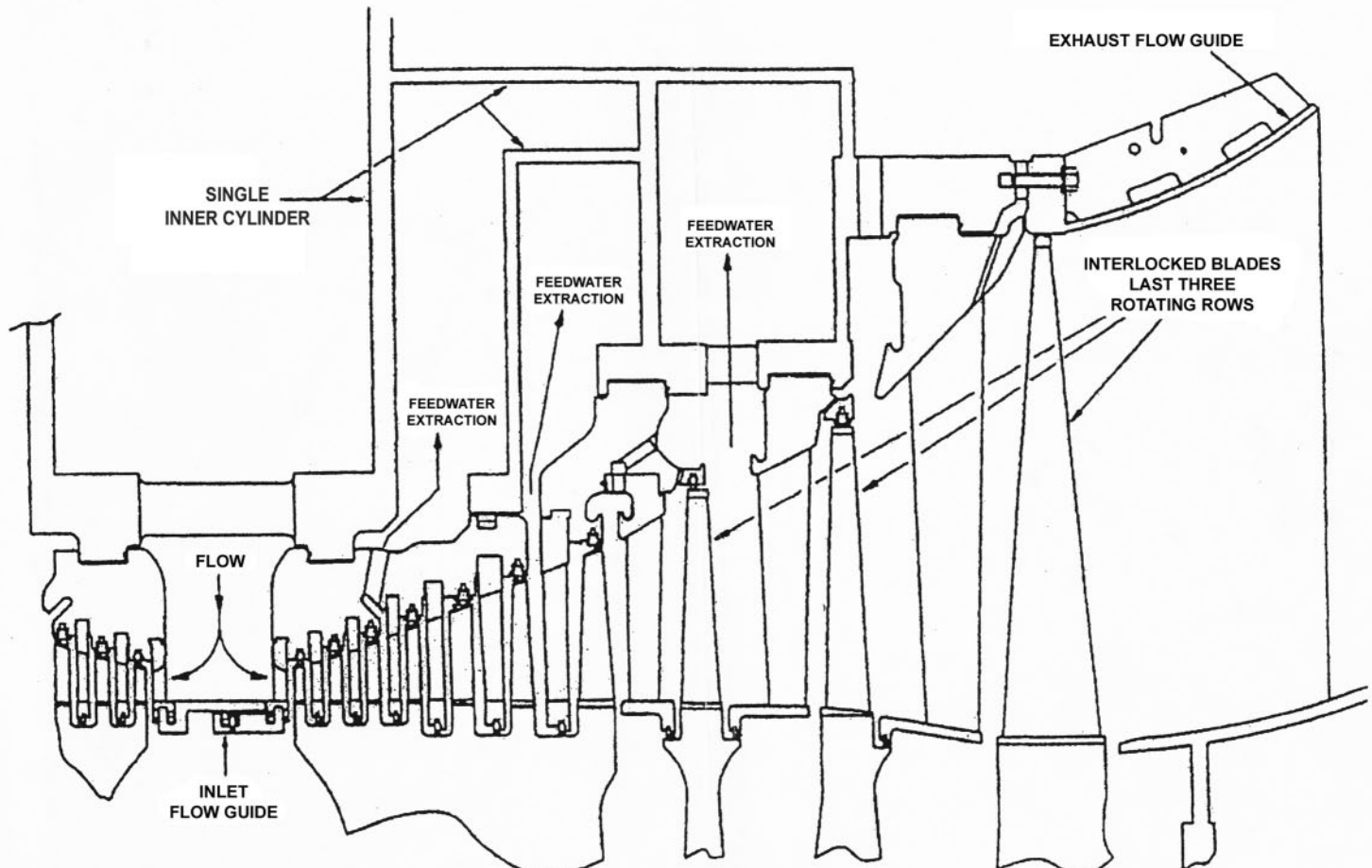


**Fig. 3–21.** LP steam path configuration for a typical Westinghouse wet-steam turbine

Source: E. P. Cramer, J. A. Moreci, C. W. Camp, et al.<sup>38</sup>

Dense Pack turbine design concept, with its increased number of stages.<sup>37</sup> The Dense Pack turbines have a higher reaction degree compared to a classic impulse-type concept. These ideas seem especially relevant for wet-steam turbines, with their taller stages. For 3-D steam path designs incorporating curved and bowed vanes and buckets, the reaction can also considerably vary along the stage height, even for relatively short HP stages.

As a rule, both impulse- and reaction-type stages of modern wet-steam turbines are designed with shrouded rotating blades (except LSBs in some cases), and with highly developed overshroud and undershroud seals (for reaction-type stages) or diaphragm seals (for impulse-type stages) to minimize the parasitic steam leakages besides the primary steam path (Figs. 3-22 and 3-23). Advanced seals allow turbine designers to reduce these leakages by as much as 50% without limiting the relative thermal expansion of the rotors.

For impulse-type stages, it is also important to arrange a proper steam flow through the clearance between the disk and diaphragm near the inlet blade root to minimize the energy losses (Fig. 3-24). Any suction of steam from the preceding diaphragm seal into a turbine blade row decreases the stage efficiency, because this steam does not possess enough energy to be of any use and also disturbs and retards the major steam streamline. At the same time, some steam leakage from the blade root zone even decreases the blade energy losses, ejecting the bottom steam layers with the end vortices from the nozzle row. For this reason, pressure-balance holes in the disks are very advisable for withdrawing the leaking steam from the blade root, even if these holes are not necessary to balance the axial thrust (for example, in double-flow rotors).

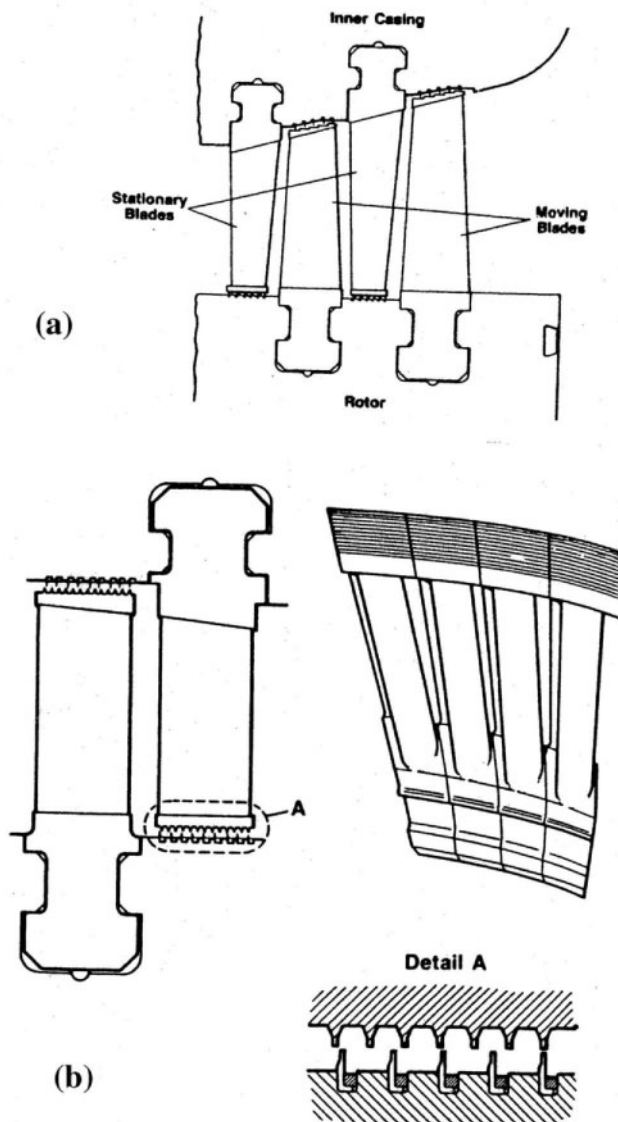


**Fig. 3-22.** Typical HP steam path stages (a) and double-strip stage seals of first LP stages (b) for Siemens' wet-steam turbines

Source: K. D. Weschenfelder, H. Oeynhausen, D. Bergmann, P. Hosbein, and H. Termuehlen<sup>38</sup>

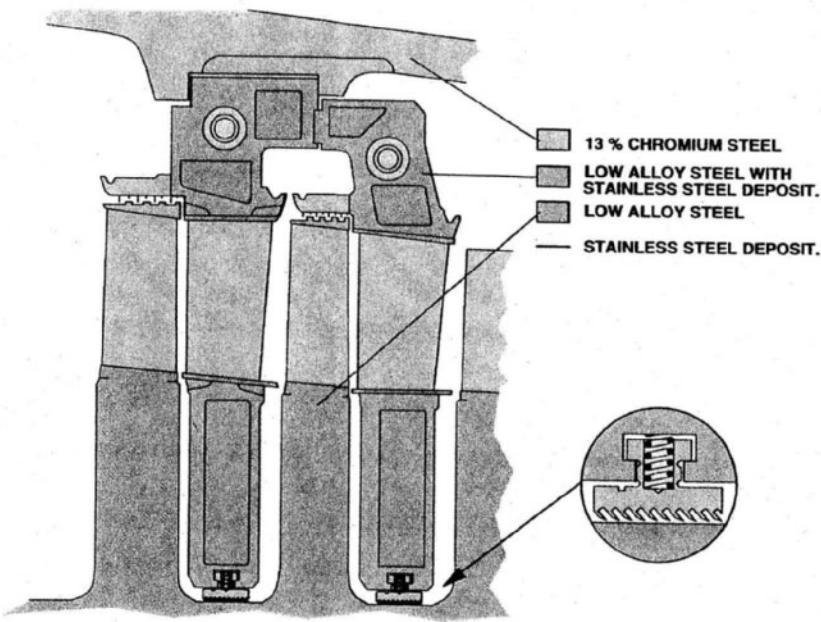


**Fig. 3-23.** Typical HP stages for ALSTOM's 1,500-MW wet-steam turbine  
Source: J. C. Franc and D. Gilchrist<sup>39</sup>

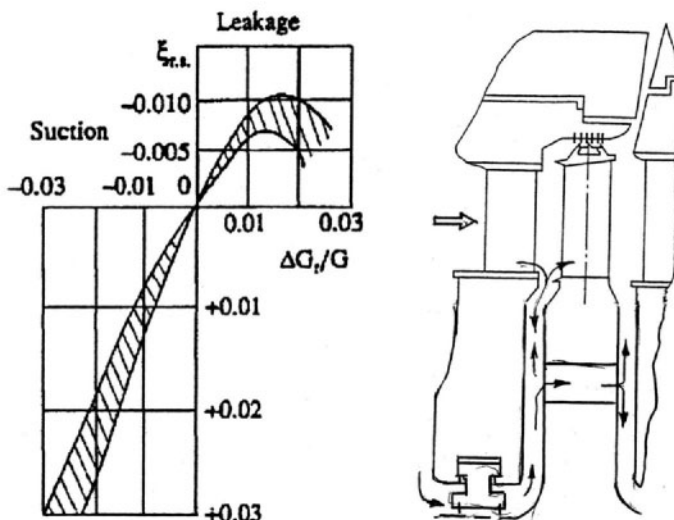


**Fig. 3-24.** Influence of steam leakage (or suction) in the blade root zone of an impulse-type stage on its efficiency  
Source: Data from A. V. Shcheglyaev<sup>40</sup>

The end gland seal designs of wet-steam turbines were well worked up at superheated-steam turbines and now provide few possibilities for further decreases in steam losses. As a result, they do not differ much from those of fossil fuel power plant turbines with moderate steam parameters. However, special attention needs to be paid to the single-circuit power units (with BWR or RBMK-type reactors) whose turbines work with radioactive steam. The end gland seals of the turbine itself (as well as those of the HP valve stems) play an important role in preventing the steam from leaking into the turbine hall. For this purpose, the last chambers of the end gland seals are kept under rarefaction, and clean steam from an outside source or special evaporator is piped into the next-to-last chambers (Fig. 3-25).

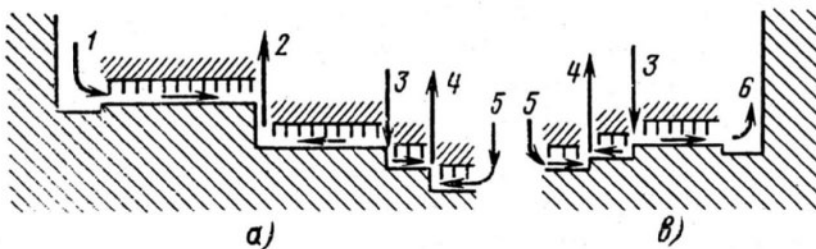


**Fig. 3-25.** Scheme of end gland seals for double-flow HP (a) and LP (b) cylinders for wet-steam turbines operating with radioactive steam (1: steam from the HP exhaust port; 2: steam to an LP regenerative heater; 3: "clean" steam from an outside source; 4: connection to a gland seal ejector; 5: ambient turbine room air; 6: steam to the LP exhaust port)

The gland seals are prone to erosion-corrosion wear (ECW) by wet-steam flow. This should be taken into account in the turbine design, especially considering the turbine's long-term operation performances. For non-alloy (carbon) steels, the ECW rate can be estimated with the use of an empirical approach developed by Siemens experts, based on long operational experiences from early wet-steam turbines:<sup>41</sup>

$$s = k_t \times K_f \times c \times \sqrt{y}$$

where,  $s$  is the expected rate of maximal local erosion-corrosion wear ( $\text{mm}/10^4 \text{ h}$ );  $c$  is the steam flow velocity ( $\text{m/s}$ );  $y$  is the steam wetness (%); the dimensionless factor  $k_t$  reflects the temperature influence,

and the flow configuration factor,  $K_f$ , for the end and diaphragm seals is taken equal to 0.08. Values of the temperature factor,  $k_t$ , significantly vary in the range from 40 to 260°C—Figure 3-26a. The most severe ECW damage takes place at about 180°C. The ECW rate falls off at lower temperatures because of a slower rate of chemical reactions and at higher temperatures due to formation of a protective layer of magnetite on the surface of metal.

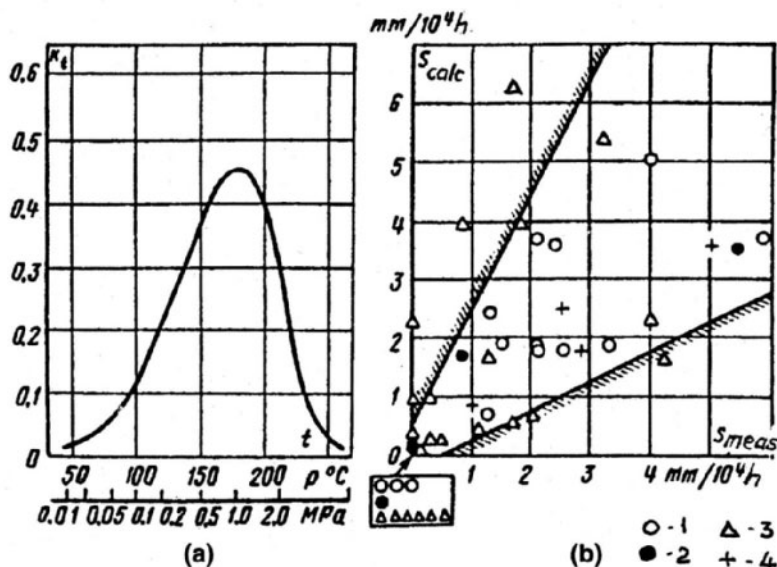


**Fig. 3-26.** Influence of temperature on ECW rate for carbon steels (a) and comparison of expected and measured ECW rate (b) (1: for horizontal joints; 2: for diaphragm visors, overshroud seals, and water traps; 3: for elbows, joints, and pipe junctions; 4: for stagnation areas, such as across steam path pipes)  
Source: Data from W. Engelke<sup>42</sup>

The same approach is also employed for estimating the ECW rate of other wet-steam turbine stator elements suffering from miscellaneous erosion-corrosion processes combined with water drop erosion. Depending on the steam flow pattern, the flow configuration factor,  $K_f$ , varies from 0.04 (for steam flowing in straight pipes) to 1.0 (for objects placed directly against a wet-steam flow, or for steam line T-joints). For example, for peripheral diaphragm visors and water traps,  $K_f = 0.3$ , assuming a typical steam flow velocity,  $c$ , equal

to the tip circumferential blade speed and for nontight flange joints,  $K_f = 0.08$ , with the steam flow velocity calculated from the pressure drop. This approach gives rather qualitative estimates. It is clear from Siemens' data presented in Figure 3-26b, where the expected, calculated ECW rates are plotted against their actual measured values for several wet-steam turbines.

Experimental and calculated data show that for stator elements fabricated from carbon steels the ECW rate can reach as much as 4–5 mm/yr ( $\approx 200$  mil/year). The most characteristic places for ECW in the HP cylinder of the Turboatom K-220-44 turbine are pointed out in Figure 3-27. The maximum ECW occurs with a steam wetness of over 5% and a temperature range of 160–200°C, which completely corresponds with the Siemens data, as well as the zones of most intense ECW outlined in the Mollier diagram in Figure 2-3.

Along with ECW, crevice erosion is prevalent in the flange joints of casings, rings, and diaphragms, and its rate often exceeds the mean rate expected based on local steam conditions. For these elements, it is especially important to prevent a through steam leakage across their joints that bears a positive feedback; the greater the leakage, the more abrasion there is due to wear. Leakage through the HP cylinder's outer casing flanges is especially unacceptable for turbines working with radioactive steam. To enhance the tightness of the flange joints in their K-220-44 turbines, Turboatom had to increase the tightening force for the bolts in the rigid belt zone and bolt the diaphragm halves together.<sup>43</sup> Some other wet-steam turbine producers also had to increase the number of bolts in the flange joints of HP cylinder casings.

Intense ECW could be prevented by using high-alloy chromium steels for endangered elements or by plating the exposed areas with similar materials. Erosion-corrosion wear of elements composed of 2.5% chromium steel drops to approximately one quarter of that expected with carbon steel, and elements made from 12–13% chromium steel suffer almost no ECW at all. Comparative calculations for the LMZ K-1000-60/3000 turbine showed that it is finally more profitable to fabricate the HP cylinder casings upon the whole from stainless steel (Fig. 3-14).<sup>44</sup> The HP cylinder casings of some ALSTOM's 1,000-MW and 1,350-MW turbines are made from 13% Cr steel, with

stainless steel piping. Along with this, many turbine manufacturers prefer to protect the endangered elements with special shields or stainless steel deposits (Figs. 3-23 and 3-28). In addition, the surfaces of flange joints are built up by welding or spraying with highly resistant alloys.

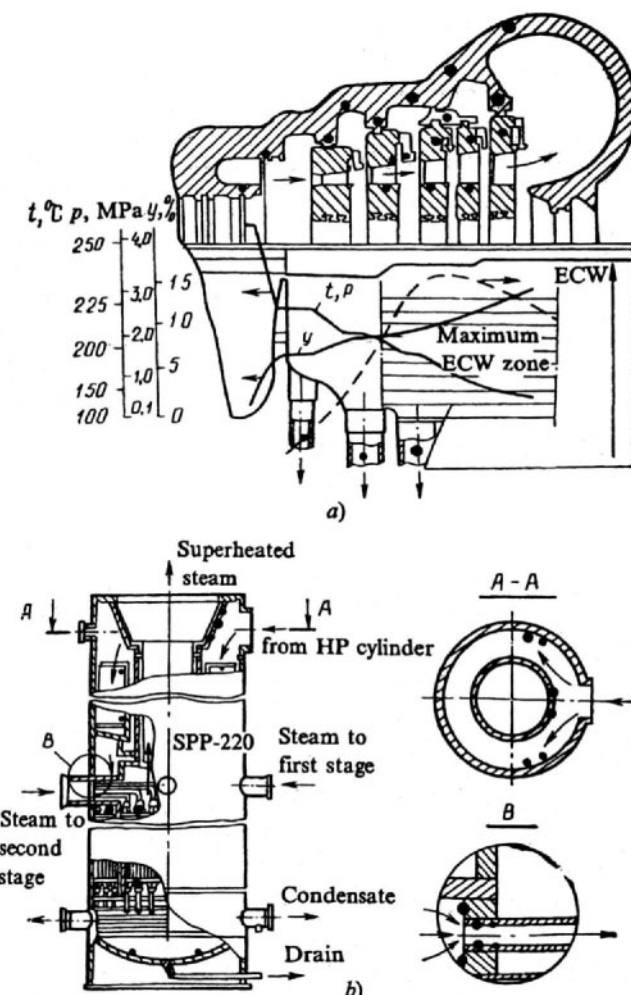


**Fig. 3-27.** Typical ECW locations in the HP cylinder (a) and MSR (b) of Turboatom's K-220-44 turbine (the black dots denote areas of the most intense ECW, with their sizes corresponding to the relative ECW rate)  
Source: O.A. Povarov, G.V.Tomarov, and V.N. Zharov<sup>45</sup>

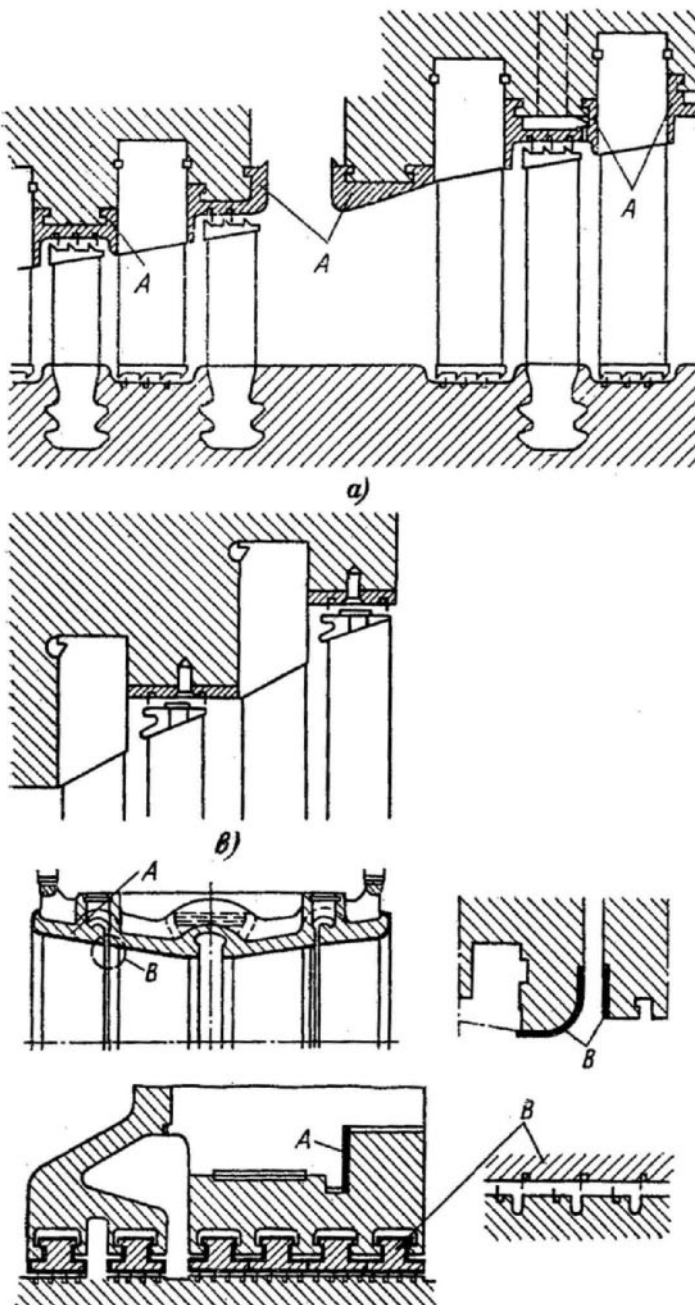


**Fig. 3-28.** Areas of corrosion-erosion protection in the turbine steam path and gland seals of ABB's (a) and Siemens' (b) wet-steam turbines

[Previous Page](#)

## 148 Wet-Steam Turbines for Nuclear Power Plants

### Steam admission elements

Huge steam flow amounts for large wet-steam turbines require special attention to their steam admission elements. With raising the turbine output, the size of the turbine valves and the energy amounts dissipated in them also increase. Simultaneously, it becomes more difficult to provide their tightness. Increased valve size results in lower natural frequencies of the moving elements (the valve itself and the valve stem). This also increases a risk of high-amplitude vibrations of the valves. There is a rule of thumb that calls for limiting the steam velocity in HP valves and their inlet pipes to 75 m/s ( $\approx 250$  ft/s). This standard has stood the test of time, but designers of large wet-steam turbines are often forced to ignore it.

To reduce pressure drops, some turbine manufacturers integrate the HP stop and control valves into a combined unit using sometimes even a common saddle. An example of such a combined valve unit developed by Brown Boveri is shown in Figure 3-29a. It resembles the HP valve unit developed by the same company for the supercritical 1,300-MW turbines manufactured for U.S. fossil fuel power plants.<sup>46</sup> In particular, the valve unit shown in Figure 3-29a is applied to the 1,160-MW wet-steam turbine installed at the Donald C. Cook nuclear power plant; the turbine is furnished with four such units (Fig. 3-10b). A more traditional design of the stop and control valves integrated in a unit with the common saddle is presented in Figure 3-30a, as developed for Turboatom's 1,000-MW-class low-speed wet-steam turbines. Another design, this one used in the HP steam admission unit (one of four) in LMZ's 1,000-MW wet-steam turbine, is presented in Figure 3-31. In this case, a traditional stop valve is replaced by a turn-gate, a kind of butterfly valve.

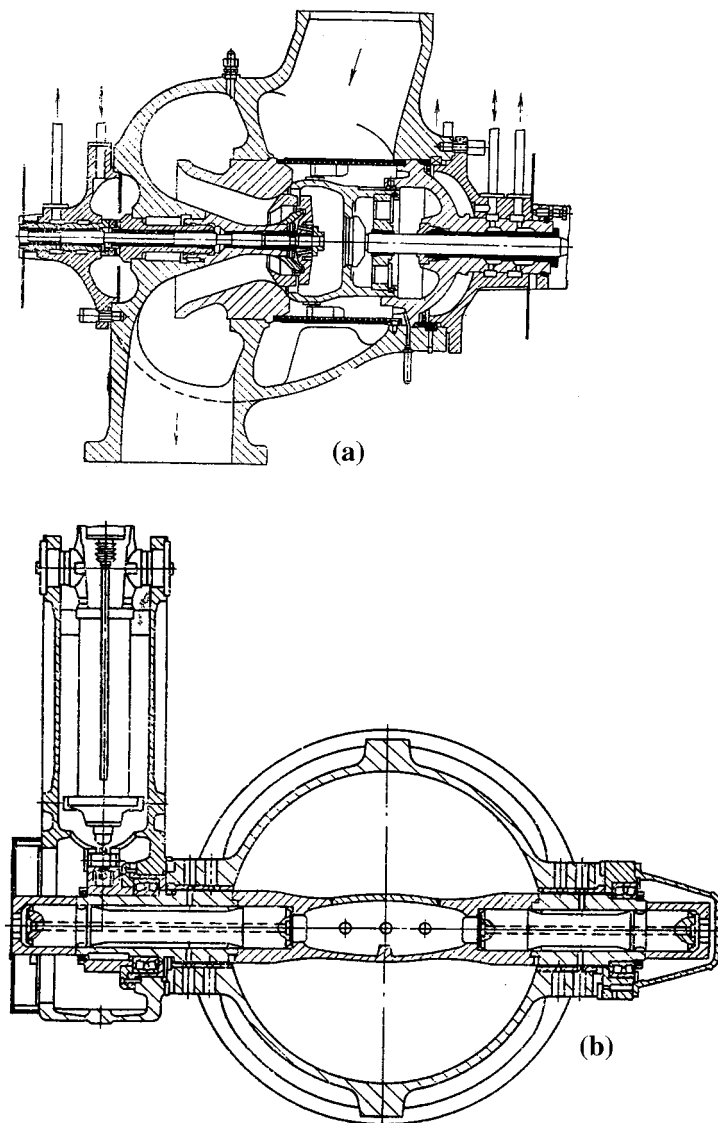


**Fig. 3-29.** One of four combined HP stop and control valve units (a) and butterfly-type intercept valve (b) for Brown Boveri's large wet-steam turbines  
Source: B. M. Troyanovskii<sup>47</sup>

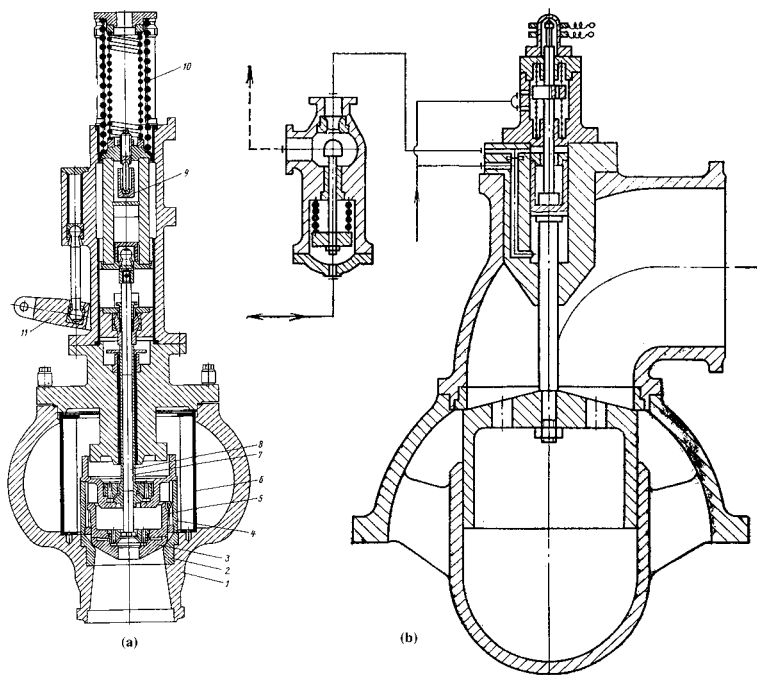


**Fig. 3-30.** Combined HP stop and control valve unit (a) (1: casing; 2: saddle; 3: control valve; 4: stop valve; 5: relief cylinder; 6: steam sieve; 7: stop valve stem; 8: control valve stem; 9: crossarm; 10: springs; 11: stop valve lever) and intercept valve (b) for Turboatom's low-speed wet-steam turbines

Source: By courtesy of Turboatom

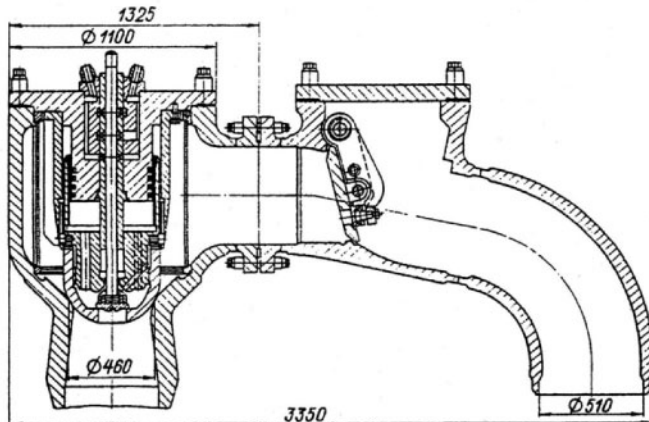


**Fig. 3-31.** HP control valve and stop turn-gate for LMZ's K-1000-60/3000 turbine

Source: By courtesy of LMZ

Two other design schemes for the HP stop and control valve units are presented in Figures 3-32a and 3-33. These are implemented in the GEC Alsthom's 630-MW wet-steam turbine, and various Siemens turbines, respectively.

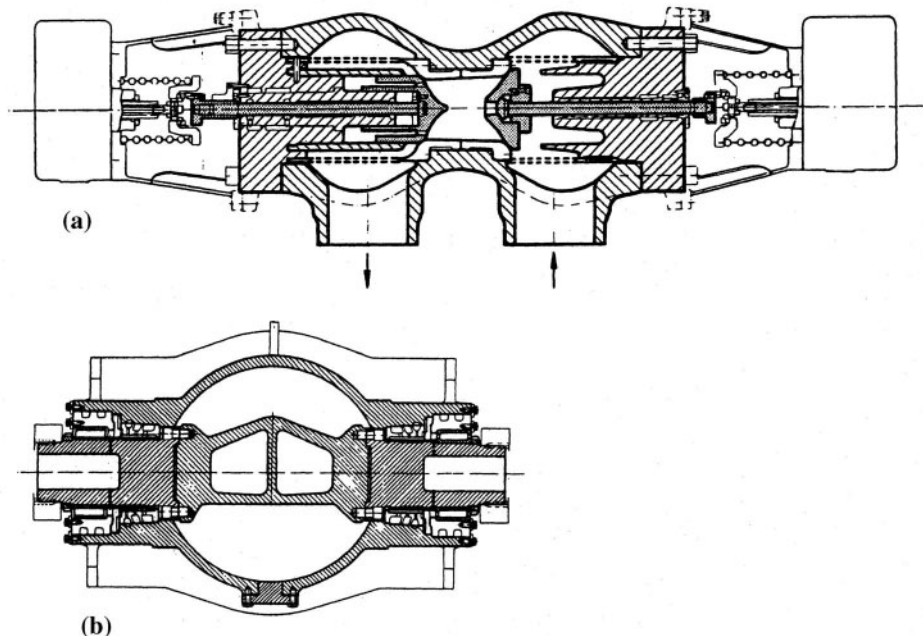


**Fig. 3-32.** HP stop and control valve unit (a) and LP butterfly valve (b) for GEC Alsthom's 630-MW wet-steam turbine  
Source: Data from J.A. Hesketh and J. Muscroft<sup>48</sup>

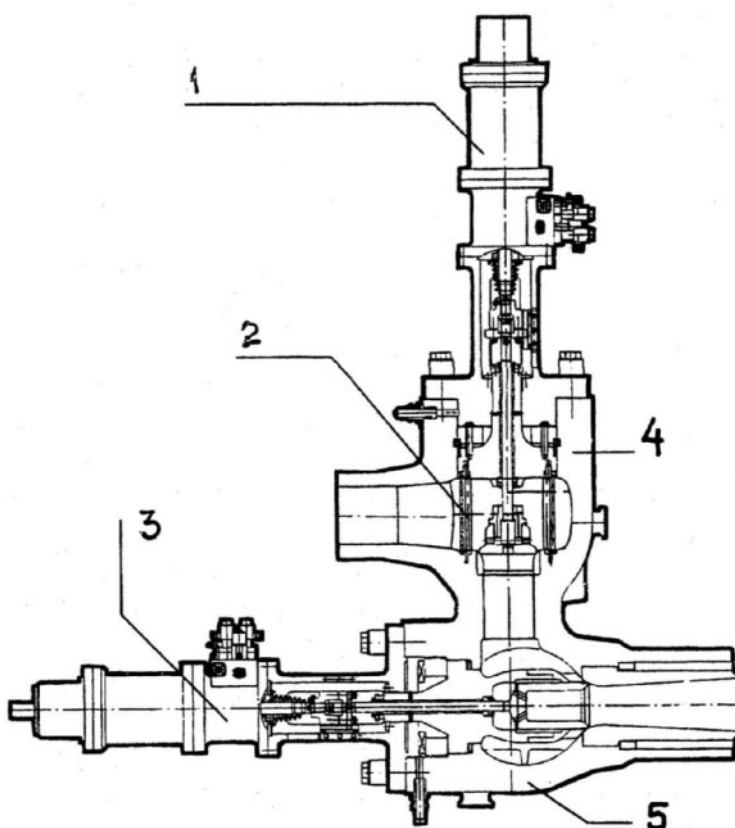


**Fig. 3-33.** HP stop and control valve unit for Siemens' wet-steam turbines  
(1: actuator; 2: steam strainer; 3: actuator; 4: stop valve; 5: control valve)

Source: Data from U. Sill and W. Zörner<sup>49</sup>

Significant potential for improving valve aerodynamics by means of streamlining the valve's geometric shape were revealed by ALSTOM while developing the control valves for their 1,500-MW *Arabelle* turbine.<sup>50</sup> The resultant design is presented in Figure 3-34. Serial wind tests were performed on scale models to classify the different geometric forms. These experiments were then completed by actual-size tests at one of the 1,000-MW nuclear power units and led to the design of the control valves mounted on the *Arabelle*.

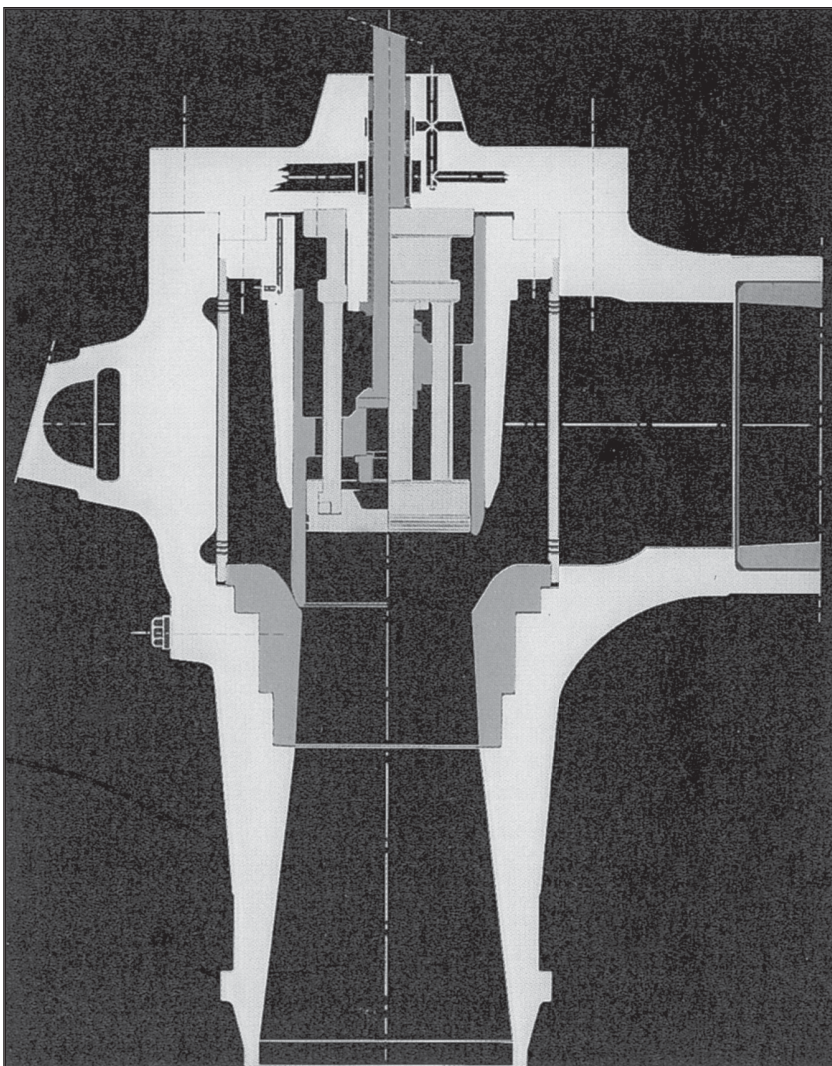


**Fig. 3-34.** HP control valve of ALSTOM's 1,500-MW wet-steam turbine  
Source: Data from ALSTOM

Most wet-steam turbines are designed with a throttle control, that is, with full-arc HP steam admission. In doing so, all of the HP control valves are handled simultaneously as if they were a single valve, and the steam flow entering the turbine is forwarded to the

entire nozzle arc of the first HP stage. When the turbine operates under a partial load, the entire steam flow is throttled in the control valves down to a pressure value approximately proportional to the current turbine load. Such a way of control, combined with a relatively small available heat drop for the turbine as a whole, leads to considerable efficiency losses under partial-load operating conditions. Thus, for the Siemens 1,300-MW turbine, the decrease of the load to 52% of MCR results in a 12% increase in the heat rate (Fig. 3-8). The lower the initial main steam pressure and available heat drop, the greater the efficiency loss.

It is well known that the nozzle-group control mode is more efficient for partial-load operating conditions. Nevertheless, the Turboatom K-220-44 turbine with its nozzle-group control is an exception (Fig. 3-4). Turbines with throttle control are simpler in design—they do not need a special nozzle box and a control stage with an enlarged diameter and greater enthalpy drop; the first HP stage does not differ from the other stages, and, as a result, the HP casing gains a more favorable outline. In addition, with everything else being equal, turbines with nozzle-group control are always a little less efficient under a full load because of the energy losses in the first stage related to its partial-arc steam admission. More importantly, nuclear power units are commonly assumed to predominantly operate under base-load conditions, producing the maximum possible output, because their power production costs are mainly defined by capital expenditures and are less dependent on fuel costs. This reasoning is absolutely correct, but in reality it is not always possible to keep nuclear power units operating under continuous full load, especially with the higher reliance of power systems on nuclear power. In many cases, individual nuclear power units ought to participate in covering the variable part of the power consumption graphs and operate under a lessened load. Nevertheless, most wet-steam turbine producers prefer to design them with throttle control.

Turbine manufacturers try to make the steam path between the HP and LP cylinders, including the MSR, as compact as possible to reduce the amount of latent energy stored in the enclosed water, and minimize turbine overspeeding after load rejections with switching off the generator. The overspeed tests performed by Siemens on their early wet-steam turbines for nuclear power plants (one with an output of 662 MW and rotation speed of 1,500 rpm

and another with an output of 477 MW and rotation speed of 3,000 rpm) demonstrated a speed increase of approximately 12-13% in 6-8 seconds after the turbine trip.<sup>51</sup> From correlation of the calculated and measured data, it was estimated that the average water film thickness in the wet-steam region of the HP cylinder and MSR is equal to approximately 3 mm ( $\approx$ 120 mil). When the turbine's stop valves are closed and the steam pressure throughout the steam path falls, this water evaporates, and the formed steam rushes into the LP cylinder, speeding up the turbine.

In order to reduce the overspeeding after load rejections, the turbines are furnished with fast-opening bypass valves that connect the cold reheat steam lines to the condenser and blow down the cross-over path after the HP cylinder, including the MSR. In addition, a load rejection can make the controlled vacuum breaker valves open, and the resultant increased backpressure in the condenser slows down the turbine rotation. In many cases these measures are sufficient to limit the overspeeding by allowable values that were proved by field tests.<sup>52</sup> Actual full-load rejection oscillograms for the 1,300-MW Biblis Unit A turbine are presented in Figure 3-35. Nevertheless, in some cases, these countermeasures turn out to be insufficient, and calculations show that to prevent excessive overspeeding, it is necessary to install intercept valves ahead of the LP cylinders, like that shown in Figure 3-30b. Along with traditional valve design decisions, butterfly-type valves are commonly used for this purpose, because in the open position they provide minimal pressure drops (approximately 1% of the current steam pressure). Examples of such valves can be seen in Figures 3-29b and 3-32b.

## 156 Wet-Steam Turbines for Nuclear Power Plants

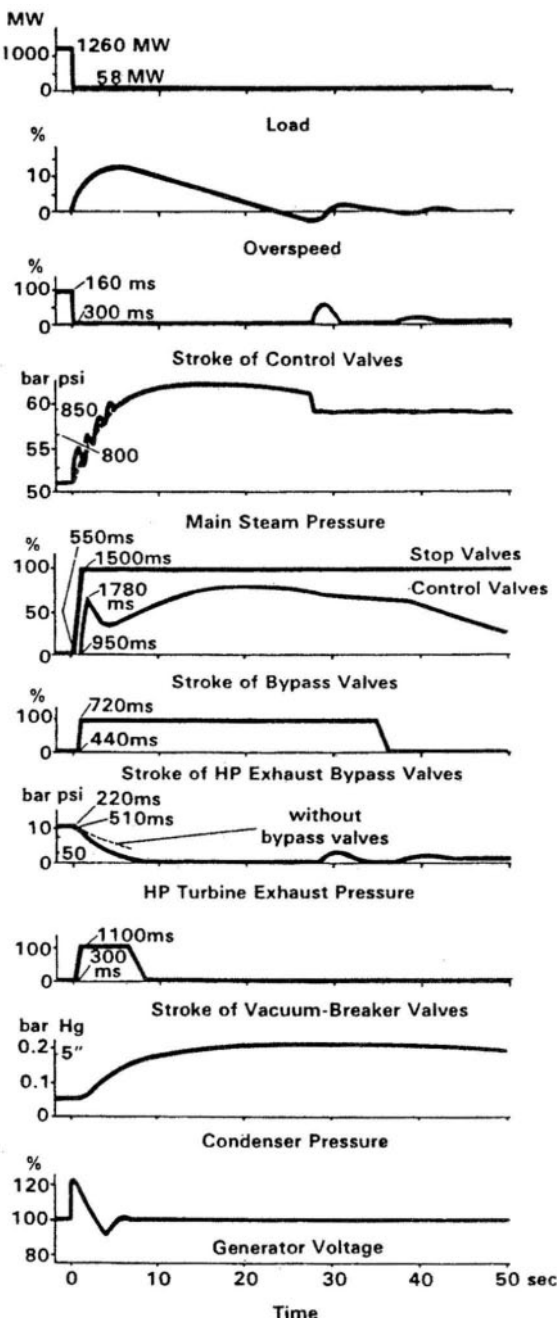


**Fig. 3-35.** Full-load rejection oscillograms for Siemens' 1,300-MW Biblis Unit A turbine

Source: Data from F.J. Spalthoff, H. Haas, and F Heinrichs<sup>53</sup>

[Previous Page](#)

Design 157

## Bearings

Large wet-steam turbines feature large-diameter journal necks—up to 800–900 mm (30–35 in) for the largest low-speed turbines and up to 520–560 mm (20–22 in) for high-speed turbines. Due to a large circular speed on the neck surface, the lubricating oil in the clearance between the rotor neck and the journal bearing shell is rapidly turbulentized, and the energy losses caused by friction sharply rise. That is why the journal bearings for large high-speed turbines are frequently made with multi-wedge, or segment, shells. In this case, the lubricant is delivered to each segment, forming separate oil wedges, and has no time for turbulization because of a small distance between segments. A sketch of such a four-segment journal bearing employed by Turboatom is given in Figure 3–36. This type of journal bearing is used in their high-speed wet-steam turbines, with the single capacities of 500 MW and 750 MW. For low-speed wet-steam turbines, despite greater diameters of their journal necks, the circular speed on the neck surface is considerably less than that for high-speed turbines and, as a rule, their journal bearings can be built with single-wedge shells.

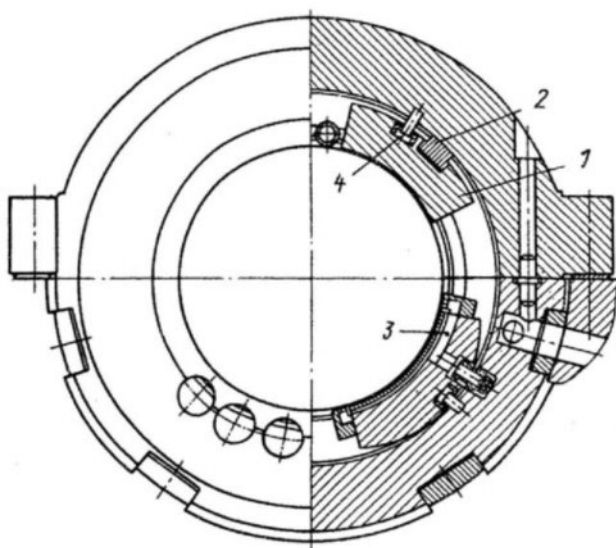


**Fig. 3–36.** Turboatom's four-segment journal bearing for high-speed wet-steam turbines (1: segment; 2: segment support; 3: oil supply channel; 4: adjusting pin)

Source: Turboatom

For large steam turbines, especially low-speed wet-steam turbines, with their heavy rotors, in order to avoid dry friction in the bearings when the turbine is shut down and is rotated by the turning gear, the bearings are additionally supplied with lubricant under increased pressure to jack the rotors.

Steam turbines commonly have voluminous, multi-branched high-pressure hydraulic and low-pressure lubrication oil systems. In order to prevent oil fires in the turbine hall, it is advisable to use synthetic fire-resistant fluids (FRFs) instead of petroleum oil because of their higher self-ignition temperature. While this value for petroleum oil is about 370°C (700°F), for FRFs it usually exceeds 750°C (1,380°F). Even if a quantity of FRF spills on a high-temperature steam line or other hot surface, it does not ignite, and even if it is ignited by a local high-temperature spot or open fire, it does not keep burning. There also exist special antirad additives developed to allow the use of FRFs at single-circuit nuclear power units. It is noteworthy that modern phosphate-ester-based FRFs, as distinct from their earlier analogs, belong to the same toxicity class as conventional petroleum oil and do not require any special precautions in service. Presently, more than 1,000 gas and steam turbines from the world's leading turbine producers operate with FRFs in their governing systems.<sup>54</sup>

Along with this, there exist alarming statistics of oil fires in the power industry, including nuclear power plants, and many of these fires originated from the turbine lubrication systems with the use of flammable petroleum oil as a lubricant.<sup>55</sup> One of the latest fires of this kind took place in December 2003 at Novovoronezh Unit 5, when the leaked lubricant oil soaked the turbine's thermal insulation and ignited; the turbine was shut down; the fire was put out and, fortunately, did not have any serious consequences. Of importance is that the danger of oil fires considerably increases for the largest steam turbines with their high-pressure lubricant circuits after jack oil pumps. At the same time, modern FRFs feature excellent lubricating properties and can successfully replace petroleum oil in both hydraulic and lubrication systems. There has been significant experience using FRFs for lubrication at power plants in the former Soviet Union and European countries. In particular, an FRF with the brand name OMTI has been used in hydraulic circuits for more than 200 steam turbines for their governing systems, and since the mid-1980s a number of units have successfully

operated with OMTI in their lubrication systems as well, including two 1,000-MW and two 220-MW nuclear wet-steam turbines.<sup>56</sup>

The use of FRFs allows turbine designers to install special backup lubrication oil reservoirs on top of the bearing casings (Figs. 3-13, 3-14, 3-16, and 3-18). These back-up reservoirs provide the bearings with lubricant during turbine coast-downs when the lubrication pumps are switched off, whereas with petroleum oil such reservoirs would pose a significant fire hazard. Similar backup lubricant reservoirs are situated on top of the LP cylinder casing of the Turboatom K-220-44-5 turbine (Fig. 3-6).

The use of FRFs as a lubrication oil has definitely prevented several serious oil fires at nuclear power plants. For example, in 1995, because of a rupture of an oil pipeline, approximately 30 metric tons of lubrication poured out onto the turbine hall floor at the 1,000 MW Khmelnitskaya nuclear power unit in Ukraine. If the turbine had operated with petroleum oil, a severe fire with possible complete destruction of the turbine hall would have been unavoidable. With OMTI in the turbine lubrication system, the incident did not have any serious consequences.

Two different design concepts take place in the shaft arrangement for large wet-steam turbines: some of them have two separate journal bearings for each rotor, whereas others use a common bearing for the adjacent HP and LP rotors. Manifestation of the first concept can be seen in Figures 3-1, 3-2, 3-4, 3-5, 3-8, 3-10 through 3-14, 3-16, 3-18, and 3-20, and the second approach, which allows for some decrease in the overall turbine length, is presented in the turbines shown in Figures 3-6 and 3-7. Both of these design concepts can be employed by the same turbine producers for turbines of different types and generations. So, for example, the Turboatom turbines K-220-44 were originally designed according to the first concept, but their later two-cylinder modifications were built with a common journal bearing between the HP and LP cylinders (Figs. 3-4a and 3-6). Siemens' high-speed wet-steam turbine also has the common journal bearing installed between the HP and LP cylinders, whereas for their heavier low-speed turbines, each rotor is furnished with two separate journal bearings (Figs. 3-7 and 3-8). The first shaft arrangement approach, with two journal bearings per rotor, was used for the first series of

French 1,000-MW turbines; however, their next series of 1,000-MW and 1,350-MW turbines were designed with the common bearing for the HP and first LP rotors, but for the 1,500-MW turbine *Arabelle*, ALSTOM returned to the two-bearings-per-rotor concept (Figs. 3-1 and 3-2).<sup>57</sup> International experience shows that out-of-balance forces that may affect rotor vibration are always weaker for shaft-lines with two bearings per rotor. In addition, such turbines are easier to assemble and repair. Along with this, reduction of the bearing number owing to the use of the common bearing for the adjacent HP and LP rotors allows designers to make the turbine shorter and cheaper and can be expedient for relatively light turbines of medium output.

For wet-steam turbines, with their large number of heavy LP cylinders (up to four for the largest high-speed machines), it seems especially advisable to use a thermal expansion arrangement with fixed bearing pedestals—a design concept that has been used with some large steam turbines for fossil fuel power plants. Such a scheme was implemented by MAN at the Martin Creek power plant's 850-MW turbine, and a similar approach was developed by Siemens for its 1,000-MW turbine series.<sup>58</sup> With this concept, in order to facilitate the turbine's thermal expansion, the bearing casings are rigidly mounted on the foundation, and the outer casings of the high-temperature cylinders and the inner casings of the LP cylinders rest on the adjacent bearing pedestals, and the cylinder casings can slide about them freely along the axial keys. Of importance, especially for turbines with a great number of cylinders, is that this system reduces a few times the frictional forces hampering the thermal expansion of the turbine, and precludes the danger of jamming in the longitudinal keys.

A similar scheme is used in the LMZ K-1000-60/3000 turbine shown in Figure 3-14. Its thermal expansion arrangement is presented in Figure 3-37. All four of its LP cylinders have their own fix-points, and all the bearing pedestals are also fixed on the foundation by means of a system of axial and lateral keys. Thus, each bearing casing contains two journal bearings. The HP cylinder, located between the second and third LP cylinders, rests with its paws on the chairs of the adjacent bearing pedestals. The lateral keys of the bearing pedestal between the second LP and HP cylinders form the fix-point of the HP cylinder. The integrated journal-thrust bearing is placed in the same casing. By contrast, the paws resting on the chairs of the bearing pedestal between the HP cylinder and the third LP cylinder do not

have lateral keys and slide along the chair surfaces. Thus, both the HP casing and the turbine shaft expand away from the bearing between the second LP cylinder and the HP cylinder.

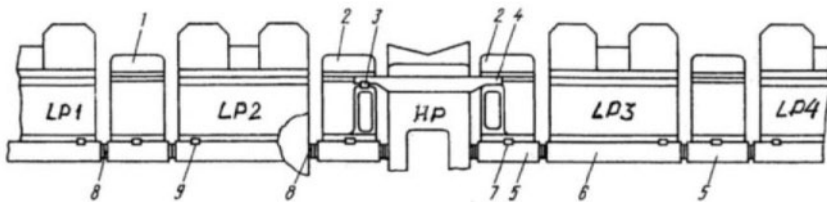


**Fig. 3-37.** Thermal expansion arrangement for LMZ's K-1000-60/3000 turbine (1: LP cylinders' fixed bearing pedestals; 2: fixed intermediate bearing pedestal; 3: lateral keys forming fix-point of HP cylinder; 4: HP cylinder casing's sliding paws; 5 & 6: foundation frames of bearings and LP cylinders; 7: lateral keys fixing bearing pedestals; 8: vertical keys; 9: lateral keys forming fix-points of LP cylinders)

Source: Data from LMZ

## Last Stage Blades

### Length of the last stage blades

The last stage blades (LSBs) are a key design element of wet-steam turbines that dictate main design decisions for these turbines, including the choice of the rotation speed and number of LP cylinders. The LSBs also, to a great degree, determine the turbine's operating performances.

At the taken rotation speed,  $n$ , the LSB length is mainly limited by the material strength under the action of centrifugal stress,  $\sigma_r$ . If the bucket is not shrouded, it is free standing (that is, not tied with the neighboring buckets), and its profile is invariable lengthwise of the blade height, the tensile radial stress in the bucket's root section caused by centrifugal forces is accounted as equal to:

$$\sigma_r = 0.5 \rho \omega^2 l_2 d_2$$

where  $\rho$  is the material density,  $\omega = 2\pi n$  is the angular velocity, and  $l_2$  and  $d_2$  are the length and mean diameter of the blade, respectively. In reality, the LSB profile changes along its height, decreasing in area from the root value,  $f_r$ , to the tip value,  $f_t$  (Fig. 3-38). This can be approximated by entering a factor for unloading the root stress,  $k_{dist} \approx 0.35 + 0.65 \times (f_r / f_t)^{-1}$ . With regard to this factor and taking the LSB annular exit area as  $F = \pi d_2 l_2$ , the tensile radial stress in the bucket's root section is:

$$\sigma_r = k_{dist} \times 2\pi F \times \rho n^2 \quad (3.3)$$

The area ratio,  $f_r / f_t$  typically lies in the range 7-10, which corresponds to  $k_{dist} \approx 0.4$ . For LSB buckets manufactured from stainless steel,  $\rho \approx 8.0 \times 10^3 \text{ kg/m}^3$ , and thus:

$$F \approx \frac{\sigma_r}{2\pi k_{dist} n^2 \rho} \approx 0.48 \times 10^{-4} \frac{\sigma_r}{n^2} \quad (3.4)$$

where  $\sigma_r$  is measured in Pa,  $n$  in  $s^{-1}$ , and  $F$  in  $m^2$ .

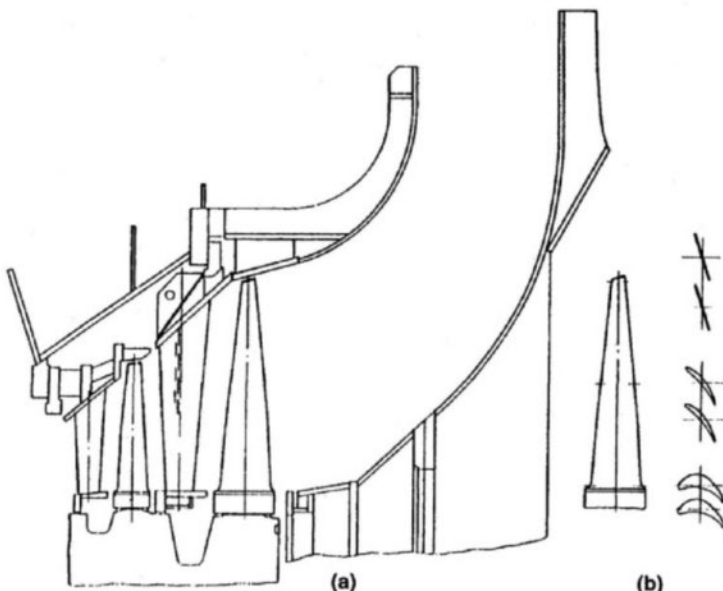


**Fig. 3-38.** Typical last LP stages of a large steam turbine (a) and the LSB with its profiles at the tip, mean, and root diameters (b).

Development of new blade steels with advanced strength properties has promoted additional progress in the development of new, longer blades. It follows that for a high-alloy steel, with the admissible stress value equal to approximately 620 MPa, the maximum accessible exit annular area of an LSB row can approach  $11.9 \text{ m}^2$  ( $128 \text{ ft}^2$ ) for  $n = 50 \text{ Hz}$  and  $8.3 \text{ m}^2$  ( $89 \text{ ft}^2$ ) for  $n = 60 \text{ Hz}$ . If  $d/l \approx 2.7$ , these annular area values can be achieved with the LSB length of 1,220 mm (48 in) for  $n = 3,000 \text{ rpm}$ , and 1,016 mm (40 in) for  $n = 3,600 \text{ rpm}$ . These values coincide with specifications of the actual steel LSB recently developed by GE and Toshiba (Table 3-3).<sup>59</sup>

**Table 3-3.** Main characteristics of some LSBs for high-speed steam turbines of various manufacturers

Length (mm [in])	Length-to-Mean Diameter Ratio	Material	Developer	Annular Exit Area per Flow ( $\text{m}^2$ [ $\text{ft}^2$ ])	Tip Circumfer- ential Speed (m/s [ $\text{ft}/\text{s}$ ])	Notes
60-Hz turbines (3,600 rpm)						
N/A	N/A	titanium	Siemens	11.1 (120)	N/A	Under development
1,169 (46)	N/A	titanium	Hitachi	N/A	N/A	Under development
1,150 (45)	0.41	titanium	MHI	10.1 (109)	746 (2,446)	
1,067 (42)	0.40	titanium	Siemens	10.3 (111)	705 (2,311)	
1,016 (40)	0.41	steel	MHI	7.8 (84)	654 (2,147)	
1,016 (40)	0.38	titanium	GE/ Toshiba	8.5 (92)	693 (2,273)	
1,016 (40)	0.39	titanium	Hitachi	8.4 (90)	689 (2,226)	
1,016 (40)	0.41	steel	GE/ Toshiba	8.3 (89)	682 (2,236)	Available since 2003
955 (38)	0.38	steel	Siemens	8.7 (94)	658 (2,158)	
858 (34)	0.41	steel	Turboatom	5.7 (61)	559 (1,834)	
852 (33.5)	0.37	steel	Hitachi, Toshiba	6.2 (67)	594 (1,948)	

852 (33.5)	0.37	steel	GE	6.2 (66)	594 (1,948)	
813 (32)	0.34	steel	Siemens	6.9 (74)	605 (1,092)	
50-Hz turbines (3,000 rpm)						
1,500 (59)	0.40	titanium	LMZ	17.9 (193)	832 (2,729)	Under development
N/A	N/A	titanium	Siemens	16.0 (172)	N/A	Under development
1,372 (54)	0.41	titanium	MHI	14.6 (157)	744 (2,441)	Under development
1,360 (53.5)	0.40	titanium	ALSTOM	14.7 (157)	750 (2,460)	Under development
1,220 (48)	0.39	steel	GE/Toshiba	11.9 (128)	679 (2,228)	Available since 2003
1,220 (48)	0.41	steel	MHI	11.3 (122)	655 (2,148)	
1,220 (48)	N/A	titanium	GE/Toshiba	N/A	N/A	
1,200 (47)	0.37	steel, titanium	ABB	12.2 (132)	697 (2,286)	
1,200 (47)	0.40	titanium	LMZ	11.3 (122)	658 (2,158)	In operation since 1979
1,146 (45)	0.38	steel	Siemens	12.5 (135)	658 (2,158)	Available since 1997
1,130 (44.5)	0.38	steel	ALSTOM	10.5 (113)	642 (2,106)	
1,100 (43)	0.37	steel	Turboatom	10.4 (116)	644 (2,112)	Under development
1,093 (43)	N/A	steel	Siemens	N/A	N/A	
1,092 (43)	0.37	steel	Hitachi	10.1 (109)	634 (2,080)	
1,085 (43)	0.39	steel	Skoda	9.5 (102)	608 (1,994)	
1,067 (42)	0.38	steel	Toshiba	9.5 (103)	613 (2,011)	
1,050 (41.5)	0.36	steel	ABB	9.7 (104)	568 (1,863)	
1,050 (41.5)	0.41	steel	Turboatom	8.4 (95)	565 (1,853)	

1,030 (40.5)	0.35	steel	MHI	9.4 (102)	618 (2,027)	
1,030 (40.5)	0.41	steel	Turboatom	8.2 (88)	560 (1,837)	
1,021 (40)	0.37	titanium	GE	8.8 (95)	591 (1,938)	
1,016 (40)	0.37	titanium	Toshiba, Hitachi	8.8 (94)	590 (1,935)	
1,000 (40)	0.37	steel	ALSTOM (ABB)	8.5 (91)	580 (1,902)	
975 (38)	0.34	steel	Siemens	10.0 (108)	605 (1,092)	
960 (38)	0.39	steel, titanium	LMZ	7.5 (81)	540 (1,771)	
950 (37.5)	0.33	steel	ALSTOM (ABB)	8.5 (92)	596 (1,955)	
940 (37)	0.33	steel	Turboatom	8.4 (90)	594 (1,948)	
915 (36)	0.36	steel	Siemens	8.0 (86)	543 (1,781)	

Transitioning to a half-speed turbine theoretically allows designers to quadruple the annular exit area by doubling the LSB length. But in practice, the maximum LSB length of low-speed turbines does not exceed one-and-a-half times that of high-speed turbines (compare Tables 3-3 and 3-4). The explanation for this lies in the fact that the increased length unavoidably lowers the aerodynamic quality of the blades and makes their design more complicated because of the large length-to-mean diameter ratio and an increased pitch of the meridional stage profile. Maintaining an optimal circumferential speed-to-steam velocity ratio, the increased mean diameter results in an increased enthalpy drop and, as a result, a greater difference in the specific steam volume values between the blade row entrance and exit. High, supersonic steam velocities and their great variations along the row height hinder the achievement of optimal aerodynamic performances. In addition, the erosion impact of wet steam becomes more serious with longer LP stage blades. Thus, the closer the LSB is to its limiting length, the smaller the gain in efficiency, and the higher the cost of this gain. Nevertheless, there still exists a substantial margin for increasing the size of low-speed steel LSBs, whereas for high-speed steel LSB, such a margin has practically run out.

**Table 3-4.** Main characteristics of some LSBs for low-speed steam turbines of various manufacturers

Length, mm (inch)	Length-to-mean diameter ratio	Material	Developer	Annular exit area, $m^2$ ( $ft^2$ ) per flow	Tip circumferential speed, m/s (ft/s)	Notes
60 Hz turbines (1,800 rpm)						
1,375 (54)	N/A	steel	MHI	N/A	N/A	
N/A	N/A	steel	ALSTOM	18.0 (194)	N/A	Under development
1,320 (52)	0.34	steel	GE, Hitachi	15.8 (170)	485 (1,591)	
1,320 (52)	0.33	steel	Hitachi, Toshiba	16.7 (180)	504 (1,653)	
1,320 (52)	0.33	steel	ABB	16.4 (176)	498 (1,630)	
1,220 (48)	N/A	steel	Hitachi	N/A	N/A	
1,194 (47)	0.33	steel	ALSTOM, Westinghouse	13.4 (144)	449 (1,473)	
1,170 (46)	0.32	steel	Siemens	13.4 (144)	448 (1,469)	
1,170 (46)	0.34	steel	MHI	12.5 (134)	427 (1,400)	
1,170 (46)	0.35	steel	ASTOM	12.2 (131)	420 (1,377)	
1,143 (45)	0.33	steel	GE	12.3 (132)	431 (1,414)	
1,118 (44)	0.33	steel	Siemens	N/A	N/A	
1,118 (44)	N/A	steel	Westinghouse	11.8 (127)	422 (1,383)	
1,092 (43)	0.33	steel	GE, Hitachi	11.5 (124)	419 (1,374)	
1,041 (41)	0.34	steel	MHI	10.0 (108)	391 (1,282)	
1,016 (40)	0.34	steel	Westinghouse	9.6 (103)	379 (1,242)	

50 Hz turbines (1,500 rpm)						
1,850 (73)	0.37	steel	ALSTOM	28.8 (310)	534 (1,751)	Under development
1,830 (72)	0.37	steel	Siemens	28.1 (302)	528 (1,730)	Commercially available
1,650 (65)	0.36	steel	Turboatom	23.6 (254)	48 (1,597)	Under development
1,524 (60)	N/A	steel	GE	N/A	N/A	Under development
1,450 (57)	0.35	steel	ALSTOM	19.2 (207)	445 (1,459)	
1,450 (57)	0.35	steel	Turboatom	18.9 (203)	440 (1,443)	
1,375 (54)	N/A	steel	MHI	N/A	N/A	
1,372 (54)	0.33	steel	Westinghouse	17.8 (192)	431 (1,414)	
1,365 (54)	0.32	steel	Siemens	18.4 (198)	443 (1,453)	
1,320 (52)	0.33	steel	Hitachi, Toshiba	16.72 (180)	420 (1,378)	
1,250 (49)	0.32	steel	Skoda	15.4 (166)	406 (1,333)	
1,250 (49)	0.34	steel	MHI	14.5 (128)	388 (1,273)	
1,220 (48)	0.31	steel	ALSTOM	15.3 (165)	409 (1,343)	
1,200 (47)	0.29	steel	ABB	15.8 (170)	424 (1,392)	
1,118 (44)	0.33	steel	MHI, Westinghouse	11.8 (127)	351 (1,151)	

This is evident in the diagram composed by ABB and shown in Figure 3-39, where the dimensions of actual LSBs developed by various turbine manufacturers are plotted against their theoretical size limits. In theory, besides the tensile stress caused by centrifugal force, the LSB length is also limited by some additional factors, including: the bending stress in the root section caused by steam forces, blade vibration frequency, and tensile stress in the LP rotor due to the centrifugal load from the LSB. However, more often than not, these factors are rather secondary.

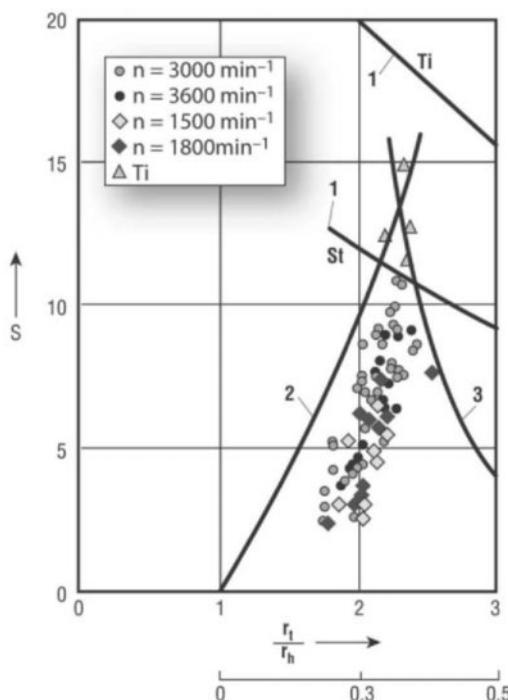


**Fig. 3-39.** Parameters of actual LSBs provided by various manufacturers (1: combined blade stress and cascade geometry limit; 2: rotor stress limit; 3: blade frequency limit; St: steel LSBs; Ti: titanium LSBs; S: annular exhaust area per flow;  $r_t$ : tip radius;  $r_b$ : hub radius;  $b$ : blade height;  $d_m$ : mean blade diameter)  
*Source: A. P. Weiss<sup>60</sup>*

It is not currently possible to radically increase the length and annular exit area of high-speed LSBs other than by transition to manufacturing the blades from titanium alloys (for example, Ti-6Al-4 V). As a rule, titanium alloy blades are called merely "titanium." The density of titanium alloys is approximately 1.8 times less than that of steel, with the same, or even greater, strength. Because of this, the length of titanium buckets can be extended appreciably. On the other hand, titanium LSBs are considerably more expensive compared to steel ones and are much harder to machine. Nevertheless, even former critics of titanium LSBs have presently turned to developing and implementing them, and every major turbine producer disposal has made turbines with titanium blades commercially available. The effectiveness of titanium LSBs has been well proven in operational practice.<sup>61</sup> A typical modern 1,093-mm (43-in) titanium LSB (for the rotation speed of 3,000 rpm) developed by Hitachi is shown in Figure 3-40.

An important additional advantage of titanium is its lesser susceptibility to erosion and corrosion compared to stainless steels. Because of this, some turbine producers also proposed using titanium blades for intermediate LP stages operating in the Wilson region, even though this might turn out to be too expensive in practice.

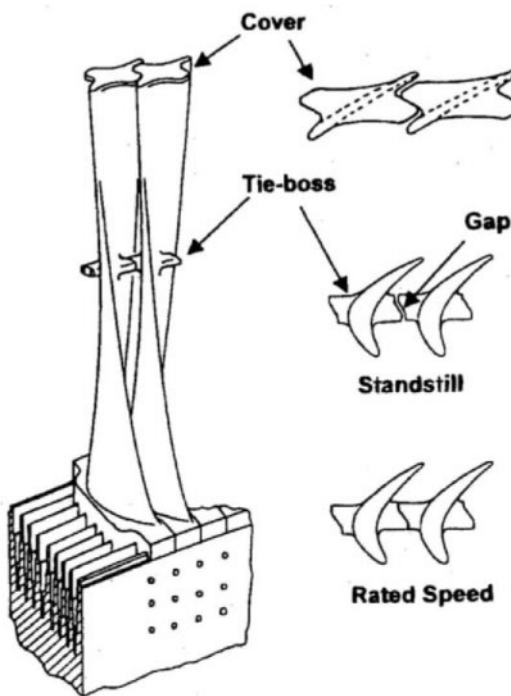


**Fig. 3-40.** Hitachi's 43-in titanium-alloy LSB  
Source: M. Machida, H. Yoda, E. Saito, and K. Namura<sup>62</sup>

With an increase in the length of the LSB, not only does the tensile stress caused by centrifugal forces grow, but the danger of WDE also increases. Longer LSBs are also more intensely heated under operating conditions of low flow and high backpressure because of friction and fanning in the ambient steam. This also lowers the blades' strength and requires special attention to be paid to the operating conditions. These phenomena are not specific to wet-steam turbines, but are rather typical for all modern condensing steam turbines with long LSBs.

## Roots, shrouds, and snubbers

For many years, the most widespread type of attachment bases for LSBs was a prong-and-finger (or fork-shaped) root with varying number of prongs. For example, Hitachi's 1,016-mm (40-in) and 1,092-mm (43-in) titanium LSBs were made with seven- and nine-prong roots, as shown in Figure 3-40. However, in recent years, most modern LSBs have been designed with curved-entry fir-tree roots. This attachment type is employed by almost all of the world's major steam turbine manufacturers<sup>63</sup>

For computational calculations of the blade stress state, the LSB is digitally modeled together with its attachment base and the adjacent steeples on the rotor surface with regard to possible clearances in the joint. An example of such a 3-D finite-element model for an MHI 1,143-mm (45-in) steel LSB with a fir-tree root (for the rotation speed of 3,600 rpm) is presented in Figure 3-41. Another 3-D finite-element model example with the resultant relative stress field for Toshiba's 1,067-mm (42-in) steel LSB (for the rotation speed of 3,000 rpm) is given in Figure 3-42. The 3-D models sometimes comprise several buckets connected by a shroud, tie-bosses, or arch bands.<sup>64</sup>

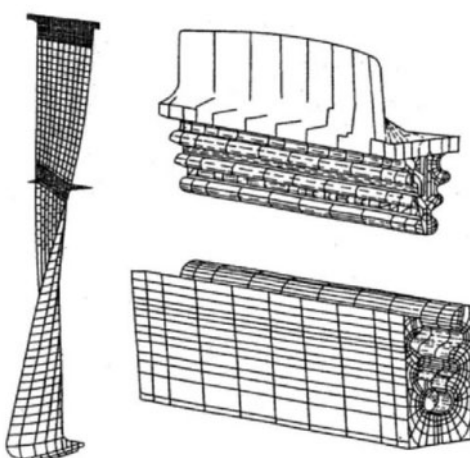


**Fig. 3-41.** Computational 3-D model for calculating the stress state and vibrational characteristics of MHI's 1,143-mm titanium LSB with its root and adjacent steeple

Source: E. Watanabe, H. Ohyama, Y. Kaneko, et al.<sup>65</sup>

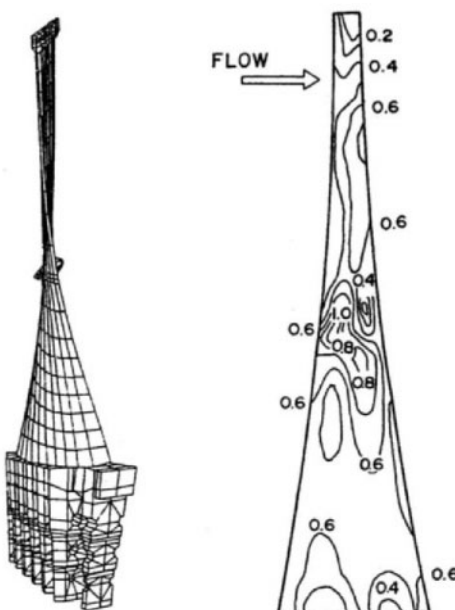


**Fig. 3-42.** Three-dimensional calculation mesh and relative stress field for Toshiba's 1,067-mm LSB

Source: S. Hisa, T. Matsuura, and H. Ogata<sup>66</sup>

The curved-entry fir-tree dovetail is currently the most suitable attachment structure for the longest LSBs. The compactness of the dovetail enables a thinner wheel configuration, and it reduces the centrifugal stress in the rotor body. In addition, the fir-tree root does not have any sharp edges or pin holes. This is especially important for blades made of titanium alloys, which are relatively brittle and sensitive to notches. In determining the dovetail shape and its machining tolerance, the difference in elasticity between the materials of the blade root and disk wheel should be considered. Of special importance for the curved entry fir-tree dovetail is a uniform distribution of load on all the blade root hooks.<sup>67</sup> The stress contours and maximum stress values related to the tensile strength for the blade and wheel dovetail of Hitachi's 1,016-mm (40-in) LSB under conditions of the rated rotation speed of 3,600 rpm are shown in Figure 3-43a. The maximum centrifugal stresses take place at the corner of the top hook for the blade root and at the corner of the bottom hook for the wheel dovetail. Their values are sufficiently lower than the material tensile strength. The load on each hook ranges from approximately 20% to 30% of the total load under normal conditions.

However, these fractional loads can be affected by errors while machining the dovetail, with resultant initial clearances on the individual hook surfaces. In Figure 3-43b, the dotted line indicates the total load on all the hooks, and the solid lines refer to the load on the individual hooks. As the rotor speed increases, the lower hooks come into contact, and the load on the hooks is equalized, but the portion for the top hook remains approximately 5% higher compared with normal conditions.

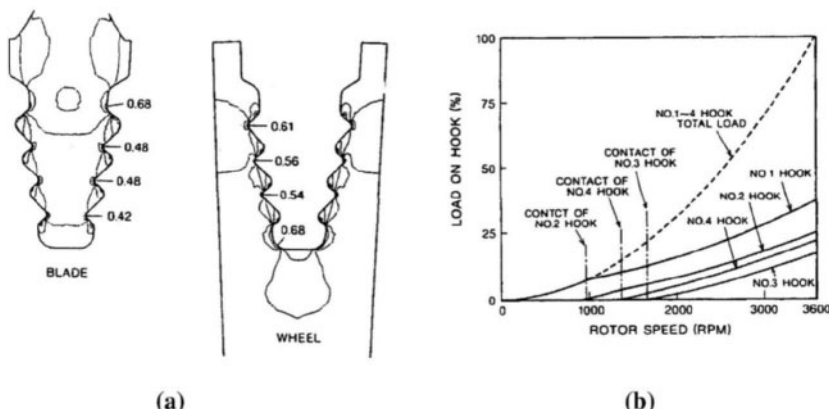


**Fig. 3-43.** Centrifugal stress contours and maximum stress values related to the tensile strength for 1,016-mm titanium LSBs with a fir-tree dovetail (a) and load distributions on hooks with machining errors (b)

Source: T. Suzuki, M. Watanabe, and M. Aoyama<sup>68</sup>

Modern turbine blades, including LP ones, are mainly manufactured integrally shrouded—the shrouding elements are milled together with the bucket's profiled body. The shrouding elements of the individual blades are connected by special inserts in a wedge-shaped groove like a dovetail joint or are designed with special wedge-shaped edges that engage the blades in mesh under action of centrifugal forces. This second approach is predominantly applied to modern LSBs (Fig. 3-44). To increase the rigidity of the entire blade structure, the blades are additionally coupled with a *snubber*—integral tie-bosses at the midspan of the blade height (Fig. 3-40). Their edges also engage under action of centrifugal forces. As a result, when the turbine rotates, all of the LSBs are tied together, forming a continuous ring of blades. One of the major advantages of such a continuous

annular blade structure, compared with blade sectors (several units of several blades each) more conventional in the past, is that it has fewer resonance points during rotation. An example of a vibration mode analysis of an LSB wheel is presented in Figure 3-45. This type of engaging LSBs is widely used by Japanese turbine producers (Hitachi, MHI, and Toshiba), as well as some European manufacturers. According to ALSTOM, this structure, with two contact supports (tie-bosses situated at 70% of the blade height and an integral shroud at the blade tip), applied to a 1,360-mm steel LSB (for the rotation speed of 1,500 rpm), reduces the maximum additional dynamic (vibrational) stress in the blade body by a factor of two to three times as much as that for free-standing blades. This type of connection produces well-defined and easily controlled vibration modes and significantly reduces the buffeting stresses arising when the LSBs are subjected to low steam flow and high back-pressure conditions.<sup>69</sup>

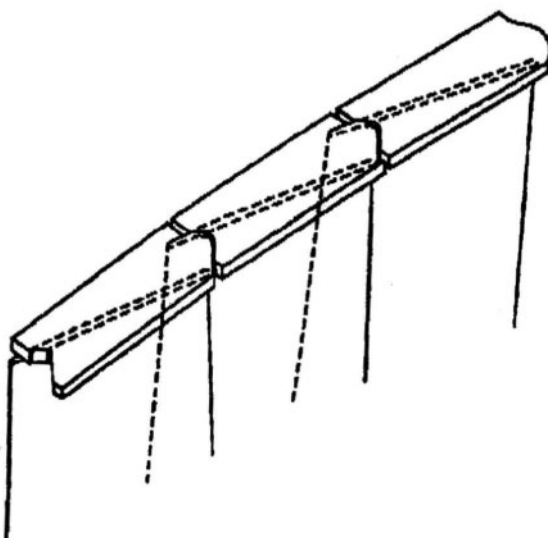


**Fig. 3-44.** Connection of shrouding elements of the LSB with wedge-shaped edges

Source: E. V. Levchenko, V. P. Sukhinin, B. A. Arkad'ev, et al.<sup>70</sup>

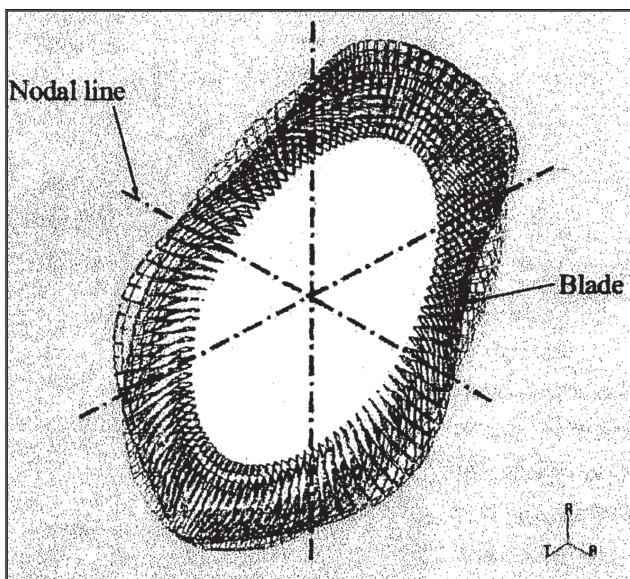


**Fig. 3-45.** Example of vibration mode analysis for a last stage wheel with “continuous cover blades” of Hitachi

Source: M. Machida, H. Yoda, E. Saito, and K. Namura<sup>71</sup>

Some other leading turbine producers, including Siemens and ABB, for many years have successfully used free-standing LSBs, not connected by shrouds, mid-span damping wire ties, or tie bosses. It might be well to note that although shrouding the blades typically reduces leakage losses, this is compensated by more effective peripheral water separation for unshrouded blades. In turn, the mid-span damping devices cause the increase in the airfoil thickness in their neighborhood, increasing profile losses. In addition, all of the obstacles in the interblade channels (like tie-bosses or wire ties) disrupt the steam flow and lead to additional energy losses. Of importance is that any local wetness concentration in the stage channels contributes considerably to blade erosion. In particular, this concerns wire ties and tie-bosses between the blades and brings another point in favor of using free-standing LSBs, as well as shrouded blades without any additional ties in the preceding stages. Free-standing LSBs manufactured by ABB and Siemens can be seen in Figures 3-7, 3-8, and 3-10a. New families of free-standing LSBs developed by Siemens for newly designed and refurbished turbines, including those for nuclear power plants, are shown in Figure 3-46.<sup>72</sup> Along with this, the use of free-standing LSBs is possible only up to a certain threshold length.

So the newest Siemens titanium LSBs, with annular exit areas of 16 m<sup>2</sup> and 11.1 m<sup>2</sup> per flow (for the rotation speeds of 3,000 and 3,600 rpm, respectively), are characterized by an interlocked design and feature an integral shroud, as well as a mid-span snubber.

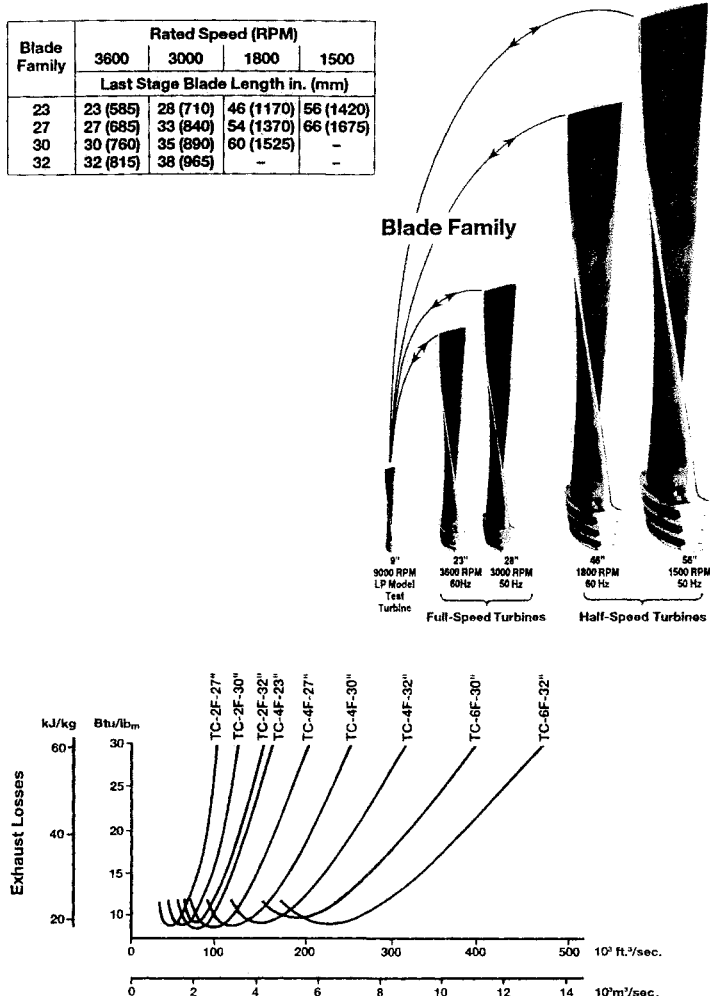


**Fig. 3-46.** Families of Siemens LSBs and selection diagram for 3,600-rpm turbines

Source: M. Gloger, K. Neumann, D. Bermann, and H. Termuehlen<sup>73</sup>

Unshrouded blades allow a more precise determination of their vibrational characteristics and thus a more reliable tuning out of the blades. In addition, for unshrouded LSBs, it is easier to arrange their non-contact continuous vibrational monitoring.<sup>74</sup> Such a non-contact vibration measuring system developed by Siemens is shown in Figure 3-47. Figure 3-48 gives an idea on how the tip of a vibrating free-standing blade is moving, and Figure 3-49 presents a Campbell diagram for a 965-mm (38-in) LSB (for the rotation speed of 3,000 rpm) with the plotted results of actual measurements from a typical 1,000-MW high-speed wet-steam turbine. An operation principle of a similar optical measuring system developed by ABB for a 1,200-mm free-standing steel LSB is shown in Figure 3-50. The calculated vibrational characteristics were confirmed by bench tests in a vacuum chamber.

Some institutions also managed to develop noncontact vibration measuring systems as applied to shrouded LSBs, too. In this case, the primary sensors are installed at the wheel side.<sup>75</sup>

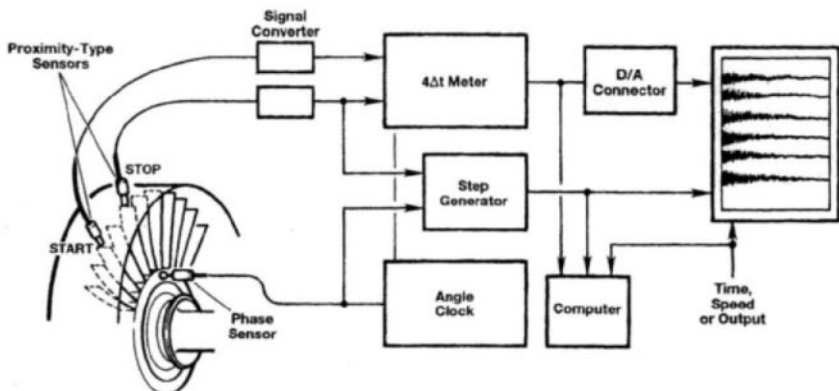


**Fig. 3-47.** Schematic diagram of a dual-sensor, proximity-type blade vibration measuring system developed by Siemens

Source: M. Gloer, K. Neumann, D. Bermann, and H. Termuehlen<sup>76</sup>

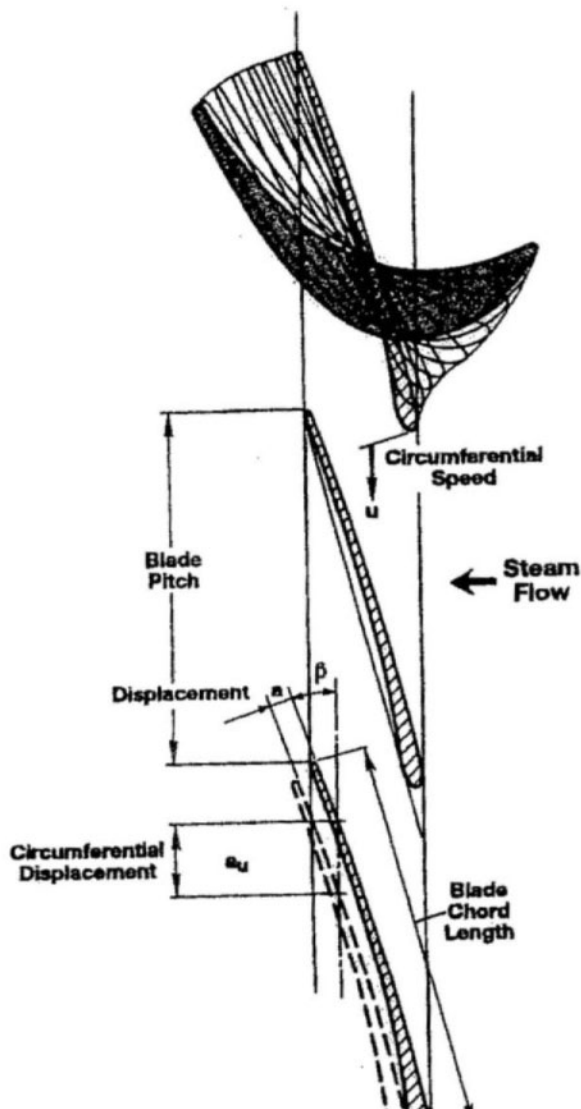
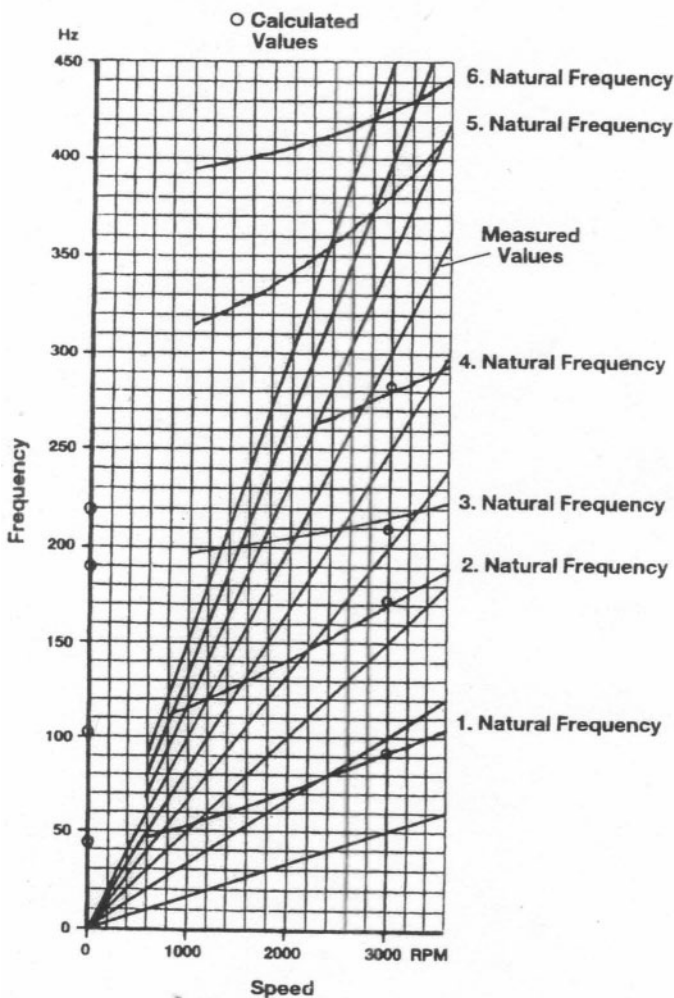
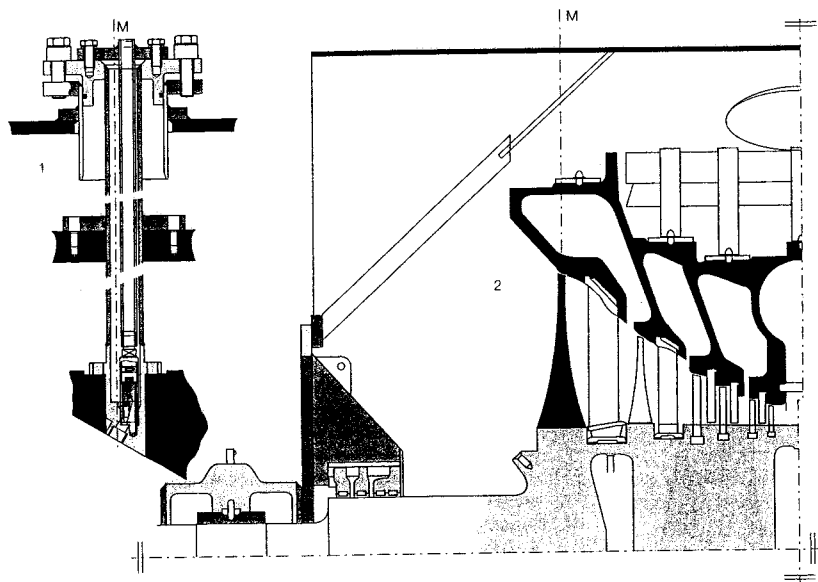
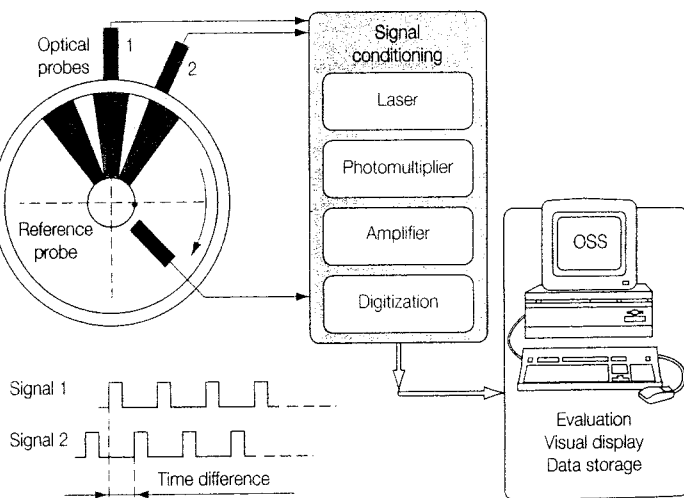


Fig. 3-48. Movement of a tip of a vibrating free-standing LSB  
Source: M. Gloger, K. Neumann, D. Bermann, and H. Termuehlen<sup>77</sup>



**Fig. 3-49.** Campbell diagram (see note) for a 965-mm LSB according to measurements at a Siemens 1,000-MW-class 3,000-rpm wet-steam turbine.  
Source: M. Gloger, K. Neumann, D. Bermann, and H. Termuehlen<sup>78</sup>

Note: A Campbell diagram presents the dynamic frequency of certain tones for the blade, blade packet, or entire stage wheel, plotted against the turbine rotational speed. It also includes lines from the coordinate origin showing changes in rotational speed of the perturbing force frequency for different harmonics. The abscissas of the intersection of these lines with the blades' dynamic frequency lines (or ranges) determine the resonant rotational speeds for each perturbing harmonic.



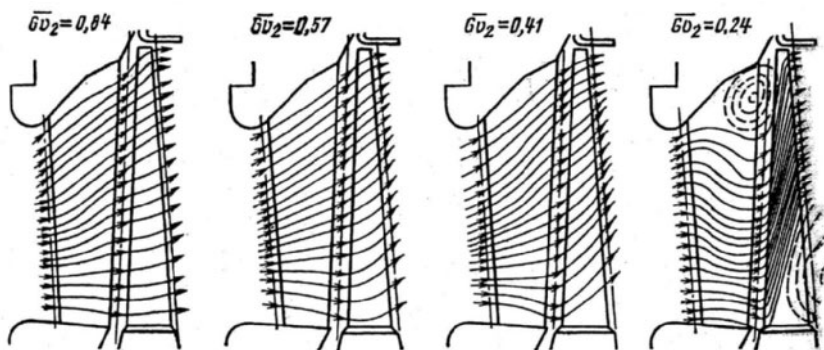
**Fig. 3–50.** Operation principle of ABB's optical blade vibration measuring system (a), optical probe (b), and its installation at the LP exhaust (c)  
*Source: E. Krämer and E. Plan<sup>79</sup>*

## Aerodynamics of LSBs

The LSB geometry is derived from complex aerodynamic calculations. The aerodynamic design is confirmed by experiments at test cascades and model turbines with model and actual buckets. If the geometry of the developed actual blade is completely similar to that of the model bucket and their dimensions are in inverse proportion to the rotation speed, all of the aerodynamic, vibrational, and strength properties of both the model and actual blades are the same. This enables creating families of standard LSBs for different rotation speeds (1,500 rpm, 1,800 rpm, 3,000 rpm, and 3,600 rpm) based on a single model version to cover a wide range of output and vacuum values. Several families of Siemens LSBs are presented in Figure 3-46. Similar LSB families are commonly developed and employed by all of the turbine manufacturers.

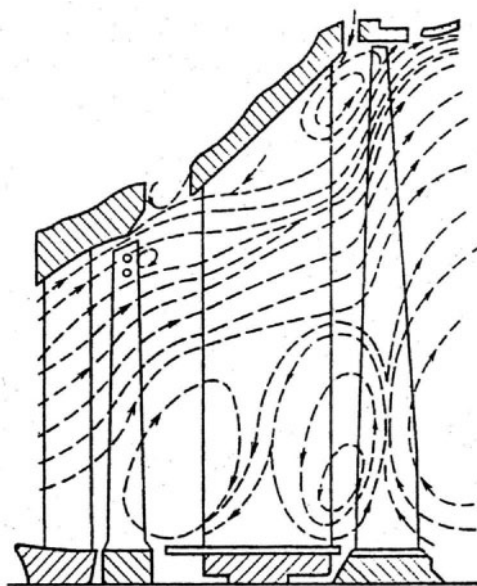
The advent of newer, longer, more efficient LSBs allows replacement of older ones at steam turbines in service in the course of their refurbishment. Thus, for example, in the process of refurbishing the 1,300-MW low-speed wet-steam turbine (similar to that shown in Fig. 3-8) at the German Unterweser nuclear power plant, the existing LSBs were replaced by 1,422-mm (56-in) buckets of blade family 23 (see the table in Figure 3-46); and at the Spanish Trillo nuclear power plant, new 965-mm (38 in) LSBs of blade family 32 were installed at the 1,000-MW, high-speed wet-steam turbine (similar to that shown in Fig. 3-7), producing a considerable gain in the turbine output (see chapter 5). The energy losses with the exit velocity for a full-speed 60-Hz (the rotation speed of 3,600 rpm) turbine, depending on the volumetric exhaust steam flow amount and the number and size of the LP exhausts, are plotted in Figure 3-46b. So, for a wet-steam turbine with an exhaust steam flow amount of 539 kg/s ( $9,945 \text{ m}^3/\text{s}$ ) and the backpressure of 8 kPa (the volumetric exhaust steam flow amount in this case will be equal to  $9,945 \text{ m}^3/\text{s}$ ), transitioning from TC-6F30 to TC-6F32 (replacement of 760-mm buckets by 815-mm LSBs in three double-exhaust LP cylinders) reduces the exhaust losses by approximately 14.5 kJ/kg, which is equivalent to a gain in the turbine output of approximately 7.8 MW (see the flow chart diagram in Fig. 2-1).

When designing the last stages, it is especially important not only to obtain the high efficiency under the nominal (rated) operating conditions, minimizing the energy loss with the exit velocity. It is also necessary to ensure stable stage operation at reduced volumetric flow amounts, as well as to maintain the stage efficiency as high as possible under these variable conditions. Significant changes in the calculated steam flow patterns, as applied to the 1,450-mm LSB developed for Turboatom's series of 1,000-MW low-speed wet-steam turbines while operating under load in the range between 84% and 24% MCR, are shown in Figure 3-51. Under no-load operating conditions and minimal loads, these changes become even more significant with the appearance of reverse vortex motion in the tip and root sections, capturing even the nozzle row and the preceding stage blade (Fig. 3-52).



**Fig. 3-51.** Changes in a streamline pattern with variations in volumetric steam flow amount through the last stage

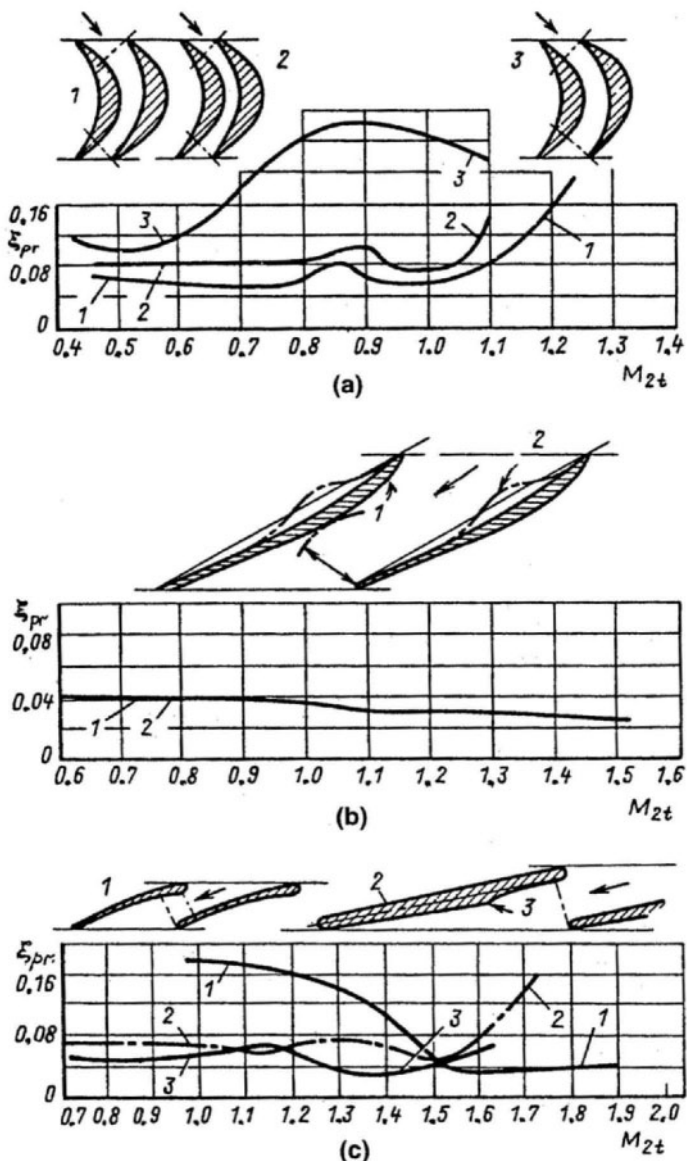
Source: Y. I. Shnee, Y. F. Kosyak, V. N. Ponomarev, et al.<sup>80</sup>



**Fig. 3-52.** Appearance of reverse vortex motion in the last two LP stages at low (14%) volumetric steam flow amount

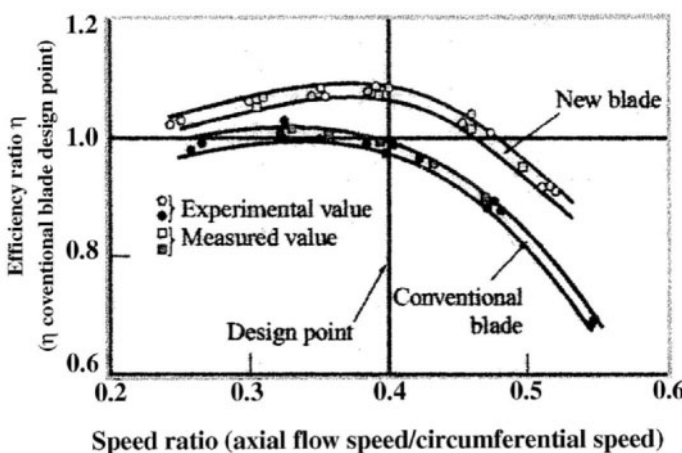
Source: A.V. Shcheglyev<sup>81</sup>

Besides the streamline pattern, with the steam flow amount there also change the ratios of the steam velocities to the current acoustic velocity, that is, the Mach numbers. Because the steam velocity diagrams, steam flow patterns, and Mach numbers essentially vary lengthwise of the stage height, the applied blading profiles also must be different for different sections. The diagrams shown in Figure 3-53 demonstrate the profile types proposed to obtain minimum profile losses in the wide range of Mach number values for the different LSB sections. Development of new, often nontraditional, profiles (especially for LSBs operating with high values of the Mach number and their sharp variations along the stage height) produces considerable gains in the stage efficiency, as seen, for example, in Figure 3-54, which compares the stage efficiencies for conventional and newly developed Hitachi LSBs with the length of 660 mm (26 in) for the rotation speed of 3,600 rpm.<sup>82</sup>



**Fig. 3-53.** Typical blade rows and dependencies of profile losses on Mach number for the LSB's root section (a) (1: row with convergent channels; 2: purely impulse blading; 3: row with divergent channels), mean section (b) (1: common row; 2: row with double-convex profiles), and tip section (c) (1: row with divergent channels and common profiles; 2: row with convergent channels and common profiles; 3: row with convergent channels and a ridge on the back of the profile)

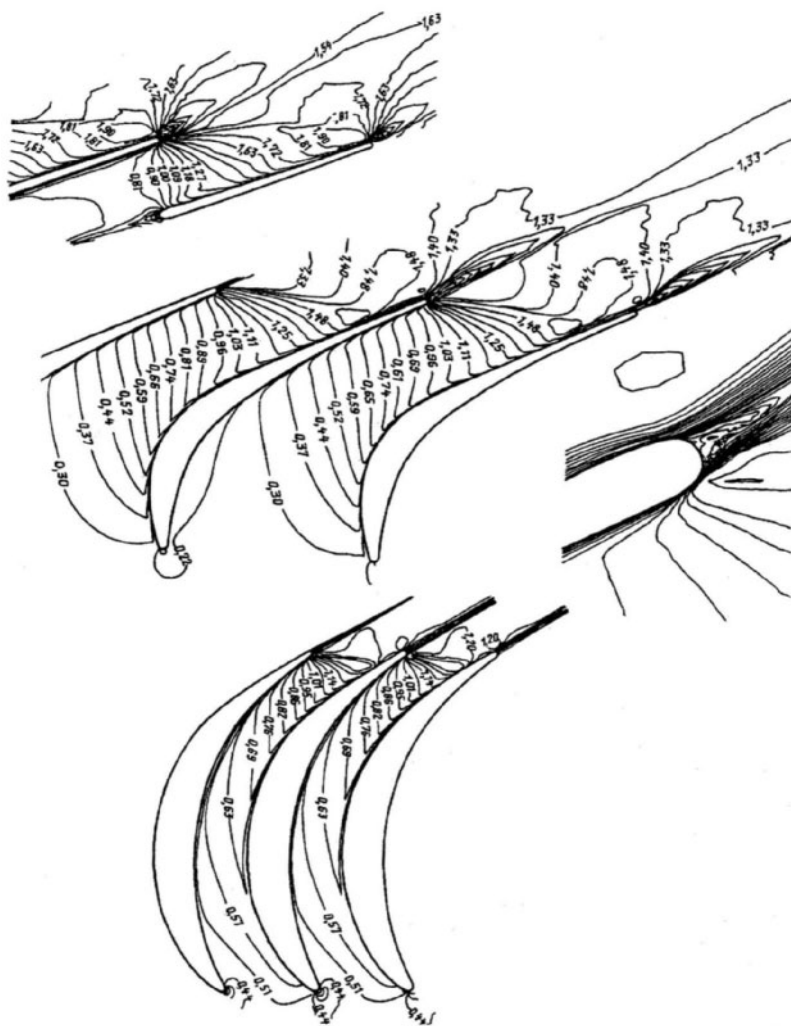
Source: A. V. Shcheglyayev<sup>83</sup>



**Fig. 3-54.** Comparison of stage efficiencies for conventional and newly developed, advanced Hitachi 26-in LSBs

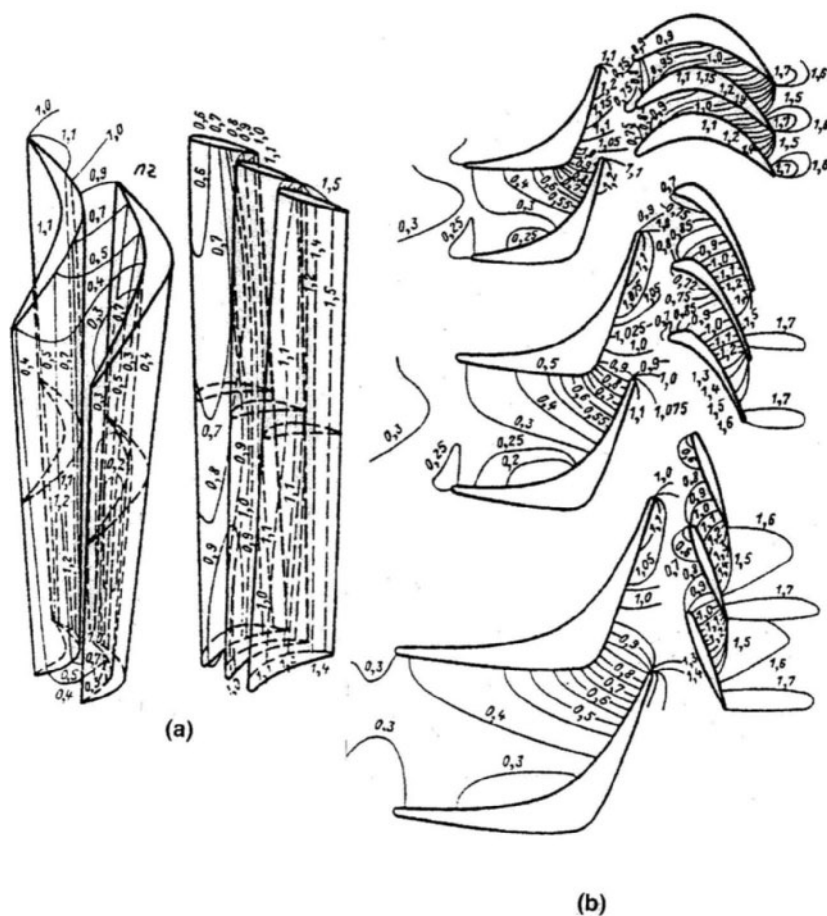
Source: M. Machida, H. Yoda, E. Saito, and K. Namura<sup>84</sup>

The world's leading turbine producers presently conduct 3-D aerodynamic calculations of LP steam paths with regard to the steam viscosity, taking into consideration the complex shape of the row profiles, the appearance of local supersonic velocities, and the wave phenomena that accompany them. Some computer programs have also been developed to solve the reverse problem—to obtain row profiles on the basis of the set stream lines and distribution of the steam flow conditions. Because of the extreme complexity of such a problem, all the applied approaches and computer programs unavoidably adopt some more or less serious assumptions. Nevertheless, they allow researchers and designers to obtain detailed space nets of meridional stream lines for the given boundary conditions, find lines of constant relative velocities,  $\lambda$  or  $M$ , (isotachs) and pressure values (isobars) for different sections, distribution of energy losses along the stage height, and so on. Three-dimensional computations also result in a field of velocities at the exit edge that lead to the possibility of optimizing the exit edge shape. The relative steam velocity fields for the tip, median, and root sections of a typical modern LSB are presented in Figure 3-55. Figure 3-56 illustrates some results of such calculations for the last LP stage of Turboatom's 1,000-MW low-speed turbines, and Figure 3-57 shows the isotach field for the LP steam path of three stages developed by MHI with 1,143 mm (45-in) titanium LSBs for the rotation speed of 3,600 rpm.



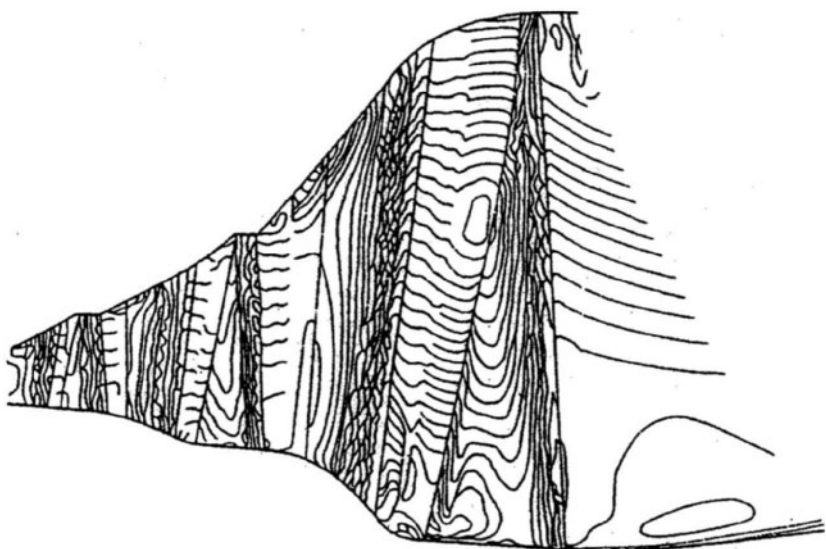
**Fig. 3-55.** Isotachs for the tip, median, and root sections of a typical modern LSB

Source: F. P. Borisov, M. Y. Ivanov, A. M. Karelkin, et al.<sup>85</sup>



**Fig. 3-56.** Isotach fields on the surfaces of the vane and bucket profiles (a) and in the interprofile channels (b) for the last stage of Turboatom's 1,000-MW low-speed turbine

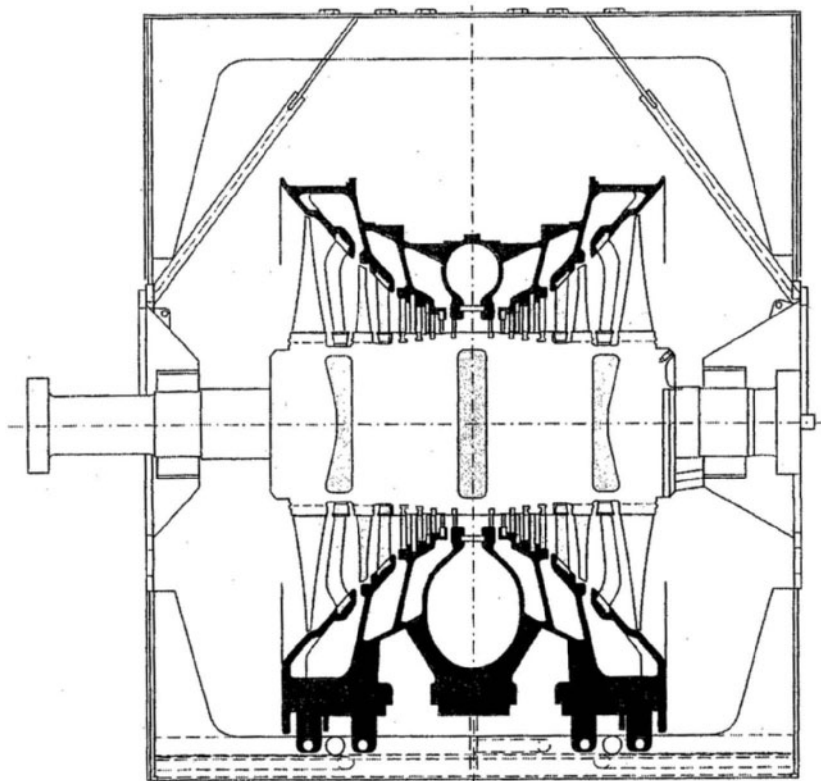
Source: A. V. Shcheglyayev<sup>86</sup>



**Fig. 3-57.** Calculated isotach field for the steam path of three last LP stages with 1,143-mm titanium LSB of MHI's 3,600-rpm turbine  
*Source:* By courtesy of Mitsubishi Heavy Industries

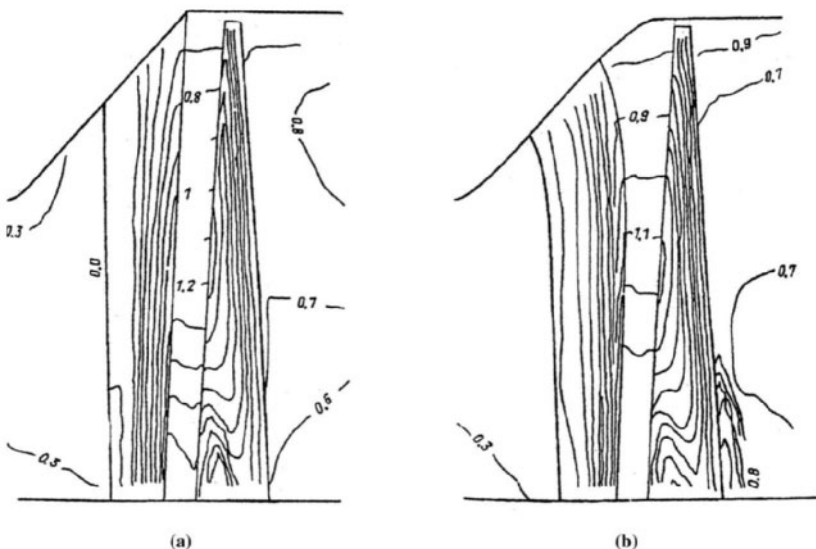
Vanes and buckets of axial turbine stages were traditionally configured radially; that is, the projection of the line through the centers of gravity of their profiles onto the plane perpendicular to the turbine axis was radial. Along with this, it has been known that some co-rotational incline of the vanes provides the steam flow with a favorable sweep in the root zone, increases the root reactivity, reduces the end (root) loss, and decreases the stage efficiency reduction when the steam flow amount varies. However, such an incline can be unfavorable for the peripheral stage sections. That is why, as long ago as the early 1960s, G.A. Filippov and Huang Chungchi of MEI proposed and investigated what they called saber-type vanes with a variable incline (that is, with the angle of inclination decreasing from the stage root to its outlying sections).<sup>87</sup> Currently, the inclined and curved (bowed) vanes and blades are widely used by almost all steam turbine manufacturers.<sup>88</sup> Analysis shows that the use of such blades is most effective in the last LP stages. Replacement of traditional (radial) blades and/or vanes by advanced, saber-type for these stages brings a great effect and is especially advisable at retrofitting the turbines in service.<sup>89</sup> Such an inclined and curved vane of the last LP stage developed by

ABB and its influence on the meridional steam flow stream lines are shown in Figure 2-25. An advanced LP cylinder with a last stage of this type is presented in Figure 3-58. The field of relative steam velocities (Mach numbers) for a similar last LP stage developed by LMZ for reconstructed and newly designed turbines is shown in Figure 3-59b. It can be seen that the use of saber-type vanes makes the steam velocity field more uniform as compared with a conventional stage (Fig. 3-59a). The resultant velocity field also favorably influences the exhaust port characteristics, thereby making it possible to exclude a local supersonic zone in the divergent section of the port, even with relatively high average Mach numbers.



**Fig. 3-58.** ABB's advanced LP cylinder with highly three-dimensional geometry in the last stage vanes

Source: A.P.Weiss<sup>90</sup>



**Fig. 3-59.** Isotach fields for the last LP stages of LMZ's newly designed and refurbished turbines with conventional (a) and saber-type (b) vanes

Source: F. P. Borisov, M. Y. Ivanov, A. M. Karelkin, et al.<sup>91</sup>

The rapidly increasing specific volume of the steam flowing in the LP steam path requires a sharp increase in the annular outlet area of the stages and leads to a large casing pitch angle. Modern large turbines, including wet-steam ones, feature high length-to-mean diameter ratios for the LSBs. The value of this ratio can be considered an indicator of the three-dimensionality for the steam flow through the last stage, as well as through the LP steam path as a whole. This ratio ( $l_2/d_2$ ) commonly varies in a range from 0.33 to 0.41 for modern high-speed turbines and from 0.31 to 0.37 for low-speed turbines. The higher the ratio value, the more complicated is the aerodynamic design of the steam path. For high-speed turbines with steel LSBs, in order to achieve the maximum annular exhaust area with regard to the limits for tensile stress, this ratio should be equal to approximately 0.35–0.4 (Fig. 3-39).

According to a classic approach to the LP cylinder design, the root (hub) diameters of the stages are either constant (as in Fig. 3-58) or slightly decrease toward the last stage (as in the cases with most of the previously mentioned turbines). In these cases and in situations with high values for the length-to-mean-diameter ratio for the LSBs, the peripheral stream line pitch angles can be as high as 60°. Under such circumstances, transition from a broken, piece-linear peripheral outline of the steam path

[Previous Page](#)

## 190 Wet-Steam Turbines for Nuclear Power Plants

to a conical meridional profile provides a noticeable gain in the local stage efficiency for the tip sections. This also refers to integrally shrouded rotating blades and requires a corresponding arrangement of the blade shrouds (Fig. 3-60).

Substantially lowering the stage hub diameter toward the last stage reduces the peripheral pitch angle, as shown in Figure 3-57. In this case, the designers increased the length-to-mean-diameter ratio for the LSBs up to the highest value of as much as 0.41 and even more.

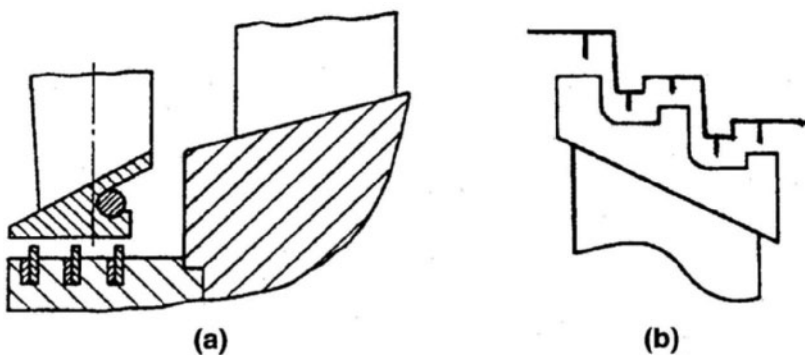


**Fig. 3-60.** Two different types of shrouds for LP stages with conical meridional profiles

### Last stage blade protection against WDE

The circumferential speed of modern steel LSBs used in high-speed turbines reaches 700 m/s ( $\approx 2,300$  ft/s) and can reach as much as 800–830 m/s (2,620–2,730 ft/s) for titanium LSBs (Tables 3-3 and 3-4). Even for low-speed turbines, the circumferential speeds reach 500–530 m/s (1,640–1,740 ft/s). Although the mean steam wetness at the LSBs is never more than about 12–14%, the local steam wetness at the stage periphery can be significantly greater and more dangerous, because the water drops are mainly concentrated in the tip region. The coarse-grained water, which presents the main threat of blade erosion, lags behind the steam stream and, as a result, impacts the blade back at the row inlet (see Fig. 2-17).

In order to protect steel LSBs against WDE, the blade surfaces are covered by Stellite laminas (shields or strips) brazed to the blade surface (Stellite is a cobalt-based, 60–65%, alloy also containing 25–28% chromium and 4–5% tungsten. It has a high hardness and a very high resistance to erosion wear).<sup>92</sup> The erosion resistance of Stellite exceeds that of stainless steel by 8–9 times and is 5–6 times higher compared with titanium alloys. Water drop erosion mainly affects the upper third of the LSB back near the leading (inlet) edge, and the Stellite laminas are attached only at this surface. This method is commonly used for steam turbines of both fossil fuel and nuclear power plants. Its disadvantage is that it creates some discontinuity in the blade profile, resulting in performance losses. In addition, during turbine operation, individual Stellite laminas sometimes break away from the blade surface, causing local abrasion of the blade profile, as well as changes in the blade's vibrational characteristics. Nevertheless, Stellite laminas have remained the most common measure of protecting steel blades against WDE.

However, the use of Stellite is unacceptable for turbines operating with radioactive steam, because cobalt is washed out of the Stellite and brought into the reactor, where it is activated and then is deposited on the equipment surfaces in the forms of various oxides. Because Co-60 has a relatively long half-life period, in this case all of the equipment pieces would have to be thoroughly deactivated before repairs could be attempted. These deactivation processes would take much time. For this reason, instead of covering with Stellite laminas, the blade surfaces are often hardened with electric-spark machining. (This method is also applied to the first stage blades of fossil fuel turbines to protect them against solid particle erosion.<sup>93</sup>) In the course of machining, numerous micro discharges between the blade surface and the electrode result in the electrode material being deposited on the blade surface. Because the applied electrodes contain ferrochrome, nickel-boron, or other erosion-resistant materials, they shape the layer of protective alloy on the blade surface. Another promising method of protecting the LSBs against WDE is coating them with clustered chromium.<sup>94</sup>

Instead of Stellite strips, the leading edges of steel blades can be protected by a welded bar-nose, which combines an erosion-resistant cobalt-free insert with a weld filler of Inconel® 82, which is a very

ductile material with high fracture toughness. This method has been well proven for years in plant operational practice, including English Electric's 1,060-MW wet-steam turbine at Fermi Unit 2 with BWR.<sup>95</sup> Welding allows complete restoration of the airfoil profile, leaving no surface discontinuity. The use of ductile weld filler also protects the blade parent material from crack propagation through the leading edge in the event of extensive water impact.

Titanium alloys are less prone to WDE than are stainless blade steels, even though titanium is inferior to Stellite in this regard. The first commercially employed titanium-alloy LSBs were originally protected by a nithinol coating, but long-term experience has proven the possibility of their use without antierosion protection.<sup>96</sup> Nevertheless, for the newest shrouded LSBs with tip circumferential speed of 700 m/s and more, it is recommended to protect the shroud and the very tip portion of the blade with an erosion shield made of Ti-15 Mo-5 Zr-3 Al, which is electron-beam welded to the leading edge. An example of such a shield is shown in Figure 3-61 as applied to Hitachi's 1,116-mm titanium LSB.<sup>97</sup> Although the operational experience for these titanium LSBs is not as long as that for conventional 12% Cr steel blades with Stellite protection, the first operational data match the predicted erosion rate for more than 120,000 operation hours (Fig. 3-62).

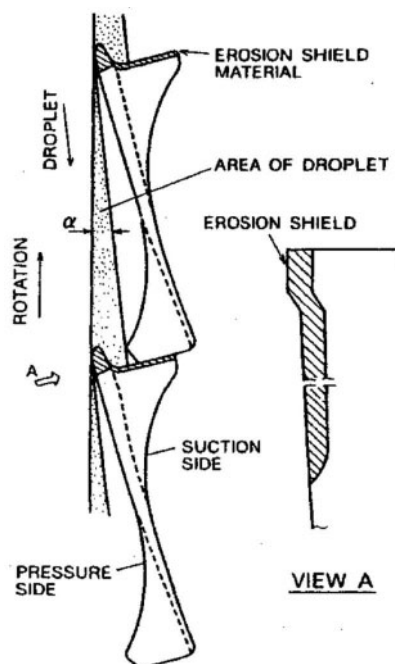


**Fig. 3-61.** Protection against WDE in the tip section and shroud of Toshiba's 1,016-mm titanium LSB

Source:T. Suzuki, M. Watanabe, and M.Aoyama<sup>98</sup>

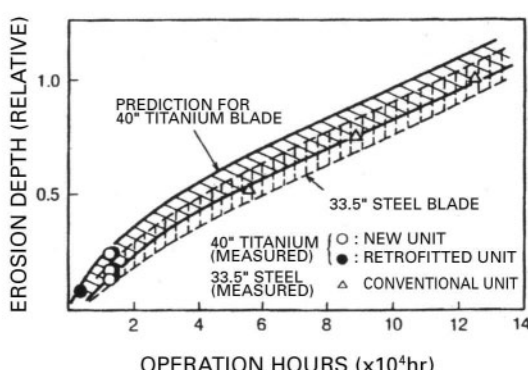


**Fig. 3-62.** Estimation of WDE for Toshiba's 1,016-mm titanium LSB

Source:T. Suzuki, M. Watanabe, and M.Aoyama<sup>99</sup>

The erosion rate at the leading edge of LSBs can also be influenced by certain design measures. For example, according to Toshiba,<sup>100</sup> the erosion rate noticeably reduces with an increase in the gap between the stationary and rotating blades, because this gives more space for the water drops leaving the nozzles from the steam flow. This effect was well confirmed by experiments on model turbines. The more effective the water separation and removal from the steam flow is, the less the erosion rate (as shown, for example, in Fig. 2-38c).

Along with the leading edge in the tip zone, LSBs also suffer from WDE at the trailing (outlet) edge in the lower (root) and median zones. This phenomenon is mainly stipulated by reverse motion of steam and vortices in the root stage portion under low-flow transient operating conditions (Fig. 3-52). These steam streams commonly bring large-sized water drops that erode the LSBs, especially their thin outlet edges. All of these unfavorable processes are additionally promoted by steam discharged into the condenser from the cold reheat and main steam-lines through the turbine steam bypasses, which come into operation exactly at low-flow transients. Sprays cool the discharged steam, and the resultant steam-water mixture is often injected by the reverse steam streams to the LSBs. That is why the correct location of these devices in the condenser port and the correct design of the turbine exhaust hood are so important.

## Water Removal from Turbines

For wet-steam turbines, with the large moisture content in the operating steam, it is desirable to remove as large a portion of this moisture from the steam flow as possible. Primarily, this is necessary to reduce the rate of erosion damage to the turbine components and secondarily to improve the blading efficiency. The water extraction devices employed in wet-steam turbines could be subdivided into two functional classes: 1) those designed to remove potentially hazardous water drops directly from the blade path and 2) more sophisticated separators intended to dry the steam flow altogether by removing the free water.<sup>101</sup> However, in practice, it seems more convenient and obvious to classify the water extraction devices not by their functional purposes, but by their designs. On this basis, it makes sense to consider separately two completely different methods of water separation and

removal: 1) internal—that is, directly from the steam path and 2) external, with the use of special MSRs placed outside (or, more accurately, beside or alongside) the turbine.<sup>102</sup> The measures for internal water extraction include devices of peripheral moisture separation and removal, intrachannel water extraction, and special stage separators.

### **Peripheral moisture separation and removal between the stage rows**

Some water is separated and removed from the steam path due to the circumferential component of the wet-steam motion—under action of centrifugal forces drawing the water drops out to the stage periphery. This separation takes place within the stages, in the gaps between the stationary and rotating blade rows. The separated water can be captured and gathered in water trap belts (as shown, for example, in Figure 2-26 as applied to the Turboatom K-220-44 turbine's HP cylinder), but the efficiency of this natural separation is not great. The separation efficiency,  $\psi$ , is defined as the ratio between the amount of the removed water and the total water contents in the steam flowing through the stage. Its value depends on the steam wetness, the steam velocity and circumferential rotation speed at the blade tip, the portion of the coarse-grained water drops in the wet steam flow, the shape, size, and location of the water-taking channels and water traps, as well as numerous other factors.

A major contributor to the moisture separation process is the centrifugation of water from the surface of the rotating blades (see Fig. 2-41). To intensify this process, turbine manufacturers such as GE, Hitachi, and Toshiba have sometimes furnished the rotating blades (mainly in the HP stages) with special lengthwise (radial) furrows on the back surface near the leading edge, which in this case is not covered by the shroud (Fig. 3-63). According to GE, based on their tests at Dresden Unit 1, such a design decision effectively prevents erosion of the blades in subsequent stages. The experimental data showing the separation efficiency for the furrowed rotating blades, as dependent on the steam pressure and wetness, are presented in Figure 3-64. Moisture removal can be additionally enhanced by suction of the steam-water mixture from the water trap chambers to the lower pressure steam chambers. An example of such a design decision with furrowed rotating blades and the water trap belts situated after the stationary blade rows is presented in Figure 3-63.

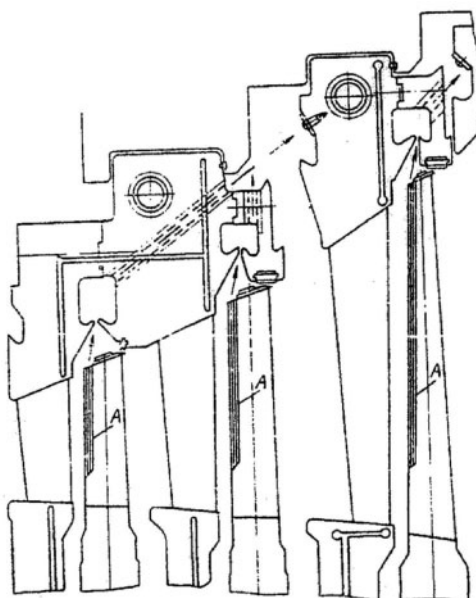


**Fig. 3-63.** LP stages with furrowed rotating blades and water traps between the nozzle and blade rows connected to the condenser (A: radial furrows on the back surface near the inlet edge)

Source: B. M. Troyanovskii<sup>103</sup>

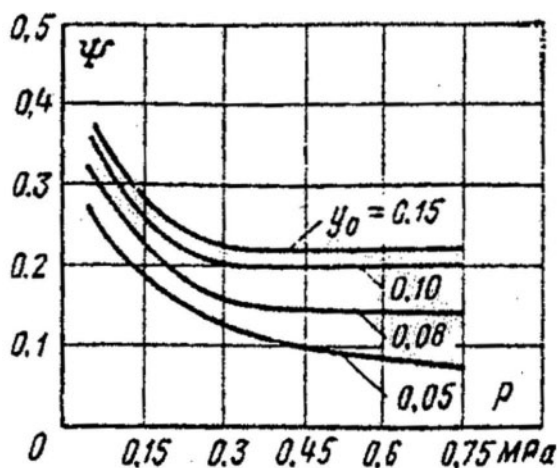


**Fig. 3-64.** GE experimental data on separation efficiency for furrowed rotating blades

Source: B. M. Troyanovskii<sup>104</sup>

Some turbine designers place the water trap belts between the stationary and rotating blades of the stage, as shown in Fig. 3-63; others prefer to position them after the rotating blade rows, as shown in Figure 3-65. The water amounts to be captured and removed come from three sources:

- $W_c$  — water that enters the stage from the preceding stages (having not been removed by their separation devices) and moves mainly along the peripheral side of the nozzle;
- $W_n$  — water that is deposited on the stationary blade surfaces and joins the  $W_c$  flow; and
- $W_r$  — water that is centrifuged by the rotating blades.

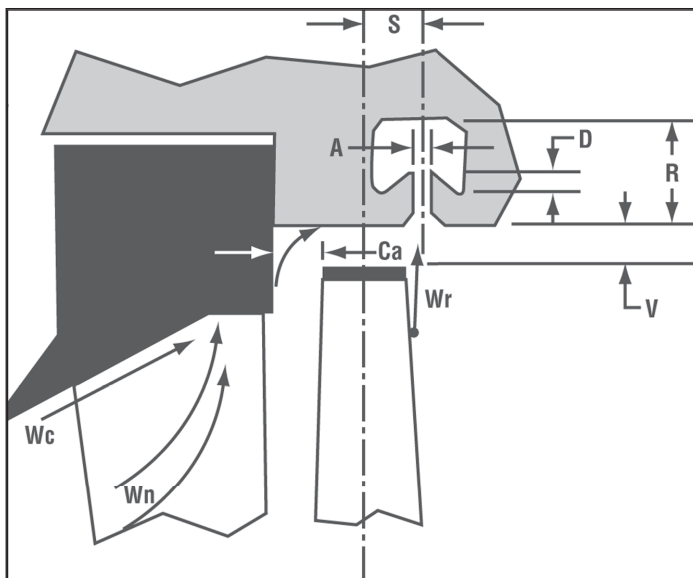


**Fig. 3-65.** Water trap positioned after the stage  
Source: W. P. Sanders<sup>105</sup>

All of the variables in Figure 3-65, characterizing the position, shape, and size of the water trap ( $Ca$ ,  $V$ ,  $S$ ,  $A$ ,  $D$ , and  $R$ ), are to be optimized to increase the separation efficiency. To capture more of the water flow ( $Wr$ ), it is rather advisable, as distinct from the picture of Figure 3-65, to have the meridional profile of the casing ring across

the rotating blades and near the water trap belt's inlet sloping and the trailing edge of the rotating blades overlapping both the shroud and the water trap belt's inlet edge. Positioning the water trap belt after the stage is also preferable for stages with unshrouded rotating blades.

Along with the captured water, the water trap belts also withdraw some amount of steam, usually estimated to be as much as 0.5% of the total steam flow through the stage. The energy of this steam can be utilized if the withdrawn water-steam mixture is forwarded into the regenerative feed-water heaters. The turbine's regular steam extraction chambers for steam bleedings also play a role of water traps. The HP steam path of an impulse-type low-speed wet-steam turbine with the water trap belts located after the rotating blade rows and connected to the lower pressure steam bleedings is shown in Figure 3-66.

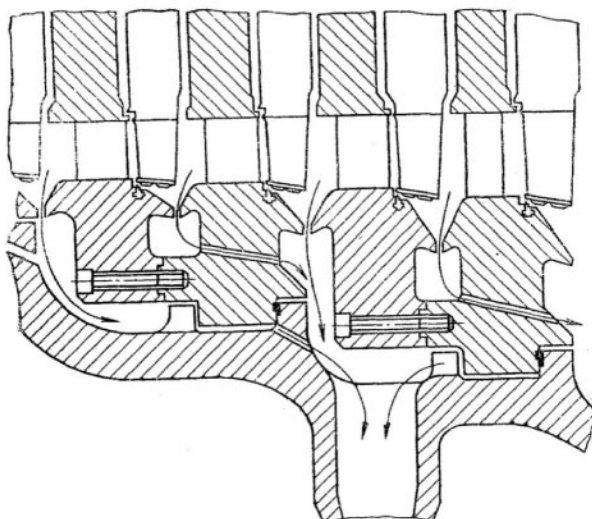


**Fig. 3-66.** Water removal from HP steam path of an impulse-type wet-steam turbine

Source: B. M. Troyanovskii<sup>106</sup>

Open chambers of the water trap belts such as those shown in Figures 3-63 and 3-65 slightly impair the aerodynamic properties of the steam path and increase the energy losses. For these reasons, some

researchers propose not using these chambers (apart from those used for steam bleedings) and substitute them with specially fluted surfaces above the rotating blades for the deposition and subsequent removal of water. A possible appearance of such a surface-type water trap is shown in Figure 3-67. The captured water is to be gathered and drained from the casing ring.

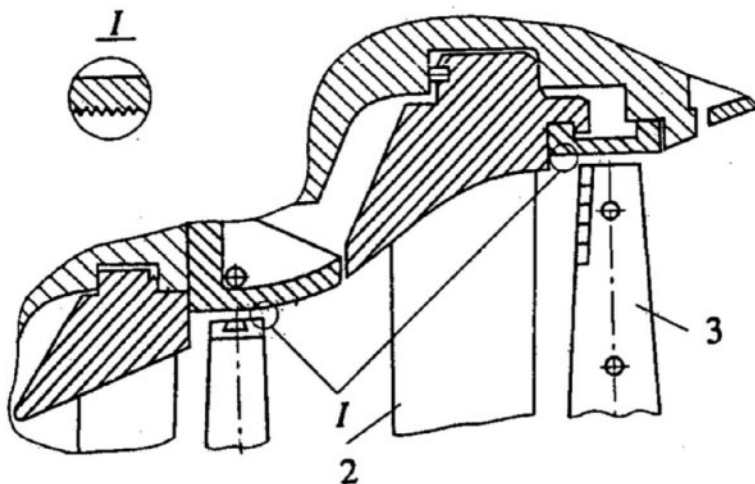


**Fig. 3-67.** Possible design for a surface-type water trap for LP steam path  
Source: I. I. Kirillov and G.G. Shpenzer<sup>107</sup>

### Intrachannel moisture separation

The diaphragms of the last and next-to-last LP stages of modern wet-steam turbines are often made with hollow nozzle vanes, which are either stamped and welded, or solid and drilled (Figs. 3-68 and 3-69). Apertures or slots connect the nozzle surface with the internal vane space, the ends of which are drained to the turbine condenser. As a result, the water film is withdrawn from the nozzle surface instead of being pulverized into drops and eroding the subsequent rotating blades.

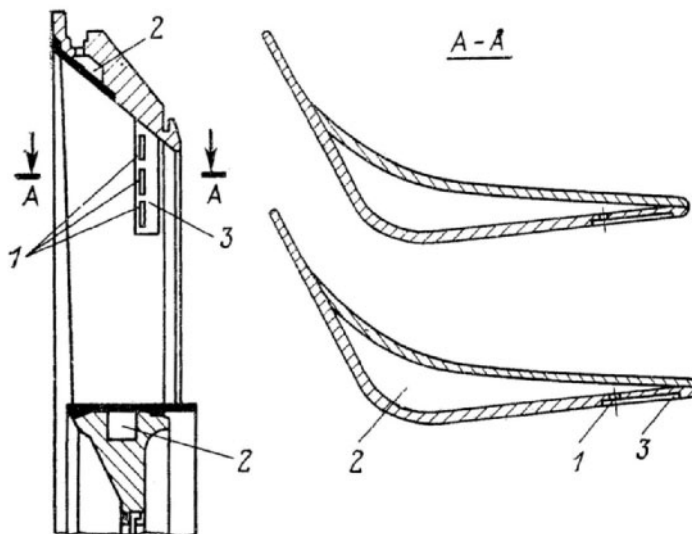


**Fig. 3-68.** Turboatom's hollow stationary blades with intrachannel water removal (1: water-taking apertures; 2: water-taking internal channels; 3: suction slots)

Source: B. M. Troyanovskii, Y. F. Kosyak, M. A. Virchenko, et al.<sup>108</sup>

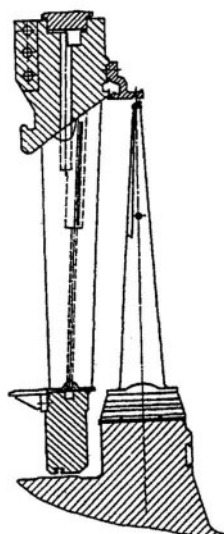


**Fig. 3-69.** Typical last stage of LMZ with intrachannel water separation and removal

Source: I. I. Pichugin, A. M. Tsvetkov, and M. S. Simkin<sup>109</sup>

Different designers locate the water-taking suction slots in different areas of the nozzle surface: on the back surface near the inlet, on the face surface where the steam flow turns (see Figs. 3-68 and 3-69), directly in the exit (trailing) edge, and so on. To increase the separation efficiency, it is reasonable to have at least two slots in different areas. Under conditions of common internal space of the vane, to avoid water being pumped from one slot to another, these slots should be located at places on the nozzle surface with equal steam pressure. For example, in Figure 3-70, the suction slot pairs could be positioned at points 1 and 2 or 3 and 4 along the nozzle profile. Suction slots on the back and face surfaces of the nozzle vane can be seen in Figure 3-71, as applied to Toshiba's 1,016-mm (40-in) titanium LSB (similar to points 3 and 4 in Fig. 3-70). The combined influence of peripheral and intrachannel water separation and removal on the blade erosion rate is shown in Figure 2-38c. The intrachannel water extraction decreases the relative erosion rate by as much as a factor of two, and additional peripheral water extraction with an increased distance between the stationary and rotating blades further decreases this rate by another 0.1–0.2.

The separation efficiency of the intrachannel water removal also significantly depends on the amount of steam withdrawn along with the water—the separation efficiency increases with the steam amount until a certain threshold, and then remains almost invariable. The quantitative characteristics of these dependencies substantially change with the shape of the suction slots and their position on the nozzle surface.

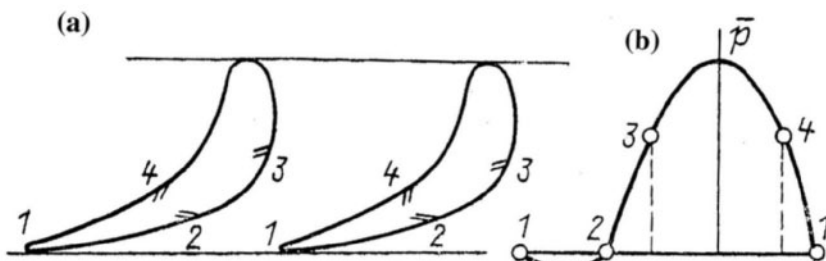


**Fig. 3-70.** Possible position of suction slots for intrachannel water removal (a) and distribution of specific steam pressure along the vane profile (b)  
Source: V.I. Kiryukhin, G.A. Filippov, O.A. Povarov, and V.I. Dikarev<sup>110</sup>

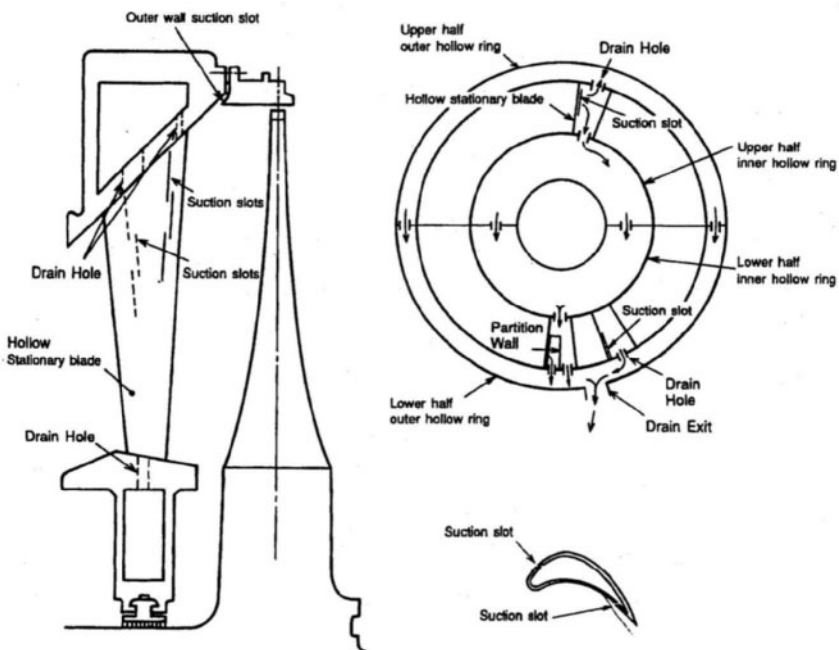


**Fig. 3-71.** Toshiba's last stage with intrachannel water separation and removal

Source: T. Sakamoto, S. Nagao, and T. Tanuma<sup>111</sup>

The water separation factor,  $\psi$ , for hollow nozzle vanes with intrachannel moisture separation can be estimated with the use of a diagram shown in Figure 3-72 as a function of the steam pressure at the stage inlet,  $p_0$ , and the Mach number for the midsection exit of the nozzle row,  $M_1 = (c_1/a_1)_m$ . It is assumed that the nozzles have two suction holes with a slot width of approximately 0.7–0.9 mm (28–36 mil): on the profile back and in the trailing edge (points 1 and 2 in Fig. 3-70) along the entire vane height for relatively short stages or in the upper third or half of the stage height for relatively long stages ( $l/d_m > 0.17$ ). There are many other factors influencing the separation efficiency (such as the geometric forms of the nozzle vanes and the slot, the moisture dispersion, the velocity ratio, the Reynolds number, and so on), but they can be considered only as applied to the actual geometry and operating conditions of specific stages.

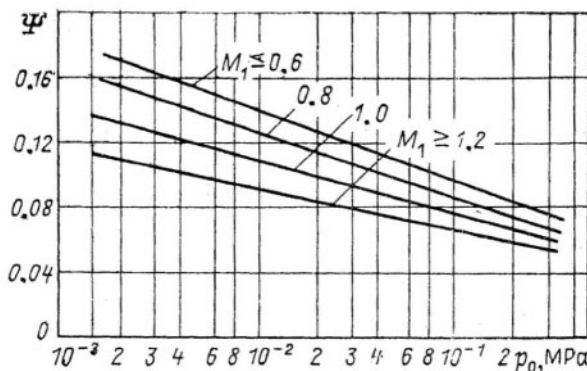


**Fig. 3-72.** Estimation of the water separation factor for hollow nozzle vanes with two suction slots

Source: B. M. Troyanovskii, G. A. Filippov, and A. E. Bulkin<sup>112</sup>

The LP steam path of a Siemens low-speed (1,500 rpm) wet-steam turbine, with a 1,365-mm (54-in) LSB and intrachannel water removal from the last stage nozzle surfaces, is shown in Figure 3-73. In addition to (or instead of) the intrachannel water removal, for cases with very high erosion coefficients, Siemens also has proposed heating the last LP stage stationary nozzle vanes with steam taken from one of the LP steam extractions (Fig. 3-74).

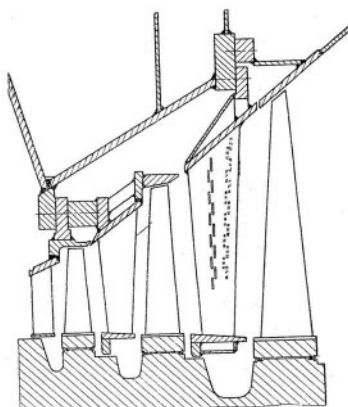


**Fig. 3-73.** Steam path of Siemens' low-speed wet-steam turbine with water removal from last stage nozzle surfaces

Source: B. M. Troyanovskii<sup>113</sup>

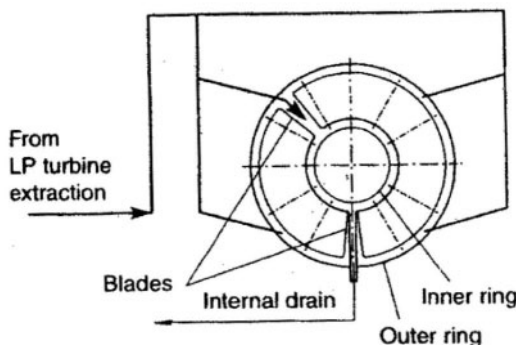


**Fig. 3-74.** Heating hollow nozzle vanes for the last stages of Siemens' turbines

Source: H. Oeynhausen, G. Roettger, J. Ewald, et al.<sup>114</sup>

### Moisture separating stages, or stage-separators

The quest for more effective water separation in the blade rows has led to the creation of special moisture separating stages, or moisture stage-separators (MSSs), which have been proposed at the Moscow Power Engineering Institute (MEI).<sup>115</sup> Some of the previously mentioned turbine stages do have a somewhat increased separation capacity thanks to certain design features such as radial furrows and a shortened shroud of the rotating blades (Fig. 3-63). Nevertheless, these stages do not differ in principle from the adjacent ones. The specially designed MSSs provide increased separation efficiency at the expense of the stage efficiency. In the ultimate scenario, MSSs do not produce any useful work at all and can be completely removed from the turbine, resting on independent bearings. In this case, such an MSS, called a rotor-type separator, turns into an external MSR.

An MSS, if it remains in the steam path along with the other, “regular” stages, features a low enthalpy drop, an increased axial clearance between the nozzle and blade rows, a low pitch-to-chord ratio for the rotating blade rows, and special profiling and machining of both the stationary and rotating blades. Some results of experimental investigations for a few different types of MSSs are presented in Figure 3-75. In the experiments, it was found that the moisture separation efficiency varies differently with the speed to velocity ratio,  $u/c_0$ , for chambers positioned across the leading (inlet) or trailing (outlet) edges of the rotating blades. The total separation efficiency (for both the chambers), however, remains virtually invariable, accounting to over 60%.

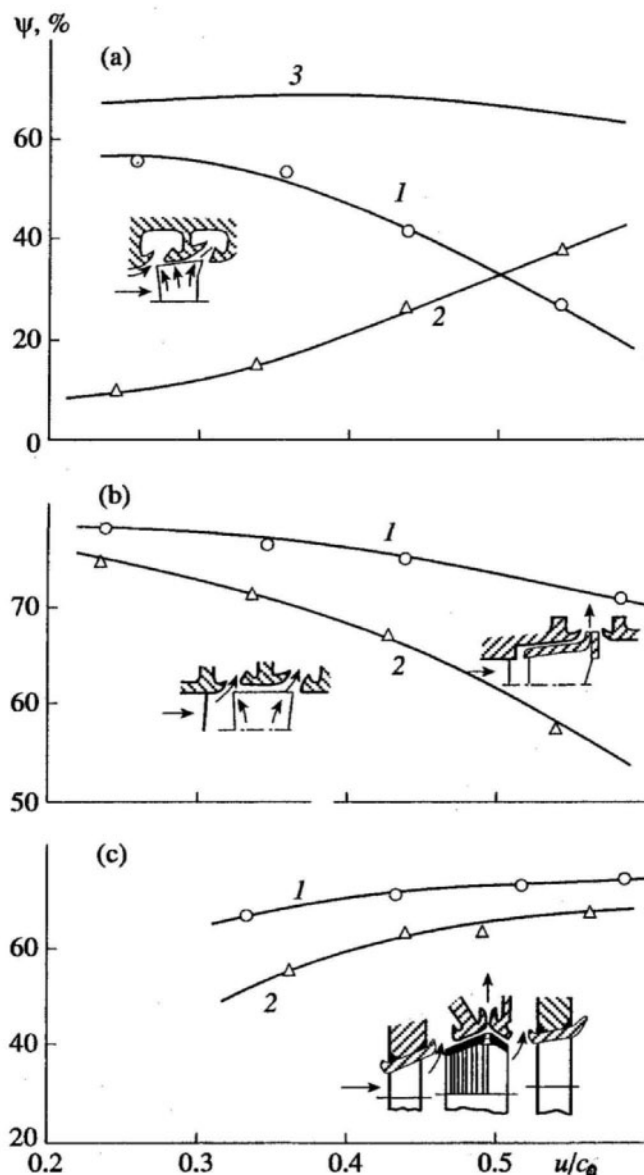


**Fig. 3-75.** Efficiency of moisture removal for different types of MSSs depending on the speed-to-velocity ratio,  $u/c_0$  (1: for the chamber across the leading edge of the rotating blades; 2: for the chamber across the trailing edge of the rotating blades; 3: total for both chambers)

Source: V.I. Kiryukhin, G.A. Filippov, and O. I. Nazarov<sup>116</sup>

MSSs can be designed either unshrouded or with a specially drilled roof-shaped shroud (Fig. 3-75c). The separation efficiency of MSSs in the power plant conditions was investigated at several turbines manufactured by Kaluga Turbine Works to drive the feed water pumps of nuclear power units with VVER-1000 reactors. The MSSs, made of titanium alloy, replaced the seventh stages in the turbines. The driving turbines have 450-mm (17.7-in) LSBs made of 13% Cr steel with the tip circumferential speed of up to 339 m/s (1,111 ft/s). The flow path has an advanced system of peripheral separation, and the diaphragms of the last two (ninth and tenth) stages are made hollow, with intrachannel water separation. Eight turbines operated in total for more than 70,000 combined hours with the seventh stages replaced by the MSSs. The rate of erosion in the LSBs for these turbines was about 2.5 times lower than that for similar turbines without the MSSs. The MSSs themselves were not affected by erosion.

## External moisture separators and reheaters

Almost all modern wet-steam turbines are equipped with external MSRs, which are usually combined in common vessels, two or four MSRs per turbine. The MSRs are located after the turbine's HP cylinder (section), before the IP section (if it exists) or the LP cylinders. Strictly speaking, external MSRs are not a portion of wet-steam turbines themselves, but rather represent a kind of turbine auxiliaries—along with the condenser, feed-water heaters, and so on—and so are not considered here in detail. More thorough information about external MSRs can be found in various sources.

Traditional external MSRs are made up of three parts: 1) an outer shell (a cylindrical vessel, often with formed heads welded to each end), 2) the moisture separator's packing, (usually with chevron plates, or merely *chevrons*, which are also called *louverplated* or *corrugated-plate separator*, or knitted wire mesh, which is also called a *demister*), and 3) one or more tube bundles for reheating the working (cycle) steam by the heating steam of a higher pressure. Different versions of MSRs have been designed with heating steam flowing either within the tubes or between them. Steam for reheating is commonly taken from the main steam-lines. For wet-steam turbines with two-stage steam reheat, the first stage is fed with the heating steam taken from the HP cylinder (see Fig. 2-1).

As a rule, both the separating and reheating surfaces of the MSR are composed as separate modules to make their replacement easier. Some turbine producers (for example, ALSTOM, GE, Hitachi, MHI, and Westinghouse) use horizontal MSRs exclusively (Figs. 3-3, 3-10b, and 3-12b). Other manufacturers (such as Turboatom) prefer vertical MSRs (Fig. 3-27b). Some use both types, such as Siemens (Figs. 3-9 and 3-76). Vertical MSRs appear to be more compact, although in some cases, especially for single-circuit nuclear power units with hermetically sealed turbines boxes, it is difficult to fit large vertical MSRs in the turbine enclosure.

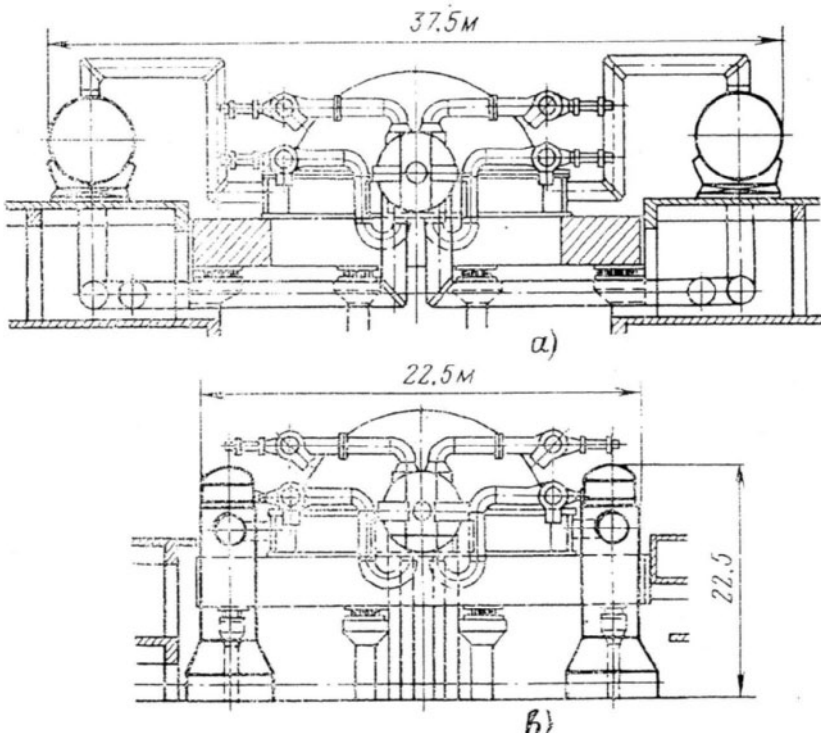


**Fig. 3-76.** Front views of Siemens' 1,200-MW wet-steam turbines with horizontal (a) and vertical (b) MSRs  
*Source:* By courtesy of Siemens Power Generation

Both types of traditional external MSRs (with chevron plates and knitted wire mesh) can be called inertial separators, because it is just the inertia of water drops that prevents the water from following the steam streamlines. As the steam-water flow passes through the separator's chevron plates or knitted wire mesh, the moisture particles drop out of the flow, and the impinged water then passes to the feed water system through drains. The separation efficiency improves with the increase of water drop size and steam velocity and with the decrease in the size of the collection elements (mesh or chevrons). For the knitted wire mesh, this size is determined by the wire diameter, which is about 0.1 mm (4 mil), and for chevron plates, the effective element size is equal to a half corrugation wavelength, which is normally not less than 10 mm (0.4 in). With increasing steam velocity, a breakthrough point is reached at which the deposited water is ejected by the steam flow again. This breakthrough velocity for the knitted wire mesh is significantly less than that for the chevron plates.

A principle scheme of horizontal MSR developed by Westinghouse is presented in Figure 3-77. It is considered to be the third MSR generation.<sup>117</sup> The first-generation MSR had a demister section of stainless steel wire mesh. While mesh is able to effectively remove moisture, large areas placed in a horizontal configuration are needed. Because of this, meshes were replaced by vertical chevrons in second-generation MSR designs, allowing 45% more steam to pass through the unit. Third-generation units shown in Figure 3-77 were actually made up of two second-generation MSRs connected by a common inlet section. To improve the thermal cycle efficiency, two-stage steam reheat was used instead of single-stage reheat. The working steam from the HP cylinder exhausts passes to the MSR's steam inlet manifold and is directed to the chevron plate separators (Fig. 3-78). The dried saturated steam passes over the outside of low-profile, integrally finned tubes. The heated steam leaves the MSR through outlets on top of the vessel and flows into the LP cylinders.

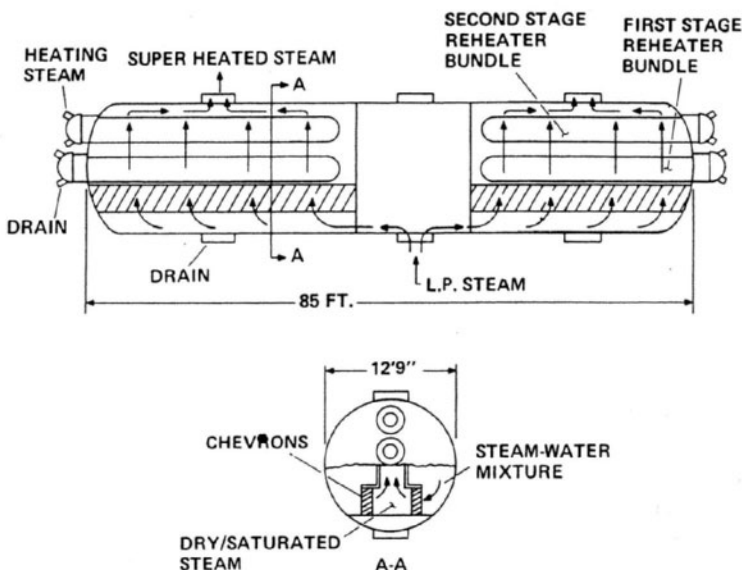


**Fig. 3-77.** Principle schematic of Westinghouse's third-generation MSR  
 Source: R. L. Coit, P. D. Ritland, T. F. Rabas, and P.W. Viscovich<sup>118</sup>

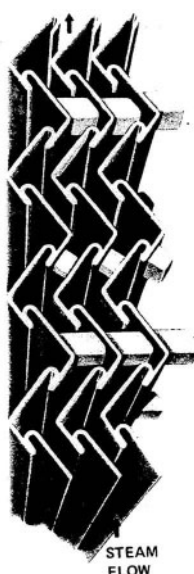


**Fig. 3-78.** Part of a chevron-plate separator  
 Source: R. L. Coit, P. D. Ritland, T. F. Rabas, and P.W. Viscovich<sup>119</sup>

Other turbine producers went through similar design stages. Therewith, MSRs of different manufacturers and even of the same manufacturer but different generations may differ significantly in the arrangement of the steam and water flows and packing of the internal space. By way of illustration, Figure 3-79 demonstrates two types of horizontal MSRs developed by Stein Industrie for French nuclear power units with individual capacities of 1,000 and 1,350 MW. Vertical MSRs also feature many different designs. Figure 3-80 shows a vertical MSR developed for Turboatom's K-220-44 turbines (Figs. 3-4 and 3-6). Figure 3-81 depicts another vertical MSR used in Siemens' 1,300-MW turbines.

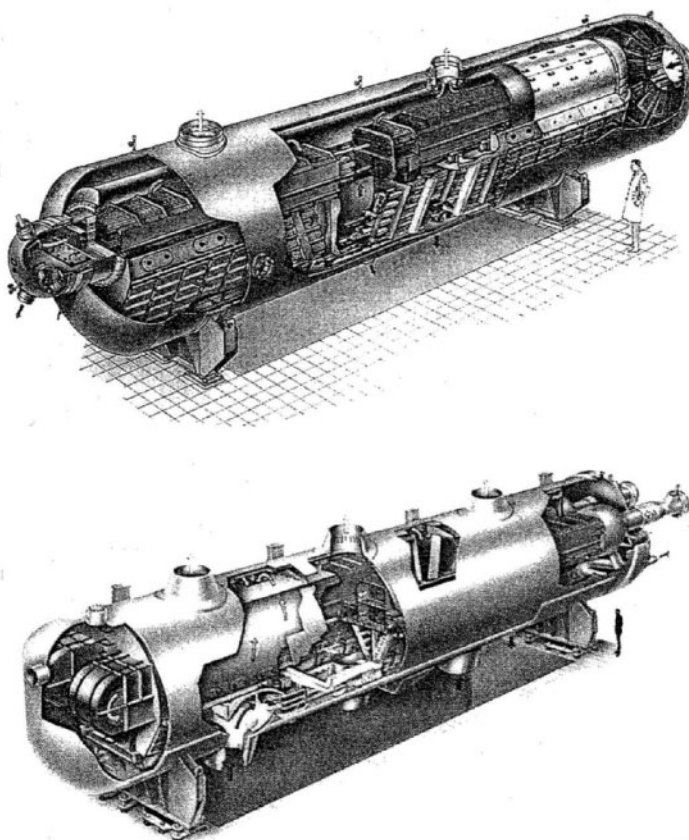


**Fig. 3-79.** Stein Industrie's horizontal MSRs for French nuclear power units of 1,000-MW and 1,350-MW output  
Source: J. C. Franc and D. Gilchrist<sup>120</sup>

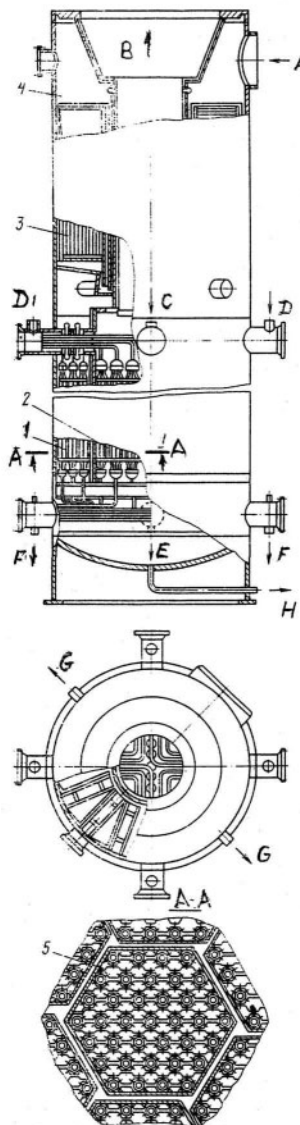


**Fig. 3-80.** Vertical MSR for Turboatom's K-220-44 turbines (1: first steam reheater stage; 2: second steam reheater stage; 3: separator; 4: steam distribution chamber; 5: steam reheater's tube assembly; A: working steam inlet; B: superheated steam outlet; C: heated steam supply for the first steam reheater stage; D: heated steam supply for the second steam reheater stage; E: heated steam condensate outlet from the first steam reheater stage; F: heated steam condensate outlet from the second steam reheater stage; G: separated water outlet; H: drain)

Source: By courtesy of Turboatom

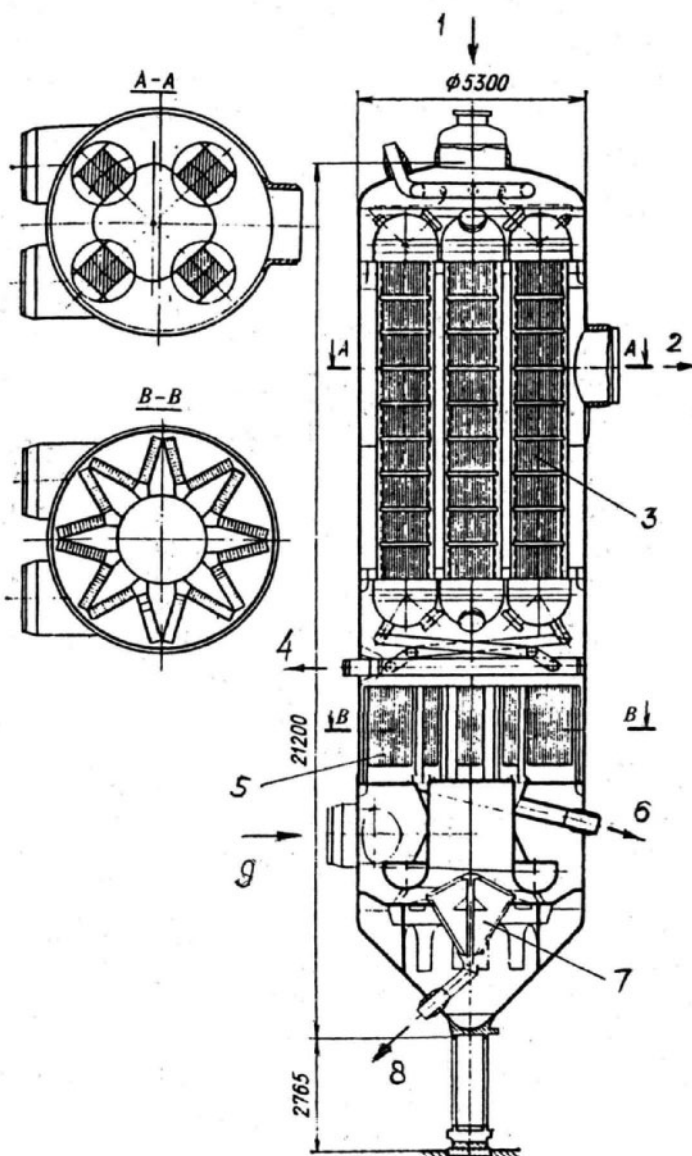


**Fig. 3-81.** One of two vertical MSRs for Siemens' 1,300-MW wet-steam turbines (1: working steam inlet; 2: superheated steam outlet; 3: steam reheat coil; 4: heated steam condensate outlet from steam reheat coil; 5: separator's modules; 6: separated water outlet; 7: preseparator; 8: drain; 9: working steam inlet)  
*Source:* By courtesy of Siemens Power Generation

Designers always quest to make their MSRs more compact. Hitachi, for example, reduced the overall length of its horizontal MSRs by 28% by means of increasing the steam flow velocities in the MSR reheater tubes and removing the drain tanks from the MSR shell.<sup>121</sup>

Some turbine and MSR manufacturers have experimented with different nontraditional design decisions for moisture separation. In 1989, ABB developed and tested a new MSR system built in the LP crossover pipes between the HP and LP cylinders. This system was implemented at several nuclear power units with the outputs ranging from 720 to 1,100 MW (Fig. 3-82).<sup>122</sup> This system consisted of four moisture preseparators (MOPSSs), one at each HP turbine exhaust, mainly separating the moisture flowing along the turbine walls, and special cross-under pipe separators (SCRUPS) installed in the cross-over pipe elbows after the MOPSSs. The main SCRUPS components are turning vanes installed in the internal chamber at the 90° elbows. In particular, the system was installed and tested at the Swiss nuclear power plant Leibstadt. The steam quality was measured using the sodium tracer method. These tests showed a separation efficiency of approximately 97% downstream of the SCRUPS and verified the predicted performance of the system. In eight of 10 other nuclear power units, measurements showed total separation efficiencies of more than 98%, with decreases in the pressure drop along the crossover (cross under) pipes. Observed increases in turbine output varied from 3 to 10 MW. In all cases, the installation of the MOPS/SCRUPS system significantly reduced erosion-corrosion effects in the crossover pipes and the separators themselves. At the Swiss nuclear power plant Mühleberg, the wear on these carbon steel components decreased from 95 kg/yr to 3.1 kg/yr. Nevertheless, this system has not found wide acceptance.

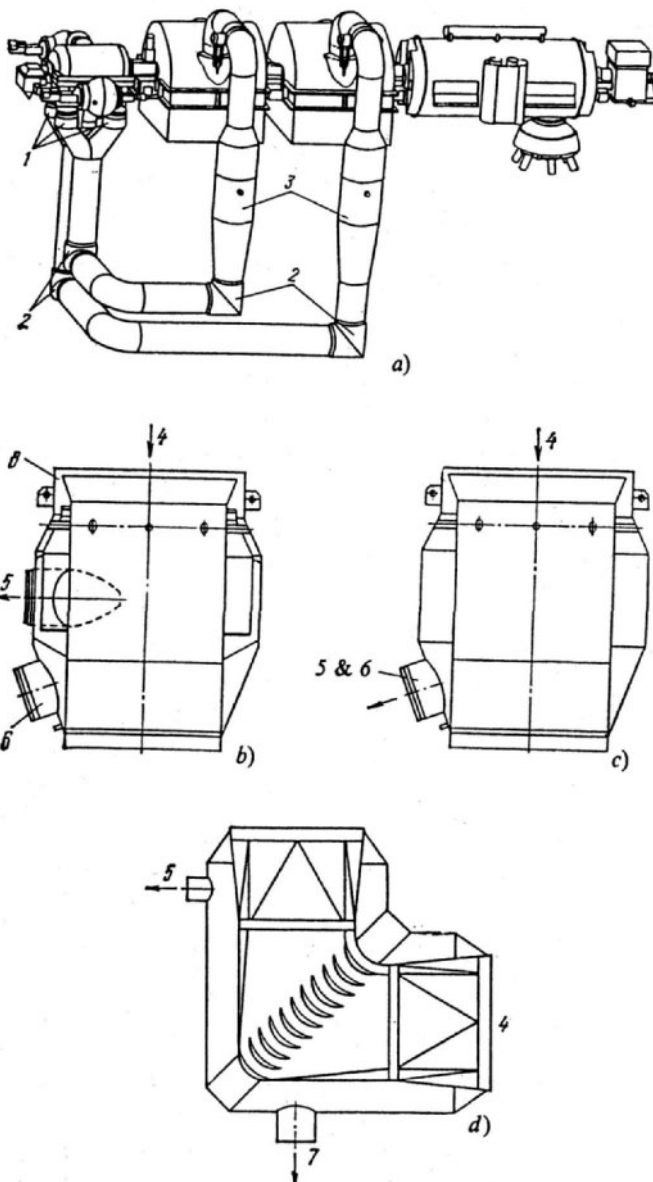


**Fig. 3-82.** (a) General view of ABB's three-cylinder wet-steam turbine with "distributed" MSR system (a) (1: preseparators; 2: separators at the crossover pipe elbows; 3: steam reheaters); (b) preseparator with phase separation; (c) preseparator without phase separation; (d) separator (4: working steam flow; 5: steam extraction to feed water heater; 6: separated water extraction; 7: drain)

Source: P. von Boeckh, M. Stiefel, and U. Frick<sup>123</sup>

Centrifugal-type devices called high-velocity separators (HVS) were developed and implemented at several French nuclear power plants by EdF in collaboration with Stein Industrie.<sup>124</sup> The main advantage of these MSRs is a ten-fold reduction in size compared to common chevron-plate separators due to much higher steam velocities—up to 50 m/s. However, the same circumstance, that is, the smaller size, causes larger pressure drops in HVSs, which is its main disadvantage.

Scientists of MEI investigated different kinds of external *turbo separators* with different types of rotating elements settled in the crossover pipes between the HP and LP sections.<sup>125</sup> Extensive experimental research was conducted to analyze the separation efficiency of external turbo separators, and many design improvements were developed to increase their effectiveness.

## References

- 1 International Atomic Energy Agency. 2001. *Operating Experience with Nuclear Power Stations in Member States in 2000* Vienna: International Atomic Energy Agency.
- 2 Stanley, W. 1969. The impact of changing economics on electric utilities *Proceedings of the American Power Conference* 31: 7-16.
- 3 Moriya, K., M. Ohtsuka, M. Aoyama, and M. Matsuura. 2001. Development study of nuclear power plants for the 21st century. *Hitachi Review* 50 (3): 61-67.
- 4 Leyzerovich, A. 1997. *Large Power Steam Turbines: Design & Operation*, Vols. 1-2. Tulsa, OK: PennWell Publishing, 1997.
- 5 Troyanovskii, B. M. 1978. *Turbines for Nuclear Power Plants*, 2d ed. (in Russian). Moscow: Energiya, 1978.
- 6 1997. *Arabelle—A World Record. Chooz B Power Station, France. 2×1531 MW*. Paris: ALSTOM, 1997.
- 7 Leyzerovich, *Large Power Steam Turbines*.
- 8 Drahy, J. 1976. Progress in steam turbine field of Shkoda (in Czech). *Shkoda Review* 1976, no. 11: 19-30.
- 9 Levchenko, E. V. 1995. Steam turbines manufactured by Turboatom NPO, their specifics, and ways of improving them. *Thermal Engineering* 42 (1): 13-20.
- 10 Troyanovskii, *Turbines for Nuclear Power Plants*.
- 11 Leyzerovich, *Large Power Steam Turbines*
- 12 Petrenya, Y. K., L. A. Khomenok, I. A. Kovalev, and Y. Y. Kachuriner. 2003. Prospects for the development of high-speed steam-turbine installations for nuclear power-generating units with a capacity of 1500 MW and higher. *Thermal Engineering* 50 (2): 112-119.
- 13 Pichugin, I. I., Y. N. Nezhentsev, and B. M. Troyanovskii. 1990. Development of a low-pressure cylinder of increased throughout for large steam turbines. *Thermal Engineering* 37 (5): 225-230.
- 14 Kosyak, Y. F. 1978. Development by Turboatom of turbine construction for nuclear power plants. *Thermal Engineering* 34 (8): 405-408.
- 15 Bannister, R. L., and G. J. Silvestri, Jr. 1989. The evolution of central station steam turbines. *Mechanical Engineering* 111 (2): 70-78.
- 16 Jacobsen, G., H. Oeynhausen, and H. Termuehlen. 1991. Advanced LP turbine installation at 1300 MW nuclear power station Unterweser. *Proceedings of the American Power Conference* 53: 991-1001.
- 17 Ibid.
- 18 2004. Site work underway on Finland's 1600 MWe EPR. *Modern Power Systems* 24 (3): 30-34.

- 19 Harris, F. R. 1984. The Parsons centenary—A hundred years of steam turbines. *Proceedings of the Institute of Mechanical Engineers* 198A(9): 183–224.
- 20 Spalthoff, F. J., H. Haas, and F. Heinrichs. 1976. First year of operation of the world's largest tandem compound turbine-generator. *Proceedings of the American Power Conference* 38: 555–569.
- 21 Troyanovskii, *Turbines for Nuclear Power Plants*.
- 22 Gyarmathy, G. 1990. Innovation and tradition in steam turbine engineering. *Proceedings of the Institute of Mechanical Engineers, Part A: Journal of Power and Energy* 204: 217–231.
- 23 Hesketh, J. A., and J. Muscroft. 1990. Steam turbine generators for Sizewell 'B' nuclear power station. *Proceedings of the Institute of Mechanical Engineers* 204 (Ser. A3): 183–191.
- 24 Kosyak, Y. F. 1978. Development by Turboatom of turbine construction for nuclear power plants, 405–408.
- 25 Levchenko, E. V. 1995. Steam turbines manufactured by Turboatom NPO, their specifics, and ways of improving them, 13–20.
- 26 Ogurtsov, A. P., V. K. Ryzhkov, Y. N. Nezhentsev, and L. Y. Bal'va. 1981. Steam turbines of LMZ for nuclear power industry. *Thermal Engineering* 28 (9): 497–504.
- 27 Kosyak, Y. F., M. A. Virchenko, V. P. Sukhinin, et al. 1980. The problem of selecting speed of turbines for nuclear power stations. *Thermal Engineering* 27 (5): 256–259.
- 28 Buzulukov, V. A., M. G. Teplitskii, A. A. Maksimenko, and T. V. Poruchinskii. 1989. Full-scale testing of the KhTZ K-1000-60/1500-2 turbine plant at Zaporozhe nuclear power station. *Thermal Engineering* 36 (2): 69–75.
- 29 Kosyak, Y. F., M. A. Virchenko, V. A. Matveenko, et al. 1985. Turbine plants with noncontrolled pressure in the extractions for combined generation of power and heat. *Thermal Engineering* 32 (7): 359–365.
- 30 Arkad'ev, B. A. 1986. *Operating Conditions of Steam Turbosets for Nuclear Power Plants* (in Russian). Moscow: Energoatomizdat, 1986.
- 31 Virchenko, M. A., B. A. Arkad'ev, and V. Y. Ioffe. 1982. The use of high-capacity condensing turbine plant as a source of heat supply. *Thermal Engineering* 29 (4): 188–191.
- 32 de Paul, M. V., M. Wallon, and A. Anis. 1989. Twenty years' progress in steam turbine aerodynamics. *Proceedings of the American Power Conference* 51: 166–173.
- 33 Arkad'ev, *Operating Conditions of Steam Turbosets*.
- 34 Safonov, L. P., V. I. Nishnevich, M. V. Bakuradze, et al. 1981. Future 2000 MW turbine unit for nuclear power stations. *Thermal Engineering* 28 (9): 505–508.

- 35 Simon, V., and H. Oeynhausen. 1998. 3DV three-dimensional blades—A new generation of steam turbine blading. In *Proceedings of International Joint Power Generation Conference*, PWR-Vol. 33, Part 2, 89–96. New York: ASME, 1998.
- 36 Cramer, E. P., J. A. Moreci, C. W. Camp, et al. 1998. Advanced LP turbine retrofits: An economical approach to gain competitiveness. In *Proceedings of the International Joint Power Generation Conference*, PWR-Vol. 33, 79–87. New York: ASME, 1998.
- 37 Maughan, J. R., L. D. Willey, J. M. Hill, and S. Goel. 2000. Development of the dense pack steam turbine: A new design methodology for increased efficiency. In *Proceedings of the International Joint Power Generation Conference*, 1–11. New York: ASME, 2000.
- 38 Weschenfelder, K. D., H. Oeynhausen, D. Bergmann, P. Hosbein, and H. Termuehlen. 1994. Turbine steam path replacement at the Grafenrheinfeld nuclear power station. *Proceedings of the American Power Conference*, 56: 1522–1529.
- 39 Franc, J. C. and D. Gilchrist. 1994. Continuing progress and experience with turbines for nuclear power stations—Ten million hours of operation. In *Symposium on Steam Turbines and Generators*, 1–16. Monaco: GEC Alsthom, 1994.
- 40 Shcheglyayev, A. V. 1993. *Steam Turbines*, 6th ed., Vols. 1–2 (in Russian). ed. B. M. Troyanovskii. Moscow: Energoatomizdat, 1993.
- 41 Engelke, W., K. Schleithoff, H.-A. Jestrich, and H. Termuehlen. 1983. Design, operating and inspection considerations to control stress corrosion of LP turbine disks. *Proceedings of the American Power Conference* 45: 196–206.
- 42 Engelke, W. 1976. Operating experience of wet-steam turbines. In *Two-Phase Steam Flow in Turbines and Separators: Theory, Instrumentation, Engineering*, ed. M. J. Moore and C. H. Sieverding, 291–315. Washington, D.C.: Hemisphere Publishing Corp., 1976.
- 43 Virchenko, M. A. 1986. Adjustment and improvement of KhTGZ wet-steam turbines. *Thermal Engineering* 33 (6): 297–303.
- 44 Ryzhkov, V. K., V. A. Pakhomov, Y. N. Nezhentsev, and A. P. Ogurtsov. 1978. Steam turbine K-1000-60/3000 for nuclear power plants. *Thermal Engineering* 25 (6): 5–12.
- 45 Povarov, O. A., G. V. Tomarov, and V. N. Zharov. 1990. Erosion-corrosion of saturated-steam turbine plant elements. *Thermal Engineering* 37 (12): 643–647.
- 46 Leyzerovich, *Large Power Steam Turbines*.
- 47 Troyanovskii, *Turbines for Nuclear Power Plants*.
- 48 Hesketh, Steam turbine generators for Sizewell ‘B’, 183–191.
- 49 Sill, U., and W. Zörner. 1996. *Steam Turbine Generators Process Control and Diagnostics*. Erlangen, Germany: Publicis MCD Verlag, 1996.
- 50 de Paul, Twenty years' progress in steam turbine aerodynamics, 166–173.

220 *Wet-Steam Turbines for Nuclear Power Plants*

- 51 Engelke, Operating experience of wet-steam turbines, 291–315.
- 52 Spalthoff, First year of operation of the world's largest tandem compound turbine-generator, 555–569.
- 53 Ibid.
- 54 Fragin, M., A. Leyzerovich, and M. Shapiro. 2001. Fire resistant fluids seek to expand application into turbine lubrication systems. *Power Engineering* 105 (11):106–112.
- 55 Bruns, S., and T. Cooper. 2003. Prevention of turbine fires and loss. *Energy-Tech* Special Issue: Rotating Equipment: 18–22.
- 56 Vilyanskaya, G. D., V. V. Lysko, M. S. Fragin, and A. G. Vainshtein. 1991. VTI fire-resistant turbine oils and the part played by them in increasing fire protection at thermal and nuclear power stations. *Thermal Engineering* 38 (7): 38–41.
- 57 Franc, Continuing progress and experience with turbines for nuclear power stations.
- 58 Leyzerovich, *Large Power Steam Turbines*.
- 59 Mujezinovic, A. 2003. Bigger blades cut costs. *Modern Power Systems* 23 (2): 25–27.
- 60 Weiss, A. P. 1998. Aerodynamic design of advanced LP steam turbines. *ABB Review* 5: 4–11.
- 61 Kaneko, R., K. Ikeuchi, A. Okabe, et al. 1990. Development of 40-inch titanium blades using titanium alloys. In *Titanium Steam Turbine Blading*, 111–128. New York: Pergamon Press, 1990.
- 62 Machida, M., H. Yoda, E. Saito, and K. Namura. 2002. Development of long blades with continuous cover blade structure for steam turbines. *Hitachi Review* 51 (5): 143–147.
- 63 Bütikofer, J., and U. Wieland. 1991. Modern LP steam turbines. (in German). *VGB Kraftwerkstechnik* 71 (4): 341–346.
- 64 Kishimoto, M., M. Hojo, M. Mase, et al. 1994. Development of 3600 rpm 40 inch titanium blade and actual operating results. *MHI—Technical Review* 31 (2): 61–65.
- 65 Watanabe, E., H. Ohyama, Y. Kaneko, et al. 2002. Development of new advanced low-pressure end blades for high efficiency steam turbine. *JSME International Journal, Series B* 45 (3): 552–558.
- 66 Hisa, S., T. Matsuura, and H. Ogata. 1983. The improvement in efficiency and reliability of last stage blades for steam turbines. *Proceedings of the American Power Conference* 45: 207–213.
- 67 Suzuki, T., M. Watanabe, and M. Aoyama. 1993. Mechanical design of a titanium last stage blade for 3600 rpm large steam turbines. In *The Steam Turbine Generator Today: Materials, Flow Path Design, Repair and Refurbishment*, PWR-Vol. 21, 153–159. New York: ASME, 1993.
- 68 Ibid.

- 69 1995. Improved 1500 MWe Arabelle begins operation. *Modern Power Systems* 15 (10): 49-52.
- 70 Levchenko, E. V., V. P. Sukhinin, B. A. Arkad'ev, et al. 1994. Development of the last stages of the steam turbines of Turboatom Research and Production Association. *Thermal Engineering* 41 (4): 246-251.
- 71 Machida, Development of long blades, 143-147.
- 72 Gloger, M., K. Neumann, D. Bermann, and H. Termuehlen. 1992. Advanced LP turbine blading: A reliable and highly efficient design. In *Steam Turbine-Generator Developments for the Power Generation Industry*, PWR-Vol. 18, 41-51. ASME, 1992.
- 73 Ibid.
- 74 Gloger, M., M. Jung, H. Wolf, and H. Termuehlen. 1995. Blade vibration information system BeSSI for power plant operation. *Proceedings of the Joint International Power Generation Conference*, PWR-Vol. 28, Part 3: 375-387. New York: ASME, 1995.
- 75 Shibata, M., Y. Mitsuyama, and H. Fukuda. 2000. Development of noncontact blade vibration measuring system. *Mitsubishi Heavy Industries—Technical Review* 37 (3): 97-100.
- 76 Gloger, Advanced LP turbine blading: A reliable and highly efficient design, 41-51.
- 77 Ibid.
- 78 Ibid.
- 79 Krämer, E., and E. Plan. 1997. Optical vibration measured system for long, free-standing LP rotor blades. *ABB Review* 5: 4-9.
- 80 Shnee, Y. I., Y. F. Kosyak, V. N. Ponomarev, et al. 1978. The main results of developing and gas-dynamic investigations of the last stage of the K-500 and K-1000-60/1500 turbines. *Thermal Engineering* 25 (9): 1-7.
- 81 Shcheglyayev, *Steam Turbines*.
- 82 Machida, Development of long blades. 143-147.
- 83 Shcheglyayev, *Steam Turbines*.
- 84 Machida, Development of long blades. 143-147.
- 85 Borisov, F. P., M. Y. Ivanov, A. M. Karelkin, et al. 1993. Steam turbine high-efficiency stage design using ideal and viscous gas-flow calculations. *Thermal Engineering* 40 (5): 375-381.
- 86 Shcheglyayev, *Steam Turbines*.
- 87 Deich, M. E., B. M. Troyanovskii, and G. A. Filippov. 1990. An effective way of improving the efficiency of turbine stages. *Thermal Engineering* 37 (10): 31-35.
- 88 Troyanovskii, B. M. 1996. Improving the flow path of steam turbines. *Thermal Engineering* 43 (1): 9-18.

222 *Wet-Steam Turbines for Nuclear Power Plants*

- 89 Simoyu, L. L., N. N. Gudkov, M. S. Indursky, et al. 1998. The influence of the saber shape of the nozzle vanes on the performance of the last stage in a steam turbine. *Thermal Engineering* 45 (8): 659–664.
- 90 Weiss, Aerodynamic design of advanced LP steam turbines. 4–11.
- 91 Borisov, Steam turbine high-efficiency stage design. 375–381.
- 92 Leyzerovich, *Large Power Steam Turbines*.
- 93 Ibid.
- 94 Rezinskikh, V. F., A. F. Bogachev, A. L. Lebedeva, et al. 1996. An investigation of promising protective coatings for the exhaust blades of steam turbines. *Thermal Engineering* 43 (12): 990–993.
- 95 Beaudry, R. J., and K. S. McLeod. 1992. The development and application of welded cobalt-free erosion shields for low pressure steam turbine blades. In *Steam Turbine-Generator Developments for the Power Generation Industry*, PWR-Vol. 18, 63–68. New York: ASME, 1992.
- 96 Pichugin, Development of a low-pressure cylinder of increased throughout for large steam turbines, 225–230.
- 97 Suzuki, Mechanical design of a titanium last stage blade for 3600 rpm large steam turbines, 153–159.
- 98 Ibid.
- 99 Ibid.
- 100 Sakamoto, T., S. Nagao, and T. Tanuma. 1992. Investigation of wet steam flow for steam turbine repowering. In *Steam Turbine-Generator Developments for the Power Generation Industry*, PWR-Vol. 18, 33–39. New York: ASME, 1992.
- 101 Smith, A. 1976. Experimental development of wet-steam turbines. In *Two-Phase Steam Flow in Turbines and Separators: Theory, Instrumentation, Engineering*, ed. M. J. Moore and C. H. Sieverding, 261–290. Washington, D.C.: Hemisphere Publishing Corp., 1976.
- 102 Faddeev, I. P., S. V. Radik, and M. V. Mokravtsov. “Some ways of improving the reliability and economic efficiency of wet-steam power turbines.” *Thermal Engineering* 40, no. 3 (1993): 187–190.
- 103 Troyanovskii, *Turbines for Nuclear Power Plants*.
- 104 Ibid.
- 105 Sanders, W. P. 2001. *Turbine Steam Path. Maintenance & Repair*, Vols. 1–2. Tulsa, OK: PennWell Publishing, 2001.
- 106 Troyanovskii, *Turbines for Nuclear Power Plants*.
- 107 Kirillov, I. I., and Shpenzer, G. G. 1993. Problems of steam-water separation and water drainage when designing flow path elements of steam turbines. *Thermal Engineering* 40 (3): 191–193.

- 108 Troyanovskii, B. M., Y. F. Kosyak, M. A. Virchenko, et al. 1977. Experience with operation of saturated steam turbines at nuclear power stations. *Thermal Engineering* 24 (2): 15–23.
- 109 Pichugin, I. I., A. M. Tsvetkov, and M. S. Simkin. 1993. Features of steam turbine design at the Leningrad Metallic Works. *Thermal Engineering* 40 (5): 355–366.
- 110 Kiryukhin, V. I., G. A. Filippov, O. A. Povarov, and V. I. Dikarev. 1975. Investigation of inside-channel separation of moisture in a multistage turbine. *Thermal Engineering* 22 (8): 26–29.
- 111 Sakamoto, Investigation of wet steam flow for steam turbine repowering.
- 112 Troyanovskii, B. M., G. A. Filippov, and A. E. Bulkin. 1985. *Steam and Gas Turbines for Nuclear Power Plants* (in Russian). Moscow: Energoatomizdat, 1985.
- 113 Troyanovskii, *Turbines for Nuclear Power Plants*.
- 114 Oeynhausen, H., G. Roettger, J. Ewald, et al. 1987. Reliable disk-type rotors for nuclear power plants. *Proceedings of the American Power Conference* 49: 113–122.
- 115 Filippov, G. A., and O. A. Povarov. 1980. *Moisture Separation in Nuclear Power Plants' Turbines* (in Russian). Moscow: Energiya, 1980.
- 116 Kiryukhin, V. I., G. A. Filippov, and O. I. Nazarov. "A study of the moisture separation systems of turbine units for nuclear power stations." *Thermal Engineering* 45, no. 8 (1998)(8): 619–625.
- 117 Coit, R. L., P. D. Ritland, T. F. Rabas, and P. W. Viscovich. 1976. External moisture separator-reheaters. In *Two-Phase Steam Flow in Turbines and Separators: Theory, Instrumentation, Engineering*, ed. M. J. Moore and C. H. Sieverding, 337–366. Washington, D.C.: Hemisphere Publishing Corp., 1976.
- 118 Ibid.
- 119 Ibid.
- 120 Franc, Continuing progress and experience with turbines for nuclear power stations. 1–16.
- 121 Haraguchi, M., Q. Liu, and S. Oda. 2001. Steam-turbine equipment for inshan phase-III nuclear power station in China. *Hitachi Review* 50 (3): 95–99.
- 122 Gyarmathy, Innovation and tradition in steam turbine engineering, 217–231.
- 123 von Boeckh, P., M. Stiefel, and U. Frick. 1986. Experience with the moisture preseparators (MOPS) and with the special cross under pipe separator (SCRUPS) in the Leibstadt nuclear plant. *Proceedings of the American Power Conference* 48: 718–725.
- 124 Dueymes, E., and J. P. Peyrelongue. 1991. A wider range of application for the high velocity separators (HVSs). In *Design, Repair, and Refurbishment of Steam Turbines*, PWR-Vol. 13, 127–131. New York: ASME, 1991.
- 125 Povarov, O. A., A. I. Derkach, and V. F. Chertushkin. 1989. The effectiveness of turbo separators. *Thermal Engineering* 36 (2): 87–90.

## Bibliography

- Arabelle—A World Record. Chooz B Power Station, France. 2×1531 MW.* 1997. Paris: ALSTOM, 1997.
- Arkad'ev, B. A. 1986. *Operating Conditions of Steam Turbosets for Nuclear Power Plants* (in Russian). Moscow: Energoatomizdat, 1986.
- Aubry, P., S. Bayard, and A. Anis. 1986. Nuclear LP turbine design and operating experience. *Proceedings of the American Power Conference* 48: 166–171.
- Bannister, R. L., and G. J. Silvestri, Jr. 1989. The evolution of central station steam turbines. *Mechanical Engineering* 111 (2): 70–78.
- Beaudry, R. J., and K. S. McLeod. 1992. The development and application of welded cobalt-free erosion shields for low pressure steam turbine blades. In *Steam Turbine-Generator Developments for the Power Generation Industry*, PWR-Vol. 18, 63–68. New York: ASME, 1992.
- Borisov, F. P., M. Y. Ivanov, A. M. Karelkin, et al. 1993. Steam turbine high-efficiency stage design using ideal and viscous gas-flow calculations. *Thermal Engineering* 40 (5): 375–381.
- Bruns, S., and T. Cooper. 2003. Prevention of turbine fires and loss. *Energy-Tech*, Special Issue: Rotating Equipment: 18–22.
- Bütikofer, J., M. Händler, and U. Wieland. 1980. ABB low-pressure steam turbines—the culmination of selective development. *ABB Review* (8/9): 9–16.
- , and U. Wieland. 1991. Modern LP steam turbines. (in German). *VGB Kraftwerkstechnik* 71 (4): 341–346.
- Buzulukov, V. A., M. G. Teplitskii, A. A. Maksimenko, and T. V. Poruchinskii. 1989. Full-scale testing of the KhTZ K-1000-60/1500-2 turbine plant at Zaporozhe nuclear power station. *Thermal Engineering* 36 (2): 69–75.
- Coenca, H. 1986. Progress achieved in steam drying: The high velocity separator. *Alsthom Review* (4): 19–25.
- Coit, R. L., P. D. Ritland, T. F. Rabas, and P. W. Viscovich. 1976. External moisture separator-reheaters. In *Two-Phase Steam Flow in Turbines and Separators: Theory, Instrumentation, Engineering*, ed. M. J. Moore and C. H. Sieverding, 337–366. Washington, D.C.: Hemisphere Publishing Corp., 1976.
- Cramer, E. P., J. A. Moreci, C. W. Camp, et al. 1998. Advanced LP turbine retrofits: An economical approach to gain competitiveness. In *Proceedings of the International Joint Power Generation Conference*, PWR-Vol. 33, 79–87. New York: ASME, 1998, Part 2.
- de Paul, M. V., M. Wallon, and A. Anis. 1989. Twenty years' progress in steam turbine aerodynamics. *Proceedings of the American Power Conference* 51:166–173.
- Deich, M. E., B. M. Troyanovskii, and G. A. Filippov. 1990. An effective way of improving the efficiency of turbine stages. *Thermal Engineering* 37 (10): 31–35.

- Drahý, J. 1976. Progress in steam turbine field of Shkoda (in Czech). *Shkoda Review* (11): 19–30.
- Dueymes, E., and J. P. Peyrelongue. 1991. A wider range of application for the high velocity separators (HVSs). In *Design, Repair, and Refurbishment of Steam Turbines*, PWR-Vol. 13, 127–131. New York: ASME, 1991.
- Egorov, N. P., I. A. Kovalev, L. I. Chernyavskii, and A. E. Yazykov. 1991. Study of a system of back-up oil supply for a turbine plant with fire-resistant oil. *Thermal Engineering* 38 (2): 117–118.
- Engelke, W. 1976. Operating experience of wet-steam turbines. In *Two-Phase Steam Flow in Turbines and Separators: Theory, Instrumentation, Engineering*, ed. M. J. Moore and C. H. Sieverding, 291–315. Washington, D.C.: Hemisphere Publishing Corp., 1976.
- . Schleithoff, H.-A. Jestrich, and H. Termuehlen. 1983. Design, operating and inspection considerations to control stress corrosion of LP turbine disks. *Proceedings of the American Power Conference* 45: 196–206.
- Faddeev, I. P., S. V. Radik, and M. V. Mokravtsov. 1993. Some ways of improving the reliability and economic efficiency of wet-steam power turbines. *Thermal Engineering* 40 (3): 187–190.
- Filippov, G. A., and O. A. Povarov. 1980. *Moisture Separation in Nuclear Power Plants' Turbines* (in Russian). Moscow: Energiya, 1980.
- Fragni, M., A. Leyzerovich, and M. Shapiro. 2001. Fire resistant fluids seek to expand application into turbine lubrication systems. *Power Engineering* 105 (11): 106–112.
- Franc, J. C. and D. Gilchrist. 1994. Continuing progress and experience with turbines for nuclear power stations—Ten million hours of operation. In *Symposium on Steam Turbines and Generators*, 1–16. Monaco: GEC Alsthom, 1994.
- Gardner, G. C. 1976. Performance of knitted wire mesh and corrugated plate separators. In *Two-Phase Steam Flow in Turbines and Separators: Theory, Instrumentation, Engineering*, ed. M. J. Moore and C. H. Sieverding, 317–337. Washington, D.C.: Hemisphere Publishing Corp., 1976.
- Gloger, M., M. Jung, H. Wolf, and H. Termuehlen. 1995. Blade vibration information system BeSSI for power plant operation. *Proceedings of the Joint International Power Generation Conference*, PWR-Vol. 28, Part 3: 375–387. New York: ASME, 1995.
- , K. Neumann, D. Bermann, and H. Termuehlen. 1992. Advanced LP turbine blading: A reliable and highly efficient design. In *Steam Turbine-Generator Developments for the Power Generation Industry*, PWR-Vol. 18, 41–51. ASME, 1992.
- Günter, R. 1997. Operating experience with synthetic fluids in the control and governing systems of steam turbines. *VGB PowerTech* 77 (12): 930–934.
- Gyamarthy, G. 1960. *A Theory of Wet-Steam Turbines* (in German). Zurich: Juris-Verlag, 1960.

- . 1990. Innovation and tradition in steam turbine engineering. *Proceedings of the Institute of Mechanical Engineers, Part A: Journal of Power and Energy* 204: 217-231.
- Haraguchi, M., Q. Liu, and S. Oda. 2001. Steam-turbine equipment for inshan phase-III nuclear power station in China. *Hitachi Review* 50 (3): 95-99.
- Harris, F. R. 1984. The Parsons centenary—A hundred years of steam turbines. *Proceedings of the Institute of Mechanical Engineers* 198A (9): 183-224.
- Hayes, J. K., S. A. Trovato, S. Misilo, and J. Burger. 1991. An investigation and assessment of methods to improve moisture removal and reheating of PWR cycle system. In *Design, Repair, and Refurbishment of Steam Turbines*, PWR-Vol. 13, 115-126. New York: ASME, 1991.
- Hesketh, J. A., and J. Muscroft. 1990. Steam turbine generators for Sizewell 'B' nuclear power station. *Proceedings of the Institute of Mechanical Engineers* 204, Ser. A3: 183-191.
- His, S., T. Matsuura, and H. Ogata. 1983. The improvement in efficiency and reliability of last stage blades for steam turbines. *Proceedings of the American Power Conference* 45: 207-213.
- Improved 1500 MWe Arabelle begins operation. 1995. *Modern Power Systems* 15 (10): 49-52.
- Jacobsen, G., H. Oeynhausen, and H. Termuehlen. 1991. Advanced LP turbine installation at 1300 MW nuclear power station Unterweser. *Proceedings of the American Power Conference* 53: 991-1001.
- Kaneko, R., K. Ikeuchi, A. Okabe, et al. 1990. Development of 40-inch titanium blades using titanium alloys. In *Titanium Steam Turbine Blading*, 111-128. New York: Pergamon Press, 1990.
- Keller, H. 1974. Erosion-corrosion of wet-steam turbines (in German). *VGB Kraftwerkstechnik* 26 (5): 292-295.
- Kirillov, I. I., and Shpenzer, G. G. 1993. Problems of steam-water separation and water drainage when designing flow path elements of steam turbines. *Thermal Engineering* 40 (3): 191-193.
- Kiryukhin, V. I., G. A. Filippov, D. I. Demicheva, et al. 1998. Operating experience with feed-pump turbine drives having a special moisture separator stage at nuclear power stations. *Thermal Engineering* 45 (4): 325-328.
- , G. A. Filippov, and O. I. Nazarov. 1998. A study of the moisture separation systems of turbine units for nuclear power stations. *Thermal Engineering* 45 (8): 619-625.
- , G. A. Filippov, O. A. Povarov, and V. I. Dikarev. 1975. Investigation of inside-channel separation of moisture in a multistage turbine. *Thermal Engineering* 22 (8): 26-29.
- Kishimoto, M., M. Hojo, M. Mase, et al. 1994. Development of 3600 rpm 40 inch titanium blade and actual operating results. *MHI—Technical Review* 31 (2): 61-65.

- Kosyak, Y. F. 1978. Development by Turboatom of turbine construction for nuclear power plants. *Thermal Engineering* 34 (8): 405–408.
- , G. A. Filippov, Y. E. Yushkevich, et al. 1978. Investigation of moisture separation in the HPC of the K-220-44 turbine. *Thermal Engineering* 25 (6): 9–12.
- , M. A. Virchenko, V. A. Matveenko, et al. 1985. Turbine plants with noncontrolled pressure in the extractions for combined generation of power and heat. *Thermal Engineering* 32 (7): 359–365.
- , M. A. Virchenko, V. P. Sukhinin, et al. 1980. The problem of selecting speed of turbines for nuclear power stations. *Thermal Engineering* 27 (5): 256–259.
- Krämer, E., and E. Plan. 1997. Optical vibration measured system for long, free-standing LP rotor blades. *ABB Review* (5): 4–9.
- Levchenko, E. V. 1995. Steam turbines manufactured by Turboatom NPO, their specifics, and ways of improving them. *Thermal Engineering* 42 (1): 13–20.
- , V. N. Galatsan, V. P. Sukhinin, and B. A. Arkad'ev. 1993. Turbines of the new generation of Turboatom NPO. *Thermal Engineering* 40 (5): 367–374.
- , V. P. Sukhinin, B. A. Arkad'ev, et al. 1994. Development of the last stages of the steam turbines of Turboatom Research and Production Association. *Thermal Engineering* 41 (4): 246–251.
- Leyzerovich, A. 1997. *Large Power Steam Turbines: Design & Operation*, Vols. 1–2. Tulsa, OK: PennWell Publishing, 1997.
- Machida, M., H. Yoda, E. Saito, and K. Namura. 2002. Development of long blades with continuous cover blade structure for steam turbines. *Hitachi Review* 51 (5): 143–147.
- Maughan, J. R., L. D. Willey, J. M. Hill, and S. Goel. 2000. Development of the dense pack steam turbine: A new design methodology for increased efficiency. In *Proceedings of the International Joint Power Generation Conference*, 1–11. New York: ASME, 2000.
- McCloskey, T. H., R. B. Dooley, and W. P. McNaughton. 1999. *Turbine Steam Path Damage: Theory and Practice*, Vols. 1–2. Palo Alto, CA: EPRI, 1999.
- Miyawaki, T., H. Tashiro, M. Honjo, and E. Watanabe. 1992. Improvement of LP turbine efficiency by fully 3D designed blade. In *Steam Turbine-Generator Developments for the Power Generation Industry*, PWR-Vol. 18, 75–80. New York, ASME, 1992.
- Moinaud, C. 1992. Arabelle is EDF's new prime mover. *Modern Power Systems*, 12 (10): 49–53.
- Moriya, K., M. Ohtsuka, M. Aoyama, and M. Matsuura. 2001. Development study of nuclear power plants for the 21st century. *Hitachi Review* 50 (3): 61–67.
- Mujezinovic, A. 2003. Bigger blades cut costs. *Modern Power Systems*, 23 (2): 25–27.

- Oeynhausen, H., A. Droszdiok, H. Ulm, and H. Termuehlen. 1996. Advanced 1000 MW tandem-compound reheat steam turbines. *Proceedings of the American Power Conference* 58: 686–698.
- , G. Roettger, J. Ewald, et al. 1987. Reliable disk-type rotors for nuclear power plants. *Proceedings of the American Power Conference* 49: 113–122.
- Ogurtsov, A. P., V. K. Ryzhkov, Y. N. Nezhentsev, and L. Y. Bal'va. 1981. Steam turbines of LMZ for nuclear power industry. *Thermal Engineering* 28 (9): 497–504.
- International Atomic Energy Agency. 2001. *Operating Experience with Nuclear Power Stations in Member States in 2000* Vienna: International Atomic Energy Agency, 2001.
- Petrenya, Y. K., L. A. Khomenok, I. A. Kovalev, and Y. Y. Kachuriner. 2003. Prospects for the development of high-speed steam-turbine installations for nuclear power-generating units with a capacity of 1500 MW and higher. *Thermal Engineering* 50 (2): 112–119.
- Pitchugin, I. I. and I. A. Kovalev. 1994. Develop titanium-alloy blades for large steam turbines. *Power*, 138 (5): 77–80.
- , Y. N. Nezhentsev, and B. M. Troyanovskii. 1990. Development of a low-pressure cylinder of increased throughout for large steam turbines. *Thermal Engineering* 37 (5): 225–230.
- , A. M. Tsvetkov, and M. S. Simkin. 1993. Features of steam turbine design at the Leningrad Metallic Works. *Thermal Engineering* 40 (5): 355–366.
- Povarov, O. A. 1980. Problems of moisture separation in turbine plants of nuclear power stations. *Thermal Engineering* 27 (2): 84–89.
- , A. I. Derkach, and V. F. Chertushkin. 1989. The effectiveness of turbo separators. *Thermal Engineering* 36 (2): 87–90.
- , G. V. Tomarov, and V. N. Zharov. 1990. Erosion-corrosion of saturated-steam turbine plant elements. *Thermal Engineering* 37 (12): 643–647.
- Rezinskikh, V. F., A. F. Bogachev, A. L. Lebedeva, et al. 1996. An investigation of promising protective coatings for the exhaust blades of steam turbines. *Thermal Engineering* 43 (12): 990–993.
- Riollet, G. 1989. New French impulse turbines feature innovative steam flow. *Nuclear Engineering International* (1): 28–35.
- Ryzhkov, V. K., V. A. Pakhomov, Y. N. Nezhentsev, and A. P. Ogurtsov. 1978. Steam turbine K-1000-60/3000 for nuclear power plants. *Thermal Engineering* 25 (6): 5–12.
- Safonov, L. P., V. I. Nishnevich, M. V. Bakuradze, et al. 1981. Future 2000 MW turbine unit for nuclear power stations. *Thermal Engineering* 28 (9): 505–508.
- Saito, E., Y. Yamazaki, K. Namura, et al. 1998. Development of a 3000 rpm 43-in. last stage blade with high efficiency and reliability. In *Proceedings of International Joint Power Generation Conference*, PWR-Vol. 33, Part 2, 89–96. New York: ASME, 1998.

- Sakamoto, T., S. Nagao, and T. Tanuma. 1992. Investigation of wet steam flow for steam turbine repowering. In *Steam Turbine-Generator Developments for the Power Generation Industry*, PWR-Vol. 18, 33-39. New York: ASME, 1992.
- Sanders, W. P. 2001. *Turbine Steam Path. Maintenance & Repair*; Vols. 1-2. Tulsa, OK: PennWell Publishing, 2001.
- Schenk, K., E. Höxtermann, and J. Hartwig. 1998. Operation of turbines with fire-resistant fluids, including the lubrication system." In *Proceedings of the International Joint Power Generation Conference*, PWR-Vol. 33, Part 2, 799-806. New York: ASME, 1998.
- Shcheglyayev, A. V. 1993. *Steam Turbines*, 6th ed., Vols. 1-2 (in Russian). ed. B. M. Troyanovskii. Moscow: Energoatomizdat, 1993.
- Shibata, M., Y. Mitsuyama, and H. Fukuda. 2000. Development of noncontact blade vibration measuring system. *Mitsubishi Heavy Industries—Technical Review* 37 (3): 97-100.
- Shnee, Y. I., Y. F. Kosyak, V. N. Ponomarev, et al. 1978. The main results of developing and gas-dynamic investigations of the last stage of the K-500 and K-1000-60/1500 turbines. *Thermal Engineering* 25 (9): 1-7.
- Sill, U., and W. Zörner. 1996. *Steam Turbine Generators Process Control and Diagnostics*. Erlangen, Germany: Publicis MCD Verlag, 1996.
- Simon, V., and H. Oeynhausen. 1998. 3DV three-dimensional blades—A new generation of steam turbine blading. In *Proceedings of International Joint Power Generation Conference*, PWR-Vol. 33, Part 2, 89-96. New York: ASME, 1998.
- \_\_\_\_\_, H. Oeynhausen, R. Bürkner, and K.-J. Eich. 1997. Impulse blading? Reaction blading? Variable blading! *VGB Kraftwerkstechnik* 77 (9): 648-652.
- Simoyu, L. L., N. N. Gudkov, M. S. Indursky, et al. 1998. The influence of the saber shape of the nozzle vanes on the performance of the last stage in a steam turbine. *Thermal Engineering* 45 (8): 659-664.
- Site work underway on Finland's 1600 MWe EPR, 2004. *Modern Power Systems* 24 (3): 30-34.
- Smith, A. 1976. Experimental development of wet-steam turbines. In *Two-Phase Steam Flow in Turbines and Separators: Theory, Instrumentation, Engineering*, ed. M. J. Moore and C. H. Sieverding, 261-290. Washington, D.C.: Hemisphere Publishing Corp., 1976.
- Spalthoff, F. J., H. Haas, and F. Heinrichs. 1976. First year of operation of the world's largest tandem compound turbine-generator. *Proceedings of the American Power Conference* 38: 555-569.
- Stanley, W. 1969. The impact of changing economics on electric utilities *Proceedings of the American Power Conference* 31: 7-16.
- Strauss, S. D. 1997. World's largest unit advances nuclear power for next century. *Electric Power International*, Sept. 1997: 27-30.

- Suzuki, T., M. Watanabe, and M. Aoyama. 1993. Mechanical design of a titanium last stage blade for 3600 rpm large steam turbines. In *The Steam Turbine Generator Today: Materials, Flow Path Design, Repair and Refurbishment*, PWR-Vol. 21, 153–159. New York: ASME, 1993.
- Tanuma, T., and T. Sakamoto. 1991. The removal of water from steam turbine stationary blades by suction slots. *Proceedings of the Institute of Mechanical Engineers*, C423/022 (1991): 179–189.
- Titanium Steam Turbine Blading, Workshop Proceedings*. 1988. Palo Alto, CA: Electric Power Research Institute, 1988.
- Troyanovskii, B. M. 1996. Improving the flow path of steam turbines. *Thermal Engineering* 43 (1): 9–18.
- . 1986. New designs of separators for the turbine plants of nuclear power stations abroad. *Thermal Engineering* 33 (1): 56–57.
- . 2003. The new design of the low-pressure cylinders of Mitsubishi steam turbines. *Thermal Engineering* 50 (2): 170–172.
- . 1986. Turbine plants of thermal and nuclear power stations. *Thermal Engineering* 33 (6): 291–296.
- . 1978. *Turbines for Nuclear Power Plants*, 2d ed. (in Russian). Moscow: Energiya, 1978.
- . 1993. Ways of improving the efficiency of steam turbines. Part 1. *Thermal Engineering* 40 (5): 386–393.
- . 1993. Ways of improving the efficiency of steam turbines. Part 2. *Thermal Engineering* 40 (7): 528–536.
- , G. A. Filippov, and A. E. Bulkin. 1985. *Steam and Gas Turbines for Nuclear Power Plants* (in Russian). Moscow: Energoatomizdat, 1985.
- , Y. F. Kosyak, M. A. Virchenko, et al. 1977. Experience with operation of saturated steam turbines at nuclear power stations. *Thermal Engineering* 24 (2): 15–23.
- Vilyanskaya, G. D., V. V. Lysko, M. S. Fragin, and A. G. Vainshtein. 1991. VTI fire-resistant turbine oils and the part played by them in increasing fire protection at thermal and nuclear power stations. *Thermal Engineering* 38 (7): 38–41.
- , V. V. Lysko, and W. D. Phillips. 1990. Recent operating experience in Europe and the Soviet Union with fire-resistant turbine lubrication. *Proceedings of the American Power Conference* 52: 704–708.
- Virchenko, M. A.. 1986. Adjustment and improvement of KhTGZ wet-steam turbines. *Thermal Engineering* 33 (6): 297–303.
- , B. A. Arkad'ev, and V. Y. Ioffe. 1982. The use of high-capacity condensing turbine plant as a source of heat supply. *Thermal Engineering* 29 (4): 188–191.

- von Boeckh, P., M. Stiefel, and U. Frick. 1986. Experience with the moisture preseparators (MOPS) and with the special cross under pipe separator (SCRUPS) in the Leibstadt nuclear plant. *Proceedings of the American Power Conference* 48: 718-725.
- \_\_\_\_\_, P., M. Stiefel, and U. Frick. 1990. Operating experience with new moisture preseparators and special cross under pipe separators. *ABB Review* (3): 3-10.
- Wallon, M. 1987. Last-stage blading: a key factor in steam turbine development. *Alsthom Review* (9): 3-16.
- Watanabe, E., H. Ohyama, Y. Kaneko, et al. 2002. Development of new advanced low-pressure end blades for high efficiency steam turbine. *JSME International Journal, Series B* 45 (3): 552-558.
- Weiss, A. P. 1998. Aerodynamic design of advanced LP steam turbines. *ABB Review*, (5): 4-11.
- Weschenfelder, K. D., H. Oeynhausen, D. Bergmann, P. Hosbein, and H. Termuehlen. 1994. Turbine steam path replacement at the Grafenrheinfeld nuclear power station. *Proceedings of the American Power Conference* 56: 1522-1529.
- Wichtmann, A., N. Schindler, and W. Ulm. 2003. Advanced large steam turbines for saturated steam conditions. Paper presented at PowerGen, 2003.

## 4

---

---

# Operation

## Operating Conditions of Wet-Steam Turbines

As a rule, nuclear power plants cover the base part of power consumption graphs; that is, they are operated in a base-load mode with minimal participation in governing the power system's load (Fig. 4-1). First of all, this is a high portion of capital expenditures and relatively low contributions from the fuel constituent in the power generation predetermined by the costs of nuclear power plants. As a result, it is reasonable and profitable to exploit these plants with as large a utilization factor value as possible. In addition, stationary operating conditions provide the most favorable safety environment for nuclear power plants. For all of these reasons and thanks to high operating reliability (see chapter 1), the annual average capacity factor for the world's nuclear power plants is remarkably high, making up 78.9% in 2001 (compared to 76.4% in 2000). The power utilities of such countries as Belgium, China, the Czech Republic, Finland, Germany, Hungary, the Netherlands, Romania, South Korea, Spain, Switzerland, and

the United States managed to maintain the national average capacity factors of their nuclear power plants above 85%.<sup>1</sup> Table 4-1 ranks the top 50 nuclear power units worldwide in 2001 by the annual capacity factor. A nuclear power unit had to operate at a capacity factor value above 95% to be included on this list.

An ideal operation diagram of a nuclear power unit (1,365-MW Unit 2 of the German power plant Neckar) operating in the base-load mode is presented in Figure 4-2a. The average annual capacity factor for this unit was 95.4 % in 2001 and 88.7% in 2002, which included a scheduled, unavoidable outage for refueling, as well as gradual unloading to extend the operation campaign.<sup>2</sup>

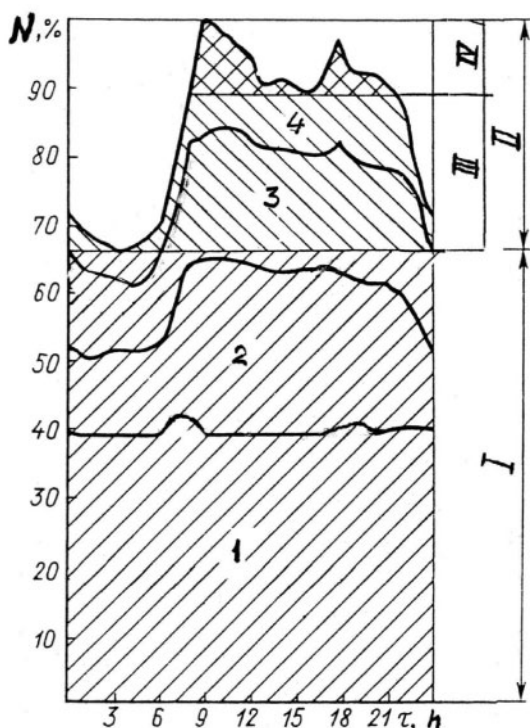


**Fig. 4-1.** Participation of different types of power plants in covering daily power consumption (I: base-load zone; II: variable-load zone; III: medium-load zone; IV: peak-load zone; 1: nuclear and cogeneration power plants, renewable power sources; 2: fossil fuel power units with supercritical-steam parameters; 3: fossil fuel power units with subcritical-steam parameters; 4: gas-turbines and hydroelectric power plants)

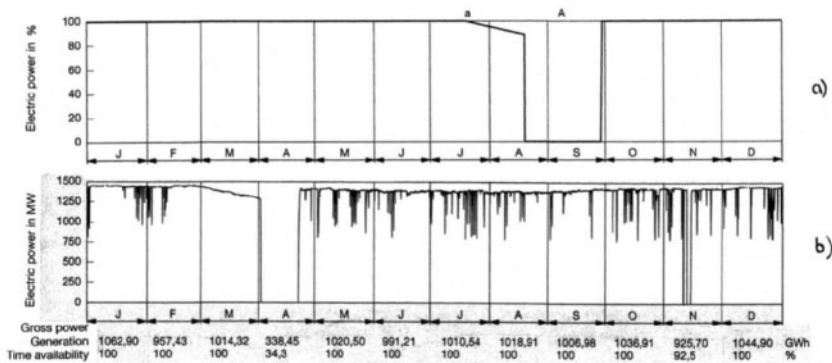


**Fig. 4-2.** Operation diagrams for German nuclear power units Neckar 2 (a) and Grohnde (b) in 2002 (a: stretch out, unloading before refueling A)  
Source: "Operating results with nuclear power plants in 2002"<sup>3</sup>

**Table 4-1.** Top 50 nuclear power plant units worldwide with the highest annual capacity factor in 2001

Rank	Country	Plant name, unit	Reactor type	Unit capacity, MW (gross)	2001 capacity factor, %
1	S. Korea	Yonggwang, 1	PWR	950	104.36
2	S. Korea	Yonggwang, 3	PWR	1,000	103.61
3	US	Limerick, 1	BWR	1,163	102.73
4	US	La Salle, 1	BWR	1,137	101.83
5	US	Byron, 1	PWR	1,242	101.56
6	US	La Salle, 2	BWR	1,137	100.21
7	US	Arkansas, 2	PWR	943	100.06
8	Japan	Tomari, 1	PWR	579	99.99
9	Japan	Takahama, 4	PWR	870	99.99
10	Japan	Shika, 1	BWR	540	99.97
11	Japan	Mihama, 3	PWR	826	99.97
12	Japan	Shimane, 2	BWR	820	99.96
13	US	Comanche Peak, 2	PWR	1,173	99.92
14	US	Wolf Creek	PWR	1,226	99.87
15	US	Davis-Besse	PWR	925	99.81
16	Japan	Fukushima ii, 4	BWR	1,100	99.75
17	US	Catawba, 1	PWR	1,205	99.66

18	Japan	Kashiwazaki, 5	BWR	1,100	99.62
19	US	Vogtle, 1	PWR	1,215	99.57
20	US	Ginna	PWR	517	99.35
21	US	Sequoyah, 2	PWR	1,181	99/15
22	Spain	Almaraz, 1	PWR	974	99.13
23	US	Browns Ferry, 3	BWR	1,155	99.08
24	US	Point Beach, 2	PWR	523	98.88
25	Spain	Vandellos, 2	PWR	1,087	98.49
26	US	Waterford, 3	PWR	1,153	98.49
27	Japan	Sendai, 1	PWR	890	98.32
28	India	Kakrapar, 2	PHWR	220	97.80
29	Finland	Olkiluoto, 1	BWR	870	97.57
30	US	Diablo Canyon, 1	PWR	1,164	97.56
31	Argentina	Embalse	PHWR	648	97.54
32	US	Beaver Valley, 2	PWR	888	97.20
33	US	Millstone, 2	PWR	889	96.93
34	US	Byron, 2	PWR	1,210	96.91
35	Switzerland	Beznau, 1	PWR	380	96.78
36	US	San Onofre, 2	PWR	1,181	96.59
37	US	Braidwood, 2	PWR	1,210	96.54
38	US	Hatch, 1	BWR	924	96.31
39	US	Quad Cities, 1	BWR	833	96.26
40	Germany	Isar, 2	PWR	1,475	95.93
41	US	Brunswick, 1	BWR	895	95.65
42	Spain	Cofrenetes	BWR	1,025	95.60
43	US	McGuire, 2	PWR	1,225	95.54
44	US	Braidwood, 1	PWR	1,242	95.49
45	Japan	Ikata, 1	PWR	566	95.20
46	US	Clinton	BWR	985	95.18
47	S. Korea	Wolsong, 2	PHWR	715	95.11
48	S. Korea	Kori, 4	PWR	950	95.08
49	Finland	Olkiluoto, 2	BWR	870	95.06
50	US	Watts Bar, 1	PWR	1,210	95.03

Source: *B. Schwieger, M. Leonard, S. Taylor, et al.*<sup>4</sup>

In countries where nuclear power plants are of great concern in the power industry, there arises a challenge to involve individual nuclear power units in covering the power consumption graphs and governing the power system's load. So, for example, some German nuclear power plants from time to time are required to operate in a power mode according to the dispatcher's schedule. Such occasional involvement is illustrated by the annual operation diagrams for the nuclear power units Grohnde (with the rated gross capacity of 1,430 MW) for 2002 and Stade (with the rated gross capacity of 672 MW) for 1999 (Figs. 4-2b and 4-3, respectively).<sup>5</sup> Despite this, the average annual capacity factor of these units remains quite high (for example, 93.8% for Grohnde in 2002), and the time availability is kept almost invariably at a level of approximately 100%.

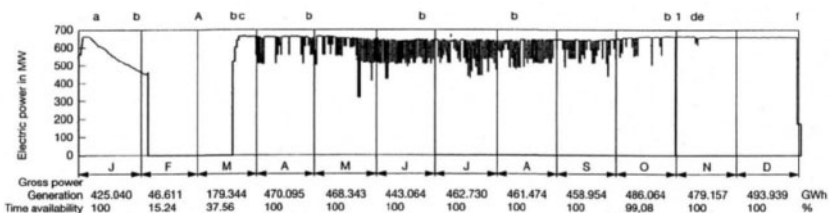


**Fig. 4-3.** Operation diagram for the German nuclear power unit Stade in 1999 (a: stretch out; A: unloading before refueling; b: operation in a planned power mode with occasional output changes according to dispatcher instructions; c: conditioning the reactor core; d: turbine trip during turbine tests; e: incorrect rod insertion; f: shutdown for standby; 1: turbine trip/reactor scram during turbine test)

Source: "Operating results with nuclear power plants in 2000"<sup>6</sup>

Since 1983, Japanese nuclear power plants have been operated in the mode of following the power system's load, thus facilitating system load control. Over 70% of the total installed capacity of Japanese nuclear power plants are supposedly involved in this process, providing a possibility of deep unloading if necessary.<sup>7</sup> The same pattern takes place in France, where nuclear power plants constitute more than half of the installed capacity of all power plants and generate more than 75% of the electricity, whereas fossil fuel plants provide only about 10%. As a rule, nuclear power units participate in covering the variable part of power consumption graphs by varying their load within the governed range, as shown, for example, in Figure 4-4.

The width of this range and the rate of load variations are exclusively dictated by the reactor and its control mode. French nuclear power units with PWR-type reactors allow load variations at the rate of up to 10% MCR (maximum continuous rating) per minute. The governed range changes during the reactor operation campaign, but it is usually not less than 20% MCR. Similar processes are also typical for some other countries.

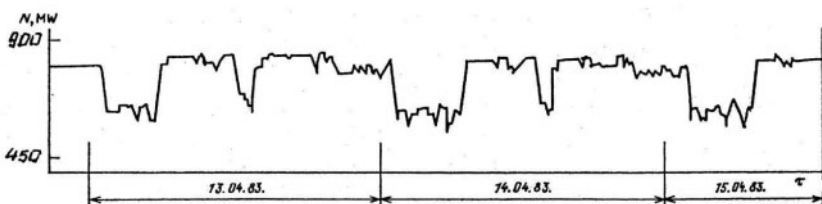


**Fig. 4-4.** Daily load variations of the 900-MW French nuclear power unit Tricastin 3

Source: V. N. Proselkov and V. D. Simonov<sup>8</sup>

For double-turbine nuclear power units (one reactor and two turbines), especially if the turbines have throttle steam admission control, it is advisable to unload the unit by reducing the load of one turbine, keeping the second one under maximum output. In addition to more efficient power generation, this provides a higher final feed water temperature. If the reactor output is to be substantially lowered (by 50% or more) for a relatively long period (an hour or more), it may be reasonable to shut down one of the turbines. Another option is to close the steam inlet to this turbine, but keep it rotated by the generator as a motor. Both of these scenarios were thoroughly researched for nuclear power units with different turbine types.<sup>9</sup> Results of these investigations showed that wet-steam turbines are quite flexible and suitable for system load control. However, the true flexibility of nuclear power units is eventually determined not by the turbine, but the reactor. Nevertheless, it is important to know that wet-steam turbines do not generally limit the rate of transients, but incorrect arrangements of these operating conditions and improper operation can lead to undesirable consequences for the turbine, causing damage even with rare, individual transient operating conditions.

A typical start-up diagram for a nuclear power unit is shown in Figure 4-5 (Kashiwazaki-Kariwa Unit 7 with an ABWR, the rated output

of 1,356 MW and steam pressure of 7.1 MPa [1,030 psi]).<sup>10</sup> The turbine is started up (rolled up and loaded) after the main steam pressure reaches its rated level. This is quite typical for wet-steam turbines of nuclear power plants with different reactor types and different start-up systems, as well as for different types of start-ups. As can be seen in the presented start-up diagram, after the reactor reaches criticality, the steam pressure is raised following the reactor water temperature change rate ( $10\text{--}55^{\circ}\text{C/h}$  [ $5\text{--}30^{\circ}\text{F/h}$ ]) by withdrawing the control rods. After the generator is switched on to the grid, the reactor is controlled in the generator power control mode by adjusting the control rod position to the target generator output and rate of its change.

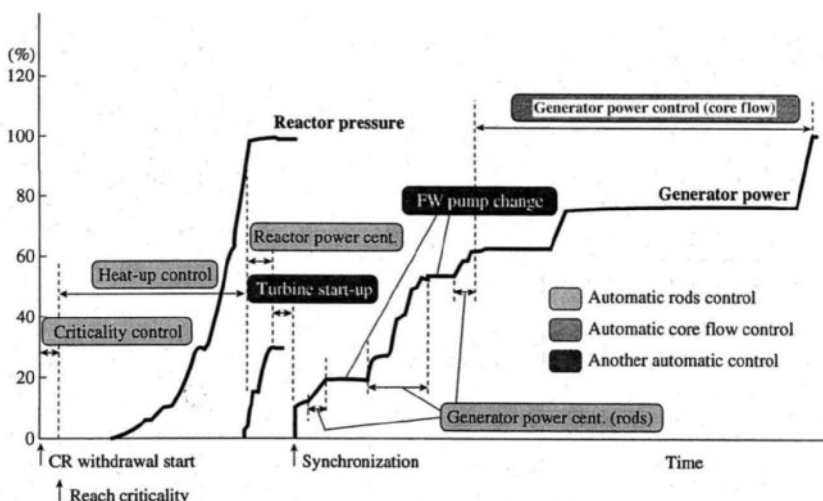


**Fig. 4-5.** Cold start-up of 1,356-MW Kashiwazaki-Kariwa Unit 7 with ABWR  
Source: F. Mizuki, Y. Miyamoto, and T. Seiji<sup>11</sup>

Wet-steam turbines for nuclear power plants are commonly designed with throttle steam flow control (see chapter 3). Thus, any unloading of the turbine and decrease of the steam flow amount through the turbine is accompanied by a decrease in the power generation efficiency. To avoid, or at least reduce this effect, most superheated-steam turbines of fossil fuel power units, especially those with throttle steam flow control, are mostly operated with a sliding, variable main steam pressure. In this case, the line of steam expansion in the HP section shifts to the right in the Mollier diagram; the enthalpy drop somewhat increases as compared to the case of throttling the

steam, and the turbine's heat rate decreases. The same phenomenon takes place in wet-steam turbines, but the effect depends more on the level of initial steam pressure and the depth of steam throttling. What is more, reduction of the throttle steam pressure also results in some decrease of the steam temperature after the steam reheater fed by main steam as the heating fluid.

The steam expansion processes for a wet-steam turbine for full and partial steam flow amounts under constant and sliding main steam pressure are shown in the Mollier diagram in Figure 4-6.

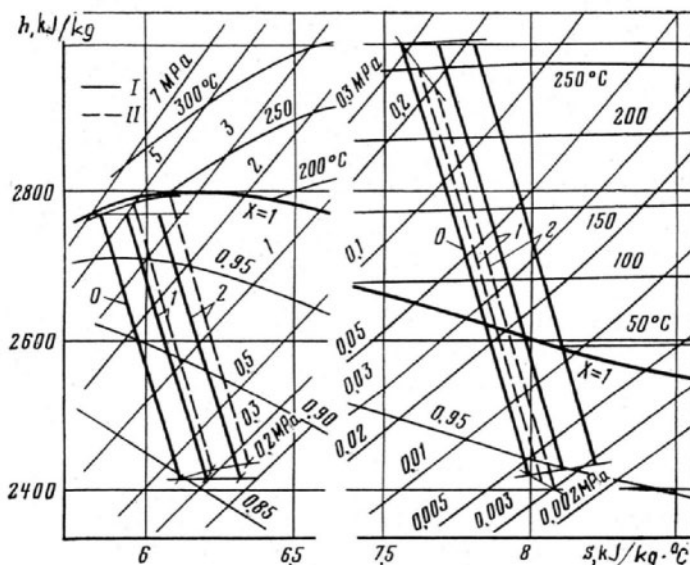


**Fig. 4-6.** Steam expansion processes for a wet-steam turbine with full and partial steam flows under constant (I) and sliding (II) main steam pressure (0: 100% steam flow; 1: 80% steam flow; 2: 60% steam flow; I: constant main steam pressure; II: sliding main steam pressure)

Source: B.A.Arkad'ev<sup>12</sup>

Even with sliding pressure, the main steam remains on the saturation line. If the main steam pressure is more than 3 MPa, its reduction with unloading the turbine increases both the initial enthalpy value and the enthalpy drop and decreases the final steam wetness in the HP section, thereby increasing its efficiency. A reduction in the main steam pressure also decreases the reheat steam temperature and the

enthalpy drop for the turbine section after the MSR, but the final steam wetness remains approximately the same. When the turbine is unloaded with a constant main steam pressure, the reheat steam temperature almost does not change and even slightly rises, and the final steam wetness decreases, thus increasing turbine efficiency. Because wet-steam turbines of contemporary nuclear power units are designed with a relatively low main steam pressure (less than 7 MPa), the influence of all these effects on turbine efficiency is not as great as that for modern fossil fuel power units of, for example, supercritical steam pressure.

Experimental investigations conducted at the Kola nuclear power plant, which uses PWR-type VVER-440 reactors with the rated main steam pressure of 4.3 MPa, showed that unloading the unit to 80% MCR under sliding steam pressure causes a heat rate decrease of approximately 0.6% as compared with unloading under constant main steam pressure. This effect should be more for nuclear power units with a higher main steam pressure and with regard to a possible additional reduction of the energy expenditures for feed water pumps.<sup>13</sup>

Light-water nuclear reactors should be stopped periodically for refueling. When the reactor's reactivity margin expires due to fuel burn-out, the reactor can no longer operate under full load with the rated parameters (point A in Fig. 4-7) and should begin to shut down with gradual unloading. This *stretch-out* process can be seen in Figures 4-2 and 4-3, as well as in line AB of Figure 4-7. Transferring the power unit to the sliding main steam pressure makes it possible to prolong the unit's operation campaign before refueling. Reduction of the main steam pressure causes a decrease of the average coolant temperature in the reactor and changes the energetic spectrum of neutrons and their mean free path. This also results in production of additional amounts of energy due to deeper burning of the fuel. If, at the end of the operation campaign, the turbine valves are kept completely open and the main steam pressure gradually decreases along with the decrease in the reactor load, the stretch-out process can be extended (line AC in Fig. 4-7). In doing so, if the feed water and hence steam flow amounts are increased, for some time the turbine load can be kept at the rated level with reduced main steam pressure, even with a reduced reactor capacity (line AD in Fig. 4-7). Then, the reactor output gradually reduces, whereas the turbine's control valves remain fully open (line DE in Fig. 4-7). In this case, the stretch-out process and operation campaign can be prolonged to an even greater degree.

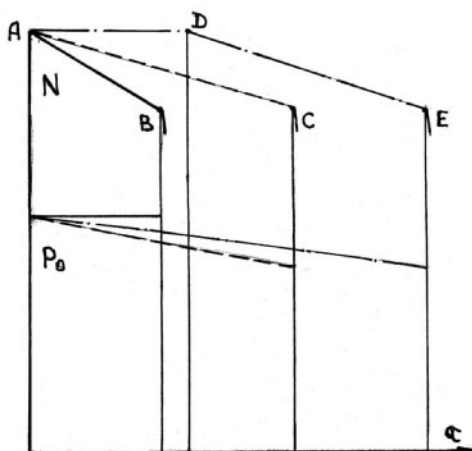


**Fig. 4-7.** Load capacity diagrams for a light-water reactor at the end of operation campaign with constant and sliding main steam pressure  
Source: B.A.Arkad'ev<sup>14</sup>

In the process of experiments at the Kola nuclear power plant, it was shown to be possible to keep the power unit's electric output at the rated level for eight additional days, keeping the turbines' control valves fully open and reducing the main steam pressure. In this way, the reactor's operation campaign was prolonged by 115 days (84 "effective" days) with additional power production of 900 million kWh. During this process, the power unit's electric output decreased from 410 MW to 260 MW; the main steam pressure fell from 4.3 MPa to 2.2 MPa (from 624 psi to 320 psi), and the mean water temperature in the reactor decreased from 284°C to 231°C (from 543°F to 448°F).<sup>15</sup>

Even if nuclear power units are operated in a purely base-load mode, they unavoidably go through some transient operating conditions: scheduled and unscheduled shutdowns with subsequent start-ups, load changes, turbine trips, and so on. Despite low heating steam temperatures, quite high temperature differences and unsteady thermal stresses can arise in wet-steam turbines during these transient operating conditions, especially start-ups, due to great dimensions of the main turbine design components and high heat transfer conditions for wet steam. More often than not, for the largest contemporary wet-steam turbines, the design components experiencing the highest thermal stresses are the turbine's rotors. This refers to not only the HP rotors, but also the welded or forged LP ones.

Typical temperature fields in the outer casing and rotor of the integrated HP-IP cylinder of Turboatom's 500-MW low-speed turbine, as in Figure 3-18, for a typical start-up instant, based on experimental measurements and calculations, are presented in Figure 4-8. The diagram of shutting down the turbine and its subsequent start-up after a one-day outage can be seen in Figure 4-9. The next images of Figure 4-10 show characteristic calculated temperature fields in the welded LP rotor of a Turboatom high-speed (3,000 rpm) wet-steam turbine for a typical start-up instant and stationary operating conditions.

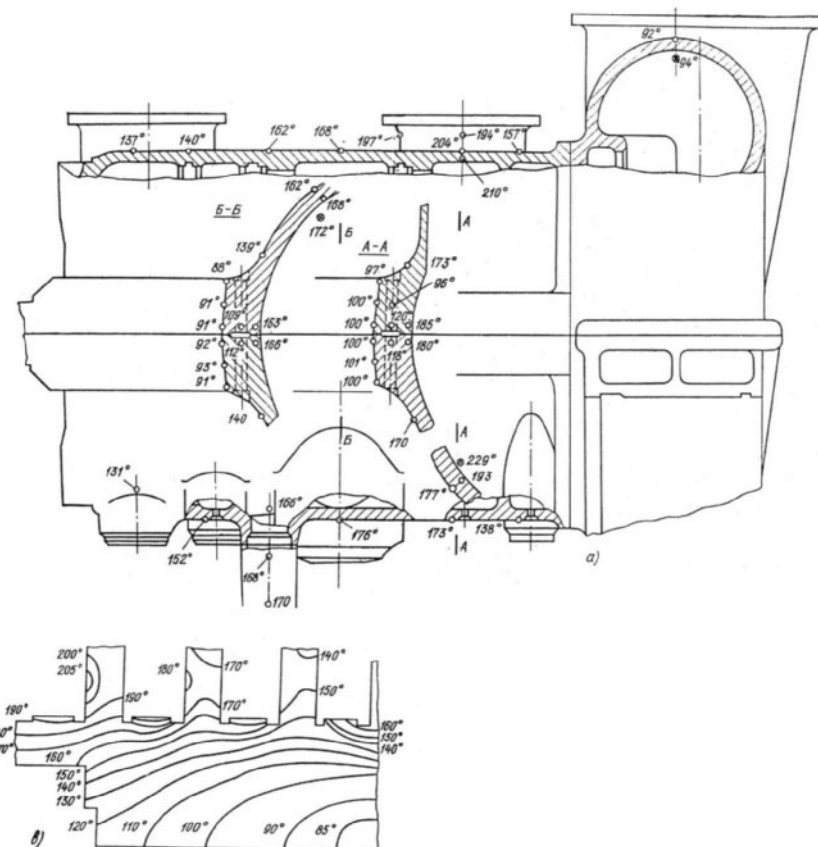


**Fig. 4-8.** Measured temperature distribution ( $^{\circ}\text{C}$ ) in outer casing (a) and calculated temperature field in rotor in the first IP stages zone (b) for the integrated HP-IP cylinder of Turboatom's K-500-60/1500 turbine for a typical start-up instant

Source: V.S Akerman, N.S. Gabrijchuk, V.B. Kirillov, A. S. Leyzerovich, et al.<sup>16</sup>

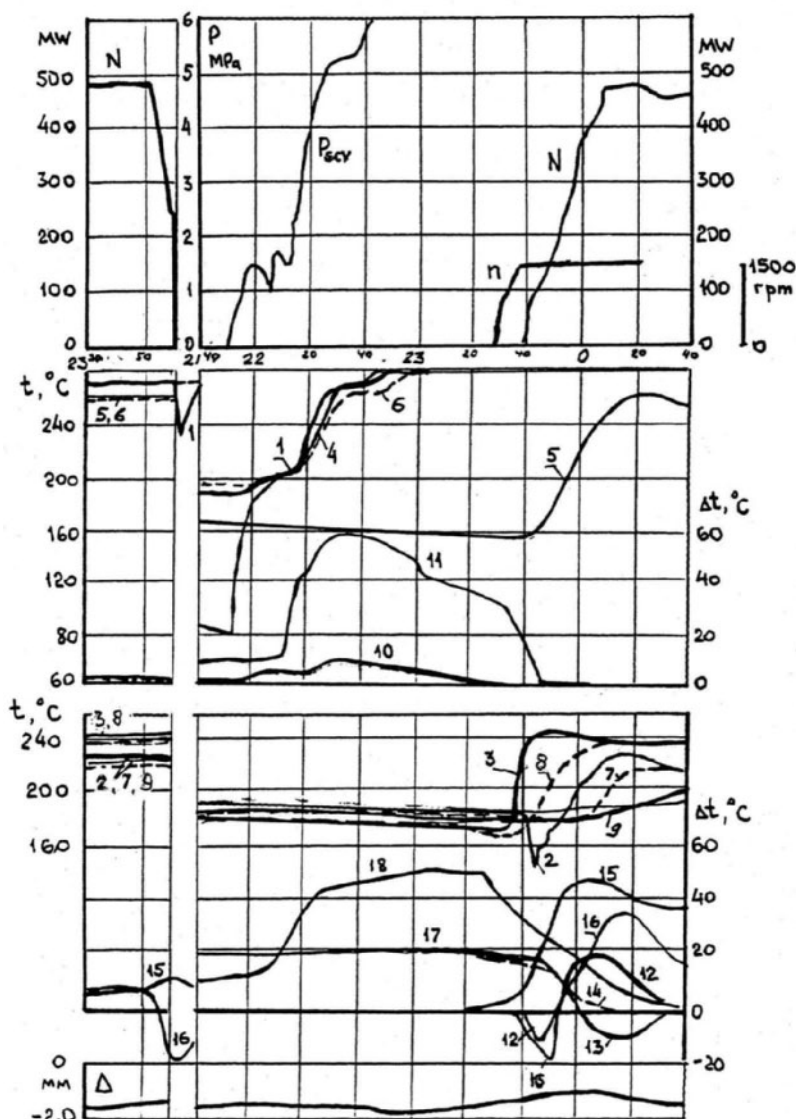


**Fig. 4-9.** Shutdown and start-up after one-day outage for Turboatom's K-500-60/1500 turbine at the Novovoronezh nuclear power plant (Steam temperatures: 1: in the steam chest of the stop/control valve (SCV); 2: in the first steam extraction chamber; 3: in the IP steam admission chamber. Metal temperatures: 4: main steam-line between the main gate valve (MGV) and SCV; 5: crossover pipe downstream from the SCV; 6: steam-chest wall of the

SCV; 7: wall of the HP-IP casing in the first steam extraction zone; 8: wall of the HP-IP casing in the IP steam admission zone; 9: external surface of the HP-IP casing flange in the HP steam admission zone. Temperature differences: 10: across the wall thickness of the SCV steam chest; 11: between top and bottom of the HP steam admission sleeve; 12: across the wall thickness of the HP-IP casing in the first steam extraction zone (on top); 13: across the wall thickness of the HP-IP casing in the IP steam admission zone (underneath sleeves); 14: across the wall thickness of the HP-IP casing in the IP steam admission zone (on top, between the sleeves); 15: across the HP-IP casing flange width in the first extraction zone; 16: across the HP-IP casing flange width in the IP steam admission zone; 17: between top and bottom of the HP-IP casing in the first steam extraction zone; 18: between top and bottom of the HP-IP casing in the IP steam admission zone;  $\Delta$ : relative expansion of the HP-IP rotor;  $P_{SCV}$ : steam pressure after the MGV in the SCV steam-chest  
 Source: VS Akerman, NS Gabrijeljuk, VB Kirillov, A S Lezzerovich, et al.<sup>17</sup>

Source: V.S Akerman, N.S. Gabrijchuk, V.B. Kirillov, A. S. Leyzerovich, et al.<sup>17</sup>

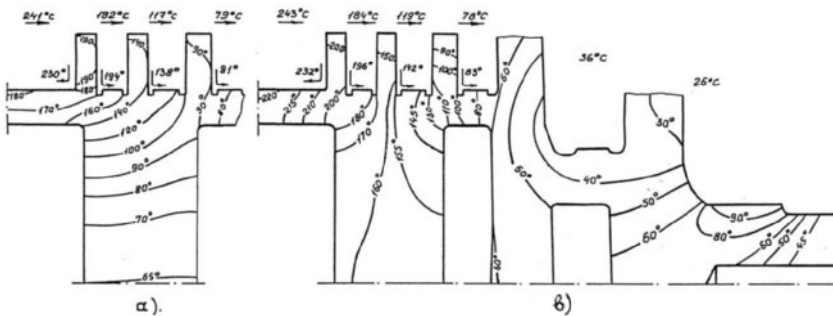


**Fig. 4-10.** Calculated temperature fields ( $^{\circ}\text{C}$ ) for the first-stage disk of a welded double-flow LP rotor of a Turboatom high-speed turbine at cold start-up (a) and the right half of the same rotor at stationary operating conditions under load (b)

Unsteady tensile thermal stresses in the rotors at turbine start-ups, combined with centrifugal stresses, can cause brittle fracture of the rotors. Repeated transients with high alternating thermal stresses can cause low-cycle (thermal) fatigue cracks on the rotor surfaces in the vicinity of stress concentrators. High unsteady thermal stresses in the casings can cause their cracking and distortion with resulting steam leakages. To prevent these effects, the transients should be run observing limits for the temperature differences and thermal stresses in the most stressed components. The diagram of

Figure 4-11 demonstrates an emulation of a start-up and subsequent load changes under control of an automated system developed for the 500-MW high-speed turbines of the Chernobyl nuclear power plant. The transients' rates are limited by a so-called "effective" radial temperature difference in the welded HP rotor. This difference is in proportion to the thermal stress on the rotor surface in its most stressed section and is monitored by means of mathematical modeling of the rotor temperature state. The limits for the monitored temperature difference are set differently for start-ups and load changes, with regard to different frequencies of these transients and thus their different expected contributions to thermal fatigue of the turbine metal. A calculated temperature field in the first stages' disk of the HP rotor for a characteristic start-up instant and emulated start-up diagrams for "hot," "warm," and "cold" initial temperature states of the turbines are presented in Figure 4-12.

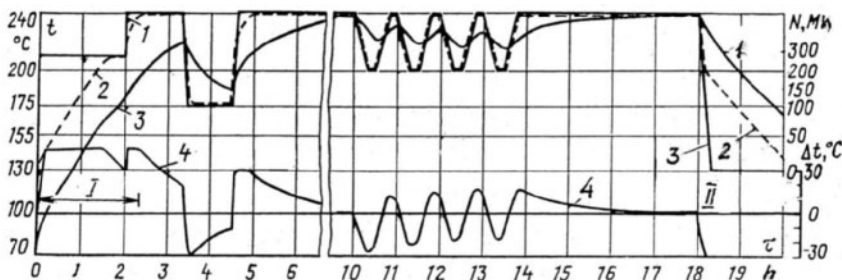


**Fig. 4-11.** Emulation of automated start-up and load changes for Turboatom's K-500-65/3000 turbine with limits for temperature difference and thermal stress in the HP rotor (1: set turbine load; 2: actual turbine load and metal temperature on the rotor surface in the most stressed section; 3: average integral metal temperature of the rotor in the same section; 4: effective radial temperature difference in the rotor, in proportion to the maximum thermal stress; I: start-up; II: shutdown)

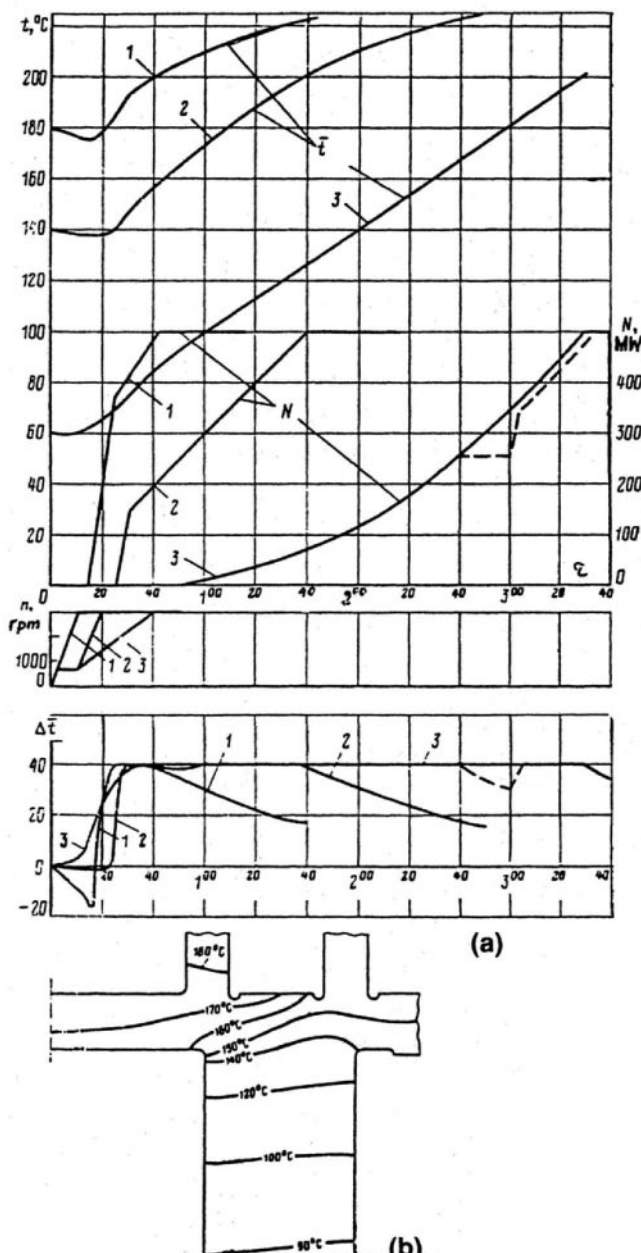
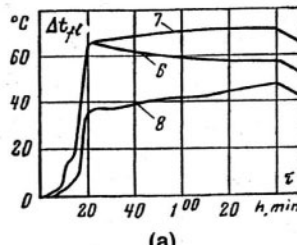
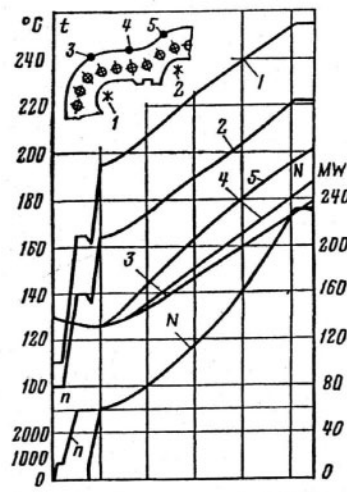


**Fig. 4-12.** Mathematical modeling of automated start-ups from hot (1), warm (2), and cold (3) initial states for Turboatom's K-500-65/3000 turbine (a) and temperature field for the first-stage disk of the HP rotor (b)  
Source: A. S. Leyzerovich and V.B. Kirillov<sup>18</sup>

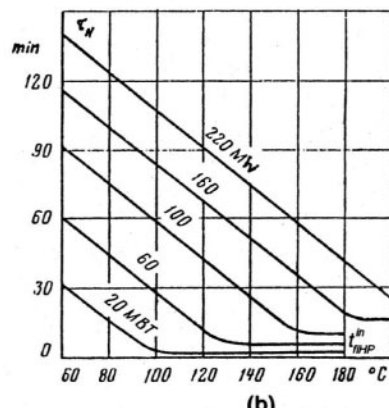
High temperature differences and thermal stresses can also occur during the transients in the thick-walled stator components, such as the HP valve steam-chests and cylinder casings, potentially causing their cracking. The highest temperature differences can arise in flange joints, causing their distortion and loss of tightness, with subsequent progressive crevice corrosion of the joint surfaces. In such cases, the start-up diagrams should be developed based on the condition of maintaining the temperature differences across the flange width at a predetermined level, not exceeding it, as in Figure 4-13a. The resulted schedule of loading the 220-MW turbine shown in Fig. 4-13b was included in the start-up instruction for this turbine.

**Fig. 4-13.** Optimization of loading schedules for Turboatom's K-220-44 turbine (a: optimized diagram of warm start-up; b: generalized schedule of loading at start-ups from different initial temperature states. Steam temperatures: 1: in the steam admission chamber; 2: in the first-stage chamber metal temperatures on the external surface of the HP flange; 3: in section after the third stud bolt; 4: in section after the fifth stud bolt; 5: in section after the eighth stud bolt. Temperature differences across the HP flange width: 6: after the third stud bolt; 7: after the fifth stud bolt; 8: after the eighth stud bolt;  $t_{\text{HP,in}}$ : initial HP flange metal temperature on the external surface in section after the fifth stud bolt before the generator is switched on to the grid)

Source: A. S. Leyzerovich, V. B. Kirillov, S. P. Kruzhkova, et al.<sup>19</sup>



(a)

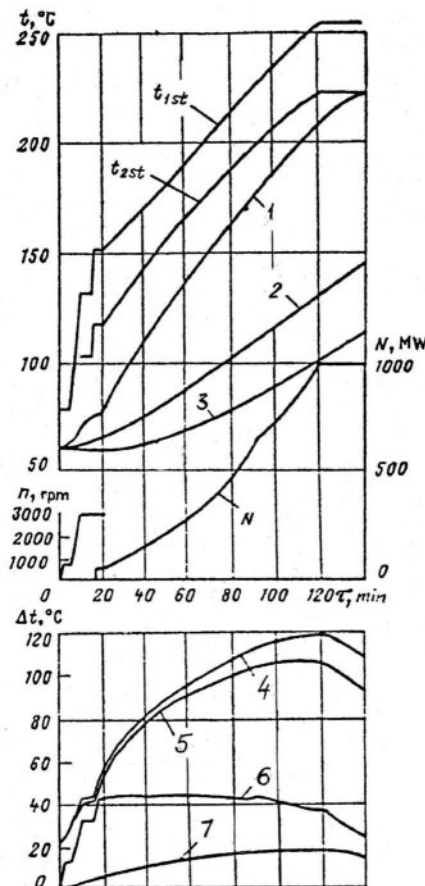


(b)

For some turbines, the start-up rate for different types of start-ups or at different start-up stages can be alternately limited by the thermal-stress state of different design components and different indications—for example, by the temperature differences across the HP casing's flange width, or the effective radial temperature difference in the HP rotor. Such a situation can be illustrated by the calculated cold start-up diagram of Figure 4-14 for LMZ's 1,000-MW high-speed turbine. At the initial loading stage, the start-up rate is limited by the radial temperature in the rotor, and at the concluding stage, it is limited by the temperature difference across flange width.

**Fig. 4-14.** Calculated diagram of optimized cold start-up for LMZ's 1,000-MW high-speed turbine ( $t_{1st}$ : steam temperature at first HP stage;  $t_{2st}$ : steam temperature at second HP stage. HP cylinder metal temperatures: 1: average integral of the HP rotor in section near the first stage; 2: stud bolt at mid-height of the upper flange; 3: external surface at mid-height of the upper flange. metal temperature differences: 4: across the upper flange width; 5: across the lower flange width; 6: along the rotor radius; 7: between the flange (near the heated surface) and stud bolt at mid-height of the upper flange)

Source: A. S. Leyzerovich, B. L. Levchenko, and V. B. Kirillov<sup>20</sup>



At fossil fuel power plants, in order to prevent the appearance of inadmissible unsteady temperature differences and thermal stresses in the main turbine components, as well as significant relative rotor expansions (RRE), and decrease the total start-up duration, the

start-up operations of the boiler and turbine are partially overlapped. The turbine start-ups are run with sliding steam parameters in such a way that the heating steam temperatures within the turbine match the turbine metal temperatures, and raising the heating steam temperatures goes at the rate in proportion to the desirable heating for the most-stressed turbine components. Running start-ups under variable steam conditions makes the factors limiting the start-up rate more controllable. When the start-up is finished and the turbine is operating under load, keeping the turbine control valves in a fixed position (that is, allowing the main steam pressure to slide with the steam flow amount or turbine load) also improves the unit's flexibility, because the heating steam temperatures in the HP section vary with the turbine load much less than they do when operating under constant main steam pressure.<sup>21</sup>

By contrast, wet-steam turbines of nuclear power units are generally operated under constant main steam pressure. Even during the start-up process, more often than not main steam is given to the turbine only after the reactor reaches the rated steam pressure; meanwhile, the generated steam is discharged through the turbine bypasses into the main or auxiliary ("technological") condenser(s). When the start-up process is finished and the turbine is operating under load, all of the load changes commonly occur with constant main steam pressure, with the turbine control valves following the load changes. Nevertheless, it does not practically affect the turbine's flexibility, because the major turbine components (more accurately, those of the HP section) are swept and heated by wet steam, with the saturation temperatures at the corresponding pressures varying in proportion to the steam flow amount through the turbine, independently of the main steam pressure value. Because the heat transfer coefficients for wet steam are sufficiently high (in the order of  $10^4 \text{ W/m}^2 \times ^\circ\text{C}$ ), the heated surface temperatures may be thought of as following the saturation temperatures.

The main steam pressure and its possible variations matter only for the HP valve steam-chests. However, when the turbine is started up, the valve steam-chests are generally heated before the valves are opened and steam passes into the turbine. If the turbine is furnished with combined stop/control HP valves and they are directly connected to the main steam lines after the reactor (or its steam generator), their steam-chests are heated in the process of raising the main steam

pressure after the reactor. This commonly happens with a relatively low rate and does not cause any problems for the valve steam-chests. However, if the HP valves are separated from the main steam lines with main gate valves (MGVs) and the main steam can pass into the valve steam-chests with the rated pressure, the “temperature shock” with opening the MGVs can cause fairly high temperature differences and thermal stresses in these steam-chests. This situation takes place, for example, at double-turbine nuclear power units—during start-up of the second turbine when the first one already operates under load. In this case, it is advisable to have a special bypass of the MGVs with a governing valve of a limited flow capacity in order to raise the steam pressure in the HP valve steam-chests gradually before passing steam into the turbine. This process can be seen in Figure 4-9. When the turbine operates under load, any ordinary variations in the main steam pressure cannot cause significant temperature unevenness in the HP valve steam-chests, because the heating steam temperature (that is, the steam saturation temperature) varies insignificantly.

After steam is passed into the turbine and while running up the turbine at start-up, the steam flow amount through the turbine is not more than 6–8% MCR. The corresponding saturation steam temperatures in the HP steam path are not sufficient to cause any significant temperature differences in the HP metal, even at cold start-ups. Unlike superheated-steam turbines of fossil fuel power plants (especially those with a common main steam line, which are started up with the rated main steam conditions), the temperature state of wet-steam turbines does not limit the rate of running up. More likely, in contrast, at hot start-ups, it is desirable not to linger at this stage to prevent cooling down the turbine with throttled steam entering the HP section.

One of the most serious problems for superheated-steam turbines in fossil fuel power plants during start-ups is a danger of brushing and rubbing in the seals and their resultant wearing out due to excessive relative rotor expansions (RREs) for the turbine cylinders, especially the HP one. The main causes of this phenomenon are: 1) much greater heat transfer coefficients from steam to the rotating surfaces of the rotors as compared with those for the motionless stator components and 2) a much more favorable ratio of the heat transfer surface area and the mass for the rotor as compared to this ratio for the casing. Sometimes, the difference in the thermal expansion coefficients for the rotor's and casing's steels can play a role, but more often than not

this difference is of minor importance. For wet-steam turbines, the heat transfer coefficients from steam to the HP rotor's and stator's surfaces are of the same order, and the mass of the HP rotor is commonly much more commensurable with the mass of the casing than takes place for superheated-steam turbines. In addition, a much lower temperature level makes the final thermal expansions of both the rotor and casing and hence the difference in their thermal expansion much less. Because of all these circumstances, for wet-steam turbines, variations of the HP RRE during start-ups are usually insignificant and do not limit the rate of start-ups (Fig. 4-9). In some cases, especially for wet-steam turbines with massive HP rotors, there can even appear a negative RRE. When the turbine is running up, the rotors additionally shorten, due to Poisson's effect, because of the growing centrifugal forces that radially "tense" the rotors. For typical HP rotors of wet-steam turbines, this decrease of the rotor length can amount to approximately 1–1.5 mm (0.04–0.06 in), and for LP rotors it can reach 4–5 mm (0.16–0.20 in).<sup>22</sup> This effect should be taken into consideration while setting the axial clearances in the turbine steam path.

The turbine parts after the external moisture separators and reheaters MSRs, that is, the IP section (if it exists) or LP cylinder(s), are swept and heated by superheated steam. Unlike the HP section, the heating of these parts is determined by two factors: 1) the heat transfer conditions from steam to the heated surfaces, depending on the turbine load, as it takes place in the superheated-steam turbines, and 2) the reheat steam temperature after the MSR. The reheat steam temperature also depends on the turbine load because of the MSR's static characteristics—that is, changes of the reheat temperature with the main steam flow amount (Fig. 4-54). If the turbine has a separate IP section or cylinder (as, for example, Turboatom's K-500-60/1500 and K-1000-60/1500 turbines and ALSTOM's 1,500-MW turbine, the *Arabelle*, shown in Figs. 3-1, 3-16, and 3-18), the main factors that could limit the increase of the reheat steam temperature are the temperature differences along the IP rotor radius or across the IP casing flange width (as, for example, for the previously mentioned Turboatom turbines with the thin-walled, drum-type welded rotor of the HP-IP or IP cylinders). If the turbine is designed without an IP section, with either welded or forged LP rotors, the limiting factor could be the temperature stresses in the rotors added to the tensile centrifugal stresses near the steam admission zone.

Because the heat transfer conditions for superheated steam under fairly low pressure are not very great and change significantly with increases in steam density, these changes tell remarkably on the rate of heating the considered design components. Under these conditions, it can be reasonable to raise the reheat steam temperature nonmonotonously: 1) with a rapid rise up to the rated value while the turbine is idling, 2) fall to an intermediate value after switching on the generator to the grid and accepting an initial load, and 3) gradual rise up to the rated level again in the process of further loading, as is shown in Figure 4-15. This method can be carried out without problems due to specific static characteristics of the MSRs (Fig. 4-54).

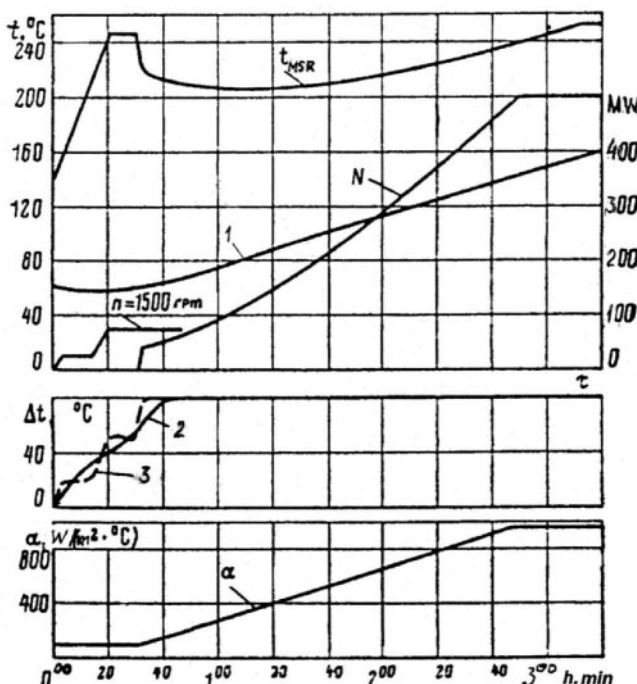


**Fig. 4-15.** Calculated optimization of a cold start-up of Turboatom's 500-MW low-speed turbine ( $t_{MSR}$ : reheat steam temperature after MSR; 1: metal temperature on the external surface of the upper flange at mid-height in the IP steam admission zone; 2 and 3: metal temperature differences across the HP-IP casing flange width in the IP and HP steam admission zones;  $\alpha$ : heat transfer coefficient from steam to metal of the outer casing in the IP steam admission zone)

Source: A. S. Leyzerovich and V.B. Kirillov<sup>23</sup>

In many cases, reactors can be emergently shut down because of improper functioning of their monitoring and protection systems or because of some accidental actions. Usually, in these situations, the turbines are also shut down; their main gate valves, stop, and intercept valves are closed, and the generators are switched off from the grid. It commonly takes the operator 20 to 180 minutes to detect and eliminate the causes of such operating actions, and then the power unit can be restarted. In order to make this restart easier, it can be advisable not to switch off the generator, and leave the turbine rotated by the generator as a motor. That is, the turbine run in a hot spinning reserve (standby) mode for as long as it takes to clarify the emergency situation. This allows avoiding the subsequent necessity of running up the turbine and synchronizing the generator during restart. The same method of so-called "motor operating conditions" can also be employed at double-turbine nuclear power units in the case of a deep short-term unloading of the reactor to less than 50% MCR.<sup>24</sup> The same approach was proposed for fossil fuel power units and was implemented at some power plants in the former Soviet Union. Experimental investigations at the Kola nuclear power plant with Turboatom K-220-44 turbines with 852-mm (33.5-in) LSBs (see Fig. 3-4) showed that the turbine can be handled under motor operating conditions for at least 2 hours without steam flowing through the LP cylinders, and for an unlimitedly long time period if the LP cylinders are supplied with cooling steam passing into the LP crossover pipes after the intercept valves and the condenser is kept under vacuum.

Motor operating conditions are also inherent in the cases of emergency load discharges if the generator is not switched off from the grid. The main problem in these cases, as well as in other no-load conditions, with small (or relatively small) steam flow amounts into the condenser, is a possible overheating of the rotating blades, because of energy losses due to friction and fanning. Such no-load conditions are also characteristic for the initial start-up stages, especially idling, before the generator accepts the load. The severity of this problem grows with the increase in the LSB length, as well as for turbines with relatively high back-pressure (for example, with dry cooling towers or with warm cooling water).<sup>25</sup> To prevent the LSBs from overheating, the duration of the no-load conditions can be limited. Another way to prevent overheating is the forced cooling of the LP steam path by a water injection

with special sprays into the exhaust hoods. However, these sprays must provide good atomization of the injected water, otherwise they can only cause additional problems with WDE of the LSBs.

With the reduction of the volumetric steam flow amount into the condenser, the axial exit velocity in the LSB root zone falls to zero, and at a certain instant in this zone, a reverse steam motion arises, accompanied by an appearance of mighty vortices (see Figure 3-51). With a further decrease of the steam flow amount, the vortex zone occupies a greater portion of the stage height, even taking over the previous stage, and another vortex zone arises around the blade tip (see Fig. 3-52). These vortices incite intense vibration in the rotating blades, causing a sharp increase of dynamic stresses in them (Fig. 4-16). In addition, the vortices cause intense erosion of the blades (Fig. 4-17). If water sprayed into the exhaust hood is not well atomized, the erosion hazard sharply increases.

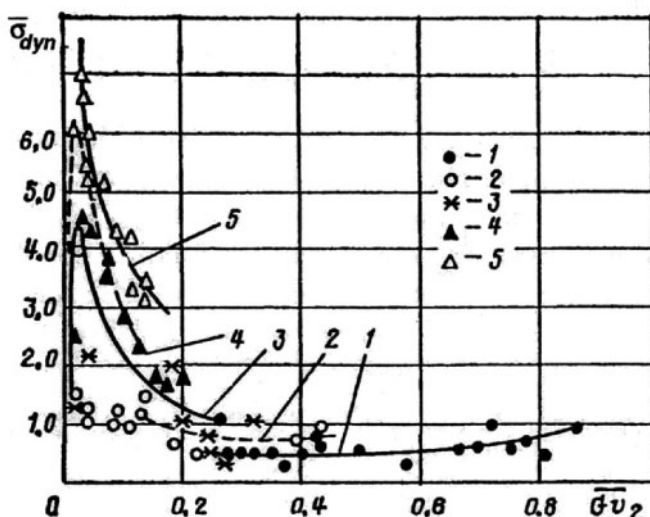


**Fig. 4-16.** Change of relative dynamic stresses in LP LSBs with back pressure and volumetric steam flow in the condenser (Pressure in condenser of: 1: 3-7 kPa [0.435-1.015 psia]; 2: 10-12 kPa [1.45-1.74 psia]; 3: 14-16 kPa [2.03-2.32 psia]; 4: 24-26 kPa [3.48-3.77 psia]; 5: 34-37 kPa [4.93-5.37 psia])

Source: N. N. Gribov, A. S. Shemonaev, and E. S. Mandryka<sup>26</sup>

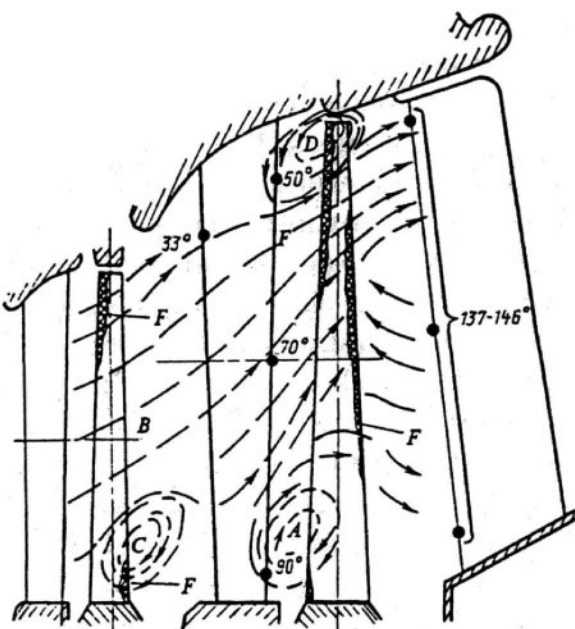


**Fig. 4-17.** Pattern of steam flows and steam temperatures and zones of increased erosion wear of blades in last stages of the LP steam path at a low-flow steam rate

Source: V.A. Khaimov, P.V. Khrabrov, Y.A. Voropaev, and O. E. Kotlyar<sup>27</sup>

Scheduled shutdowns of wet-steam turbines commonly go in parallel with unloading the reactor. When the turbine load decreases, the heating steam temperatures in the HP section decrease following the decrease of steam pressures with the steam flow amount. This makes the HP section cool down. If the turbine is unloaded too quickly, it can cause undesirable negative temperature differences in the turbine's most stressed components, so the unloading process should be governed and monitored just as the loading process is during start-ups. While unloading, the turbine can be cooled much more intensely than in the process of natural cool-down, so the initial temperature conditions of the subsequent start-ups are more dependent on the shutdown process than on the outage duration. Deep unloading of the turbine is desirable when the turbine is shut down for repairs and inspections. If the turbine outage is expected to be only for a short period, the turbine should not be kept under partial loads, and it is advisable to close the turbine valves at a load level of not lower than 50% MCR, to preserve the turbine's thermal state (Fig. 4-9).

Turbine load discharges, as well as overly rapid increases in the steam flow amount through the turbine during start-ups (for example, while running up the turbine), can cause water induction into the turbine from the connected steam lines, with unpleasant consequences. Water induction commonly can be revealed with the use of fast-acting steam-temperature measurements within the turbine chambers.<sup>28</sup> Such events are accompanied with impulse-type declines of the measured steam temperature in the turbine chamber where water inducts. An example of such an event is shown in Figure 4-44.

The cool-down characteristics of turbine components when the turbine is stopped are less important for wet-steam turbines than for superheated-steam ones, because, as said before, the pre-start thermal conditions of the turbine are determined more by the unloading process than the outage duration. The cool-down characteristics themselves are of concern only for the HP valve steam-chests and main steam-lines, to schedule in advance the duration of their pre-start heating. Analysis of cool-down data for the main steam lines can also be used to reveal possible water induction sources (Fig. 4-59). At the same time, the cool-down characteristics of the HP and IP sections can be used for estimating the quality of thermal insulation for their casings. Its insufficient quality can result in excessive temperature differences across the flange width. Relying on data from numerous field tests and analyses of recorded regular measurements at power plants with steam turbines of diverse types, the cool-down constant,  $m$ , for the HP (or HP-IP) cylinder casings of large wet-steam turbines can be expected to be approximately 0.010–0.015 (the cooling time constant,  $K \approx 67\text{--}100$  h). For the HP valve steam-chests, the expected value of the cool-down constant is  $m \approx 0.015\text{--}0.020$  ( $K \approx 50\text{--}65$  h), and for the main steam-lines  $m \approx 0.025\text{--}0.033$  ( $K \approx 30\text{--}40$  h).

Note that the value of the cool-down constant is determined from the cool-down characteristic for the measured metal temperature,  $t_m$ , presented in its exponential form:  $t_m(\tau) \approx t_a + [t_m(0) - t_a] \times \exp(-m\tau)$ , where  $t_a$  is the ambient temperature in the turbine room,  $\tau$  is the cool-down time period, and  $K = 1/m$ .

## Efficiency of Wet-Steam Turbines and Heat-Rate Performance Tests

Because nuclear power units are mainly operated in the base-load mode, the operating efficiency of wet-steam turbines, in addition to their safety, reliability, and availability, is especially important. However, in this case, the matter is not the quest for the lowest heat rate in order to decrease fuel expenditures and thus reduce power generation costs due to the fuel constituent, as it is for fossil fuel power plants. With nuclear power plants, the goal is to generate the maximum amount of energy from the reactor's available thermal capacity in order to substitute power generation by fossil fuel power plants and thus reduce environment pollution. The lower cost of electricity generated by nuclear power units is also of concern. That is why the wet-steam turbine efficiency is frequently estimated in terms of an additional output that can be obtained with the same thermal capacity of the reactor, rather than in terms of a decrease in the heat rate value.

If the gross efficiency of the best modern superheated-steam turbines for fossil fuel power plants approaches 50% (see chapter 2), wet-steam turbines rank significantly lower in their efficiency because of much lower steam parameters, as well as additional energy losses due to the steam wetness. The heat rate performance data for some "nuclear" wet-steam turbines of the mid-1980s are listed in Table 4-2.<sup>29</sup> Even though these values have been transcended by more advanced turbines launched since then (as, for example, the French 1,500-MW *Arabelle* turbines), as well as some recently refurbished turbines (see chapter 5), the data shown in Table 4-2 remain quite representative even now. The benchmark in efficiency for wet-steam turbines of the new generation has been set at the level of about 36.5%, reached for Siemens' 1,300-MW turbines after their refurbishment.<sup>30</sup> For Siemens' newest and largest in the world wet-steam turbine with the rated individual capacity of 1,720 MW to be commissioned in 2009 at Finnish Olkiluoto Unit 3, the net efficiency is expected to be at the level of 37%.<sup>31</sup>

**Table 4-2.** Comparative efficiency data for some wet-steam turbines of different manufacturers operated at NPP of different countries (as of 1986)

Nuclear power unit, country	Reactor type	Turbine manufacturer	In service since	Turbine rated capacity/ rotation speed, MW/ rpm	Guarantee heat rate (efficiency), kJ/kWh (%)
Grohnde, Germany	PWR	Siemens/KWU	1984	1361 / 1500	9,959 (36.1)
S.-Ukrainian-1, Ukraine	PWR	Turboatom	1983	1100 / 1500	10,020* (35.9)
Ohi-2, Japan	PWR	MHI	1978	1175 / 1800	10,035* (35.9)
Ohi-1, Japan	PWR	MHI	1977	1175 / 1800	10,040* (35.9)
Philippsburg-1, Germany	PWR	Siemens/KWU	1984	1349 / 1500	10,047 (35.8)
Fitzpatrick, USA	BWR	GE	1975	848 / 1800	10,155* (35.5)
Catawba-1, USA	PWR	GE	1985	1205 / 1800	10,190 (35.3)
Saint Alban-1, France	PWR	Alsthom	1985	1048 / 1500	10,194 (35.3)
Doel-4, Belgium	PWR	BBC (ABB)	1985	1059 / 1500	10,198 (35.3)
Biblis-B, Germany	PWR	Siemens/KWU	1976	1303 / 1500	10,244* (35.1)
Wolf Creek-1, USA	PWR	GE	1985	1197 / 1800	10,259 (35.1)
Fermi-2, USA	BWR	English Electric	1985	1154 / 1800	10,273 (35.0)
Tihange-3, Belgium	PWR	Alsthom	1985	1048 / 1500	10,305 (34.9)
Takahama-3, Japan	PWR	MHI	1984	870 / 1800	10,358* (34.8)
Ignalina-1, Lithuania	RBMK	Turboatom	1983	800 / 3000	10,383 (34.7)
Pilgrim-1, USA	BWR	GE	1972	691 / 1800	10,434* (34.5)
Byron-1, USA	PWR	Westinghouse	1985	1175 / 1800	10,450 (34.4)
Takahama-4, Japan	PWR	MHI	1984	870 / 1800	10,496* (34.3)
Kola-3, Russia	PWR	Turboatom	1983	220 / 3000	10,528* (34.2)
Crystal River-3, USA	PWR	Westinghouse	1977	860 / 1800	10,548* (34.1)

Loviisa, Finland	PWR	Turboatom	1980	235 / 3000	10,549* (34.1)
Gundremmingen B and C, Germany	BWR	Siemens/KWU	1984	1310 / 1500	10,553 (34.1)
Fukushima-2, Japan	BWR	Hitachi	1983	1100 / 1500	10,570 (34.1)
Kashiwazaki-1, Japan	BWR	Toshiba	1985	1100 / 1500	10,777 (33.4)

\* According to heat-rate test results

Source: Y.F. Kosyak<sup>32</sup>

The main and most reliable source of data on the wet-steam turbine efficiency is the heat-rate performance test. They are often conducted as acceptance tests to verify the efficiency data guaranteed by the turbine producer and to ascertain the actual performance of the turbine. Performance tests can also pursue the goals of tracking changes in turbine efficiency during operation or estimating the effectiveness of modifying the turbine design, that is, refurbishing the turbine. Some simplified heat-rate performance tests are carried out before and after turbine overhauls to evaluate the quality of turbine operation and maintenance. The specific heat-rate test scenarios, applied methods, instrumentation setup, and operating conditions can differ depending on the test goals, and they should be agreed upon prior to conducting the tests.

The main approaches to preparing for and conducting the heat-rate performance tests, as well as processing and analyzing their results, are in particular described in the author's *Large Power Steam Turbines: Design & Operation*. This description is mainly based on general requirements of the *ASME Performance Test Codes: Code on Steam Turbines* (PTC 6) developed by ANSI and ASME<sup>33</sup> and experience conducting such tests in the former Soviet Union, generalized by A. M. Sakharov.<sup>34</sup>

The philosophy of PTC 6, as is that of all the ASME Performance Test Codes, is to "provide test procedures which yield results of the highest level of accuracy consistent with the best engineering knowledge and practice currently available." This philosophy can be traced back to the 1915 Test Code, which provided the directive: "Ascertain the specific object of the test and keep this in view, not

only in the work of preparation, but also during the progress of the tests and do not let it be obscured by devoting too close attention to matters of minor importance. Whatever the object of the test might be, accuracy and reliability must underlie the work from beginning to end.<sup>35</sup> This refers to the entire test process, beginning with developing the scheme of measurements and scheduling the operating conditions for the tests and up to after-the-fact comparative analysis of the calculated data. Inattentiveness, carelessness, or errors at any stage of planning and conducting the tests and processing the measured data can depreciate the value of the obtained results.

Success of turbine heat-rate performance tests primarily depends on furnishing the turbine with all of the necessary measurements of proper accuracy, correct location, and proper arrangement. The general concepts for shaping the schema of measurements for heat-rate performance tests are described in the following paragraph.

All of the measuring instruments should be calibrated according to the appropriate national standards. The main variables, such as steam and water flow amounts, temperature and pressure values, and electrical load at the generator terminals, should be measured with instruments of the highest accuracy. It is desirable to duplicate main measurements to increase their reliability and representativeness. In particular, the ASME Code specifies duplicate instrumentation for measuring certain types of data that have been found to be especially troublesome and for which duplication is readily available. These measurements are mostly the flow-nozzle differentials and working-fluid temperatures. Several measurements require confirming each other by tracing their pattern across multiple test points. Duplication of other types of instrumentation should be seriously considered to ensure successful use of the instruments, to detect trouble, and to reduce uncertainty by averaging the results of the duplicated instruments.

A typical, somewhat simplified diagram of measurements for heat-rate performance tests as applied to "nuclear" wet-steam turbines according to PTC 6 is shown in Figure 4-18. This diagram refers to the turbines with the feed water heater drain pumped forward, and there is another diagram proposed for turbines with cascading drains of all the feed water heaters into the condenser.<sup>36</sup> Similar recommendations have been used in practice in Europe and the former Soviet Union. They are mainly grounded on the same approaches.

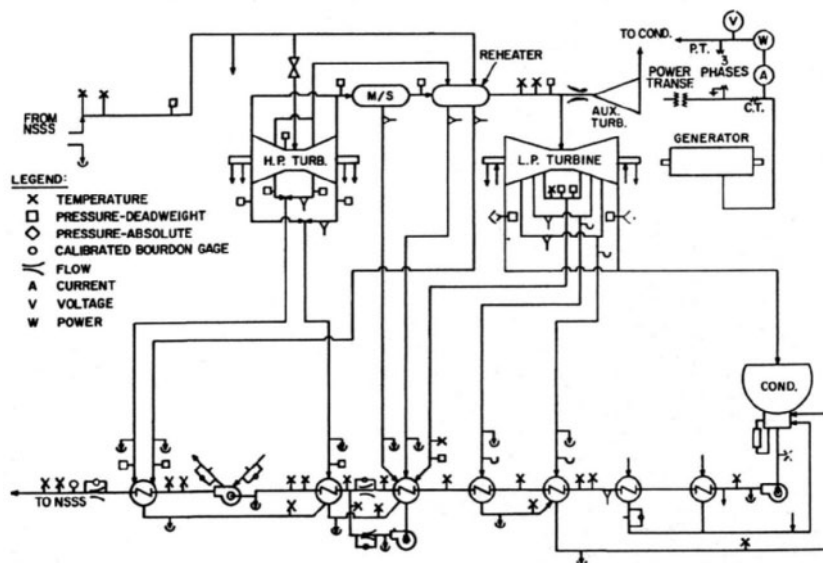


**Fig. 4-18.** Location and type of main measurements at a wet-steam turbine for heat-rate performance tests according to PTC 6 (NSSS: nuclear steam supply system; M/S: moisture separator)

Source: B. Bornstein and K. C. Cotton<sup>37</sup>

The main method of primary-flow measurements is based on the use of calibrated throat-tap nozzles to measure the differential pressure at the nozzle. If the turbine has two or more strings of feed water heaters, then two or more feed water flow measurement devices are used in parallel, one for each string. The type of instrumentation and the technique for measuring secondary flows are determined by the accuracy requirements, based on calculation of the expected flow amounts and their effect on the overall results. It is accepted that the combined error of these measurements should not affect the resultant heat-rate value by more than 0.1%. In particular, any secondary flow measurements requiring less than 5.0% error must be performed with calibrated flow-measuring devices. If the extraction steam is superheated (after the MSR in wet-steam turbines), its flow amount can be determined by heat balance calculations. The accuracy of the result decreases as the temperature rise across the heater diminishes. Errors in the temperature measurements will be carried over to the error in determining the extraction flow amount. In wet-steam cycles, extraction flow amounts can be determined from heater drain flow measurements, using calibrated flow-measuring devices.

Acceptable temperature measurement systems are mainly based on the use of suitable thermocouples with integral cold junctions, as well as platinum resistance-type thermometers. Their accuracy for the most important measurements is desirable to be 0.1%. This might be the most critical limitation in the use of regular instruments for heat-rate performance tests, because the accuracy of regular temperature measurements is commonly 0.5% or even worse. The temperatures that have the greatest influence on the test results should be measured, at least, at two different nearby points, and the fluid temperature should be calculated as the average. Discrepancies between two readings must be resolved if they exceed 0.5°C (1°F).

According to the ASME Code, pressure measurements are mostly performed with calibrated deadweight gauges for pressures greater than 240 kPa (35 psia) and with calibrated manometers for pressures less than this value. For exhaust pressure measurements at condensing turbines, absolute pressure gauges or calibrated manometers are used. To fit modern data monitoring and processing equipment, the ASME Codes allows the use of pressure transmitters.

The electric output of the generator is normally measured using separate test instruments for each phase. The two-wattmeter method can also be employed to test a generator operating with a grounded neutral. It is also desirable to measure the power output by several independent methods, including the meter of output electric energy. Commonly, these measurements, as well as the measurements of electric energy expenditures for turbine auxiliaries (primarily motor-driven pumps), are performed according to the special standards and instructions for electric measurements in power circuits. If the feed water pump is driven from the turbine shaft, additional measurements must be made to determine as accurately as possible the power supplied by the turbine for the driven pump and any associated hydraulic couplings.

A big problem for wet-steam turbines, as well as for LP turbine cylinders of fossil fuel power plants, is the measurement of the quality of wet steam, that is, the steam wetness. According to the ASME Code, the following methods, listed in order of preference, can be used to determine the steam wetness: 1) radioactive tracer technique (for main and extracted steam), 2) heater drain flow measurements (extraction steam only), and 3) heat balance calorimeters for direct

determination of wetness (main steam only). The radioactive tracer technique has the advantage of not requiring a representative sample of the water-steam mixture—only a water sample is required.

A conventional measurement diagram for an actual Brown Boveri 1,100-MW low-speed wet-steam turbine is presented in Figure 4-19 (the general view and longitudinal section of such a turbine are shown in Fig. 3-10). The tests were conducted jointly by Brown Boveri and American Electric Power Service Corporation (AEP), the nuclear power plant's owner, in strict accordance with the PTC 6 requirements and with regard to European practice.<sup>38</sup> Because of the very large mass of the feed water flow, three throat-tap nozzles were installed in parallel in the feed-pump suction lines. The nozzles were laboratory-calibrated both before and after the tests. Dual sets of differential pressure taps on each nozzle were connected to precision quartz Bourdon tubes. At significant points in the cycle where the temperature has a great influence on the test results, anywhere from two to four measurements were settled. For example, at each of the turbine's LP crossover pipes (between the MSR and LP cylinders), four thermocouples were placed 90° apart in one plane. Approximately 140 individual temperature measurements were installed. Most pressures were measured with deadweight gauges. For pressures less than approximately 0.3 MPa (45 psia), calibrated, temperature-compensated Bourdon tube gauges of test-class accuracy (0.1%) were used. The turbine exhaust pressures were measured with mercury-filled absolute-pressure gauges; special precautions were taken to minimize the risk of an accidental introduction of mercury into the cycle. The total number of individual pressure measurements was approximately 115. Moisture flows in the wet-steam bleeding lines were measured using the radioactive tracer technique. An elaborate setup for this purpose was supplied and operated by BBC. Approximately 25 injection points and 65 sample taps were employed. The test results showed that the turbine performed better than the manufacturer's heat rate guarantees by about 1.0% over a wide range of load changes (from the rated output to approximately 10% MCR). The tests showed a commensurably high accuracy of the manufacturer's heat-rate calculations. Along with this, the obtained results revealed some noticeable errors in assessing the swallowing capacity of the turbine's steam path—the actual measured steam flow amounts occurred to be larger than had been expected on the basis of calculations and laboratory measurements. According to both the turbine's manufacturer and operator, the obtained results completely justified the high cost of the tests.

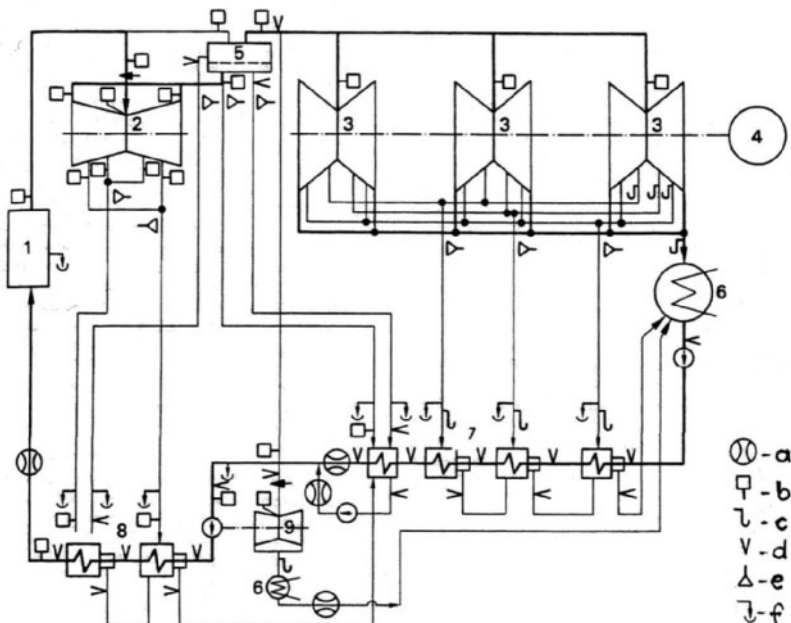


**Fig. 4-19.** Instrumentation diagram for heat-rate performance tests of Brown Boveri's 1,100-MW wet-steam turbine (1: steam generator; 2: HP cylinder; 3: LP cylinders; 4: generator; 5: MSR; 6: condensers; 7: LP feed water heater; 8: HP feed water heater; 9: feed water pump's driving turbine; a: calibrated flow section; b: deadweight gauge; c: U-tube manometer; d: thermocouple; e: tracer injection; f: water sample)

Source: R. I. Pawliger, A. Roeder, E. Mueller, and Z. S. Stys<sup>39</sup>

Even though the full-range heat-rate tests according to PTC-6 are very informative and fairly representative, their high costs and complexity discourage many power plant owners and operators. According to some data, only about one-tenth of all nuclear power units have been subjected to such full-range tests.<sup>40</sup> Because of this, ASME appointed an *ad hoc* committee to evaluate the cost effectiveness of various test procedures, and (after thorough analysis) the committee recommended an “alternative” heat-rate test procedure that is simpler and less costly than the traditional full-range ASME acceptance tests, yet only slightly less accurate.<sup>41</sup> This simplified procedure has been accepted by the ASME and was first published as an *Interim Test Code for an Alternative Procedure for Testing Steam Turbines*.<sup>42</sup> The new procedure was verified in the course of the “alternative” heat-rate performance tests of GE’s 570-MW tandem-compound steam turbine

at the Laramie River fossil fuel power plant in Wyoming.<sup>43</sup> Results of these tests were not significantly different from those of the full-range ASME tests. The main difference of the simplified tests is the use of fewer high accuracy measurements, which are employed only for measuring the feed water flow, temperature, and pressure values around the highest-pressure feed water heater (to establish its complete performance), steam flows for auxiliary turbine drives (if applicable), and the generator's electric output. All other measurements can utilize the power plant's regular instrumentation calibrated in place. The comparative error analysis for the simplified acceptance tests showed a total error of 0.38%, compared to 0.27% for the full-scale ASME Code test.

According to the latest version of PTC 6, the uncertainty of the full-scale performance tests "for steam turbines operating predominantly within the moisture region" makes up approximately 0.375%, whereas the uncertainty for the alternative simplified tests is 0.5%.<sup>44</sup> Despite the higher uncertainty level for the simplified tests, it can be considered low enough to accept the test results without applying a measuring tolerance. Because the instrumentation for the simplified heat-rate tests can be permanently installed, the turbine cycle performance can be monitored by repeating the tests periodically. The use of a laboratory-calibrated flow test section for direct measurements of the feed water flow permits the owners of nuclear power plants with light-water reactors to operate them closer to the licensed full capacity without exceeding it.<sup>45</sup>

Heat-rate performance tests of wet-steam turbines in other countries are based on similar principles, although individual approaches differ. For example, according to the heat-rate test practice at power plants in the former Soviet Union, measuring the feed water flow amount is commonly supplemented by direct measurements of the main steam flow on the main steam-lines, as well as the steam flows to the driving turbines of the feed-water pumps and the first and second reheat stages of the MSR. In addition, the steam wetness is commonly measured with the use of a so-called calorimetric method, and more attention is paid to the performance properties of the MSR and its components.<sup>46</sup>

A typical instrumentation diagram for the heat-rate tests of Turboatom's 1,000-MW low-speed (1,500 rpm) K-1000-60/1500-2 turbine, as in Figure 3-13, at Zaporozhe Unit 1 is shown in Figure 4-20.<sup>47</sup> The turbine has four cylinders: one double-flow HP cylinder and three LP ones. This turbine, unlike the preceding K-1000-60/1500 model, is designed without an IP section and with basement condensers instead of side condensers. The LSBs are 1,450 mm (57 in) long. The rated back pressure in the condenser at a load of 1,114 MW is 3.92 kPa (0.57 psi), and the cooling water temperature and flow rate are 15°C and 168,800 m<sup>3</sup>/h, respectively. The turbine was put into operation in December 1984 and by the beginning of the performance tests had operated for 8,700 hours with 60 start-ups. The system of measurements was arranged in such a way that the most important variables were determined by no less than two independent methods. A special system was developed for measuring the main steam wetness based on throttling the steam samples to a superheated state and determining their thermodynamic characteristics; the resultant error was assessed as not exceeding 0.1%.

The same approaches were employed in the heat-rate performance tests of some other wet-steam turbines of Turboatom, including the K-500-65/300, K-500-60/1500, K-750-65/3000, and K-1000-60/1500 models, at the Sosnovy Bor, Novovoronezh, Ignalina, and South Ukrainian nuclear power plants.<sup>48</sup>

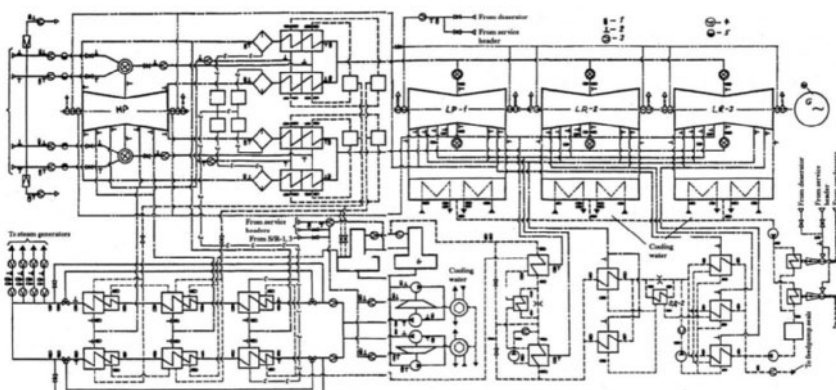


**Fig. 4-20.** Instrumentation diagram for heat-rate performance tests of Turboatom's K-1000-60/1500-2 turbine (Points of measuring: 1: temperatures; 2: pressures; 3: flows (pressure drops); 4: power; 5: steam wetness)  
Source: V.A. Buzulukov , M. G. Teplitskii, A.A. Maksimenko, and T.V. Poruchinskii<sup>49</sup>

The main results of the heat-rate tests for the K-1000-60/1500-2 turbine are given in Figure 4-21, and Table 4-3 shows a comparison of the obtained heat-rate data with the data guaranteed by the turbine manufacturer. With the maximum main steam flow rate of 6,370 t/h, the HP control valves completely open, and with main steam pressure of 5.88 MPa (853 psi), the turbine load made up 1,171 MW, which matched the guaranteed maximum capacity. With the turbine load of 1,095 MW, which corresponds to the rated thermal production capacity of the reactor, the main steam flow amount was 5,900 t/h, the pressure drop in the HP stop and control valves was 0.58 MPa (84 psi), or 9.7%, and pressure losses in the main steam-lines were approximately 0.3 MPa (43.5 psi). With a reduction of the turbine load, the turbine efficiency decreased, and the heat rate increased by 3.6% with a turbine load equal to 70% MCR. Apart from throttling in the control valves, such a significant increase in the heat rate is explained by switching over the steam supply of the deaerator.

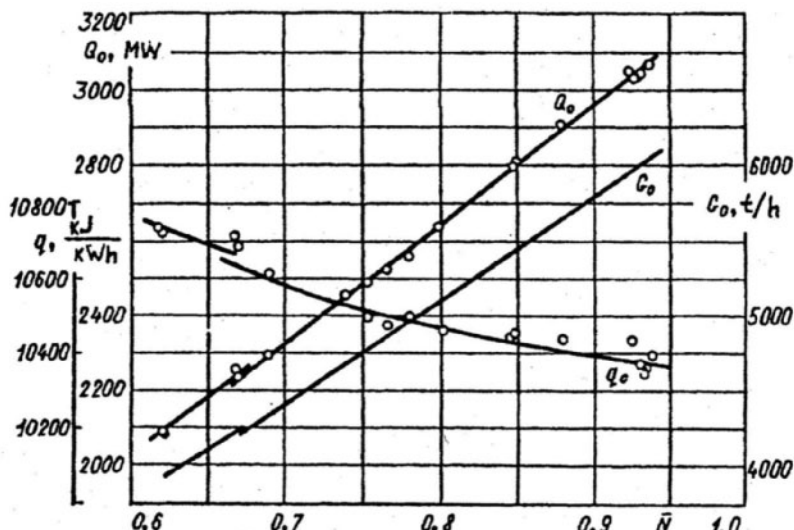


**Fig. 4-21.** Heat-rate and steam-rate performances for Turboatom's K-1000-60/1500-2 turbine according to heat-rate performance tests at the Zaporozhe nuclear power plant

Source: V.A. Buzulukov, M. G. Teplitskii, A.A. Maksimenko, and T.V. Poruchinskii<sup>50</sup>

**Table 4-3.** Heat-rate performances of Turboatom's turbine K-1000-60/1500-2 according to the acceptance tests at Zaporozhe nuclear power plant

Output at the generator terminals, MW	Heat rate, kJ/kWh (Btu/kWh) / Efficiency, %		Discrepancies, %	
	guaranteed	obtained	kJ/kWh (Btu/kWh)	%
808	10501 (9953)/ 34.28	10505 (9957)/ 34.27	4 (4)	0.04
1010	10321 (9782)/ 34.88	10346 (9806)/ 34.80	25 (24)	0.24

Source: V.A. Buzulukov, M.G. Teplitskii, A.A. Maksimenko, and T.V. Poruchinskii<sup>51</sup>

Similar performance data were obtained for the K-1000-60/1500 turbine at South Ukrainian Unit 1.<sup>52</sup> In both cases, the heat-rate tests showed that the overall capacity of the HP cylinders of both turbines is too high in relation to the steam-generation capacity of the reactor (VVER-1000), causing excessive throttling in the HP control valves. With the reactor's rated thermal capacity of 3,000 MW, the overall main steam flow to the K-1000-60/1500 turbine was 5,975 t/h, with a 12.8% pressure drop in the HP stop-and-control valves of 0.75 MPa (109 psi). Based on the test results, the turbine manufacturer somewhat decreased the overall capacity of the HP cylinder for both turbine types by reducing the height of the first stage's fixed and rotating blades. The results of this change were investigated in the process of the repeated heat-rate tests on the K-1000-60/1500 turbine at South Ukrainian Unit 1 and the K-1000-60/1500-2 turbine at Zaporozhe Unit 4. According to the data of these tests, the increase in turbine capacities amounted to 13.9 MW in the first case and 21 MW in the second case. As a result, at the rated reactor capacities, the overall output and efficiency figures for the two turbines were 1,065 MW and 36.0% for the K-1000-60/1500 turbine and 1,043 MW and 35.7% for the K-1000-60/1500-2 turbine.<sup>53</sup>

Heat-rate performance tests are important for verifying certain assumptions and the use of conventional methods employed in the process of designing and calculating turbines, providing data for corrective actions, if necessary, and proving the resultant effectiveness of fulfilled alterations.

In the early and mid-1990s, Siemens conducted a series of heat-rate performance tests on their “nuclear” wet-steam turbines before and after refurbishing them. These refurbishments mainly included replacement of the turbine’s LP rotor(s) and inner casing(s). Such a replacement (at one of three LP cylinders), with the accompanying heat-rate performance tests, was first accomplished on the 1,300-MW turbine at the German nuclear power plant Unterweser.<sup>54</sup> The refurbishment was related to the development of an advanced eight-disk LP rotor to replace the existing 10-disk LP rotors that had been used at Siemens’ large low-speed wet-steam turbines in service since the mid-1970s (see Fig. 3-8). By that time, problems arose with corrosion cracking of disk-type LP rotors (see the next section), and Siemens initiated a special program of ultrasonic inspections of all their disk-type rotors of turbines installed at nuclear power plants. In 1987, indications of corrosion cracking were found on one of the turbine disks at Unterweser (the only instance among 310 inspected disks), and it was decided to replace the damaged rotor with a new advanced one. The newly developed eight-disk rotor exhibited significantly reduced levels of the tensile centrifugal stresses and had a more efficient steam path. The comparative performance heat-rate tests were considered to be of utmost importance because an increase in the turbine output due to the refurbishment of even one LP cylinder would provide a benchmark for the future wide program based only on the turbine efficiency advantage, not even touching on the reliability aspects.

In order to conduct the comparative performance tests (before and after the refurbishment) with the highest possible repeatable accuracy, the Unterweser turbine was equipped with a number of additional measuring devices, including some specially calibrated meters. The power plant’s data acquisition system and computer were updated for gathering and processing the test data. The test results showed an increase in the turbine output of 15.4 MW. After correcting the results for the generator efficiency, back pressure, and extraction leakage losses, the final gain in the output related to the replacement of the LP-3 cylinder’s steam path was assessed as 17.9 MW. It meant that replacement of all the three LP sections would bring a total increase of 53.7 MW. The initial turbine efficiency, according to the acceptance tests, accounted to 35.01%; the prereplacement tests

showed the efficiency value of 35.11%, and the post-replacement tests result was 35.60%. Assuming the replacement of all three LP sections, this value would rise to 36.56%.<sup>55</sup> The results of comparative heat-rate tests for other Siemens wet-steam turbines that underwent similar refurbishments are shown in Table 4-4. Comparative performance tests at wet-steam turbines before and after refurbishing them have also been performed by other turbine manufacturers.<sup>56</sup> Arrangement of such tests in strict accordance with PTC 6 requirements at turbines in service often encountered serious difficulties, and special attention was paid to the uncertainty of the obtained test results.

**Table 4-4.** The increase in output for wet-steam turbines of Siemens due to their refurbishment according to their comparative heat-rate performance tests

Power plant	Initially rated turbine output, MW	Replacement	Guaranteed output increase, MW	Measured and corrected output increase, MW
Unterweser	1300 (1500 rpm)	One (of 3) LP rotors and inner casings	9	17.9
Phillipsburg-2	1362 (1500 rpm)	One (of 3) LP rotors and inner casings	12	13.6
Trillo (Spain)	1032 (3000 rpm)	Three (of 3) LP rotors and inner casings	26	41.6
Emsland	1363 (1500 rpm)	Two (of 2) LP rotors and inner casings	32	32.0
Gundremmingen	1310 (1500 rpm)	HP and two (of 2) LP rotors and inner casings	48	52.0
Grafenrheinfeld	1300 (1500 rpm)	HP and two (of 2) LP rotors and inner casings	40.4	45.3

Source: K.D.Weschenfelder, H. Oeynhausen, D. Bergman, et al.<sup>57</sup>

One of the most serious difficulties is measuring the quality of wet steam, or steam wetness. Previously mentioned methods of this measuring are rather complicated, laborious, and not suited to automated processing. This situation could improve with the appearance of moisture gauges to allow continuous measuring. In particular, such a goal was pursued by EPRI in their development of a probe, based on the principle of light scattering when passing through a two-phase flow. It was originally intended for installing in LP cylinders of steam turbines at fossil fuel power plants. In 1997–98, steam wetness measurements with the use of this probe were performed at 10 locations, and in 2001 an improved fiber optic system matching the cycle measurement requirements of PTC 6 was planned for validation in a benchmark test at the TVA's Martin Lake lignite-fired power plant.<sup>58</sup> Unfortunately, the first tests were not completely successful—the traverse using the probe resulted in steam wetness measurements that were several percentage points higher than the moisture values determined by the ASME PTC 6 test. Some new steam wetness measurement methods and devices are under development by other institutions in various countries, but for the time being they have not been successful. Hopefully, in the future, such measurements will be brought to commercial use at wet-steam turbines.

The heat-rate tests make it possible to estimate more accurately the influence on the turbine output and efficiency of deviations of the actual operating conditions from the rated conditions. This primarily refers to variations of vacuum in the condensers, depending on the mass steam flow amount through the turbine exhausts into the condenser (which is approximately equivalent to the current turbine load) and the cooling water's temperature and flow rate. In turn, the volumetric flow amount through the LSBs varies, depending on both the mass steam flow amount and the back pressure at the turbine exhaust. However, the steam velocities and energy losses in the last stage depend only on the resultant volumetric steam flow, no matter what factors were involved. This allows calculating a so-called “universal” correction curve for the vacuum, which shows the dependence of the turbine output and its changes on the mass steam flow amount into the condenser and the pressure in the condenser, with additional correction for the exhaust hood resistance. The methodology of such calculations is well worked out.<sup>59</sup> It takes into consideration changes of

the enthalpy drop in the last stages after the last regenerative bleeding and steam extraction flow into this bleeding, the internal efficiency of the last stage, the integral energy loss with the exit steam velocity (with regard to its change along the stage height), and the power losses in the exhaust hood. These correction curves, plotted with respect to changes in the turbine output and pressure in the condenser, as related to the mass steam flow into the condenser, can be used for different turbines if they are designed with the same LSBs and exhaust hoods. Examples of such universal curves of correction for vacuum as applied to Turboatom steam turbines (per exhaust flow) are presented in Figure 4-22. It is of importance that these curves are linear over the largest portion of the change range.

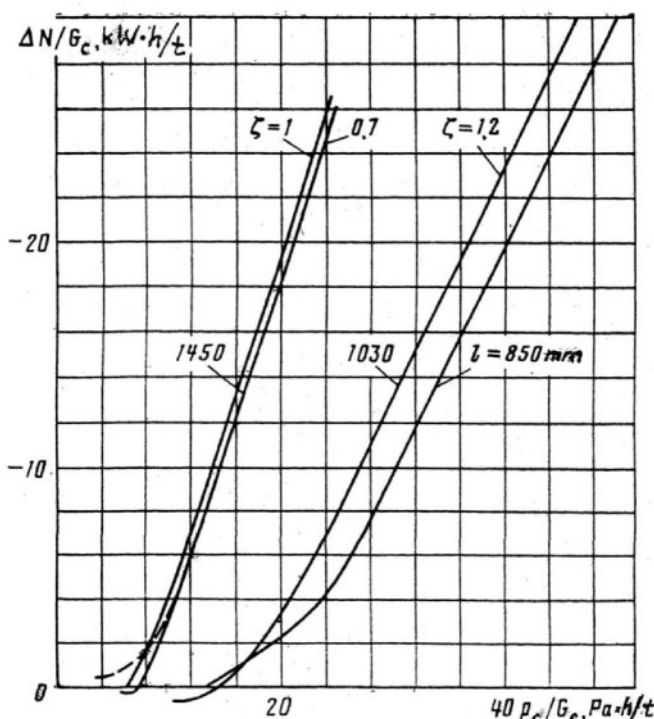


**Fig. 4-22.** Calculated “universal” curves of correction for vacuum for Turboatom’s steam turbines (per exhaust flow) with different LSBs and exhaust hoods ( $\zeta$ : coefficient of resistance for exhaust hood [0.7 for side condensers;  $\geq 1.0$  for basement-mounted condensers])

Source: B.A.Arkadyev<sup>60</sup>

The heat-rate test results allow verifying these calculation curves and assessing the influence of the operating back pressure variations on the turbine output more accurately. For example, according to the heat-rate tests of the K-1000-60/1500-2 turbine, correction of the turbine capacity for vacuum makes up  $\pm 9,800$  kW per 1 kPa of variations in pressure in the condensers.<sup>61</sup>

For the most efficient operation of the turbine, it is also helpful to know the corrections for deviations of other controllable variables. First of all, this refers to the main steam pressure and steam quality at the turbine inlet and after the separator. As an example, such characteristics for Turboatom's K-1000-60/1500 turbine are given in Figure 4-23. They are built under the assumption that all the other operating conditions do not deviate from the rated values.

According to Siemens, as applied to a 1,300-MW wet-steam turbine, a decrease in the main steam quality of 0.5% results in a loss of the turbine output of 2 MW; reduction of the cooling water flow rate by 10% also results in an output loss of approximately 2 MW; bypassing one feed water heater takes approximately 7 MW; an increase of the terminal temperature differences (TTD) in the MSR or in a mean feed water heater by 1°C decreases the output by 1.5 MW, and the same (1°C) increase of the TTD in the condenser results in an output loss of approximately 2 MW.<sup>62</sup> Knowledge of the cost of these deviations makes the operator pay more attention to observing the rated operating conditions.

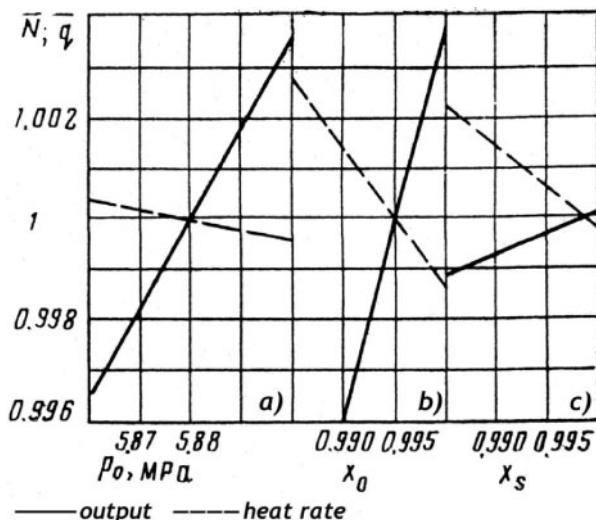


**Fig. 4-23.** Corrections for deviations of steam conditions for the output (1) and heat rate (2) for Turboatom's K-1000-60/1500 turbine (a: main steam pressure; b: main steam quality; c: steam quality after the separator [before the reheater])

Source: B.A.Arkad'yev<sup>63</sup>

At times it can be read that "in nuclear power plants...deterioration of the performance can be normally neglected."<sup>64</sup> In fact, the turbine efficiency can remain practically unchanged during long-term operation periods. For example, the gross efficiency of the 1,300-MW Unterweser turbine after 11 years of operation was found equal to 35.11% against the initial value of 35.01% from the acceptance tests.<sup>65</sup> (This does not mean that the turbine became more efficient in operation, because such a difference lies within the range of the test uncertainty.). In any event, the heat-rate performance deterioration for wet-steam turbines is remarkably less on the average than that for superheated-steam turbines of fossil fuel power plants. To a great degree, this can be explained by a smaller probability of increasing the clearances in the turbine steam path and gland seals due to wearing out caused by brushing and rubbing. Wet-steam turbines are also less prone to other factors affecting their performance. Nevertheless, these turbines are not ensured against some damages related specifically to wet-steam turbines, and it is desirable to monitor their state during the operation process.

[Previous Page](#)

## 276 Wet-Steam Turbines for Nuclear Power Plants

Under conditions of regular scheduled outages of nuclear power units with light-water reactors for refueling, it is reasonable to arrange condition-oriented, predictive maintenance of wet-steam turbines on the basis of their continuous performance monitoring. In this case, the turbines are opened and repaired during the outages for refueling only if it is absolutely necessary to restore their conditions. Continuous monitoring of the steam pressures at a few characteristic points in the steam path, with statistical processing of the measured data to account for the influence of varying operating conditions, can effectively replace full-scale on-line heat-rate monitoring. Such an approach to revealing on-line potential damages in the steam turbine path was developed and implemented for fossil fuel power units,<sup>66</sup> and it could be even more effective for wet-steam turbines.

## Some Generic Damages of Wet-Steam Turbines and Their Causes

The operating reliability and availability indices of modern nuclear power plants and their wet-steam turbines are sufficiently high (see Table 1-7). According to *International Journal for Nuclear Power*, in the period between 1992 and 2002, the average annual time-availability factor for nuclear power plants worldwide increased from 75.3% to 85.5%, whereas the unplanned outage rate declined from 6.9% to 3.0%.<sup>67</sup>

The reliability and availability of wet-steam turbines are influenced to a great degree by their substantially low steam parameters and a predominantly base-load operation mode. Because of these factors, wet-steam turbines avoid many of problems characteristic of large superheated-steam turbines of fossil fuel power plants. A low steam temperature level and a more favorable correlation of the

mass and heat-transfer conditions for the rotors and casings make wet-steam turbines less prone to significant changes in RRE and, as a result, decreases in axial clearances in the gland seals, with possible brushing and rubbing as a consequence. Great rigidity of the rotors also diminishes the hazard of increased vibration and radial brushing. On the other hand, the operating reliability of wet-steam turbines is hindered by the fact that almost the entire turbine path is swept with wet steam featuring a high content of coarse-grained water, which promotes the intensity of corrosion-erosion processes. In addition, the combination of a large individual capacity and low steam parameters leads to the design of wet-steam turbines with a great number of cylinders and long LSBs, which can also lead to problems in operation.

The comparative influence of different damage mechanisms on the steam paths for different types of steam turbines is presented in Table 4-5.<sup>68</sup> The specific focus of this table is damage to the fixed and rotating blades, as well as to the blade attachments (including both the blade roots and the attachment areas on the disk or shaft), lacing and tie wires, shrouds, tenons, and so on. The table does not cover specific damages to rotor bodies, casings, casing rings, seals, valves, pipes and other components beyond the steam path. Nevertheless, it is obvious that wet-steam turbines are not prone to many factors that are influential for superheated-steam turbines of high steam conditions. In particular, this refers to the phenomena of creep, creep-fatigue, solid particle erosion, and copper deposition. If wet-steam turbines are operated in a base-load mode, it is understandable that they are not prone to low-cycle (thermal) fatigue. Thus, the primary causes of damages to wet-steam turbines are water erosion and corrosion, in all of their different forms. Considerations of damage that are common to steam turbines of both fossil fuel and nuclear power plants can be found in various editions. In addition, a general outline of operating experiences relating to damages of wet-steam turbines is presented in special articles. Some damages that are most generic to wet-steam turbines are considered below, although they can also be observed in LP cylinders of superheated-steam turbines.

**Table 4-5.** Relevance of steam path damage mechanisms for various steam-turbine types

Damage mechanism	Superheated-steam fossil fuel turbines	Wet-steam turbines for NPP	Steam turbines of CC units	Feed-water pumps driving turbines	Geothermal turbines
Creep and creep-fatigue in blades and blade attachments	X	UC	X	X	UC
Solid-particle erosion	XX	UC	UC	UC	XX
Copper deposition	XX	UC	UC	X	UC
Fatigue in LP blading	XX	X	X	X	UC
Fatigue in HP blading	X	X	X	X	UC
Localized corrosion	XX	XX	X	X	XX
Corrosion fatigue	XX	XX	X	X	XX
Stress corrosion cracking in disc-rim attachments	XX	XX	UC	UC	XX
Stress corrosion cracking in blading	X	X	UC	UC	XX
Liquid droplet erosion	XX	XX	X	X	XX
Water induction	XX	XX	X	X	X
Flow-accelerated corrosion	X	XX	X	X	X
Fretting	X	X	X	X	X

Notes: "XX" indicates damages commonly found or presenting a major problem when found;

"X" indicates damages that can be found but present a lesser problem;

"UC" indicates damages uncommon to have occurred in this type of turbines.

Source: T.H. McCloskey, R.B. Dooley, and W.P. McNaughton<sup>69</sup>

## Stress-corrosion and corrosion-fatigue cracking

Corrosion-assisted fatigue has been responsible for the cracking and failures of many rotors and wheel disks of wet-steam turbines. Cracking of the LP rotors of AEG's 660-MW low-speed (1,500 rpm) turbine at Würgassen is one of the best-known instances of this type of damage.<sup>70</sup> Cracks were detected in the metal of both LP rotors in 1974 after 6,800 hours of operation. The turbine was stopped because of a high level of shaft and bearing vibration. Examinations revealed the cracks initiating from the axial stress-relief slot at the transition from the seating of the generator-side disk to the central thrust collar (Fig. 4-24). The crack in the LP-1 rotor reached a maximum depth of 245 mm (10 in), with the shaft diameter of 978 mm (38.5 in), and the crack in the LP-2 rotor had a maximum depth of 50 mm (2 in), at the same location on the shaft.

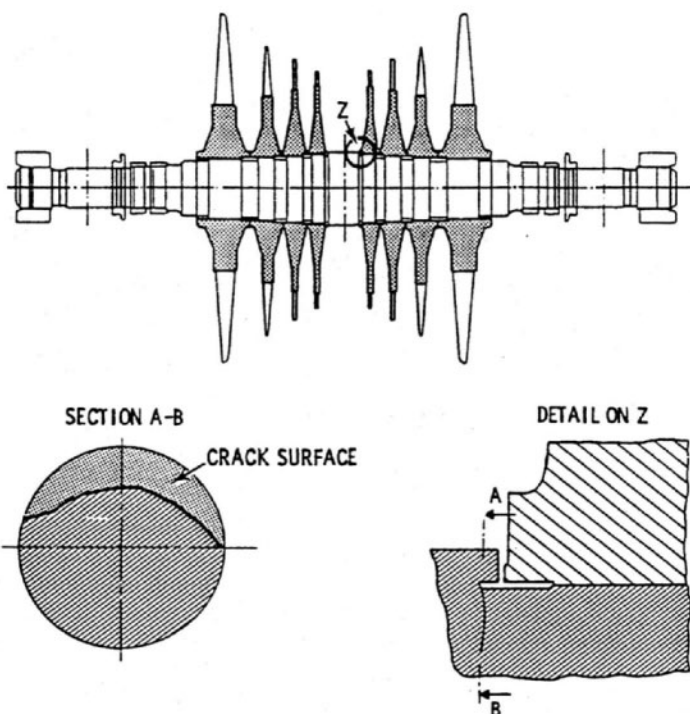


**Fig. 4-24.** Crack damage on the LP-1 rotor of AEG's 660-MW wet-steam turbine at Würgassen

Subsequent analysis showed that the cracks were caused by high-cycle fatigue under the action of altering bending stresses due to the incorrect fit of the shrunk-on wheel disks. Rotating the turbine with a high-speed (100-rpm) turning gear caused stresses that probably initiated the cracks, whereas the much smaller high-frequency dynamic stresses caused by operating at the nominal speed were responsible for their growth. Calculations showed that in an air or pure steam atmosphere, these alternating stresses were insufficient for the cracks to progress as far as they did. The residual time to final fracture of the rotor at the instant when the turbine was stopped was estimated to be 1.5 hours. Thus, the cracks were caused by the combined effects of high-cycle fatigue and corrosion.

Very similar cracks occurred on three LP rotors with shrunk-on disks in the 500-MW turbines at the British fossil fuel power plant Ferrybridge "C", and on the IP rotor's coupling of BBC's 1,300-MW cross-compound turbine at TVA's fossil fuel power plant Cumberland.<sup>71</sup>

Thereafter, most cases of damages with wheel disks have been experienced on wet-steam turbines and LP cylinders of superheated-steam turbines. The damages sometimes led to failures of the turbine rotors. Except for the cracks due to creep-rupture in the blade grooves of the high-temperature stages, almost all of the disk damages and failures were caused by *stress corrosion*—that is, corrosion acting under high-stress conditions. As in all the previously mentioned cases, corrosion cracks most frequently originated in places where liquid concentrates of steam contaminants could gather and be stored for a long time. Corrosion is stimulated by such mechanisms as deposition, evaporation, and drying. Impurities are consolidated on the disk surfaces in various slots, recesses, grooves, and other design *crevices*,

or occasional fissures or pores in the metal, which simultaneously become places of stress concentration. This phenomenon was the subject of special consideration and analysis in numerous investigations.<sup>72</sup> According to specialists of ABB, for stress corrosion cracking (SCC) to occur, three conditions must be satisfied: a sufficiently *high tensile stress* must be applied to a *susceptible steel* in a *corrosive environment*.<sup>73</sup> Combination of all three factors creates a real menace of the appearance and propagation of SCC.

There are over 150 various steam contaminants, but the most aggressive mediums promoting stress corrosion are such compounds as NaOH, NaCl, Na<sub>2</sub>SO<sub>4</sub>, Na<sub>3</sub>PO<sub>4</sub>, NaNO<sub>3</sub>, Na<sub>2</sub>SiO<sub>3</sub>, NH<sub>4</sub>Cl, Na<sub>2</sub>CO<sub>3</sub>, organic and inorganic acids, and ferric and cupric oxides. The most indicative factors of steam impurity are the steam pH level, conductivity, cation conductivity, and the concentration of such chemicals as oxygen and sodium chloride. The latter should be kept to concentrations of few parts per billion (ppb) or less. There were some accidents in which, when after a damaged rotor had been replaced, the stress corrosion cracks reappeared at the same wheel disks in the Wilson region. In these cases, the power plant operators managed to avoid the repeated appearance and propagation of cracks only by means of radical improvements in water treatment and steam chemistry monitoring. The formation of corrosive media and their deposition on steam path surfaces in the phase transition zone and the effect of these media on the SCC processes were the subject of special experimental and analytical investigations.<sup>74</sup> Proper water treatment and proper material selection can diminish and even minimize corrosion attacks. The effect of the pH level of the steam/water cycle on the specific corrosion rate is shown in Figure 4-25; the rate drastically reduces with a pH level above 9.0.<sup>75</sup> Replacing carbon steel components with 2.5% chromium steel components increases the resistance to erosion-corrosion from 0% to approximately 97–99%.

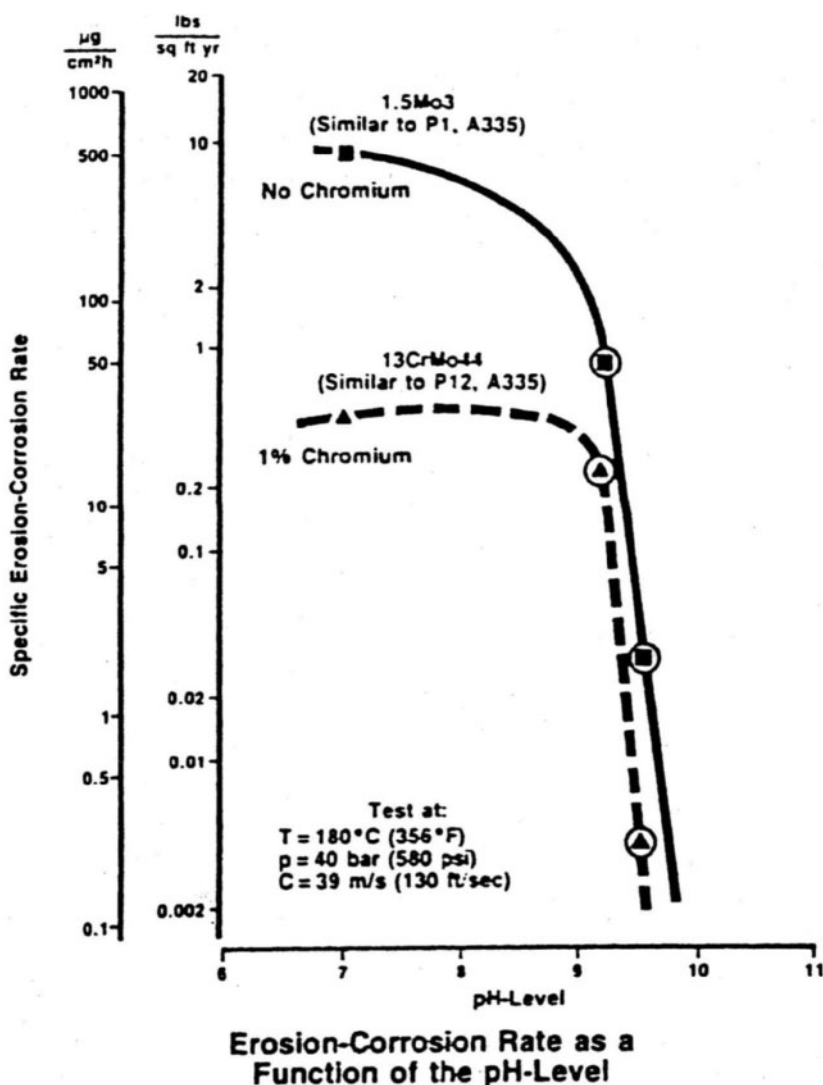


**Fig. 4-25.** Influence of pH level on the erosion-corrosion rate of various steels

Source: W. Engelke, K. Schleithoff, H.-A. Jestrich, and H. Termuehlen<sup>76</sup>

The most general explanation of SCC is given by its electrochemical theory. According to this concept, the main factor affecting crack propagation is anodal dissolving of metal in the crack root. Under certain circumstances, a protective film appears on the metal surface (a phenomenon known as *passivation*). If the passive layer is

broken under action of, for example, mechanical stresses, the crack root turns out to be under conditions of chemical activity, and the metal begins to dissolve actively with continuous depassivation. This process is accompanied by hydrogenization of metal on the juvenile surface at the crack root and results in embrittlement of the metal. Some ideas exist that this process is intensified if the turbine operates under conditions of frequent load changes, with resultant shifts of the phase transition zone and variations of the steam pressure at the turbine stages working in this zone. In particular, this also means that the Wilson region at transient operating conditions embraces a greater number of stages, and more disks are involved in this process.

Along with the steam/water chemistry, the intensity of stress corrosion to a great degree depends on the composition and heat treatment of the steel applied to the disks, as well as their design features. So, stress corrosion of disks has been almost absent, not only at power plants in countries with a traditionally high culture of steam/water chemistry, but also at steam turbines made by ABB and Siemens, for example, even if these turbines were operated at power plants without high-quality water treatment. The only indication of cracks found in wheel disks of Siemens' turbines was related to insufficient local heat treatment.<sup>77</sup> In contrast, steam turbines manufactured by U.S. producers were prone to stress corrosion to a large degree. From the late 1970s to July 1980, inspections were carried out on 72 wet-steam turbines at 32 U.S. nuclear power plants; at 20 of these turbines, cracks were discovered in 70 disks of 36 different LP rotors.<sup>78</sup> By 1996, of 110 U.S. nuclear units surveyed, 33% of 290 LP rotors had to be retrofitted, including 18% of 119 LP rotors on the turbines manufactured by Westinghouse and 35% of 150 LP rotors produced by GE.<sup>79</sup> The cracks took place in the stages in the Wilson region and ranged in depth from 2.5 to 75 mm (0.1–3 in). The rate of crack growth varied from 0.1 to 10 mm/yr (4–400 mil/yr). Because of SCC in the shrunk-on wheel disk keyways, for example, of four 820-MW turbines at the nuclear power plants Dresden (Units 2 and 3) and Quad Cities, all of the 12 LP rotors with shrunk-on disks were replaced with rotors of the welded type delivered by another manufacturer.<sup>80</sup> Similar damages were revealed in the LP cylinders of many turbines at fossil fuel power plants. The most typical zones of disk damages are shown in Figure 4-26. Among 131 damaged disks that were inspected, 38% had cracks in the blade attachment zone, 29% on the side surfaces, and 30% on the bore surface, including 26% with cracks in key slots.

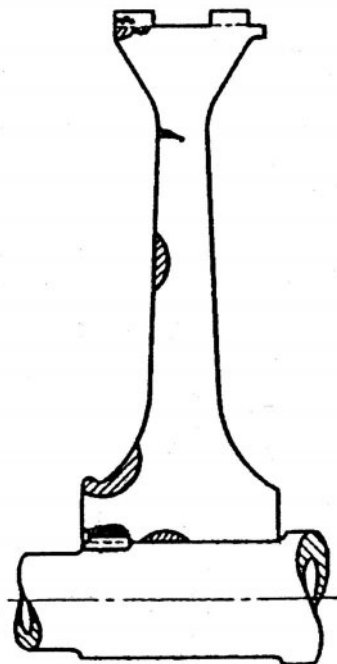


**Fig. 4-26.** Typical zones of stress corrosion cracking in shrunk-on wheel disks of wet-steam turbines at U.S. power plants (late 1970s)

Cracks in the blade attachment zone can entail rupture of the disk rim and blade liberation, with the potential consequences of avalanche-shaped damages in the steam path, sudden rise in shaft vibration, damages to bearings, and so on (Fig. 4-27). Cracks on the bore surface can be equally or even more dangerous, because their propagation can cause fracture of the whole disk, resulting in subsequent destruction of the turbine. One of the most serious failures of this type happened at the British nuclear power plant Hinkley Point A,<sup>81</sup> and presently similar failures bear this name. Three wheel disks on the LP rotor burst; the shaft of the 93-MW turbine was broken in three places; the entire steam path crashed, and two neighboring turbines were also severely damaged. The process originated from stress-corrosion cracks in the semicircular axial keyway in the shrunk-on disks and on their bore surfaces. The cracks propagated, remaining unnoticed, and resulted in brittle fracture when the turbine ran through an ordinary overspeed test and reached a rotation speed of 3,200 rpm (with the synchronous speed of 3,000 rpm) (Fig. 4-28). Immediately after this failure, 810 wheel disks on 102 rotors were inspected, and stress-corrosion damages were discovered on 124 disks of 50 rotors.

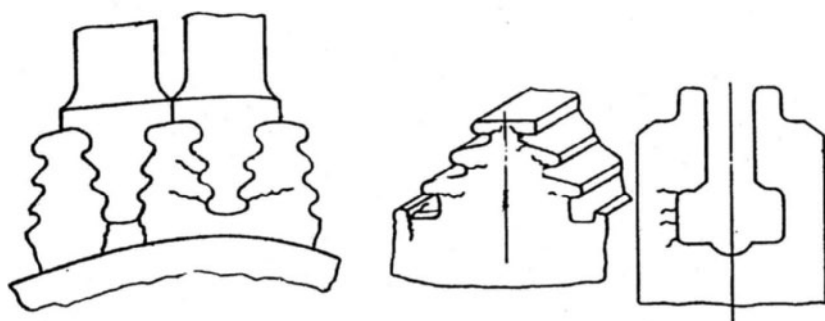


Fig. 4-27. Stress corrosion cracks at a disk rim in the blade attachment zone

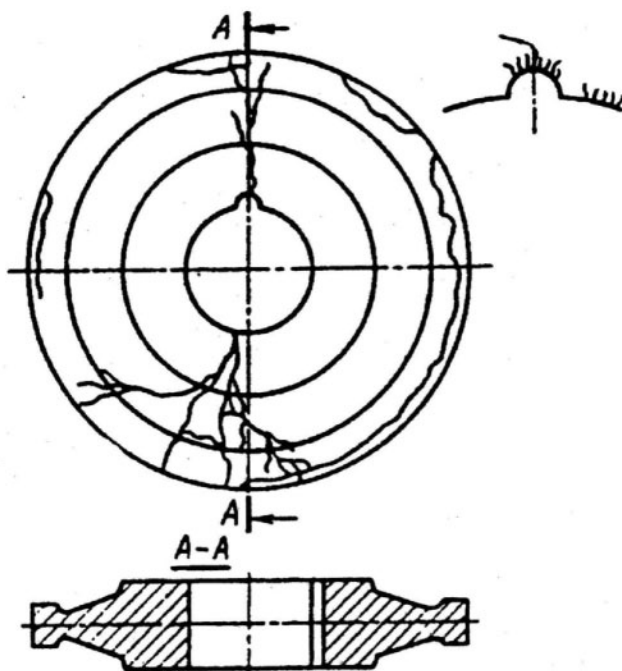


Fig. 4-28. Brittle fracture of shrunk-on disk due to propagation of stress corrosion cracks from the bore surface at the British nuclear power plant Hinkley Point A

If a turbine operates under conditions of aggressive steam (with undesirable impurities) and the disk steel with regard to its heat treatment is prone to stress corrosion, the probability of stress corrosion

damages for the wheel disks in the Wilson region practically approaches 100% (Fig. 4-29). These statistical data for Westinghouse turbines are very similar to those for turbines made by AEG, GE, NEI Parsons, and TMZ. On the basis of field measurements for 40 damaged wheel disks, Westinghouse researchers derived an empirical equation for crack growth, which can be recast as follows:

$$\ln(v) = -16.829 - \frac{4057}{t} + 0.04 \times \sigma_{0.2},$$

where  $v$  is the crack growth rate in m/s;  $t$  is the metal temperature in °C; and  $\sigma_{0.2}$  is the conventional yield limit in MPa.

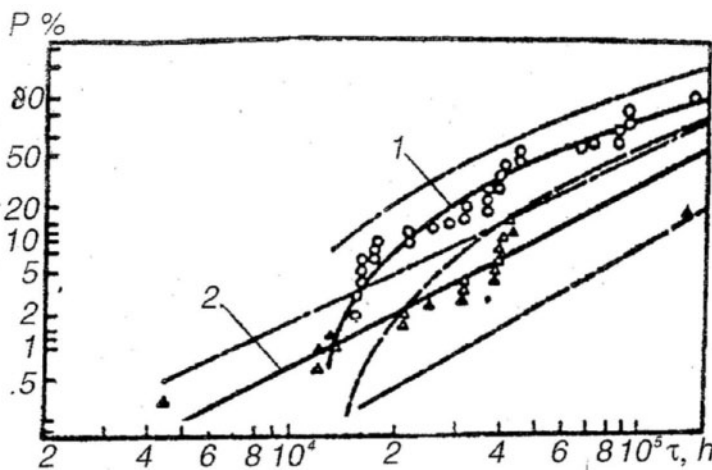


**Fig. 4-29.** Probability of damages in the key slot (1) and on other surfaces (2) of wheel disks in the Wilson region  
Source: O.A. Povarov and E.V. Velichko<sup>82</sup>

According to investigations of EPRI, the crack growth rate mostly depends on the steel composition and tempering temperature, yield limit, and disk metal temperature. For standard NiCrMoV steels used for LP wheel disks and rotors, the most influential components of the steel composition are manganese, vanadium, nickel, and sulfur. If the sulfur content rises to 0.01%, the crack growth rate increases, but any additional increase of sulfur content is accompanied by a decrease

in the crack growth rate. It is assumed that the manganese content is the most representative, and the crack growth rate can be estimated using an empirical equation based on this value, as well as the tempering temperature:

$$\ln(v) = -4.82 - \frac{5,150}{t+273} + 0.0048\sigma_{0.2} + 4.53Mn - 0.0127(t_t + 273),$$

where  $Mn$  is the manganese content (%), and  $t_t$  is the tempering temperature. As can be seen from the aforesaid equations, the crack growth rate increases appreciably with the disk metal temperature, and steels with higher strength properties (yield limit) are more sensitive to stress corrosion.

All of these factors are taken into consideration by turbine manufacturers when they choose the material for wheel discs. Presently, there are some steel grades used in manufacturing LP disks and rotors that have extremely high resistance to stress corrosion. These steels are used in newly designed and retrofitted turbines, as well as for substituting for the damaged wheel disks. At the same time, it is the power plant's responsibility to maintain proper steam/water chemistry in order to prevent stress-corrosion cracking.

The intensity of the stress corrosion processes essentially depends on the shrunk-on wheel disk design decisions, especially the keyway shape. For example, large-scale cracking was observed in turbines of AEG (prior to its merging with Siemens). The combined LP rotors of these turbines were mostly made with rectangular-shaped keyways in the shrunk-on wheel disks. According to inspections conducted by Siemens on 16 turbines at three South African fossil fuel power plants, corrosion cracks were revealed on 49 of 128 disks examined. All told, 42 of 61 disks with rectangular-shaped keyways were damaged, and in 40 cases, the cracks were revealed only in the keyway zones.<sup>83</sup> All of the disk cracks demonstrated an intergranular crack pattern with ramified crack propagation. The crack initiation locations were often pitted and heavily expanded by corrosion. Corrosion products penetrated to the crack tips, and after analysis they were found to be magnetite ( $Fe_3O_4$ ). The maximum crack depth found in one of the 128 inspected disks was 18 mm (0.7 in).

In order to avoid damages such as those just described, some turbine manufacturers, including Westinghouse and Siemens, recommended a transition from rectangular to circular keys and keyways.<sup>84</sup>

Because the highest tensile stresses in shrunk-on disks occur at the shrink fit, in the wet-steam turbines for the French CP-1 nuclear power plant series (which had shrunk-on LP rotors), instead of common axial keys between the shaft and disks, ALSTOM used round radial keys between the disks in the lower stress zone of their hub face (Fig. 4-30). This design makes the adjacent disks interconnected, and the entire disk chain is connected to the shaft by a sleeve that experiences very low centrifugal stresses. This allows the use of a light shrink for this sleeve, relieving its stress state.<sup>85</sup>

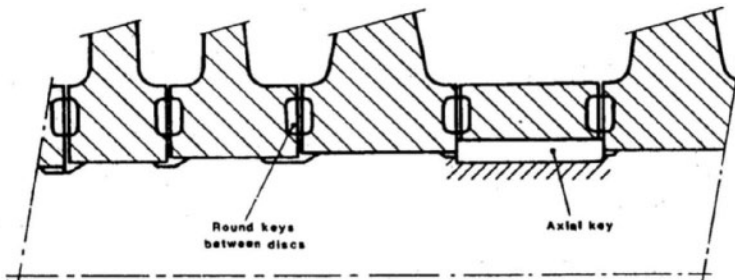


**Fig. 4-30.** Disk keying for the LP rotors of ALSTOM's wet-steam turbines for the French CP-1 nuclear power plant series

Source: P.Aubry, S. Bayard, and A.Anis<sup>86</sup>

SCC has never been seen on wheel disks of welded and forged rotors. According to ABB, by 1996, some of their wet-steam turbines with welded LP rotors had been in operation for over 200,000 hours; more than 50 LP rotors had been running for over 150,000 hours, and SCC failures had never occurred at these turbines.<sup>87</sup> This is the reason why some nuclear power plants have replaced shrunk-on LP rotors in their wet-steam turbines in service with the welded rotors.<sup>88</sup> In particular, such a replacement was carried out at the U.S. nuclear power plant Zion with the wet-steam turbines of a domestic manufacturer.

The LP rotors in the turbines at this plant had numerous cracks after six years of operation, and the new welded LP rotors showed no signs of SCC after 47,000 hours operation.<sup>89</sup>

Without shrunk-on disks, welded or forged LP rotors feature much more even stress fields, with smaller stresses on the surfaces swept by steam, no stress concentrators, and no fissures or crevices where aggressive steam contaminants can gather.

Along with this, it is well known that Siemens' steam turbines with shrunk-on LP rotors (in particular, low-speed wet-steam turbines with the output of up to 1,475 MW as shown in Figure 3-8) have a long experience of operation without any indications of SCC. By 1987, a total of 40 rotors of this type were in operation, averaging close to seven years of service; 11 of these rotors had been in operation for an average of 59,000 hours, with a maximum of 83,000 hours, before the first ultrasonic inspection was carried out. No stress corrosion cracks were identified by these inspections, which covered 100% of the entire disk hub bore area and keyway zone of all the rotor disks.<sup>90</sup> By now, the current lifetime of some Siemens turbines with shrunk-on wheel disks has reached the level of 200,000 hours without any signs of SCC.

In the 1980s, in connection with the development of a new, more efficient LP steam path, Siemens proposed an advanced design of the LP rotors with shrunk-on wheel disks.<sup>91</sup> The stress states of the rotor shaft and disks were thoroughly investigated with the use of a finite-element method employing a grid shown in Figure 4-31; an example of the rotor's calculated temperature field used for calculating the rotor's stress state can be seen in Figure 4-61. The design configuration of the shrink fit and the keyway section, presented in Figure 4-32, was completely adopted from the preceding vintage's rotor design, which had a long and successful operating experience. This design features the following approaches: 1) the keyways are located on the downstream side of the disks in order to eliminate condensation during steady-state operation;

2) a larger-than-1-mm (40-mil) gap between the shaft and disks opens up the keyways and the circumferential stress relief groove in order to avoid crevice conditions; 3) large radii of the stress relief grooves at the shaft and disks are designed to minimize stress concentration, and 4) the shaft outline is specifically designed for the lowest high-cycle fatigue stressing caused by shaft bending. All of the LP disk forgings, as well as the rotor shaft, are manufactured of NiCrMoV steel with 3.5% nickel and 1.5% chromium content, with advanced fracture resistance and consistent yield strength. This is achieved by specifying a proper chemical composition with low phosphorus, sulfur, and silicon contents. To diminish the tensile surface stresses and thus reduce the potential for SCC, the residual stresses on the shaft surface are eliminated by rolling the machined surface, and residual compressive stresses are artificially developed at the surfaces of the disk forgings, so that the residual tensile stresses remain only inside the forgings. How the compressive stresses are formed at the disk forging surfaces is illustrated in Figure 4-33. The first step is to build up compressive hub bore stresses by an optimized water spraying process during the heat treatment of the disk forgings. Shot peening the disks is the next step, and rolling and honing are applied in the keyways to produce compressive stresses after the disks have been shrunk onto the shaft in order to eliminate any potential keyway cracking. These compressive stresses continue to act during the later turbine operation, preventing SCC in the keyway.

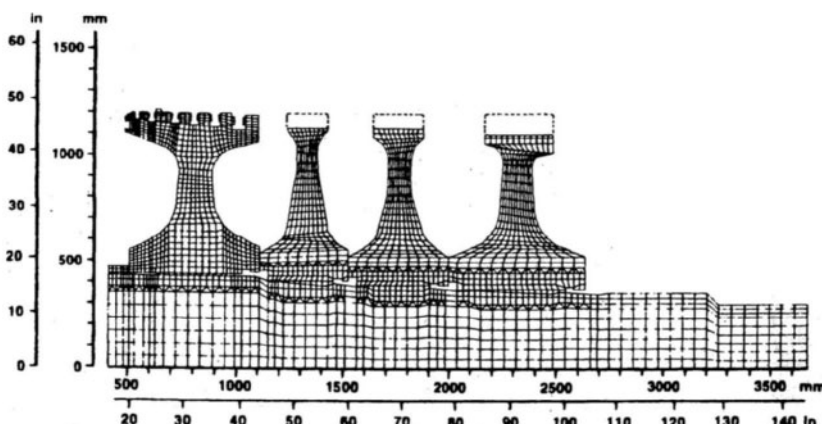


**Fig. 4-31.** Finite element mesh for calculating stress state of the shaft and disks for a combined LP rotor of Siemens

Source: H. Oeynhausen, G. Roettger, J. Ewald, et al.<sup>92</sup>

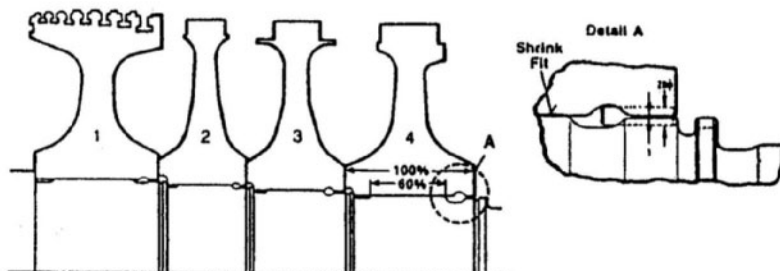


**Fig. 4-32.** Keyway design for combined LP rotors of Siemens' turbines for nuclear power plants

Source: H. Oeynhausen, G. Roettger, J. Ewald, et al.<sup>93</sup>

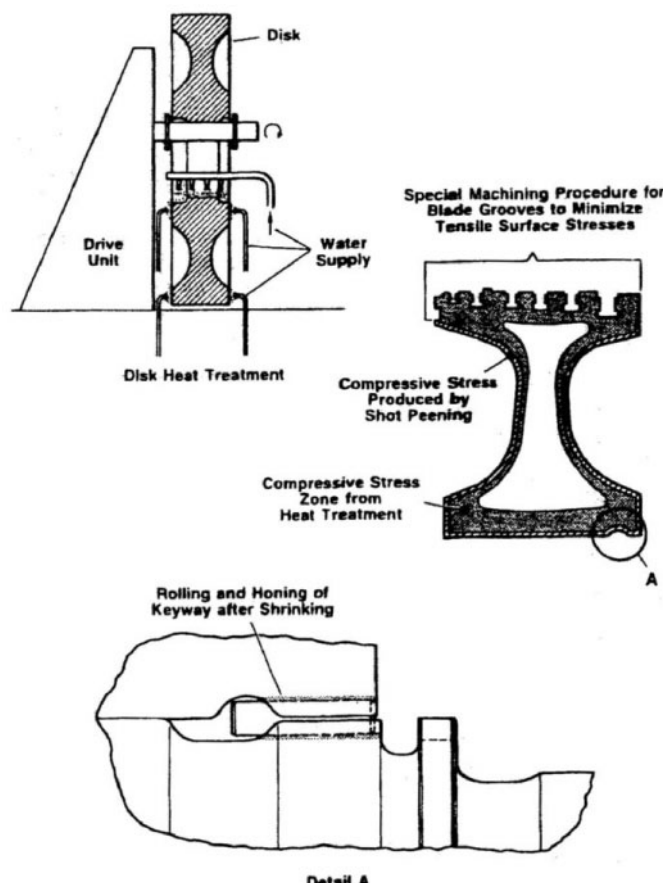


**Fig. 4-33.** Measures to produce residual compressive stresses at surfaces of disk forgings for combined LP rotors of Siemens' turbines for nuclear power plants

Source: H. Oeynhausen, G. Roettger, J. Ewald, et al.<sup>94</sup>

Stress corrosion can also cause damage to the blades operating in the phase transition zone if they experience high local vibrational stresses. In particular, such damages occurred in the IP cylinder of Turboatom's K-1000-60/1500 turbine at the South Ukrainian nuclear power plant.<sup>95</sup> If the turbine operates with a somewhat decreased reheat steam temperature, the damaged turbine stage occurs under conditions of initial condensation, instead of operating with superheated steam.

Corrosive effects can also occur in the blade attachment zones. For example, corrosion cracks were revealed in the LSB's curved fir-tree fastenings of some ABB turbines.<sup>96</sup> The cracks occurred predominantly in the two upper hooks of the fir-tree groove, in both the convex and concave bearing shoulders (Fig. 4-34). Metallographic examinations showed that the cracks were caused by pitting corrosion, and the crack growth was accelerated by crack opening corrosion, but no causal connection was found with the number of operating hours or start-ups of the turbines. As a result, the most probable cause of pitting corrosion was assumed to be the environmental conditions of the LP exhaust space during outages. It is crucial to prevent penetration of wet air with carbon dioxide content into the blade attachment crevices.

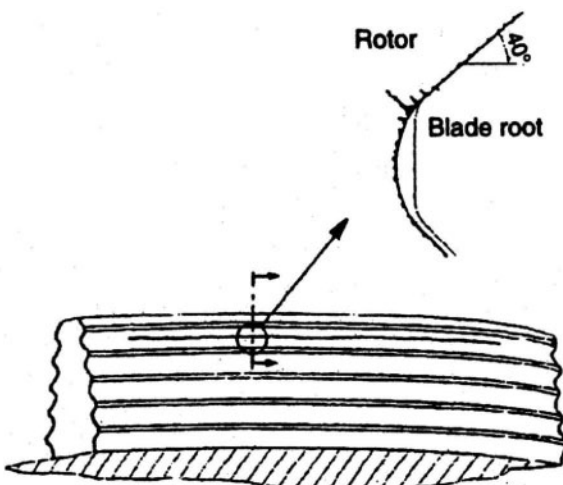


**Fig. 4-34.** Crack locations in the fir-tree grooves of ABB's LP last stage blades  
Source: L. Busse, D. Heiberger, and E. Krämer<sup>97</sup>

## Erosion-corrosion of turbine casings

Most often, wear on turbine stator elements is caused by miscellaneous erosion-corrosion processes combined with water drop erosion (Fig. 4-35). As well as for the rotating elements, the intensity of these processes for the turbine stator elements essentially depends on numerous factors, such as steam/water chemistry (in particular, its hydrogen indicator pH level), steam impurities, local steam flow features, the employed steel grade and its corrosion resistance, specific design decisions applied, and local steam wetness and temperature (see Fig. 3-26a).

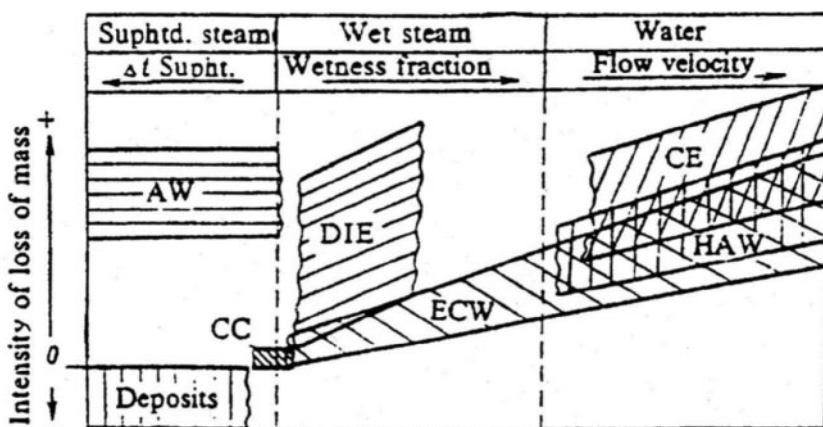


**Fig. 4-35.** Different patterns of wear for metal of wet-steam turbines due to erosion and erosion-corrosion processes (AW: abrasive wear; CC: corrosion cracking (stress corrosion); CE: cavitation erosion; DIE: drop impact erosion (water drop erosion); ECW: erosion-corrosion wear; HAW: hydroabrasive wear)  
Source: O.A. Povarov, G.V.Tomarov, and V.N. Zharov<sup>98</sup>

There are some empirical approaches that make it possible to foresee the rate of these processes with regard to the factors mentioned, but they give rather qualitative results. This is clear from Siemens' data in Figure 3-26b, where the expected ECW rate values are plotted against the actual measured values for several wet-steam turbines. It can be seen that for stator elements fabricated from carbon steels, the ECW rate reaches as much as 4–5 mm/yr (120–200 mil/yr).

Experimental data of bench tests and observations on actual wet-steam turbines in service allowed determining the areas of various ECW rates in the two-phase region (see Fig. 2-3). The greatest ECW intensity threatens the steam path and bleeding steam-lines of the HP cylinder, crossover pipes to the MSR, and the moisture separator. The data of Figures 2-3 and 3-26b are valid for structural carbon steels. For alloyed steels, the characteristic ECW areas are the same, qualitatively, differing in a level of the ECW rates. Evidently, there is also a similar effect caused by steam/water chemistry conditions. The menace of ECW for LP cylinder casings, casing rings, and diaphragms to a degree depends on the steam-expansion process features. The ECW rate rises with an increase in the reheat (partition) steam pressure and a decrease in the corresponding steam temperature, especially if steam reheat does not exist.

As for HP sections of wet-steam turbines, Figure 3-27 shows the most typical locations for ECW in the HP cylinder of Turboatom's K-220-44 turbine, and Figure 4-36 demonstrates the erosion wear for the outer HP casing of two actual K-500-65/3000 turbines after different operation periods. Analysis of statistical data for the K-220-44 turbines shows that the maximum ECW occurs with a steam wetness of more than 5% and in the temperature range of 160–200°C. These data completely correspond to the Siemens data presented in Figure 3-26a.

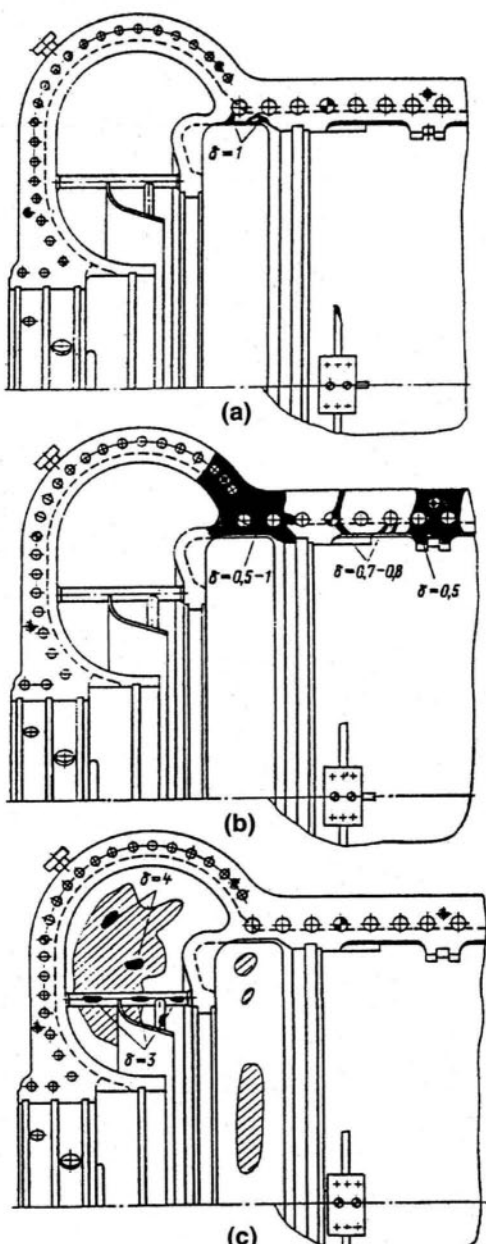


**Fig. 4-36.** Erosion wear for outer casing bottoms of two Turbotatom K-500-65/3000 turbines (a: sample 1 after 6,000 hours in service; b: sample 1 after 12,000 hours; c: sample 2 after 14,000 hours;  $\delta$ : depth of wear in mm)  
Source: B. M. Troyanovskii, Y. F. Kosyak, M. A. Virchenko, et al.<sup>99</sup>

Crevice erosion is prevalent in the joints of casings, rings, and diaphragms, and its rate often exceeds the mean rate expected for the local steam conditions. For this reason, it is especially important to prevent steam leakage through the flange joints, which acts as a positive feedback: the greater the leakage, the more the wear increases. To enhance the tightness of the flange joints, Turboatom had to increase the tightening force for the bolts in the rigid belt zone of their K-220-44 turbines and fastened the diaphragm halves together with bolts; in some places, the stud bolts were replaced by bolts of enlarged diameters.<sup>100</sup> In some cases, ABB and Siemens also increased the number of bolts in the flange joints of the HP casings.

Many turbine manufacturers apply surfacing (building up by welding or spraying) the flanges with highly resistant materials. However, the most drastic way to reduce or completely eliminate ECW is to fabricate these elements from alloyed and stainless steels. Replacing carbon steel by steel with 2.5% Cr reduces the ECW rate by a factor of four, and the use of steel with 12% Cr almost completely eliminates erosion of the stator elements. Comparative calculations showed that it is finally more profitable to fabricate the HP cylinder of the K-1000-60/3000 turbine from stainless steel rather than cheaper alloyed steels (see Fig. 3-14).

For turbines in service, building up the eroded surfaces such as the horizontal joints of the casings, cylinder rings, and diaphragms by welding with an erosion-resistant material can be accomplished when the turbine is being overhauled. No post-weld stress relief is needed in most cases.

## Damages to blading

Blade damages tend to develop and propagate like a chain reaction. If, for whatever cause, a blade loses its pieces, the fragments broken off come between the rotating and fixed components and can cause destruction of the next stage blades; then, fragments from those blades fall into the next stage, ruining their blades, and so on. Increased vibration of the rotor due to a weight imbalance can progress following the same pattern. Failures of long LP LSBs are especially harmful and dangerous. Tearout of even the tip of such a blade results in an intensive growth in vibration, necessitating the shutdown of the turbine as soon as possible to prevent further damages, potentially even the complete destruction of the turbine.

Usually, when a blade breaks, it is only the final stage in a long destructive process that begins well before the breakage with the appearance of an initial crack in the blade, caused by fatigue or corrosion, for example. The crack continues to grow until reaching its critical size, at which point the blade breaks. The crack's critical size depends to a great degree on the blade's stress state: the more stress, the smaller the range in which the crack has grown before breaking. The appearance of a crack not only causes a decrease in the blade's cross-section area and an increase in the stress, but also creates conditions for the potential brittle fracture of the blade, with all of the attendant consequences.

One example of this is an accident with a wet-steam turbine of an 895-MW nuclear power unit after four years of operation.<sup>101</sup> The turbine consisted of one double-flow HP cylinder and three double-flow LP cylinders. The turbine was designed with nozzle group control and partial steam admission. For its initial six months of operation, the turbine operated under a two-valve mode. The remaining three and a half years were operated under "three-valves-plus-20%" conditions. A single blade, the third of a four-blade group located in the governor-end row of the control stage, failed catastrophically and left the rotor. Cracks had occurred within the blade attachment zone, at both the middle and lower blade hooks. On inspection, 63 other blades were also found to be cracked in their attachment regions. Some cracking of the control stage disk had also occurred. Considerable pounding damage and fretting corrosion were found on the adjacent blade platform faces throughout both of the control-stage rows. There was no evidence of corrosion or breach marks on the failure surface or other cracked surfaces, which suggested that the cracks had propagated rapidly following initiation, and that relatively pure steam conditions existed. In situ vibration tests were conducted on a similar turbine owned by another utility, and their results were analyzed to identify the natural frequencies of the blade group. It was concluded that the blade failure was due to high-cycle fatigue, mainly caused by the two-valve steam admission operation. This was apparent from the metallographic test results, and it was confirmed by the fatigue life calculations. After this failure, the turbine operation was restricted to full-arc steam admission to minimize variable loading of the blades. This was expected to cause some loss of efficiency in operation, but would have a favorable effect on the blade fatigue life.

When the first large-capacity wet-steam turbines were conceived, most apprehensions were about WDE of their rotating blades, caused by the increase of both the steam wetness and high circumferential velocity of the blades with increases in turbine output and blade length. However, thanks to withdrawing water from the steam path, external moisture separation and reheat, and special protection of the rotating blades (see chapter 3), WDE has never been a decisive factor for wet-steam turbine reliability.

The problems of WDE for the rotating blades of both superheated- and wet-steam turbines are considered in detail by many authors. Most often, the WDE severity for rotating blades is assessed with the use of a so-called WDE criterion,  $E$ , even though the methods of calculating it and the admissible boundaries employed by different researchers and turbine producers are substantially different. Two examples of empirical expressions for calculating this value are presented in chapter 3 (Equations 3.1 and 3.2). According to Siemens, the erosion rate as a function of the operating conditions for a particular turbine can be ascertained from the following equation:<sup>102</sup>

$$E = y_0^2 \times u^3 \times K/p_0 \quad (4.1)$$

where  $E$  is the WDE criterion in  $\text{m}^4/(\text{s} \times \text{kg})$ ;  $y_0$  and  $p_0$  are the moisture content (steam wetness) and steam pressure ahead of the stage, respectively;  $u$  is the blade tip speed in  $\text{m/s}$ ; and  $K$  is an empirical coefficient representing the influence of the steam path design features. The two main factors, influencing  $K$  and affecting the WDE rate, are the axial distance between the stage's fixed and rotating blade rows and the thickness of the trailing edge of the vanes (fixed blades) (Fig. 4-37). The considerable influence of the distance between the stationary and rotating blades on the LSB erosion rate was also demonstrated in experiments conducted by Toshiba.<sup>103</sup>

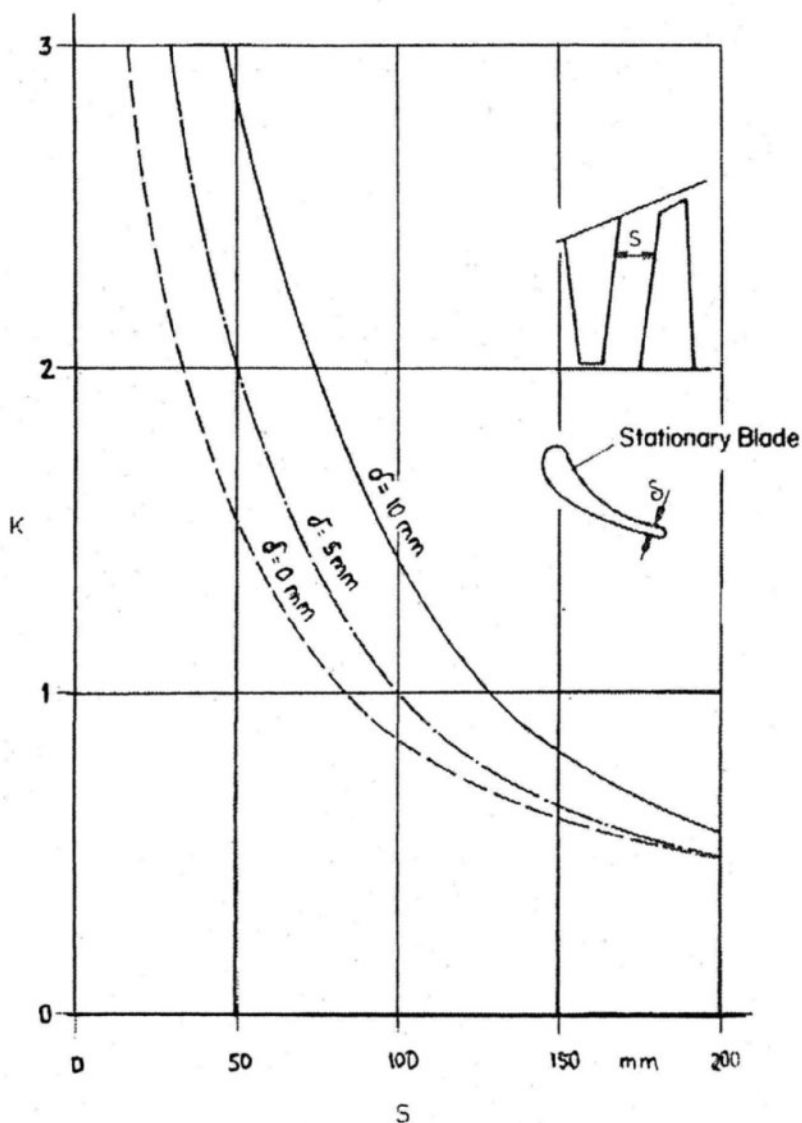
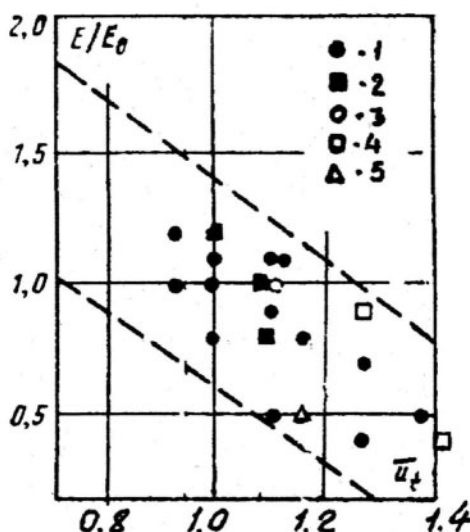


Fig. 4-37. Influence of various design parameters on the WDE rate of rotating blades

Source: W. Engelke<sup>104</sup>

The WDE criterion values,  $E$ , calculated according to methodology of ABB for some newly designed and employed LSBs with various values of the peripheral (circumferential) speed (up to 600 m/s for a 1,000-mm LSB) are plotted in Figure 4-38. The exposed values for  $E$  are related to the characteristics for the LSB with the peripheral speed,  $u$ , of 424 m/s and the moisture content ahead of the blade row ( $y_1$ ) of 10.7%. Although newly designed stages are assumed to be resistant to erosion if the  $E/E_0$  ratio is less than 1.0, some stages in service have reliably worked with  $E/E_0 = 1.1-1.2$ . It can also be seen that for longer LSBs, particularly those installed in wet-steam turbines of nuclear power plants with their greater peripheral speed, the erosion rate even decreases, due to applied design measures, as well as relatively rare transients and no-load operating conditions causing unfavorable steam flows and, as a result, more intense erosion (Fig. 4-17). However, this problem remains topical.



**Fig. 4-38.** Variation of relative WDE criterion with the LSB's peripheral speed for different ABB steam turbines (1: superheated-steam turbines with rotation speed of 3,000 rpm; 2: superheated-steam turbines with rotation speed of 3,600 rpm; 3: wet-steam turbines with rotation speed of 3,000 rpm; 4: wet-steam turbines with rotation speed of 1,500 rpm; 5: wet-steam turbines with rotation speed of 3,600 rpm)  
Source: B. M. Troyanovskii<sup>105</sup>

As mentioned previously, the leading edges of the last and next-to-last LP stages' steel blades are commonly shielded in their peripheral parts against liquid droplet impacts by Stellite laminas (either shields or strips) brazed to the blade surface. Instead of Stellite strips, the leading edges can also be formed by an inlay nose produced from the protective shield material and welded to the blade body. This may or may not preserve the aerodynamic shape of the blade profile. Sometimes the profile shape is purposefully broken in such a way as to produce a discontinuity that causes premature separation of water drops from the boundary layer,<sup>106</sup> but more often than not the shield is designed to preserve the aerodynamic form of the edge (Fig. 4-39). If the shield material is poorly chosen, it can make the blade susceptible to welding-related cracks that eventually cause the blade to break; such failures were observed, for example, at the nuclear power plant Dresden.<sup>107</sup>

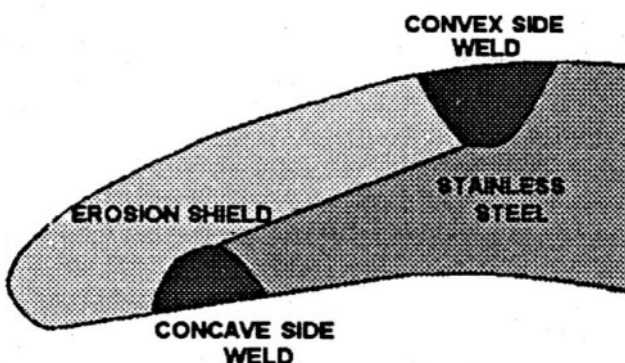


**Fig. 4-39.** Shielding the leading edge of a steel last stage blade from WDE  
Source: J. M. Chynoweth, G. S. Gerzen, and R. W. Tomala<sup>108</sup>

At wet-steam turbines with nozzle group control, there occurred repeated failures of the control stage's blades. The turbine control stages face large pulse loads caused by partial steam admission, causing forced high-frequency blade oscillations. It is almost impossible to tune these blades to prevent them from resonating due to these oscillations. In addition, the first stages of wet-steam turbines work under conditions of nonstationary spontaneous condensation, which also

can cause steam flow oscillations close to the natural frequency of the nozzle vanes, resulting in flaking of their trailing edges. These types of damages, as well as fatigue cracks in the fastening zone and, in some cases, failures of the rotating blades, were found, for example, in some of Turboatom's 220-MW turbines operating with nozzle group control. After transition to throttle control, with the simultaneous opening of the HP control valves, and removal of the wall between the separate nozzle boxes, such damages have not been found.<sup>109</sup>

On the other hand, it should be noted that these types of damages to the first HP stages can also be associated with water induction into the HP cylinder from the main steam lines. This possibility was also revealed with the Turboatom 220-MW turbines, and the potential water induction sources were also eliminated practically simultaneously with the transition of these turbines to throttle control. Repeated damages to the rotating blades of the first HP stages also occurred in Siemens' low-speed 1,200-MW turbines with throttle steam admission control.<sup>110</sup>

Nonstationary spontaneous condensation also takes place in the LP steam path in the phase transition zone, promoting the appearance of tiny pits and scratches on the blade surfaces. This pitting corrosion often combines with stress corrosion processes and can lead to fatigue cracking and eventual failure of the blades.<sup>111</sup>

In the 1970s and 1980s, several instances of blade cracks and failures were reported in large steam turbines at nuclear and fossil fuel power plants that were caused by electrical disturbances between the generator and the electric grid. The electrical disturbances included different types of short circuits at the generator or transformer terminals or in the electric grid with subsequent successful or unsuccessful automatic high-speed reclosing (HSR), switching on the ill-synchronized generator to the grid, subsynchronous resonance in the grid, and so on.<sup>112</sup> Because the turbine rotor presents a complex system that includes a shaft, disks, and blades, oscillations cause not only torsional oscillating stresses in the rotor itself, but also additional bending tangential stresses in the blades, and can lead to considerable fatigue for the last and next-to-last stage blades (Fig. 4-40). In particular, such failures due to torsional resonance took place at the U.S. nuclear power plant Prairie Island with ABB's 560-MW high-speed turbines.<sup>113</sup>

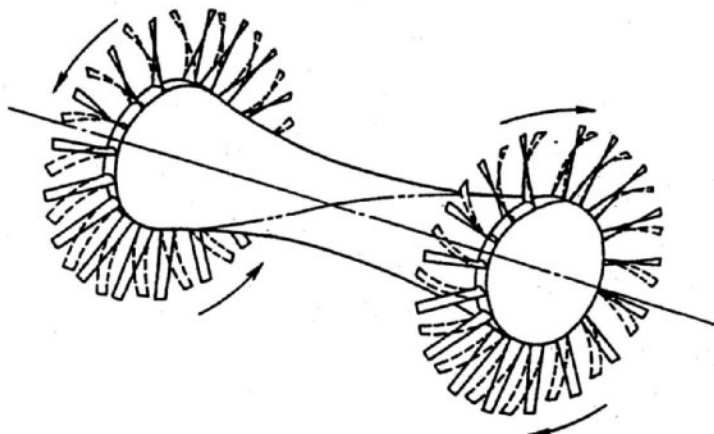
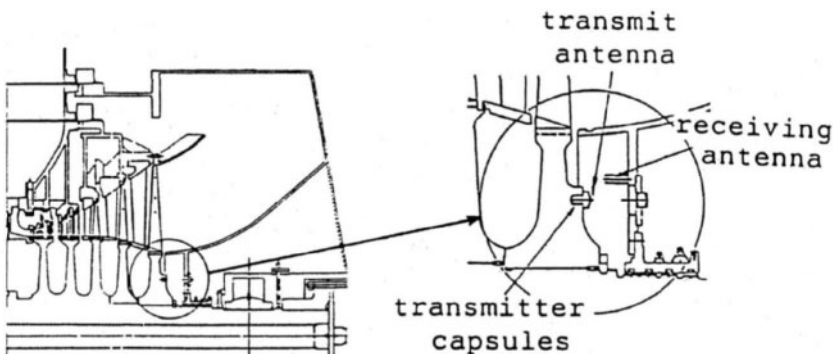


Fig. 4-40. Phenomenon of shaft-blade coupled torsional oscillations  
Source: E. Tsunoda, H. Mimuro, S. Hisa, et al.<sup>114</sup>

These events are associated with variations in the generator rotation speed and entail a slip of magnetic fields in the generator's stator and rotor. Thus, the electromagnetic and mechanical oscillations occur to be bound together. The excited oscillations are damped by internal friction in the rotor metal, aerodynamic resistance of steam in the turbine steam path, and friction in the bearings. According to numerous calculations performed in the late 1970s by U.S., European, and Japanese researchers as applied to different types of large steam turbines in service, the specific fatigue due to these torsional oscillations can reach several tens of percent in the most serious cases.<sup>115</sup> The most dangerous events are subsynchronous resonance, out-of-phase synchronization of the generator, and both successful and unsuccessful HSR after different types of faults in the grid.<sup>116</sup>

Forced torsional oscillations of the turbine-generator shafting caused by the interaction of the generator with the electric grid occur with both single and double grid frequencies. The natural frequencies of the shafting, considered as a multi-mass and multi-support rotating system, must be sufficiently segregated from the grid frequency and its doubled value, with regard to all of the possible inaccuracies of the applied mathematical models. It is especially important to be sure that the LP blades are well tuned against the double-synchronous frequency (100 or 120 Hz), which is the most dangerous in relation to torsional vibration.

Special telemetry measurements were carried out, in particular, on MHI's low-speed (1,800 rpm) 1,160-MW turbine at Unit 2 of the Japanese nuclear power plant Tsuruga. The telemetry system that was used to transmit the blade vibration stress signals to outside observers is shown in Figure 4-41. A special experiment was conducted with a short circuit between two phases at the generator terminals. The measurements confirmed that the LSBs were well tuned out from the double-frequency resonance.<sup>117</sup>



**Fig. 4-41.** Telemetry system for transmitting blade vibration stress measurements of MHI's 1,160-MW turbine at the Tsuruga nuclear power plant  
Source: M. Higuchi and T. Tsuda<sup>118</sup>

Along with this, there is another way of looking at this problem. Analysis and testing of Southern California Edison's San Onofre Nuclear Generating Station (SONGS) turbine No. 3 (a low-speed turbine made by English Electric, with output of 1,181 MW) revealed natural torsional frequencies close to 120 Hz. The standard practice would be to move the natural frequency of the LSB away from this dangerous point. Another possible approach would be to perform thorough direct measurements of the blade stress in response to controlled torsional oscillations from the generator, in order to determine with due confidence if the torsional oscillations could damage the turbine. Both of these approaches were found to be unrealistic, and after long discussion it was concluded that the normal grid operation around SONGS was sufficiently stable and any possible faults would not cause dangerous consequences.<sup>119</sup>

# Protection and Preservation of Steam/Water Paths Using Microadditives of Amines-Based Surfactant

Along with stress corrosion and water drop erosion, the turbine steam path can suffer serious damage from so-called *downtime corrosion*—that is, atmospheric corrosion under the action of ambient wet air during long-term outages. This causes the destruction of a protective oxide film on the inner surfaces of equipment, resulting in the pitting of these surfaces. Downtime corrosion can affect the entire steam/water circuit, including the turbine itself and its auxiliaries, steam-lines, and feed water pipelines. When a power unit (no matter whether it is fossil fuel or nuclear) is started up after a long outage, its working fluid is seriously contaminated by various impurities, including the products of downtime corrosion, and the steam/water path should be “washed out” for a long time period, withdrawing the contaminated water from the cycle until the water chemistry indices reach their normal values. If a turbine is shut down for more than seven days, some national rules and standards for operation and maintenance of power plants advise preservation of the steam/water path.

This in full measure refers to wet-steam turbines of nuclear power plants. First, these turbines have to be stopped for about a month every one or one-and-a-half years when the reactor is refueled and it is not necessary to open and repair them. In addition, some older nuclear power units are shut down because of the expiration of their operating license, but this decommissioning often turns out to be only provisional, and with time they may be relicensed and returned to service. Sometimes, nuclear power units are also temporarily shut down for cold standby, due to an unfavorable economic or political situation in the country where they are located. In all of these cases, it is desirable to preserve the turbine and steam/water path to prevent them from downtime corrosion.

The methods of preservation used in various countries can be subdivided into two groups. The first one is based on creating and maintaining an anticorrosive environment in the inner spaces of equipment to be protected. The second group involves forming

protective films on the inner surfaces of equipment. As applied to steam turbines, the most widely applied approaches involve blowing hot dry air through the steam path or filling up the turbine with nitrogen or volatile inhibitors. Preservation of condensers and feed water heaters is most frequently accomplished by washing them with a hydrazine-ammonia solution or filling them up with nitrogen. Special conservation lubricants or glycerin are used for valves.

Nowadays, preservation of the power unit's entire steam/water path with its diverse types of equipment can be accomplished substantially easier and more effectively with the use of microdoses of film-forming surface-acting fluids (surfactants) added to the working fluid before the power unit's outage. Such an amines-based surfactant, octadecylamine ( $C_{18}H_{37}NH_2$ ), also called ODA (brand name ODACON-ODA conditioned), was developed by Russian (of VNIIAM and MEI) and German (of REICON) specialists. They also developed and have widely implemented an effective technology for its use in fossil fuel and nuclear power plants.<sup>120</sup> This reagent is industrially produced in Germany and has a European certificate of quality. The technology for its use completely meets European ecological requirements.

ODA inhibits corrosion by forming a molecular hydrophobic film on internal equipment surfaces. This film protects metal from oxygen, carbonic acid, and other corrosive and aggressive substances contained in air. Experiments showed that ODA adsorption on the main structural power equipment materials (of both the turbine and its auxiliaries) is approximately equal for carbon and austenitic steels, copper, and brass. Gravimetric bench tests for coupons of carbon and stainless steels in wet media demonstrate the decrease of the corrosion rate by a factor of more than 20n (Fig. 4-42). These results were well corroborated by electrochemical studies.

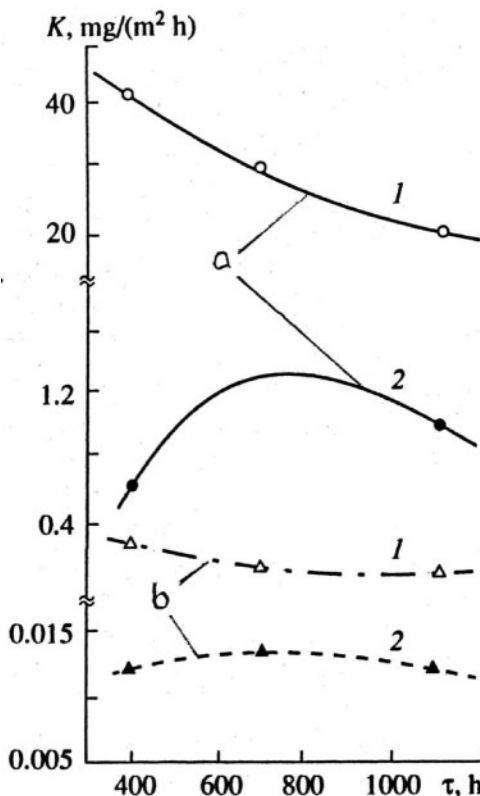


**Fig. 4-42.** Corrosion rate of carbon-steel (a) and stainless-steel (b) coupons in wet medium without preliminary treatment (1) and with pretreatment by ODA for 8 hours (2)

Source: G.A. Filippov, A. N. Kukushkin, G.A. Saltanov, et al.<sup>121</sup>

The preservation ODA-technology was applied to the secondary steam/water circuit and related equipment, including the 220-MW wet-steam turbines, of the Armenian nuclear power plant with two PWR-type VVER-440 reactors. The power plant was shut down after the destructive Armenian earthquake in December 1988, even though the power plant itself was not damaged. Conservation was fulfilled

while the power units were operating under load. The ODA reagent was added into the feed water pump suction sleeves in the form of a 2% water emulsion. The initial concentration of ODA in the feed water after the HP heaters was 1 mg/l, and it was increased over the course of the preservation procedure to 5–8 mg/l. The total duration of the procedure amounted to 100 hours and 160 hours at Units 1 and 2, respectively. All of the secondary-circuit equipment elements were visually examined just after shutdown, and the examinations were then repeated at least twice a year, supplemented by periodic measurements of the specific ODA sorption and water repellency of the surfaces. The total length of the preserved steam-lines and pipelines made of carbon steels, which are greatly prone to atmospheric corrosion, was more than 60,000 m. Unit 2 was restarted in November 1995 after a 69-month outage, without replacing any equipment. The turbine and all of the secondary-circuit elements, including the steam generators, condenser, feed water heaters, steam lines, and pipelines, were examined before the restart by an international commission, and the state of all these elements was found to be quite satisfactory, without any signs of atmospheric corrosion. All of the water chemistry indices achieved admissible values in just a few hours after the start-up, whereas previously, when the unit had been operated and then stopped for several weeks without ODA preservation, this process had taken about a day or more.<sup>122</sup> The same preservation technology was also employed at decommissioned nuclear power plants of the former Eastern Germany.

Added to the working fluid during the operation process, ODA promotes the protection of the rotating blades, disks, and other elements of the turbine steam path from SCC by washing out chlorides and other aggressive deposits from the surfaces swept by steam. What is perhaps more important, ODA-additives reduce the WDE rate by approximately 30% due to a better dispersion of the steam/water flow with reducing water drop sizes and thus reducing the intensity of drop impact erosion. This effect is obvious from the images presented in Figure 4-43, which compares a water drop impact against a solid surface for “pure” wet steam, without any ODA additions, and with ODA added to the steam (4 mg/l).<sup>123</sup>

The influence of the ODA additives on wet-steam turbine reliability and efficiency was first studied at experimental 4-MW and 12-MW turbines of MEI, then was carried over to an industrial 70-MW wet-steam turbine at the nuclear power plant Rainsberg in Eastern

Germany, and finally to the 220-MW turbines of the Kola nuclear power plant in Russia. All of these investigations indicated that the presence of ODA microadditives in the wet-steam flow increases the turbine efficiency by approximately 1.5–2%, with a simultaneous decrease in the droplet impact erosion intensity by approximately 30%.<sup>124</sup> The addition of microdoses of ODA to the working fluid has proven to be a good method for wet-steam turbines to increase their efficiency and reliability.

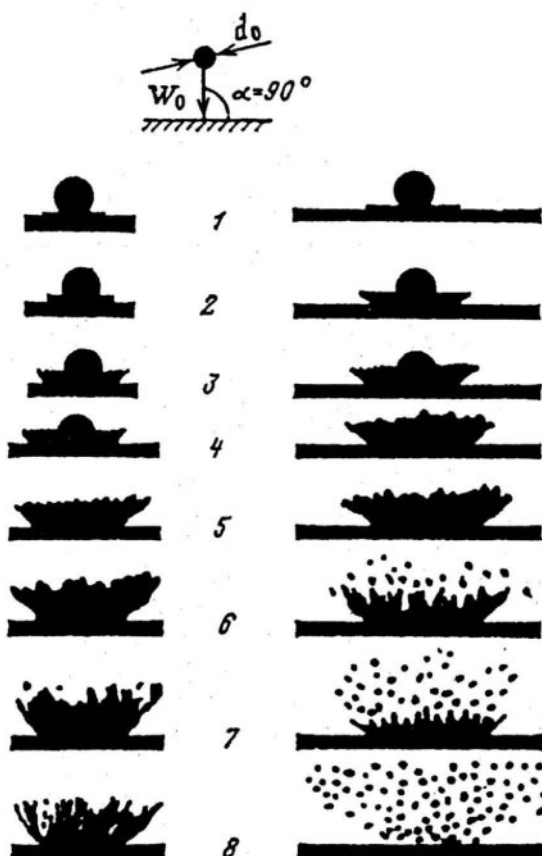


**Fig. 4-43.** The effect of adding microdoses of ODA into wet-steam stream line on the interaction between water droplets and a solid surface (mean droplet size,  $d_0 = 200 \text{ mkm}$ ; steam/water mixture velocity,  $v_0 = 50 \text{ m/s}$ ; a: without ODA; b: with ODA concentration = 4 mg/l; instants after impact: 1:  $0.35 \times 10^{-6} \text{ s}$ ; 2:  $0.85 \times 10^{-6} \text{ s}$ ; 3:  $1.35 \times 10^{-6} \text{ s}$ ; 4:  $1.85 \times 10^{-6} \text{ s}$ ; 5:  $2.35 \times 10^{-6} \text{ s}$ ; 6:  $2.85 \times 10^{-6} \text{ s}$ ; 7:  $2.35 \times 10^{-6} \text{ s}$ ; 8:  $3.85 \times 10^{-6} \text{ s}$ )

Source: G.A. Filippov, G.A. Saltanov, O. I. Martynova, et al.<sup>125</sup>

[Previous Page](#)310 *Wet-Steam Turbines for Nuclear Power Plants*

# Experimental Research and Calculation of Transients for Wet-Steam Turbines

## Start-up tests of wet-steam turbines

Just as the field heat-rate performance tests remain the main and most reliable source of data on the actual efficiency for steam turbines in service, even though the turbine efficiency indices are thoroughly calculated when the turbine is designed, experimental field researches of the turbine transients, along with the actual daily operation practice, lie at the heart of all the operational instructions and manuals, schedules, and diagrams of turbine transients.

Field tests provide researchers with valuable information on the turbine's unsteady-state temperature and thermal-stress states and their changes during transient operating conditions. Start-up tests are the most important and representative part of these field tests. This term is often used in reference to all types of field tests related to the transients. According to a traditional methodology of start-up tests developed in the late 1950s, their primary aim is the experimental reproduction of start-up conditions for the most characteristic prestart temperature states. These start-ups had to be carried out for the shortest possible time periods without exceeding the admissible values of the observed criteria. For the turbines of that time, these criteria mostly included the relative rotor expansion (RRE) and heating-up rates of the high-temperature casings and steam-lines, as well as a few temperature differences in these casings (for example, the temperature differences between the top and bottom halves, across the flange width, and across the wall thickness). This predetermined the nomenclature of the measured values for these tests: they were mainly based on measuring the metal temperatures at the turbine casings and steam-lines. The pursued aims of the tests were attained through numerous repetitions of the laborious and expensive experiments to select the final, most suitable start-up schedules and diagrams of raising the steam parameters and flow rate through the turbine (that is, rotation speed and load). For other types of transients, field tests similarly led to recording the results

of experiments and evaluating whether the operating conditions carried out were fit to be recommended for actual operation.

This approach based on this trial-and-error method is still used by some researchers. It is obvious that the diagrams of the transients that are obtained in such a manner too often turn out to be far from optimum. In addition, for modern large steam turbines, with the rate of their transients mainly limited by the thermal stresses in the rotors, the primary emphasis should be given only to the unsteady temperature fields of the rotors, but their direct thermometry presents a real challenge to researchers, and the number of start-up tests that have actually been conducted with such measurements can be counted on one hand. Automated control of the transients also creates new tasks for the start-up tests. In particular, automation requires knowing the dynamic characteristics for all of the main indications employed to control the turbine state. To gain the dynamic characteristics experimentally, the operating conditions should be subjected to relatively large and sharp disturbances. Often, these disturbances can pose a severe hazard to the turbine's reliability, and sometimes, especially for nuclear power plants, they are completely inadmissible for safety reasons.

A new methodology for steam turbine start-up tests, which met new requirements and was based on a combination of experimental investigations of transients and their mathematical modeling, was developed in the late 1960s by E. R. Plotkin and the author.<sup>126</sup> This methodology was originally developed as applied to start-up tests of subcritical-pressure 200-MW and supercritical-pressure 300-MW power units with K-200-130 and K-300-240 turbines of various modifications, operated with different types of boilers and start-up systems. Then, this methodology was carried over to other power objects, and was further developed by the author as applied to wet-steam turbines of nuclear power plants. Even operated in the base-load mode, these turbines have to experience start-ups, load changes, and other transients, and even individual transients, if they run incorrectly, can damage the turbine or significantly affect its performance. The methodology was also further advanced to accommodate the needs of automated control and monitoring during the transients.<sup>127</sup>

What distinguishes the new methodology from the original one is that the main purpose of the start-up tests is aimed at the acquisition of information necessary for mathematical modeling and calculation optimization of turbine transients, rather than at the direct reproduction of operating conditions that could be directly advised for service. The mathematical modeling replaces many laborious and challenging field experiments. It also makes it possible to construct diagrams and schedules of the transients close to the theoretically optimal ones for the entire spectrum of transients and variations in the turbine conditions, taking into consideration the temperature and thermal-stress states of all the turbine components, including both casings and rotors. It should be noted that these mathematical models could significantly differ from those traditionally used by turbine designers pursuing different goals. Special mathematical models can also help to determine the optimal structure of automated control devices, tune them, and foresee and compare the operating processes under action of different automated control programs. These results can be achieved not only for turbines in service, but also for newly designed turbines and units in the design stage, provided that the developed models and numerical values of their factors were applicable to the considered objects and that the necessary boundary conditions for the considered turbine design elements were known.

In order to materialize the mentioned potentialities, the field start-up tests should provide all of the required data for the mathematical modeling, as well as verify the developed models through a minimum scope of special experiments at the actual turbines in service. In doing so, the field tests do not depreciate themselves. Their results remain the principal criterion to determine whether the developed and applied mathematical models and speculative schemas are valid. In addition, the measurements at the turbines in service often reveal new effects that could not be foreseen from the previous experience. Finally, new technological decisions and approaches for improving transients, as well as their scenarios, can be worked out and put into effect only through the field tests and subsequent turbine operation.

The traditional sequence of experiments followed by calculations based on the experimental results has been replaced by a calculation-experimentation-calculation sequence, which corresponds to the contemporary practice of planning experiments. As applied

to turbine start-up tests, this triple sequence can turn into a tetrad: preliminary calculation, first-stage experimentation, calculation verification, and, finally, second-stage experimentation. In so doing, the field tests are divided into two series.

The mathematical models for potentially critical turbine elements are developed in the preliminary calculation stage, preceding the first series of field tests. The main goals of this stage are to estimate the turbine's preliminary flexibility characteristics, evaluate the thermal stress state and dynamics of heating for the expected critical elements, evaluate the validity of their temperature monitoring, and construct advanced diagrams and schedules of the transients. An analysis of the obtained results helps to determine the number and location of temperature measurements for the subsequent field start-up tests.

For the first test series, some typical transients must be reproduced. However, they do not have to be carried out with as much accuracy as that required by the traditional methodology. For example, the data shown in Figures 4-8 and 4-9 were recorded during an ordinary regular shutdown and start-up. The number of experiments decreases, because it is not necessary to conduct them closely to the assigned programs, which are in turn altered during the testing. Thus, the first test series needs to include start-ups from the most typical initial temperature states. During the tests, partial-load and, if possible, full-load discharge operating conditions are also simulated. In particular, these conditions are used to analyze their influence on the prestart turbine temperature state.

The recorded results of measuring the heating-steam and metal temperatures allow determination of the static and, if necessary, dynamic dependencies for boundary heat transfer conditions as applied to the most thermally-stressed (*critical*) turbine design elements. These characteristics can be made more statistically representative by using data recorded during regular operating conditions, including stationary ones.

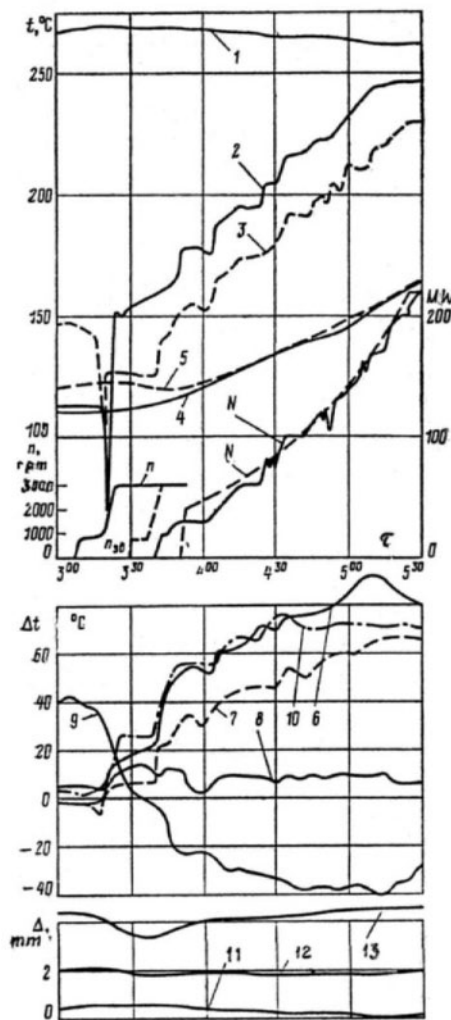
The first test series is followed by the calculation verification stage, which includes processing the data of the preceding experiments. In particular, the recorded data are used to verify the applied mathematical models that were developed earlier and to refine the numerical

values of their factors by comparing the measured data with the results of mathematical simulations. The corrected, if necessary, models are then used for the repeated and refined optimization of the transients, taking into account improvements in technology and transient scenarios according to the results of the first-stage experimentation.

The final verification of the developed recommendations comprises the main goal and contents of the second series of field tests. During this series, it is desirable to reproduce the calculated diagrams of the transients as exactly as possible (Fig. 4-44). The scope of this series of field tests depends on the set tasks of research.

**Fig. 4-44.** Experimental verification of the set start-up diagram for a K-220-44 turbine at field start-up tests at the Kola nuclear power plant (Steam and metal temperatures: 1: stop valve steam-chest; 2: steam in nozzle chamber downstream from the first control valve; 3: wall of the HP control-stage chamber on top; 4: the HP flange's external surface after the 5th stud bolts; 5: the HP flange's external surface after the 9th stud bolts. Differences in the measured metal temperatures: 6: across the HP flange width after the 5th stud bolt; 7: across the HP flange width after the 9th stud bolt; 8: across the thickness of the HP casing wall in the steam admission zone at the bottom; 9: between top and bottom in the steam admission section; 10: calculated metal temperature difference across the HP flange width in the steam admission zone; relative rotor expansions: 11: HP RRE; 12: LP-1 RRE; 13: LP-2 RRE)

Source: A. S. Leyzerovich, V. B. Kirillov, S. P. Kruzhkova, et al.<sup>128</sup>



This methodology was applied to investigations of the flexibility characteristics for main standard Soviet steam turbines used in fossil fuel power units, with individual capacities of 200, 300, and 800 MW. The results of these investigations were used as the basis of constructing the standard instructions for start-ups and shutdowns of these units. But most obviously, rich opportunities of this methodology manifested themselves in the field tests of nuclear power units with K-220-44, K-500-60/1500, and K-1000-60/3000 wet-steam turbines. Due to a widespread use of mathematical modeling, the amount of special operating conditions for these tests was minimized. As applied to the last two turbine types, it became possible to restrict the field work to only the recording of readings for ordinary stationary operating conditions and regular start-ups and shutdowns, without any additional interference with operation. Because of this, the first- and second-stage series of field start-up tests for these turbines were practically merged into a single experimentation stage, without intermediate calculations. The obtained results were used to revise the operating instructions and start-up diagrams.<sup>129</sup> When the K-220-44 turbines in service were remodeled, by transferring them from nozzle group control to throttle control, the start-up diagrams were recalculated and reconstructed without additional start-up tests. The obtained test results lie at the heart of algorithms and programs for the first wet-steam turbine start-up automaton, which was developed for the K-220-44 turbine and successfully put into operation at the Kola nuclear power plant.<sup>130</sup> Owing to high confidence in the developed mathematical models, they were used for calculated optimization of start-up diagrams, design of automated control for transients, and arranging information support for operational personnel during transients as applied to other types of wet-steam turbines, even without special start-up tests for them.<sup>131</sup>

As an illustration of preparing a wet-steam turbine to field start-up tests, the location of steam and metal temperature measurements at the outer casing of the integrated HP-IP cylinder of the 500-MW low-speed K-500-60/1500 turbine (see Fig. 3-18) at Novovoronezh Unit 5 can be seen in Figure 4-8. The unit is of a double-turbine scheme with the pilot PWR-type VVER-1000 reactor. Some results of these temperature measurement readings during shutdown and start-up are presented in Figure 4-9.<sup>132</sup>

The scope of the metal temperature measurements should provide researchers with the required information about initial temperature conditions for the major turbine design elements and steam-lines. These data are used as the initial conditions for calculating the heating-up of

the turbine at transient. It is also important to have the possibility of comparing the measured metal temperatures with their calculated values. Comparisons of the measured and calculated temperature fields in the HP casing flanges for K-220-44 and K-500-60/1500 wet-steam turbines based on their start-up tests are shown in Figures 4-45 and 4-46.

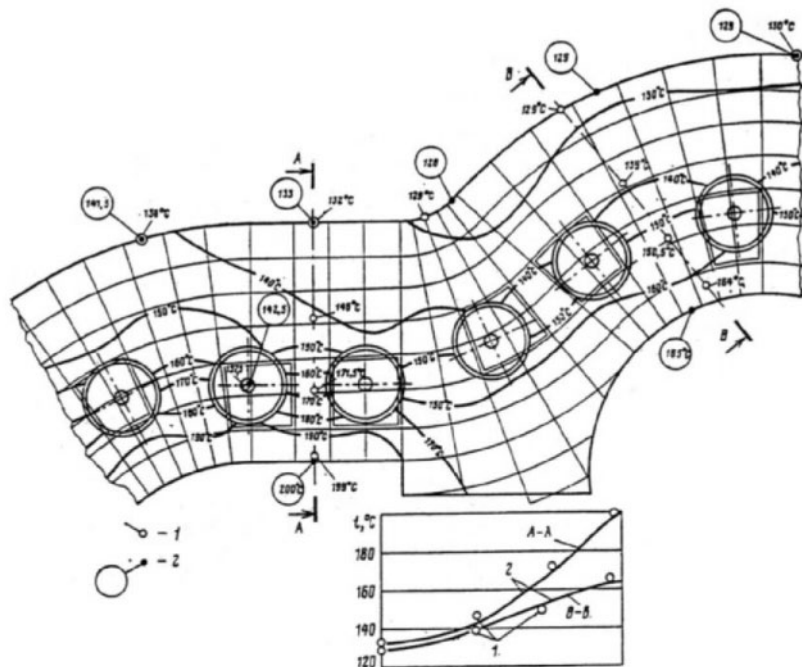


**Fig. 4-45.** Comparison of measured (1) and calculated (2) temperature fields in HP casing flanges of K-220-44 turbine based on start-up tests at the Kola nuclear power plant

Source: A. S. Leyzerovich, V. B. Kirillov, S. P. Kruzhkova, et al.<sup>133</sup>

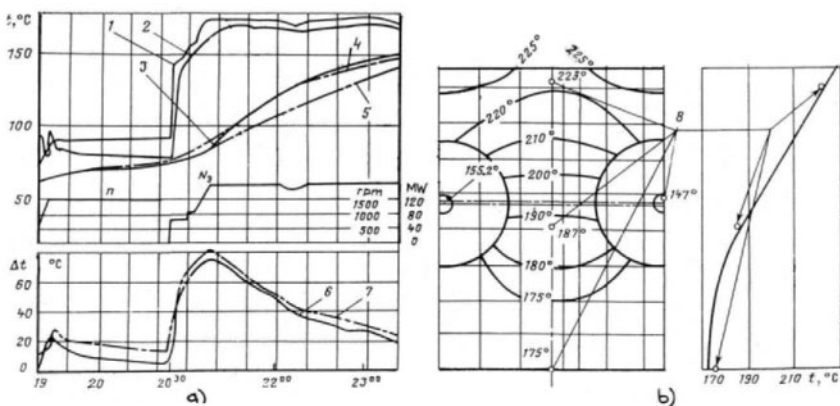


**Fig. 4-46.** Comparison of measured and calculated metal temperatures in the HP flange (a) and IP flange (b) of the HP-IP cylinder casing of a K-500-60/1500 turbine at start-up (measured temperatures in the HP section: 1: steam in the intercasing space; 2: flange metal near the heated surface; 3: flange metal on the external insulated surface; calculated metal temperatures: 4: flange metal on the external insulated surface, 5: stud bolt at flange mid-height, 6: measured metal temperature differences across the HP flange width; 7: calculated metal temperature difference across the HP flange width; 8: measured metal temperatures in the IP steam admission chamber)

Source: V.A. Akerman, N. S. Gabrijchuk, V. B. Kirillov, A. S. Leyzerovich, et al.<sup>134</sup>

Choosing the number and location of metal temperature measurements should be based on the implied mechanism for shaping the stress state and the assumed schema of stress calculations. For bulky and potentially critical high-temperature stator elements, the set of metal temperature measurements should provide all of the means to estimate the thermal-stress state of these elements. In addition to radial temperature differences, axial and circular temperature unevenness can also play a significant role. However, because the corresponding thermal fluxes are of secondary importance, they can be estimated by using temperature measurements on the external surface of the considered element, with emphasis placed on the temperature distribution across the element thickness. It is especially desirable to measure the metal temperature as close as possible to the heated surface where the metal temperature gradient is the greatest.

Experimental acquisition of the data about the boundary heat conditions in the whole range of their variations may be the most important part of the start-up tests. This primarily concerns the temperature of steam sweeping the potentially critical elements. Depending on the turbine design features, they may be the steam-chests of the HP stop and control valves, casings of the high-temperature cylinders in the inlet and first-stage chamber zones, and/or rotors in the steam admission and first-stage zones. For wet-steam turbines, the boundary conditions are somewhat easier to determine, because for most of the critical elements, the heating steam temperature can be considered equal to the saturation temperature at the corresponding pressure, and the heat transfer coefficients for wet-steam are so high (in the order of  $10^4 \text{ W/m}^2 \times {}^\circ\text{C}$  or greater) that an error in setting this value cannot significantly affect the calculation results. During start-up tests and regular load changes, it is necessary to establish static dependences of the heating steam pressures on the steam flow amount through the turbine (that is, the turbine load), which makes it possible to plot the static dependence for the heating steam temperatures equal to the saturation temperatures. Such a static dependence for the heating steam temperature in the first HP steam extraction chamber of the K-500-60/1500 turbine is shown in Figure 4-47a.

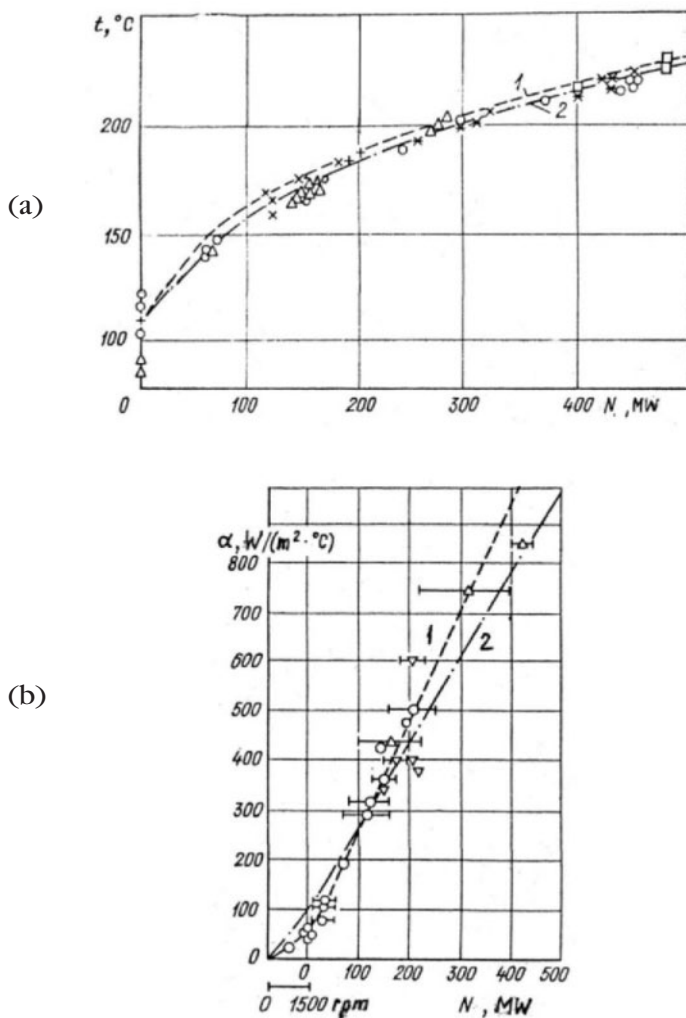


**Fig. 4-47.** Static dependencies on turbine load for heating steam temperature in the first steam extraction chamber (a) and heat transfer conditions in the IP steam admission chamber (b) of the HP-IP cylinder of a K-500-50/1500 turbine based on start-up tests at the Novovoronezh nuclear power plant (1: approximate generalization of calculated procession of experimental data; 2: approximate generalization of preliminary calculated data)

Source: V.A. Akerman, N. S. Gabrijchuk, V. B. Kirillov, A. S. Leyzovich, et al.<sup>135</sup>

For wet-steam turbines, deep steam throttling in the HP control valves at low steam flow rates can result in the appearance of superheated steam in the first stages of the HP steam path. This effect was fixed in the start-up tests of the K-220-44 turbine, with the main steam pressure of 4.3 MPa (44 atm; 625 psi) (Fig. 4-48). In this case, the steam flow rate through the turbine is estimated from the total load of the main and house (auxiliary power) generators. If the metal temperature is lower than the steam saturation temperature, and the heat flux from the heated surface into the metal thickness is more than that from steam to the heated surface, even with superheated steam, the turbine is heated with steam condensation on the heated surfaces, as it is with wet steam. Otherwise, the heat transfer process is determined by thermal convection, as it is in superheated-steam turbines.

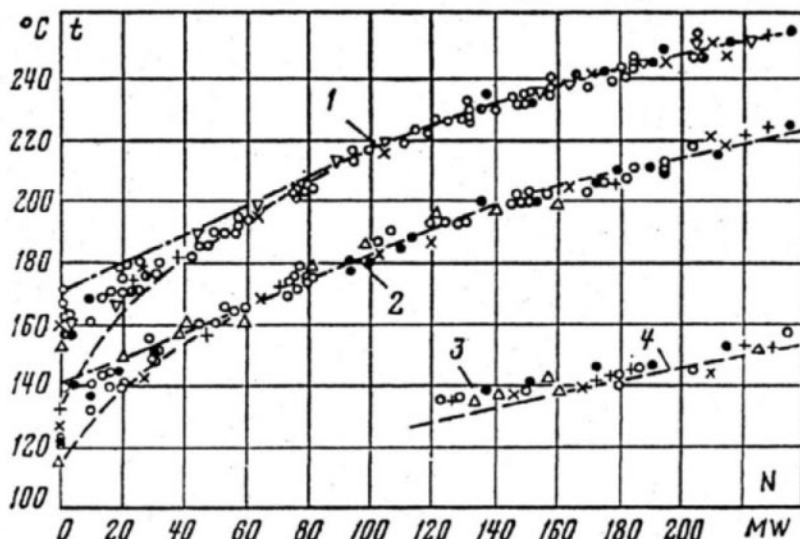


**Fig. 4-48.** Static dependencies on the total turbine load for heating steam temperatures in the HP cylinder chambers of a K-220-44 turbine based on start-up tests at the Kola nuclear power plant (1: in the steam admission chamber downstream from the first two control valves (with nozzle-group steam control); 2: at the control stage; 3: in the front seal first chamber (connected to the fourth steam extraction); 4: in the fourth steam extraction chamber)

Source: A. S. Leyzerovich, V. B. Kirillov, S. P. Kruzhkova, et al.<sup>136</sup>

Similar heat transfer conditions take place in the IP section, if it exists, and in the first stages of the LP cylinders if the IP section is absent. For power steam turbines, the heat transfer convection processes can be regarded as stationary or quasi-stationary, because any real nonstationary effects manifest themselves only during very short time periods incommensurable with the heating duration.

The temperature fields of elements of wet-steam turbines that are heated by superheated steam are shown in Figure 4-8 (the IP portion of the integrated HP-IP rotor and the outer casing cross-section for the IP steam admission chamber) and Figure 4-10a (the first stages' disk of the LP rotor). For the casing elements, the heat transfer conditions in the casing chambers can be determined in the same manner as for superheated-steam turbines. The methodology for determining these data was described in detail in the author's previous publications.<sup>137</sup> Experimental data of the heat transfer conditions for the integrated HP-IP cylinder's IP steam admission chamber of the K-500-60/1500 turbine are presented in Figure 4-47b in the form of a static dependence on the turbine load. The generalization of these data combined with experimental data for similar chambers with tangential steam admission for superheated-steam turbines allows description of this dependence in the dimensionless criterial form (Fig. 4-49):

$$\text{Nu} = 0.021 \times \text{Re}^{0.8} \times \text{Pr}^{0.43},$$

where the Nusselt and Reynolds numbers (Nu and Re, respectively) are calculated based on a conventional circular steam velocity in the chamber and the equivalent diameter of the chamber cross-section. According to experiments conducted by Turboatom, the heat transfer conditions in the HP steam admission chamber of the K-220-44 turbine, when it is swept by superheated steam, are on the order of 180–200 W/(m<sup>2</sup> × °C), which agrees well with estimates based on criterial equations.<sup>138</sup>

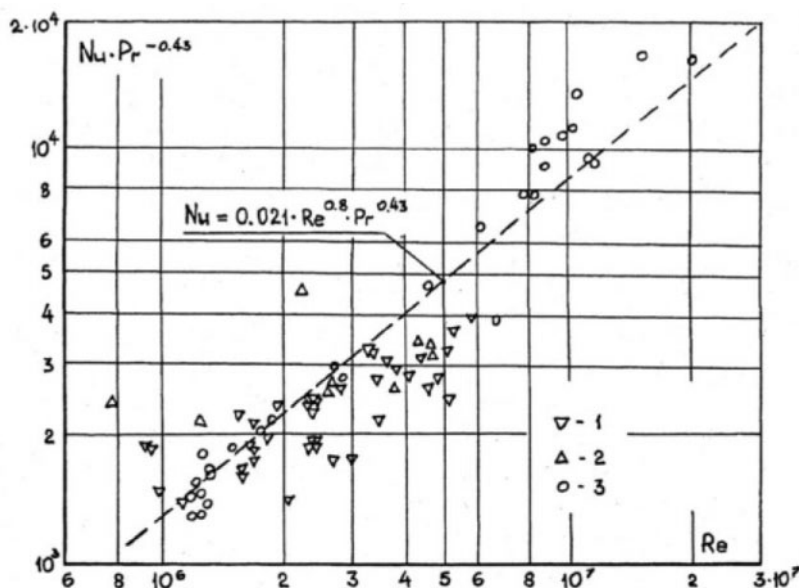


**Fig. 4-49.** Generalization of static dependence for heat transfer conditions from steam to casing in the IP steam admission chambers of various turbines on the basis of their start-up tests (1: LMZ's K-200-130 turbine; 2: LMZ's K-300-240 turbine; 3: Turboatom's K-500-60/1500 turbine)

As to the rotors (IP or LP) heated by superheated steam, the heat transfer conditions for their typical surfaces can be calculated with the use of well-known experimental data already presented in the form of dimensionless criterial equations. Some of these equations were presented in the author's previous book,<sup>139</sup> and more detailed, comprehensive data on this point can be found in numerous papers, special monographs on heat transfer conditions in turbomachinery, and technical guidelines on calculation temperature fields in steam turbine rotors and casings.

While calculating the temperature fields of the rotors, their heating steam temperatures are often taken to be equal to the steam temperatures at the inlet (or outlet) of the adjacent blade rows (Figs. 4-8b, 4-10, and 4-12b). Yet, in many cases, the heating steam temperatures near the heated surfaces of the rotor body can significantly differ from the steam temperatures in the steam path's main stream. For large steam turbines with relatively great stage heights and especially three-dimensional steam path designs, the steam temperature significantly varies along the stage height. This pattern becomes more intricate with regard to

steam leaking out or, on the contrary, sucking into the main stream through the root seals. Depending on the stage features, there could appear different patterns of steam movement through the diaphragm gland seals and pressure balance holes.<sup>140</sup> Because of this, it is always desirable to have data on heating steam temperature conditions near the rotor surfaces measured experimentally.

This task was included in the scope of start-up tests for the Turboatom K-220-44 turbine, with standard welded LP rotors, at the Kola nuclear power plant (see Fig. 3-4). Welded rotors are widely used for large wet-steam turbines (see chapter 3), and in the absence of an IP section, the thermal-stress state of such rotors can severely limit the rate of raising the steam reheat temperature (after the MSR) at start-ups.

The system of experimental temperature measurements that were installed in the LP cylinder of one of the Kola turbines is shown in Figure 4-50. Diagrams of the measured steam temperatures during shutdown and start-up of the turbine can be seen in Figure 4-51, and results of generalizing and processing them in the form of static dependencies on the turbine load for steam temperature decreases relating to the inlet steam temperature are given in Figure 4-52.<sup>141</sup> The temperatures of steam sweeping the rotor body surfaces, particularly in the diaphragm seals, are considerably higher than the steam temperatures in the main stream at the inlet of the corresponding stages at the mid-height of the nozzles. This is explained by the fact that the gland seals are mainly fed by steam from the previous stage's root section, which has a higher temperature due to the end energy losses. The steam temperature drops in the stages along the main steam stream remain practically independent of the steam flow rate. Unlike this, the steam temperature differences between the main steam stream and the diaphragm seal inlet are invariable only at significantly high flow rates through the turbine, and these differences fall almost to zero with approaching no-load conditions. At the same time, for stages working with saturated or wet steam (in this case, these are the fourth and fifth stages), the measured steam temperatures in the diaphragm seals and the main steam stream do not practically differ, and correspond to the saturation temperature for the steam pressure at the stage inlet. The temperature of steam sweeping the rotor in the steam admission zone is lower than the stagnation temperature at the LP cylinder inlet, apparently due to steam leaking through the axial clearances between the fixed blades and disks of the first stages of both flows of the cylinder.

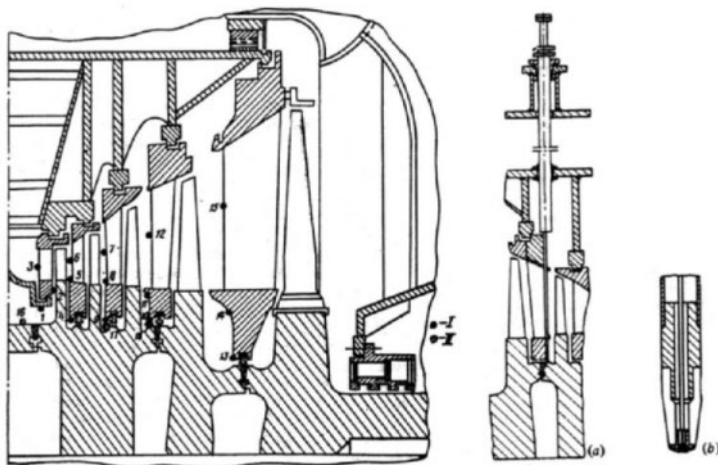


**Fig. 4-50.** Experimental temperature measurements in the LP cylinder of a K-220-44 turbine for investigating the boundary and initial conditions of heating for the rotor (I: steam temperature measurements [1-15]; II: rotor metal surface temperature measurements at stopped turbine [16-18]); installation (a) and head (b) of a temperature probe for measuring the rotor surface temperature

Source: B. N. Lyudomirskii, A. S. Leyzerovich, and Y. N. Kolomtsev<sup>142</sup>

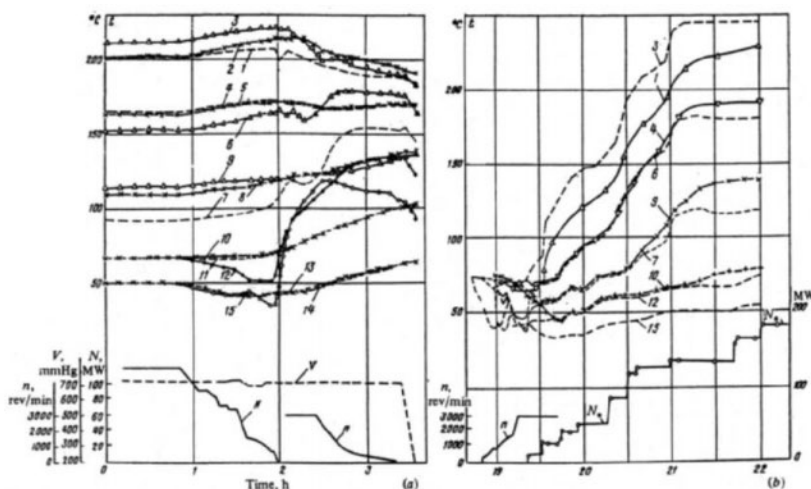


**Fig. 4-51.** Variation in measured steam temperatures in the LP cylinder of a K-220-44 turbine during shutdown (a) and subsequent start-up (b) (numbering of temperature curves is given in accordance with designations in Fig. 4-50; V: vacuum in condenser)

Source: B. N. Lyudomirskii, A. S. Leyzerovich, and Y. N. Kolomtsev<sup>143</sup>

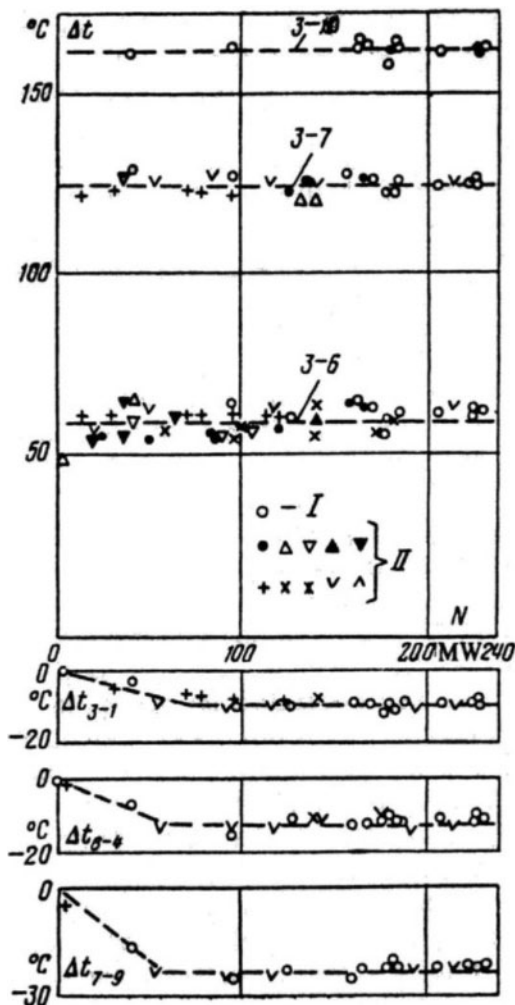


**Fig. 4-52.** Static dependencies of steam temperature decreases in the LP cylinder of a K-220-44 turbine (numbering of temperature curves is given in accordance with designations in Fig. 4-50; I: measurement under stationary operating conditions; II: measurements at start-ups and shutdowns)

Source: B. N. Lyudomirskii, A. S. Leyzerovich, and Y. N. Kolomtsev<sup>144</sup>

Processing the obtained experimental data for transients also showed that if the steam temperatures in the main steam stream,  $t_c(\tau)$ , follow the variation in the steam temperature at the cylinder inlet with virtually no lag, for the steam temperatures in the diaphragm seals,  $t_s(\tau)$ , this time lag is significant, and the dynamics of these temperatures as

related to the main stream steam temperatures can be described with sufficient accuracy by the following transfer function:

$$W(s) = \frac{L(t_s)}{L(t_c - \Delta t_s)} \approx (1 + Ts)^{-1}, \quad (4.1)$$

where  $L$  and  $s$  are the Laplace operator and Laplace transfer parameter, respectively;  $\Delta t_s$  is the static difference of the steam temperatures,  $t_c(\tau)$  and  $t_s(\tau)$ ; and  $T$  is the time constant. In the case of a piecewise linear approximation of the main stream steam temperature variation,  $t_c(\tau)$ , the change in temperature for steam sweeping the rotor surface,  $t_s(\tau)$ , will be :

$$t_s(\tau) = t_c(\tau) - \Delta t_s - [wT + (\delta t_s - wT) \times \exp(-\tau_1/T)], \quad (4.2)$$

where  $w = \text{const}$  is the rate of a linear piecewise approximation of the steam temperature change,  $t_c(\tau)$ , within the considered time period;  $\tau_1$  is the amount of time counted from the beginning of varying  $t_c(\tau)$  at the rate  $w$ , and  $\delta t_s = t_c - t_s - \Delta t_s$  at  $\tau_1 = 0$ . Numerical solution of this equation with reference to  $T$  for the steam temperatures at the stage inlet,  $t_c(\tau)$ , and near the rotor surface,  $t_s(\tau)$ , taken from the measured results give an average value  $T \approx 10$  min. The scatter of the calculated values depends considerably on the assigned accuracy of the solution, and with an allowable error of  $\pm 2$  °C, it amounted to  $\pm 5$  min. Under these conditions, it is hardly possible to establish more detailed connections between variations of  $T$  and load, relative rotor expansion, and other factors. It is of interest that these static and dynamic dependencies are quite close to experimental results obtained for the IP rotor of a supercritical-pressure 800-MW turbine.<sup>145</sup>

The obtained generalized dependencies were used for calculating the heating steam temperatures for the main rotor surfaces at start-ups with arbitrary changes in the steam temperature at the LP cylinder inlet (after the MSR). Comparison of these calculations with the measured data for an actual start-up is shown in Figure 4-53. The steam temperature determination error did not exceed 10°C in dynamics and 1–2°C for stationary conditions, which is quite satisfactory for practical purposes.

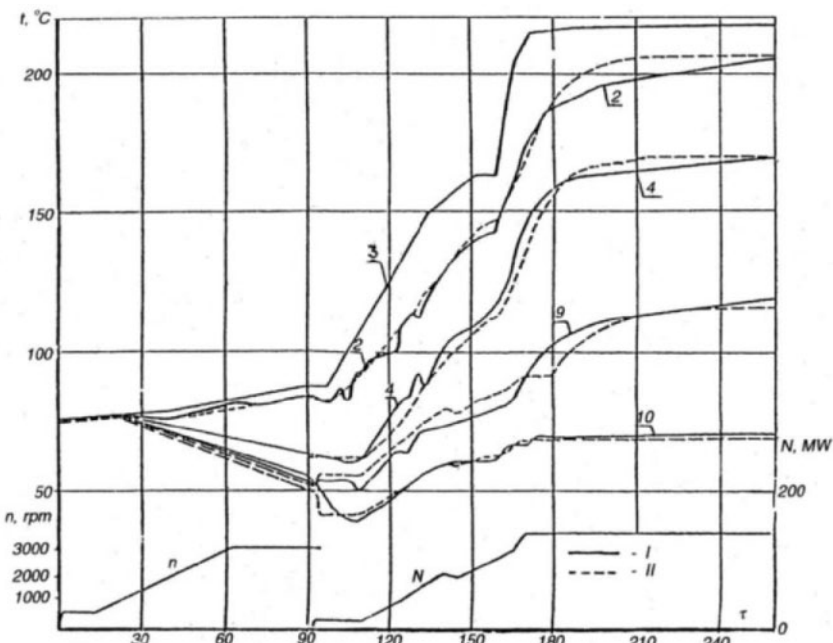


**Fig. 4-53.** Comparison of measured (I) and calculated (II) steam temperatures in the LP cylinder of K-220-44 turbine at start-up (numbering of temperature curves is given in accordance with designations in Fig. 4-50)

The obtained static and dynamic (Equation 4.1) characteristics refer to the steam temperature at the LP cylinder inlet, after the MSR (Fig. 4-52). However, this reheat steam temperature itself changes with the flow amounts of the heated and heating steam in the MSR. Knowledge of these dependencies is important to govern the reheat steam temperature at start-ups. As can be seen, for example, from results of heat-rate performance tests, with the full flow rate of the main heating steam to the MSR's second stage, the reheat steam temperature slightly increases with a decrease in the turbine load.<sup>146</sup> However, with partially opened valves at the steam-lines of heating steam, the pattern drastically changes. A qualitative pattern of static dependencies of the reheat steam temperature on the turbine load and position of the valve governing the heating steam flow is shown in Figure 4-54a. This graph is based on heat balance calculations and some experimental measurements (Fig. 4-54b). Switching on the generator to the grid and accepting the initial load sharply decreases the reheat steam temperature. The dynamics of these variations also substantially depend on the heated steam flow amount. According to

the start-up tests for the K-220-44 turbines of the Kola nuclear power plant in Figure 4-55 and K-500-65/3000 turbines of the Chernobyl plant, the dynamics of the steam temperature after the MSR, regarding disturbances by the heating steam flow amount, is characterized by an initial delay (with a subsequent change in the exponential law) and can be approximated by the following transfer function:

$$W(s) = [\exp(-sT_1)]/(1 + sT_2) \quad (4.3)$$

For the K-220-44 turbine, the time constants are  $T_1 \approx 1-2$  min and  $T_2 \approx 5-15$  min, linearly decreasing with the increase in the turbine load. If the heating steam flow rate decreases, the reheat steam temperature changes are about 1.5 times more inertial than those with an increase in the heating steam flow rate, all else being equal.

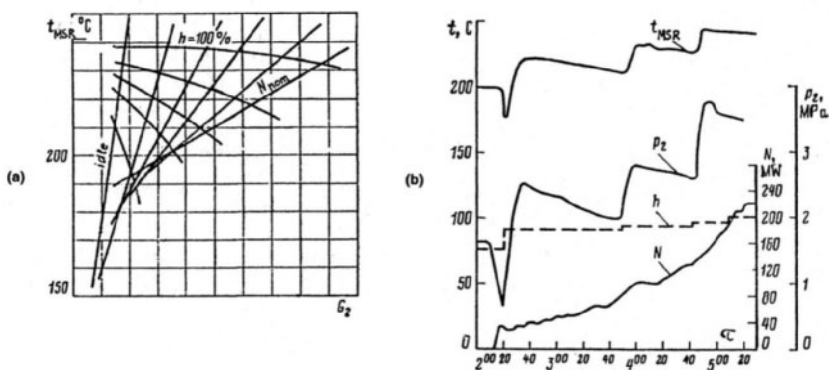


**Fig. 4-54.** Qualitative static characteristics of the reheat steam temperature after the MSR and heating steam flow rate related to the turbine load and heating steam valve position (a) and variation of steam temperature after the MSR for the K-220-44 turbine at start-up (b), according to field start-up test data ( $G_2$ : heating steam flow rate to the MSR's second stage;  $h$ : position of the valve governing heating steam flow rate to MSR;  $p_z$ : steam pressure after the valve)

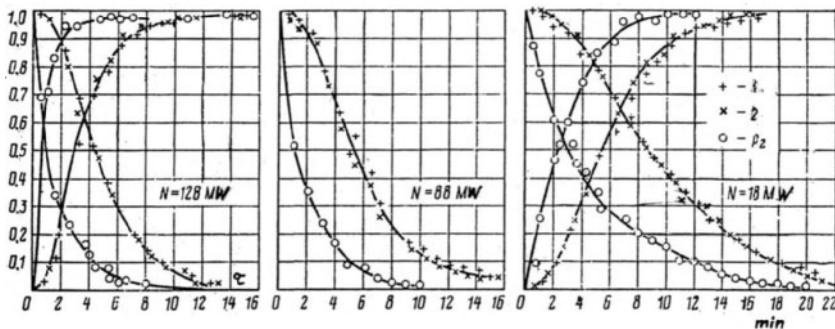


**Fig. 4-55.** Response of reheat steam temperature and heating steam pressure to disturbances by the valve governing the heating steam flow to the MSR of a K-220-44 turbine (1 and 2: steam temperatures after the MSRs on the left and right turbine sides, respectively;  $p_2$ : steam pressure after the valve governing the heating steam flow amount to the MSRs)

In most cases, the initial, prestart temperature state of the turbine rotors can be taken relying on the measured casing metal temperatures, except for the LP cylinders.<sup>147</sup> A relatively simple and original method of obtaining the cooling-down characteristics of the LP rotor was developed and employed in the previously mentioned start-up tests of the K-220-44 turbine at the Kola nuclear power plant.<sup>148</sup> The metal temperatures on the external surface of the LP rotor body at several characteristic sections were measured with special temperature probes at the stopped turbine (Fig. 4-50). The design features of the LP cylinder made it possible to use these probes in only three sections: in the steam admission zone and after the disks of the second and third stages. The probe was developed and manufactured as a long (about 3.5 m, or 11.5 feet) system of steel tubes, 14–40 mm in diameter (0.5–1.6 in). The thin, bottom end of the probe was furnished with a copper measuring head fixed in a fluoroplastic collar. The collar provided the head's electric and thermal insulation from the main probe body. Measuring the rotor temperature was carried out by pressing the head to the rotor surface. To lead the probes to the measurement spots, three radial guide tubes were assembled in the bottom half of the cylinder. At the one end, these tubes were welded to the inner cylinder casing and entered to the level of the

external diameter of the diaphragms. The opposite ends passed out of the outer casing via special glands that, being sufficiently tight, at the same time provided a freedom of thermal expansion for the tubes. The tubes were assembled so that the measuring heads of the probes fitted the smooth cylindrical portion of the rotor surface between the disk fillet and diaphragm gland seal, with regard to the relative thermal displacement of the rotor, and the probes were sunk in the radial grooves made in the diaphragm bodies. In the steam admission zone, the temperature probe reached the rotor surface through a special hole in the casing ring. Preliminarily, before installing at the turbine, the probe design and the procedure of measuring were worked up at a special bench, verifying the sensitivity of the measuring head. Measurements of the rotor surface temperatures were begun immediately after the turbine was shut down and the rotor ran down. Measurements were conducted approximately each hour, with the turning gear switched off for the period of measuring. Each set of measurements took no more than 4–6 min with steam supplied to the end glands and up to 10–12 min when sealing steam was not supplied. The sealing steam temperatures were measured in addition to the measurement set shown in Figure 4-50.

Results of measuring the LP rotor metal temperatures for two turbine outages are shown in Figure 4-56. Steam supply to the end seals during about one hour after closure of the turbine valves hardly affected the metal temperature near the first stages. The high cool-down rate of the rotor is noteworthy. The metal temperature on the rotor surface in the steam admission zone and in the vicinity of the first two stages decreased over 24 hours from 170–210°C to 85–90°C, with the cooling-down rate constant equal to  $0.043 \text{ h}^{-1}$ . (To compare, the cooling-down rate constant for the HP casing was approximately  $0.012 \text{ h}^{-1}$ .) In addition, an irregular nature of the cool-down process that manifests itself in a considerable difference of the cooling-down rate constants for different portions of the rotor is noteworthy.

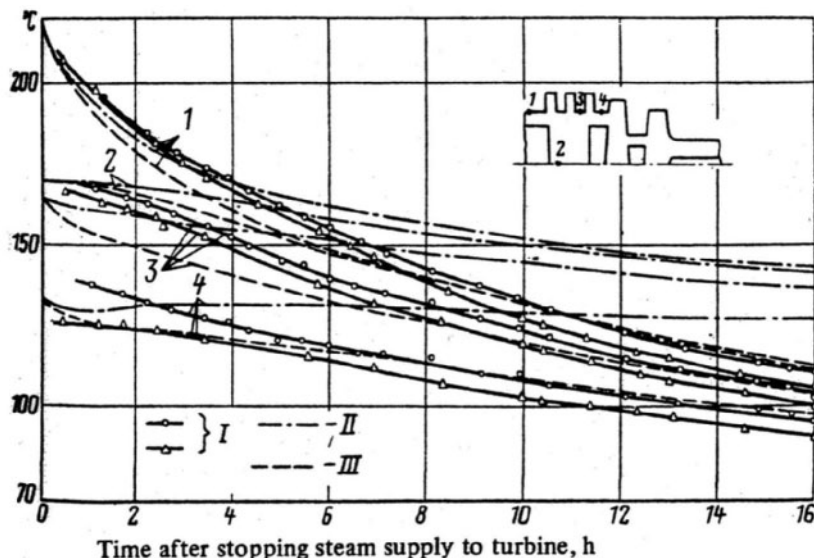


**Fig. 4-56.** Cool-down characteristics of a welded LP rotor for the K-220-44 turbine (numbering of temperature curves [1, 2, 3, 4] follows notations in inset; I: experimental measured data for two outages; II: calculated data with no heat transfer from rotor surfaces within cylinder space; III: calculated data with regard to natural convection within cylinder space)

Source: B. N. Lyudomirskii, A. S. Leyzerovich, and Y. N. Kolomtsev<sup>149</sup>

To analyze the influence of individual factors on the cooling-down process and connect the rotor's surface metal temperatures with the temperature state in the rotor thickness, the cooling-down characteristics of the LP rotor were also calculated with the use of various models. The initial temperature field of the rotor was taken relying on the results of calculations for the stationary operating conditions (Fig. 4-10b). According to many traditional approaches and recommendations, the cooling-down process for LP rotors is mainly due to the heat transfer from the metal to the lubricating oil in the adjacent journal bearings, without any heat transfer from the rotor surfaces within the casing space. However, in this case, the calculation results considerably disagreed with the experimental data, and only an allowance of the natural convection heat transfer from the rotor surface to the wet air within the cylinder space yielded a satisfactory agreement with the experimental data. The intracylinder space is connected to the condenser and steam bleedings, except for the steam admission section shielded by the first stage's casing ring. The heat transfer coefficients for the rotor surfaces were calculated on the basis of well-known criterial

equations for free convection around a ribbed horizontal cylinder. The calculation results confirmed a considerable unevenness in the cooling-down rates for different parts of the rotor during virtually the entire cooling-down process.

The developed approach was later used in a more sophisticated computer program for calculating the cooling-down characteristics of turbine rotors.<sup>150</sup> Results of two such calculations for the aforesaid LP rotor of the K-220-44 turbine and another welded LP rotor of Turboatom's low-speed K-1000-60/1500 turbine (see Fig. 3-16) are shown in Figure 4-57. In the second case, the rotor cools down considerably more slowly because of its greater mass and greater thermal resistance to the axial heat fluxes with thermal conduction toward the journal bearings.

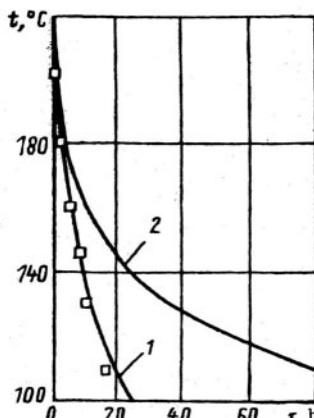


**Fig. 4-57.** Calculated cool-down characteristics of welded LP rotors for K-220-44 (1) and K-1000-60/1500 (2) turbines (first stage disks) (points denote experimental data from the Kola nuclear power plant)

Source: V. M. Kapinos, Y.Y. Matveev, V.N. Pustovalov, and V.A. Palei<sup>151</sup>

The measurements also showed that with a cooling duration of less than 1-2 days, the sealing steam cannot provide prestart warming of the LP rotors, but rather conserves the temperature state attained by the instance of giving the sealing steam to the end glands. Even for cold start-ups, prestart warming by sealing steam does not make it possible to reach rotor metal temperatures greater than the saturation

temperature corresponding to the back pressure in the condenser, and the warming process takes approximately 2-2.5 hours because of the great mass of the rotor.

More than 30 fast-response experimental temperature measurements were installed in the steam path of the LP cylinder at another K-220-44 turbine also operated at the Kola nuclear power plant to investigate the possibility of keeping the turbine rotating without steam, using the generator as a motor.<sup>152</sup> As already said, such so-called *motor operating conditions* can be helpful to decrease the amount of time it takes to restart the power unit after shutting down the reactor for a relatively short term. These conditions are also inherent in the cases of emergency load discharges if the generator is not switched off from the grid. Unfortunately, the obtained results were not processed in full measure to extend them to other turbines and operating conditions. The main result of the experiments was the finding that all of the measured temperatures in the steam path remained much lower than the permissible level (230°C; 446°F), even with the turbine being rotated by the generator up to two hours with the synchronous speed, with all the HP and LP valves closed and steam in the turbine given only to the end seals to keep the back pressure in the condenser at a level of approximately 4.5–5.0 kPa (0.65–0.72 psia). With supplying the turbine with cooling steam passed into the LP crossover pipes, these operating conditions can be maintained for as long as necessary without violating the given limitations.

The main problem of all no-load conditions, that is, operating conditions with small (or relatively small) volumetric steam flow amounts into the condenser, is a possible overheating of the rotating blades, because of energy losses with friction and fanning. The temperature distribution along the height of the 1,200-mm (47-in) titanium LSB used, in particular, in LMZ's high-speed 1,000-MW K-1000-60/3000 wet-steam turbine, in Figure 3-14, under no-load operating conditions is shown in Figure 4-58. Special experimental temperature measurements in the LP steam path at low steam flow conditions were also conducted by LMZ on a 1,200-MW supercritical-steam turbine also furnished with 1,200-mm titanium LSBs.<sup>153</sup>

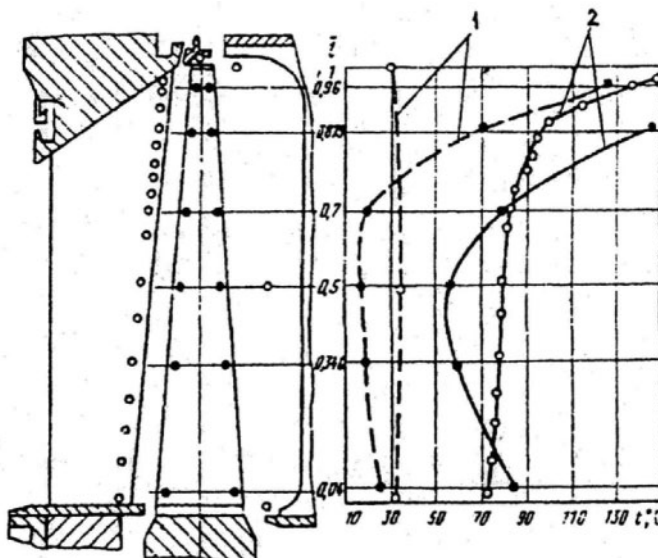


**Fig. 4-58.** Measured temperature distribution along the height of LMZ's 1,200-mm titanium LSB under no-load conditions (white points denote steam temperature measurements; black points denote metal temperature measurements; solid lines: temperatures at or near the leading edge; dashed lines: temperatures at or near the trailing edge)

Source: V.V. Malev and Y.N. Nezhentsev<sup>154</sup>

Along with temperature measurements, in situ investigations of LP steam paths can also include gas dynamic experiments under actual operating conditions, which are good supplements to bench tests on model turbines. The steam flow pattern is studied by means of special combined probes moved transverse to the steam flow over the stage radii (see Figs. 2-27 and 2-37). These probes allow measuring the main parameters of the steam flow with regard to its three-dimensional nature: static and total pressure, stagnation temperature, and so on. These field tests are more expensive, more laborious, and allow less variability in operating conditions than the bench tests, but they provide the possibility to research the influence on actual steam flow patterns of many factors that cannot easily be reproduced in the laboratory.<sup>155</sup>

Field start-up tests often reveal some unexpected factors affecting turbine operation that cannot be foreseen prior to testing. During the start-up tests at the Kola nuclear power plant, for example, the fast-response steam measurements revealed some deep impulse-type decreases in the steam temperature at the HP cylinder entrance in the instants when the control valves were opened quickly—such as when the generator is switched on to the grid and accepts the initial load (Fig. 4-44). As this takes place, any possibility of water induction from the steam generators was excluded. Similar events were also observed at other turbines when the turbine rotation speed or load was sharply increased by opening the control valves. This was regarded as a sign of water induction into the turbine from the main steam-lines, and made the researchers assume the presence of water pools in the steam-lines that remained even with a full steam flow rate through the turbine, as well as when the turbine is stopped. For power units with superheated-steam turbines when they are stopped and cool down, these pools can be revealed by measuring comparatively the metal temperatures in the top and bottom outlying lines of the pipeline. For wet-steam lines, these comparative measurements cannot help, because both the top and bottom metal temperatures are practically equal and close to the steam saturation temperature, whether or not there is water in the bottom of the steam-line.

To prove the presence of such water pools and locate them, the main steam-lines were furnished with special metal temperature measurements (Fig. 4-59a). The pools were located by means of gradually reducing the steam pressure in the plugged steam-lines by opening the drainage valves with the MSGs and with the turbine stop valves closed. While the steam pressure is decreasing and the water pool is evaporating, the metal temperature at the bottom of the steam-line drops sharply, due to heat of vaporization, whereas the top of the steam-line continues to cool slowly. If the reduction of the steam pressure is stopped, the metal temperature at the steam-line bottom gradually levels with the temperature on top. This process continues until the water completely evaporates. To prevent forming such water pools, the steam-line routes were thoroughly checked and leveled to eliminate any sags and to supply necessary inclines toward the drain lines. Implementing these measures to a great degree prevented water induction into the turbines and the resultant erosion damages to the first-stage nozzles.<sup>156</sup>

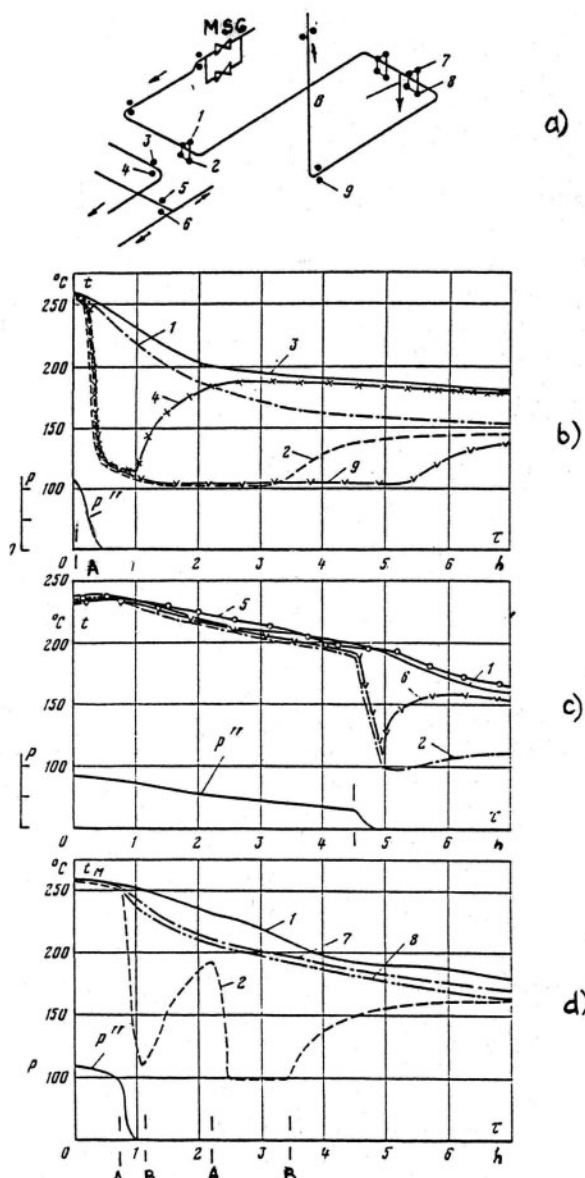


**Fig. 4-59.** Sketch of additional temperature measurements (a) and cool-down diagrams (b-d) for the main steam-lines of the K-220-44 turbine downstream from the main steam gates, according to field start-up tests at the Kola nuclear power plant (temperature curves are denoted according to measurement point numbers on the sketch; A: instants of opening drainage valves of steam lines between the MSG and stop valves; B: instants of closing drainage valves;  $p''$ : steam pressure after the MSG)

Source: V.B. Kirillov, A.S. Leyzerovich, and Y.V. Kolomtsev<sup>157</sup>

## Calculation of temperature fields for main turbine design elements

The stationary and unsteady temperature fields of the main turbine design elements should be known for subsequent calculations of the thermal stresses and for assessing the stress state of the elements with regard to the action of other factors, such as centrifugal forces for rotating elements, inner steam pressure for casings, and so on. These temperature fields can be obtained by means of digital solution of the direct heat conduction problem for the considered “critical” (potentially most thermally-stressed) elements—that is, by calculating the metal temperatures, relying on the known values of the heating steam temperatures and heat transfer conditions. Calculation optimization of the turbine transients can be accomplished by means of a combined solution of the direct and reverse heat conduction problems, where the reverse problem is solved by referring to the heating steam temperature. The problem is to find the value or variation of this temperature under conditions of limits set for the temperature field—for example, keeping a specific temperature difference at the upper allowable level (permanent or variable).

To solve the combined (direct and reverse) heat conduction problem for the critical turbine elements, the mathematical models of these elements should reflect their genuine geometrical forms and boundary heat conditions varying over time and lengthwise of the heated surfaces. For this purpose, it is not necessary to model the design elements upon the whole in all their three-dimensional complexity. It is usually sufficient to confine the model to only a fragment of the entire element in the vicinity of the sections where the leading indices (the temperature differences across the element thickness) occur. The influence of the heat fluxes on the side surfaces of the fragment on the temperature distribution across the thickness of the element should not exceed approximately 10%.<sup>158</sup>

For example, if the critical design element is the casing flange, it is advisable to consider the two-dimensional unsteady-state thermal conduction problem for the horizontal section at the flange mid-height, ignoring the heat flux in the circular direction, between the casing's flange and wall. For long casing chambers (with a chamber length-to-flange width ratio greater than 5–6), it is possible to model the flange area at a single stud bolt pitch, as shown in Figure 4-46b.

On the contrary, if the maximum temperature difference across the flange width occurs in a relatively short or bent chamber with significantly different boundary conditions than in the adjacent chambers, the calculation model should encompass the flange at a length of about three or four bolt pitches on either side of the considered cross section (Fig. 4-45). In any event, it is absolutely necessary to take into account the holes in the flanges, with air gaps between the flanges and stud bolts, as well as outward heat flux on the external flange surface through the thermal insulation. This heat flux can be assessed using the equivalent heat transfer coefficient on the external surface. Although its value depends on the actual thermal insulation quality, it cannot be formally calculated by relying on the insulation material properties listed in reference books. Comparison of calculation results achieved with the use of different calculation meshes (orthogonal, triangular, and mixed) proves that it is more important to model with due accuracy the position and area of the stud bolt holes than their true form (the holes can be represented, for example, by orthogonal or hexagonal wells). Such an approach is justified by comparison of the calculated data with results of direct temperature measurements (Figs. 4-44 through 4-46). These models cannot be accurate if the flange is additionally heated by steam leaking through the split surface of the flange—for example, if the flange loses its tightness. This is the reason for the discrepancy between the calculated and measured temperature differences at the end of the start-up process shown in Figure 4-44.

If the critical design element is a rotor, whether it is a forged or welded rotor of the HP, IP, or LP cylinder, to calculate the optimized start-up diagrams, it is sufficient to consider only a fragment of its longitudinal section in the vicinity of the considered cross section with the highest radial temperature differences. For forged rotors, as applied to turbine transients, especially start-ups, more often than not, it is allowable to use one-dimensional models, in which only the radial temperature distribution in the most thermally stressed cross-section is considered. The radial temperature differences in the most thermally stressed sections as calculated using one- and two-dimensional mathematical models do not significantly differ. The explanation is that, in the most intensely heated zones, the radial heat fluxes from the steam to the rotor surface and from the heated surface into the metal thickness are much greater than the axial heat fluxes into the adjacent less-heated zones. This is especially true for the steam admission zones

of turbine cylinders with central steam admission (as for integrated, double-flow, and loop-flow cylinders). A typical temperature field for a solid double-flow LP rotor of a Siemens high-speed 1,000-MW turbine (see Fig. 3-7) is shown in Figure 4-60. Moving away from the zone of maximum heating steam temperatures to the rotor ends, the lines of equal metal temperatures (isotherms) change from being almost horizontal to rather vertical; that is, the dominant heat fluxes become axial rather than radial. Likewise, for HP rotors in their most thermally stressed sections, the intense heat transfer conditions from wet steam make the radial heat fluxes prevail over the axial ones.

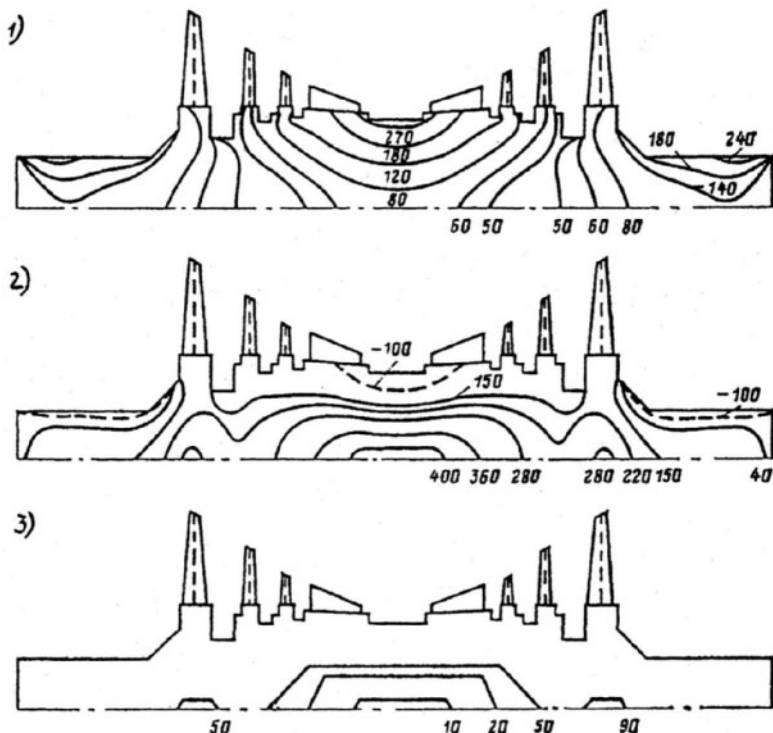


**Fig. 4-60.** Calculated temperature ( $^{\circ}\text{C}$ ) fields (1) and total stress (MPa) fields (2) for the most stressed start-up instant and admissible sizes of possible initial macrodefects (mm) (3) for the solid double-flow LP rotor of a Siemens high-speed 1,000-MW turbine

Source: W. Engelke, J. S. Joyce, D. Lambrecht, et al.<sup>159</sup>

These features of the temperature fields and character of their isotherms are also typical for the most-stressed sections of welded rotors with their more complicated geometrical shape. Temperature fields for the first stages' disks of the welded HP, IP, and LP rotors of wet-steam turbines are shown in Figures 4-8b, 4-10a, and 4-12b. Under stationary operating conditions, the rotor temperature fields become essentially two-dimensional, and often, especially for forged rotors of single-flow cylinders and welded rotors, the axial heat fluxes become more influential than the radial ones (Fig. 4-10b). The same can be said for a combined LP rotor with shrunk-on wheel disks (Fig. 4-61).

These characteristics of temperature fields at different operating conditions are typical for all types of rotors.

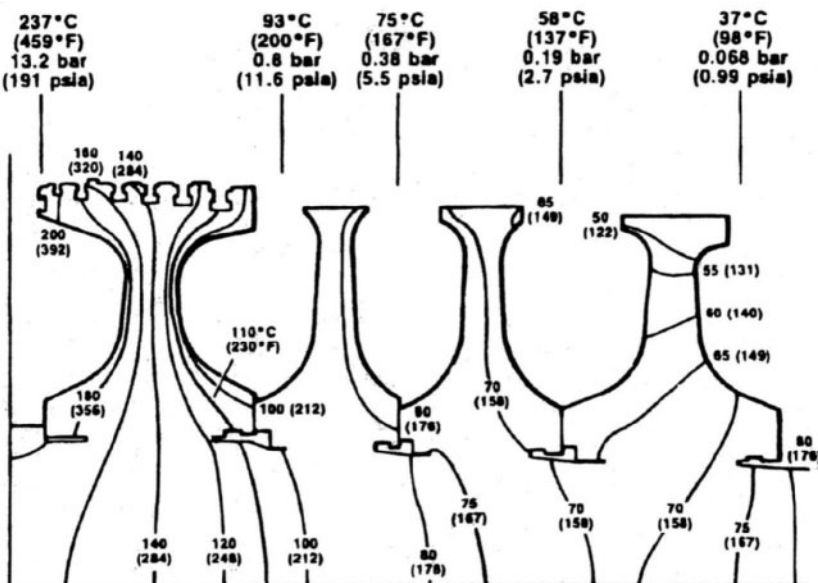


**Fig. 4-61.** Calculated temperature field for a combined LP rotor (right half)  
Source: H. Oeynhausen, G. Roettger, J. Ewald, et al.<sup>160</sup>

While calculating metal temperature fields in welded rotors, it is important to set the proper boundary heat transfer conditions on the surfaces of internal cavities. The medium (air or residual gas left from welding) that is locked within these cavities, being heated at the cavity periphery, is forced out by heavier colder gas and moves toward the rotor axes, where it transfers its heat to the metal of the colder central part of the rotor, thus reducing the radial temperature differences in the rotor. This thermal convection process takes place in a field of artificial gravity under action of centrifugal forces. For high-speed turbine rotors with rotation speed of 3,000 rpm and an outer diameter of the internal cavity of approximately 1 m ( $\approx 40$  in), which is quite typical for such turbines, the centrifugal acceleration at the periphery is more than  $6 \times 10^3$  g. Some preliminary calculations showed that heat transfer with thermal convection in a field of centrifugal forces can significantly influence the dynamics of heating the rotor, and with regard to this effect, the temperature difference along the rotor radius could noticeably decrease, but this phenomenon needs further study.

The solution of the problem of free convection in rotor cavities is seriously hindered by several circumstances: 1) the temperature distribution at the cavity boundaries varies and is itself determined by the heat transfer conditions in the cavity, which makes it necessary to solve a conjugate non-stationary two-dimensional problem of free convection in the cavity coupled with thermal conduction in the adjacent rotor body; 2) the high acceleration of centrifugal forces in the rotor cavities corresponds to the Rayleigh number ( $Ra$ ) values beyond the range for which experimental and theoretical investigations have ever been conducted, and 3) the acceleration of centrifugal forces changes significantly over the cavity height.

The considered problem was subjected to thorough analysis using specially developed mathematical models of a hollow thick-walled cylinder heated from the outside.<sup>161</sup> In the cylinder's internal cavity, free convection occurs, characterized by the Rayleigh number varying from 0 to  $10^{10}$ . Some results of this investigation are presented in Figures 4-62 and 4-63. The calculations showed that if the Rayleigh number characterizing free convection within the rotor cavity does not exceed  $10^{10}$ , the influence of the effect can be neglected, and the heat fluxes on the cavity surfaces can be taken as zero. At the same time, estimates showed that if the free convection within the rotor

cavity is artificially intensified (for example, by means of filling the cavity with a special gas or compressed air), it can result in significant decreases of the radial temperature differences and thermal stresses in the rotor.

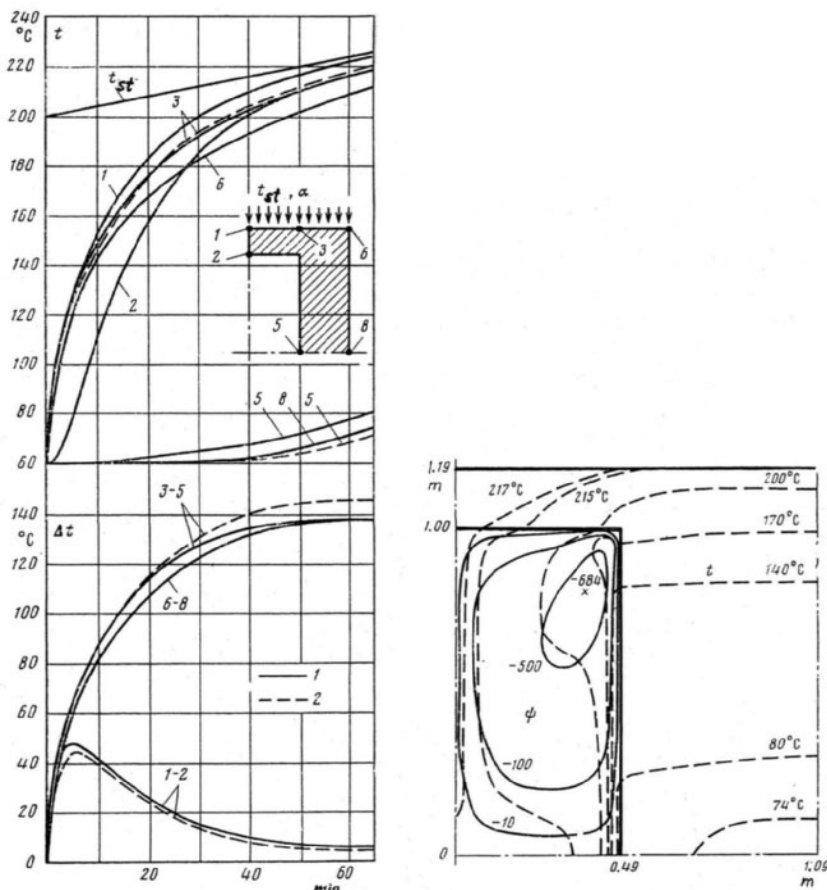


**Fig. 4-62.** Results of mathematical modeling of heating for a hollow thick-walled cylinder with and without free convection within the internal cavity and traced free convection stream lines within the cavity and isotherms for the rotor body at the end of heating (numbering of temperature curves is based on notations on sketch; 1:  $Ra = 10^{10}$ , 2:  $Ra = 0$ )

Source: V.A. Brailovskaya, V.R. Kogan, A.S. Leyzerovich, and V.A. Polezhaev<sup>162</sup>

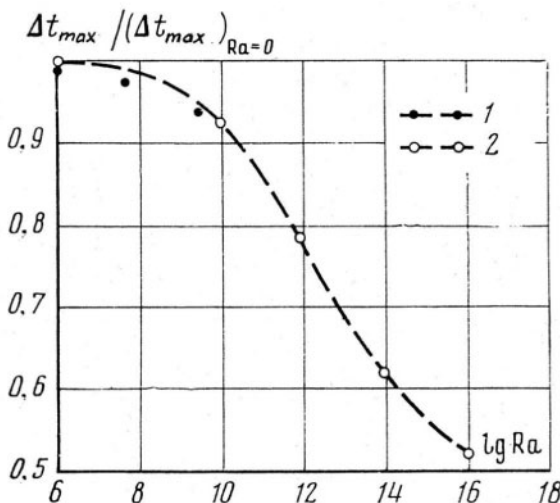


Fig. 4-63. Influence of free convection within the internal cavity of a welded rotor on its heating for a process modeling cold start-up (1: results of calculations using special mathematical model (see Fig. 4-62); 2: results of calculations using approximate engineering methodology)

Source: V.A. Brailovskaya, V.R. Kogan, A.S. Leyzerovich, and V.A. Polezhaev<sup>163</sup>

### Calculated optimization of start-up diagrams

Optimization of the turbine transients is regarded as a problem of minimizing their duration with unconditional observance of limitations caused by reliability requirements. To solve this problem, it is necessary to coin the term *leading indications* of the turbine's temperature and thermal stress state. Generally, the leading indications of the turbine state are those that limit (actually or potentially) the rate of transients in such a way that variation of these indications is determined only by the main external controlling actions, or in other words, varying the main operating parameters: the steam flow amount through the turbine (its load) and the main and reheat steam temperatures.<sup>164</sup> For modern, large, superheated-steam turbines, the leading indications are generally the temperature differences in the most-stressed (critical) turbine elements, which more often than not are the HP and IP rotors and HP stop-valve steam-chests. Depending on the turbine design, output, and steam conditions and the unit's start-up system features, certain other indications can also play such a role (for example, RRE or temperature differences across the flange width of the high-temperature cylinders).

Eventually, the problem of optimizing is formulated as searching for the diagrams of changing the turbine's operating parameters in such a way that the turbine's leading indications are maintained at their top admissible levels without exceeding them over the entire course of a transient. In this case, the duration of the transient is supposed to be minimal. However, if there are more than one leading indication and more than one controlling actions, this definition of the problem is not absolutely correct, and it is necessary to use supplementary conditions to obtain a single-valued solution.

During the first stage, it is expedient to consider the problem of the optimal heating for individual turbine elements, taking the temperature differences across their thickness as the leading indications and the change of the heating steam temperatures for these elements as controlling actions. This problem can be solved using solutions for unsteady-state heat conduction with the special boundary heat conditions on the heated surface, that is, with the surface metal temperature changing in such a way that the aforesaid temperature difference across the thickness of the element is maintained at the upper admissible level, which can be generally set as a function of the current metal temperature. Then, the known heat transfer conditions make it possible to move on from the surface metal temperature to the heating steam temperature. This can be done by means of the combined digital solution for the direct and reverse problems of unsteady heat conduction for the considered elements. In so doing, the reverse problem is solved in reference to the heating steam temperature. The solution of the direct problem gives the change in the temperature fields for the considered elements. This in turn makes it possible to solve the reverse problem with regard to the heating steam temperature. Both the direct and reverse problems can be solved for several potentially critical elements simultaneously.

The current upper admissible value of the heating steam temperature for each element can be calculated as follows:

$$[t_{sl}] = t_m + [\Delta \tilde{t}] \times \left( 1 + \frac{\lambda}{\alpha} \times \left. \frac{\partial t}{\partial x} \right|_{x=0} \right) = t_m + [\Delta \tilde{t}] \times \left( 1 + \frac{\Phi}{B\tilde{t}} \right), \quad (4.4)$$

where  $\Delta \tilde{t} = t_s - t_m$ , and  $t_s$  and  $t_m$  are the metal temperatures of the considered element on the heated surface and at a characteristic

point at distance  $\tilde{H}$  from the heated surface. This point can be fixed (for example, on the external insulated surface or at the rotor axis) or sliding (if it refers to the average integral temperature). In this case, the Biot number,  $\tilde{Bi}$ , is also calculated for  $\tilde{H}$ . In this equation,  $\Phi$  is the dimensionless temperature gradient on the heated surface. Generally speaking, all of the values in Equation 4.4 are variable quantities. For nonstationary processes,  $\Phi$  is also variable. However, if the process is close to optimal and heat removal from the insulated surface is much smaller than the heat flux from steam to metal, it is expedient to take  $\Phi$  as a constant. This assumption assures a stable solution even in the case of outside disturbances of the process.

The value of the dimensionless temperature gradient,  $\Phi$ , for simple-shaped elements under conditions of quasi-stationary heating can be found analytically. For a hollow cylinder with a radius ratio typical for forged rotors, the value of  $\Phi$ , in reference to the admissible effective temperature difference,  $[\bar{\Delta}t]$ , is approximately 1.17. For more complex cases, this value can be calculated digitally. For the HP flanges of wet-steam turbines, this value in reference to the entire temperature difference,  $\Delta t$ , across the flange width is approximately 1.2.

Even after finding the optimal change of the heating steam temperature for every critical design element, the problem of optimizing turbine transients cannot be considered solved. First, it is necessary to calculate the changes of the turbine operating parameters—the controlling actions influencing the heating steam temperatures for different elements. In addition, two or more leading indications of the turbine state can be influenced by different controlling actions to different extents. As this takes place, the change of some indications that are influenced by the same external actions can feature in their dynamics, and the change of one indication can simultaneously depend on different actions. Finally, it is necessary to take into account the existence of technological limitations in changing turbine operating parameters. These limitations can concern their absolute values, the rate of variations, and functional interrelations.

Actual transients under manual control run with almost inevitable occasional deviations from the optimized schedules. These deviations are caused by external disturbances and operator errors. Thus, the schedule must be optimized with regard to these potential deviations.

The simplest way is to decrease the upper admissible value of the leading indications by the value of the expected deviations of the heating steam temperature. However, in fact, in order to optimize the process, it is desirable to take into account the influence of the current Biot number for the considered turbine elements on dynamics of heating them, the frequency spectrum for the expected disturbances, as well as other factors.

The optimal diagrams of the transients are usually calculated using special computer programs, and their algorithms must involve all of the previously mentioned circumstances. The greater the number of interrelated controlling actions, the more complex the set problem and its solution. In the case of start-ups for superheated-steam turbines of fossil fuel units under variable steam conditions, at least four independent main controlling actions occur. They are (1) the changes in the steam flow amount through the turbine, (2) the main steam temperatures, (3) the reheat steam temperatures, and (4) the position of the turbine's control valves, even without considering the control of bypass valves.<sup>165</sup> By contrast, wet-steam turbines of nuclear power units are started-up under constant main steam conditions and have only two main external controlling actions: the changes in the steam flow amount through the turbine and the steam temperature after the MSR. Because of invariable steam parameters in the start-up process of wet-steam turbines, the heating of the HP sections practically depends solely on the steam flow amount through the turbine, that is, the turbine load,  $N$ . The steam temperature downstream from the MSR,  $t_{\text{MSR}}$ , can be governed during start-ups by means of changing the heating main-steam flow to the MSR. Thus, the changes in both of the main operating parameters ( $N$  and  $t_{\text{MSR}}$ ) can be optimized separately in accordance with variations of their "own" leading indications. The loading diagram is formed according to the temperature state of the HP cylinder, and under this condition, the diagram for raising  $t_{\text{MSR}}$  is dictated by the temperature state of the cylinder located downstream from the MSR with regard to the change of its boundary heat conditions due to loading. For wet steam in the HP cylinder, the surface metal temperature for the critical elements can be considered practically equal to the heating-steam temperature, that is, in Equation 4.4,  $\text{Bi} \rightarrow \infty$ , and  $\Phi/\text{Bi} \approx 0$ .

The transition from optimizing the heating steam temperature diagrams,  $\theta(\tau)$ , to the loading diagram,  $N(\tau)$ , is carried out through the static

dependencies between these steam temperatures and the turbine load. If the loading rate can be limited by two (or more) different leading indications for the HP cylinder, the admissible values of the heating steam temperature and load are defined for each element with inserting technological limitations for the absolute value of the current load and the rate of its change. The final admissible value is the minimum of the two (or more). The heating steam temperature values for each element are defined from the found load value, and these steam temperature values are used to calculate the temperature fields of the considered elements for the next moment in time. The static dependence,  $N(\theta)$ , and the reverse dependence,  $\theta(N)$ , are assigned based on design calculations or data of measurements at an actual turbine in service.

Depending on the turbine design features, the critical elements of the HP cylinder that determine the flexibility of a wet-steam turbine can be the rotor or the outer casing flange. The radial temperature difference in the rotor is limited by the value  $[\Delta t_r]$  from the standpoint of low-cycle (thermal) fatigue of the rotor steel, and the admissible value of the temperature difference across the flange width,  $[\Delta t_{fl}]$ , is determined by the yield strength of the casing steel. The most-stressed sections of the rotor and flanges are swept with steam of different temperatures. Under the nominal load, these temperatures are  $t_{st}^{(r)}$  and  $t_{st}^{(fl)}$ , whereas the initial metal temperatures of the rotor and flange (before the turbine is started-up) are assumed to be equal:  $t_{in}^{(r)} = t_{in}^{(fl)}$ . The flange of the HP cylinder can be eliminated as a critical element if its width,  $H$ , is smaller than the critical value, given as:

$$H = \Delta R \times \sqrt{\frac{(t_{st}^{(r)} - t_{in}^{(r)}) \times k_r}{(t_{st}^{(fl)} - t_{in}^{(fl)}) \times k_{fl}}} \times \frac{[\Delta t_{fl}] \times a_{fl}}{[\Delta t_r] \times a_r}, \quad (4.5)$$

where  $\Delta R$  is the thickness of the HP rotor in the most-stressed section;  $a_r$  and  $a_{fl}$  are the temperature conduction of steel for the rotor and flange, respectively; and  $k_r$  and  $k_{fl}$  are the shape influence factors, equal to the ratio of the temperature difference,  $\Delta t$ , for the considered element to the temperature difference in a plate of the same thickness under quasi-stationary heating. This expression was applied to various types of wet-steam turbines. For turbines with a typical correlation of the flange sizes,  $k_{fl}$  varies in the range from 1.2 to 1.5. This value takes into consideration flange holes with an air gap between the flange and bolt, as well as a heat flux on the external flange surface outward through the thermal insulation. For forged rotors,  $k_r$  is approximately 0.55–0.60.

As applied to a series of Soviet wet-steam turbines for nuclear power plants, the calculation results showed that the HP flange should be treated as the only critical element for such wet-steam turbine types as the K-220-44 (see Fig. 3-6) with the forged HP rotor and the K-500-60/1500 (see Fig. 3-18) and K-1000-60/1500 (see Figs. 3-13 and 3-16), with their welded drum-type, thin-walled HP rotors. For other turbine types (for example, the K-500-65/3000, with the welded disk-type HP rotor, or the K-750-65/3000 and K-1000-60/3000, with the forged HP rotors), both the rotor and flange could be considered as critical elements, alternating for different types of transients or their different stages (Fig. 4-14). In addition, a large factor is the quality of the HP casing's thermal insulation. This quality can be characterized by the value of the temperature difference across the flange width under stationary operating conditions, and it significantly influences the values of allowable changes to the turbine load without rate limitations.

The critical elements for the cylinders downstream from the MSR are usually welded or forged LP rotors. Sometimes, however, if the turbine has a separate IP section (like some wet-steam turbines of ALSTOM, Siemens, and Turboatom), its rotor or casing flanges can become the critical elements. The heat transfer coefficients from superheated steam after the MSR to the metal of these elements (IP casing flanges, IP or LP rotors) are relatively low and vary appreciably with an increase in the steam flow through the turbine (Fig. 4-47b). Under these conditions, in order to heat these elements more efficiently, it is reasonable to raise the steam temperature after the MSR to the nominal level, while the turbine is rolling-up and idling and the heat transfer coefficients are quite low, then decrease this temperature when the generator is switched on to the grid and accept an initial load (with a significant increase in the heat transfer conditions in the cylinder), and, finally, gradually raise the steam temperature again to the nominal value during loading. This nonmonotonous steam temperature diagram is accomplished relatively easily, because the steam temperature after the MSR,  $t_{MSR}$ , decreases with an increase in the heated steam flow rate if the valve governing the heating-steam flow is partially opened (Fig. 4-54).

The diagrams for raising the steam temperature after the MSR are also optimized on the basis of Equation 4.4. In doing so, the diagrams of turbine rolling-up and loading determine the change in the

Biot number for the critical element(s). Results of such optimization as applied to a cold start-up of Turboatom's K-500-60/1500 turbine with an integrated HP-IP cylinder are presented in Figure 4-15. The diagrams for both loading and raising the steam temperature after the MSR are determined by the temperature differences in the outer casing of the HP-IP cylinder.

Another example of the diagram for the steam temperature after the MSR being close to optimal at actual start-up under automated control as applied to the K-220-44 turbine can be seen in Figure 4-80. In this case, the diagram is conditioned by the thermal stresses in the welded LP rotors.

It becomes more difficult to optimize the diagrams for raising the steam temperature after the MSR if the individual capacity of the turbine is 1,000 MW or more. In this case, the long LSBs are intensively heated under no-load conditions and do not permit an increase in the steam temperature before the LP cylinder. On the other hand, large LP rotors of large turbines are heated with greater inertia and have no time to be heated effectively while the turbine is rolling-up, even if the heating-steam temperature were raised as much as possible. This can be seen, for example, with LMZ's K-1000-60/3000 turbine (Fig. 4-64). The radial temperature difference in the LP rotors reaches its maximum value in 60–75 minutes after the steam temperature increase. This is commensurable with the length of the entire start-up time. For the original design version of this turbine with welded LP rotors, it was necessary either to slow down the loading process at warm start-ups because of the thermal stress in the LP rotors or to allow accepting the nominal load while  $t_{MSR}$  was far below the nominal value. Transition to forged, solid LP rotors without a central bore removed this problem, because the metal of these rotors permits greater thermal stresses (see Fig. 3-14).

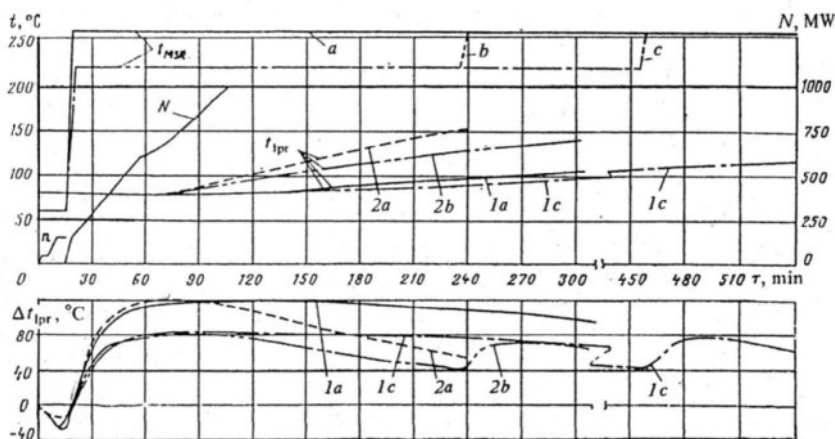


**Fig. 4-64.** Calculation of heating for welded (1) and solid (2) LP rotors of LMZ's K-1000-60/3000 turbine at warm start-ups ( $t_{LPR}$ : LP rotor metal temperature at the axis in the section through the second-stage diaphragm seal;  $\Delta t_{LPR}$ : entire temperature difference along the LP rotor radius in the same section)

Source: A. S. Leyzerovich, B. L. Levchenko, and V. B. Kirillov<sup>166</sup>

The described methodology was verified during field tests for different types of wet-steam turbines (Fig. 4-44). Results of start-up optimization for different turbines are presented in Figures 4-12 through 4-15. For some of them, the start-up rate is limited by the temperature differences across the HP casing flange width (Figs. 4-13 and 4-15); for others, the critical element is the HP rotor (Fig. 4-12); and sometimes, as with LMZ's high-speed 1,000-MW turbine, the critical elements are alternately either the HP rotor or the outer casing flange. The diagram for raising  $t_{MSR}$  can also be dictated by the heating of either the IP casing flanges or the LP or IP rotor(s).

The optimized start-up diagrams for different initial temperature conditions should be generalized and unified in their structure (Figs. 4-12, 4-13, and 4-65). This is important for constructing both start-up instructions for manual control and start-up programs for automated control.

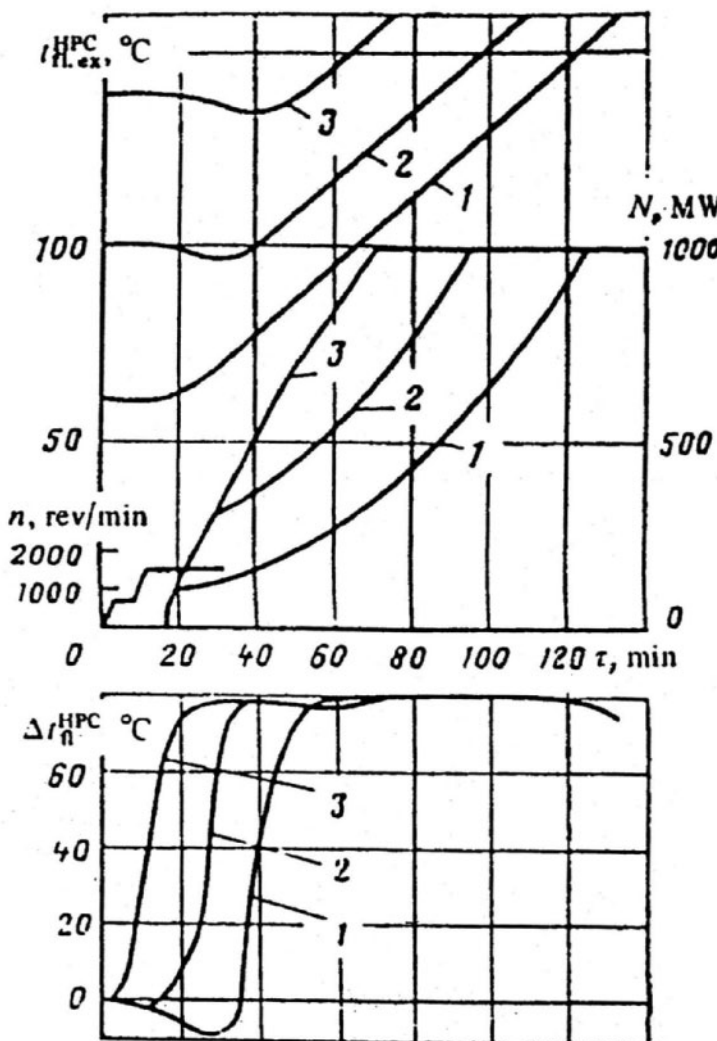


**Fig. 4-65.** Optimized calculated schedules of hot (1), warm (2), and cold (3) start-ups for Turboatom's K-1000-60/1500 turbine ( $t_{fl,HPC}$ : metal temperature on the external HP flange surface;  $\Delta t_{fl,HPC}$ : temperature difference along the flange width in the HP steam admission zone)

Source: A. S. Leyzerovich, V.B. Kirillov, V.A. Paley, and V.L. Yasnogorodsky<sup>167</sup>

For the no-load operating conditions of wet-steam turbines, the heated steam temperatures for the critical elements of the HP cylinder do not differ substantially from the initial metal temperatures, except for the very hot start-ups after the turbine trips with a load discharge,

when the turbines have no time to cool down. As a result, no undesirable temperature differences and thermal stresses can be expected in the HP cylinder elements while the turbine is running up. Raising the turbine rotation speed can be done in the way that will be most comfortable for the operator, and the running-up diagrams can be unified for the turbine start-ups from almost all the initial temperature conditions. This way, the running up diagrams can be reduced to four discrete operations: 1) rolling up the turbine from the turning gear to a certain intermediate rotation speed, 2) holding at this level while listening to the turbine, 3) raising the rotation speed to the synchronous level, and 4) holding at the synchronous (or subsynchronous) speed until the generator is ready to synchronize and accept the initial load. The rate of raising the rotation speed can be maintained constant in the entire range of the rotation speed changes and independent of the start-up type. The amount of time the turbine is held at the intermediate rotation speed level should not depend on the turbine temperature state, except for hot start-ups, when it is desirable to omit any delay before the turbine is brought up to the synchronous speed and the generator is switched on to the grid.

For cold start-ups, there is little point in slowing down the running up process to heat the IP or LP rotors at the intermediate rotation speed—it is too ineffective because of low heat transfer conditions. It is more reasonable to heat the rotors by steam passed to the end gland seals before the start-up begins. However, this process takes a significant amount of time and goes only up to the saturation temperature; that is why this prestart heating is advisable to conduct with a decreased vacuum in the condenser. Some calculated curves for prestart heating of welded LP rotors with an external body diameter of approximately 1,200 mm (47 in) are shown in Figure 4-66 (the metal temperature shown in the diagram refers to the rotor axis). These rotors are standard for Turboatom's high-speed wet-steam turbines with individual capacities of 220, 500, and 750 MW. The cool-down characteristic of such a rotor is presented in Figure 4-56. For other rotors, the time taken for heating varies as the square of the rotor diameter.

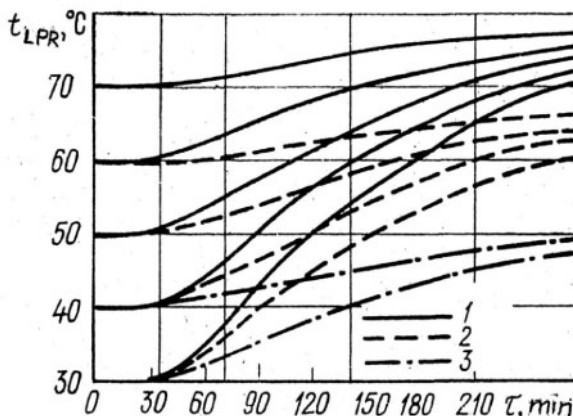


**Fig. 4-66.** Calculated temperature curves for prestart heating of standard welded LP rotors of Turboatom high-speed wet-steam turbines with different initial temperature conditions and vacuum in the condenser (1: for vacuum of 400 mm Hg [7.7 psi]; 2: 540 mm Hg [10.4]; 3: 650 mm Hg [12.5 psi])

The loading diagrams for start-ups from different initial conditions can also be subjected to unification. Optimizing the loading process allows developers to present it consisting of two parts: 1) the initial loading, with the maximum rate, up to a level depending on the initial temperature state of the HP cylinder and 2) subsequent loading, with the rate determined by the current load value. Examples of these dependencies for Turboatom's K-220-44 turbines with nozzle-group and throttle control are presented in Figure 4-67. The same approach can also be used for other wet-steam turbines if their loading rate is determined by the only indication of the HP section's temperature state (the temperature difference across the flange width or along the rotor radius). Loading diagrams constructed with this approach and laid in the basis of instructive start-up diagrams for the most characteristic initial temperature conditions of Turboatom's low-speed 1,000-MW turbines are shown in Figure 4-65.<sup>168</sup> If the loading rate can be alternately limited by two or more indications (for example, the temperature difference across the flange width and along the rotor radius), the start-up diagrams take somewhat more complicated, individual forms (Fig. 4-14).

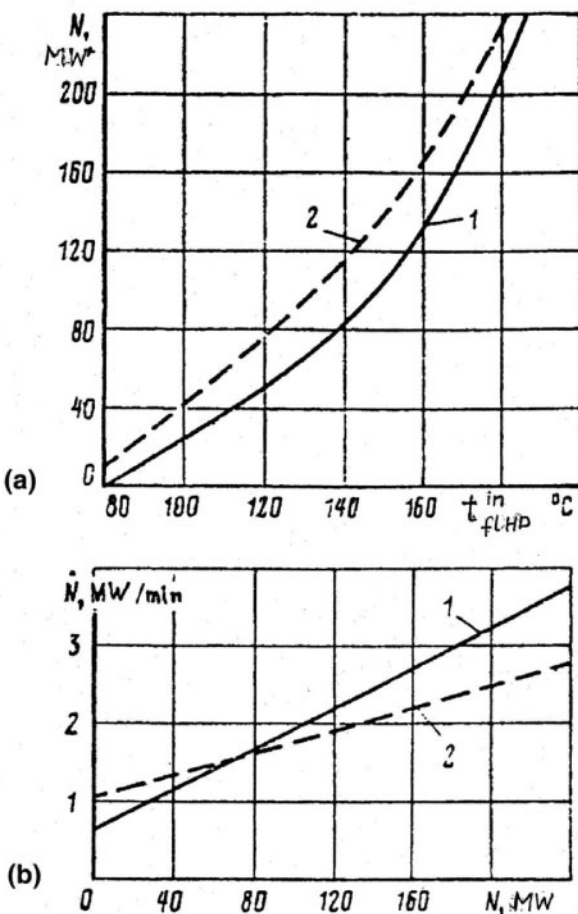


**Fig. 4-67.** Dependencies of the upper level of initial loading with the maximum rate on the initial temperature state (a) and the rate of further loading on the current load (b) for Turboatom's K-220-44 turbines with nozzle group (1) and throttle (2) control ( $t_{fHP}^{in}$ : initial metal temperature of the HP casing flange)

Optimal control of the reheat steam temperature after the MSR for most wet-steam turbines during start-ups begins with opening the valve(s) on the steam lines feeding the steam reheater with heating steam up to an intermediate position while the turbine is rolling-up and until reaching the synchronous rotation speed (for turbines with two-stage steam reheaters, this refers to steam passed to the second stage; the steam-lines to the first stages should be completely open from the beginning). This makes the reheat steam temperature rise to near the rated value. Accepting the initial load after switching on

the generator causes some decrease in the reheat steam temperature. While loading the turbine, the heating steam valve(s) should be gradually opened all the way. The resultant diagrams for the reheat steam temperature can be seen in Figures 4-15 and 4-80. Specific recommendations depend on the turbine design features (a danger of overheating the LSBs under no-load conditions, the presence or absence of an IP section, the LP rotor type, and so on).

For wet-steam turbines with combined LP rotors (with shrunk-on wheel disks), if the steam temperature at the LP cylinder entrance (after the MSR) is not controlled, a rapid increase in the metal temperature of the disks and the resultant high tensile thermal stress on the disk bore surfaces can unshrink the disks, and this factor alone can limit the rate of raising the reheat steam temperature after the MSR. If the maximum load achievable under the partial reheat steam temperature is limited, any delays in raising this temperature can hamper the loading process.

Optimizing the start-up loading diagrams for wet-steam turbines is based on two assumptions: 1) the presence of a single-valued dependence of the heating steam temperature for the critical HP elements on the turbine load and 2) diminutive, negligible differences between the metal temperatures on the heated surfaces and the heating steam temperatures (the saturation temperature for wet steam). The same principles are applicable to finding the range of admissible load changes without limitations to their rate when the turbine operates under load. The original temperature conditions determining these opportunities are characterized by the value of  $t_m$  in Equation 4.4. For wet-steam turbines with bulky welded or forged HP rotors, these changes are limited by the thermal stress state of these rotors, and the characteristic metal temperature is the average integral rotor temperature in the most thermally stressed section (Fig. 4-11).

The admissible load change ranges for the Turboatom K-1000-60/1500 turbine are shown in Figure 4-68. For this turbine, the leading indication is the temperature difference across the HP outer casing flange width. Under the original load,  $N$ , the characteristic metal temperature on the external flange surface,  $t_m$ , depends on the initial (stationary) value of this temperature difference. Therefore, the limitations on the turbine load changes are different depending on whether

[Previous Page](#)356 *Wet-Steam Turbines for Nuclear Power Plants*

they are to increase or decrease the turbine load. This difference also depends on the thermal insulation quality of the HP flange: the better this insulation, the less the initial (stationary) temperature difference across the flange width and the less the difference between the admissible load changes for loading and unloading.

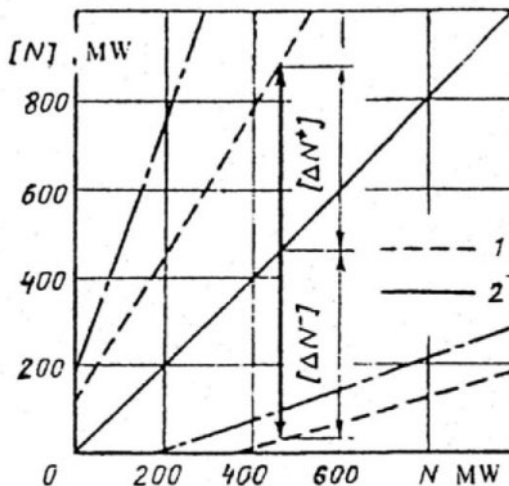


**Fig. 4-68.** Range of admissible load changes for the Turboatom K-1000-60/1500 turbine with various qualities of thermal insulation of the HP casing (1: steady-state temperature difference across the HP casing flange width equal to 40 °C; 2: steady-state temperature difference across the HP casing flange width equal to 20 °C)

Source: V.B. Kirillov and A. S. Leyzerovich<sup>169</sup>

## Information Support for Operators and Automated Control During Turbine Transients

Control and instrumentation (C&I) systems for nuclear power plants should support the operational personnel in observing the state of equipment. These systems should provide the operator with proficient, timely, and comprehensive information about equipment condition during stationary and transient operating conditions, as well as well-grounded assistance in alarming or ambiguous situations,

relying on the properly processed measured data. In modern practice, these objectives are mainly attained with the help of highly computerized data acquisition and control systems (DACS). An example of such a relatively up-to-date system is a digital complex called the Nuclear Power Plant Control Complex with Advanced Man-Machine Interface 90 (NUCAMP-90), developed by Hitachi in the mid-1990s and adopted for nuclear power units with ABWR-type reactors. In particular, this complex is implemented at Japanese Kashiwazaki-Kariwa Unit 7 with the rated output of 1,356 MW.<sup>170</sup> The complex includes a main control panel that comprises an intensively arranged set of principal operation and observation devices and a wide display panel that provides the main bulk of information on the entire power unit, so as to make the man-machine interface obvious, comfortable, and practical (Fig. 4-69). The display panel contains 226 fixed mimic displays, 231 hard switches, and 170 annunciators arranged so as to make the current status of the power unit comprehensible at a glance. The number of operation devices on the operator console of the main control panel is minimized and concentrated so that they can be easily observed from a sitting position. This was done by incorporating touch-screen operation, positioning flat displays (FDs) and color cathode ray tubes (CRTs) for easy observation, and expanding the scope of automatic control. As a whole, the main control panel has 465 CRTs and 153 FDs available for playback, and includes 325 hard switches, 15 FD push buttons, and 235 CRT annunciators. The operator load is reduced to a large extent owing to automatic power control, particularly at start-ups, shutdowns, and other transients, including program and logic control of the turbine and its auxiliaries, such as motor- and turbine-driven feed water pumps, and so on. The diagram of starting up the unit under automated control is shown in Figure 4-5.

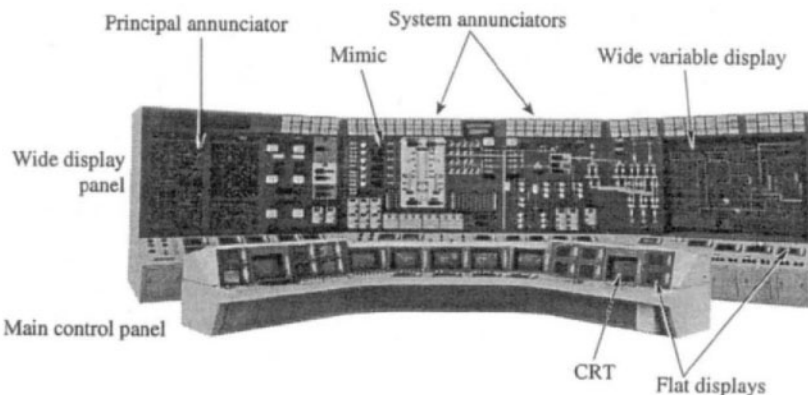


**Fig. 4-69.** Main control board of NUCAMM-90 for the 1,356-MW Kashiwazaki-Kariwa Unit 7

Source: F. Mizuki, Y. Miyamoto, and T. Seiji<sup>171</sup>

The continuing progress in information technology has opened the way for further development of supervisory and control systems, in particular, to extend their capabilities.<sup>172</sup> The core of these systems has become supervisory operation via CRT terminals. Owing to multi-window displays, main parameters can be displayed and operations are performed without interrupting the monitoring process. Because the majority of technological operations are performed automatically (using sequential, or logic, control), the operator can focus his or her attention on continuous monitoring and control. For a clearer understanding of the unit's equipment conditions, the operator can use numerous diagrams, charts, and trend graphs that show the current and forecasted (to a degree) operational status of the monitored objects. An example of a multi-window screen of a supervisory and control system for nuclear power plants is shown in Figure 4-70.

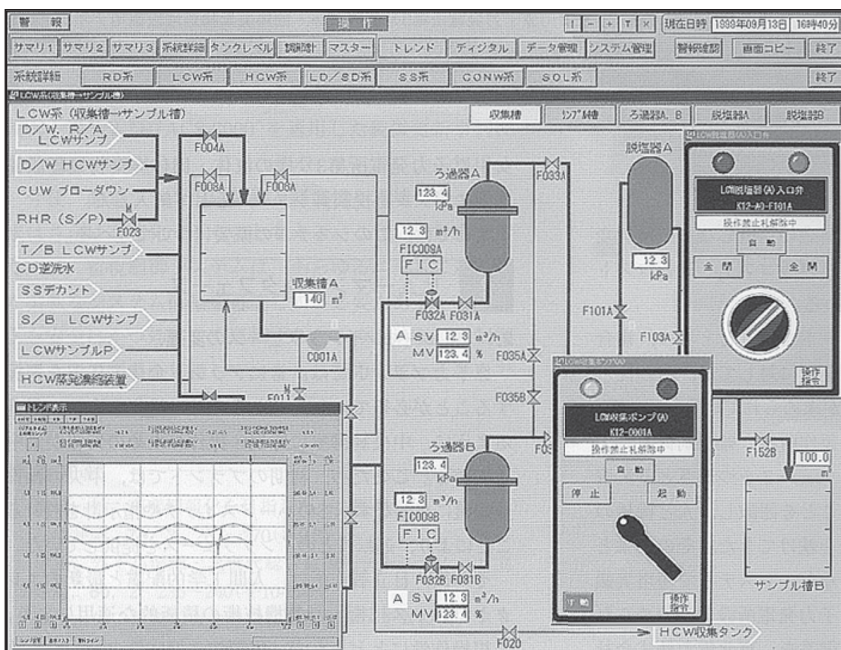


**Fig. 4-70.** Multiwindow CRT operation display of Hitachi's supervisory and control system for nuclear power plants

Source: T.Yamamori, T.Ichikawa, S.Kawaguchi, and H.Honma<sup>173</sup>

Along with this, data acquisition and control systems for many older nuclear power plants were designed based almost entirely on analog or electromechanical C&I techniques that have now almost exhausted their lifetime, becoming less reliable, requiring more maintenance, and looking rather obsolete and ineffective compared with modern systems. For these reasons, the owners of some nuclear power plants are striving to upgrade their surveillance and control systems. For example, the analog C&I system at the Ignalina nuclear power plant in Lithuania, with two RBMK-1500 power units, is being replaced by one of the largest digital-control systems to be applied to a nuclear power plant anywhere in the world; the renovation involves the entire data acquisition and presentation system.<sup>174</sup> Similar projects are also under way at other nuclear power plants.<sup>175</sup>

New, up-to-date C&I techniques provide many possibilities for better information support of the operational personnel and advanced automated control, in particular as applied to steam turbines. At the

same time, even relatively out-of-date (from the standpoint of today) C&I means used at older nuclear power plants provide possibilities of significantly better information support.

In parallel with the aim of providing the operator with more detailed and complete information, there is the problem of presenting this information in more compact and obvious forms. An abundance of information on the control board and supervisory terminals can frequently overwhelm and irritate an operator. As a rule of thumb, any irrelevant, excessive information on the control board is detrimental to the operation quality and should be considered harmful, because it diverts the operator's attention. Because of surplus flows of information on the control panel, in many cases the operator never uses most of the data presentation options, relying instead on just a few of the most informative and convenient windows with relatively limited informative capabilities. As a result, along with an abundance of information, the operator is often short of some specific data and timely relevant advice. This information should be presented to the operator preprocessed and in the most capacious and representative graphic forms. For example, as applied to possible needs of varying the current turbine load, the operator, instead of tracing the current values of the dispersed set of parameters and indications—such as turbine output, metal temperatures, and temperature differences with nothing that relates them to each other—would prefer to see combined images where all of these data would be presented with their interrelations and allowable change ranges.<sup>176</sup>

For wet-steam turbines with a single leading indication of temperature conditions limiting the load change rate, this problem can be solved by presenting both the load and the leading indication to be monitored in the form of an  $N-t_m$  diagram, where  $t_m$  is the characteristic metal temperature of the critical element. The leading indication, by definition, is the temperature difference across the thickness of the critical element and can be seen in the same diagram. An example of such an  $N-t_m$  diagram is given in Figure 4-71 as applied to Turboatom's K-220-44 turbine. In this case, the characteristic metal temperature is that on the external surface of the HP casing flange,  $t_{fl,ext}$ , in the section of the greatest temperature difference, and the leading indication is the temperature difference across the flange width in this section,  $\Delta t_{fl}$  (Figs. 4-13 and 4-45). The diagram is supplied with lines of constant temperature differences ( $\Delta t_{fl}$ -isolines). Because the metal temperature on the heated

surface can be considered equal to the saturation temperature, which in turn is treated as unequivocally dependent on the steam flow amount through the turbine (see Fig. 4-48), the actual value of the temperature difference across the flange width at any given instant is defined by the current correlation of the measured coordinate values  $N$  and  $t_{fl,ext}$  in the isoline field. The vertical distance from this point to the isoline of the upper admissible temperature difference gives the range of the permissible load step change. During transients, the optimal loading should be led in such a way that the trajectory of the condition point in the given coordinates would move along the upper admissible isoline, just as in the case of the automated start-up shown in Figure 4-71c. During the entire process of loading (except the beginning stage and with forced suspensions), the temperature difference across the flange width was held at the set admissible level of  $80^{\circ}\text{C}$  ( $144^{\circ}\text{F}$ ).

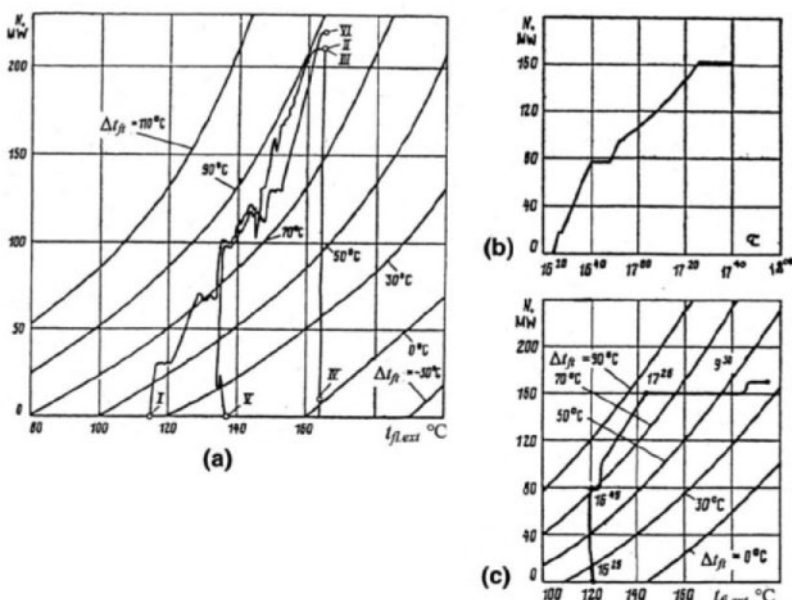


**Fig. 4-71.** Two-coordinate loading diagram for Turboatom's K-220-44 turbine and its application to start-ups at the Kola nuclear plant (a: daily loading diagram with two start-ups [I: 3:40 A.M.—generator is switched on to grid after two-day outage; II: 5:30 A.M.—turbine reaches the final load of 210 MW; III: 11:40 A.M.—turbine unloading begins; IV: 12:00 P.M.—generator is switched off; V: 9:07 P.M.—generator is repeatedly switched on to the grid; VI: 10:45 P.M.—turbine reaches the final load of 220 MW]; b: loading diagram of automated start-up after two-day outage; c:  $N$ - $t$  diagram of the same automated start-up after two-day outage)

Such diagrams were first implemented at the Kola nuclear power plant using special two-coordinate analogous recorders. Similar diagrams for the K-500-60/1500 and K-1000-60/1500 turbines at the Novovoronezh and Zaporozhe nuclear power plants were later presented on CRT displays of the computerized DACSs.

If the critical design element of the turbine is its HP rotor and the leading indication of the turbine's thermal stress state is the effective radial temperature difference (between the heated surface and the integral average metal temperatures in the most stressed section), this temperature difference should be monitored by means of mathematical modeling of heating the rotor. For the purpose of operational monitoring, a one-dimensional calculation model provides sufficient accuracy (as well as in the case with temperature monitoring for the HP and IP rotors for steam turbines of fossil fuel power plants), which makes it possible to rely on minimum input measurements.<sup>177</sup> Because the metal temperature variations for wet-steam turbines are quite limited, in this case, the mathematical model can be linearized—that is, the thermal conduction of the rotor steel is taken as invariable. Due to the high heat transfer conditions from wet steam, the heated surface temperature can be considered equal to the saturation temperature; but if the turbine is shut down, the HP rotor temperature is close to the measured metal temperature of the HP casing near the steam admission zone. All of these suppositions significantly simplify the problem of modeling as compared to that for rotors of superheated-steam turbines.

For forged or welded HP rotors without a central bore and for a unit-step function, that is, for the boundary conditions of  $t_s = t(R, \tau) = 1$  and  $t(r, 0) = 0$ , the average integral metal temperature variation over time can be described by the following expression:

$$\bar{t}(\tau) = 1 - \sum_{n=1}^{\infty} B_n \times \exp(-\mu_n^2 Fo), \quad (4.6)$$

where  $Fo = (\alpha \tau / R^2)$  is the Fourier number, and  $\mu_n$  ( $n = 1, 2, 3, \dots$ ) are the roots of the characteristic equation for the simple geometric form modeling the rotor (for forged, welded, or monoblock rotors without a central bore, the characteristic equation is  $J_0(\mu) = 0$ , and  $B_n = 4/\mu_n^2$ ). With an increase of  $n$ , the values of  $\mu_n$  rise rapidly and monotonously,

and the values of  $B_n$  tend toward zero, thus for some numbers  $n > m$ , the value of  $B_n$  can be considered equal to zero, and Equation 4.6 becomes:

$$\bar{t}(\tau) \approx 1 - \sum_{n=1}^m B_n [1 - \exp(-\mu_n^2 F_0)] + \left( 1 - \sum_{n=1}^m B_n \right) \quad (4.7)$$

Equation 4.7 with  $m = 3$  corresponds to the functional chart of the device for the temperature monitoring of an HP rotor for wet-steam turbines shown in Figure 4-72. The device's outputs correspond to the average integral metal temperature,  $\bar{t}$ , and the effective radial temperature difference,  $\Delta\bar{t} = t_s - \bar{t}$ , in proportion to the thermal stress on the heated surface in the considered section. In the same way, though with somewhat less accuracy for the same  $m$ , it is possible to derive the metal temperature at the rotor axes,  $t_0$ , and the full temperature difference across the rotor radius,  $\Delta t = t_s - t_0$ .<sup>178</sup>

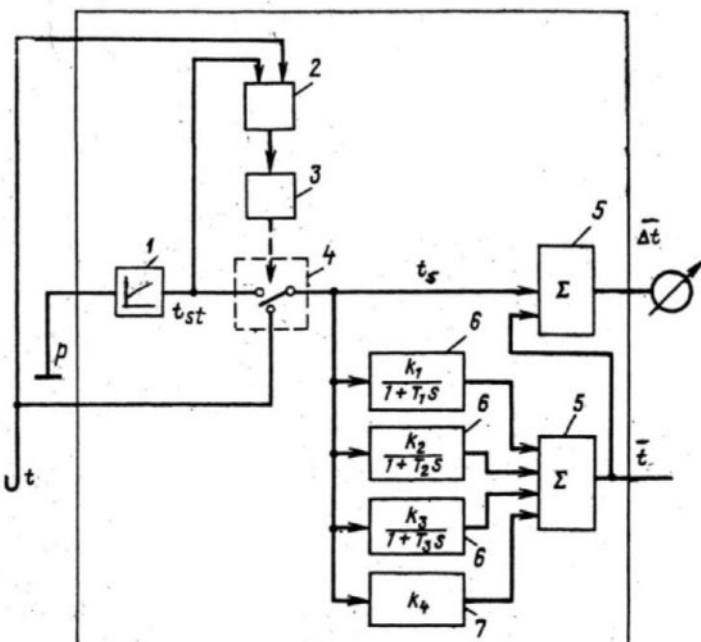


**Fig. 4-72.** Functional chart of a device for temperature monitoring of the HP rotor for wet-steam turbines (1: nonlinear transducer; 2: logic element; 3: switchboard; 4: switch; 5: summators; 6: aperiodic elements; 7: amplifier)

For a welded disk-type HP rotor, Figure 4-73 compares the changes in the metal temperatures and temperature differences along the rotor radius calculated using different mathematical models: 1) a "precise" two-dimensional model, taking into consideration the axial temperature fluxes in the rotor metal (Fig. 4-12b); 2) a "precise" one-dimensional model, and 3) an approximate, simplified model, corresponding to the block chart of Figure 4-72 and used as the basis for the temperature monitoring device. The main source of inaccuracy lies in neglecting the two-dimensionality of the rotor temperature field, whereas the simplification of the one-dimensional model (rejecting the row terms with  $n > 3$  in Equation 4.6, that is, transition to the form of Equation 4.7) does not affect the final result as much. The total modeling errors do not exceed 5–8°C, and that seems quite acceptable.

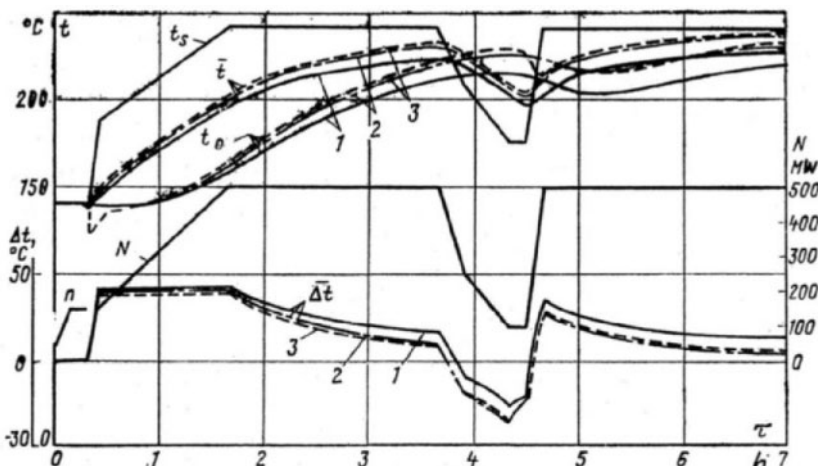


**Fig. 4-73.** Calculation of heating-up the HP rotor of a K-500-65/3000 turbine during start-up and subsequent load change using different mathematical models (1: precise two-dimensional model; 2: precise one-dimensional model; 3: approximate one-dimensional model simulating the device for temperature monitoring of the rotor)

A similar functional chart was also developed for the welded and monoblock LP rotors of wet-steam turbines without an IP section.<sup>179</sup> The model in Figure 4-74 is closer to those developed for the HP and IP rotors of large superheated-steam turbines for fossil fuel power plants and takes into consideration the variation over time of the heat transfer conditions from steam to the rotor surface, depending on the steam flow rate through the turbine. In this case, the heat flow from

steam to the heated surface is determined as the difference between the heated steam and surface temperatures multiplied by the Biot number. In turn, the Biot number,  $Bi$ , is taken as a nonlinear function of the steam pressure at the cylinder inlet; this dependence is calculated using known dimensionless, criterial equations. Relying on results of experimental investigations, as shown in Figure 4-52, the heating steam temperature for the most thermally stressed section of the rotor is determined in reference to the measured reheat steam temperature after the MSR at the cylinder inlet, with some correction taken as a nonlinear function of the measured steam pressure at the cylinder inlet. The average integral metal temperature of the rotor section is determined by integrating the heat flow from the heated surface with the time constant,  $T_0 = R^2/2a$  (where  $R$  is the external radius of the rotor body, and  $a$  is the thermal conduction of the metal). The metal temperatures on the heated surface and the rotation axis are calculated by summing the outputs of the aperiodic elements with the time constant,  $T_n = R^2/(a \times \mu_n^2)$ , where  $\mu_n$  are the roots of the characteristic equation  $J_1(\mu) = 0$ . As applied to the scheme of Figure 4-74,  $m$  is taken equal to 2. For the external surface ( $\rho = r/R = 1$ ) and the rotor axis ( $\rho = r/R = 0$ ), the influence factors for the aperiodic elements are calculated as follows:

$$k_n = 2 \times J_0(\mu_n \rho) / [\mu_n^2 \times J_0(\mu_n)]$$

Unlike the HP and IP rotors, the initial, prestart metal temperature of the LP rotor cannot be set by measuring the metal temperature of the casing. So, when the turbine is shut down, the decrease of the average integral metal temperature of the rotor is assumed to follow an exponential curve, and the cooling time constant,  $T_c$ , is established on the basis of experiments or calculations based on experimental data (Figs. 4-56 and 4-57).

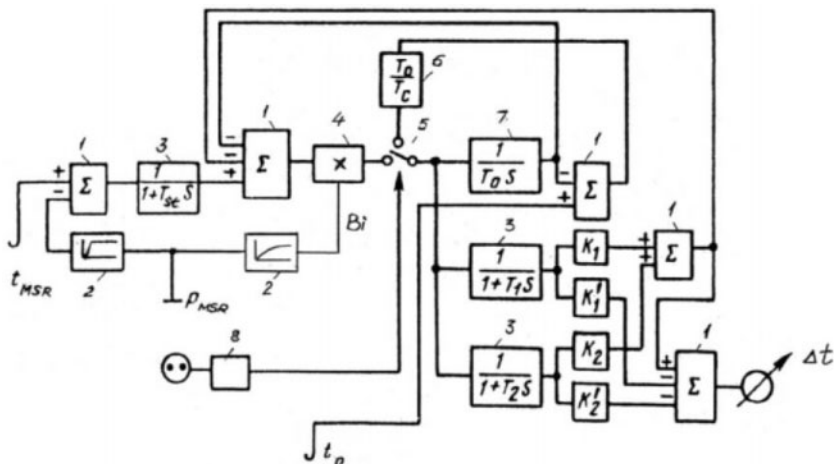


**Fig. 4-74.** Functional chart of a device for temperature monitoring of LP rotors for wet-steam turbines (1: summators; 2: nonlinear transducers; 3: aperiodic elements; 4: multiplier; 5: switch; 6: amplifier; 7: integrator; 8: switchboard;  $t_{MSR}$ : steam temperature after MSR;  $p_{MSR}$ : steam pressure after MSR;  $\Delta t$ : complete temperature differences along the rotor radius)

If the turbine's most thermally stressed element is the HP rotor and the turbine is furnished with a device for the temperature monitoring of the rotor (or if the turbine's critical element is the HP casing flange and the metal temperature on the external flange surface in the most stressed section can be reliably measured), the operator can be continuously provided with the data of the current upper and lower boundaries for admissible load changes. This can be done using Equation 4.4 and the characteristic metal temperature,  $t_m$ , which is set equal to either the calculated (modeled) average integral metal temperature of the HP rotor or the measured metal temperature on the insulated external surface of the casing flange—depending on the turbine design. For some turbines, the admissible load boundaries should be determined with regard to the current temperature state of both the HP rotor and flange.

The described devices for the temperature monitoring of the HP and LP rotors and determining the admissible load change boundaries were consecutively developed as applied to the use of different kinds of computational techniques, such as analogous devices, microprocessor-based programmable controllers, special microprocessors built into the turbine's electrohydraulic governing system, computers of the power unit's DACS, and PCs specially built

into DACSs. In particular, these devices were included as part of the regular automated control and surveillance complexes delivered by Turboatom with various modifications of their K-750-65/3000 and K-1000-60/1500 turbines, as well as built into projects of DACSs for newly designed nuclear power units with K-500-65/3000 turbines.<sup>180</sup> Emulations of automated start-ups and load changes for such a turbine are shown in Figures 4-11 and 4-12, and the diagram of an actual start-up of this turbine at the Chernobyl power plant with experimental samples of such devices is shown in Figure 4-75.

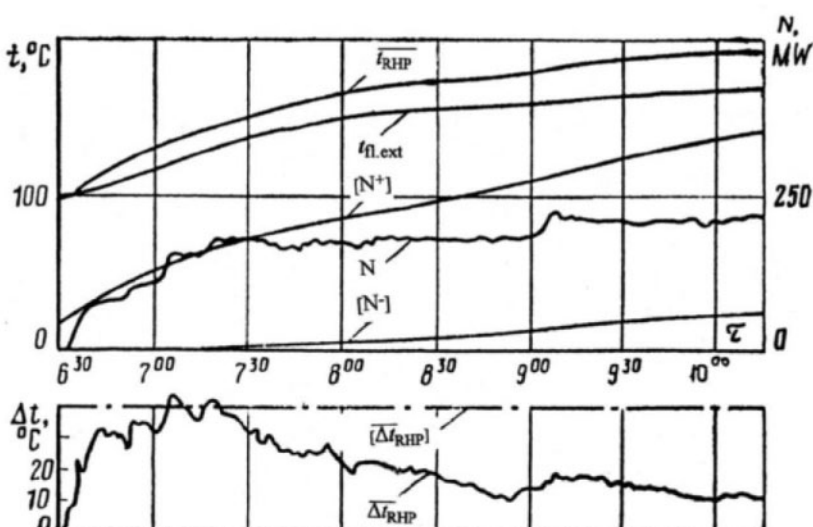


**Fig. 4-75.** Cold start-up of Turboatom's K-500-65/3000 turbine at the Chernobyl nuclear power plant with current admissible load boundaries based on the HP rotor's monitored thermal stress state as presented to the operator

The devices shown in Figures 4-72 and 4-74 were constructed using mathematical models based on the method of approximate transfer functions. With the use of different kinds of computational techniques, other approximate mathematical models can be more convenient—for example, based on the definite difference method, which has been successfully used in many developments.

Automated control of transients, predominantly start-ups, promotes more reliable power plant operation. One of the world's first automated devices and systems of this kind for wet-steam turbines was a start-up automaton developed for Turboatom's K-220-44 turbine

and put into commercial operation at the Kola nuclear power plant as early as in the mid-1970s.<sup>181</sup> Its control desk is shown in Figure 4-76. Presently, it looks rather archaic, with its multitude of indicators, switches, buttons, and signal lamps, because now all of their functions are performed with greater effectiveness and ergonomic comfort based on modern computer technologies. Nevertheless, the technology essence of this automaton remains quite valid.

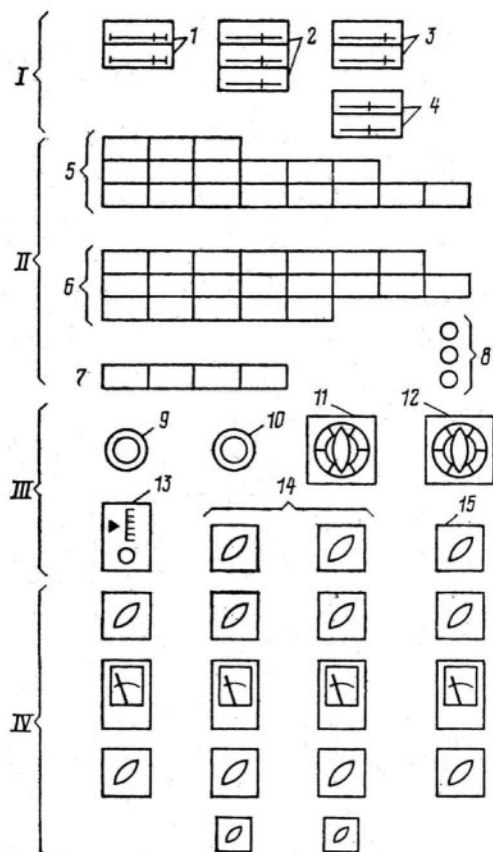


**Fig. 4-76.** Control desk of the start-up automaton for the K-220-44 turbine at the Kola nuclear power plant (I: indicators for current actual and set values of controlled parameters: 1: steam pressure downstream of MSG (at the stage of prestart heating); 2: steam temperature downstream of MSR; 3: rotation speed (at the stage of running up); 4: load (at the stage of loading); II: signal panels and lamps: 5: causes of deviations from the normal technological course (stage by stage); 6: accomplishment of start-up operations (stage by stage);

7: general signals for all stages (accomplishment of the stage, suspension of accomplishment, return to the previous stage, switching all the control actions off); 8: readiness to execute the set stage; III: devices controlled by the operator: 9: permission button to begin the executing stage; 10: permission button to repeat the stage operation after return to the previous stage; 11: multi-position switch of the mode which the automaton functions; 12: multi-position switch of the start-up stage; 13: set point device for the final load value; 14: input of information about accomplishment of preliminary manual operations; 15: input of permission to raise the rotation speed up to the synchronous rate (listening to the turbine is finished); IV: remote control devices, including start-up governors and position indicators for governing valves)

*Source:* A. S. Leyzerovich, A. D. Melamed, V. B. Kirillov, et al.<sup>182</sup>

The entire start-up process under automated control is divided into three steps: 1) the prestart heating of the main steam lines and HP valve steam-chests (for power units without a main steam gate between the reactor's steam-generator and the turbine's stop valves, this stage is omitted), 2) running-up to the subsynchronous rotation speed, and 3) loading to the rated or set final output. The automaton (or any other automated start-up system) should comprise special program governors and logical controllers influencing the turbine's discrete position objects, including the start-up governors. Of importance are the collaboration between the operator and the automated devices and friendly human-machine interface. The operator should be able to trace the course of the automated operations, and the entire progression of operations should be tied to the actions accomplished by the operator.

The automaton's running-up programs were unified for all types of start-ups (Fig. 4-77). When the generator was switched on to the grid and the loading governor was brought into operation, the turbine load was initially raised at the maximum admissible rate up to the primary load level, and then increased according to the set program (Fig. 4-78). Two types of loading programs were tested and then used in different projects: 1) a program derived from Equation 4.4, based on tracing the current value of the monitored metal temperature on the HP casing flange's external surface and 2) a "program-in-time" of loading the turbine at the rate changed depending on the current load value (Fig. 4-67b).

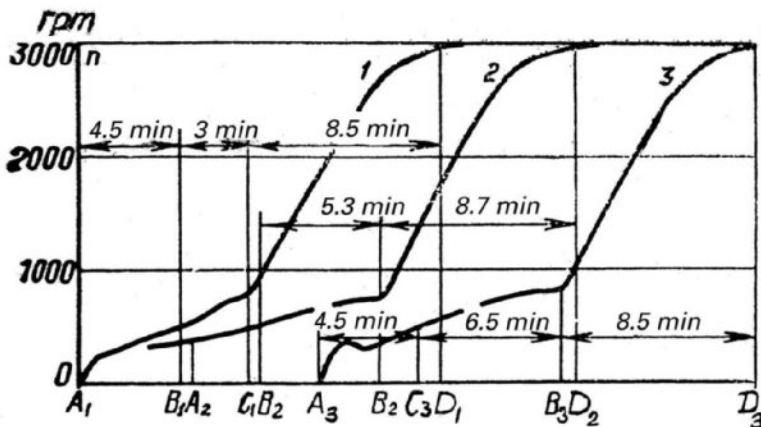


**Fig. 4-77.** Experimental automated running-up of the turbine for various start-ups (1: cold start-up with vacuum of 710 mm Hg [13.7 psi]; 2: hot restart just after rolling-down; 3: hot start-up with vacuum of 600 mm Hg [11.6 psi]; A: beginning of opening HP control valves and passing heating steam to MSR; B: signal to the operator to listen to the turbine; C: permission of the operator for further increase of the rotation speed; D: reaching a subsynchronous rotation speed, signal to prepare the generator to be synchronized and switched on to the grid)

Source: A. S. Leyzerovich, A. D. Melamed, V. B. Kirillov, et al.<sup>183</sup>

The loading program-in-time is presented in the form of a linear dependence for the rate of increasing the set on its current value:

$$\dot{N}_{set} = \frac{\partial N_{set}}{\partial \tau} = \frac{\partial N_{set}}{\partial p} \times \frac{\partial p}{\partial t_s} \times [\dot{t}_m] \approx a + bN_{set}, \quad (4.8)$$

where  $\dot{t}_m$  is the rate of heating up the critical element necessary to keep its leading indication at the upper admissible level (for wet-steam turbines, it is possible to neglect the influence of the metal temperature on the metal temperature conduction and take  $\dot{t}_m = \text{const}$ );  $\partial p / \partial t_s$  is the dependence between the steam pressure and saturation temperature, which can be regarded as a linear function of pressure with an error less than 5–10% in the pressure range from 1.2 to 6.5 MPa (175–950 psi), and  $\partial N / \partial p \approx \text{const}$  is the proportional coefficient between the turbine load and heating steam pressure for the critical element. The initial load value,  $t_{set}^{in}$ , that can be reached with an unlimited, maximum admissible rate is set according to the initial metal temperature of the critical element,  $t_m^{in}$ . The dependencies  $N_{set}(N_{set})$  and  $N_{set}^{in}(t_m^{in})$  for K-220-44 turbines are presented in Figure 4-67.

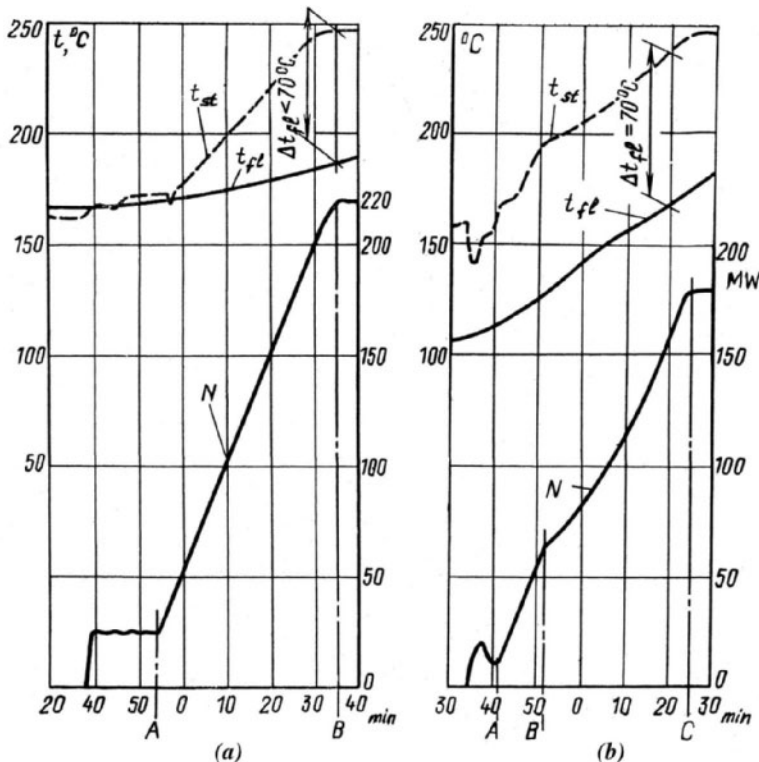


**Fig. 4-78.** Experimental automated loading of the turbine at hot (a) and warm (b) start-ups (A: switching on the loading governor; B: finish of the initial loading stage at the maximum rate; C: reaching the set final load level;  $t_{st}$ : steam temperature in the HP steam admission chamber,  $t_{ft}$ : metal temperature on the HP casing flange's external surface)

Source: A. S. Leyzerovich, A. D. Melamed, V. B. Kirillov, et al.<sup>184</sup>

The ordinary loading programs-in-time have a principal disadvantage: if execution of such a program is interrupted or suspended, the controlled process thereafter differs from the optimal one in principle. This is especially typical for loading wet-steam turbines at start-ups, when the loading process is often suspended by regular operations with the reactor. If the turbine load is kept constant, the heating steam temperatures within the turbine do not vary, and the value of the leading indication (the temperature difference in the critical element) decreases almost exponentially with the time constant  $T$ . After the loading process is resumed, it is possible to increase the load at the maximum admissible rate within the load range, the value of which depends on the duration,  $\Delta\tau$ , of the previous suspension:

$$\Delta N = A(N) \times [1 - \exp(-\Delta\tau/T)], \quad (4.9)$$

where  $A(N)$  is the admissible step-like load change after holding the load at a constant level for an uncertainly long amount of time.

A principle block-chart of the automated device for loading wet-steam turbines during start-up is shown in Figure 4-79. The set on the turbine load, measured by the sensor (11), is worked out by the governor (2) influencing the turbine control valves (1).The set for the governor is formed by the integrator (3), which is connected through the switch (5) to pulsers (either 6 or 7) of the program and maximum upper admissible rates of loading, respectively. At the beginning stage of the loading process, until the turbine output reaches the initial value corresponding to the prestart metal temperature measured by the sensor (10), the rate of loading is set to the maximum. As soon as the turbine load reaches this value, obtained at the outlet of the nonlinear transducer (9), the logical device (8) switches over the programmer (6) to the inlet of the integrator (3), instead of the other pulser (7). This programming device (6) is provided with positive feedback from the outlet of the integrator (3).

This system also comprises another logical device (16) influencing the switch (4) between the integrator and its pulsers. It may be done by the operator or a logical control device of a higher range (for example, if loading the reactor is suspended). In this case, the switch (14) is closed, and the dynamic converter (15) begins forming the value  $\Delta N$  depending on the time length of the suspension,  $\Delta\tau$ , according to Equation 4.9. When the process of loading is resumed, the switch (4) is closed, the switch (14) is opened, and the third logical device (12), influencing the switch (5), provides loading at the maximum rate allowable within the value of  $\Delta N$ .Then the turbine is again loaded with the program rate formed by the pulser (6).

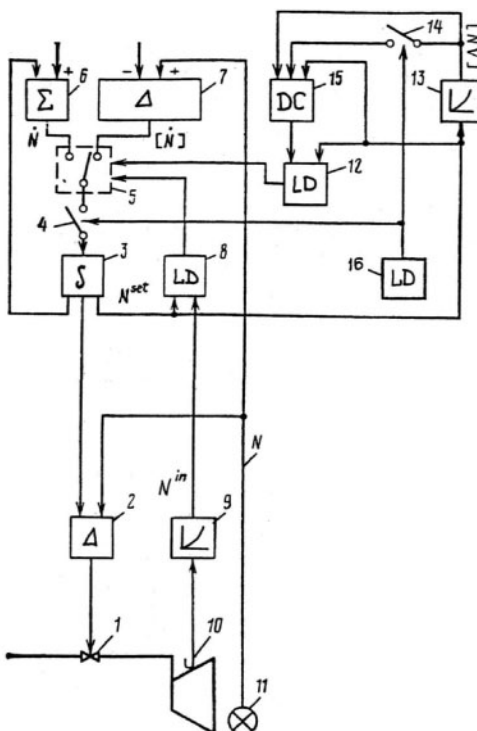


**Fig. 4-79.** Principle block-chart of automated device for loading a wet-steam turbine during start-ups (1: turbine control valve(s); 2: executing governor; 3: integrating set-point device for executing governor; 4, 5, 14: switches; 6, 7: pulsers (as programmers); 8, 12, 16: logic devices; 9, 13: nonlinear transducers; 10: metal temperature sensor; 11: turbine load sensor; 15: dynamic converter)

Both of these types of programs were later used for start-up automation of other wet-steam turbines. A diagram of one of regular automated turbine start-ups at the Kola nuclear power plant is shown in Figure 4-80. The leading indication for the turbine (the temperature difference across the HP flange width) is kept close to the upper admissible level, approximately 80°C, and the reheat steam temperature after the MSR is raised in a manner providing close to optimal heating of the LP rotors. The loading process for another regular automated start-up is shown in Figure 4-71.

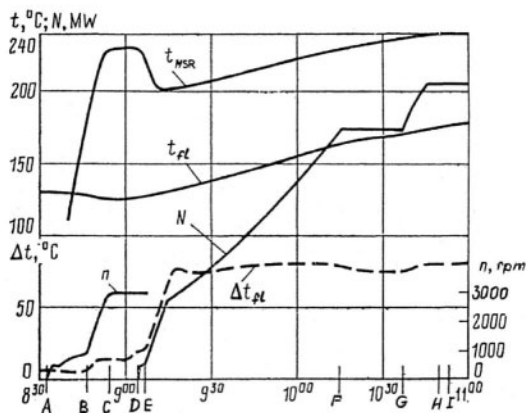


**Fig. 4-80.** Automated start-up of a K-220-44 turbine at the Kola power plant (A: the operator switches on the start-up automaton, and steam enters the turbine; B: the operator confirms completion of listening to the turbine, and the turbine rotation speed begins increase to the synchronous value, with the program governor for the reheat steam temperature switched on automatically; C: the turbine reaches 3,000 rpm, and the operator takes over control for synchronizing and switching on the generator; D: the operator switches the generator on, and the turbine accepts an initial load; E: the operator permits further loading; F-G: the operator suspends loading to switch on the HP feed water heaters; G: the operator increases the set final load value; H: the final load value is reached; I: the automated start-up is completed, and the operator switches off the automaton)

Source: A. S. Leyzerovich, A. S., A. D. Melamed, V. B. Kirillov, et al.<sup>185</sup>

## References

- 1 Schwieger, B., M. Leonard, S. Taylor, et al. 2002. First annual top plants survey. *Power* 46 (4): 27-70.
- 2 2002. Operating results with nuclear power plants in 2001 (in German). *VGB PowerTech* 82 (5): 27-67.
- 3 2003. "Operating results with nuclear power plants in 2002" (in German). *VGB PowerTech* 83 (5): 37-73.
- 4 Schwieger, First annual top plants survey. 27-70.
- 5 2000. Operating results with nuclear power plants in 1999. *VGB PowerTech* 80 (5): 17-53.
- 6 2001. Operating results with nuclear power plants in 2000 (in German). *VGB PowerTech* 81 (5): 29-66.
- 7 Sekine, Y. 1993. Nuclear power generation in Japan—Present status and future prospects. *Proceedings of the Institute of Mechanical Engineers* 207 (A4): 233-246.
- 8 Proselkov, V. N., and V. D. Simonov. 1989. Technical problems associated with participation of nuclear power plants in governing load of power systems (in Russian). *Energokhozyajstvo za Rubezhom* 3: 11-15.
- 9 Kirillov, V. B., and A. S. Leyzerovich. 1985. Flexibility characteristics of wet-steam turbines of nuclear power stations. *Thermal Engineering* 32 (7): 366-370.
- 10 Mizuki, F., Y. Miyamoto, and T. Seiji. 1998. Control and instrumentation for ABWR plant. *Hitachi Review* 47 (5): 164-167.
- 11 Ibid.
- 12 Arkad'ev, B. A. 1986. *Operating Conditions of Steam Turbosets for Nuclear Power Plants* (in Russian). Moscow: Energoatomizdat, 1986.
- 13 Ibid.
- 14 Ibid.
- 15 Ibid.
- 16 Akerman, V. S., N. S. Gabrijchuk, V. B. Kirillov, A. S. Leyzerovich, et al. 1984. Results of field start-up tests for K-500-60/1500 turbine (in Russian) *Elektricheskie Stantsii* 2: 5-10.
- 17 Ibid.
- 18 Leyzerovich, A. S., and V. B. Kirillov. 1976. Optimization of start-ups of turbines at nuclear power stations by a method of mathematical simulation. *Thermal Engineering* 23 (2): 30-34.
- 19 Leyzerovich, A. S., V. B. Kirillov, S. P. Kruzhkova, et al. 1976. Investigating start-up operating conditions of the K-220-44 wet-steam turbines at Kola nuclear power plant (in Russian). *Elektricheskie Stantsii* 5: 34-39.

- 20 Leyzerovich, A. S., B. L. Levchenko, and V. B. Kirillov. 1983. Mathematical investigation of variable operational conditions of the LMZ K-1000-60/3000 turbine. *Thermal Engineering* 30 (1): 20–25.
- 21 Leyzerovich, 1997. *Large Power Steam Turbines: Design & Operation*, Vols. 1–2. Tulsa, OK: PennWell Publishing, 1997.
- 22 Ibid.
- 23 Leyzerovich, A. Optimization of start-ups of turbines. 30–34.
- 24 Madoyan, A. A., and L. N. Kobzarenko. 1986. About expediency of motor conditions for steam turbines of nuclear power plants (in Russian). *Teploenergetika* 33 (3): 8–10.
- 25 Bergmann, D., M. Gloger, G. May, and G. Gartner. 1985. High temperature control in high backpressure LP turbines. *Proceedings of the American Power Conference* 47: 219–229.
- 26 Gribov, N. N., A. S. Shemonaev, and E. S. Mandryka. 1988. Vibrational state of moving blades in the final stage of the low pressure section of a high-capacity steam turbine as a function of the volumetric flow of steam. *Soviet Energy Technology* 5: 24–27.
- 27 Khaimov, V. A., P. V. Khrabrov, Y. A. Voropaev, and O. E. Kotlyar. 1991. Low-flowrate operating modes and the reliability of the T-250/300-23.5 turbine. *Thermal Engineering* 38 (11): 594–597.
- 28 Leyzerovich. *Large Power Steam Turbines*.
- 29 Kosyak, Y. F. 1987. Development by Turboatom of turbine construction for nuclear power plants. *Thermal Engineering* 34 (8): 405–408.
- 30 Jacobsen, G., H. Oeynhausen, and H. Termuehlen. 1991. Advanced LP turbine installation at 1300 MW nuclear power station Unterweser. *Proceedings of the American Power Conference* 53: 991–1001.
- 31 2004. Site work underway on Finland's 1600 MWe EPR. *Modern Power Systems* 3: 30–34.
- 32 Kosyak, Development by Turboatom. 405–408.
- 33 ASME. 1976. *ASME Performance Test Codes: Code on Steam Turbines*. ANSI/ASME-PTC 6-1976. New York: ASME, 1976.
- 34 Sakharov, A. M. 1990. *Heat-Rate Performance Tests of Steam Turbines* (in Russian). Moscow: Energoatomizdat, 1990.
- 35 Pawliger, R. I., A. Roeder, E. Mueller, and Z. S. Stys. 1982. Experience in heat-rate acceptance tests of steam-turbine generators. *Proceedings of the American Power Conference* 44: 320–329.
- 36 Bornstein, B., and K. C. Cotton. 1981. A simplified ASME acceptance test procedure for steam turbines. *Combustion* March: 40–47.
- 37 Ibid.
- 38 Pawliger, Experience in heat-rate acceptance tests. 320–329.

- 39 Ibid.
- 40 Egli, A. J., and R. U. Danz. 1993. Experiences in testing the refurbished LP turbines in the Maanshan nuclear power plant. In *The Steam Turbine Generator Today: Materials, Low Path Design, Repair and Refurbishment*, PWR-Vol. 21, 7-19. New York: ASME, 1993.
- 41 Bornstein, A simplified ASME acceptance test procedure. 40-47.
- 42 ASME. 1983. *Interim Test Code for an Alternative Procedure for Testing Steam Turbines*. ASME-PTC 6-1983. New York: ASME, 1983.
- 43 Cotton, K. C., H. S. Shafer, T. H. McCloskey, and R. Boettcher. 1983. Demonstration and verification of the alternative ASME steam turbine-generator acceptance test. *Proceedings of the American Power Conference* 45: 169-176.
- 44 ASME. 1996. *ASME Performance Test Codes: Code on Steam Turbines*. ANSI/ASME-PTC 6-1996. New York: ASME, 1996.
- 45 Bornstein, A simplified ASME acceptance test procedure. 40-47.
- 46 Sakharov, *Heat-Rate Performance Tests of Steam Turbines*.
- 47 Buzulukov, V. A., M. G. Teplitskii, A. A. Maksimenko, and T. V. Poruchinskii. 1989. Full-scale testing of the KhTZ K-1000-60/1500-2 turbine plant at Zaporozh'e nuclear power station. *Thermal Engineering* 36 (2): 69-75.
- 48 Konovalov, G. M., V. D. Kanaev, F. M. Sukharev, et al. 1984. Thermal tests of the KhTZ K-500-60/1500 turbine plant. *Thermal Engineering* 31 (4): 188-193.
- 49 Buzulukov, Full-scale testing of the KhTZ K-1000-60/1500-2 turbine Plant. 69-75.
- 50 Ibid.
- 51 Ibid.
- 52 Teplitskii, M. G. 1986. Investigating the efficiency of the KhTZ K-1000-60/1500 turbine plant and the 1000 MW generating unit at the Southern-Ukrainian nuclear power station. *Thermal Engineering* 33 (12): 649-656.
- 53 Garbuзов, I. P., L. B. Oberman, M. G. Teplitskii, and Y. V. Flak. 1991. Experiments and calculations to determine the effectiveness of modernizing the flow section of the high-pressure cylinder in KhTZ K-1000-60/1500 turbines. *Thermal Engineering* 38 (2): 61-65.
- 54 Jacobsen, Advanced LP turbine installation. 991-1001.
- 55 Ibid.
- 56 Aubry, P., S. Bayard, and A. Anis. 1986. Nuclear LP turbine design and operating experience. *Proceedings of the American Power Conference* 48: 166-171.
- 57 Weschenfelder, K. D., H. Oeynhausen, D. Bergman, et al. 1994. Turbine steam path replacement at the Grafenrheinfeld nuclear power station. *Proceedings of the American Power Conference* 56: 1522-1529.

- 58 2001. EPRI seeks additional participants in development of turbine probe. *Power Engineering* 105 (3): 18.
- 59 Samoylovich, G. S., and B. M. Troyanovskii. 1982. *Variable and Transient Operation Conditions in Steam Turbines*, 2d ed. (in Russian). Moscow: Energoatomizdat, 1982.
- 60 Arkad'ev, *Operating Conditions of Steam Turbosets*.
- 61 Buzulukov, Full-scale testing of the KhTZ K-1000-60/1500-2 turbine Plant. 69-75.
- 62 Sill, U., and W. Zörner. 1996. *Steam Turbine Generators Process Control and Diagnostics*. Erlangen, Germany: Publicis MCD Verlag, 1996.
- 63 Arkad'ev, *Operating Conditions of Steam Turbosets*.
- 64 Weschenfelder, Turbine steam path replacement at the Grafenrheinfeld nuclear power station. 1522-1529.
- 65 Jacobsen, Advanced LP turbine installation at 1300 MW nuclear power station Unterweser. 991-1001.
- 66 Gordinsky A., E. Plotkin, E. Benenson, and A. Leyzerovich. 2000. A new approach to statistic processing of steam parameter measurements in the steam turbine path to diagnose its condition. In *Proceedings of the 2000 International Joint Power Generation Conference*, 1-5. New York: ASME, 2000.
- 67 Wesselmann, C. 2003. Nuclear power production (in German). *Brennstoff-Wärme-Kraft (BWK)* 55 (6): 40-47.
- 68 McCloskey, T. H., R. B. Dooley, and W. P. McNaughton. 1999. *Turbine Steam Path Damage: Theory and Practice*, Vols. 1-2. Palo Alto, CA: EPRI, 1999.
- 69 Ibid.
- 70 Bush, S. H. 1982. Failures in large steam turbine rotors. In *Rotor forgings for Turbines and Generators* (Proceedings of the International Workshop, Palo Alto, Calif., Sept. 1980). 1.1-1.27. New York: Pergamon Press, 1982.
- 71 Leyzerovich, A. *Large Power Steam Turbines*.
- 72 Lyle, F. F., Jr., A. McMinn, and G. R. Leverant. 1985. Low-pressure steam turbine disc cracking—An update. *Proceedings of the Institute of Mechanical Engineers* 199 (A1): 59-67.
- 73 Krämer, E., H. Huber, and B. Scarlin. 1996. Low-pressure steam turbine retrofits. *ABB Review* 5: 4-13.
- 74 Martynova, O. I., O. A. Povarov, O. A. Petrova, et al. Formation on corrosive media in the region of the phase transition in steam turbines. *Thermal Engineering* 45 (7): 568574.
- 75 Engelke, W. 1976. Operating experience of wet-steam turbines. In *Two-Phase Steam Flow in Turbines and Separators: Theory, Instrumentation, Engineering*, ed. M.J. Moore and C.H. Sieverding, 291-315. Washington, D.C.: Hemisphere Publishing Corp., 1976.

- 76 Engelke, W., K. Schleithoff, H.-A. Jestrich, and H. Termuehlen. 1983. Design, operating and inspection considerations to control stress corrosion of LP turbine disks. *Proceedings of the American Power Conference* 45: 196-206.
- 77 Jacobsen, Advanced LP turbine installation at 1300 MW nuclear power station Unterweser. 991-1001.
- 78 Joyce, J. S., and D. Lambrecht. 1979. Monitoring the fatigue effects of electrical disturbances of steam turbine-generators. *Proceedings of the American Power Conference* 41: 1153-1162.
- 79 1996. As the steam turbine turns, SCC still comes a calling. *Power* 140 (6): 6-8.
- 80 Chynoweth, J. M., G. S. Gerzen, and R. W. Tomala. 1996. Root cause of low pressure turbine blade failure. *Proceedings of the American Power Conference* 58: 1230-1236.
- 81 Kalderon, D. 1972. Steam turbine failure at Hinkley Point A. *Proceedings of the Institute of Mechanical Engineers* 186 (31): 341-377.
- 82 Povarov, O. A., and E. V. Velichko. 1989. Corrosion cracking in the metal of steam turbines. *Soviet Energy Technology* 4: 10-18.
- 83 Engelke, Design, operating and inspection considerations. 196-206.
- 84 Cheruvu, N. S., and B. B. Seth. 1993. Key variable affecting the susceptibility of shrunk-on discs to stress corrosion cracking. In *The Steam Turbine Generator Today: Materials, Flow Path Design, Repair and Refurbishment*, PWR-Vol. 21, 43-53. New York: ASME, 1993.
- 85 Aubry, Nuclear LP turbine design and operating experience. 166-171.
- 86 Ibid.
- 87 Krämer, Low-pressure steam turbine retrofits. 4-13.
- 88 Aubry, P., B. Billerey, and J. P. Goffin. 1996. Retrofit of LP rotors on nuclear turbines in Belgium. *Proceedings of the American Power Conference* 58: 166-171.
- 89 Krämer, Low-pressure steam turbine retrofits. 4-13.
- 90 David, W., G. Röttger, K. Schleithoff, et al. 1993. Disk-type LP turbine rotors experience. In *The Steam Turbine Generator Today: Materials, Flow Path Design, Repair and Refurbishment*, PWR-Vol. 21, 83-91. New York: ASME, 1993.
- 91 Oeynhausen, H., G. Roettger, J. Ewald , K. Schleihoff, and H. Termuehlen. 1987. Reliable disc-type rotors for nuclear power plants. *Proceedings of the American Power Conference* 49: 113-122.
- 92 Ibid.
- 93 Ibid.
- 94 Ibid.

- 95 Virchenko, M. A., E. V. Levchenko, B. A. Arkad'ev, et al. 1997. Corrosion fatigue of rotating blades. *Thermal Engineering* 44 (6): 464–468.
- 96 Busse, L., D. Heiberger, and E. Krämer. 1997. Corrosion effects in curved fir-tree fastenings. *VGB Kraftwerkstechnik* 77 (10): 729–732.
- 97 Ibid.
- 98 Povarov, O. A., G. V. Tomarov, and V. N. Zharov. 1990. Erosion-corrosion of saturated-steam turbine plant elements. *Thermal Engineering* 37 (12): 643–647.
- 99 Troyanovskii, B. M., Y. F. Kosyak, M. A. Virchenko, et al. 1977. Experience with operation of saturated steam turbines at nuclear power stations. *Thermal Engineering* 24 (2): 15–23.
- 100 Kosyak, Y. F., M. A. Virchenko, B. M. Troyanovskii, and M. Y. Grabovskii. 1983. Experience with operation of saturated-steam turbines at nuclear power stations. *Thermal Engineering* 30 (1): 7–11.
- 101 Leyzerovich, *Large Power Steam Turbines*.
- 102 Engelke, Operating experience of wet-steam turbines. 291–315.
- 103 Sakamoto, T., S. Nagao, and T. Nanuma. 1992. Investigation of wet steam flow for steam turbine repowering. In *Steam Turbine-Generator Developments for the Power Generation Industry*, PWR-Vol. 18, 33–39. New York: ASME, 1992.
- 104 Engelke, Operating experience of wet-steam turbines. 291–315.
- 105 Troyanovskii, B. M. 1978. *Turbines for Nuclear Power Plants*, 2d. ed. (in Russian). Moscow: Energiya, 1978.
- 106 McCloskey, *Turbine Steam Path Damage: Theory and Practice*.
- 107 Chynoweth, Root cause of low pressure turbine blade failure. 1230–1236.
- 108 Ibid.
- 109 Troyanovskii, *Turbines for Nuclear Power Plants*.
- 110 Spalthoff, F. J., H. Haas, and F. Heindrichs. 1976. First year of operation of the world's largest tandem compound turbine-generator. *Proceedings of the American Power Conference* 38: 555–569.
- 111 Sokolov, V. S., A. I. Lebedeva, and V. I. Nogin. 1998. An estimate of the damage to the blade surface by pitting corrosion. *Thermal Engineering* 45 (8): 665–667.
- 112 Leyzerovich, *Large Power Steam Turbines*.
- 113 Steigleder, K., and E. Krämer. 1989. Coupled vibrations of steam turbine blades and rotors due to torsional excitation by negative sequence current. *Proceedings of the American Power Conference* 51: 94–101.
- 114 Tsunoda, E., H. Mimuro, S. Hisa, et al. 1989. Torsional vibration evaluation technique for large-capacity steam turbines. *Proceedings of the American Power Conference* 51: 109–114.
- 115 Leyzerovich, *Large Power Steam Turbines*.

- 116 Joyce, J. S., and D. Lambrecht. 1979. Monitoring the fatigue effects of electrical disturbances of steam turbine-generators. *Proceedings of the American Power Conference* 41: 1153-1162.
- 117 Higuchi, M., and T. Tsuda. 1989. Telemetry test of blade shaft coupled torsional vibration at the Tsuruga no. 2 power plant. *Proceedings of the American Power Conference* 51: 103-108.
- 118 Ibid.
- 119 Chetwynd, R., M. Hojati, and D. Pilmer. 1999. An evaluation of the limits to safe operation for low pressure nuclear turbines with low margins from torsional resonance. In *Proceedings of the Joint Power Generation Conference*. PWR-Vol. 34, Part 2, 395-402. New York: ASME, 1999.
- 120 Filippov, G. A., A. N. Kukushkin, G. A. Saltanov, et al. 1999. Preservation of thermal power equipment using reagents based on film-forming amines. *Thermal Engineering* 46 (9): 789-794.
- 121 Ibid.
- 122 Filippov, G. A., A. N. Kukushkin, G. A. Saltanov, et al. 1998. Experience of commissioning the secondary coolant circuit of power unit no. 2 at the Armenian nuclear power station after its preservation using film-forming amines. *Thermal Engineering* 45 (5): 397-400.
- 123 Filippov, G. A., A. N. Kukushkin, G. A. Saltanov, et al. 1997. Protection, cleaning and preservation of steam/water paths of fossil-fuel and nuclear power plants using film-forming amine-based microadditives. *Proceedings of the American Power Conference* 59: 936-940.
- 124 Deich, M. E., A. V. Kurshakov, A. A. Tishchenko, and V. M. Leonov. 1986. The effect of adding octadecylamine on the structural and power characteristics of two-phase flows. *Thermal Engineering* 33 (9): 482-486.
- 125 Filippov, G. A., G. A. Saltanov, O. I. Martynova, et al. 1990. The physico-technical problems involved in improving the reliability and efficiency of thermal power plant based on the use of microdoses of surfactants. *Thermal Engineering* 37 (2): 94-96.
- 126 Leyzerovich, *Large Power Steam Turbines*.
- 127 Leyzerovich, A. S. 1978. Rational monitoring of heating and control of transients for wet-steam turbines (in Russian). *Elektricheskie Stantsii* 6: 4-8.
- 128 Leyzerovich, Investigating start-up operating conditions of the K-220-44. 34-39.
- 129 Akerman, V. S., N. S. Gabrijchuk, V. B. Kirillov, A. S. Leyzerovich, et al. 1984. Results of field start-up tests for K-500-60/1500 turbine (in Russian) *Elektricheskie Stantsii* 2: 5-10.
- 130 Leyzerovich, A. S. 1983. *Technological Fundamentals of Power Steam Turbine Start-up Automation* (in Russian). Moscow: Energoatomizdat, 1983.
- 131 Kirillov, Flexibility characteristics of wet-steam turbines of nuclear power stations. 366-370.

*382 Wet-Steam Turbines for Nuclear Power Plants*

- 132 Akerman, Results of field start-up tests for K-500-60/1500 turbine. 5-10.
- 133 Leyzerovich, Investigating start-up operating conditions of the K-220-44. 34-39.
- 134 Akerman, Results of field start-up tests for K-500-60/1500 turbine. 5-10.
- 135 Ibid.
- 136 Leyzerovich, Investigating start-up operating conditions of the K-220-44. 34-39.
- 137 Leyzerovich, *Large Power Steam Turbines*.
- 138 Kosyak, Y. F., V. N. Galatsan, and V. A. Paley. 1983. *Operating Nuclear Power Plant Turbines* (in Russian). Moscow: Energoatomizdat, 1983.
- 139 Leyzerovich, *Large Power Steam Turbines*.
- 140 Ibid.
- 141 Lyudomirskii, B. N., A. S. Leyzerovich, and Y. V. Kolomtsev. 1979. An experimental investigation of the conditions of heating up the welded rotor of the low pressure cylinder of a nuclear station turbine when starting. *Thermal Engineering* 26 (11): 664-668.
- 142 Ibid.
- 143 Ibid.
- 144 Ibid.
- 145 Leyzerovich, *Large Power Steam Turbines*.
- 146 Teplitskii, Investigating the efficiency of the KhTZ K-1000-60/1500 turbine plant. 649-656.
- 147 Leyzerovich, *Large Power Steam Turbines*.
- 148 Lyudomirskii, An experimental investigation. 664-668.
- 149 Ibid.
- 150 Kapinos, V. M., Y. Y. Matveev, V. N. Pustovalov, and V. A. Palei. 1988. Modeling the cooling-down process in high-capacity steam turbines. *Thermal Engineering* 35 (4): 196-200.
- 151 Ibid.
- 152 Madoyan, A. A., and L. N. Kobzarenko. 2002. Investigation of a K-220-4.3 turbine of KhTZ under motor operating conditions. *Thermal Engineering* 49 (12): 996-1001.
- 153 Levchenko, B. L., V. S. Shargorodskii, N. N. Gudkov, and S. A. Ivanov. 1993. No-load temperature conditions of a K-1200-23.5 turbine. *Thermal Engineering* 40 (11): 874-880.
- 154 Malev, V. V., and Y. N. Nezhentsev. 1992. New developments in steam turbine construction at Leningrad Metalworking Factory. *Thermal Engineering* 39 (6): 289-293.

- 155 Kaneko, R., K. Ikeuchi, A. Okabe, et al. 1990. Development of 40-inch titanium blades using titanium alloys. In *Titanium Steam Turbine Blading*, 111-128. New York: Pergamon Press, 1990.
- 156 Kirillov, V. B., A. S. Leyzerovich, and Y. V. Kolomtsev. 1979. Temperature state of the main steam-lines of K-220-44 turbine at transients (in Russian). *Elektricheskie Stantsii* 9: 10-13.
- 157 Ibid.
- 158 Leyzerovich, *Large Power Steam Turbines*.
- 159 Engelke, W., J. S. Joyce, D. Lambrecht, et al. 1982. Rotor forgings for KWU-designed turbine generators. In *Rotor Forgings for Turbines and Generators (Proceedings of the International Workshop)*, Palo Alto, CA, Sept. 1980), 3.147-3.163. New York: Pergamon Press, 1982.
- 160 Oeynhausen, "Reliable disc-type rotors for nuclear power plants." 113-122.
- 161 Brailovskaya, V. A., V. R. Kogan, A. S. Leyzerovich, and V. I. Polezhaev. 1980. Influence of free convection within the internal cavity on heating of welded rotors of large steam turbines at start-ups (in Russian). *Izvestiya Akademii Nauk SSSR: Energetika i Transport (Proceedings of the Academy of Sciences of the USSR: Power Engineering and Transport)* 5: 109-116.
- 162 Ibid.
- 163 Ibid.
- 164 Leyzerovich, *Large Power Steam Turbines*.
- 165 Ibid.
- 166 Leyzerovich, Mathematical investigation of variable operational conditions. 20-25.
- 167 Leyzerovich, A. S. A. S., V. B. Kirillov, V. A. Paley, and V. L. Yasnogorodsky. 1978. Flexibility characteristics of steam turbines for nuclear power plants (in Russian). *Flexibility of Large Power Plant Units (Proceedings of the VTI, No. 14)*, 153-156. Moscow: Energiya, 1978.
- 168 Kirillov, Flexibility characteristics of wet-steam turbines of nuclear power stations. 366-370.
- 169 Ibid.
- 170 Mizuki, F., Y. Miyamoto, and T. Seiji. Control and instrumentation for ABWR plant. *Hitachi Review* 47 (5): 164-167.
- 171 Ibid.
- 172 Seiji, T., Y. Ohga, and M. Koyama. 2001. Advanced supervisory and control systems for nuclear power plants. *Hitachi Review* 50 (3): 79-167.
- 173 Yamamori, T., T. Ichikawa, S. Kawaguchi, and H. Honma. 2000. Recent technologies in nuclear power plant supervisory and control systems. *Hitachi Review* 49 (2): 61-65.

- 174 Butkus, K., and M. Pakstys. 2000. Major process computer upgrade improves safety at Lithuania's nuclear giant. *Modern Power Systems* 20 (2): 45–46.
- 175 2000. European nuclear plants upgrade controls. *Power* 144 (2): 12, 14.
- 176 Leyzerovich, *Large Power Steam Turbines*.
- 177 Ibid.
- 178 Leyzerovich, A. S. 1981. Mathematical modeling the heating of steam turbine rotors for operating monitoring (in Russian). *Izvestiya Akademii Nauk SSSR. Energetika i Transport (Proceedings of Academy of Sciences of the USSR. Power Engineering and Transport)*, 1: 123–131.
- 179 Ibid.
- 180 Kosyak, *Operating Nuclear Power Plant Turbines*.
- 181 Leyzerovich, *Technological Fundamentals of Power Steam Turbine Start-up Automation*.
- 182 Leyzerovich, A. S., A. D. Melamed, V. B. Kirillov, et al. 1976. Experience of automation of start-up operating conditions of the nuclear-plant turbine (in Russian). *Elektricheskie Stantsii* 11: 29–34.
- 183 Ibid.
- 184 Ibid.
- 185 Ibid.

## Bibliography

- Akerman, V. S., N. S. Gabrijchuk, V. B. Kirillov, A. S. Leyzerovich, et al. 1984. Results of field start-up tests for K-500-60/1500 turbine" (in Russian). *Elektricheskie Stantsii* (2): 5–10.
- Arkad'ev, B. A. 1986. *Operating Conditions of Steam Turbosets for Nuclear Power Plants* (in Russian). Moscow: Energoatomizdat, 1986.
- , V. A. Palei, V. Y. Ioffe, et al. 1976. Use of varying pressure of main steam for controlling the power generating units at nuclear power stations. *Thermal Engineering* 24 (1): 34–36.
- As the steam turbine turns, SCC still comes a calling. 1996. *Power* 140 (6): 6–8.
- Asai, K., E. Saito, K. Namura, S. Sakurai, and K. Nomura. 2002. Corrosion fatigue life evaluation method for the bladed disk attachments of low-pressure steam turbines. In *Proceedings of the 2002 International Joint Power Generation Conference*, 495–501. New York: ASME, 2002.
- ASME Performance Test Codes: Code on Steam Turbines*. 1976. *ANSI/ASME-PTC 6-1976*. New York: ASME, 1976.
- . 1996. *ANSI/ASME-PTC 6-1996*. New York: ASME, 1996.
- Aubry, P., S. Bayard, and A. Anis. 1986. Nuclear LP turbine design and operating experience. *Proceedings of the American Power Conference* 48: 166–171.
- , B. Billerey, and J. P. Goffin. 1996. Retrofit of LP rotors on nuclear turbines in Belgium. *Proceedings of the American Power Conference* 58 (1996): 166–171.
- Bergmann, D., M. Gloger, G. May, and G. Gartner. 1985. High temperature control in high backpressure LP turbines. *Proceedings of the American Power Conference* 47 (1985): 219–229.
- Bornstein, B., and K. C. Cotton. 1981. A simplified ASME acceptance test procedure for steam turbines. *Combustion* March 1981: 40–47.
- Brailovskaya, V. A., V. R. Kogan, A. S. Leyzerovich, and V. I. Polezhaev. 1980. Influence of free convection within the internal cavity on heating of welded rotors of large steam turbines at start-ups (in Russian). *Izvestiya Akademii Nauk SSSR: Energetika i Transport (Proceedings of the Academy of Sciences of the USSR: Power Engineering and Transport)*, 1980 (5): 109–116.
- Brown, R. D., F. Y. Simma, and R. J. Chetwood. 2000. Efficiency improvement features of recent ABB-ALSTOM HP-LP turbine retrofit at Southern California Edison's San Onofre Nuclear Generating Station. In *Proceedings of the ASME International Joint Power Generating Conference*. 85–93. New York: ASME, 2000.
- Bush, S. H. 1982. Failures in large steam turbine rotors. In *Rotor Forgings for Turbines and Generators (Proceedings of the International Workshop, Palo Alto, Calif., Sept. 1980)*. 1.1–1.27. New York: Pergamon Press, 1982.
- Busse, L., D. Heiberger, and E. Krämer. 1997. Corrosion effects in curved fir-tree fastenings. *VGB Kraftwerkstechnik* 77 (10): 729–732.

- Butkus, K., and M. Pakstys. 2000. Major process computer upgrade improves safety at Lithuania's nuclear giant. *Modern Power Systems* 20 (2): 45–46.
- Buzulukov, V. A., M. G. Teplitskii, A. A. Maksimenko, and T. V. Poruchinskii. 1989. Full-scale testing of the KhTZ K-1000-60/1500-2 turbine plant at Zaporozh'e nuclear power station. *Thermal Engineering* 36 (2): 69–75.
- Cheruvu, N. S., and B. B. Seth. 1993. Key variable affecting the susceptibility of shrunk-on discs to stress corrosion cracking. In *The Steam Turbine Generator Today: Materials, Flow Path Design, Repair and Refurbishment*, PWR-Vol. 21, 43–53. New York: ASME, 1993.
- Chetwynd, R., M. Hojati, and D. Pilmer. 1999. An evaluation of the limits to safe operation for low pressure nuclear turbines with low margins from torsional resonance. In *Proceedings of the Joint Power Generation Conference*. PWR-Vol. 34, Part 2, 395–402. New York: ASME, 1999.
- Chynoweth, J. M., G. S. Gerzen, and R. W. Tomala. 1996. Root cause of low pressure turbine blade failure." *Proceedings of the American Power Conference* 58: 1230–1236.
- Cotton, K. C., H. S. Shafer, T. H. McCloskey, and R. Boettcher. 1983. Demonstration and verification of the alternative ASME steam turbine-generator acceptance test. *Proceedings of the American Power Conference* 45: 169–176.
- David, W., G. Röttger, K. Schleithoff, et al. 1993. Disk-type LP turbine rotors experience. In *The Steam Turbine Generator Today: Materials, Flow Path Design, Repair and Refurbishment*, PWR-Vol. 21, 83–91. New York: ASME, 1993.
- Deich, M. E., A. V. Kurshakov, A. A. Tishchenko, and V. M. Leonov. 1986. The effect of adding octadecylamine on the structural and power characteristics of two-phase flows. *Thermal Engineering* 33 (9) : 482–486.
- Egli, A. J., and R. U. Danz. 1993. Experiences in testing the refurbished LP turbines in the Maanshan nuclear power plant. In *The Steam Turbine Generator Today: Materials, Low Path Design, Repair and Refurbishment*, PWR-Vol. 21, 7–19. New York: ASME, 1993.
- Engelke, W. 1976. Operating experience of wet-steam turbines. In *Two-Phase Steam Flow in Turbines and Separators: Theory, Instrumentation, Engineering*, ed. M. J. Moore and C. H. Sieverding, 291–315. Washington, D.C.: Hemisphere Publishing Corp., 1976.
- , J. S. Joyce, D. Lambrecht, et al. 1982. Rotor forgings for KWU-designed turbine generators. In *Rotor Forgings for Turbines and Generators (Proceedings of the International Workshop, Palo Alto, CA, Sept. 1980)*, 3.147–3.163. New York: Pergamon Press, 1982.
- , K. Schleithoff, H.-A. Jestrich, and H. Termuehlen. 1983. Design, operating and inspection considerations to control stress corrosion of LP turbine disks. *Proceedings of the American Power Conference* 45 (1983): 196–206.
- EPRI seeks additional participants in development of turbine probe. 2001. *Power Engineering* 2001 (3): 18.
- European nuclear plants upgrade controls. 2000. *Power*, 144 (2): 12, 14.

- Filippov, G. A., A. N. Kukushkin, G. A. Saltanov, et al. 1998. Experience of commissioning the secondary coolant circuit of power unit no. 2 at the Armenian nuclear power station after its preservation using film-forming amines. *Thermal Engineering* 45 (5): 397-400.
- \_\_\_\_\_, A. N. Kukushkin, G. A. Saltanov, et al. 1999. Preservation of thermal power equipment using reagents based on film-forming amines. *Thermal Engineering* 46 (9): 789-794.
- \_\_\_\_\_, A. N. Kukushkin, G. A. Saltanov, et al. 1997. Protection, cleaning and preservation of steam/water paths of fossil-fuel and nuclear power plants using film-forming amine-based microadditives. *Proceedings of the American Power Conference* 59 (1997): 936-940.
- \_\_\_\_\_, O. I. Martynova, A. N. Kukushkin, et al. 1994. Preservation of the equipment of thermal and nuclear power stations by means of film-forming amines. *Thermal Engineering* 46 (4): 307-311.
- \_\_\_\_\_, and O. A. Povarov. 1986. *Erosion-Corrosion in Steam Turbines* (in Russian). Moscow: Energiya, 1986.
- \_\_\_\_\_, G. A. Saltanov, O. I. Martynova, et al. 1990. The physico-technical problems involved in improving the reliability and efficiency of thermal power plant based on the use of microdoses of surfactants. *Thermal Engineering* 37 (2): 94-96.
- Garbuzov, I. P., L. B. Oberman, M. G. Teplitskii, and Y. V. Flak. 1991. Experiments and calculations to determine the effectiveness of modernizing the flow section of the high-pressure cylinder in KhTZ K-1000-60/1500 turbines. *Thermal Engineering* 38 (2): 61-65.
- Gloger, M. 1970. Problems of water withdrawal in wet-steam turbines (in German). *Brennstoff-Wärme-Kraft (BWK)* 22 (5): 417-420.
- Gordinsky A., E. Plotkin, E. Benenson, and A. S. Leyzerovich. 2000. A new approach to statistic processing of steam parameter measurements in the steam turbine path to diagnose its condition. In *Proceedings of the 2000 International Joint Power Generation Conference*, 1-5. New York: ASME, 2000.
- Gribov, N. N., A. S. Shemonaev, and E. S. Mandryka. 1988. Vibrational state of moving blades in the final stage of the low pressure section of a high-capacity steam turbine as a function of the volumetric flow of steam. *Soviet Energy Technology* (5): 24-27.
- Groenendaal, J. C., L. G. Fowls, R. Subbiah, et al. 1996. LP turbine retrofit modernization: Improvements in performance and operation. *Proceedings of the American Power Conference* 58, Part 2 (1996): 1224-1229.
- Higuchi, M., and T. Tsuda. 1989. Telemetry test of blade shaft coupled torsional vibration at the Tsuruga no. 2 power plant. *Proceedings of the American Power Conference* 51: 103-108.
- Hishinuma, Y., K. Hoshino, and T. Tamatsukuri. 1995. Current trends in thermal and hydraulic power technologies. *Hitachi Review* 44 (1): 1-6.

- Hodge, J. M., and I. L. Mogford. 1979. UK experience of stress corrosion cracking in steam turbine discs. *Proceedings of the Institute of Mechanical Engineers* 193 (11): 93-109.
- Hurley, J. D., and S. A. Welhoelter. 1989. Turbine-generator design, analysis, and testing for prevention of double-frequency torsional resonance. *Proceedings of the American Power Conference* 51: 87-93.
- Huster, J., L. Eckert, and F. Pohle. 1998. Calculation and measurement of torsionals in large steam turbosets. *ABB Review* (3): 31-41.
- Interim Test Code for an Alternative Procedure for Testing Steam Turbines.* 1983. ASME-PTC 6-1983. New York: ASME, 1983.
- Ivanov, V. A. 1986. *Operating Conditions of Large Steam-Turbine Power Plants* (in Russian). Leningrad: Energoatomizdat, 1986.
- Jacobsen, G., H. Oeynhausen, and H. Termuehlen. 1991. Advanced LP turbine installation at 1300 MW nuclear power station Unterweser. *Proceedings of the American Power Conference* 53: 991-1001.
- Jonas, O. 1985. Steam turbine corrosion. *Materials Performance* 24 (2): 9-18.
- Joyce, J. S., and D. Lambrecht. 1979. Monitoring the fatigue effects of electrical disturbances of steam turbine-generators. *Proceedings of the American Power Conference* 41: 1153-1162.
- Kalderon, D. Steam turbine failure at Hinkley Point A. *Proceedings of the Institute of Mechanical Engineers* 186 (31): 341-377.
- Kaneko, R., K. Ikeuchi, A. Okabe, et al. 1990. Development of 40-inch titanium blades using titanium alloys. In *Titanium Steam Turbine Blading*, 111-128. New York: Pergamon Press, 1990.
- Kapinos, V. M., Y. Y. Matveev, V. N. Pustovalov, and V. A. Palei. 1988. Modeling the cooling-down process in high-capacity steam turbines. *Thermal Engineering* 35 (4): 196-200.
- Khaimov, V. A., P. V. Khrabrov, Y. A. Voropaev, and O. E. Kotlyar. 1991. Low-flowrate operating modes and the reliability of the T-250/300-23.5 turbine. *Thermal Engineering* 38 (11): 594-597.
- Kirillov, V. B., and A. S. Leyzerovich. 1985. Flexibility characteristics of wet-steam turbines of nuclear power stations. *Thermal Engineering* 32 (7): 366-370.
- , A. S. Leyzerovich, and Y. V. Kolomtsev. 1979. Temperature state of the main steam-lines of K-220-44 turbine at transients (in Russian). *Elektricheskie Stantsii* 1979 (9): 10-13.
- Komarov, N. F., and E. V. Yurkov. 1991. Corrosion damage to the blading and discs of steam turbines. *Thermal Engineering* 38 (2): 66-70.
- Kondakov, A. Y., L. L. Simoyu, V. P. Lagun, et al. 1986. Investigation of the resistance to vibration of the moving blades of the low-pressure cylinders of a high-capacity steam turbines. *Thermal Engineering* 33 (12): 665-669.
- Konovalov, G. M., V. D. Kanaev, F. M. Sukharev, et al. 1984. Thermal tests of the KhTZ K-500-60/1500 turbine plant. *Thermal Engineering* 31 (4): 188-193.

- Kosyak, Y. F. 1987. Development by Turboatom of turbine construction for nuclear power plants. *Thermal Engineering* 34 (8): 405–408.
- , ed. 1978. *Steam-Turbine Installations for Nuclear Power Plants* (in Russian). Moscow: Energiya, 1978.
- , V. N. Galatsan, and V. A. Paley. 1983. *Operating Nuclear Power Plant Turbines* (in Russian). Moscow: Energoatomizdat, 1983.
- , M. A. Virchenko, B. M. Troyanovskii, and M. Y. Grabovskii. 1983. Experience with operation of saturated-steam turbines at nuclear power stations. *Thermal Engineering* 30 (1): 7–11.
- Krämer, E., H. Huber, and B. Scarlin. 1996. Low-pressure steam turbine retrofits. *ABB Review* 1996 (5): 4–13.
- Krzyzanowski, J. 1991. *Erosion of Steam Turbine Blades* (in Polish). Wrocław, Poland: Wydawnictwo Polskiej Akademii Nauk, 1991.
- Levchenko, B. L., V. S. Shargorodskii, N. N. Gudkov, and S. A. Ivanov. 1993. No-load temperature conditions of a K-1200-23.5 turbine. *Thermal Engineering* 40 (11): 874–880.
- Leyzerovich, A. S. 1997. *Large Power Steam Turbines: Design & Operation*, Vols. 1–2. Tulsa, OK: PennWell Publishing, 1997.
- . 1981. Mathematical modeling the heating of steam turbine rotors for operating monitoring (in Russian). *Izvestiya Akademii Nauk SSSR. Energetika i Transport (Proceedings of Academy of Sciences of the USSR. Power Engineering and Transport)*, 1981 (1): 123–131.
- . 1980. Monitoring thermal-stress state of LP rotors for large steam turbines (in Russian). *Teploenergetika* 27 (8): 17–21.
- . 1978. Rational monitoring of heating and control of transients for wet-steam turbines (in Russian). *Elektricheskie Stantsii* 1978 (6): 4–8.
- . 1983. *Technological Fundamentals of Power Steam Turbine Start-up Automation* (in Russian). Moscow: Energoatomizdat, 1983.
- , and V. B. Kirillov. 1976. Optimization of start-ups of turbines at nuclear power stations by a method of mathematical simulation. *Thermal Engineering* 23 (2): 30–34.
- , V. B. Kirillov, S. P. Kruzhkova, et al. 1976. Investigating start-up operating conditions of the K-220-44 wet-steam turbines at Kola nuclear power plant (in Russian). *Elektricheskie Stantsii*, 1976 (5): 34–39.
- , V. B. Kirillov, V. A. Paley, and V. L. Yasnogorodsky. 1978. Flexibility characteristics of steam turbines for nuclear power plants (in Russian). *Flexibility of Large Power Plant Units (Proceedings of the VTI, No. 14)*, 153–156. Moscow: Energiya, 1978.
- , B. L. Levchenko, and V. B. Kirillov. “Mathematical investigation of variable operational conditions of the LMZ K-1000-60/3000 turbine.” *Thermal Engineering* 30, no. 1(1983): 20–25.

- , A. D. Melamed, and L. Y. Gushchina. 1980. Development of automated control system for the functional group ‘turbine’ of nuclear power plant unit with RBMK-1000 reactor (in Russian). *Automation of Nuclear Power Plants (Proceedings of VTI, No. 25)*, 55–64. Moscow: Energiya, 1980.
- , A. D. Melamed, V. B. Kirillov, et al. 1980. Experience of automation of start-up operating conditions of the nuclear-plant turbine (in Russian). *Elektricheskie Stantsii*, 1976 (11): 29–34.
- Lyle, F. F., Jr., A. McMinn, and G. R. Leverant. 1985. Low-pressure steam turbine disc cracking—An update. *Proceedings of the Institute of Mechanical Engineers* 199 (A1): 59–67.
- Lyudomirskii, B. N., A. S. Leyzerovich, and Y. V. Kolomtsev. 1979. An experimental investigation of the conditions of heating up the welded rotor of the low pressure cylinder of a nuclear station turbine when starting. *Thermal Engineering* 26 (11): 664–668.
- Madoyan, A. A., and L. N. Kobzarenko. 1986. About expediency of motor conditions for steam turbines of nuclear power plants (in Russian). *Teploenergetika* 33 (3): 8–10.
- , and L. N. Kobzarenko. 2002. Investigation of a K-220-4.3 turbine of KhTZ under motor operating conditions. *Thermal Engineering* 49 (12): 996–1001.
- Malev, V. V., and Y. N. Nezhentsev. 1992. New developments in steam turbine construction at Leningrad Metalworking Factory. *Thermal Engineering* 39 (6): 289–293.
- Martynova, O. I., O. A. Povarov, O. A. Petrova, et al. 1998. Formation on corrosive media in the region of the phase transition in steam turbines. *Thermal Engineering* 45 (7): 568–574.
- McCloskey, T. H., R. B. Dooley, and W. P. McNaughton. 1999. *Turbine Steam Path Damage: Theory and Practice*, Vols. 1–2. Palo Alto, CA: EPRI, 1999.
- Mizuki, F., Y. Miyamoto, and T. Seiji. 1998. Control and instrumentation for ABWR plant. *Hitachi Review* 47 (5): 164–167.
- Oeynhausen, H., G. Roettger, J. Ewald, K. Schleihoff, and H. Termuehlen. 1987. Reliable disc-type rotors for nuclear power plants. *Proceedings of the American Power Conference* 49: 113–122.
- Operating results with nuclear power plants in 1999. 2000. *VGB PowerTech* 80 (5): 17–53.
- Operating results with nuclear power plants in 2000 (in German). 2001. *VGB PowerTech* 81 (5): 29–66.
- Operating results with nuclear power plants in 2001 (in German). 2002. *VGB PowerTech* 82 (5): 27–67.
- Operating results with nuclear power plants in 2002 (in German). 2003. *VGB PowerTech* 83 (5): 37–73.
- Pawliger, R. I., A. Roeder, E. Mueller, and Z. S. Stys. 1982. Experience in heat-rate acceptance tests of steam-turbine generators. *Proceedings of the American Power Conference* 44: 320–329.

- Pizzica, J., J.-E. Berilsson, and E. Thommen. 1988. Replacement of LP-turbine rotors in nuclear power stations Dresden and Quad Cities. *Proceedings of the American Power Conference* 50: 77-86.
- Plotkin, E. R., and A. S. Leyzerovich. 1980. *Start-ups of Power Unit Steam Turbines* (in Russian). Moscow: Energiya, 1980.
- Povarov, O. A., V. N. Semenov, and B. V. Bogomolov. 1986. The effect of corrosive media on reliability of steam turbines. *Thermal Engineering* 33 (10): 542-547.
- \_\_\_\_\_, G. V. Tomarov, and V. N. Semenov. 2002. Investigations and experience in introducing the technology of protection against corrosion of the metal of steam turbines. *Thermal Engineering* 49 (12): 987-995.
- \_\_\_\_\_, G. V. Tomarov, and V. N. Zharov. 1990. Erosion-corrosion of saturated-steam turbine plant elements. *Thermal Engineering* 37 (12): 643-647.
- \_\_\_\_\_, and E. V. Velichko. 1989. Corrosion cracking in the metal of steam turbines. *Soviet Energy Technology* 1989 (4): 10-18.
- Presson, J. H., Jr., R. R. Hess, C. W. Rose, and R. D. Scott. 1995. Improved nuclear LP turbine inspection strategy—A team approach. In *Proceedings of the International Joint Power Generating Conference*, PWR-Vol. 28, 321-325. New York: ASME, 1995.
- Probe improves tracking of turbine efficiency. 2000. *EPRY Annual Report*, 2000: 9-10.
- Proselkov, V. N., and V. D. Simonov. Technical problems associated with participation of nuclear power plants in governing load of power systems (in Russian). *Energokhozyajstvo za Rubezhom* 1989 (3): 11-15.
- Raczkowski, C., and G. C. Kung. 1978. Turbine-generator torsional frequencies—Field reliability and testing. *Proceedings of the American Power Conference* 40: 1116-1123.
- Sakamoto, T., S. Nagao, and T. Nanuma. 1992. Investigation of wet steam flow for steam turbine repowering. In *Steam Turbine-Generator Developments for the Power Generation Industry*, PWR-Vol. 18, 33-39. New York: ASME, 1992.
- Sakharov, A. M. 1990. *Heat-Rate Performance Tests of Steam Turbines* (in Russian). Moscow: Energoatomizdat, 1990.
- Samoylovich, G. S., and B. M. Troyanovskii. 1982. *Variable and Transient Operation Conditions in Steam Turbines*, 2d ed. (in Russian). Moscow: Energoatomizdat, 1982.
- Sanders, W. P. 2001. *Turbine Steam Path Maintenance & Repair*, Vols. 1-2. Tulsa, OK: PennWell Publishing, 2001.
- Schwieger, B., M. Leonard, S. Taylor, et al. 2002. First annual top plants survey. *Power* 146 (4): 27-70.
- Seiji, T., Y. Ohga, and M. Koyama. 2001. Advanced supervisory and control systems for nuclear power plants. *Hitachi Review* 50 (3): 79-167.

- Sekine, Y. 1993. Nuclear power generation in Japan—Present status and future prospects. *Proceedings of the Institute of Mechanical Engineers* 207 (A4): 233–246.
- Shnee, Y. I., Y. F. Kosyak, V. N. Ponomarev, et al. 1978. The main results of development and gas-dynamic investigation of the last stage of the K-500 and K-1000-60/1500 turbines.” *Thermal Engineering* 25 (9): 1–7.
- Sill, U., and W. Zörner. 1996. *Steam Turbine Generators Process Control and Diagnostics*. Erlangen, Germany: Publicis MCD Verlag, 1996.
- Sokolov, V. S., A. I. Lebedeva, and V. I. Nogin. 1998. An estimate of the damage to the blade surface by pitting corrosion. *Thermal Engineering* 45 (8): 665–667.
- Spalthoff, F. J., H. Haas, and F. Heindrichs. 1976. First year of operation of the world’s largest tandem compound turbine-generator. *Proceedings of the American Power Conference* 38: 555–569.
- Springer, G. S. 1976. *Erosion by Liquid Impact*, New York: Wiley, 1976.
- Steigleder, K., and E. Krämer. 1989. Coupled vibrations of steam turbine blades and rotors due to torsional excitation by negative sequence current. *Proceedings of the American Power Conference* 51: 94–101.
- Sugitani, T., and K. Kawamoto. 1988. Reliability enhancement of turbine-generator system against blade-shaft coupled vibration. *Proceedings of the American Power Conference* 50: 72–76.
- Teplitskii, M. G. 1986. Investigating the efficiency of the KhTZ K-1000-60/1500 turbine plant and the 1000 MW generating unit at the Southern-Ukrainian nuclear power station. *Thermal Engineering* 33 (12): 649–656.
- Termuehlen, H. 2001. *100 Years of Power Plant Development: Focus on Steam and Gas Turbines as Prime Movers*. New York: ASME, 2001.
- Tomarov, G. V. 2001. The physicochemical processes and regularities of the metal of the power equipment in two-phase flow. *Thermal Engineering* 48 (9): 761–770.
- Troyanovskii, B. M. 1978. *Turbines for Nuclear Power Plants*, 2d. ed. (in Russian). Moscow: Energiya, 1978.
- \_\_\_\_\_, Y. F. Kosyak, M. A. Virchenko, et al. 1977. Experience with operation of saturated steam turbines at nuclear power stations. *Thermal Engineering* 24 (2): 15–23.
- Tsunoda, E., H. Mimuro, S. Hisa, et al. 1989. Torsional vibration evaluation technique for large-capacity steam turbines. *Proceedings of the American Power Conference* 51: 109–114.
- Virchenko, M. A., E. V. Levchenko, B. A. Arkad’ev, et al. 1997. Corrosion fatigue of rotating blades. *Thermal Engineering* 44 (6): 464–468.

- Weschenfelder, K. D., H. Oeynhausen, D. Bergman, et al. 1994. Turbine steam path replacement at the Grafenrheinfeld nuclear power station. *Proceedings of the American Power Conference* 56: 1522-1529.
- Wesselmann, C. 2003. Nuclear power production (in German). *Brennstoff-Wärme-Kraft (BWK)* 55 (6): 40-47.
- Yamamori, T., T. Ichikawa, S. Kawaguchi, and H. Honma. 2000. Recent technologies in nuclear power plant supervisory and control systems. *Hitachi Review* 49 (2): 61-65.

## 5

# Refurbishment

## Retrofitting Versus Repairing

Omitting so-called corrective (or, as it is sometimes termed, reactive) maintenance necessarily carried out in cases of sudden failures, the most conventional practice of maintaining large power steam turbines is their *preventive maintenance* (PM), which includes regular, previously scheduled inspections, repairs, overhauls, and replacements. The goal of PM is to reveal accumulated damages, remove them and their consequences, and provide reliable operation until the next scheduled inspections and repairs. It is also intended to restore the turbine efficiency deteriorated in the course of previous operation.

In recent years in the power industry, there have also been increasingly frequent appeals for a transition from traditional PM to so-called *predictive maintenance* (PdM), also known as condition-oriented maintenance (COM), reliability-centered maintenance (RCM), and efficiency-oriented maintenance (EOM). With PdM, the operated equipment is stopped for repairs not on a regular calendar basis, as with PM, but only if the equipment condition has significantly changed for the worse, and further operation is either dangerous in terms of reliability or unprofitable in terms of efficiency.<sup>1</sup>

This kind of maintenance, which is presently applied more and more frequently in different fields of industry, is based on the intense use of technical diagnostics, continuous monitoring, and analysis of stored operating performance data. All of these measures should provide a possibility of continually evaluating current equipment condition and its changes during the operation process and revealing any imminent failure at a very early stage. The more complicated the operated equipment is and the more factors influence its condition, the more problematical and responsible is a transition from PM to PdM. The problem is that the employed diagnostic means should reliably provide early detection of any possible serious fault or approaching failure. An essential prerequisite for the development and possible application of this maintenance technology is the knowledge of all the vulnerable points with regard to possible defects and failures, and the capability of noticing them in the inspected data. In other words, the considered equipment should be completely diagnosable. If any factor that could potentially produce dangerous changes in the equipment condition cannot be monitored, and the corresponding equipment condition changes have a chance to remain unnoticed, such equipment cannot be considered ready for COM, and any attempt of transition to this technology can have possibly dangerous or at least undesirable consequences. Currently, large power steam turbines cannot be said to completely meet the requirements of their diagnosability.<sup>2</sup> That is why even though PdM has already been successfully used for some relatively simple kinds of power equipment, as applied to large power steam turbines, this transition to PdM seems somewhat premature. It should be also pointed out that under actual conditions of operating power systems, shutdowns of large power capacities should be planned in advance to avoid substantial financial losses.

All of these circumstances refer in full measure to wet-steam turbines of nuclear power plants. In addition, because light-water reactors of nuclear power plants need to be regularly stopped for refueling, these outages are commonly used for inspecting and repairing the turbines, so the PM technology might be considered as if inherent in them. Along with this, if some of the turbine components are really furnished with representative means of technical diagnostics, and if operators have a possibility to evaluate the current condition of these components and forecast their state until the next scheduled refueling, there is no necessity for special examinations and repairs of these components during each outage. With regard to these possibilities

and because of different vulnerability and different susceptibility to damages, different wet-steam turbine components (for example, the HP and LP cylinders, MSR, and so on) can have different PM cycles. The most vulnerable components of wet-steam turbines are, as a rule, the LP cylinders and their rotating parts, which are subjected to the greatest degree to WDE and SCC. Methods for revealing and repairing these damages in the turbine steam paths are considered in detail in other publications,<sup>3</sup> and their consideration is beyond the scope of this book.

Repairs are aimed at returning the turbine to its initial conditions whenever possible, without any serious alternatives to its original design decisions. If the turbine was damaged, the repair actions, as a rule, do not eliminate the source(s) of the damages, but rather eradicate the damages themselves. Even if it is necessary to remove irreversibly damaged parts, the proposed design alterations commonly are not beyond the initial design concept. The maintenance of wet-steam turbines is managed so that as many of the repair actions as possible are accomplished while refueling the reactor, within the available time window, to avoid extra power generation losses. Steady efforts to reduce duration of the refueling outages make the turbine repairs more intense, so they commonly take approximately two to three weeks to perform.

Repairs are always somewhat palliative in nature. A typical example is the experience of repairing the LP rotors of three 1,350-MW wet-steam turbines at the Palo Verde Nuclear Generating Station in Arizona.<sup>4</sup> The turbines were manufactured by GE and commissioned in the mid-1980s. They are low-speed (1,800 rpm) four-cylinder machines with one double-flow HP cylinder and three double-flow LP cylinders, with LSB length of 1,093 mm, or 43 in (TC6F-43). The LP rotors are made with shrunk-on disks and rotating blades mounted on the periphery of the disks with dovetail attachments. In 1995, after approximately 50,000 operating hours, intergranular stress corrosion cracking was detected on the wheel disks of the third and fourth from the exhaust LP stages (L-2 and L-3) near the tangential entrance notches. This area is subjected to the highest stress, because the centrifugal load of the locking blade is additionally transferred to the adjacent blades through the axially mounted crosskeys. The mentioned stages are also most susceptible to crack initiation, because they work in the zone of thermodynamic transition from superheated to

saturated steam, with unfavorable steam temperatures. What is more, the stage design features allow steam contaminants to be trapped in crevices, promoting SCC. Repair welding of turbine wheels with dovetail cracking is a common and successful solution for forged rotors. However, any experience of such welding for shrunk-on disks, even though theoretically feasible, has been absent, at least at U.S. nuclear power plants. In addition, the current welding technology would not allow for the completion of the weld operations within the refueling window, and the removal and reinstallation of the wheel disks were shown to be both cost and time prohibitive. Complete removal of the rotating blades in the damaged stages might be another possible solution; however, it would result in reduction of the turbine output by as much as 25–35 MW per stage.

An alternative was found in a process known as *longshanking*. It involves re-machining new dovetail blade attachments for the existing disks. After all of the damaged material and all of the crack indications are removed, the new dovetails are machined at a lower radius on the wheel. New blades are manufactured, featuring an extra long shank between the blade root and the blade airfoil section. The shank serves to raise the airfoil of the rotating blades (that is, their working portion) back to their original radial position in the steam path. In October 2000, longshanking was performed on one LP rotor at Palo Verde. Successful completion of this operation within a 15-day window met the station goals of returning the safe rotor to service without impacting the outage schedule and losing power generation. A disadvantage of longshanking is the higher stress caused by the longer blades, but enhancements to the dovetail profile combined with the use of individual titanium blades in some selected locations helped to minimize this adverse impact. The repair was preceded by thorough strength and vibration calculations for the repaired stages, accompanied by a new nondestructive test procedure. According to GE and EPRI, this procedure allowed the detection of crack indications with greater accuracy compared to previous technologies and helped to determine the critical flaw size with more certainty. The remaining life of the rest of the cracked rotors was assessed with the use of a special calculation program developed by EPRI. In the following two years, the remaining eight LP rotors at Palo Verde were subjected to the same repair. Afterward, the LP cylinders of all three turbines were retrofitted, and all of the nine LP rotors that had been previously repaired were replaced with new mono-block rotors manufactured by GE. The first three repaired LP rotors were replaced with solid rotors in the summer of 2003.

Steam turbine repairs can include improvements in the steam path to raise the turbine efficiency by decreasing or eliminating some energy losses. However, these alterations mainly refer to rather particular improvements as, for example, optimizing the correlation of clearances in the steam path, improving the design of seal glands and water traps, and so on. According to Turboatom, optimization of the axial clearances between the fixed and rotating blades of HP stages of wet-steam turbines in service enables the stage efficiency to be increased by approximately 0.8–1.0%.<sup>5</sup> At best, the repairs can include the replacement of blading for individual stages with the use of more advanced profiles, or even involve such serious alterations as transition from nozzle group to throttle control (as was done by Turboatom for all their K-220-44 turbines of early vintages). Nevertheless, after repairing the turbine, all of the main design features of its generation are kept.

In contrast to repairs, refurbishing, or retrofitting, more radical, more fundamental changes of the turbine design are made with replacement of all of the entire large turbine components, as for example, individual cylinders. It might be well to note once more that wet-steam turbines with their moderate initial steam parameters are not prone to high-temperature effects like creep, and, in addition, because they are operated predominantly in a base-load mode, they suffer less from low-cycle (thermal) fatigue. Because of this, for wet-steam turbines, longevity problems are not as important as they are for high-temperature steam turbines of fossil fuel power plants. The lifetime of nuclear power units is mainly determined by reactors, rather than by turbines, and thus the refurbishment of wet-steam turbines pursues the goal of extending their lifetime to a lesser degree. Nevertheless, refurbishing wet-steam turbines becomes especially topical with aging nuclear power plants and the necessity to make decisions about their further fate. For example, by 2000, 11 out of 28 Japanese nuclear power units with BWR-type reactors and nine units with PWRs had been operating for 20 years or more, and these numbers will almost double by 2010.<sup>6</sup> Along with advanced inspections and diagnosis for the reactors, replacing individual equipment components, and renewing the data acquisition and control systems, refurbishment of the turbines is also an important issue in these cases. The service time of wet-steam turbines is primarily determined by the lifetime of their rotors. Experience with large superheated-steam turbines of fossil fuel power plants, as well as special investigations for wet-steam turbines, has proved that the current condition and remaining lifetime

of both HP and LP rotors of different types can be reliably estimated based on existing ultrasonic techniques.<sup>7</sup> Replacing the turbine rotors while refurbishing the turbines postpones any replacement decision on it for years, and perhaps for the lifetime of the unit.

The problem of aging nuclear power plants is topical for many countries: as of January 2001, 156 reactors in the world had operated for 20 years or more, and by 2011 that number will increase to 376,<sup>8</sup> and owners and operators of nuclear power plants directly face the problem of refurbishing wet-steam turbines while relicensing or restarting their nuclear power units.

In the first place, turbine refurbishment is aimed mainly at decisive solutions to the most topical problems of reliability (for example, SCC of LP rotors) based on new approaches, compared to the initially accepted design concepts. Along with this, retrofitting commonly involves increasing the turbine efficiency to a greater degree than is possible with the use of some particular measures characteristic for repairs and thus increasing the output of the nuclear power unit without even enlarging the reactor capacity. An increase in the output (or efficiency) itself can also be a target of a turbine refurbishment. Moreover, in many cases, the focus of retrofitting moves to this goal from the aim of increasing the turbine's mechanical integrity, strength, and longevity, which is rather paramount for fossil fuel power plants. Modern advanced 3-D computer-based CFD approaches make it possible to greatly increase the internal turbine efficiency and avoid energy losses inherent in older wet-steam turbines that were designed and produced in the 1970s and 1980s, but such retrofitting requires quite noticeable changes in the turbine steam path configuration.

Because of the limited duration of refueling outages used for refurbishment, it is advisable to retrofit "nuclear" turbines gradually, step-by-step, i.e., refurbishing only individual sections or cylinders in each outage. The optimal strategy consists in determining the parts that most need refurbishment (or whose refurbishment will provide the most considerable gain in the turbine output or efficiency) and retrofitting these parts first. So the LP cylinders of wet-steam turbines are usually retrofitted before the HP cylinders.

As a rule, large steam turbines were traditionally refurbished by their original equipment manufacturers (OEMs). The situation has changed sharply in recent years, and refurbishment of steam turbines in service is now as important a field of activity for turbine manufacturers as is production of new turbines. Mergers of many former wet-steam turbine manufacturers and the redistribution of their spheres of influence in the world power market open wide possibilities for the use of new design approaches that can be alien even to the OEM. If an early retrofitting experience has focused mainly on the elimination of long-standing reliability concerns, usually for LP rotors, later this experience has been broadened. The deregulation of electricity generation markets provided financial incentives for power plant owners and operators to maximize the economic competitiveness of their steam turbines in service and to raise their availability and efficiency using new approaches that had not necessarily been offered by the OEMs.<sup>9</sup> According to data presented at the Nuclear Plant Performance Improvement Seminar, held in the United States in 1996, out of 110 U.S. nuclear power units surveyed, 33% of their 290 LP rotors had been retrofitted, including 18% of 119 rotors on turbines supplied by Westinghouse and 35% of 150 rotors supplied by GE.<sup>10</sup> The retrofits were mostly done to avoid the losses associated with turbine unreliability, rather than to improve the turbine efficiency. In other words, the prospects of minimizing the outage time by replacing existing rotors with more reliable ones offset the expenditures for retrofitting more than any potential gains in performances. In these cases, ABB and Siemens, foreign manufacturers that had originally delivered only four wet-steam turbines for U.S. nuclear power plants, were actively involved in retrofitting turbines originally produced by U.S. manufacturers. The most widespread reason for the retrofitting was SCC of the LP rotors, their wheel disk attachments, bores, and keyways. Similar trends took place in other countries, too. Over time, the situation has somewhat changed, and, more often than not, retrofitting wet-steam turbines is presently performed in order to achieve increases in the efficiency and power output more than to eliminate losses caused by unreliability.

# Retrofitting LP Cylinders

## Replacing disk-type rotors with welded ones (experience of ALSTOM)

One of possible radical ways to solve the problem of SCC for LP rotors with shrunk-on disks (combined or disk-type rotors) is their replacement with rotors manufactured from forged disks welded together (welded rotors), as shown in Figure 5-1. Due to the inherent features of such rotors, they are not usually subjected to SCC. Because of the absence of a center bore, these rotors typically exhibit much lower stress levels compared to shrunk-on disks, all other things being the same. As a result, welded rotors can be made of materials with lower yield strength, which are less prone to SCC. And even with regard to the lower yield strength, the major stresses in these rotors can be kept below 50% of the yield limit, which significantly reduces the probability of SCC occurring. It is also important that the highest stress areas are not in contact with steam and its impurities.

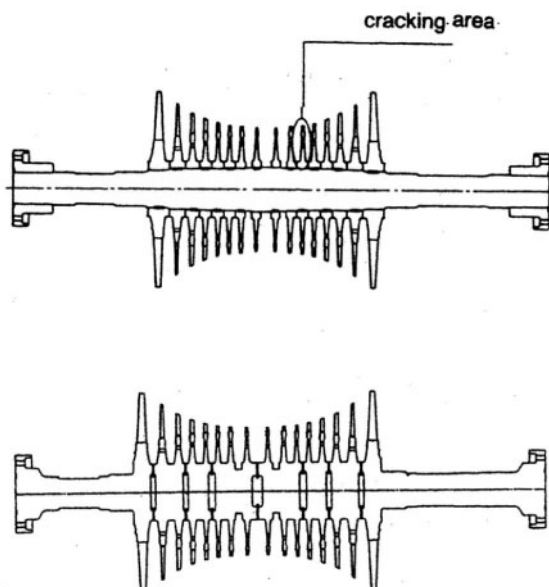


**Fig. 5-1.** Replacement of an LP rotor with shrunk-on disks (a) with a welded rotor (b)

Source: J. Pizzica, J.-E. Bertilsson, and E. Thommen<sup>11</sup>

The replacement of existing disk-type LP rotors with welded rotors has been proposed by ABB for wet-steam turbines produced by different OEMs and operated at nuclear power plants throughout the world. Therewith, welded rotors have been successfully used by ABB (later ALSTOM) in large steam turbines for nuclear and fossil fuel plants for decades.<sup>12</sup> In particular, such replacements were accomplished for 12 identical and interchangeable LP rotors at Dresden Units 2 and 3 (each with a capacity of 794 MW) and Quad Cities Units 1 and 2 of (789 MW each) in the United States.<sup>13</sup> Because the LP casings and stationary blades were not changed, the rotating blade profiles and clearances were chosen to match those of the stationary parts, and the LP steam paths remained practically unchanged. Similar retrofits of LP cylinders were done in the mid-1980s at two 1,200-MW turbines at San Onofre, two 1,040-MW turbines at Zion, and at some other U.S. nuclear power plants.<sup>14</sup> It was specially emphasized that the retrofit at Zion was accomplished during a regular 14-week outage.

Along with other features, welded rotors are more rigid than those with shrunk-on disks. As a result, the static deflection at the supports of the turbine with welded rotors is approximately half that of rotors with shrunk-on disks, and the curvature of the turbine shaft-line should be modified. The corresponding change in the static shaft-line curvature as applied to GEC-Alsthom's 900-MW turbines is shown in Figure 5-2.

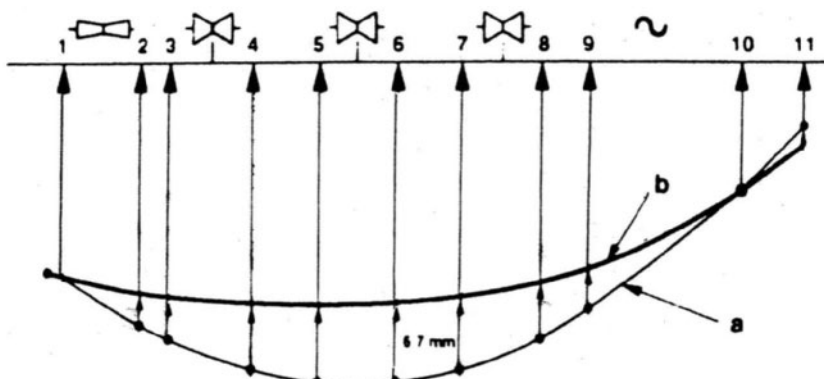


**Fig. 5-2.** Change in the static shaft-line curvature due to replacement of LP disk-type rotors (a) with welded ones (b) (The numbers denote the turbine bearings)

Source: P.Aubry, B.Billerey, and J.P.Goffin<sup>15</sup>

The original LP rotors were replaced by welded ones on 24 GEC Alsthom 900-MW turbines for the first French PWR program (CPO-CP), as well as similar turbines supplied to nuclear power units in Belgium (Tihange Unit 2 and Doel Unit 3) and South Africa (two units of Koeberg).<sup>16</sup> Replacement of the LP rotors changed the duration of the turbine start-ups, especially cold start-ups (Fig. 5-3). For rotors with shrunk-on disks, if the steam temperature at the LP cylinder entrance (after the MSR) is not controlled, a rapid increase in the metal temperature of the disks and the resultant high tensile thermal stress on the disk bore surfaces can unshrink the disks, and the turbine should be loaded slower to make the heat transfer from steam to the LP rotor metal less intense. With welded LP rotors, this problem does not exist, and the rate of loading can be increased. According to the manufacturer's instructions, the total duration of a cold start-up for a 900-MW turbine is reduced from 6 hours to 3 hours and 40 minutes. In addition, after replacement, it is no longer required to turn on the turbine during at least 6 hours to reduce the risk of damages caused by alternating bending stresses in the shaft in the course of running-up the turbine. Due to their greater rigidity, welded rotors are also less prone to torsional oscillation problems. According to ABB, successful operation experience of turbines with retrofitted LP cylinders allows customers to extend the interval between major inspections with opening the cylinders up to 10-12 years.<sup>17</sup>

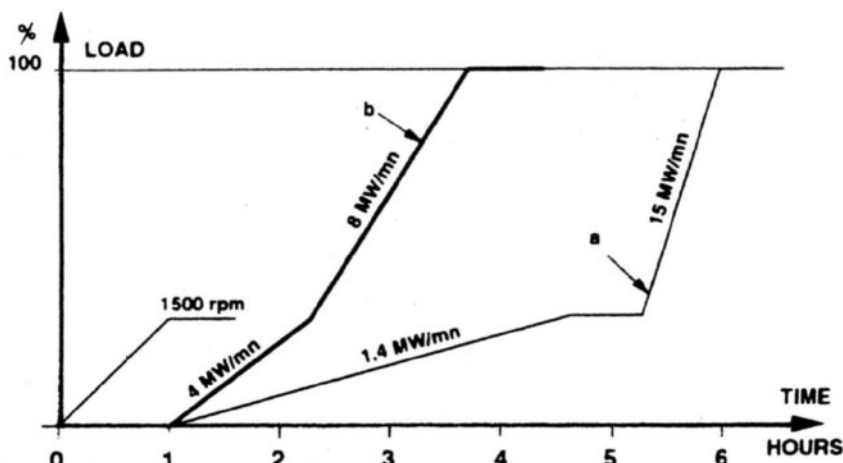


**Fig. 5-3.** Change of a cold start-up diagram for ALSTOM's 900-MW wet-steam turbine after replacement of disk-type LP rotors (a) with welded rotors (b)  
Source: P.Aubry, B.Billerey, and J.P.Goffin<sup>18</sup>

In some instances, replacement of the LP rotors was accompanied with refurbishment of the LP exhaust diffusers and hoods, which allowed a reduction in the exhaust losses. Today, very complicated flow patterns in the turbine exit can be resolved in detail using modern 3-D CFD tools that enable designers to predict and optimize diffuser and hood performances for a given application range to a much greater degree than was possible even few years ago. This type of refurbishment was performed by ABB on two 1,040-MW turbines at the Zion nuclear power plant, and resulted in an increase in the efficiency and output of 1.67%, that is, approximately 17 MW.<sup>19</sup> Similar improvements to the exhaust hood, without refurbishment of the steam path, were accomplished at two 1,120-MW turbines at the San Onofre plant, with a resultant increase in the output of approximately 5 MW for 18 months preceding the main steam path retrofit.<sup>20</sup>

In some other cases, ABB performed more complete refurbishments of LP cylinders by changing the steam path outline from a piecewise linear shape to a conical peripheral shape and increasing the steam exhaust annular area due to the use of longer LSBs (Fig. 5-4). According to bench tests of ABB, only the transition to a conical flow path outline gives an efficiency gain of approximately 2%.<sup>21</sup> For the Swiss nuclear power plant Leibstadt's 1054-MW turbine, its retrofit fulfilled in 1994 after 74,000 hours of service produced an increase in output of 46 MW. A similar retrofit of the steam turbine's LP cylinders at Finnish Olkiluoto Unit 1 (the gross capacity of 735 MW) after 17 years of trouble-free operation resulted in the power output increase of 36 MW, that is, almost 5%.<sup>22</sup> This value was obtained from the series of heat-rate performance tests: a baseline test carried out prior to any changes being made, an intermediate test after the refurbishment of LP3 and LP4 cylinders, and a final, verification test carried out after the replacements in LP1 and LP2 cylinders. Complete heat-rate performance tests according to ASME's PTC 6/6.1, at Taiwan's Maanshan nuclear power plant with two 950-MW turbines yielded the output increases of 12.17 MW and 12.11 MW.<sup>23</sup>

An additional gain can be achieved with the use of 3-D curved and inclined vanes in the last stage with modern blading profiles, as in Figure 3-58, and, on occasion, a scroll-type steam inlet with radial-axial first stages (Fig. 5-5).<sup>24</sup>

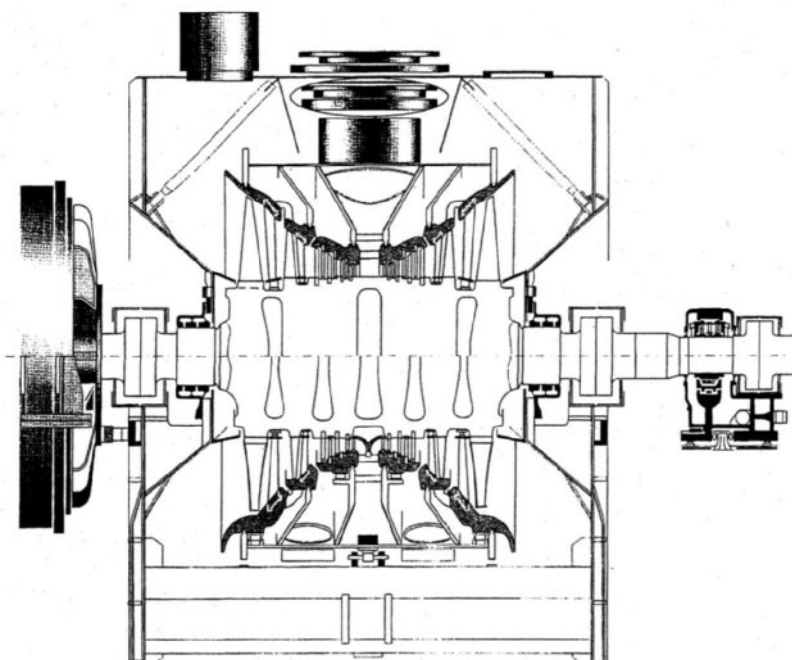


**Fig. 5-4.** Refurbishment of the LP cylinder of an ABB wet-steam turbine for efficiency improvement (top: improved design; bottom: original version)  
Source: E. Krämer, N. Lannefors, and B. Scarlin<sup>25</sup>

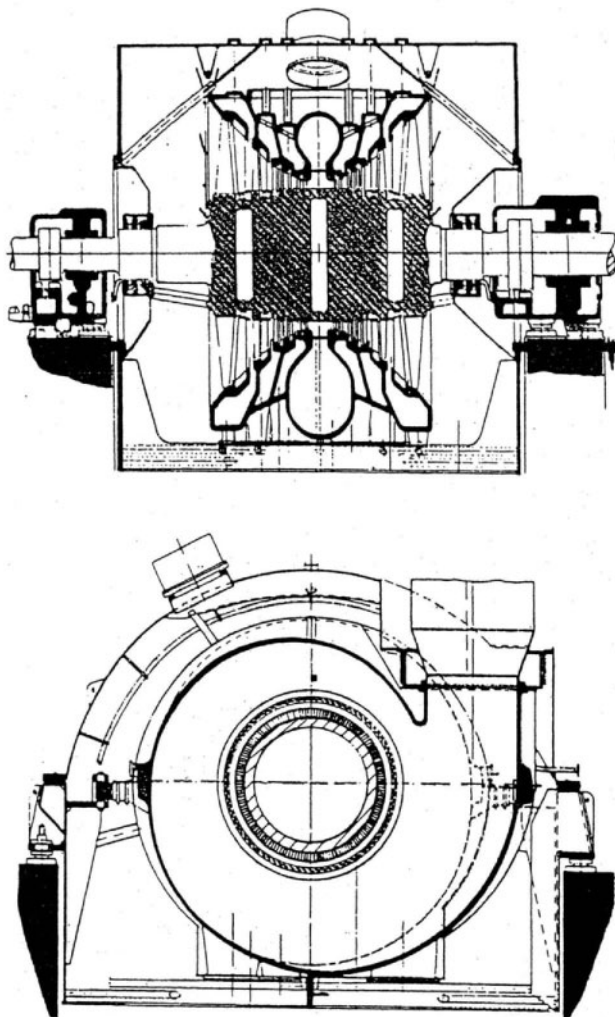


**Fig. 5-5.** Longitudinal and cross sections of ABB's LP cylinder with a scroll type steam inlet

Source: J. Bütkofer, M. Händler, and U. Wieland<sup>26</sup>

## Replacing LP disk-type rotors with solid ones (experience of Westinghouse)

An alternative to replacing LP disk-type rotors prone to SCC with welded rotors is the use of monoblock rotors (solid forged rotors without a central bore). The absence of a central bore (as with welded rotors) considerably reduces the level of maximum centrifugal stresses in the rotor, and the absence of separate disks with their bore surfaces and keyways eliminates the danger of cracking in these areas. Lower maximum stresses allow the use of more corrosion- and erosion-resistant materials for the rotors.

As mentioned above, GE replaced the repaired disk-type LP rotors with monoblock rotors on the 1,350-MW turbines at Palo Verde. As well, MHI replaced the original disk-type rotors with monoblock rotors on Westinghouse's 566-MW low-speed turbine (TC4F-44) at Japanese Ikata Unit 2. In turn, Westinghouse accumulated its own experience in manufacturing monoblock LP rotors for large steam turbines, including low-speed rotors, and retrofitting LP cylinders with the use of such rotors. So, for example, six LP rotors were replaced by Westinghouse on two 400-MW turbines originally produced by English Electric at the Swedish nuclear power unit Ringhals with a double-turbine configuration (Fig. 5-6).<sup>27</sup>

In 1986, Westinghouse introduced a new design concept, called a *ruggedized LP turbine*, especially for retrofit applications.<sup>28</sup> This design approach was originally conceived to improve turbine reliability by means of avoiding primarily SCC problems. However, the application of modern technologies in designing blade paths more efficiently, reducing exhaust and leakage losses, and a significant increase in the annular exit area have provided considerable performance improvement in addition to improved reliability. The ruggedized concept is characterized by the use of solid LP rotors with no central bore, freestanding LSBs, and integrally shrouded blades in the upstream rows. A typical ruggedized LP cylinder design with a 1,194-mm (47-in) freestanding LSB for retrofitting low-speed (1,800 rpm) wet-steam nuclear turbines is shown in Figure 5-7. The design decisions employed in this case provide greater resistance to SCC in the rotor attachment area because of the improved side-entry blade root design, which features lower peak stresses. The developed LSBs are intended to replace the original 44-in and 45-in LSBs in retrofit applications, offering improved efficiency due

to their longer length and hence greater annular exhaust area, optimized profiling, and an advanced exhaust flow guide design. These LSBs also provide the turbine's improved operational flexibility at low loads and high back pressure due to better airfoil design and increased structural stiffeners. The steam path has an enhanced resistance to moisture erosion because of increased axial spacing and improved wraparound Stellite strips. Some improved resistance to the blading WDE also came from the use of moisture trap grooves, moisture drainage slots in the honeycomb seals, and specially designed moisture drainage slot holes in the inner casing structure.

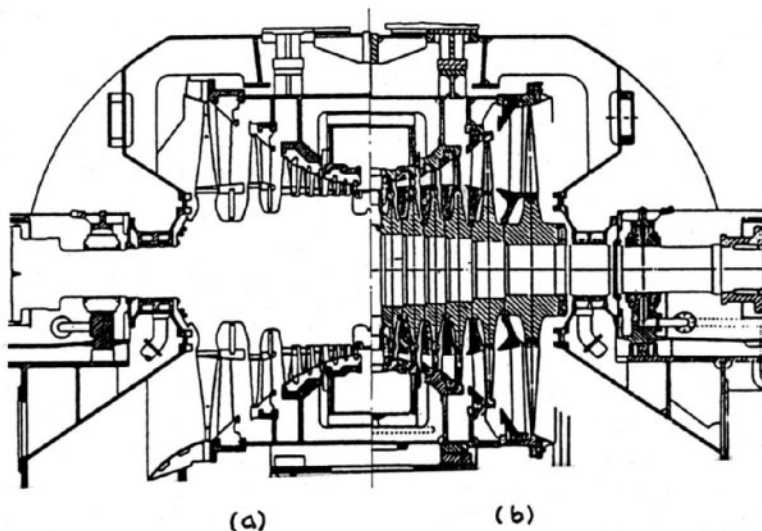


**Fig. 5–6.** LP cylinder of a low-speed turbine after (a) and before (b) retrofitting by Westinghouse

Source: J. C. Groenendaal, L. G. Fowls, R. Subbiah, et al.<sup>29</sup>

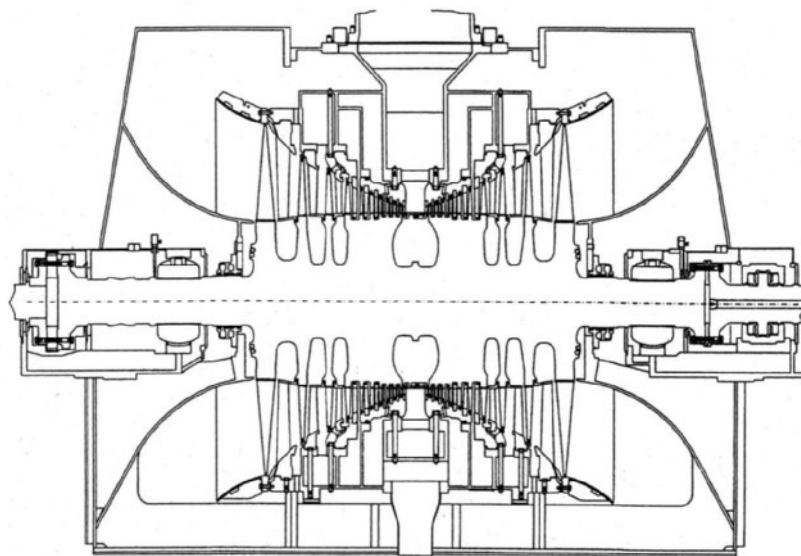


**Fig. 5-7.** Ruggedized LP cylinder of Westinghouse for retrofitting nuclear steam turbines

Source: E.P. Cramer, J.A. Moreci, C.W. Camp, et al.<sup>30</sup>

A ruggedized LP design was used to retrofit the 1,154-MW low-speed four-cylinder turbine (one double-flow HP cylinder and three LP cylinders) at the U.S. BWR-type Columbia nuclear power unit put into commercial operation in 1984. Originally, the turbine was delivered with disk-type LP rotors. During the second yearly refueling outage in April 1987, a single instance of a smallest detectable size crack initiation in a disk keyway was found on one of the LP rotors in the process of their first inspection. This entailed a decision to replace and retrofit all of the turbine's LP rotors, and the proposal of Westinghouse was chosen as the best overall technical solution with regard to a cost/benefit analysis of the warranty, the guaranteed amount of the input increase, the required duration of the retrofit, and the recommended frequency of following inspections. The output increase was guaranteed to be 15.5 MW. Heat-rate tests of the unit proved the load improvement of 22.9 MW at the reactor's rated thermal level, that is, exceeding the contract guarantee by 7.4 MW.<sup>31</sup>

Another example is the upgrading of Prairie Island Units 1 and 2, with the net outputs of 530 MW each, and Point Beach Units 1 and 2, with the net outputs of 500 MW each. These units have essentially identical low-speed turbines consisting of one HP cylinder and two LP cylinders. The retrofit at the Prairie Island Unit 1 turbine took 28 days, with the contract outage window of 35 days. The pre- and post-heat-rate tests showed an increase in turbine efficiency and output of 2.7% that is, by approximately 0.5% above the guaranteed gain.<sup>32</sup>

### Retrofitting LP cylinders with disk-type rotors (experience of Siemens)

For large, high-speed (3,000 and 3,600 rpm) steam turbines for both fossil fuel and nuclear power plants, Siemens uses monoblock LP rotors (see Fig. 3-7), and LP rotors with shrunk-on disks are employed only for low-speed (1,500 and 1,800 rpm) nuclear turbines (see Fig. 3-8). Due to careful design decisions and proper choice of disk material and its heat treatment, Siemens' disk-type LP rotors practically do not suffer from SCC. There was only one case of SCC found among 310 disks of Siemens wet-steam turbines inspected at nuclear power plants by the late 1980s,<sup>33</sup> whereas similar disk-type LP rotors made by other turbine manufacturers were greatly affected by SCC. That is why Siemens' developments of advanced LP cylinders, first, have relied on the well-proven concept of disk-type rotors for low-speed turbines and, second, have been aimed primarily at increasing turbine efficiency. These developments were intended particularly for retrofitting aging wet-steam turbines in service, and thus assumed replacement of both the LP rotors and inner casings to improve the steam path. Along with this, serious attention was paid to supporting the high reliability of the LP rotors and their high resistance to SCC. Siemens' advanced LP rotor designs were developed to be fully competitive with any monoblock or other rotor designs.

Siemens' original 10-disk rotor, which had been used since 1987, was redesigned for the eight-disk rotor, and then, in 1995, for the six-disk rotor, as shown in Figure 5-8. The disk forgings are thermally treated to provide the yield strength and fracture toughness levels well below the threshold values, so that even if SCC commenced, its rate would be small enough to reach the critical crack size for the time period significantly exceeding the

turbine's lifetime. Because of the relatively wide disk forgings, a special treatment is applied to form compressive stresses at the disk surfaces, including the blade attachments, that increases the margin against potential SCC initiation (see Fig. 4-33).<sup>34</sup>

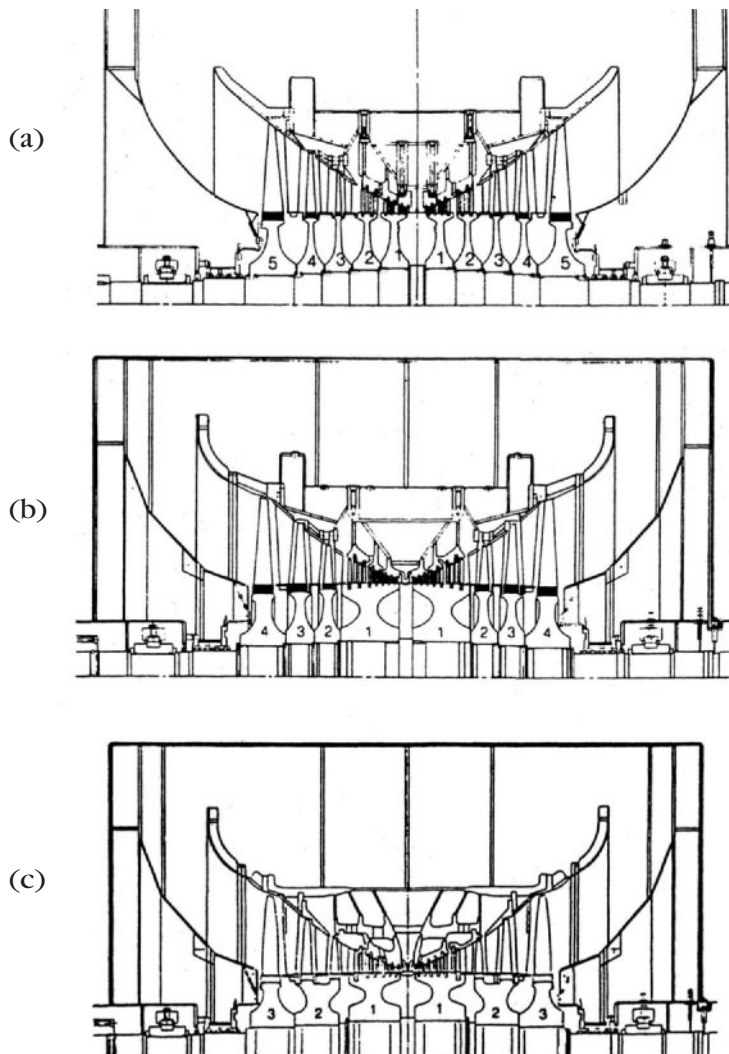


**Fig. 5-8.** Improvements of the LP cylinder design for Siemens' low-speed wet-steam turbines (from a ten-disk rotor to a six-disk rotor)  
Source: By courtesy of Siemens

The advanced LP steam path includes improved, integrally shrouded blading for the first LP rows, increasing the stage group efficiency by approximately 1.0–1.5%. The improved performance is achieved owing to, in particular, a continuous curvature of the blade profile's suction side, resulting in minimum velocity reduction and avoidance of flow separation. The blunt nose makes the profile immune to changes in the incident flow angle, and the narrow trailing edges minimize the exit losses. Another improvement in performance is achieved by utilizing double-strip interstage seals for the stationary and rotating blades, as shown in Figure 3-22b. These interstage seals minimize leakage losses, but allow relative axial expansion between the rotating and stationary components. A leakage flow reduction of up to 50% is expected as compared with previous designs. In order to achieve the speed ratio nearer to the optimum value, an extra stage is added to each flow, and this improves the stage group efficiency by approximately 1.5%. The internal efficiency of the last three stages has been proven to be as much as 7% better than that of the previously employed stages. The better stage efficiency is achieved with a relatively low reaction at the outer diameter to reduce the exhaust losses at the blade tip and a slight increase in the low reaction at the hub section to avoid flow separation at the blade root. This improvement in the last stage blading, with local transonic velocities and high supersonic exhaust velocities, resulted in the development of tapered and forward-curved, tangentially inclined stationary blades. In the outlet area, where the steam flow exits the optimized diffusers downstream of the last stages, flow baffles were positioned in the upper center of the enclosure and underneath the lower part of the diffusers to reduce vortices in the outflowing steam. The improved outflow to the condenser also reduces the local pressure drop. Steam stream lines with and without baffles are compared in Figure 5-9. This improvement was combined with an increase in the size of the inflow cross-section to even out the inlet steam flow along the steam admission arc. This resulted in an estimated increase in the turbine output of approximately 3 MW. The total results of retrofitting LP cylinders on Siemens turbines at various power plants are presented in Table 4-4.<sup>35</sup>

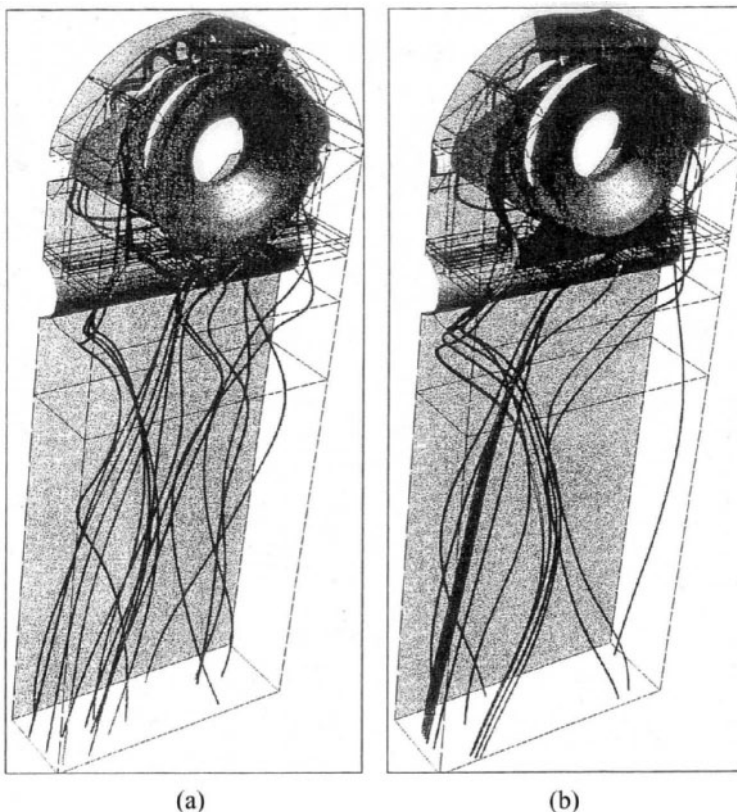


**Fig. 5-9.** Steam stream lines in the outflow to the condenser for old (a) and improved (b) Siemens turbine designs

Source: H. Oeynhausen, H.-P. Classen, and J. Riehl<sup>36</sup>

According to the heat-rate test conducted at the 1,300-MW Unterweser nuclear power unit, the initial gross efficiency of the turbine-generator was 35.01%; measurements before the retrofit (pre-test) gave the value of 35.11%, and after retrofitting one of three LP cylinders (post-test) the net efficiency value was 35.6%, with the gross output at the generator terminals equal to 1,310.8 MW. Estimations allow assessing the gross efficiency of the turbine after retrofitting all the three LP cylinders as equal to 36.56%.<sup>37</sup>

Special considerations were taken and studies performed to make sure that all of the LP cylinder's inner components could be easily replaced during the annual refueling outage. As a result, the

replacement of the LP rotor and inner casing at the Unterweser plant was accomplished within the preapproved scheduled period of one month,<sup>38</sup> but similar works at the German nuclear power plant Emsland took only 15.5 days.<sup>39</sup>

## Complete Upgrading of Turbines Including Both HP and LP Cylinders

The upgrading of wet-steam turbines at nuclear power plants mostly focuses on the refurbishment of LP cylinders, because they provide the largest part of the turbine output and are the turbine's most vulnerable components. It can be said that their reliability determines the turbine availability more than any other component does. Along with this, as most paramount problems with the LP cylinders are solved, more attention is paid to retrofitting the HP cylinders. This is mainly tied with significant advances in the design of HP blading achieved in recent years. Upgrading the HP steam path with blading of modern design provides an additional substantial increase in the power output, with a relatively short payback period.<sup>40</sup> If possible, the HP cylinder is retrofitted in parallel with retrofits of the LP cylinders during the same turbine outage; otherwise, it is commonly performed later, during the next outage.

### Upgrade experience of Siemens

After the successful refurbishment of the LP cylinders at several German nuclear power units, as discussed above, a more complete upgrading with the retrofit of both the HP and LP cylinders was undertaken at the German nuclear power plants Grafenrheinfeld and Gundremmingen, both with low-speed (1,500 rpm) 1,300-MW turbines.<sup>41</sup> The turbines include one double-flow HP cylinder and two LP cylinders, with 1,365-mm ( $\approx$ 54-in) LSBs.

A comparison of the previous and advanced HP cylinder designs can be seen in Figure 5-10. To improve the velocity ratio, the first stage is changed from a traditional 50% reaction-type blading to an impulse-type stage with tilted stationary blades (Fig. 5-10c).

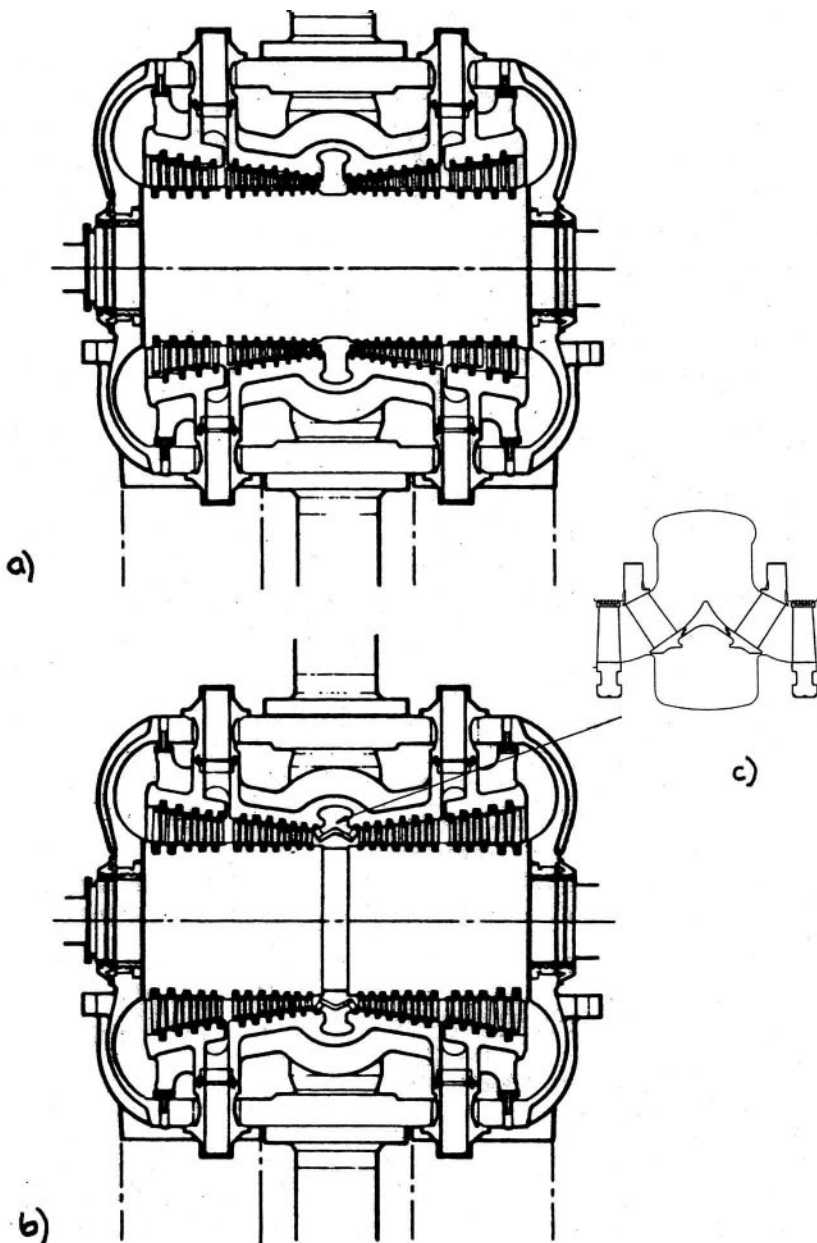


**Fig. 5-10.** Comparison of previous (a) and advanced (b) HP cylinders for retrofitted Siemens wet-steam turbines; steam inlet segment (c)  
Source: K. D. Weschenfelder, H. Oeynhausen, D. Bergman, et al.<sup>42</sup>

An inlet steam guide ring is added to optimize flow conditioning and eliminate any leakage losses around the first stage. An enhanced reaction profile is employed for the cylindrical intermediate stages. The leading edge, with a large radius of curvature characteristic for this profile, makes it relatively insusceptible to changes in the angle of the steam flow approach, and the slender trailing edge reduces the losses induced by trailing-edge wakes. Twisted integrally shrouded blades are used at the exhaust ends, considerably reducing the profile and secondary-flow losses. The interstage seal system features a larger number of labyrinth seal strips (see Fig. 3-22a). The inner casing's exhaust configuration is modified to optimize the diffuser section. On the basis of all these improvements, an increase in the HP section efficiency of approximately 3% is expected.

At the Grafenrheinfeld nuclear power unit, the entire refurbishment, including the replacement of all three rotors and inner casings (in the HP and two LP cylinders) was performed during the regular refueling outage from May 29 to July 7, 1993, taking five-and-a-half weeks. The heat-rate test results showed an increase in the power output from 1,305.8 MW to 1,365.2 MW, that is, by 59.4 MW, or 4.5%. After applying all of the correction factors (especially the correction for the back pressure), the performance improvement was determined to be 45.3 MW, whereas the guaranteed figures were assessed equal to 7.8 MW for the HP cylinder and 32.6 MW for the two LP cylinders (an aggregate 40.4 MW). Even better results were achieved at the Gundremmingen nuclear power unit (see Table 4-4).<sup>43</sup>

If Siemens' original upgrade projects referred to their own turbines, later Siemens also accomplished the complete refurbishment of several turbines (both their HP and LP sections) produced by other manufacturers. One of the best known projects was the retrofit of two 1,160-MW low-speed (1,800 rpm) turbines at the U.S. nuclear power plant Limerick with BWR-type reactors.<sup>44</sup> The original turbines were produced by GE and comprised one double-flow HP cylinder and three double-flow LP cylinders with disk-type rotors, 966-mm (38-in) LSBs, and steam flowing down into a multi-pressure condenser. The OEM's LP rotors and inner casings were replaced because of SCC on the shrunk-on disks and severe crevice corrosion of the LP casings and diaphragms. The HP steam path was retrofitted only from considerations of efficiency improvement.

The new HP cylinder is very similar to that shown in Figure 5-10b, with a mono-block rotor and 12 stages per flow. The first stage is of an impulse type with tilted stationary blades. Both ends of the rotor forging are made with a deposit of corrosion-resistant weld overlay in the shaft seal area. All of the HP stages are designed fully three-dimensional, tapered, and twisted (3DST<sup>TM</sup>), with integrally shrouded blades. The new HP inner casing is made of stainless steel to avoid erosion-corrosion problems. The original HP outer casing of the OEM required in-place modifications to accept the new components, and special inlet L-seals were installed to provide sealing between the inner and outer casings.

For this project, Siemens used its six-disk version of the LP rotor with freestanding 1,170-mm (46-in) LSBs, which provided an annular exhaust area of 13.4 m<sup>2</sup> (144.2 ft<sup>2</sup>) per flow (Fig. 5-8c). The project was adapted to fit into the existing exhaust hoods and condenser with some alterations and existing turbine bearings, even though the new LP rotors were approximately 30% heavier than the original rotors. The new LP cylinders were furnished with special ports for boroscopic inspections of the LP blading. The turbine missile probability for the LP cylinders is assessed to be within the acceptable NRC limit of 1/100,000 per year for a 10-year period between full inspections with opening the cylinders, providing valve tests every three months.

Limerick Unit 1 was first retrofitted in spring 1998. Post-outage heat-rate test indicated an increase in the power output of 42 MW, which was attributed solely to the turbine retrofit. The actual retrofitting time to restore the turning gear operation was 41 days and 7 hours. The lessons learned from the Limerick Unit 1 retrofit contributed to shortening the retrofit time for Unit 2 to 35.5 days.

The Susquehanna nuclear power plant's 1,065-MW Unit 2 with a BWR-type reactor was put into commercial operation in 1985 (Unit 1 was launched two years earlier). A routine refueling outage of Unit 2 in April 2003 was used by Siemens Westinghouse Power Corporation to retrofit the turbine with replacement of the rotors and inner casings of its HP cylinder and three LP cylinders.<sup>45</sup> During its first four years of commercial operation, Susquehanna had experienced SCC in the LP rotors. As a result, the plant replaced the original disk-type rotors with solid rotors. The new rotors had a six-year inspection interval

that was later extended to eight years. Although the SCC problem of the disks was resolved, other problems occurred subsequently, including SCC of the dovetail attachments in the LP steam paths and erosion of the LP inner casings. These problems and the need to increase the unit performance led to the decision to retrofit both of the plant's turbines all over again. Even though there were no specific problems with the HP cylinders, it was decided to upgrade them, too. The retrofit project was very similar to that performed at the Limerick unit. A similar refurbishment is to be performed at Susquehanna Unit 1.

Siemens is also planning to upgrade two 1,150-MW turbines at the U.S. nuclear power plant Salem (the turbines were manufactured by Westinghouse and put into operation in 1977 and 1981).<sup>46</sup> New HP cylinders in both turbines and three LP cylinders in the first turbine are supposed to increase the power plant output by approximately 90 MW. Unit 2 was to be upgraded during the annual refueling outage of 2003, with Unit 1 to follow it during the refueling outage of 2004. The LP cylinders of the second turbine are scheduled to be replaced in 2006.

Similarly, an order for four new LP cylinders for the U.S. nuclear power plant Comanche Peak with two 1,150-MW turbines is a continuation of a previous retrofit of the HP cylinders performed by Siemens in 1999. These measures will provide additional output of more than 70 MW. Siemens is also scheduled to retrofit three LP cylinders of the ABB-built 1,200-MW turbine at the Swedish nuclear power plant Forsmark's Unit 3 during the refueling outage of 2004. It should increase the turbine output by approximately 30 MW.

## Upgrade experience of Mitsubishi Heavy Industries

Mitsubishi Heavy Industries has conducted refurbishing their own nuclear wet-steam turbines, as well as those of other manufacturers, since 1993. Twelve turbines have undergone replacement of the LP steam path with transition to 3-D integrally shrouded blading and replacing, if necessary, the LP rotors with forged rotors. No SCC has been found in the new forged rotors after 390,000 cumulative operating hours.

In 1999, MHI performed a combined refurbishment of a 1,000-MW-class turbine at the Spanish nuclear power plant Vandellos' Unit 2 with a PWR-type reactor. The turbine was originally manufactured by Westinghouse and put into operation in 1988. It is a low-speed (1,500 rpm) four-cylinder machine (TC-6F44) with one double-flow HP cylinder and three LP cylinders with disk-type rotors and grouped 44-in LSBs. The turbine retrofit was aimed at both the enhancement of the LP rotors' endurance against SCC and the increase in the turbine output and efficiency. The retrofit involved replacement of the HP rotor, including its rotating blades, associated stationary blades, and casing rings, as well as replacement of three LP rotors, including their rotating blades, associated stationary blades, and inner casings. The refurbished HP and LP cylinders are shown in Figure 5-11. All of the rotors are forged. The HP and LP steam paths comprise fully 3-D integrally shrouded blades, including 1,245-mm (49-in) LSBs.

The entire refurbishment process was accomplished in May 1999 during an ordinary refueling outage and took 40 days. A comparison of performance test results before and after the refurbishment showed an increase in the turbine output of approximately 8% (from 1,004 MW to 1,085 MW), which includes an increase of approximately 4.5% due to improvements in thermal efficiency.

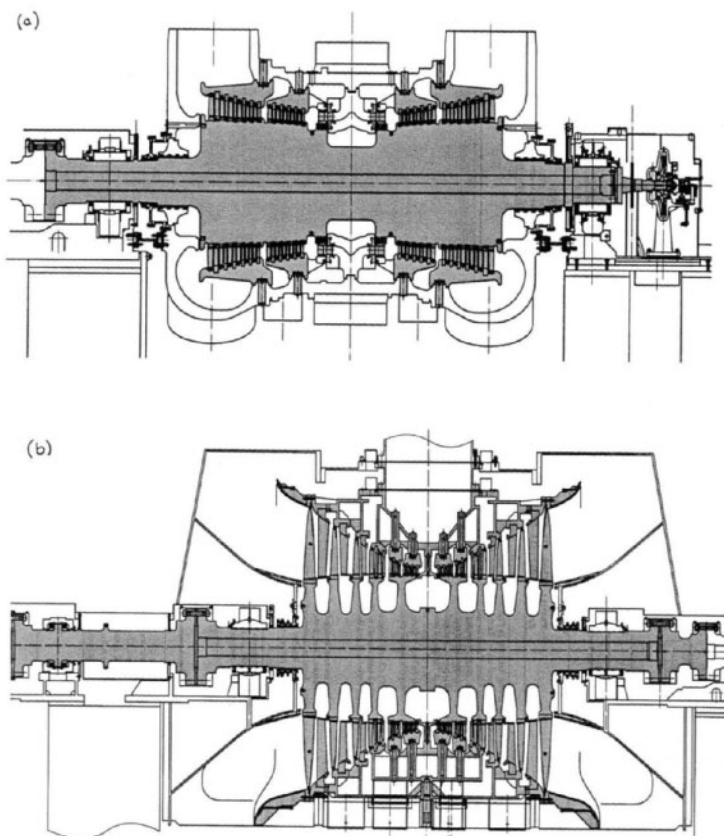


**Fig. 5-11.** Refurbished HP (a) and LP (b) cylinders of the 1,000-MW-class wet-steam turbine at Vandelllos Unit 2 (replaced components are shaded)

Source: By courtesy of Mitsubishi Heavy Industries

## Upgrade experience of ALSTOM at SONGS

In 1999, during regular refueling outages, ABB ALSTOM Power (later ALSTOM) performed integrated retrofits of two units with PWR-type reactors at the San Onofre Nuclear Generating Station (SONGS) in Southern California.<sup>47</sup> Operation of the power plant's low-speed (1,800 rpm) 1,127-MW turbines, originally produced by English Electric, commenced in 1983 and 1984. Each turbine comprises a double-flow HP cylinder and three LP cylinders with 1,144-mm (45-in) LSBs. By the time of retrofitting, each unit had accumulated more than 100,000 operating hours.

During operation, intergranular SCC of the steam generator tubes manifested itself as one of the most significant lifetime limiting factors for these units. This phenomenon is known to be thermally activated and can be somewhat mitigated by lowering the operating temperature. Initially, the units were designed for the main steam pressure of 5.9 MPa (855 psi), which corresponds to the saturation temperature of approximately 274°C (525°F). In order to extend the steam generators' lifetime in lieu of their replacement and avoid the power output losses because of plugging individual, damaged tubes, it was decided to reduce the operating temperature. Afterward, the final reactor coolant system temperature was lowered by 7°C (13°F). This entailed decreasing the main steam pressure, which also meant a decrease in the reactor's coolant system temperature and, as a result, a potential decrease in the plant output, because the maximum steam flow amount through the HP steam path is proportional to the inlet steam pressure. Keeping up the main steam flow amount through the turbine with the lower inlet steam pressure necessitates increasing the flow capacity of the HP steam path. This was done by fitting new nozzle vanes with larger throat areas for the three first HP stages. In addition, the steam generators were chemically cleaned to remove heat-transfer retarding deposits from the inner tube surfaces. All of these measures allowed passing the original full steam flow amount through the turbines. The new fixed blades for the refurbished HP stages were manufactured with integral root and tip platforms that could be welded directly into the diaphragm rings.

The main reason for retrofitting the LP cylinders was SCC in the disk rim and balance-hole zones of the LP disk-type rotors. These cracks were first found at several stages in 1995, and their propagation was retarded by skim cutting, dressing out the larger defects, drilling out the steam balance holes, and shot peening the surfaces. The discovery of large-scale SCC at the LP disk-type rotors, together with a possibility of further SCC propagation, as well as its initiation at other vulnerable points, led to heightened inspection requirements, with a possibility of extended or even additional outages. A secondary reliability problem for the original LP rotors, shown in Figure 5-12a, was that their natural torsional oscillation frequencies were very close to the value of 120 Hz associated with possible phase unbalance or bulk power disturbances in the power system. Retrofitting the LP rotors could also provide a considerable gain in the power output.

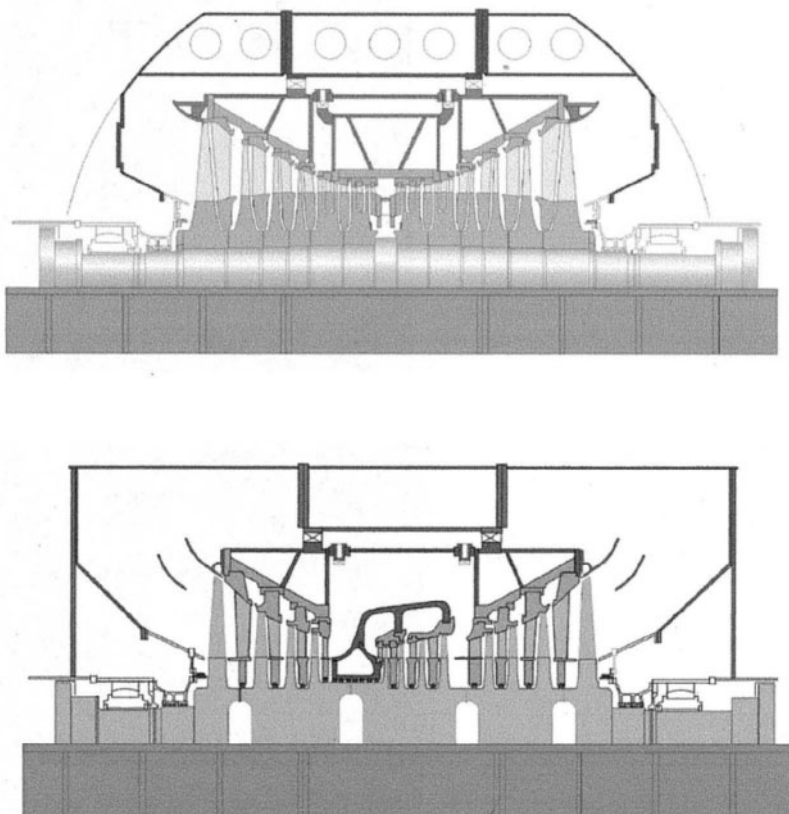


**Fig. 5-12.** Original design of disk-type LP rotors of SONGS' 1,127-MW turbines (a) and their retrofitted optiflow configuration design (b)

Source: R. D. Brown, F.Y. Simma, and R. J. Chetwynd<sup>48</sup>

The LP cylinders were refurbished based on concepts of welded rotors and so-called *optiflow* configuration (Fig. 5-12b). Forked-pinned root attachments were used for the rotating blades of all the LP stages except for the last and next-to-last ones (L-0 and L-1) instead of the former fir-tree (straddle) type. All other things being equal, the pinned roots feature lower peak stresses in the disk rim than fir-tree roots. This, as well as the lower centrifugal stresses due to a bore-free design, allowed the use of rotor metal with the yield strength lower by 15–20% than that for the metal of shrunk-on disks.

The optiflow concept of an LP cylinder with a special, separate single-flow IP section placed within a double-flow LP cylinder originated from Alsthom.<sup>49</sup> (In particular, this concept was realized in several moderate-output wet-steam turbines—for example, 510-MW high-speed turbines of Belgian double-turbine Tihange Unit 1<sup>50</sup>). The use of a single-flow IP section instead of the first stages of a double-flow LP section working with superheated steam allows a decrease in energy losses due to an increase in the blade length. A separate single-flow IP section integrated with a single-flow HP section in one cylinder was also used by Alsthom for large low-speed wet-steam turbines with the rotation speed of 1,500 rpm (see Fig. 3-1); similar designs were sometimes applied by other turbine manufacturers, as well (see, for example, Fig. 3-18). As distinct from them, the combination of a single-flow IP section and a double-flow LP steam path within one cylinder features the optiflow concept. According to Alsthom, increases in turbine efficiency due to replacement of the first LP stages with longer IP stages outweighs the sum of energy losses because of flow reversal after the IP section and with the exit velocity, as well as because of the leakage through the inner gland seal between the IP and LP section inlets.

The retrofitted LP steam path is formed with the use of modern CFD-designed profiles of an advanced efficiency and 1,194-mm (47-in) LSBs. The longer LSBs with greater annular exhaust areas reduce the energy losses with the exit velocity. The LSBs are highly twisted and are furnished with integral snubbers and curved axial-entry fir-tree roots. The freestanding rotating blades of the previous, next-to-last (L-1) stage have a root of the same type. Excepting the two last stages, all of the other ones in the LP cylinders have integrally shrouded rotating blades. The stepped shrouds permit the application of both a smooth conical outer outline for the steam path (on the shroud underside) and highly efficient overshroud labyrinth seals (on the shroud topside) as shown in Figure 3-60b. Spring-backed, slant-finned diaphragm seals provide lesser steam leakage than the original design, with its straight-finned, caulked-in seals.

The original LP exhaust hoods, with their curved shape and short axial steam space, presented significant restrictions to the steam exhausting from the LSB annulus (Fig. 5-12a). These restrictions were eliminated due to the use of new, generously sized hoods and aerodynamically designed diffusers (Fig. 5-12b). The new hoods

and diffusers were installed separately two years before the LP rotor replacements.

The individual constituents of the expected performance improvement due to retrofitting the LP cylinders are presented in Table 5-1.

**Table 5-1.** Constituents of performance improvement due to retrofitting LP cylinders for 1127-MW turbines of SONGS

Measures	Turbine output increase, %
Modern fixed and rotating blade profiles, and “optiflow” design	1.1
Integral shrouds	0.1
Improved diaphragm seals and overshroud seals of the rotating blades	0.3
Longer LSBs	0.15
Exhaust hood improvement	0.5
LP steam path degradation recovery	0.15
Total	2.30

Source: R.D. Brown, F.Y. Simma, and R.J. Chetwynd<sup>51</sup>

The complete retrofits at two units of SONGS were accomplished in 41 and 32 days, respectively. Heat-rate performance tests to assess the actual contribution of the retrofit measures to the power output were conducted at SONGS Unit 2 and arranged as alternative tests, with uncertainties higher than those for a full-scale ASME PTC 6 test. The overall test uncertainty was estimated to be  $\pm 0.17\%$  with a confidence level of 95%. This corresponds to an overall back-to-back test uncertainty of approximately  $\pm 3.5$  MW, which was considered adequate for the particular test purposes. The pre-test was performed 65 days before the planned outage, and the first post-retrofit estimate was done five days after the unit reached full load. The corrected and averaged power increase attained due to the LP retrofit, with regard to the reduced main steam pressure, amounted to 22.62 MW, compared with an expected value of 21.5 MW. With regard to an additional output increase of approximately 5.5 MW due to the refurbishment of the exhaust hoods and diffusers, the overall LP retrofit improved the unit output by approximately 28.1 MW.

## References

- <sup>1</sup> Jäger, G., and D. Dibelius. 1988. Condition-oriented maintenance using turbine generator sets as an example (in German). *VGB Kraftwerkstechnik* 68 (12): 1239–1243.
- <sup>2</sup> Leyzerovich A. 1996. General requirements on diagnosability of power unit equipment—First approach to standardization. *Proceedings of the American Power Conference* 58, (Part 2): 1463–1467.
- <sup>3</sup> McCloskey, T. H., R. B. Dooley, and W. P. McNaughton. 1999. *Turbine Steam Path Damage: Theory and Practice*, Vols. 1-2. Palo Alto, CA: EPRI, 1999.
- <sup>4</sup> Glover, J. J., A. Beecher, and J. Beverly. 2001. Evaluation, redesign, and repair of a nuclear steam turbine low-pressure rotor suffering from intergranular stress corrosion cracking. In *Proceedings of the International Joint Power Generating Conference*, 1-10. New York: ASME, 2001.
- <sup>5</sup> Levchenko, E. V. 1995. Steam turbines manufactured by Turboatom NPO, their specifics, and ways for improving them. *Thermal Engineering* 42 (1): 13–20.
- <sup>6</sup> Ikegami, T., T. Shimura, and M. Koike. 2001. Plant life management technologies for nuclear power plants. *Hitachi Review* 50 (3): 84–88.
- <sup>7</sup> Matsubara, M., and A. Nitta. 1995. Remaining life assessment of actual steam turbine rotors using the ultrasonic method. In *Service Experience, Structural Integrity, Severe Accidents, and Erosion in Nuclear and Fossil Plants*, PVP-Vol. 303, 49–55. New York: ASME, 1995.
- <sup>8</sup> 2001. *Operating Experience with Nuclear Power Stations in Member States in 2000*. Vienna: International Atomic Energy Agency.
- <sup>9</sup> Hesketh, A., and J. McCoach. 2002. Fulfilling the need for turbine retrofits which match demand on “date and duration” of outage. In *Proceedings of the International Joint Power Generating Conference*, 475–483. New York: ASME, 2002.
- <sup>10</sup> 1996. As the steam turbine turns, SCC still comes a calling. *Power* 140 (6): 6–8.
- <sup>11</sup> Pizzica, J., J.-E. Bertilsson, and E. Thommen. 1988. Replacement of LP-turbine rotors in nuclear power stations Dresden and Quad Cities. *Proceedings of the American Power Conference* 50: 77–86.
- <sup>12</sup> Hohn, A., and A. Roeder. 1984. ABB solution for low pressure rotors endangered by stress corrosion cracking. *BBC Review* 71 (3/4): 160–168.
- <sup>13</sup> Pizzica, Replacement of LP-turbine rotors. 77–86.
- <sup>14</sup> Hesketh, Fulfilling the need for turbine retrofits. 475–483.
- <sup>15</sup> Aubry, P., B. Billerey, and J. P. Goffin. 1996. Retrofit of LP rotors on nuclear turbines in Belgium. *Proceedings of the American Power Conference* 58: 166–171.
- <sup>16</sup> Ibid.

- 17 Krämer, E., H. Huber, and B. Scarlin. 1996. Low-pressure steam turbine retrofits. *ABB Review* 5: 4-13.
- 18 Aubry, Retrofit of LP rotors in Belgium. 166-171.
- 19 La Fontaine, J., and G. J. Heim. 1994. Rotor retrofit boosts turbine output and efficiency by 1.67%. *Power Engineering* 98 (4): 42-44.
- 20 Hesketh, Fulfilling the need for turbine retrofits. 475-483.
- 21 Krämer, Low-pressure steam turbine retrofits. 4-13.
- 22 Lindström, B., C.-H. Ahrbom, and L.-G. Karlson. 1998. Steam turbines retrofitted in record time. *ABB Review* 3: 27-32.
- 23 Egli, A. J., and R. U. Danz. 1993. Experiences in testing the refurbished LP turbines in the Maanshan nuclear power plant. In *The Steam Turbine Generator Today: Materials, Flow Path Design, Repair and Refurbishment*, PWR-Vol. 21, 7-19. New York: ASME, 1993.
- 24 Bütikofer, J., M. Händler, and U. Wieland. 1980. ABB low-pressure steam turbines—the culmination of selective development. *ABB Review* 8/9: 9-16.
- 25 Krämer, E., N. Lannefors, and B. Scarlin. 1994. Advanced reliable low-pressure steam turbine retrofits. In *Advances in Steam Turbine Technology for the Power Generation Industry* PWR-Vol. 26, 89-98. New York: ASME, 1994.
- 26 Bütikofer, ABB low-pressure steam turbines. 9-16.
- 27 Groenendaal, J. C., L. G. Fowls, R. Subbiah, et al. 1996. LP turbine retrofit modernization: Improvements in performance and operation. *Proceedings of the American Power Conference* 58 (Part 2): 1224-1229.
- 28 Cramer, E. P., J. A. Moreci, C. W. Camp, et al. 1998. Advanced LP turbine retrofits: An economical approach to gain competitiveness. In *Proceedings of the International Joint Power Generating Conference* PWR-Vol. 33, Part 2, 79-87. New York: ASME, 1998.
- 29 Groenendaal, LP turbine retrofit modernization. 1224-1229.
- 30 Cramer, Advanced LP turbine retrofits. 79-87.
- 31 Parker, J., and I. Aneja. 1993. Today's technology application in modernization: Reliability and MW improvements in large steam turbines. In *The Steam Turbine Generator Today: Materials, Flow Path Design, Repair and Refurbishment* PWR-Vol. 21, 175-180. New York: ASME, 1993.
- 32 Cramer, Advanced LP turbine retrofits. 79-87.
- 33 Jacobsen, G., H. Oeynhausen, and H. Termuehlen. 1991. Advanced LP turbine installation at 1300 MW nuclear power station Unterweser. *Proceedings of the American Power Conference* 53: 991-1001.
- 34 Eckel, M., W. Braitsch, and M. Jansen. 1995. Upgrading of turbine generator sets operated by Bayernwerk AG. *VGB Kraftwerkstechnik* 75 (5): 376-384.
- 35 Classen, H.-P., H. Oeynhausen, and J. Riehl. 2000. Upgrading of the low-pressure steam turbines of nuclear power plants. *Power Journal* 1: 26-29.

- <sup>36</sup> Oeynhausen, H., H.-P. Classen, and J. Riehl. 2003. Upgrading the low-pressure turbines of the Emsland nuclear power plant. *VGB PowerTech* 83 (1/2): 85–90.
- <sup>37</sup> Jacobsen, Advanced LP turbine installation. 991–1001.
- <sup>38</sup> Ibid.
- <sup>39</sup> Classen, Upgrading of the low-pressure steam turbines. 26–29.
- <sup>40</sup> Marlow, B. A., and R. D. Brown. 1998. Upgrading of HP turbines for nuclear power plants. *Proceedings of the American Power Conference* 60: 260–264.
- <sup>41</sup> Eckel, Upgrading of turbine generator sets. 376–384.
- <sup>42</sup> Weschenfelder, K. D., H. Oeynhausen, D. Bergman, et al. 1994. Turbine steam path replacement at the Grafenrheinfeld Nuclear Power Station. *Proceedings of the American Power Conference* 56: 1522–1529.
- <sup>43</sup> Ibid.
- <sup>44</sup> Atkinson, R. B., G. R. Sealy, and M. W. Smiarowski. 1999. Turbine retrofit project overview at Limerick Generating Station for reliability and performance improvement. *Proceedings of the American Power Conference* 61: 899–904.
- <sup>45</sup> Smith, D. J. 2003. Steam turbine upgrades improve reliability. *Power Engineering* 107 (6): 38–41.
- <sup>46</sup> 2002. Siemens PG sheds UK staff. *Modern Power Systems* 22 (9): 11.
- <sup>47</sup> Brown, R. D., F. Y. Simma, and R. J. Chetwynd. 2000. Efficiency improvement features of recent ABB-ALSTOM HP-LP turbine retrofit at Southern California Edison's San Onofre Nuclear Generating Station. In *Proceedings of the International Joint Power Generating Conference* 85–93. New York: ASME, 2000.
- <sup>48</sup> Ibid.
- <sup>49</sup> Riolett, G. 1983. Outlook for the large steam turbines of tomorrow. *Modern Power Systems* 3 (1): 35–37.
- <sup>50</sup> Aubry, Retrofit of LP rotors in Belgium. 166–171.
- <sup>51</sup> Brown, Efficiency improvement features. 85–93.

## Bibliography

- As the steam turbine turns, SCC still comes a calling. 1996. *Power* 140 (6): 6-8.
- Atkinson, R. B., G. R. Sealy, and M. W. Smiarowski. 1999. Turbine retrofit project overview at Limerick Generating Station for reliability and performance improvement. *Proceedings of the American Power Conference* 61: 899-904.
- Aubry, P., B. Billerey, and J. P. Goffin. 1996. Retrofit of LP rotors on nuclear turbines in Belgium. *Proceedings of the American Power Conference* 58: 166-171.
- Brown, R. D., F. Y. Simma, and R. J. Chetwynd. 2000. Efficiency improvement features of recent ABB-ALSTOM HP-LP turbine retrofit at Southern California Edison's San Onofre Nuclear Generating Station. In *Proceedings of the International Joint Power Generating Conference*, 85-93. New York: ASME, 2000.
- Bütikofer, J., M. Händler, and U. Wieland. 1980. ABB low-pressure steam turbines—the culmination of selective development. *ABB Review*, 1980 (8/9): 9-16.
- \_\_\_\_\_, and U. Wieland. 1991. Modern LP steam turbines (in German). *VGB Kraftwerkstechnik* 71 (4): 341-346.
- Classen, H.-P., H. Oeynhausen, and J. Riehl. 2000. Upgrading of the low-pressure steam turbines of nuclear power plants. *Power Journal*, January 2000: 26-29.
- Cramer, E. P., J. A. Moreci, C. W. Camp, et al. 1998. Advanced LP turbine retrofits: An economical approach to gain competitiveness. In *Proceedings of the International Joint Power Generating Conference*, PWR-Vol. 33, Part 2, 79-87. New York: ASME, 1998.
- Davids, J., R. E. Warner, M. E. Schlatter, and L. R. Southal. 1988. Testing and service experience with ruggedized turbine designs. *Proceedings of the American Power Conference* 50: 65-71.
- Eckel, M., W. Braitsch, and M. Jansen. 1995. Upgrading of turbine generator sets operated by Bayernwek AG. *VGB Kraftwerkstechnik* 75 (5): 376-384.
- Egli, A. J., and R. U. Danz. 1993. Experiences in testing the refurbished LP turbines in the Maanshan nuclear power plant. In *The Steam Turbine Generator Today: Materials, Flow Path Design, Repair and Refurbishment*, PWR-Vol. 21, 7-19. New York: ASME, 1993.
- German nuclear plant gains 'free' capacity. 2000 *Power*, 144 (5): 11-12.
- Gloger, M., K. Neumann, D. Bermann, and H. Termuehlen. 1992. Advanced LP turbine blading: A reliable and highly efficient design. In *Steam Turbine-Generator Developments for the Power Generation Industry*, PWR-Vol. 18, 41-51. ASME, 1992.
- Glover, J. J., A. Beecher, and J. Beverly. 2001. Evaluation, redesign, and repair of a nuclear steam turbine low-pressure rotor suffering from intergranular stress corrosion cracking. In *Proceedings of the International Joint Power Generating Conference*, 1-10. New York: ASME, 2001.

- Groenendaal, J. C., L. G. Fowls, R. Subbiah, et al. 1996. LP turbine retrofit modernization: Improvements in performance and operation. *Proceedings of the American Power Conference* 58 (Part 2): 1224-1229.
- Hesketh, A., and J. McCoach. 2002. Fulfilling the need for turbine retrofits which match demand on “date and duration” of outage. In *Proceedings of the International Joint Power Generating Conference*, 475-483. New York: ASME, 2002.
- Hesketh, J. A., H. Tritthart, and P. Aubry. 1994. Modernisation of steam turbines for improved performances. In *Proceedings of Symposium on Steam Turbines and Generators*. Monaco: GEC-Alsthom, 1994.
- Hohn, A., and A. Roeder. 1984. ABB solution for low pressure rotors endangered by stress corrosion cracking. *BBC Review* 71 (3/4): 160-168.
- Ikegami, T., T. Shimura, and M. Koike. 2001. Plant life management technologies for nuclear power plants. *Hitachi Review* 50 (3): 84-88.
- Jacobsen, G., H. Oeynhausen, and H. Termuehlen. 1991. Advanced LP turbine installation at 1300 MW nuclear power station Unterweser. *Proceedings of the American Power Conference* 53: 991-1001.
- Jäger, G., and D. Dibelius. 1988. Condition-oriented maintenance using turbine generator sets as an example (in German). *VGB Kraftwerkstechnik* 68 (12): 1239-1243.
- Krämer, E., H. Huber, and B. Scarlin. 1996. Low-pressure steam turbine retrofits. *ABB Review*, 1996 (5): 4-13.
- , N. Lannefors, and B. Scarlin. 1994. Advanced reliable low-pressure steam turbine retrofits. In *Advances in Steam Turbine Technology for the Power Generation Industry*, PWR-Vol. 26, 89-98. New York: ASME, 1994.
- La Fontaine, J., and G. J. Heim. 1994. Rotor retrofit boosts turbine output and efficiency by 1.67%. *Power Engineering*, April 1994: 42-44.
- Levchenko, E. V. 1995. Steam turbines manufactured by Turboatom NPO, their specifics, and ways for improving them. *Thermal Engineering* 42 (1): 13-20.
- , V. N. Galatsan, B. A. Arakd'ev, et al. 1997. Modernization of the 220 MW turbines of NPO Turboatom for nuclear power stations. *Thermal Engineering* 44 (7): 535-541.
- Leyzerovich A. S. 1996. General requirements on diagnosibility of power unit equipment—First approach to standardization. *Proceedings of the American Power Conference* 58 (Part 2): 1463-1467.
- Lindström, B., C.-H. Ahrbom, and L.-G. Karlsson. 1998. Steam turbines retrofitted in record time. *ABB Review*, 1998 (3): 27-32.
- Marlow, B. A., and R. D. Brown. 1998. Upgrading of HP turbines for nuclear power plants. *Proceedings of the American Power Conference* 60: 260-264.
- Matsubara, M., and A. Nitta. 1995. Remaining life assessment of actual steam turbine rotors using the ultrasonic method. In *Service Experience, Structural Integrity, Severe Accidents, and Erosion in Nuclear and Fossil Plants*, PVP-Vol. 303, 49-55. New York: ASME, 1995.

- McCloskey, T. H., R. B. Dooley, and W. P. McNaughton. 1999. *Turbine Steam Path Damage: Theory and Practice*, Vols. 1-2. Palo Alto, CA: EPRI, 1999.
- Oeynhausen, H., H.-P. Classen, and J. Riehl. 2003. Upgrading the low-pressure turbines of the Emsland nuclear power plant. *VGB PowerTech* 83 (1/2): 85-90.
- \_\_\_\_\_, G. Roettger, J. Ewald, et al. 1987. Reliable disk-type rotors for nuclear power plants. *Proceedings of the American Power Conference* 49: 113-122.
- Operating Experience with Nuclear Power Stations in Member States in 2000*. 2001. Vienna: International Atomic Energy Agency, 2001.
- Parker, J., and I. Aneja. 1993. Today's technology application in modernization: Reliability and MW improvements in large steam turbines. In *The Steam Turbine Generator Today: Materials, Flow Path Design, Repair and Refurbishment*, PWR-Vol. 21, 175-180. New York: ASME, 1993.
- Peltier, R. 2002. Steam turbine advances transform new and existing plants. *Power* 146 (1): 26-34.
- Pizzica, J., J.-E. Bertilsson, and E. Thommen. 1988. Replacement of LP-turbine rotors in nuclear power stations Dresden and Quad Cities. *Proceedings of the American Power Conference* 50: 77-86.
- Presnak, R., M. Maras, W. Woyshner, and R. Matusheski. 1997. Predictive maintenance assessment for a competitive edge. *Proceedings of the American Power Conference* 59 (Part 1): 116-122.
- Riolett, G. 1983. Outlook for the large steam turbines of tomorrow. *Modern Power Systems* 3 (1): 35-37.
- Sanders, W. P. 2001. *Turbine Steam Path Maintenance & Repair*, Vols. 1-2. Tulsa, OK: PennWell Publishing, 2001.
- Schimmoller, B. K. 2000. Accelerating outages & extending intervals. *Power Engineering*, 104 (11): 42-50.
- Siemens PG sheds UK staff. 2002. *Modern Power Systems* 22 (9): 11.
- Smiarowski, M. W., and T. J. Otterlee. 1999. Design overview of the state-of-the-art turbine replacement at Limerick Generating Station. In *Proceedings of the Joint Power Generation Conference*. PWR-Vol. 34, Part 2, 223-229. New York: ASME, 1999.
- Smith, D. J. 2001. Predictive and preventive maintenance pays dividends. *Power Engineering*, 105 (2): 39-41.
- Smith, D. J. 2000. Retrofit options increase steam turbine efficiency. *Power Engineering*, 104 (3): 34-36.
- Smith, D. J. 2003. Steam turbine upgrades improve reliability. *Power Engineering* 107 (6): 38-41.
- Stephen, D. 2001. Optimized plant retrofits. In *Proceedings of the 2001 International Joint Power Generating Conference*, JPGC2001/PWR-19175, 1-7. New York: ASME, 2001.
- Taag, H.-J. 1999. Reliability-centered maintenance (RCM). *VGB PowerTech* 79 (12): 58-61.

- Termuehlen, H. 1997. Replacement of nuclear LP turbine rotors and inner casings. Paper presented at the American Power Conference, Chicago, IL, 1997.
- . 2001. *100 Years of Power Plant Development: Focus on Steam and Gas Turbines as Prime Movers*. New York: ASME, 2001.
- Valenti, M. 2000. Sound as a dollar. *Mechanical Engineering Power* 2000 (5): 18-22.
- Weiss, A. P. 1998. Aerodynamic design of advanced LP steam turbines. *ABB Review* 1998 (5): 4-11.
- Weschenfelder, K. D., H. Oeynhausen, D. Bergman, et al. 1994. Turbine steam path replacement at the Grafenrheinfeld Nuclear Power Station. *Proceedings of the American Power Conference* 56: 1522-1529.
- Yokoyama, A., and H. Haruyama. 1992. MHI nuclear service experience with operating PWRs in Japan. In *Service Experience and Life Management in Operating Plants*, PWP-Vol. 240, 23-28. New York: ASME, 1992.
- Young, K. 1998. Converting a PM program to an RCM basis. *Maintenance Technology* 1998 (1): 22-29.
- Zink, J. C. 1998. Competition dictates maintenance decisions. *Power Engineering* 102 (5): 22-26.

To my wife Lucy,  
our elder daughter Olga,  
and to the memory of our younger daughter Irina—  
with love

*Thee in thy panoply, thy measur'd dual throbbing and thy beat convulsive,  
The black cylindric body, golden brass and silvery steel, ...  
Thy metrical, now swelling pant and roar ....*



*And thy wet and hot breath that precipitates with heavy  
water dust on my hands and forehead...*

*Excerpt from "To a Locomotive in Winter" by Walt Whitman*

# List of Illustrations

Figure 1–1	Westinghouse nuclear wet-steam turbine (100-MW, 1,800 rpm) used at Shippingport Station, 1957. ....	2
Figure 1–2	U.S. nuclear power plants. ....	11
Figure 1–3	Schematic diagram for a nuclear power unit with PWR. ....	18
Figure 1–4	Schematic diagram for a nuclear power unit with BWR. ....	19
Figure 1–5	Schematic diagram for a nuclear power unit with PHWR. ....	22
Figure 1–6	Schematic diagram for a nuclear power unit with LWGR (RBMK) ....	23
Figure 2–1	Schematic diagram of a large double-circuit nuclear power unit turboset with operating conditions corresponding to 100% MCR ....	40
Figure 2–2	Mollier diagram with characteristic steam expansion lines for wet-steam turbines compared to superheated steam turbines of fossil fuel plants. ....	41
Figure 2–3	Areas of various levels intensity of erosion-corrosion processes in the wet-steam region for turbine stator elements made of carbon steels. ....	43
Figure 2–4	Influence of the end steam pressure in the condenser, $p_c$ , on wet-steam turbine thermal efficiency ....	48
Figure 2–5	Gain in the output (a) and efficiency (b) for a 750-MW wet-steam turbine with three serially connected condensers, related to the turbine load and cooling water inlet temperature ....	50
Figure 2–6	Configurations of wet-steam turbines with different combinations of external moisture separators (MS) and single-stage and two-stage reheaters (R) ....	51
Figure 2–7	Influence of partition steam pressure (between the HP and LP cylinders) on wet-steam turbine efficiency, according to GE ....	52
Figure 2–8	Various forms of water existing in a wet-steam turbine stage ....	54
Figure 2–9	Changes of maximum achievable subcooling temperature and critical droplet radius with initial saturated steam pressure, $p_{os}$ , and steam expansion velocity. ....	56
Figure 2–10	Steam expansion process with subcooling shown on h-s axes ....	57

Figure 2–11	Energy loss with subcooling of wet steam depending on pressure ratio . . . . .	58
Figure 2–12	Drop paths of water in a nozzle channel depending on the drop size . . . . .	60
Figure 2–13	General pattern of water motion within a nozzle channel . . . . .	60
Figure 2–14	Experimental characteristics of energy losses (a) and flow amount factor (b) for slightly superheated and wet steam. . . . .	61
Figure 2–15	Influence of wetness in the exit section of a turbine blade row on the flow amount factor. . . . .	62
Figure 2–16	Influence of initial steam pressure, $p_0$ , and wetness, $y_0$ , on the slide factor for a supersonic nozzle . . . . .	63
Figure 2–17	Velocity triangles of a wet-steam turbine stage for steam and water . . . . .	64
Figure 2–18	Changes in the internal efficiency and reaction degree for tip and root zones related to velocity ratio and initial steam wetness for an experimental turbine stage . . . . .	65
Figure 2–19	Changes in optimal velocity ratio and internal stage efficiency for turbine stages with different median-diameter-to-height ratios, depending on initial wetness . . . . .	66
Figure 2–20	Influence of initial wetness on changes in efficiency related to different rotating blade profiles . . . . .	66
Figure 2–21	Influence of wetness on efficiency for reaction-type turbine stages . . . . .	68
Figure 2–22	Influence of wetness on efficiency for impulse-type turbine stages . . . . .	69
Figure 2–23	Distribution of exit wetness along the height of an individual stage, depending on the coarse-grain wetness portion . . . . .	70
Figure 2–24	Development of reaction-type, integrally shrouded blades for Siemens turbines . . . . .	71
Figure 2–25	Changes in meridional steam flow behavior in LP stages of ABB turbines, due to using 3-D, bowed, and inclined vanes in the last stage . . . . .	72
Figure 2–26	Variation in wet-steam conditions along the steam path of the HP cylinder of a K-220-44 turbine . . . . .	75
Figure 2–27	Installation of research probes into an LP turbine section . . . . .	76

Figure 2–28	Typical distribution of coarse-grain water before the last LP stage of a 500-MW turbine .....	77
Figure 2–29	Steam wetness variation over the height of an individual stage.....	79
Figure 2–30	Wetness distribution along the length of the last turbine stage inlet, according to experimental data from Westinghouse (1) and AEI (2) turbines .....	79
Figure 2–31	Optical attenuation probe for measuring fog droplet size.....	81
Figure 2–32	Microvideo probe used for coarse-grain water drop measurements .....	81
Figure 2–33	Experimental distributions of fog droplets and large drops downstream of the LSB.....	82
Figure 2–34	Calculated energy losses due to wetness for LP stages of a low-speed 600-MW wet-steam turbine .....	83
Figure 2–35	System for sampling primary condensate (a) and laser probe (b) for investigating corrosive properties of wet steam on a model turbine .....	84
Figure 2–36	Content of chlorides (a) and sulfates (c) in primary condensate; variation of droplet size over the stage height for different impurity levels in steam at the turbine inlet (b).....	85
Figure 2–37	Schematic diagram of steam wetness measurement system (a); wetness distribution over the stage height at a model turbine outlet (b) .....	87
Figure 2–38	Schematic diagram for measuring water quantities withdrawn through suction slots on surfaces of the hollow vane (a); pressure distribution along the vane profile (b); relative erosion rate of the blade inlet edge (c) .....	88
Figure 2–39	Boroscope probe (a); inserted into the model turbine steam path (b); behavior of water flow at outlet edge of the nozzle vane (c) .....	89
Figure 2–40	Water motion on the pressure surface of the last stage nozzle vane .....	90
Figure 2–41	Theoretical characteristic water flow field for LP rotating blades .....	91

Figure 3–1	Longitudinal section of the HP cylinder and two of three LP cylinders of ALSTOM's 1,500-MW 1,500-rpm wet-steam turbine the <i>Arabelle</i> .....	107
Figure 3–2	Longitudinal section of the HP cylinder and one of three LP cylinders of ALSTOM's 1,200-to-1,500-MW 1,800-rpm wet-steam turbine .....	109
Figure 3–3	Outline drawing and plan view of ALSTOM's 1,200-to-1,500-MW 1,800-rpm wet-steam turbine.....	110
Figure 3–4	Longitudinal section of the HP cylinder and one of two LP cylinders (a) and cross-section of the HP cylinder (b) of Turboatom's K-220-44 wet-steam turbine .....	112
Figure 3–5	Longitudinal section of the HP cylinder and one of two LP cylinders of Skoda's 220-MW 3,000-rpm wet-steam turbine .....	113
Figure 3–6	Longitudinal section of Turboatom's K-220-44 wet-steam turbine, with one LP cylinder and a 920-mm last stage blade .....	114
Figure 3–7	Longitudinal section of the HP cylinder and one of three LP cylinders of Siemens' 1,040-MW 3,000-rpm wet-steam turbine .....	119
Figure 3–8	Longitudinal section of the HP cylinder and one of three LP cylinders of Siemens' 1,300-MW 1,500-rpm wet-steam turbine .....	120
Figure 3–9	Three-dimensional view of Siemens' 1,700-MW 1,500-rpm wet-steam turbine .....	121
Figure 3–10	Longitudinal section of the HP cylinder and one of three LP cylinders (a) and general view (b) of Brown Boveri's 1,100-to-1,300-MW 1,800-rpm wet-steam turbine .....	123
Figure 3–11	Longitudinal section of MHI's 900-MW-class low-speed wet-steam turbine .....	125
Figure 3–12	Longitudinal section and general view of GEC Alsthom's 630-MW 3,000-rpm wet-steam turbine for the double-turbine Sizewell-B nuclear power unit .....	126
Figure 3–13	Longitudinal section of the HP cylinder and one of three LP cylinders of Turboatom's 1,000-MW 1,500-rpm K-1000-60/1500-2 wet-steam turbine .....	128

Figure 3–14	Longitudinal section of a half of the HP cylinder and one of four LP cylinders of LMZ's 1,000-MW 3,000-rpm K-1000-60/3000 wet-steam turbine . . . . .	129
Figure 3–15	Schematic diagram of Turboatom's KT-1070-60/1500-3 1,000-MW wet-steam turbine with four-stage network water heating to 180°C . . . . .	130
Figure 3–16	Longitudinal section of Turboatom's K-1000-60/1500-1 1,000-MW 1,500-rpm wet-steam turbine with IP cylinder and side condensers . . . . .	132
Figure 3–17	Rear-view and cross-section of the LP cylinder for Turboatom's 500- and 1,000-MW 1,500-rpm wet-steam turbines with side condensers . . . . .	133
Figure 3–18	Longitudinal section of Turboatom's 500-MW low-speed wet-steam turbine with IP section and side condensers . . . . .	134
Figure 3–19	Hypothetical LP cylinder with 1,800-mm last stage blades for up to 2,000-MW wet-steam turbine . . . . .	135
Figure 3–20	Longitudinal section of the HP cylinder and one of the LP cylinders of Toshiba's 800-MW-class low-speed wet-steam turbine . . . . .	138
Figure 3–21	LP steam path configuration for a typical Westinghouse wet-steam turbine . . . . .	139
Figure 3–22	Typical HP steam path stages (a) and double-strip stage seals of first LP stages (b) for Siemens' wet-steam turbines . . . . .	141
Figure 3–23	Typical HP stages for ALSTOM's 1,500-MW wet-steam turbine . . . . .	142
Figure 3–24	Influence of steam leakage (or suction) in the blade root zone of an impulse-type stage on its efficiency . . . . .	142
Figure 3–25	Scheme of end gland seals for double-flow HP (a) and LP (b) cylinders for wet-steam turbines operating with radioactive steam . . . . .	143
Figure 3–26	Influence of temperature on ECW rate for carbon steels (a) and comparison of expected and measured ECW rate (b) . . . . .	144
Figure 3–27	Typical ECW locations in the HP cylinder (a) and MSR (b) of Turboatom's K-220-44 turbine . . . . .	146
Figure 3–28	Areas of corrosion-erosion protection in the turbine steam path and gland seals of ABB's (a) and Siemens' (b) wet-steam turbines . . . . .	147

Figure 3–29 One of four combined HP stop and control valve units (a) and butterfly-type intercept valve (b) for Brown Boveri's large wet-steam turbines .....	149
Figure 3–30 Combined HP stop and control valve unit (a) and intercept valve (b) for Turboatom's low-speed wet-steam turbines.....	150
Figure 3–31 HP control valve and stop turn-gate for LMZ's K-1000-60/3000 turbine .....	150
Figure 3–32 HP stop and control valve unit (a) and LP butterfly valve (b) for GEC Alsthom's 630-MW wet-steam turbine .....	151
Figure 3–33 HP stop and control valve unit for Siemens' wet-steam turbines.....	152
Figure 3–34 HP control valve of ALSTOM's 1,500-MW wet-steam turbine .....	153
Figure 3–35 Full-load rejection oscillograms for Siemens' 1,300-MW Biblis Unit A turbine.....	156
Figure 3–36 Turboatom's four-segment journal bearing for high-speed wet-steam turbines.....	157
Figure 3–37 Thermal expansion arrangement for LMZ's K-1000-60/3000 turbine .....	161
Figure 3–38 Typical last LP stages of a large steam turbine (a) and the LSB with its profiles at the tip, mean, and root diameters (b) .....	162
Figure 3–39 Parameters of actual LSBs provided by various manufacturers .....	168
Figure 3–40 Hitachi's 43-in titanium-alloy LSB.....	169
Figure 3–41 Computational 3-D model for calculating the stress state and vibrational characteristics of MHI's 1,143-mm titanium LSB with its root and adjacent steeple.....	170
Figure 3–42 Three-dimensional calculation mesh and relative stress field for Toshiba's 1,067-mm LSB .....	171
Figure 3–43 Centrifugal stress contours and maximum stress values related to the tensile strength for 1,016-mm titanium LSBs with a fir-tree dovetail (a) and load distributions on hooks with machining errors (b) .....	172
Figure 3–44 Connection of shrouding elements of the LSB with wedge-shaped edges .....	173

Figure 3–45	Example of vibration mode analysis for a last stage wheel with “continuous cover blades” of Hitachi .....	174
Figure 3–46	Families of Siemens LSBs and selection diagram for 3,600-rpm turbines .....	175
Figure 3–47	Schematic diagram of a dual-sensor proximity-type blade vibration measuring system developed by Siemens .....	176
Figure 3–48	Movement of a tip of a vibrating freestanding LSB .....	177
Figure 3–49	Campbell diagram for a 965-mm LSB according to measurements at a Siemens 1,000-MW-class 3,000-rpm wet-steam turbine .....	178
Figure 3–50	Operation principle of ABB’s optical blade vibration measuring system (a), optical probe (b), and its installation at the LP exhaust (c) .....	179
Figure 3–51	Changes in a streamline pattern with variations in volumetric steam flow amount through the last stage .....	181
Figure 3–52	Appearance of reverse vortex motion in the last two LP stages at low (14%) volumetric steam flow amount .....	182
Figure 3–53	Typical blade rows and dependencies of profile losses on Mach number for the LSB’s root section (a), mean section (b), and tip section (c) .....	183
Figure 3–54	Comparison of stage efficiencies for conventional and newly developed, advanced Hitachi 26-in LSBs .....	184
Figure 3–55	Isotaches for the tip, median, and root sections of a typical modern LSB .....	185
Figure 3–56	Isotach fields on the surfaces of the vane and bucket profiles (a) and in the interprofile channels (b) for the last stage of Turboatom’s 1,000-MW low-speed turbine .....	186
Figure 3–57	Calculated isotach field for the steam path of three last LP stages with 1,143-mm titanium LSB of MHI’s 3,600-rpm turbine .....	187
Figure 3–58	ABB’s advanced LP cylinder with highly three-dimensional geometry in the last stage vanes .....	188
Figure 3–59	Isotach fields for the last LP stages of LMZ’s newly designed and refurbished turbines with conventional (a) and saber-type (b) vanes .....	189

Figure 3–60	Two different types of shrouds for LP stages with conical meridional profiles .....	190
Figure 3–61	Protection against WDE in the tip section and shroud of Toshiba's 1,016-mm titanium LSB .....	193
Figure 3–62	Estimation of WDE for Toshiba's 1,016-mm titanium LSB.....	193
Figure 3–63	LP stages with furrowed rotating blades and water traps between the nozzle and blade rows connected to the condenser.....	196
Figure 3–64	GE experimental data on separation efficiency for furrowed rotating blades.....	196
Figure 3–65	Water trap positioned after the stage .....	197
Figure 3–66	Water removal from HP steam path of an impulse-type wet-steam turbine .....	198
Figure 3–67	Possible design for a surface-type water trap for LP steam path . . . . .	199
Figure 3–68	Turboatom's hollow stationary blades with intrachannel water removal .....	200
Figure 3–69	Typical last stage of LMZ with intrachannel water separation and removal .....	200
Figure 3–70	Possible position of suction slots for intrachannel water removal (a) and distribution of specific steam pressure along the vane profile (b) .....	201
Figure 3–71	Toshiba's last stage with intrachannel water separation and removal .....	202
Figure 3–72	Estimation of the water separation factor for hollow nozzle vanes with two suction slots.....	203
Figure 3–73	Steam path of Siemens' low-speed wet-steam turbine with water removal from last stage nozzle surfaces .....	203
Figure 3–74	Heating hollow nozzle vanes for the last stages of Siemens' turbines.....	204
Figure 3–75	Efficiency of moisture removal for different types of MSSs depending on the speed-to-velocity ratio, $u/c_0$ . . . . .	205
Figure 3–76	Front views of Siemens' 1,200-MW wet-steam turbines with horizontal (a) and vertical (b) MSRs .....	207
Figure 3–77	Principle schematic of Westinghouse's third-generation MSR .....	209

Figure 3–78	Part of a chevron-plate separator . . . . .	209
Figure 3–79	Stein Industrie's horizontal MSRs for French nuclear power units of 1,000-MW and 1,300-MW output . . . . .	210
Figure 3–80	Vertical MSR for Turboatom's K-220-44 turbines . . . . .	211
Figure 3–81	One of two vertical MSRs for Siemens' 1,300-MW wet-steam turbines . . . . .	212
Figure 3–82	General view of ABB's three-cylinder wet-steam turbine with "distributed" MSR system (a), preseparator with phase separation (b), preseparator without phase separation (c), and separator (d) . . . . .	214
Figure 4–1	Participation of different types of power plants in covering daily power consumption . . . . .	234
Figure 4–2	Operation diagrams for German nuclear power units Neckar 2 (a) and Grohnde (b) in 2002 . . . . .	235
Figure 4–3	Operation diagram for the German nuclear power unit Stade in 1999 . . . . .	237
Figure 4–4	Daily load variations of the 900-MW French nuclear power unit Tricastin 3 . . . . .	238
Figure 4–5	Cold start-up of 1,356-MW Kashiwazaki-Kariwa Unit 7 with ABWR . . . . .	239
Figure 4–6	Steam expansion processes for a wet-steam turbine with full and partial steam flows under constant (I) and sliding (II) main steam pressure . . . . .	240
Figure 4–7	Load capacity diagrams for a light-water reactor at the end of operation campaign with constant and sliding main steam pressure . . . . .	242
Figure 4–8	Measured temperature distribution (°C) in outer casing (a) and calculated temperature field in rotor in the first IP stages zone (b) for the integrated HP–IP cylinder of Turboatom's K-500-60/1500 turbine for a typical start-up instant . . . . .	243
Figure 4–9	Shutdown and start-up after one-day outage for Turboatom's K-500-60/1500 turbine at the Novovoronezh nuclear power plant . . . . .	244

Figure 4–10 Calculated temperature fields (°C) for the first stage disk of a welded double-flow LP rotor of a Turboatom's high-speed turbine at cold start-up (a) and the right half of the same rotor at stationary operating conditions under load (b) .....	245
Figure 4–11 Emulation of automated start-up and load changes for Turboatom's K-500-65/3000 turbine with limits for temperature difference and thermal stress in the HP rotor .....	246
Figure 4–12 Mathematical modeling of automated start-ups from hot (1), warm (2), and cold (3) initial states for Turboatom's K-500-65/3000 turbine (a) and temperature fields for the first stage disk of the HP rotor (b).....	247
Figure 4–13 Optimization of loading schedules for Turboatom's K-220-44 turbine.....	248
Figure 4–14 Calculated diagram of optimized cold start-up for LMZ's 1,000-MW high-speed turbine .....	249
Figure 4–15 Calculated optimization of a cold start-up of Turboatom's 500-MW low-speed turbine .....	253
Figure 4–16 Change of relative dynamic stresses in LP LSBs with back pressure and volumetric steam flow in the condenser .....	255
Figure 4–17 Pattern of steam flows and steam temperatures and zones of increased erosion wear of blades in last stages of the LP steam path at a low-flow steam rate.....	256
Figure 4–18 Location and type of main measurements at a wet-steam turbine for heat-rate performance tests according to PTC 6 .....	262
Figure 4–19 Instrumentation diagram for heat-rate performance tests of Brown Boveri's 1,100-MW wet-steam turbine .....	265
Figure 4–20 Instrumentation diagram for heat-rate performance tests of Turboatom's K-1000-60/1500-2 turbine.....	267
Figure 4–21 Heat-rate and steam-rate performances for Turboatom's K-1000-60/1500-2 turbine according to heat-rate performance tests at the Zaporozhe nuclear power plant .....	268
Figure 4–22 Calculated "universal" curves of correction for vacuum for Turboatom's steam turbines (per exhaust flow) with different LSBs and exhaust hoods .....	273

Figure 4–23 Corrections for deviations of steam conditions for the output (1) and heat rate (2) for Turboatom's K-1000-60/1500 turbine . . . . .	275
Figure 4–24 Crack damage on the LP-1 rotor of AEG's 660-MW wet-steam turbine at Würgassen . . . . .	279
Figure 4–25 Influence of pH level on the erosion-corrosion rate of various steels . . . . .	282
Figure 4–26 Typical zones of stress corrosion cracking in shrunk-on wheel disks of wet-steam turbines at U.S. power plants (late 1970s) . . . . .	284
Figure 4–27 Stress corrosion cracks at a disk rim in the blade attachment zone . . . . .	285
Figure 4–28 Brittle fracture of shrunk-on disk due to propagation of stress corrosion cracks from the bore surface at the British nuclear power plant Hinkley Point A . . . . .	285
Figure 4–29 Probability of damages in the key slot (1) and on other surfaces (2) of wheel disks in the Wilson region . . . . .	286
Figure 4–30 Disk keying for the LP rotors of ALSTOM's wet-steam turbines for the French CP-1 nuclear power plant series . . . . .	288
Figure 4–31 Finite element mesh for calculating stress state of the shaft and disks for a combined LP rotor of Siemens . . . . .	290
Figure 4–32 Keyway design for combined LP rotors of Siemens' turbines for nuclear power plants . . . . .	291
Figure 4–33 Measures to produce residual compressive stresses at surfaces of disk forgings for combined LP rotors of Siemens' turbines for nuclear power plants . . . . .	291
Figure 4–34 Crack locations in the fir-tree grooves of ABB's LP last stage blades . . . . .	292
Figure 4–35 Different patterns of wear for metal of wet-steam turbines due to erosion and erosion-corrosion processes . . . . .	293
Figure 4–36 Erosion wear for outer casing bottoms of two Turboatom K-500-65/3000 turbines . . . . .	295
Figure 4–37 Influence of various design parameters on the WDE rate of rotating blades . . . . .	299
Figure 4–38 Variation of relative WDE criterion with the LSB's peripheral speed for different ABB steam turbines . . . . .	300

Figure 4–39	Shielding the leading edge of a steel last stage blade from WDE . . . . .	301
Figure 4–40	Phenomenon of shaft-blade coupled torsional oscillations . . . . .	303
Figure 4–41	Telemetry system for transmitting blade vibration stress measurements of MHI's 1,160-MW turbine at the Tsuruga nuclear power plant . . . . .	304
Figure 4–42	Corrosion rate of carbon steel (a) and stainless steel (b) coupons in wet medium without preliminary treatment (1) and with pretreatment by ODA for 8 hours (2) . . . . .	307
Figure 4–43	The effect of adding microdoses of ODA into wet-steam stream line on the interaction between water droplets and a solid surface . . . . .	309
Figure 4–44	Experimental verification of the set start-up diagram for a K-220-44 turbine at field start-up tests at the Kola nuclear power plant . . . . .	314
Figure 4–45	Comparison of measured (1) and calculated (2) temperature fields in HP casing flanges of a K-220-44 turbine based on start-up tests at the Kola nuclear power plant . . . . .	316
Figure 4–46	Comparison of measured and calculated metal temperatures in the HP flange (a) and IP flange (b) of the HP–IP cylinder casing of a K-500-60/1500 turbine at start-up . . . . .	317
Figure 4–47	Static dependencies on turbine load for the heating steam temperature in the first steam extraction chamber (a) and heat transfer conditions in the IP steam admission chamber (b) of the HP–IP cylinder of a K-500-50/1500 turbine based on start-up tests at the Novovoronezh nuclear power plant . . . . .	319
Figure 4–48	Static dependencies on the total turbine load for heating steam temperatures in the HP cylinder chambers of a K-220-44 turbine based on start-up tests at the Kola nuclear power plant . . . . .	320
Figure 4–49	Generalization of static dependence for heat transfer conditions from steam to casing in the IP steam admission chambers of various turbines on the basis of their start-up tests . . . . .	322
Figure 4–50	Experimental temperature measurements in the LP cylinder of a K-220-44 turbine for investigating the boundary and initial conditions of heating for the rotor; installation (a) and head (b) of a temperature probe for measuring the rotor surface temperature . . . . .	324

Figure 4–51	Variation in measured steam temperatures in the LP cylinder of a K-220-44 turbine during shutdown (a) and subsequent start-up (b) .....	324
Figure 4–52	Static dependencies of steam temperature decreases in the LP cylinder of a K-220-44 turbine.....	325
Figure 4–53	Comparison of measured (I) and calculated (II) steam temperatures in the LP cylinder of a K-220-44 turbine at start-up.....	327
Figure 4–54	Qualitative static characteristics of the reheat steam temperature after the MSR and heating steam flow rate related to the turbine load and heating steam valve position (a) and variation of steam temperature after the MSR for the K-220-44 turbine at start-up (b), according to field start-up test data .....	328
Figure 4–55	Response of reheat steam temperature and heating steam pressure to disturbances by the valve governing the heating steam flow to the MSR of a K-220-44 turbine .....	329
Figure 4–56	Cool-down characteristics of a welded LP rotor for the K-220-44 turbine .....	331
Figure 4–57	Calculated cool-down characteristics of welded LP rotors for K-220-44 (1) and K-1000-60/1500 (2) turbines (first stage disks) .....	332
Figure 4–58	Measured temperature distribution along the height of LMZ's 1,200-mm titanium LSB under no-load conditions.....	334
Figure 4–59	Sketch of additional temperature measurements (a) and cool-down diagrams (b–d) for the main steam lines of the K-220-44 turbine downstream from the main steam gates, according to field start-up tests at the Kola nuclear power plant .....	336
Figure 4–60	Calculated temperature fields (1) and total stress fields (2) for the most stressed start-up instant and admissible sizes of possible initial macrodefects (3) for the solid double-flow LP rotor of a Siemens high-speed 1,000-MW turbine.....	339
Figure 4–61	Calculated temperature field for a combined LP rotor (right half) .....	340

Figure 4–62 Results of mathematical modeling of heating for a hollow thick-walled cylinder with and without free convection within the internal cavity and traced free convection stream lines within the cavity and isotherms for the rotor body at the end of heating .....	342
Figure 4–63 Influence of free convection within the internal cavity of a welded rotor on its heating for a process modeling cold start-up .....	343
Figure 4–64 Calculation of heating for welded (1) and solid (2) LP rotors of LMZ's K-1000-60/3000 turbine at warm start-ups .....	350
Figure 4–65 Optimized calculated schedules of hot (1), warm (2), and cold (3) start-ups for Turboatom's K-1000-60/1500 turbine .....	351
Figure 4–66 Calculated temperature curves for prestart heating of standard welded LP rotors of Turboatom high-speed wet-steam turbines with different initial temperature conditions and vacuum in the condenser .....	353
Figure 4–67 Dependencies of the upper level of initial loading with the maximum rate on the initial temperature state (a) and the rate of further loading on the current load (b) for Turboatom's K-220-44 turbines with nozzle group (1) and throttle (2) control .....	354
Figure 4–68 Range of admissible load changes for the Turboatom K-1000-60/1500 turbine with various qualities of thermal insulation of the HP casing .....	356
Figure 4–69 Main control board of NUCAMM-90 for 1,356-MW Kashiwazaki-Kariwa Unit 7 .....	358
Figure 4–70 Multiwindow CRT operation display of Hitachi's supervisory and control system for nuclear power plants .....	359
Figure 4–71 Two-coordinate loading diagram for Turboatom's K-220-44 turbine and its application to start-ups at the Kola nuclear plant .....	361
Figure 4–72 Functional chart of a device for the temperature monitoring of the HP rotor for wet-steam turbines .....	363
Figure 4–73 Calculations of heating-up the HP rotor of a K-500-65/3000 turbine during start-up and subsequent load change using different mathematical models .....	364

Figure 4–74	Functional chart of a device for temperature monitoring of LP rotors for wet-steam turbines .....	366
Figure 4–75	Cold start-up of Turboatom's K-500-65/3000 turbine at the Chernobyl nuclear power plant with current admissible load boundaries based on the HP rotor's monitored thermal stress state as presented to the operator .....	367
Figure 4–76	Control desk of the start-up automaton for the K-220-44 turbine at the Kola nuclear power plant .....	368
Figure 4–77	Experimental automated running-up of the turbine for various start-ups.....	370
Figure 4–78	Experimental automated loading of the turbine at hot (a) and warm (b) start-ups .....	371
Figure 4–79	Principle block chart of automated device for loading a wet-steam turbine during start-ups.....	373
Figure 4–80	Automated start-up of a K-220-44 turbine at the Kola power plant.....	374
Figure 5–1	Replacement of an LP rotor with shrunk-on disks (a) with a welded rotor (b) .....	402
Figure 5–2	Change in the static shaft-line curvature due to the replacement of LP disk-type rotors (a) with welded ones (b).....	403
Figure 5–3	Change of a cold start-up diagram for ALSTOM's 900-MW wet-steam turbine after replacement of disk-type LP disk-type rotors (a) with welded rotors (b) .....	404
Figure 5–4	Refurbishment of the LP cylinder of an ABB wet-steam turbine for efficiency improvement.....	406
Figure 5–5	Longitudinal and cross sections of ABB's LP cylinder with a scroll-type steam inlet .....	407
Figure 5–6	LP cylinder of a low-speed turbine after (a) and before (b) retrofitting by Westinghouse.....	409
Figure 5–7	Ruggedized LP cylinder of Westinghouse for retrofitting nuclear steam turbines .....	410
Figure 5–8	Improvements of the LP cylinder design for Siemens' low-speed wet-steam turbines (from a ten-disk rotor to a six-disk rotor).....	412
Figure 5–9	Steam stream lines in the outflow to the condenser for old (a) and improved (b) Siemens turbine designs .....	414

Figure 5-10 Comparison of previous (a) and advanced (b) HP cylinders for retrofitted Siemens wet-steam turbines; steam inlet segment (c) . . . . .	416
Figure 5-11 Refurbished HP (a) and LP (b) cylinders of the 1,000-MW-class wet-steam turbine at Vandellós Unit 2 . . . . .	421
Figure 5-12 Original design of disk-type LP rotors of SONGS' 1,127-MW turbines (a) and their retrofitted optiflow configuration design (b) . . . . .	423

# List of Tables

Table 1–1	Nuclear electricity production in various countries (1999) .....	6
Table 1–2	Top 50 nuclear power plant units ranked by power production (2001).....	7
Table 1–3	Top 20 U.S. nuclear power plants ranked by efficiency (1999–2001).....	12
Table 1–4	Top 20 U.S. nuclear power plants ranked by lowest non-fuel O&M costs (1999–2001) .....	13
Table 1–5	Top 20 U.S. nuclear power plants ranked by power generation (2001).....	14
Table 1–6	Nuclear power generation by countries (2001).....	15
Table 1–7	Operating performances for German nuclear power units (2002) .....	17
Table 3–1	Distribution of wet-steam turbines by gross individual capacity (as of 2001) .....	103
Table 3–2	Main characteristics of Siemens' large wet-steam turbines.....	117
Table 3–3	Main characteristics of some LSBs for high-speed steam turbines of various manufacturers.....	163
Table 3–4	Main characteristics of some LSBs for low-speed steam turbines of various manufacturers.....	166
Table 4–1	Top 50 nuclear power plant units worldwide with the highest annual capacity factor in 2001.....	235
Table 4–2	Comparative efficiency data for some wet-steam turbines of different manufacturers (1986).....	259
Table 4–3	Heat-rate performances of Turboatom's turbine K-1000-60/1500-2 according to the acceptance tests at Zaporozhe nuclear power plant .....	269
Table 4–4	The increase in output for wet-steam turbines of Siemens due to their refurbishment according to their comparative heat-rate performance tests .....	271
Table 4–5	Relevance of steam path damage mechanisms for various steam-turbine types.....	278
Table 5–1	Constituents of performance improvement due to retrofitting LP cylinders for 1127-MW turbines of SONGS .....	425

# Appendix

## List of Abbreviations and Symbols

### Abbreviations of Institutions in the Power Industry

<b>ABB</b>	Asea Brown Boveri, Germany/Switzerland/Sweden (currently merged with ALSTOM)
<b>AEG</b>	Allgemeine Electricitäts-Gesellschaft, Germany (merged with Siemens)
<b>AEP</b>	American Electric Power, United States
<b>ANSI</b>	American National Standards Institute, United States
<b>ASME</b>	American Society of Mechanical Engineers, United States
<b>BBC</b>	Brown Boveri Company (later ABB), Germany/Switzerland (currently merged with ALSTOM)
<b>BHEL</b>	Bharat Heavy Electricals Ltd., India
<b>CEM</b>	Compagnie Electro-Mecanique, France (became part of GEC Alsthom; currently merged with ALSTOM)
<b>EdF</b>	Electricité de France, France
<b>EIA</b>	Energy Information Administration, United States (part of the U.S. Department of Energy)

<b>EPRI</b>	Electric Power Research Institute, United States
<b>GE</b>	General Electric, United States
<b>GEC</b>	The General Electric Company, United Kingdom (became part of GEC Alsthom; currently merged with ALSTOM)
<b>IAEA</b>	International Atomic Energy Agency
<b>INPO</b>	Institute of Nuclear Power Operations, United States
<b>KhTGZ</b>	Kharkov Turbine Works, Soviet Union (currently Turboatom, Ukraine)
<b>KWU</b>	Kraftwerke Union AG, Germany (currently Siemens Power Generation)
<b>LMZ</b>	Leningrad Metallic Works, Russia
<b>MAN</b>	Maschinenfabrik Augsburg-Nürnberg, Germany (became part of GEC Alsthom; currently merged with ALSTOM)
<b>MEI</b>	Moscow Power Engineering Institute, Russia
<b>MHI</b>	Mitsubishi Heavy Industries, Japan
<b>NRC</b>	Nuclear Regulatory Commission, United States
<b>SONGS</b>	San Onofre Nuclear Generating Station, United States
<b>SWPC</b>	Siemens Westinghouse Power Corporation, United States (U.S. subsidiary of Siemens Power Generation)
<b>VNIIAM</b>	All-Russian (formerly All-Union) Research, Planning and Design Institute for Nuclear Power Engineering, Russia
<b>VTI</b>	All-Russian (formerly All-Union) Thermal Engineering Research Institute, Russia

## Acronyms

<b>ABWR</b>	advanced boiling water reactor
<b>AGR</b>	advanced gas-cooled reactor
<b>AW</b>	abrasive wear
<b>BWR</b>	boiling water reactor
<b>C&amp;I</b>	control and instrumentation
<b>CANDU</b>	Canada deuterium uranium (pressurized heavy water reactor)
<b>CC</b>	corrosion cracking
<b>CC</b>	cross-compound (double-shaft turbine)
<b>CE</b>	cavitation erosion
<b>CFD</b>	computational fluid dynamics

<b>COM</b>	condition-oriented maintenance
<b>CRT</b>	cathode ray tube
<b>DACS</b>	data acquisition and control system
<b>DIE</b>	drop impact erosion (see WDE)
<b>ECW</b>	erosion-corrosion wear
<b>EOM</b>	efficiency-oriented maintenance
<b>EPR</b>	European Pressurized Water Reactor (pressurized water reactor)
<b>FBR</b>	fast breeder reactor (see LMFBR)
<b>FD</b>	flat display
<b>FRF</b>	fire-resistant fluid
<b>GCR</b>	gas-cooled reactor
<b>HAW</b>	hydroabrasive wear
<b>HP</b>	high-pressure
<b>HP-IP</b>	high-pressure and intermediate-pressure (integrated turbine cylinder)
<b>HSR</b>	high-speed reclosing (of a generator)
<b>HTGR</b>	high-temperature gas-cooled reactor
<b>HVS</b>	high-velocity separator (centrifugal separator)
<b>HWR</b>	heavy-water reactor (see PHWR)
<b>IP</b>	intermediate-pressure
<b>LMFBR</b>	liquid metal fast breeder reactor
<b>LP</b>	low-pressure
<b>LSB</b>	last stage blade
<b>LWGR</b>	light-water graphite reactor (see PTGR, RBMK)
<b>LWR</b>	light-water reactor
<b>MCR</b>	maximum continuous rating
<b>MOPS</b>	moisture preseparator
<b>MGV</b>	main gate valve
<b>MS</b>	moisture separator
<b>MSR</b>	moisture separator and reheater
<b>MSS</b>	moisture separation stage
<b>NWH</b>	network water heater
<b>O&amp;M</b>	operation and maintenance
<b>ODA</b>	octadecylamine ( $C_{18}H_{37}NH_2$ ), amines-based surface-acting fluid
<b>OEM</b>	original equipment manufacturer
<b>OMTI</b>	oil of Thermal Engineering Institute (Russian acronym)

<b>PBMR</b>	pebble bed modular reactor
<b>PC</b>	personal computer
<b>PdM</b>	predictive maintenance
<b>PHWR</b>	pressurized heavy-water reactor
<b>PM</b>	preventive maintenance
<b>PTGR</b>	pressure-tube graphite reactor (see LWGR, RBMK)
<b>PWR</b>	pressurized water reactor
<b>RBMK</b>	channel reactor of large capacity (Russian acronym; see LWGR)
<b>RCM</b>	reliability-centered maintenance
<b>RRE</b>	relative rotor expansion
<b>SCC</b>	stress corrosion cracking
<b>SCRUPS</b>	special crossunder pipe separator
<b>SCV</b>	stop/control valve
<b>SG</b>	steam generator
<b>SI</b>	International System of Units
<b>TC</b>	tandem-compound (single-shaft turbine)
<b>TTD</b>	terminal temperature difference
<b>USC</b>	ultra-supercritical (steam pressure)
<b>VVER</b>	water-water reactor (Russian acronym; see PWR)
<b>WDE</b>	water drop erosion
<b>WWER</b>	(see VVER)

## Symbols

<b>Symbol</b>	<b>Units</b>	<b>Definition</b>
<i>a</i>	m/s	acoustic velocity
<i>a</i>	$\text{m}^2/\text{s}$	thermal conduction
<i>a</i>	m	distance; length
<i>b</i>	m	width; blade chord length
<i>c</i>	m/s	velocity (of steam or fluid)
<i>c<sub>p</sub></i>	$\text{kJ}/(\text{kg} \times ^\circ\text{C})$	specific heat capacity under invariable pressure
<i>d</i>	m	diameter; mean diameter
<i>F</i>	$\text{m}^2$	annular area, cross-section area
<i>f</i>	Hz; 1/s	frequency
<i>g</i>	$\text{m}/\text{s}^2$	free fall acceleration
<i>G</i>	kg/s; t/h	mass flow amount (of steam)

$H, h$	m	wall thickness, characteristic distance
$H$	kJ/kg	enthalpy
$H$	kJ/kg	available energy; enthalpy drop
$J_0(\mu), J_1(\mu)$	-	Bessel functions
$k$	-	isentropic index
$k$	-	characteristic coefficient
$l$	m	blade length
$L$	-	Laplace operator
$M$	kg	mass
$n$	rpm	rotation speed
$N$	MW	electric power output; load
$p$	MPa	pressure
$r, R$	m	radius
$s$	-	Laplace transfer parameter
$S$	-	rate of corrosion-erosion
$t$	°C	temperature
$T$	°K	absolute temperature
$T$	s	time constant
$u$	m/s	circular rotation speed
$V$	kPa	vacuum (in condenser)
$v$	m³/kg	specific volume
$v$	m/s	rate of crack growth
$w$	m/s	relative velocity (of steam or fluid)
$W_N$	MW/min	rate of ramp load change
$W_t$	°C/min	rate of ramp temperature change
$W$	-	transfer function
$x, y, z$	m	spatial coordinates
$x$	m	distance
$X$	-	steam dryness
$y = 1 - x$	-	steam wetness
$z$	-	number of stages
$\alpha, \beta$	°	exit angles
$\alpha$	W/(m²×°C)	convection heat transfer coefficient
$\beta$	°C⁻¹	coefficient of cubic expansion
$\Delta_{HP}$ , etc.	mm	relative rotor expansion (of HP cylinder, etc.)
$\Delta t$	°C	temperature difference
$\overline{\Delta t} = t_s - \bar{t}$	°C	effective temperature difference
$\Delta\beta$	-	flow turn angle
$\varepsilon$	-	pressure ratio
$\zeta$	-	energy loss factor
$\eta$	-	efficiency
$\lambda$	-	relative steam velocity

$\lambda$	-	percentage of coarse-grained drops
$\lambda$	W/(m×°C)	thermal conduction
$\mu$	-	flow amount factor
$\mu$	kg/(m×s)	dynamic viscosity
$\mu$	-	roots of a characteristic equation
$\nu$	-	Poisson's ratio
$\nu$	m <sup>2</sup> /s	kinematic viscosity
$\rho$	kg/m <sup>3</sup>	specific density
$\rho$	-	reaction degree
$\rho$	-	relative radius
$\sigma$	MPa	stress
$\sigma_{0.2}$	MPa	yield limit (yield strength)
$\tau$	s; min; h	time
$\Delta\tau$	s	time step
$\psi$	-	separation efficiency factor
$\omega$	1/s	angular rotation speed; frequency

## Subscripts and Superscripts

0	steam conditions at the stage (section, turbine) inlet
1	steam conditions between the nozzle and blade rows
2	steam conditions at the stage (section, turbine) outlet
a	axial
c	in the condenser
cr	critical
el	electric
ex	exit
ext	external (surface)
fl	across the flange width (temperature difference)
fl-b	between the flange and bolt (temperature difference)
gr	gross
in; 0	initial
ins	insulated (surface)
int	internal (surface)
lk	leakage
m	medium
m	metal
max	maximum
meas	measured
min	minimum

net	net
nom	nominal
opt	optimum
p	peripheral
r	radial; root
rh	reheat (steam)
s	surface (heated)
sat	saturation
set	set (given)
sh	superheated (main steam)
st	stationary; steam
t	tip
t	temperature (stress)
th	thermal (efficiency)
u	tangential
W	Wilson
wet	wet (steam)
z	axial
$\theta$	tangential; circumferential

## Criteria of Similarity

$$Bi = \frac{\alpha h}{\lambda} \text{ (or) } \frac{\alpha R}{\lambda} \quad \text{Biot number}$$

$$Fo = \frac{\alpha \tau}{h^2} \text{ (or) } \frac{\alpha \tau}{R^2} \quad \text{Fourier number}$$

$$Gr = \frac{g \times \beta \times \Delta \theta}{\nu^2} \times R^3 \quad \text{Grashof number}$$

$$M = \frac{c}{a} \text{ (or) } \frac{w}{a} \quad \text{Mach number}$$

$$Nu = \frac{\alpha d}{\lambda_{st}} \text{ (or) } \frac{\alpha x}{\lambda_{st}} \quad \text{Nusselt number}$$

$$Pr = \frac{c_p \mu}{\lambda} \quad \text{Prandtl number}$$

$$Ra = Gr \times Pr \quad \text{Rayleigh number}$$

$$Re = \frac{\rho w d}{\mu} \text{ (or) } \frac{\rho w x}{\mu} \quad \text{Reynolds number}$$

# Conversion Table for Main Units Used

Physical qualities	SI to US Customary System	US Customary System to SI
Length	1 m = 3.28 ft = 39.36 in	1 ft = 0.305 m; 1 in = 0.0254 m
Area	1 m <sup>2</sup> = 10.76 ft <sup>2</sup>	1 ft <sup>2</sup> = 0.093 m <sup>2</sup>
Volume	1 m <sup>3</sup> = 35.3 ft <sup>3</sup>	1 ft <sup>3</sup> = 0.0283 m <sup>3</sup>
Velocity, speed	1m/s = 3.28 ft/s	1 ft/s = 0.305 m/s
Density	1 kg/m <sup>3</sup> = 0.0624 lb <sub>m</sub> /ft <sup>3</sup>	1 lb <sub>m</sub> /ft <sup>3</sup> = 16.02 kg/m <sup>3</sup>
Force	1 N = 0.225 lb <sub>f</sub>	1 lb <sub>f</sub> = 4.45 N
Mass	1 kg = 2.205 lb <sub>m</sub>	1 lb <sub>m</sub> = 0.454 kg
Pressure, stress	1 MPa = 10 <sup>6</sup> N/m <sup>2</sup> = 10 bar = 145.0 psi (lb <sub>f</sub> /in <sup>2</sup> ) 1 kPa = 0.145 psi	1 psi = 6.9 kPa = 0.0069 MPa 1 in. Hg = 3.39 kPa
Energy, work, heat	1 kJ = 0.948 Btu	1 Btu = 1.055 kJ
Power, heat flow	1 W = 1 J/s = 3.41 Btu/h	1 Btu/h = 0.293 W
Heat flux per unit area	1 W/m <sup>2</sup> = 0.317 Btu/(h×ft <sup>2</sup> )	1 Btu/(h×ft <sup>2</sup> ) = 3.154 W/m <sup>2</sup>
Energy per unit mass, enthalpy	1 kJ/kg = 0.43 Btu/ lb <sub>m</sub>	1 Btu/ lb <sub>m</sub> = 2.33 kJ/kg
Temperature	t °C = (t °F - 32)/ 1.8 T °K = (t °F - 32)/ 1.8 + 273.16	t °F = 1.8×t °C + 32 t °F = 1.8× (T °K-273.16) + 32
Temperature difference	1 °C = 1 °K = 0.556 °F	1 °F = 1.8 °C
Specific heat capacity, entropy	1 kJ/(kg ×°C) = 0.239 Btu/ (lb <sub>m</sub> ×°F)	1 Btu/ (lb <sub>m</sub> ×°F) = 4.187 kJ/(kg×°C)
Thermal conduction	1 W/(m×°C) = 0.578 Btu/(h×ft×°F)	1 Btu/(h×ft×°F) = 1.73 (W/m×°C)
Heat transfer coefficient	1 W/(m <sup>2</sup> ×°C) = 0.176 Btu/(h×ft <sup>2</sup> ×°F)	1 Btu/(h×ft <sup>2</sup> ×°F) = 5.68 W/(m <sup>2</sup> ×°C)
Dynamic viscosity	1 kg/(m×s) = 0.672 lb <sub>m</sub> /(ft×s)	1 lb <sub>m</sub> /(ft×s) = 1.49 kg/(m×s)
Temperature conduction, cinematic viscosity	1 m <sup>2</sup> /s = 10.76 ft <sup>2</sup> /s	1 ft <sup>2</sup> /s = 0.0929 m <sup>2</sup> /s

# INDEX

---

## Index Terms

## Links

### A

Abbreviations	435
Acronyms	436
Advanced BWR (ABWR) projects	27
Advanced gas-cooled reactor (AGR)	24
Advanced PWR (APWR) projects	27
Aerodynamics	74      152      165      174
LSB design	180
Alarm	356
Algorithm	346
All-volatile treatment	83
ALSTOM upgrade experience (SONGS)	421
HP and LP cylinders	421
ALSTOM wet-steam turbines	106
Arabelle	106
Mirabelle	108
Amines-based surfactant (steam and water paths)	305
Annular exhaust	108
Antirad additive	158
APR1400 reactor	28
Arabelle wet-steam turbine	106      118      152      160
	258

This page has been reformatted by Knovel to provide easier navigation.

## Index Terms

## Links

ASME Performance Test Codes				
Code on Steam Turbines (PTC 6)	260	265	272	
Atmospheric corrosion	305			
Atomic Energy of Canada Limited				
(AECL)	28			
Automated control and information				
support (turbine transients)	350	356		
Automated control	311	350	356	
turbine operating conditions	350			
turbine transients	350	356		
information support	350	356		
automaton system	367			
Automaton system (start-up control)	367			
<b>B</b>				
Backpressure	155	169		
Base load mode	16	154	233	242
	258	276		
Basement condenser	133			
Baumann factor/rule	69	80	116	
Bearings (turbine design)	122	124	157	
Bending stress	167			
Blade damages	296			
Blade erosion	105	190	255	409
protection	190			
Blade length	49	70	105	118
	161	171	189	
design	161			

This page has been reformatted by Knovel to provide easier navigation.

<u>Index Terms</u>	<u>Links</u>
Blade profile/shape	65      71      174      187 195
bowed	71      187
curved	71      187
inclined	71      187
free-standing	174
radial	187
furrowed	195
Blade repair	398
Blade root	170      292
fork-shaped	170
Blade row	54
Blade stress	170
Blading	40      49      54      65 70      104      111      118 136      140      161      255 292      296      398      409
last stage blades	40      49      65      70 104      111      118      161 255      409
length	49      70      105      118 161      171
blade row	54
profile/shape	65      71      174      187 195
impulse-type turbine	73      136      140
reaction-type turbine	73      136      140
erosion	105      255      409
design	136      161
stress	170

This page has been reformatted by Knovel to provide easier navigation.

## Index Terms

## Links

Blading ( <i>Cont.</i> )				
root	170	292		
damages	296			
repair	398			
Bleedings	39	53	129	199
Boiling water reactor (BWR)	xxx	18	27	46
	102	104	143	
advanced BWR projects	27			
Bored rotor	122	124		
Bucket profile/shape	140	187		
curved	140			
radial	187			
Butterfly cylinder arrangement	127			
Butterfly valve	148	151	155	
Bypass valve	155			

## C

Calandria	21			
Campbell diagram	176	178		
Canada deuterium uranium PWR (CANDU)	xxx	21	28	
CANDU 6 reactor	28			
NG-CANDU	28			
Capacity factor	13	233		
Carbon dioxide	xxxi	10	24	26
Casing flange	337			
Cathode ray tube (CRT)	357			
Centrifugal stress	124	161	167	171
	245			
Centrifugation	195			

This page has been reformatted by Knovel to provide easier navigation.

<u>Index Terms</u>	<u>Links</u>
Channel reactor of large capacity (RBMK)	22      29      102      143
Chernobyl catastrophe (1986)	xxx      xxxiv      23
Chevron/chevron plate	206      208
Chromium	191
Chromium steel	145
Coal fuel	xxxii      45      104
Cobalt	191
Cold start-up	352
Commercial nuclear plant (first)	1
Common saddle valve unit	148      150
Computational fluid dynamics (CFD)	xxxiii      72      131      400 424
Condensate sampling/analysis	83
Condensation	55      73      83      301
spontaneous	55      58      301
condensation shock	55
Condenser	49      53      133
cooling water connection	49
basement	133
Condition-oriented maintenance (COM)	395
Control and instrumentation (C&I)	
systems	356
Control systems	311      350      356
automated control	311      350      356
C&I systems	356
automaton	367
Control valve	148      150      155
Conversion table	442

This page has been reformatted by Knovel to provide easier navigation.

<u>Index Terms</u>	<u>Links</u>
Cooling-down process	257 330
characteristics	257
Correction (variables)	272
Corrosion process	42 144
Corrosion rate	194 206 282
Corrosion resistant alloy	145
Corrosion-fatigue and stress-corrosion	
cracking (wet-steam turbines)	279
Corrosivity (environment/materials)	42 83 115 144
	194 206 279 305
corrosion process	42 144
corrosion resistant alloy	145
rate	194 206 282
downtime	305
Countermeasure (overspeeding)	155
Crack propagation	276
Crevice corrosion	145 280 296
Criteria of similarity	441
Critical elements (turbine operating	
condition)	315 346 355 362
	370
Cross-compound (CC) turbine	105 115
Crossover pipes	110
Curved-entry fir-tree root	170
Cylinder upgrading	415
Siemens experience	415
Mitsubishi Heavy Industries	
experience	419
ALSTOM experience at SONGS	421

This page has been reformatted by Knovel to provide easier navigation.

## Index Terms

## Links

<b>D</b>	
Damage mechanisms (steam path)	277
Damages and causes (wet-steam	
turbines)	276
steam path	277
stress-corrosion and corrosion-	
fatigue cracking	279
erosion-corrosion of turbine casings	293
blading	296
Data acquisition and control system	
(DACS)	357
data presentation	360
information storage/presentation	360
Data presentation	360
Deactivation process	191
Degaerator	39
Decommissioning	305
Demister/wire mesh	206      208
Dense pack turbine	73      137      140
design	73
Depassivation	283
Design (wet-steam turbines)	101
general design features	104
influence of single capacity and	
rotation speed	104
blading, gland seals, and protection	
against erosion–corrosion wear	136
steam admission elements	148
bearings	157

This page has been reformatted by Knovel to provide easier navigation.

## Index Terms

## Links

Design (wet-steam turbines) ( <i>Cont.</i> )	
last stage blades	161
blade length	161
roots, shrouds, and snubbers	170
aerodynamics	180
protection against WDE	190
water removal from turbines	194
moisture separation and removal	
between stage rows	195
intrachannel moisture separation	199
moisture separating stages/stage-separators	204
external moisture separators and	
reheaters	206
references	217
bibliography	225
Design features (last stage blades)	136      161
blade length	161
roots, shrouds, and snubbers	170
aerodynamics	180
protection against WDE	190
Design features (water removal	
from turbines)	194
peripheral moisture separation	
and removal between stage rows	195
intrachannel moisture separation	199
moisture separating stages/	
stage-separators	204
external moisture separators and	
reheaters	206
Disk-type rotor	402

This page has been reformatted by Knovel to provide easier navigation.

## Index Terms

## Links

Double-shaft turbine	105			
Double-turbine nuclear power unit	4	102		
Dovetail attachment	171			
Downtime corrosion	305			
<b>E</b>				
Efficiency and heat-rate performance				
tests (wet-steam turbines)	258			
Efficiency value (turbine performance)	44	52		
Efficiency-oriented maintenance (EOM)	395			
Electric output measurement	263			
Electricity production cost	9	258		
nuclear power plants	9			
fossil fuel plants	11			
Electric-spark machining	191			
Electrochemical theory	282			
Emissions/emission control	xxxii	9	26	29
Endoscope method	76	89		
boroscope	89			
End steam pressure (turbine)	47			
pressure reduction	47			
Energy Information Administration				
(EIA)	10			
Energy loss	44	50	60	63
	68	80	91	108
	136	140	157	174
	181			
Enriched nuclear fuel	21	23		
uranium	21			

This page has been reformatted by Knovel to provide easier navigation.

<u>Index Terms</u>	<u>Links</u>
Enthalpy drop	62      106      136      204 273
Erosion-corrosion process	42      144
Erosion-corrosion rate	194      206      282
Erosion-corrosion wear (ECW)	42      83      115      137 191      206      213      279 305
process	42      144
protection	137      191      296      305
resistance	145      191
rate	194      206      282
turbine casings	293
amines-based surfactant	305
Erosion-corrosion wear protection	137      191      296      305 amines-based surfactant 305
Erosion resistance	145      191
European Pressurized Water Reactor (EPR)	28      118
projects	28
Exhaust area	108      124      127      131 133      135      168
Experimental Breeder Reactor-I (EBR-I)	1
Experimental research (wet-steam flow)	74
Experimental research and calculation (turbine transients)	310
start-up tests of wet-steam turbines	310
calculation of temperature fields for	

This page has been reformatted by Knovel to provide easier navigation.

## Index Terms

## Links

Experimental research and calculation ( <i>Cont.</i> )				
main turbine design elements		337		
calculated optimization of start-up				
diagrams		343		
External moisture separator/reheater	195	206		
External water removal	195	206		
separator/reheater	195	206		
Extinction/light-scattering/				
light-attenuation method	78	80		
<b>F</b>				
Fast breeder reactor (FBR)		25		
liquid-metal FSB		25		
Field tests (turbine performance)		310		
recommendations		310		
verification		314		
Finite-element model (root)		170		
Fire hazard		158		
Fire reheat		5		
Fire-resistant fluid (FRF)		158		
OMTI		158		
Fir-tree root		170		
Fixed bearing		160		
Fixed blade channel		136		
Flow amount factor		61		
Forged rotor	122	124	288	349
Fossil fuel power unit/plant	xxx	2	40	44
	52	73	103	115
	133	148	191	251
	258	276	364	

This page has been reformatted by Knovel to provide easier navigation.

## Index Terms

## Links

France	16			
Friction	169			
Fuel fabrication expenditure	21			
Functional chart	360			
<b>G</b>				
Gas turbine–modular helium reactor (GT–MHR)	25			
Gas-cooled, graphite-moderated reactor	24			
Generation II technology	29			
Generation III technology	26			
Generation III+ technology	26			
Generation IV technology	26			
Germany	16			
Gland seal (turbine design)	136			
Greenhouse gas	xxxii      9      26      29			
Grid frequency	105      116			
Gross capacity	103      106			
Gross efficiency performance	9      44      52      103			
	106      108      258			
efficiency value	44      52			

## **H**

Half-speed/full-speed turbine	127
Heat transfer	313      315      337      348
Heat-rate performance tests (wet-steam turbines)	258
Helium	25
High-speed reclosing (HSR)	302

This page has been reformatted by Knovel to provide easier navigation.

## Index Terms

## Links

High-temperature gas-cooled reactor (HTGR)	25
High-velocity separator (HVS)	215
History (nuclear wet-steam turbine)	1
Hollow-nozzle vane	199
Hook load	171
HP cylinder upgrading	415

## I

Impulse-type turbine (blading)	73	136	140
Inconel® 82	191		
Indicatrix diagram	78		
Information storage/presentation	360		
data presentation	360		
functional chart	360		
Information support and automated control (turbine transients)	356		
Information technology	356		
Institute of Nuclear Power Operations (INPO)	14		
Instrumentation (measurement)	261		
Internal water removal	194		
International Atomic Energy Agency (IAEA)	5	102	
Intrachannel moisture separation/ extraction (turbine design)	195	199	
Isentropic index	58		
Isotach field	184	189	

This page has been reformatted by Knovel to provide easier navigation.

## Index Terms

## Links

### **J**

Journal bearing	157	159
journal neck	157	

### **K**

Keyways (disks)	289
Korean next generation reactor (KNGR)	28
APR1400 reactor	28
Korean standard nuclear plant (KSNP) project	28

### **L**

Laser probe	83			
Last stage blade (LSB)	40	49	65	70
	104	111	118	136
	140	161	255	296
	409			
length	49	70	105	118
	161	171	189	
profile/shape	65	71	174	187
	195			
erosion	105	190	255	409
design features	136	161		
protection from WDE	190			
damages	296			

This page has been reformatted by Knovel to provide easier navigation.

## Index Terms

## Links

Last stage blade design features	136	161
blade length	161	
high-speed steam turbine	163	
low-speed steam turbine	165	
roots, shrouds, and snubbers	170	
attachment base	170	
aerodynamics	180	
protection against WDE	190	
Leading indications (turbine operating condition)	343	
Leakage	140	143
Length-to-mean diameter ratio (LSB)	189	
License/relicense	29	
Light-scattering/light-attenuation method	78	80
Light-water reactor (LWR)	18	
pressurized water reactor	18	
boiling water reactor	18	
VVER/WWER reactor	18	
Light-water-cooled graphite-moderated reactor (LWGR)	22	46
RBMK reactor	22	
Liquid sodium	25	
Liquid-metal FSB	25	
Load change range	355	
Load discharge	254	
Load distribution	171	
Load rejection	155	
Loading program	353	369
program-in-time	369	

This page has been reformatted by Knovel to provide easier navigation.

## Index Terms

## Links

Longshanking	398	
Louver-plate/corrugated-plate separator	206	208
LP cylinders	408	
retrofit	411	
upgrading	415	
Lubricant/lubrication	157	

## **M**

Mach number	182	188	
Magnox reactors	24		
Main gate valve (MGV)	251		
Manufacturers (wet-steam turbine)	101		
ALSTOM	101		
Siemens Power Generation	101		
General Electric	101		
Hitachi	101		
Mitsubishi Heavy Industries	101		
Toshiba	102		
Turboatom	102		
Leningrad Metallic Works	102		
Skoda Energo	102		
Ansaldo Energia	102		
Bharat Heavy Electricals, Ltd.	102		
Donfang Steam Turbine Works	102		
Shanghai Steam Turbine Co., Ltd.	102		
Doosan Heavy Industries &			
Construction Co.	102		
Mathematical modeling	312		
Maximum continuous rating (MCR)	39	154	251

This page has been reformatted by Knovel to provide easier navigation.

## Index Terms

## Links

Measurements (heat rate performance test)	261
instrumentation	261
Mechanical-hydraulic governing system	115
Microadditives (steam and water paths)	305
Microvideo probe	80
Mirabelle wet-steam turbine	108
Mitsubishi Heavy Industries upgrade experience (HP and LP cylinders)	419
Model turbine stage	65
Moisture content (thermal efficiency)	2      42      47      50
	63      83      105      194
	263      272
Moisture preseparator (MOPS)	213
Moisture separating stage/stage-separator	195      204
Moisture separation and removal	4      39      50      53
	67      74      106      110
	122      124      155      194
	252
moisture separator	39      50      53      206
moisture separator and reheater	50      53      106      110
	122      124      155      195
	204      206      252
separation factor	67
efficiency	74
wet-steam turbine design	194
separating stage/stage-separator	195      204
moisture stage-separator	204
moisture preseparator	213

This page has been reformatted by Knovel to provide easier navigation.

## Index Terms

## Links

Moisture separation/removal				
(wet-steam turbine design)	194			
internal	194			
peripheral between stage rows	195			
separating stage/stage-separator	195	204		
intrachannel	199			
external separator and reheater	206			
Moisture separator (MS)	39	50	53	206
design	206			
Moisture separator and reheater (MSR)	50	53	106	110
	122	124	155	195
	204	206	252	
design	206			
distributed type	213			
Moisture stage-separator (MSS)	204			
Mollier diagram	40	56		
Monitoring (equipment condition)	356			
Motor operating condition	333			
Multi-cylinder nuclear power unit	4			
Multifactor influence (steam flow)	64			
Multiphase flow	53	59	62	

## **N**

Natural uranium	21		
Next generation CANDU project			
(NG CANDU)	28		
Nitric/nitrous oxide	xxxii	10	
No-load operating conditions	351	355	
Nozzle box	115		
Nozzle group control	111	154	301

This page has been reformatted by Knovel to provide easier navigation.

## Index Terms

## Links

Nozzle row	136	
Nuclear electricity production		
(worldwide)	5	
Nuclear Energy Institute (NEI)	10	
Nuclear power capacity (worldwide)	5	
Nuclear power industry prospects,		
(wet-steam turbines)	26	
Generation III technology	26	
Generation III+ technology	26	
Generation IV technology	26	
advanced BWR projects	27	
advanced PWR projects	27	
EPR projects	28	
VVER project	28	
SWR project	28	
Korean next generation reactors	28	
Korean standard nuclear plant		
project	28	
next generation CANDU project	28	
life span	29	
plant licensing/relicensing	29	
refurbishing	29	
uprating	30	
Nuclear power industry	xxx	1
wet-steam turbine history	1	
operating performance	5	
nuclear reactor types	18	

This page has been reformatted by Knovel to provide easier navigation.

## Index Terms

## Links

Nuclear power industry ( <i>Cont.</i> )	
wet-steam turbine-based nuclear	
power plants	26
references	31
bibliography	35
Nuclear Power Plant Control Complex	
with Advanced Man-Machine	
Interface 90	357
Nuclear power plants (wet-steam	
turbine)	xxx      26
Nuclear reactor types	18
light-water reactor	18
pressurized water reactor	18
boiling water reactor	18
VVER/WWER reactor	18
shutdown for refueling	19
pressure vessel	20
enriched uranium	21
Canada deuterium uranium PWR	21
light-water-cooled graphite-	
moderated reactor	22
pressure-tube graphite reactor	22
RBMK reactor	22
wet-steam turbine	23
gas-cooled, graphite-moderated	
reactor	24
advanced gas-cooled reactor	24
Magnox reactor	24
high-temperature gas-cooled reactor	25
gas turbine-modular helium reactor	25

This page has been reformatted by Knovel to provide easier navigation.

## Index Terms

## Links

Nuclear reactor types ( <i>Cont.</i> )	
pebble bed modular reactor	25
fast breeder reactor	25
liquid-metal FSB	25
Nuclear wet-steam turbine (history)	1
first power installation	1
Nucleation	55      74

## O

Octadecylamine (ODA)	306
Oil fire	158
OMTI fire-resistant fluid	158
Operating conditions	233
Operating efficiency and heat-rate	
performance tests	258
Operating mode	13      154      233      242
	254      258      276      351
	355
capacity factor	13      233
base load mode	16      154      233      242
	258      276
system load control	237
reserve/standby	254
Operating performance (nuclear plant)	9
efficiency	11
operation and maintenance costs	12
capacity factor	13
base-load mode	16
U.S. plants	13
worldwide plants	15

This page has been reformatted by Knovel to provide easier navigation.

## Index Terms

## Links

Operating performance (nuclear plant) ( <i>Cont.</i> )	
France	16
Germany	16
safety	16
Operation	233
operating conditions	233
efficiency and heat-rate performance tests	258
generic damages and their causes	276
protection and preservation of steam	
and water paths using	
microadditives of amines-based	
surfactant	305
experimental research and	
calculation of turbine transients	310
information support for operators	
and automated control during	
turbine transients	356
references	375
bibliography	385
Operation and maintenance (O&M)	
costs	12
Optical attenuation probe	80
Optical method (wet-steam structure)	78
80	
Optiflow configuration	423
Optimization calculation (turbine start-up diagrams)	343
Original equipment manufacturer (OEM)	401
Outage	396

This page has been reformatted by Knovel to provide easier navigation.

## Index Terms

## Links

Output capacity	5	30	40	103
	106	116		
worldwide	5			
Overspeeding	155			
countermeasure	155			
Oxygenated treatment (OT)	83			
<b>P</b>				
Partition-to-initial steam pressure ratio	51			
Passivation/depassivation	282			
Pebble bed modular reactor (PBMR)	25			
Performance (wet-steam turbines)	9	103	106	108
	258			
efficiency	11			
operation and maintenance costs	12			
capacity factor	13			
base-load mode	16			
U.S. plants	13			
worldwide plants	15			
France	16			
Germany	16			
safety	16			
Performance monitoring	258	395		
diagnosis	395			
Performance tests	258	310		
heat-rate tests	258			
field tests	310			
start-up tests	310			
Peripheral moisture separation/removal				
(stage row)	195			

This page has been reformatted by Knovel to provide easier navigation.

<u>Index Terms</u>	<u>Links</u>
Petroleum oil lubricant	158
pH level	281
Plutonium production	21
Power generation/output capacity	5      30      40      103
	106      116
worldwide	5
Predictive maintenance (PdM)	395
Preservation technology	305
microadditives	305
amines-based surfactant	305
Pressure-balance hole (disk)	140
Pressure drop	129      133      148
Pressure measuring	262
Pressure tube	21
Pressure vessel	20
Pressured heavy-water reactor (PHWR)	xxx      21      102
Pressure-tube graphite reactor (PTGR)	22
Pressurized water reactor (PWR)	xxx      18      27      102
	111
advanced PWR projects	27
Preventive maintenance (PM)	395
Prong-and-finger/fork-shaped root	170
Protection and preservation	
(steam and water paths)	305
microadditives	305
amines-based surfactant	305

This page has been reformatted by Knovel to provide easier navigation.

## Index Terms

## Links

### **R**

Radioactive steam	143			
RBMK reactor	22	29	102	143
Reaction-type turbine (blading)	73	136	140	
Reactor trip	22			
Refueling	19	241	254	396
	400			
shutdown	19	254		
Refurbishing (plant and equipment)	xxxi	29	180	187
	270	395		
wet-steam turbines	270	395		
Refurbishment (wet-steam turbines)	270	395		
retrofitting versus repairing	395			
retrofitting LP cylinders	402			
complete upgrading of turbines				
(HP and LP cylinders)	415			
references	427			
bibliography	431			
Regeneration/regenerative system	39	198		
Reheat/reheating	4	39	43	50
	106	110	122	124
	155	195	204	206
	252	328	346	354
reheater design	206			
Relative rotor expansion (RRE)	249	277	310	
Reliability/availability				
(wet-steam turbines)	276			
Reliability-centered maintenance				
(RCM)	395			

This page has been reformatted by Knovel to provide easier navigation.

## Index Terms

## Links

Repairing versus retrofitting (wet-steam turbines)	395
Replacement option	399
rotor replacement	402
Replacing disk-type rotors with welded rotors (ALSTOM)	402
Replacing LP disk-type rotors with solid rotors (Westinghouse)	408
Research (wet-steam flow experiments)	74
Research and calculation (wet-steam	
turbine transients)	310
start-up tests of wet-steam turbines	310
calculation of temperature fields	
for main turbine design elements	337
calculated optimization of start-up	
diagrams	343
Reserve/standby mode	254
Retarding torque	64
Retrofitting LP cylinders with disk-type	
rotors (Siemens)	411
Retrofitting LP cylinders	402
replacing disk-type rotors with	
welded rotors (ALSTOM	
experience)	402
replacing LP disk-type rotors	
with solid rotors (Westinghouse	
experience)	408
retrofitting LP cylinders with	
disk-type rotors (Siemens	
experience)	411

This page has been reformatted by Knovel to provide easier navigation.

## Index Terms

## Links

Retrofitting versus repairing (wet-steam turbines)	395			
Rotating blade	136	140		
Rotating blade channel	136			
Rotation speed	5	104	154	161
	170	173	195	352
influence on turbine design	104			
Rotor	122	124	127	160
	245	288	338	349
	399	402		
bored	122	124		
forged	122	124	288	349
solid	122	124	127	349
	408			
vibration	160			
fracture	245			
rotor cavity	341			
disk-type	402			
welded	402			
Ruggedized LP turbine	408			

## **S**

Safety (nuclear power plant)	16		
San Onofre Nuclear Generating Station (SONGS)	304		
Saturated steam	40		
Seal/sealing	140	143	
Separating stage/stage-separator (wet-steam turbine design)	195	204	
moisture stage separator	204		

This page has been reformatted by Knovel to provide easier navigation.

## Index Terms

## Links

Separation factor	67
Shaft arrangement design	159
Shield/shielding	146
Shippingport Station	1
Shrouding	124      140      170
LSB design	170
Shrunk-on wheel disk	4      122      124      127 287
Shutdown for refueling	19      254
Siemens large wet-steam turbines	116
Siemens upgrade experience (HP and LP cylinders)	415
Similarity criteria	441
Single-capacity influence (wet-steam turbine design)	104
Single-shaft turbine	104
Single-turbine nuclear power unit	102
Slide factor	62
Snubber (LSB design)	170
tie-boss	172
Software (turbine transient optimization)	346
Solid rotor	122      124      127      349 408
Special cross-under pipe separator (SCRUPS)	213
Specific volume ratio	63
Splitting pressure	51
Spontaneous condensation	55      58      301
Stage efficiency	65      180

This page has been reformatted by Knovel to provide easier navigation.

<u>Index Terms</u>	<u>Links</u>
Stage reaction optimization	73
Stage reactivity/reaction degree	136
Stainless steel	145      162      191      296
Standby mode	254
Start-up diagram optimization	343
Start-up tests (wet-steam turbines)	310
Start-up	238      242      310      343
tests	310
optimization	343
Stator elements	144
Steam admission element (wet-steam turbine design)	148
Steam and water paths protection and preservation	305
microadditives	305
amines-based surfactant	305
Steam conditions (initial, partition, and end)	39
Steam contaminants	281
Steam expansion process (wet-steam turbine)	39
initial, partition, and end steam conditions	39
wet-steam flow in turbine steam path	53
references	93
bibliography	97
Steam extraction/bleedings	39      53      129      199

This page has been reformatted by Knovel to provide easier navigation.

<u>Index Terms</u>	<u>Links</u>			
Steam flow	3	39	104	129
	136	148	165	181
	189	195	199	277
	305	323	334	346
	399	413	419	424
control	3	148		
initial, partition, and end steam				
conditions	39			
extraction/bleedings	39	53	129	199
turbine steam path	53	104	154	277
	305	334	399	413
	419	424		
amount	61	131	148	182
	189	346		
loss	67			
experimental research	74			
flow pattern	90	181	323	
velocity	131	136	148	165
	195			
Steam flow amount	61	131	148	182
	189	346		
flow amount factor	61			
Steam flow pattern	90	181	323	
Steam generator	39			
Steam moisture. <i>See</i> Steam wetness.				
Steam path	53	104	154	277
	305	334	399	413
	419	424		
turbine blade row	54			
wetness influence on efficiency	63			

This page has been reformatted by Knovel to provide easier navigation.

## Index Terms

## Links

Steam path ( <i>Cont.</i> )					
experimental research	74				
damage mechanisms	277				
protection and preservation	305				
microadditives	305				
testing	334				
Steam pressure reduction	47				
Steam reheat/reheating	4	39	43	50	
	106	110	122	124	
	155	195	204	206	
	252	328	346	354	
reheater design	206				
Steam velocity	131	136	148	165	
	195				
Steam viscosity	184				
Steam wetness (thermal efficiency)	2	42	47	50	
	63	83	105	194	
	263	272			
Steel	145	162	191	281	
	287	290	296		
Stellite laminas	3	191	301	409	
Stop valve	148	150			
Stream velocity	54	59	64		
Streamline	181	188	413		
Stress corrosion cracking (SCC)	122	127	279	308	
	397	400	402	408	
	419	422			
corrosion fatigue	279				
Stress-corrosion and corrosion-fatigue					
cracking (wet-steam turbines)	279				

This page has been reformatted by Knovel to provide easier navigation.

## Index Terms

## Links

Stretch-out process	241			
Subcooling	55	58		
Sub-critical main steam pressure	44			
Subscripts/superscripts	440			
Suction removal	195	199		
suction slot	199			
Sulfur dioxide	10			
Superheated high-pressure steam	40	53	58	320
Supersaturation	55	58		
Supervisory and control system	358			
Surface-type water trap	199			
Surfactant microadditives	305			
SWR project	28			
Symbols	438			
System load control	237			

## **T**

Tandem-compound (TC) turbine	104	111		
Temperature effect (wet-steam flow)	55			
Temperature fields calculation (main turbine design elements)	337			
Temperature measuring fields calculation	263	337	369	
Tennessee Valley Authority (TVA)	30			
Tensile radial stress	161	167	169	
Tensile strength	171	245	281	288
Terminal temperature difference (TTD)	47	274		
Terminology	436			

This page has been reformatted by Knovel to provide easier navigation.

<u>Index Terms</u>	<u>Links</u>
Test probes	76      78      80      329 334
optical attenuation probe	80
microvideo probe	80
laser probe	83
boroscope/endoscope	86      89
Thermal convection	341
Thermal efficiency (wetness influence)	2      42      47      50 63      83      105      194 263      272
Thermal expansion arrangement	160
Thermal process (wet-steam turbine)	39
initial, partition, and end steam conditions	39
wet-steam flow in turbine steam path	53
references	92
bibliography	96
Thermal stress	245      313      315      337 349
Thermodynamic conditions (steam)	53
Three-dimensional computation	71
Three Mile Island accident (1979)	xxx      29
Throttle control	47      77      153      239 320
Throttling process (steam flow)	47      77
Tie-boss	172
wire tie	174
Titanium	104      116      127      163 168      171      175      190 192

This page has been reformatted by Knovel to provide easier navigation.

## Index Terms

## Links

Torque effect	64
Torsional oscillation/resonance	302
Train cylinder arrangement	127
Tungsten	191
Turbine design elements (temperature fields calculation)	337
Turbine repair/refurbishment	270
retrofitting versus repairing	395
retrofitting LP cylinders	402
complete upgrading of turbines (HP and LP cylinders)	415
references	427
bibliography	431
Turbine stage model	65
Turbine start-up diagrams (optimization calculation)	343
Turbine start-up tests	310
Turbine steam path (wet-steam flow)	53
	104
	154
	277
	305
	334
	399
	413
	419
	424
turbine blade row	54
wetness influence on efficiency	63
experimental research	74
damage mechanisms	277
protection and preservation	305
microadditives	305
testing	334

This page has been reformatted by Knovel to provide easier navigation.

<u>Index Terms</u>	<u>Links</u>
Turbine transients	238      310
operating conditions	238
experimental research and calculation	310
monitoring	311
temperature fields	337
optimization	343
information support and automated control	356
Turboseparator	215
Turngate	148      150
Two-phase flow	53      59      62
 <b>U</b>	
U.S. nuclear power plants (statistics)	10
efficiency	11
O&M costs	12
power generation	13
U.S. Nuclear Regulatory Commission	
(NRC)	14      29
license/relicense	29
Ultra-supercritical (USC) main steam	
pressure	44
Universal correction curve	272
Upgrading of turbines (HP and LP cylinders)	415
Siemens experience	415
Mitsubishi Heavy Industries experience	419
ALSTOM experience at SONGS	421

This page has been reformatted by Knovel to provide easier navigation.

## Index Terms

## Links

Uprating (reactor output)	30
Uranium dioxide	21
<b>V</b>	
Vacuum breaker valve	155
Valve aerodynamics	152
Valve steam-chest	250
Vane profile/shape	140      187      199      405
bowed/curved	140      187
inclined	187
radial	187
saber	187
hollow-nozzle	199
Vibration	148      167      170      173
	176      191      296      302
Vortices	133      181      194      255
VVER/WWER reactors	18      28      47      102
	111

## **W**

Water channel/trap	53      195
trap belt	53      195
Water chemistry	83
Water drop erosion (WDE)	42      105      144      169
	190      293      298      308
	397      409
WDE criterion	105
last stage blade protection	190

This page has been reformatted by Knovel to provide easier navigation.

## Index Terms

## Links

Water drop size	53	59	70	77
	190	194		
Water motion	59			
Water removal from turbine (turbine				
design)	194			
internal	194			
peripheral moisture separation				
and removal between stage rows	195			
intrachannel moisture separation	199			
moisture separating stage/				
stage-separator	204			
external moisture separator and				
reheater	206			
Water trap belt	53	195		
Welded rotor	106	111	115	122
	124	127	288	340
	402			
Welding technology	398			
Wetness influence (thermal efficiency)	2	42	47	50
	63	83	105	194
	263	272		
Wet-steam flow (turbine steam path)	53			
turbine blade rows	54			
wetness influence on efficiency	63			
experimental research	74			
Wet-steam parameters	74			
Wet-steam turbine design	101	337		
manufacturers	101			
general features	104			

This page has been reformatted by Knovel to provide easier navigation.

## Index Terms

## Links

Wet-steam turbine design ( <i>Cont.</i> )	
influence of single capacity and	
rotation speed	104
blading, gland seals, and protection	
against erosion–corrosion wear	136
steam admission elements	148
bearings	157
last stage blades	161
blade length	161
roots, shrouds, and snubbers	170
aerodynamics	180
protection against WDE	190
water removal from turbines	194
moisture separation/removal	
between stage rows	195
intrachannel moisture separation	199
moisture separating stages/	
stage-separators	204
external moisture separators and	
reheaters	206
references	216
bibliography	224
Wet-steam turbine transients	238      310
operating conditions	238
experimental research and	
calculation	310
monitoring	311
temperature fields	337
information support and automated	
control	356

This page has been reformatted by Knovel to provide easier navigation.

## Index Terms

## Links

Wet-steam turbines	xxi	1	23	26
history		1		
prospects for nuclear power industry		26		
Wilson region	56	59	169	286
Wire mesh/demister	206	208		

## **X**

Xenon poisoning	22
-----------------	----

## **Z**

Zircaloy	21
----------	----

This page has been reformatted by Knovel to provide easier navigation.